UNIVERSITÄT LEIPZIG

# REPORT

## Institute für Physik
## The Physics Institutes

2008

The Physics Institutes of Universität Leipzig, Report 2008
M. Grundmann (Ed.)

Technical Editor: Gregor Zimmermann



Printed in Germany by
MERKUR Druck- und Kopierzentrum GmbH, Leipzig

online available at
http://www.uni-leipzig.de/~exph2/report_2008.pdf

**Front cover**
J. Kärger, A. Märcker, J. Gabke: "Physics Games", 129th Sunday Lecture at the Faculty of Physics and Earth Sciences, March 9 2008. Afterwards, the more than 300 attendees played the computer game "Pong" using an acousto (blowing on bottles)–electronic feedback. The game, for which an entry in the Guiness World Records is pending, was started with a bell made out of lead. It could only be tolled using a physical effect: It had to be cooled to liquid-nitrogen temperature in order to make it ring.

**Back cover**
Recent book publication.

# Institut für Experimentelle Physik I
# Institut für Experimentelle Physik II
# Institut für Theoretische Physik

## Fakultät für
## Physik und Geowissenschaften

## Universität Leipzig

# Institute for Experimental Physics I
# Institute for Experimental Physics II
# Institute for Theoretical Physics

## Faculty of Physics and Geosciences

## Universität Leipzig

# Report 2008

# Addresses

### Institute for Experimental Physics I

Linnéstraße 5
D-04103 Leipzig, Germany

Phone: +49 341 97-32551
Fax: +49 341 97-32599
WWW: http://www.uni-leipzig.de/~gasse/nysid_a/inst/exp_1.htm
Mailing address: Postfach 100 920, D-04009 Leipzig, Germany

### Institute for Experimental Physics II

Linnéstraße 5
D-04103 Leipzig, Germany

Phone: +49 341 97-32650
Fax: +49 341 97-32668
WWW: http://www.uni-leipzig.de/~exph2
Mailing address: Postfach 100 920, D-04009 Leipzig, Germany

### Institute for Theoretical Physics

Vor dem Hospitaltore 1
D-04103 Leipzig, Germany

Phone: +49 341 97-32420
Fax: +49 341 97-32548
WWW: http://www.physik.uni-leipzig.de
Mailing address: Postfach 100 920, D-04009 Leipzig, Germany

# Preface

In front of you is the 2008 report of the Physics Institutes of the Universität Leipzig. The year has brought a strong expansion of our interdisciplinary education and cooperation with chemistry and biochemistry in the framework of the Leipzig Graduate School of Natural Sciences "Building with Molecules and Nano-objects (BuildMoNa)", now hosting almost one hundred doctoral candidates. We particularly acknowledge the strong participation of our industrial partners in the teaching modules. The Graduate School is supported by the State of Saxony with two additional Research Units ("Nachwuchsforschergruppen") funded via ESF and having started in the meanwhile.

The Universität Leipzig continues to host the EU Network of Excellence SANDiE and supports research in the area of nanotechnology with its Top Level Research Area 1 "From Molecules and Nanostructures to Multifunctional Materials and Processes" ("Profilbildender Forschungsbereich 1"). The beginning of the year 2008 marks also the start of Sonderforschungsbereich 762 "Functionality of Oxidic Interfaces" intensifying the cooperation with our neighboring university in Halle on novel memory concepts.

The report presents to you an overview of our research in numerous projects, enjoyably conducted with colleagues and partners worldwide. We are grateful to our guests in the colloquium and the research groups. They have enriched our academic year. Our activities are only possible due to the generous support from various funding agencies which is individually acknowledged in the short reports.

Leipzig,
June 2008

*M. Grundmann*
*J.A. Käs*
*R. Verch*
Directors

# Contents

# 1

# Structure and Staff of the Institutes

## 1.1 Institute for Experimental Physics I

### 1.1.1 Office of the Director

Prof. Dr. Friedrich Kremer (director)
Prof. Dr. Jörg Kärger (vice director)

since June 2008:

Prof. Dr. Josef A. Käs (director)
Prof. Dr. Frank Cichos (vice director)

### 1.1.2 Molecular Nano-Photonics, Molekulare Nanophotonik [MON]

Prof. Dr. Frank Cichos

**Secretary**

Christine Adolph

**Technical staff**

Dipl.-Phys. Uwe Weber

**PhD candidates**

Subhasis Adhikari, M.Sc.
Dipl.-Phys. Nicole Amecke
Dipl.-Phys. Nils Neubauer
Dipl.-Phys. Martin Pumpa
Dipl.-Phys. Romy Radünz
Dipl.-Phys. Rebecca Wagner

**Students**

Marco Braun
Eugen Ehrenpreis
Leander Fiedler
Momchil Ivanov

Rüdiger Kürsten
Spas Nedev
Markus Selmke
Angel Topalov

### 1.1.3 Molecular Physics, Molekülphysik [MOP]

Prof. Dr. F. Kremer

**Secretary**

Karin Girke
Ines Grünwald

**Technical staff**

Tech. Hartmut Domröse
Dipl.-Ing. Jörg Reinmuth
Dipl.-Phys. Viktor Skokov

**Academic staff**

Dr. Mahdy Elmahdy
Dr. Periklis Papadopoulos

**PhD candidates**

Dipl.-Chem. Roxana Ene
Dipl.-Phys. Christof Gutsche
Ciprian Ghiorghita Iacob, M.Sc.
Dipl.-Phys. Kati Kegler
Emmanuel U. Mapesa, M.Sc.
Joshua Rume Sangoro, M.Sc.
Ilya Semenov, M.Sc.
Dipl.-Phys. Gunter Stober

**Students**

Hergen Brutzer
Benjamin Gollnick
Oliver Otto
Jan H. Peters
Wilhelm Kossack
Christina Krause
Martin Treß
Olaf Ueberschär
Carolin Wagner

### 1.1.4 Physics of Interfaces, Grenzflächenphysik [GFP]

Prof. Dr. Jörg Kärger

**Secretary**

Katrin Kunze

**Technical staff**

Dipl.-Phys. Cordula Bärbel Krause
Lutz Moschkowitz
Stefan Schlayer

**Academic staff**

Prof. Dr. Dieter Freude
Dr. Karen Friedemann
Jun. Prof. Dr. Petrik Galvosas
PD Dr. Farida Grinberg
Dr. Grit Kalies
Dr. Margarita Krutyeva
Prof. (i.R.) Dr. Dr. h.c. Harry Pfeifer †
Dr. Frank Stallmach
Dr. Rustem Valiullin

**PhD candidates**

Dipl.-Phys. Christian Chmelik
Dipl.-Phys. Muslim Dvoyashkin
Dipl.-Phys. Moisés Fernadez
Dipl.-Phys. Wadinga Fomba
Dipl.-Chem. Filipe Furtado
Dipl.-Phys. Lars Heinke
Dipl.-Phys. Aleksey Khokhlov
Dipl.-Phys. Sergej Naumov
Dipl.-Phys. Ekaterina Romanova
Dipl.-Phys. Oraphan Saengsawang
Dipl.-Phys. Denis Schneider
Dipl.-Geophys. Wiete Schönfelder
Dipl.-Ing. Despina Tzoulaki
Dipl.-Phys. Konstantin Ulrich
Dipl.-Phys. Markus Wehring

**Students**

Florian Hibbe
Carsten Horch
Tomas Binder
Marcel Gratz
Mario Grossmann
Tobias Titze
Steffen Becker

### 1.1.5 Soft Matter Physics, Physik der weichen Materie [PWM]

Prof. Dr. Josef A. Käs

**Secretary**

Claudia Honisch

**Technical staff**

Dipl. Ing. Undine Dietrich
Dipl.-Phys. Bernd Kohlstrunk
Ing. Elke Westphal

**Academic staff**

Dr. Carsten Selle

**PhD candidates**

Dipl.-Phys. Claudia Brunner
Susanne Ebert, M.Sc.
Anatol Fritsch, M.Sc.
Thomas Fuhs, M.Sc.
Brian Gentry, M.Sc.
Dipl.- Phys. Jens Gerdelmann
Markus Gyger, M.Sc.
Dipl.-Phys. Florian Huber
Dipl.-Phys. Tobias Kießling
Dipl.-Phys. Melanie Knorr
Daniel Koch, M.Sc.
Dipl.-Phys. Karla Müller
Kenechukwu David Nnetu, M.Sc.
Dipl.-Phys. Philipp Rauch
Florian Rückerl, M.Sc.
David Smith, M.Sc.
Dipl.-Phys. Dan Strehle
Björn Stuhrmann, M.Sc.
Carsten Stüber, M.Sc.
Dipl.-Phys. Franziska Wetzel
Dipl.-Phys. Lydia Woiterski

**Students**

José Alvarado
Sebastian Ehrig
Lukas Hilde
Kathleen Kirchner
Tom Kirchner
Maximilian Semmling
Jörg Schnauß
Roland Stange
Matthias Steinbeck
Johannes Stelzer
Markus Streicher
Carsten Vogt

## 1.2 Institute for Experimental Physics II

### 1.2.1 Office of the Director

Prof. Dr. Marius Grundmann (director)
Prof. Dr. Tilman Butz (vice director)

### 1.2.2 Magnetic Resonance of Complex Quantum Solids, Magnetische Resonanz Komplexer Quantenfestkörper [MQF]

Prof. Dr. Jürgen Haase

**Secretary**

Teresa Nitsch

**Technical staff**

Dipl.-Ing. Joachim Hoentsch
Dipl.-Phys. Gert Klotzsche

**Academic staff**

Dr. Marko Bertmer
Prof. Dr. Rolf-Michael Böttcher
apl. Prof. Dr. Andreas Pöppl
Dr. Damian Rybicki

**PhD candidates**

Dipl.-Phys. Ingo Hilschenz
Dipl.-Chem. Bettina Jee
Dimo Ivanov, M.Sc.
Dipl.-Phys. Pavel Sedykh

**Students**

Benno Meier
Gregor Thörmer
Michael Jurkutat
Alexander Jäger
Thomas Meißner

### 1.2.3 Nuclear Solid State Physics, Nukleare Festkörperphysik [NFP]

Prof. Dr. Tilman Butz

**Secretary**

Teresa Nitsch

**Technical staff**

Carsten Pahnke
Dipl.-Ing. Joachim Starke

**Academic staff**

Dr. Tilo Reinert
Dr. Daniel Spemann
Dr. Jürgen Vogt

**PhD candidates**

Nirav Barapatre, M.Sc.
Dipl.-Biol. Anja Fiedler
Dipl.-Phys. Steffen Jankuhn
Dipl.-Phys. (Med.-Phys.) Torsten Koal
Dipl.-Phys. Christoph Meinecke
Dipl.-Phys. Frank Menzel
Dipl.-Phys. Martin Rothermel

**Students**

Tobias Andrea
Alexander Arndt
René Feder
Katherine Guenther
Frank Heymann
Andreas Hinze
Marcus Hohlweg
Alexander Malwin Jakob
Franz Kirsten
Daniela Kolbe
Niklas Liebing
Silvio Marx
Dirk Mehlhorn
Jens Schneider
Uwe Scholz
Ronald Werner

### 1.2.4 Semiconductor Physics, Halbleiterphysik [HLP]

Prof. Dr. Marius Grundmann

**Secretary**

Anja Heck

**SANDiE Network Office**

Dr. Alexander Weber (Network Officer)
Birgit Wendisch (Secretary)

**Technical staff**

Dipl.-Phys. Gabriele Benndorf
Dipl.-Ing. Gisela Biehne
Dipl.-Ing. Holger Hochmuth

Dipl.-Phys. Jörg Lenzner
Gabriele Ramm
Roswitha Riedel

**Academic staff**

Dr. Bingqiang Cao
Dr. Karsten Goede
Dr. Nilotpal Ghosh
PD Dr. Michael Lorenz
PD Dr. Rainer Pickenhain
Prof. Dr. Bernd Rheinländer (retired)
Dr. Rüdiger Schmidt-Grund
Dr. Alexander Weber
Dr. Holger von Wenckstern

**PhD candidates**

Dipl.-Phys. Matthias Brandt
Dipl.-Phys. Christian Czekalla
Dipl.-Phys. Martin Ellguth
Dipl.-Phys. Heiko Frenzel
Susanne Heitsch, M.Sc.
Dipl.-Phys. Helena Hilmer
Dipl.-Phys. Alexander Lajn
Dipl.-Phys. Martin Lange
Dipl.-Phys. Alexander Müller
Dipl.-Phys. Matthias Schmidt
Dipl.-Phys. Chris Sturm
Dipl.-Phys. Gregor Zimmermann
Dipl.-Phys. Jan Zippel

**Students**

Uta Allenstein
Ronny Bakowskie
Lucie Behnke
Kerstin Brachwitz
Christof Dietrich
Dominik Lausch
Thomas Lüder
Annekatrin Hinkel
Fabian Klüpfel
Andreas Kraus
Philipp Kühne
Michael Lorenz
Friedrich Schein
Florian Schmidt
Stefan Schöche
Dieter Stender
Marko Stölzel
Zhang Zhipeng

### 1.2.5 Solid State Optics and Acoustics, Festkörperoptik und -akustik [FKO]

Prof. Dr. Wolfgang Grill

**Secretary**

Annette Käthner

**Technical staff**

Hans-Joachim vom Hofe
Dipl.-Ing. (FH) Ulrike Teschner
Dipl.-Phys. Horst Voigt

**Academic staff**

Dr. Reinhold Wannemacher
Dr. Evgeny Twerdowski

**PhD candidates**

Amro Abdelrahman, M.Sc.
Esam Eldin Ahmed Mohamed, M.Sc.
Umar Amjad, M.Sc.
Dipl.-Phys. Erik von der Burg
Dipl.-Phys. Moritz von Buttlar
Albert Kamanyi, M.Sc.
Zakir Hossain Muhammad, M.Sc.
Khurram Shahzad Tarar, M.Sc.

**Students**

Katrin Hahn
Angeline Kasina, M.Sc.
Toma Lazar, M.Sc.
Rico Meier, M.Sc.
The Gia Tang

### 1.2.6 Superconductivity and Magnetism, Supraleitung und Magnetismus [SUM]

Prof. Dr. Pablo Esquinazi

**Technical staff**

Dr. Winfried Böhlmann
Klaus Grünwald
Dipl.-Krist. Annette Setzer
Monika Steinhardt

**Academic staff**

Dr. José Barzola-Quiquia
Dr. German Brideaux
Dr. Roland Höhne
Dr. Detlef Spoddig
PD Dr. Michael Ziese

**PhD candidates**

Ana Ballestar, M.Sc.
Srujana Dusari, M.Sc.
Xiasong Jiang, M.Eng.
Muhammad Khalid, M.Sc.

**Students**

Francis Bern
Ingo Hilschenz
Holger Motzkau
Thomas Scheike
Thomas Scheller

## 1.3 Institute for Theoretical Physics

### 1.3.1 Office of the Director

Prof. Dr. Gerd Rudolph (director)
Prof. Dr. Klaus Kroy (vice director)

since October 2008:

Prof. Dr. Rainer Verch (director)
Prof. Dr. Klaus Kroy (vice director)

**Secretary**

Susan Hussack
Gabriele Menge
Lea Voigt

### 1.3.2 Computational Quantum Field Theory, Computerorientierte Quantenfeldtheorie [CQT]

Prof. Dr. Wolfhard Janke

**Academic staff**

Dr. Michael Bachmann
Dr. Elmar Bittner
Dr. Viktoria Blavatska
Dr. habil. Martin Hasenbusch
Dr. Bartłomiej Wacław

**PhD candidates**

Dipl.-Phys. Mathias Aust
Dipl.-Phys. Rainer Bischof
Dipl.-Phys. Mario Collura (jointly with Université Nancy)
Dipl.-Phys. Monika Möddel
Dipl.-Phys. Andreas Nußbaumer
Dipl.-Phys. Stefan Schnabel

Dipl.-Phys. Sebastian Schöbl
Dipl.-Phys. Thomas Vogel
Sandro Wenzel, M.Sc.
Dipl.-Phys. Micha Wiedenmann

**Students**

Frank Beyer
Martin Falk
Niklas Fricke
Jonathan Groß
Hannes Nagel

### 1.3.3 Molecular Dynamics / Computer Simulation, Moleküldynamik / Computersimulation [MDC]

PD Dr. Horst-Ludger Vörtler (Speaker)
PD Dr. Siegfried Fritzsche

**Academic staff**

Prof. Dr. Reinhold Haberlandt (retired)
Dr. Tanin Nanok
Prof. Dr. Liu Ping
Dr. Oraphan Saengsawang

**PhD candidates**

Rungroj Channajaree, M.Sc.
Kompichit Seehamart, M.Sc.
Somphob Thompho, M.Sc.

**Students**

Markus Knauth

### 1.3.4 Quantum Field Theory and Gravity, Quantenfeldtheorie und Gravitation [QFG]

Prof. Dr. Gerd Rudolph
Prof. Dr. Rainer Verch

**Academic staff**

PD Dr. Michael Bordag
Dr. Pjotr Marecki
Dr. Vladimir Nikolaev
Dr. Matthias Schmidt

**Retired**

Prof. em. Bodo Geyer
Prof. em. Armin Uhlmann

**PhD candidates**

Dipl.-Phys. Marcus Borris
Dipl.-Phys. Alexander Hertsch
Dipl.-Phys. Jan Schlemmer

**Students**

Jörn Boehnke
Andreas Degner
Alexander Knospe
Falk Lindner
Rainer Mühlhoff
Juliane Stanja
Martin Teuchler
Almut Tröller
Konrad Zimmermann

### 1.3.5 Statistical Physics, Statistische Physik [STP]

Prof. Dr. Manfred Salmhofer

**Academic staff**

Dr. Oliver Lauscher

**PhD candidates**

Dipl-Phys. Kay-Uwe Giering
Dipl-Phys. Christoph Husemann

**Students**

Giulio Schober
Ronald Starke

### 1.3.6 Theory of Condensed Matter, Festkörpertheorie [TKM]

Prof. Dr. Ulrich Behn (Speaker)
Prof. Dr. Klaus Kroy

Prof. Dr. Dieter Ihle (retired)
Prof. Dr. Adolf Kühnel (retired)

**Academic staff**

Dipl.-Phys. Sebastian Schöbl

**PhD candidates**

Dipl.-Phys. Jens Glaser
Dipl.-Phys. Micaela Krieger-Hauwede
Dipl.-Phys. Daniel Rings
Dipl.-Phys. Holger Schmidtchen
Dipl.-Phys. Sebastian Sturm
Dipl.-Phys. Lars Wolff

**Students**

Fridolin Groß
Steffen Grosser
Susanne Gütter
Marcel Hennes
Christian Hubert
Melanie Knorr
Andrea Kramer
Mario Thüne
Benjamin Werner
Lucas Wetzel

### 1.3.7 Theory of Elementary Particles, Theorie der Elementarteilchen [TET]

Prof. Dr. Klaus Sibold

**Academic staff**

Dr. Burkhard Eden
PD Dr. Roland Kirschner
PD Dr. Holger Perlt
PD Dr. Arwed Schiller
Dr. Mathieu Segond

# I

# Institute for Experimental Physics I

# 2

# Molecular Nano-Photonics

## 2.1 Introduction

The challenge of experimental physics on the nanoscale is to access local phenomena, that occur for example at interfaces, at specific molecular sites or at certain places within nano-structured materials. These local phenomena may control molecular dynamics, drive self-organization, cause charge separation or alter light propagation. Their importance extends to almost every field involved in future nanotechnology. The research of the molecular nano-photonics group thus aims at the development and application of optical techniques to access nanoscale (dynamical) processes in various fields such as chemical physics, biology or semiconductor physics. The understanding of these dynamical processes shall ultimately lead to a control over single molecules and other nano-objects by applying heat, flow, shear forces, electric fields or current.

The main experimental tool within our research is optical single molecule detection by ultra-sensitive microscopic techniques including time-resolved confocal microscopy, wide-field fluorescence or photothermal microscopy. Single molecules or semiconductor quantum dots provide the ideal local probes to access nanoscale physical properties inside materials while keeping the information on the heterogeneity of the system. Using these techniques recent projects focused on the

- Photothermal detection of single gold nanoparticles,
- Heat transfer on the nanoscale,
- Nanometric distance measurements with single gold nanoparticle pairs,
- Electrochemical manipulation of the emission of colloidal semiconductor nanocrystals,
- Photophysics of single silicon nanoparticles,
- Defocused imaging of single emitters in photonic crystals,
- Single molecule diffusion in ultrathin confined liquid films.

During the year 2008 the Molecular Nanophotonics Group has started experimenting on the new experimental facilities including

- confocal sample scanning optical microscope for fluorescence correlation spectroscopy and time-resolved detection,
- sample scanning photothermal microscope coupled with a fluorescence wide field and optical confocal microscope,

- fluorescence wide field microscope for high speed single molecule detection,
- single molecule wide field fluorescence microscope for defocused imaging and orientational mapping of single molecules.

The group has contributed in 2008 significant work to the DFG research unit 877 "From Local Constraints to Macroscopic Transport". Especially first collaborations with the group of Prof. Dr. Klaus Kroy (University Leipzig) and Dr. Michael Mertig (Technische Universität Dresden) have been established.

*Frank Cichos*

## 2.2 Photothermal Correlations Spectroscopy

R. Radünz, F. Cichos

Single molecule detection is meanwhile a widely used technique to study dynamical processes in complex materials, especially in biophysics. It is, however, always restricted to fluorescent probes such as organic dye molecules or quantum dots. Within this project, we analyze the capabilities of photothermal microscopy and photothermal correlation spectroscopy for the detection of single non-fluorescent nano-objects such as gold nanoparticles.

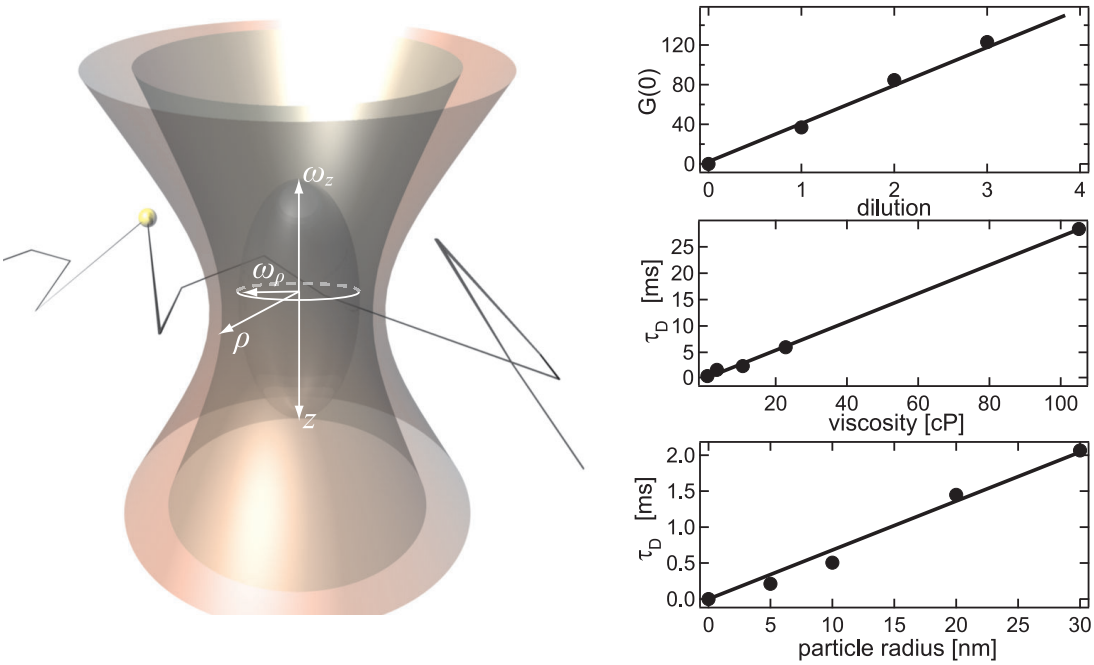


**Figure 2.1:** *Left*: Principle of the photothermal correlation spectroscopy (PhoCS). A laser is heating gold nanoparticles diffusing through the focal volume of a confocal microscope. A red laser probes the refractive index change around the nanoparticle with heterodyne detection technique. *Right*: Verification of PhoCS. The *top graph* shows the contrast obtained from the correlation function, which is a linear function of the particle concentration. The *lower two graphs* depict the particle diffusion time as a function of the viscosity and particle radius.

The detection is based on the absorption of light not on the fluorescence and therefore free of processes as for instance photo-blinking. The photothermal detection technique is based on the generation of a temperature gradient around a heated gold nanoparticle. The temperature gradient modifies the local refractive index which is used to detect single particles optically even though the scattering cross section is far below the single particle detection limit. The group has developed a variant of the photothermal detection technique – the so called photothermal correlation spectroscopy or PhoCS – which is capable of characterizing fast fluctuations of the photothermal signal. This technique can be i.e. applied to replace fluorescence correlation spectroscopy for the study of local tracer diffusion or fast distance fluctuations between gold nanoparticels as described in Sect. 2.4. By studying the diffusion of heated gold nanoparticles in water, we find that the local temperature and viscosity gradient around the hot particle speeds up diffusion. The speed up can be well described by a generalized Stokes–Einstein relation as developed in collaboration with the group of Prof. Klaus Kroy (University Leipzig).

The technique is currently extended to single nanoparticle counting for high throughput screening application techniques in biomedicine.

## 2.3 Heat Transfer on the Nanoscale

R. Radünz, F. Cichos

Single gold nanoparticles can be intentionally used as nano heat sources, allowing the fabrication of thermal nanoactuators for a variety of microfluidic tasks. As the temperature around a single optically heated gold nanoparticle decays on a lengthscale

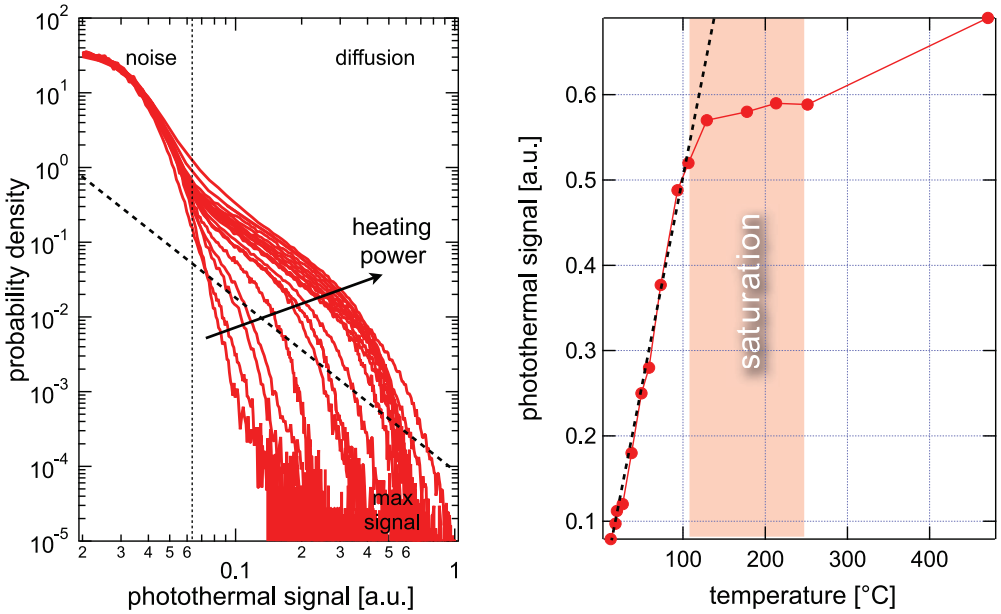


**Figure 2.2:** Left: Histogram of the photothermal signal strength of $R = 30$ nm gold nanoparticles diffusing in water at different heating power. *Right*: Cut-off signal according to the *dashed line* in the *left graph*. The cut-off photothermal signal intensity clearly shows a saturation of the signal at a particle temperature of about 100 ℃, which is presumably due to local structural changes in the liquid next to the particle surface.

of a few 10 nm, also phase transitions or just the transfer of heat across a nanoscale curved interface can be studied. Photothermal correlation spectroscopy is therefore and ideal tool, since the photothermal detection technique as presented in Sect. 2.2 is intrinsically based on the heat released from a particle to the surrounding.

We therefore couple the observation of particle mobility, which reveals thermal fluctuation strength and viscosity changes due to temperature with the observation of photothermal signal strength, which tells about the thermal gradient in the surrounding liquid. Our results demonstrate, that heat transfer at the nanoscale is influenced by the local structure of the liquid. Local structural changes at the particle surface result in an insulation layer for the heat transfered from the particle to the surrounding liquid. These local structural changes on a nanoscale lead to a saturation of heat transfer and thus the photothermal signal (see Fig. 2.2). These effects go along with a saturation of the particle mobility. The details of these changes are currently under investigation by molecular dynamics simulations.

## 2.4 Nanometric Distance Measurements with Single Gold Nanoparticle Pairs

N. Neubauer, M. Wähnert, R. Radünz F. Cichos

The number of optical techniques capable of measuring distances and distance fluctuations on the nanoscale is limited to charge and electron transfer processes. The upper limit of distances being measured with these methods is currently 10 nm and no other method is available, which fills the gap between 10 nm and 1 µm (corresponding to optical resolution). This project develops a technique based on pairs of gold nanoparticles for this intermediate distance range. Gold particles are strongly inter-

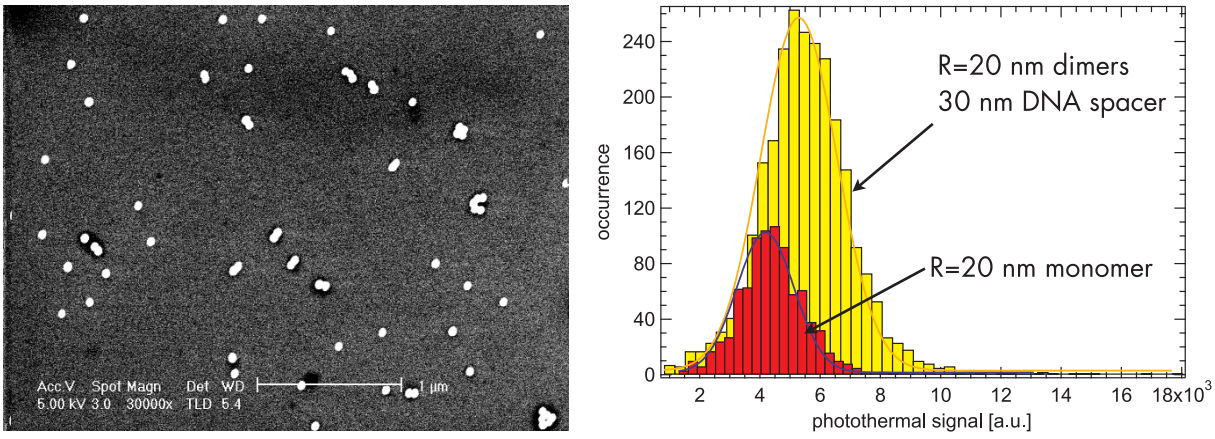


**Figure 2.3:** *Left*: Electron microscopy image of coupled gold nanoparticles ($R = 30$ nm). The nanoparticles are coupled by 30 nm double stranded DNA. The separation of the particles is not visible as a result of capillary effects during sample preparation. *Right*: Photothermal signal intensity histograms of individual $R = 30$ nm gold nanoparticles (*red*) and gold nanoparticle dimers (*yellow*). The histograms show for the first time an increased signal intensity of dimers as compared to individual nanoparticles.

acting with light due to a collective excitation of free electrons in the nanoparticle. These plasmon can be resonantly excited with visible light. The electric field associated with the plasmon resonance couples between closely spaced nanoparticles and forms a new resonance.

In collaboration with the group of Dr. Michael Mertig at the TU Dresden the group has fabricated sucessfully gold nanoparticle pairs coupled by 30 nm DNA strands (see Fig. 2.3). The pairs are synthesized by coupling two complementary single stranded DNA chains to gold nanoparticles. The complementary DNA chains then bind to form gold nanoparticle dimers, which have been further separated from monomers by gel electrophoresis. These dimers have been investigated by dark-field scattering microscopy, which reveals clear signs of plasmon coupling in the structures. Further, photothermal measurements have been carried out to investigate the photothermal signal enhancement due to the plasmon coupling. As shown in Fig. 2.3 clear enhancement effects of the photothermal signal are found, which are the first photothermal proof of coupled plasmon resonances. Currently the technique is extended to monitor distance fluctuations and to allow for screening applications on DNA.

## 2.5 Electrochemical Manipulation of the Emission of Colloidal Semiconductor Nanocrystals

N. Amecke, A. Topalov, F. Cichos

Semiconductor nanocrystals and dye molecules show an intermittent emission on timescales ranging from microseconds up to several hundred seconds. Such extremely long periods without any emission are still a mystery. They are thought to be related to photoinduced charging processes. A charge, presumably an electron is ejected from the excited state of an emitter by a tunneling process to the surrounding environment, which is often an amorphous, disordered polymer or glass. Due to the rugged energy landscape in such amorphous environments, the kintetics of “on–off” blinking in quantum dots or dye molecules follows a power law statistics being very robust, which makes the characterization of the physical processes behind the blinking very difficult.

Our studies are aimed to take control of the blinking processes. We are developing a method to study emission intermittency of quantum dots in an electrochemical cell. The electrochemical cell shall allow a controlled removal or addition of electrons to the quantum dot in solution. The fluorescence based detection with picosecond time resolution will correlate the photophysics with the charge state of the quantum dots. First experimental success showing the influence of a current on dissolved quantum dot emission is depicted in (Fig. 2.4). The present results cleary demonstrate that the emission intensity of a quantum dot ensemble in solution is strongly correlated with the applied voltage in the cell. This correlation is clearly related a change in the non-radiative decay rate of the quantum dots.

Thus current experiments demonstrate the feasibility of optically detected electrochemistry on quantum dots. Our further efforts will extend these measurements to single quantum dots to clearify the physical origins of quantum dot blinking.

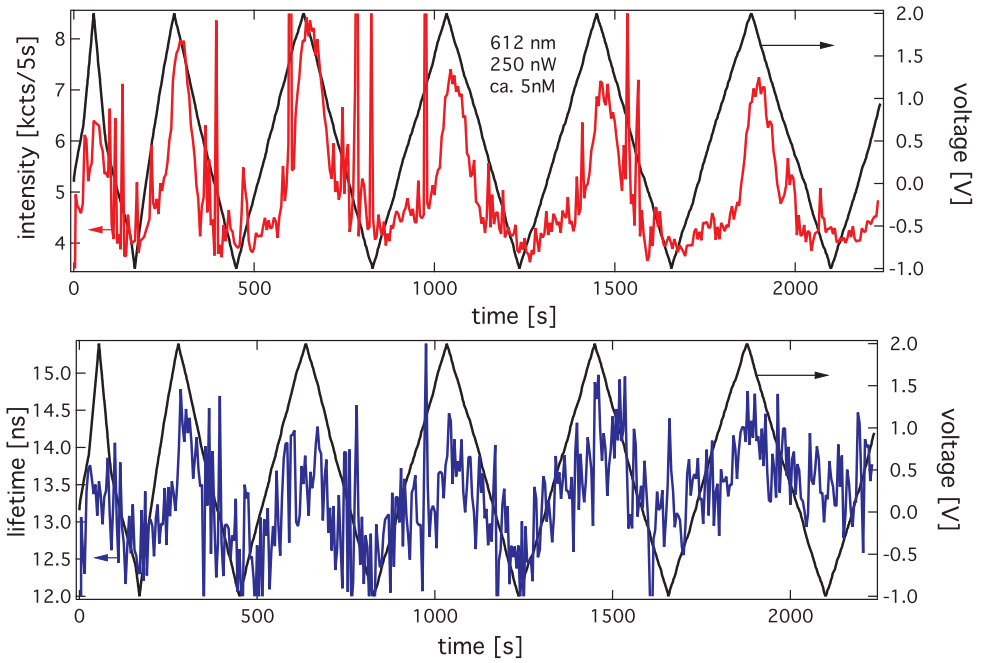


**Figure 2.4:** *Top*: Fluorescence emission intensity of CdSe quantum dots in solution as a function of the voltage applied to the electrochemical cell. The intensity clearly follows the triangular voltage applied. *Bottom*: Fluorescence emission lifetime of the quantum dots. Since the lifetime also follows the applied voltage, we assume a change in the non-radiative transition rate in the quantum dots.

## 2.6 Defocused Imaging of Single Emitters in Photonic Crystals

R. Wagner, G. Kropat, F. Cichos

Photonic crystals provide a powerful way to manipulate light on a basis, which is very similar to that of semiconductors. The photonic crystal structure can be tailored in great detail in contrast to semiconductor crystals. As in photonic crystals the refractive index is a function of the position in the crystal and thus a local property, all optical properties of emitters become also a function of their position in the crystal. This spatial change of the so called local optical density of states is difficult to explore in three dimensional systems as all local methods cannot penetrate structure. We have therefore developed a method, which is based on the imaging of single emitters inside a photonic crystal. The method employs a defocusing of single emitters (e.g. quantum dots), in which a diffraction pattern of the emitting object appears. This diffraction pattern contains information on the anisotropic light propagation in material.

This type of study reveals the anisotropic light propagation in colloidal photonic crystals from a single image of a quantum dot and is now further applied to wavelength-selective studies in colloidal photonic crystals (see Fig. 2.5). The emission diffraction pattern is studied at different incorporation depth in the photonic crystal, which gives information on the local optical density of states at various positions. Currently these methods are extended to realize emission anisotropy studies in liquid crystals as well as long range energy transfer in photonic crystals.

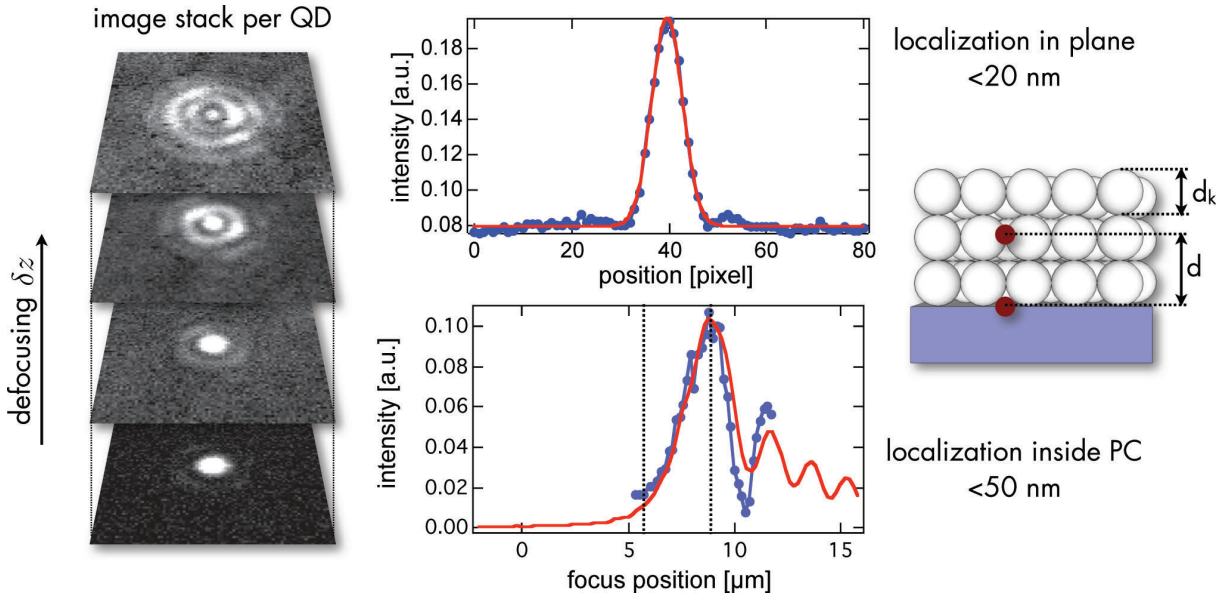


**Figure 2.5:** *Left*: Sequence of defocused fluorescence images from a single CdSe/ZnS quantum dot embedded inside an opaline photonic crystal made of 260-nm polystyrene beads. *Middle*: Emission intensity cross section of the quantum dot fluorescence image in the focal plane (*top*) and emission intensity of the central intensity maximum as a function of the focus position inside the photonic crystal. Both plots deliver a localization accuracy of the quantum dot inside the photonic crystal of 20 nm and 50 nm. *Right*: Schematics depicting the incorporation depth $d$ of the quantum dot in the photonic crystal as well as the colloidal diameter $d_k$ of the photonic crystal building blocks.

## 2.7 Single Molecule Diffusion in Thin Liquid Films and Liquid Crystals

M. Pumpa, F. Cichos

The experiments of this project are aimed at the direct manipulation of molecular mobility due to local chemical modifications of a solid surface. Chemical modifications alter locally the hydrodynamic boundary conditions which also effect the viscous drag experienced by any tracer molecule or particle at the solid surface. To proof this effect, we have applied micro-contact printing to prepare alternating stripes of hydrophilic and hydrophobic regions on a glass substrate. This glass slide is used together with a hydrophilic one to confine a liquid containing dye labeled polystyrene beads (100 nm diameter) down to a film thickness of 150 nm in a home built surface forces apparatus. This surface forces apparatus is coupled to a wide field single molecule microscope.

Single particle tracking experiments reveal a significant change in the particle mobility between hydrophobic and hydrophilic surface areas, which we can clearly attribute to modified hydrodynamic coupling to the surface (see Fig. 2.6). However, the chemically modified regions reveal themselves considerable variation in the particle mobility (see Fig. 2.6a). The spread of local mobilities in regions of hydrophobic surface modification suggests local imperfections and defects of the chemical modification. Thus particle tracking experiments as shown exemplarily can be used to sense chemical surface composition.

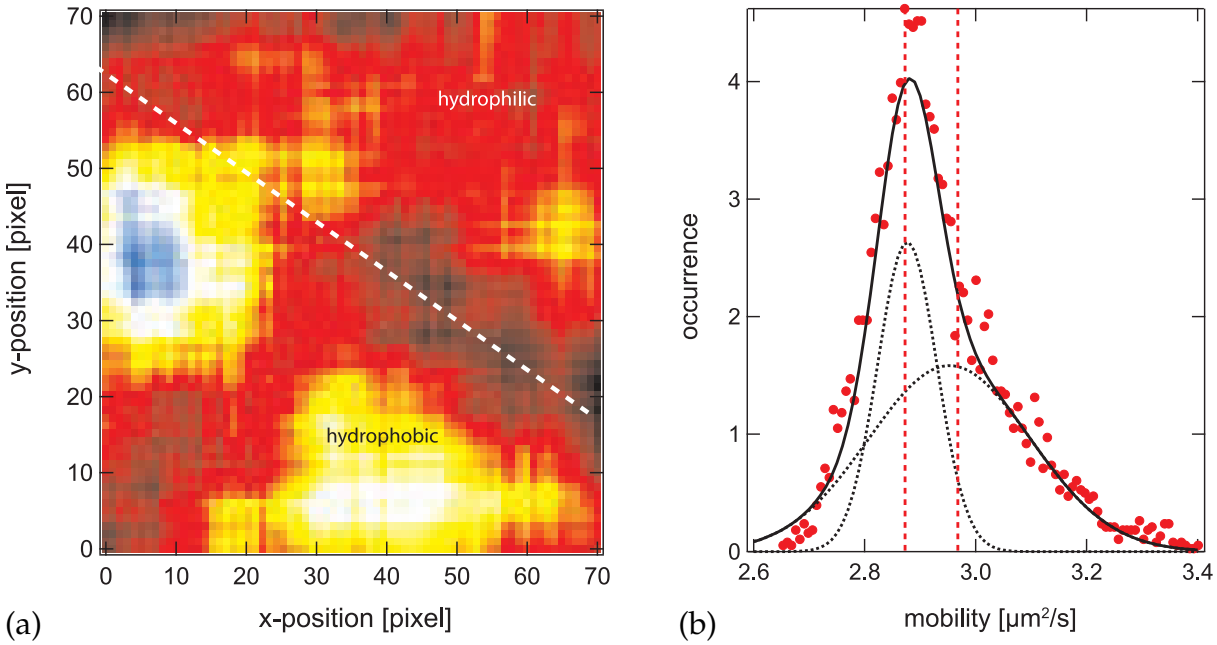


**Figure 2.6:** (**a**) Local mobility map for 100-nm polystyrene particles confined between a hydrophilic and a chemically structured glass surface (1 pixel corresponds to 140 nm). *Brighter areas* denote large particle mobility. (**b**) Histogram of local particle mobilities obtained from the *left* image. A bimodal mobility distribution is visible, which is the result of the chemical surface modification. The larger spread in the mobilities is found in the hydrophobic part, which for the first time reveals a local sensitivity of particle diffusion to chemical surface imperfections.

## 2.8 Single Molecule Nanorheology

M. Selmke, S. Adhikari, F. Cichos

A drastic slowdown of the dynamics of a liquid when approaching the transition to a disordered amorphous solid state is common to a vast variety of systems. Such systems involve simple molecular fluids of small molecules and extend to complex polymeric or polyelectrolyte systems and even to the cell's network of structural filaments. All of these systems have two things in common: structural disorder and metastability, which define the still not well understood complexity of the systems dynamics. Within this project we explore a new way to reveal the maroscopic viscoelastic properties from nanoscopic measurements. By coupling two fluorophores to a single polymer chain embedded in a polymer, we are able to measure distance fluctuations between these dye, which contain information about the viscoelastic coupling due to the local material properties. A detailed analysis of the distance fluctuations shall thus give information if the local viscoelestic response of a polymer is still corresponding to the macroscopic ones.

Current experiments of this project investigate the temperature dependence of the reorientational dynamics of single dye molecules in polymers (see Fig. 2.7). By polarization resolved fluorescence microscopy we are able to take snapshots of the orientation of single dye molecules. Our experiments reveal so far, that the polymer dynamics in the studied temperature range is spatially heterogeneous. In comparative measurements, we could for the first time directly show, that the dynamics as reported by single

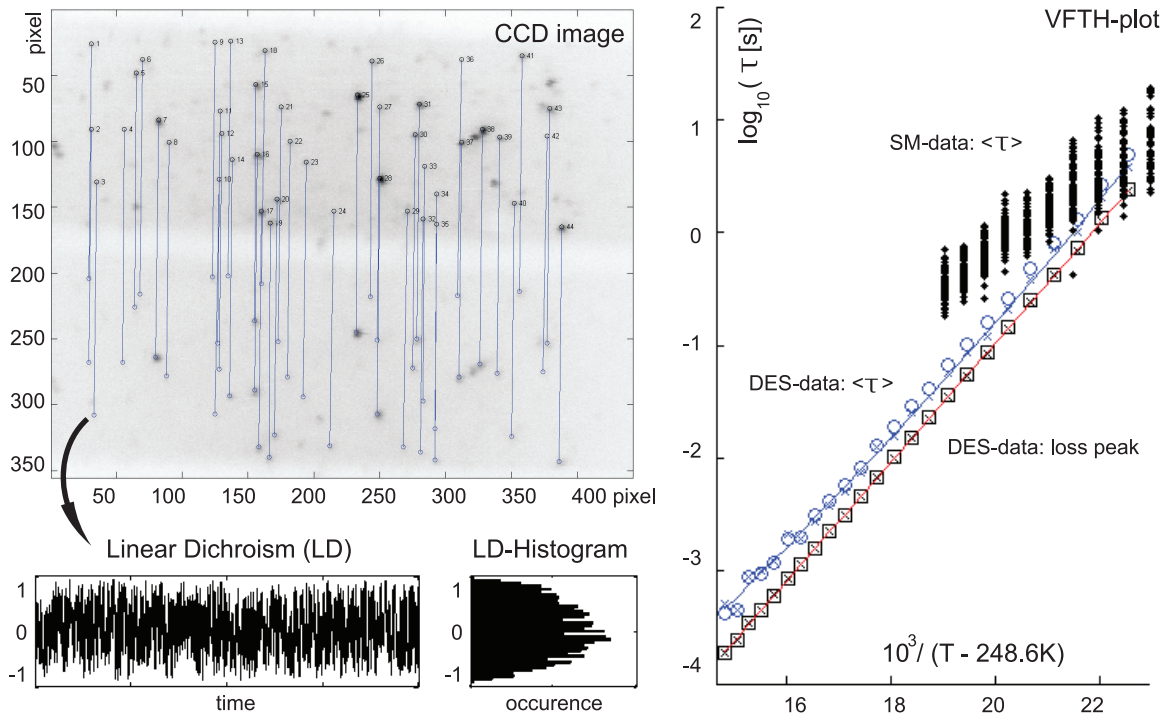


**Figure 2.7:** *Left*: Emission polarization images of single dye molecules embedded in a polymer film. These images allow the calculation of a linear dichroism, which is a measure of the dye molecule orientation in the polymer (see the text). The fluctuations of the correlation allow the extraction of a single molecule rotational diffusion time-constant. *Right*: Single molecule rotational diffusion time constants (SM-data) in comparison with dielectric measurements.

dye molecules resembles that of dielectric measurements. Further, efforts are made to synthesize doubly labeled polymer molecules, which allow for a detection of the end to end fluctuations of single polymer chains in polymer melts. This will lead to a new rheological technique applicable to a large variety of viscoelastic materials.

## 2.9 Funding

*Light Emission of Single Emitters in 3-dimensional Photonic Crystals*
Frank Cichos
Ci 33/5-1

*Ortsaufgelöste Detektion von Struktur und Dynamik in nematischen Phasen biaxialer Moleküle*
Frank Cichos
Ci 33/6-1

*FG 877: Constrained Single Molecule Dynamics in Glassy Polymer Systems*
Frank Cichos
Ci 33/7-1

## 2.10 Organizational Duties

F. Cichos

- Vorsitzender der Eignungsfeststellungskommission der Fakultät für Physik und Geowissenschaften
- Speaker DFG Research Unit 877 "From Local Constrainst to Macroscopic Transport"
- Referee: Phys. Rev. B, Phys. Rev. Lett., Nature, Chem. Phys. Lett., Appl. Phys. Lett., ACS Petroleum Research Fund

## 2.11 External Cooperations

**Academic**

- Technische Universität Chemnitz
  Prof. Dr. C. von Borczyskowski
- Universität Mainz
  Prof. Dr. T. Basché
- Technische Universität Dresden
  Dr. M. Mertig

## 2.12 Publications

**Journals**

J. Martin, F. Cichos, F. Huisken, C. von Borczyskowski: *Electron-Phonon Coupling and Localization of Excitons in Single Silicon Nanocrystals*, Nanolett. **8**, 656 (2008)

T. Blaudeck, E.I. Zenkevich, F. Cichos, C. von Borczyskowski: *Probing Wave Functions at Semiconductor Quantum-Dot Surfaces by NON-FRET Photoluminescence Quenching*, J. Phys. Chem. C **112**, 20251 (2008)

E.I. Zenkevich, T. Blaudeck, F. Cichos, M. Heidernätsch, C. von Borczyskowski: *Electron wave function tunneling in excited nanocomposites based on semiconductor CdSe/ZnS quantum dots and porphyrins*, Proc. VII Int. Conf. Laser Phys. Opt. Technol., Minsk, 228 (2008)

**Talks**

F. Cichos: *Concepts for Single Quantum object detection in diffusion processes*, SFG Symposium, Technische Universität Chemnitz, Germany, July 2008

F. Cichos: *Emission Intensity Fluctuations of Single Molecule Emitters*, 2. Workshop on Low Dimensional Structures: Properties and Applications, Aveiro, Portugal, January 2008

F. Cichos: *Emission of Single Molecules in 3D Photonic Crystals*, E-MRS 2008 Spring Meeting, Straßbourg, France, 26. – 30. May 2008

F. Cichos: *Measuring and Manipulating with Single Gold Nanoparticles*, Physical Chemistry Colloquium, Ludwig-Maximilians-Universität München, Germany, April 2008

F. Cichos: *Photothermal Fluctuation Spectroscopy on Coupled Gold Nanoparticles*, SFG Symposium, Universität Leipzig, Germany, February 2008

F. Cichos: *Tracking and Manipulating Single Molecule Diffusion in Liquids*, 72. DPG Spring Meeting, Berlin, Germany, 25. – 29. February 2008

R. Radünz: *PhoCS - Photothermal Correlation Spectroscopy*, 8. Int. Meeting Thermodiffusion (IMT 8), Bonn, 09.- 13. June 2008

R. Radünz: *PhoCS - Photothermal Correlation Spectroscopy*, Workshop for German and Korean Junior Scientists, Seoul, Korea, October 2008

R. Radünz: *Probing polymer dynamics by interfacial heat transfer at single gold nanoparticles*, 72. DPG Spring Meeting, Berlin, Germany, 25. – 29. February 2008

M. Selmke: *Single Molecule Dynamics in Polymers*, SFG Symposium, Technische Universität Dresden, Germany, November 2008

R. Wagner: *Defocused Imaging of Single Emitters in Photonic Crystals*, 72. DPG Spring Meeting, Berlin, Germany, 25. – 29. February 2008

**Posters**

N. Amecke, F. Cichos: *Investigations of single quantum dot (QD) blinking via Fluorescence Correlation Spectroscopy (FCS)*, 72. DPG Spring Meeting, Berlin, Germany, 25. – 29. February 2008

M. Pumpa, F. Cichos: *Single Molecule Diffusion on Chemically Patterned Substrates*, 72. DPG Spring Meeting, Berlin, Germany, 25. – 29. February 2008

R. Radünz, F. Cichos: *PhoCS - Photothermal Correlation Spectroscopy*, Bunsentagung 2008, Saarbrücken, Germany, 01. – 03. May 2008

R. Radünz, F. Cichos: *Probing polymer dynamics by interfacial heat transfer at single gold nanoparticles*, Bunsentagung 2008, Saarbrücken, Germany, 01. – 03. May 2008

R. Radünz, F. Cichos: *Probing polymer dynamics by interfacial heat transfer at single gold nanoparticles*, 8. Int. Meeting Thermodiffusion (IMT 8), Bonn, 09.- 13. June 2008

M. Wähnert, R. Radünz, F. Cichos: *Measuring distance fluctuations by single pairs of gold nanoparticles*, 72. DPG Spring Meeting, Berlin, Germany, 25. – 29. February 2008

S. Zimmermann, R. Wagner, F. Cichos: *Defocused Imaging of Fluorescent beads in Photonics Crystals*, 72. DPG Spring Meeting, Berlin, Germany, 25. – 29. February 2008

## 2.13 Graduations

**Diploma**

- Eugen Ehrenpreis
  *Basic considerations towards photothermal trapping*
  August 2008
- Momchil Ivanov
  *Development of Optically Detected Cyclic Voltammetry for Measurements on Single Semiconductor Quantum Dots*
  December 2008
- Rüdiger Kürsten
  *Photothermal Correlation Spectroscopy*
  September 2008
- Markus Selmke
  *Study of Polymer Dynamics with the help of Single Fluorescent Molecules*
  December 2008
- Miriam Wähnert
  *Abstandsmessungen auf der Nanometerskala mit Hilfe von Goldnanopartikelpaaren*
  December 2008
- Sven Zimmermann
  *Emission und Energietransfer in photonischen Kristallen*
  June 2008

# 3

# Molecular Physics

## 3.1 Introduction

In 2008 Ulrich Keyser and his coworkers accomplished their move to Cambridge, UK. Later in the year Anatoli Serghei moved to Amherst, USA and Mahdy Elmahdy joined the group as Postdoctoral coworker. Periklis Papadopoulos was awarded with the "Peter Debye Prize for young investigators for excellence in dielectric research", which was given to him at the IV. Annual Meeting of the International Dielectric Society (IDS) in Lyon from the chairman of the prize committee, Prof. Dr. G. Williams, Swansea, UK and the head of IDS, Prof. Dr. J. Berberian, Chapel Hill, North Carolina, USA. For her excellent diploma thesis and her very good grades Carolin Wagner was awarded with a "Diploma with distinction".

A longstanding open problem in dielectric spectroscopy, the phenomenon of electrode polarization (EP), was unraveled by Anatoli Serghei. He could show – both experimentally and theoretically – that its frequency and temperature dependence is characterized by special features, for which scaling laws exist. By that it is possible – for the first time – to deduce information concerning the bulk conductivity from the dispersion of the complex conductivity and the complex dielectric function on the very low frequency side ($\leq 10^2$ Hz). The paper is submitted to PRL, but sometimes it is not easy to convince reviewers about new ideas and concepts.

*Friedrich Kremer*

## 3.2 Apparent Changes in the Molecular Dynamics of Thin Polymer Layers due to the Impact of Interfacial Layers

M. Tress, A. Serghei, F. Kremer

The glassy dynamics of ultra-thin polymer films is currently a topic of large scientific and technological interest. Broadband Dielectric Spectroscopy has proven – based on its ability to measure molecular fluctuations over a wide frequency and temperature range – its strength in unravelling the mechanisms of confinement-effects in thin polymer layers [1]. These effects are supposed to rise due to the changes of the polymer

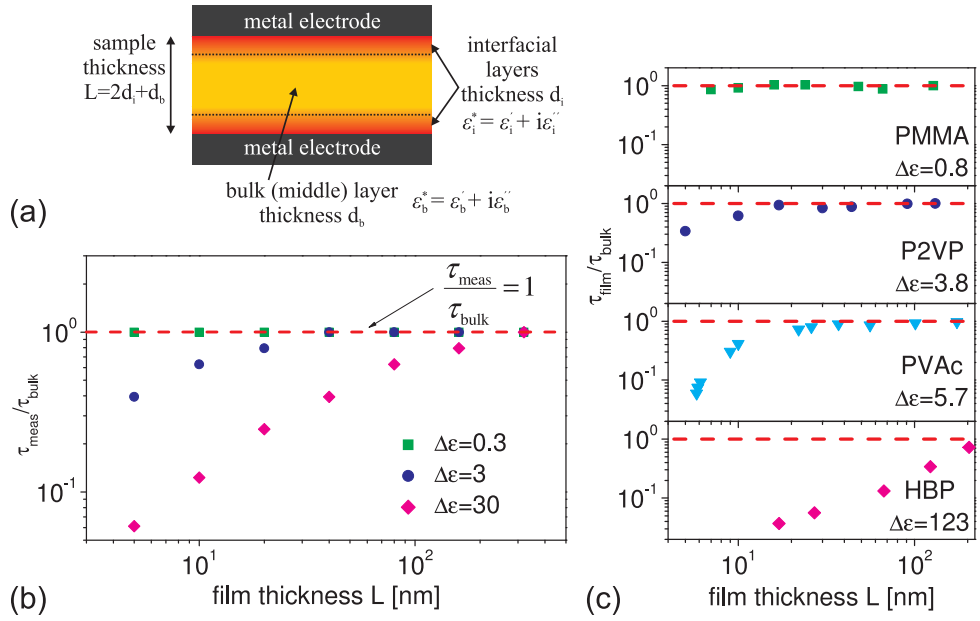


**Figure 3.1:** (**a**) Sketch of the proposed layer model of a polymer film confined in a so called capped geometry. (**b**) Calculated thickness dependence of the apparent relaxation peak of the net dielectric function of a layer arrangement like shown in (**a**) assuming constant measures of the interfacial layers. A pronounced effect is introduced by the variation of the dielectric strength $\Delta e$. (**c**) Thickness dependence of the apparent relaxation peak of several polymers having different dielectric strengths measured in a capped geometry.

glassy dynamics in the nanometric vicinity of confining interfaces (Fig. 3.1). Thus, the dielectric response of thin polymer films is calculated by taking into account possible modifications of the dielectric function in interfacial polymer sub-layers (Fig. 3.1). A multitude of mechanisms leading to an apparent faster dynamics in thin capped polymer films is revealed (Fig. 3.1). None of them corresponds to a faster molecular structural relaxation. It is shown that several reported experimental findings can be traced back to the influence of such interfacial layers: (i) no shifts in the mean-relaxation time for polymeric systems showing a weak alpha relaxation, while (ii) polymers having a large dielectric strength could experience apparent shifts already at thicknesses as large as 200 nm.

[1] A. Serghei et al.: *Apparent changes in the molecular dynamics of thin polymer layers due to the impact of interfacial layers*, J. Chem. Phys. (2009), in press

## 3.3 Electrode Polarization and Its Scaling Laws

J.R. Sangoro, A. Serghei, M. Tress, F. Kremer

Electrode polarization is a ubiquitous phenomenon taking place at the interface between an electrode and an ionic conductor. It shows a characteristic signature in the measured dielectric response of the sample cell in dependence on frequency of the applied electric field, temperature, concentration of the charge carriers and the sample

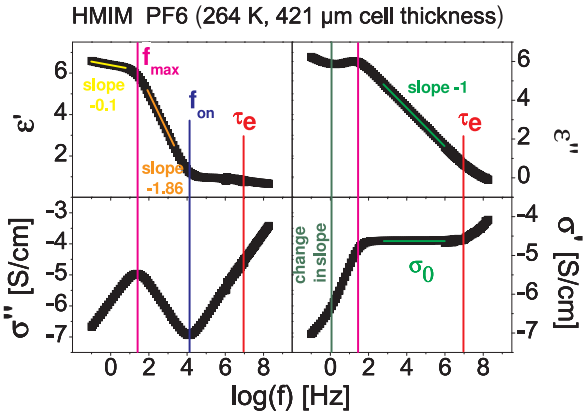


**Figure 3.2:** Dielectric properties of ionic liquids showing electrode polarization exemplified by 1-HMIM-$PF_6$, $\tau_e$: hopping time, $\sigma_0$: DC conductivity, $f_{on}$: onset of electrode polarization, slope of $-1.86$ in $\epsilon'$ for $f < f_{on}$, $f_{max}$: full development of electrode polarization, slope of $-0.1$ in $\epsilon'$ for $f < f_{max}$, change in slope of $\sigma'$ for $f < f_{max}$.

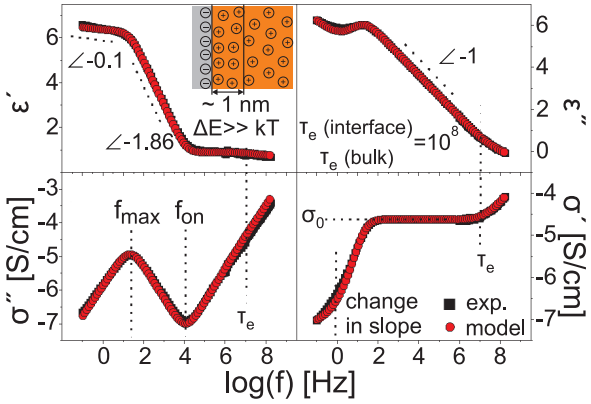


**Figure 3.3:** Measured and calculated complex dielectric permittivity and conductivity of HMIM-$PF_6$.

length (Fig. 3.2). Furthermore, it is well known that electrode polarization is strongly affected by the material of the electrodes, a finding which lacks – until now – a microscopic understanding. Despite early theoretical insights into the physics of electrolytes at solid interfaces (resulting in the electrical double layer model), no consistent description of the scaling laws governing electrode polarization effects exists (Fig. 3.3). Based on the fact that, due to coulombic interactions, the ion mobility is drastically slowed down at the interfaces, a quantitative description of electrode polarization is suggested which describes the observed scaling laws and enables one to deduce – by use of a novel formula – the bulk conductivity of the ionic charge carriers under study [1].

[1] A. Serghei et al.: *Electrode polarization and its scaling laws*, Phys. Rev. Lett., submitted (2008)

## 3.4 Universal Scaling of Charge Transport in Glass-Forming Ionic Liquids

J.R. Sangoro, C. Iacob, A. Serghei, F. Kremer

Charge transport and glassy dynamics of a variety of glass-forming ionic liquids (ILs) are investigated in a wide frequency and temperature range by means of Broadband Dielectric Spectroscopy, Differential Scanning Calorimetry and Rheology [1–4]. While the absolute values of dc conductivity and viscosity vary over more than 11 decades with temperature and upon systematic structural variation of the ILs, quantitative agreement is found between the characteristic frequency of charge transport and the structural $\alpha$-relaxation. This is traced back to dynamic glass transition assisted hopping as the underlying mechanism of charge transport (Fig. 3.4).

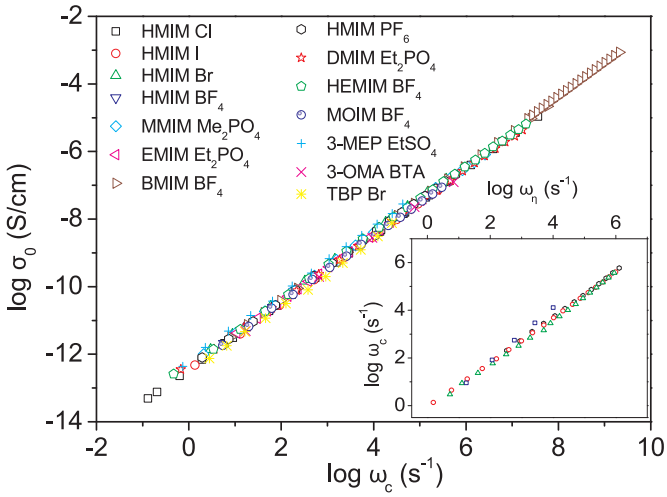


**Figure 3.4:** DC conductivity, $\sigma_0$, *versus* the characteristic frequency, $\omega_c$, for different liquids as indicated. This plot experimentally demonstrates the universality of charge transport in ionic liquids. Inset: Correlation of $\omega_c(T)$ with the characteristic frequency, $\omega_\eta(T)$, corresponding to structural relaxation time obtained from viscosity by applying the Maxwell relation.

[1] J.R. Sangoro et al.: Phys. Chem. Chem. Phys. **11**, 913 (2008), doi:10.1039/b816106b
[2] J.R. Sangoro et al.: Phys. Rev. E **77**, 051 202 (2008)
[3] J.R. Sangoro et al.: J. Chem. Phys. **128**, 212 509 (2008)
[4] J.R. Sangoro et al.: Macromolecules **42**, 1648 (2009)

## 3.5 Charge Transport and Glassy Dynamics in Imidazole-Based Liquids

C. Iacob, J.R. Sangoro, A. Serghei, F. Kremer

Broadband Dielectric Spectroscopy (BDS), differential scanning calorimetry, rheology and Pulsed Field Gradient Nuclear Magnetic Resonance (PFG-NMR) are combined to study glassy dynamics and charge transport in a homologous series of imidazole-based liquids with systematic variation of the alkyl chain length [2]. The dielectric spectra are interpreted in terms of dipolar relaxation and a conductivity contribution. By applying Einstein, Einstein–Smoluchowski and Stokes–Einstein relations, translational diffusion coefficients in quantitative agreement with PFG-NMR measurements are obtained (Fig. 3.5) [1, 3]. With increasing alkyl chain length, it is observed that the viscosity increases whereas the structural a-relaxation rate decreases in accordance with Maxwell's relation. Between the rate we of electrical relaxation and the rate wa of the structural a-relaxation scaling is observed over more than 6 decades with a decoupling index of about 2.

[1] C. Iacob et al.: J. Chem. Phys. **129**, 1 (2008)
[2] J.R. Sangoro et al.: Phys. Chem. Chem. Phys. **11**, 913 (2008), doi:10.1039/b816106b
[3] J.R. Sangoro et al.: Phys. Rev. E **77**, 051 202 (2008)

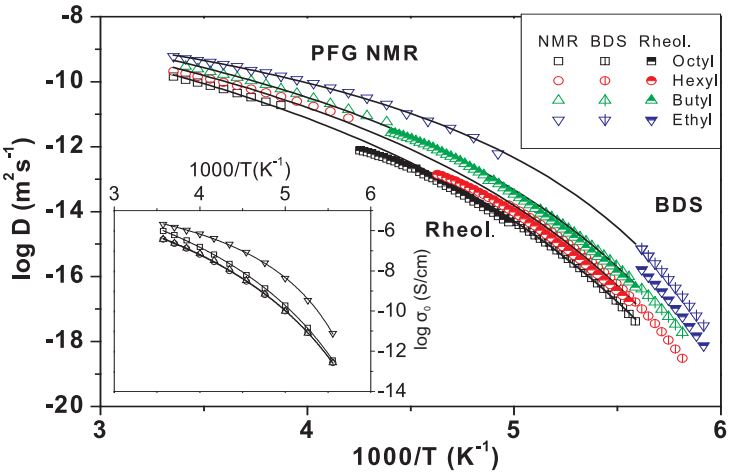


**Figure 3.5:** Diffusion coefficient $D$ vs. inverse temperature as measured by Pulsed-Field Gradient NMR (*open symbols*), BDS (*open symbols with vertical line*) and from Stokes–Einstein equation (*upper filled symbols*). *Inset*: DC conductivity $\sigma_0$ vs. inverse temperature (*open symbols with vertical line*).

## 3.6 Infrared Transition Moment Orientational Analysis in Liquid Crystalline Elastomers

P. Papadopoulos, W. Kossack, F. Kremer

A novel method is suggested for unraveling the mean orientation and the molecular order parameter in any IR-transparent or translucent material under study. It is based on the analysis of IR transmission spectra as a function of polarization and an intentional inclination of the sample. Taking advantage of the specificity of the IR spectral range, it is based on the analysis of the absorption coefficient, where is the transition dipole moment and the electric field of the IR beam, in dependence on the polarization and the angle of inclination. Additionally, for non-scattering samples, the complex refractive index tensor can be determined by using the Fresnel equations. The spatial resolution of the technique is only limited by the wavelength. The measurement setup is shown schematically in Fig. 3.6a. Polarization can be varied from $0^\circ - 360^\circ$ and inclination from $-80^\circ - +80^\circ$, allowing the electric field vector to become almost perpendicular to the sample.

The setup is used in the sample compartment of a FTIR spectrometer to determine the molecular order parameter and the spatial orientation of the director of a smectic Liquid Crystalline Elastomer (sLCE) film as a function of external strain. The molecular moieties exhibit different alignment (Fig. 3.6b,c). At 0 % strain the molecular order parameter of the main chains is 0.8, with the mesogens lying on the film plane. This result could not have been obtained by conventional polarization-dependent studies, where the electric field is only varied in the $xz$-plane. At a strain value of 190 % the order parameter is increased to 0.91 and the mesogens are slightly reoriented (by 15°) and become parallel to the stretching direction. The findings show that the technique can give detailed structural information for materials with multiple levels of organization.

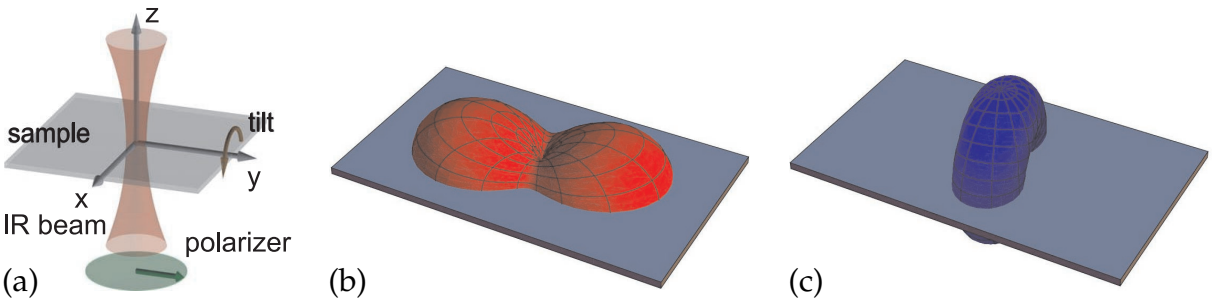


**Figure 3.6:** (**a**) Measurement principle used for the IR-TMOA technique. The electric field vector of the IR beam (*green*) can be rotated with a polarizer, while the sample can be tilted. This way the electric field can have any of the *x*,*y*,*z* directions. (**b**) Application of IR-TMOA to a smectic liquid crystalline elastomer (*grey plane*) at 0 % strain. The 3D polar plot (*red*) shows the dependence of the absorbance on the orientation of the electric field and, therefore, the distribution of transition dipole moments. In this case the corresponding transition moment (C−O stretching) is parallel to the main chains of the elastomer, which consist of the mesogen. The mean orientation is not parallel to the stretching direction (*x*-axis) and there is no cylindrical symmetry about the mean absorbance axis. (**c**) Absorbance dependence of an absorption band with a transition dipole moment perpendicular to the main chain (C=O stretching). As one would expect, no cylindrical symmetry is observed, but the lowest absorbance is found for the direction parallel to the highest absorbance in (**b**).

## 3.7 Combined Mechanical and Time-Resolved Polarization-Dependent FTIR Studies in Major and Minor Ampullate Spider Silk

R. Ene, P. Papadopoulos, F. Kremer

Minor and major ampullate spider silks are studied under varying mechanical stress by static and time-resolved FTIR-spectroscopy [1]. This enables one to trace the external mechanical excitation on a microscopic level and to determine for the different moieties the time-dependence of the molecular order parameters and corresponding band shifts (Fig. 3.7). It is concluded that the hierarchical nanostructure of both types of silk is similar, being composed of highly oriented nano-crystals which are interconnected by amorphous chains obeying the worm-like chain model and having a gaussian distribution of pre-strain [2]. By that it is possible to describe the mechanical properties of both silks by two adjustable parameters only, the center and width of the distribution. For major ampullate silk the observed variability is small in pronounced contrast to the findings for minor ampullate [3].

[1] P. Papadopoulos et al.: Eur. Phys. J. E Soft Matter **24**, 193 (2007)
[2] P. Papadopoulos et al.: Coll. Polym. Sci. **287**, 231 (2009)
[3] P. Papadopoulos et al.: *Similarities in the structural organization of major and minor ampullate spider silk*, Macromol. Rapid. Commun. (2009), in press

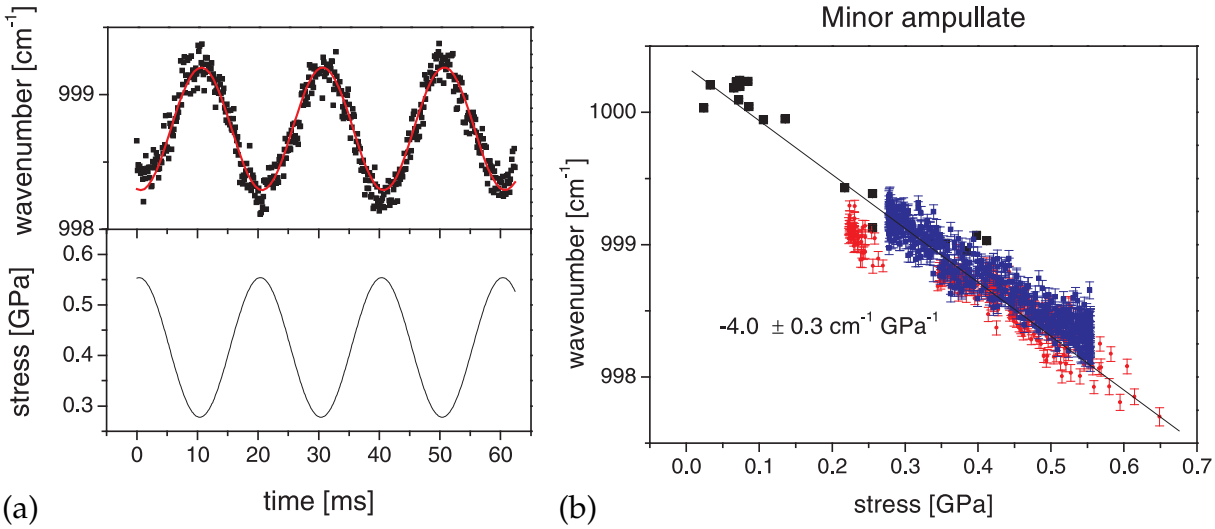


**Figure 3.7:** Stress dependence of band shift in different time scales. (**a**) Step scan measurements of the AlaGly vibration frequency in a *Nephila edulis minor* ampullate silk sample. A sinusoidal mechanical field is applied to the sample, while spectra are measured with a time resolution of 125 µs. The band shift (sinusoidal fit shown) clearly reflects the field. No phase difference is observed (±1°). (**b**) Band shift dependence on stress for static (*black*), kinetic (*red*) and step scan measurements (*blue*) of the same sample. The same linear dependence is observed for all sets, showing that macroscopic and microscopic stress are equal regardless of the time scale. The crystals must be in serial arrangement, otherwise deviations would have to be observed before reaching equilibrium.

## 3.8 In-Situ Analysis of the Forces of Interaction in Polyelectrolyte Brushes

M.M. Elmahdy, G. Dominguez, C. Gutsche, K. Kegler, F. Kremer

Optical tweezers are employed to measure the forces of interaction within single pairs of poly(acrylic acid) (PAA) grafted colloids with an extraordinary resolution of ±0.5 pN [1]. Parameters varied are the concentration and valency of the counterions (KCl, $CaCl_2$) of the surrounding medium as well as its pH. The force-separation dependence for varying pH (Fig. 3.8) at a fixed concentration of $10^{-3}$ M KCl enables one to trace – within a single pair of PAA-grafted colloids – the swelling of the polymer brush with increasing pH. The data are well described by Jusufi model of the effective interaction between spherical polyelectrolyte brushes [2]. The brush height $L$ as obtained from the fits (inset of Fig. 3.8b) shows a strong pH effect and compares well with independent ellipsometric measurements [1]. The increase in the brush height is caused by the pH-induced augment of the PAA dissociation and results in a stretching of the grafted chains.

[1] G. Dominguez et al.: Polymer **49**, 4802 (2008)
[2] A. Jusufi et al.: Coll. Polym. Sci. **282**, 910 (2004)

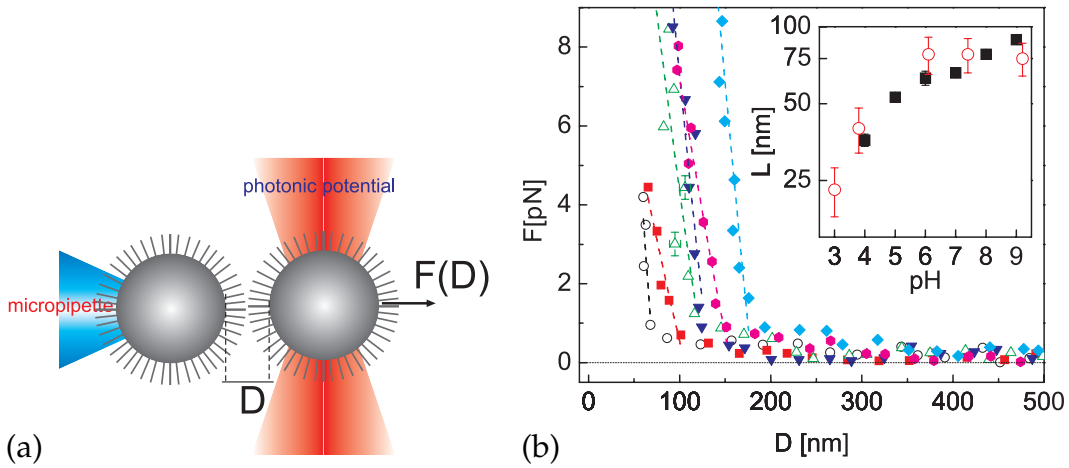


**Figure 3.8:** (**a**) Scheme of the experimental set-up. One colloid is held with a micropipette due to the capillary action, and the other is kept in an optical trap. (**b**) Force vs. separation ($D$) between the solid surfaces of two PAA-grafted particles under conditions of varying pH: 4 (*open circle*), 5 (*full squares*), 6 (*open up-triangles*), 7 (*full down-triangles*), 8 (*full hexagon*) and 9 (*full rhombus*) at $10^{-3}$ M KCl. The *dashed lines* represent the fits to the experimental data according to a model by Jusufi et al. [2]. *Inset*: brush height $L$ vs. pH at $10^{-3}$ M KCl obtained from analyzing the Optical Tweezers measurements using the Jusufi model (*full squares*) and as measured by Ellipsometry (*open circles*).

## 3.9 Polyelectrolyte-Compression Forces Between Spherical DNA-Grafted Colloids

K. Kegler, F. Kremer

The experimental investigation was based on the measurement of the force–distance dependence between two identical, negatively charged DNA-grafted colloids employing optical tweezers [1, 2]. Optical tweezers offer unprecedented accuracy down to the pN domain and 3 nm in measuring forces and position, respectively. By monitoring the force–distance dependencies between two grafted colloids it is possible to learn how the different physicochemical properties (molecular weight, grafting density, ionic strength of the surrounding medium) affect the effective interaction between the grafted colloids (Fig. 3.9). The measured force–distance relation is analyzed by means of a theoretical treatment. Quantitative agreement with the experiment is obtained for all parameter combinations. The physical system provides a convincing verification of the importance of the PE-compression mechanism in sharp contrast to most hitherto studied systems, which were dominated by counterion entropy [3].

[1] K. Kegler et al.: Phys. Rev. Lett. **98**, 058 304 (2007)
[2] K. Kegler et al.: Phys. Rev. Lett. **100**, 118 302 (2008)
[3] M. Konieczny, C.N. Likos: J. Chem. Phys. **124**, 214 904 (2006)

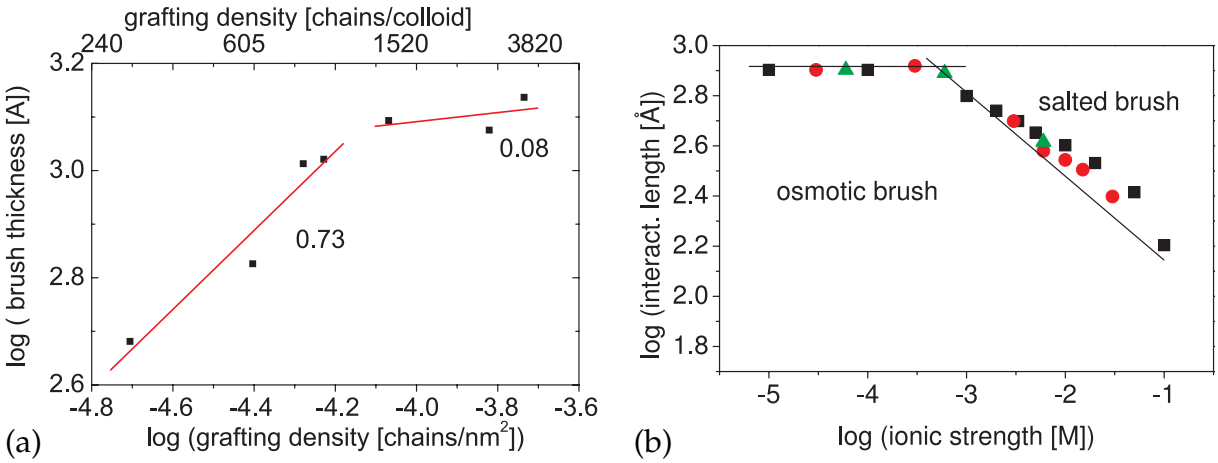


**Figure 3.9:** (**a**): Interaction length $l(f = 2\,\mathrm{pN})$ at a force of 2 pN versus grafting density for DNA (1000 bp)-grafted colloids of varying grafting density in buffered (10 mM $C_4H_{11}NO_3$, pH 8.5) solution (*square*). The scaling relationships are indicated by *straight lines*. The *circles* are predicted by the model [3]. (**b**) Double-logarithmic plot of the interaction length for a force $F = 2\,\mathrm{pN}$ versus the ionic strength of the added salt. Here, the molecular weight of the grafted DNA is $N = 1000$. Different types of symbols correspond to different salt valencies (NaCl - *circle*, $CaCl_2$ - *square*, $LaCl_3$ - *triangle*). The line of slope $-1/3$ indicates theoretical scaling law predictions for comparison.

## 3.10 Investigating Fluctuation and Dissipation of Optically Trapped Colloids

O. Ueberschär, F. Kremer

Fluctuation and dissipation as the dominant mechanisms behind the well-observable Brownian motion of micron-sized particles are investigated and quantified on a single colloid level by means of the optical tweezers technique [1–3]. Using an outstandingly fast optical diffraction image analysis routine with a sampling frequency of 10 kHz combined with an automated data acquisition loop, we deduce the precise size of the colloid under study. Moreover, we measure the colloid's entropy production and consumption along a large number of different trajectories (e.g. 6000) in a non-equilibrium steady-state. Since our micron-sized single colloid clearly does not fulfil the assumptions of the second law of thermodynamics, i.e. the limit of large numbers of particles ($N \to \infty$) and a big system size ($V \to \infty$), entropy is observed to be produced ($\delta S \geq 0$) or consumed ($\delta S \leq 0$) depending on the particular trajectory and time scale. Replacing the second law for arbitrarily system sizes, the fluctuation theorem (FT) by Evans et al. only discovered in 1993 still holds, however. It quantifies the probability of entropy production compared to entropy consumption,

$$\frac{\Pr(\delta S = +A)}{\Pr(\delta S = -A)} = \exp\left(\frac{A}{k_\mathrm{B}}\right), \tag{3.1}$$

where $A$ is an arbitrary value of entropy change. Obviously, for large positive values of entropy change, i. e. $A \gg k_\mathrm{B}$, the second law is obtained from the FT. We find quantitative agreement between our measurements and the predictions of the FT.

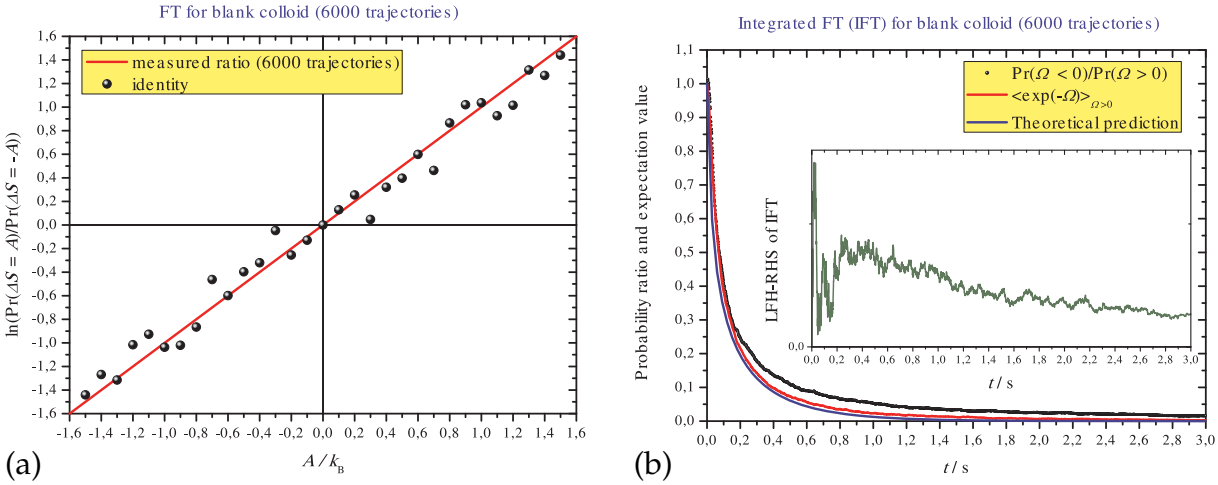


**Figure 3.10:** (**a**) Comparison of the left-hand side (LHS, *black balls*) and the right-hand side (RHS, *red line*) of the FT for 6000 single trajectories 100 ms after the initiation of a disturbance (logarithmic plot). (**b**) Comparison of the LHS and RHS of an integrated, time-dependent form of FT applied to our system (*black line* and *red line*). The theoretical prediction by stochastic dynamics is also shown (*blue line*). As expected, these three graphs almost collapse. *Inset*: LHS-RHS of IFT.

Running out measurements on both blank and DNA-grafted colloids (DNA properties: molecular weight of 4000 base pairs, contour length of approximately 1360 nm), we compare their average entropy change rates, addressing the issue if there is evidence for an additional dissipative mechanism due to the DNA coat (Fig. 3.10).

[1] G.M. Wang et al.: Phys. Rev. Lett. **89**, 050 601 (2002)
[2] G.M. Wang et al.: Phys. Rev. E **71**, 046 142 (2005)
[3] D.M. Carberry et al.: J. Opt. A **9**, S204 (2007)

## 3.11 Single Colloid Electrophoresis

I. Semenov, O. Otto, G. Stober, P. Papadopoulos, U.F. Keyser, F. Kremer

Optical Tweezers enable one to trap a single particle without any mechanical contact and to measure its position and the forces acting on it with high resolution (±4 nm, ±160 fN) [1, 2]. Single spherical polystyrene (PS) colloids of a diameter $d$ = 2.23 mm are used. The imaging system and experimental setup based on epifluorescent microscope (Fig. 3.11). The fluidic cell geometry is defined by the inner shape of the PMMA spacer (Fig. 3.11)): two reservoirs with Pt electrodes are connected by a narrow channel (width: 300 mm, height: 1 mm) that helps to obtain a uniform electric field distribution. The channel is extended to the other sides of both reservoirs and the ends are kept open to avoid back flow. For measuring of phase displacement between applied AC signal and colloidal response, a light-emitting diode (LED), connected to synchronization output of function generator is incorporated right in front of the CMOS sensor. By applying an outer electrical sinusoidal field the complex (sum of the electrophoretic and electroosmotic contributions) response of the single colloid under study can be directly

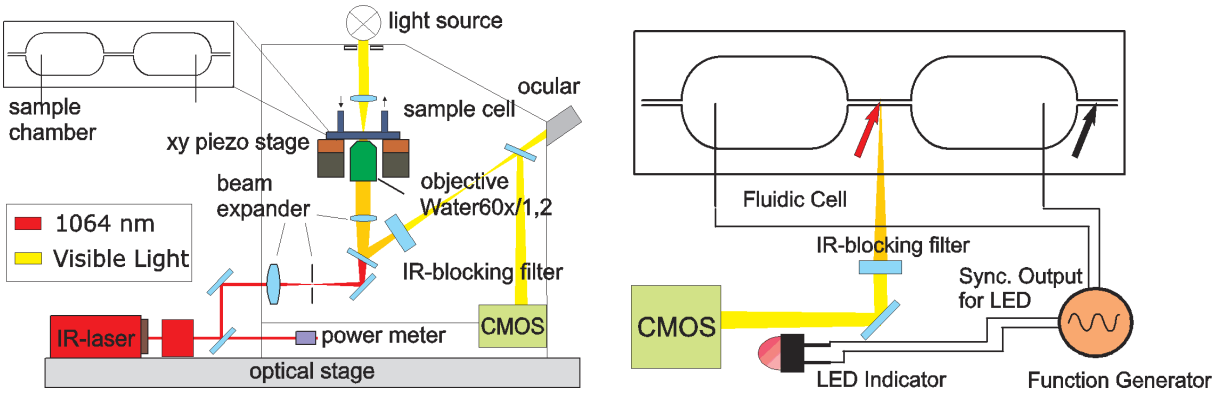


**Figure 3.11:** Scheme of the experimental setup. Particles are imaged using an epifluorescence microscope accomplished with a high resolution CMOS camera. Scheme of the sample cell used to measure the electrophoretic (colloid at position A) or the electroosmotic (colloid at position B) response. The fluidic cell consists of an open ended narrow channel (width: 300 mm, height: 1 mm) in which two reservoirs with Pt electrodes (diameter = 0.2 mm, the tip is along the axis) are incorporated. For the phase measurement of the electrophoretic response an LED flash indicates the zero-value of the external electric field.

determined. It is found that the phase is shifted with respect to the applied external field. Hence, this gives rise to observe the complex electrophoretic mobility which is theoretically described by a strongly damped driven harmonic oscillator model. The electroosmotic effect is studied separately with the result that it stays more than one order of magnitude lower than electrophoretic motion of the particle. Exchanging the medium surrounding the colloid allows deducing the (KCl) concentration dependence of a single colloidal complex response. The results are compared with conventional Zetasizer measurements.

[1] A. Delgado et al.: J. Coll. Interf. Sci. **309**, 194 (2007)
[2] O. Otto et al.: Rev. Sci. Instrum. **79**, 023 710 (2008)

## 3.12 Drag-Induced Forces on Colloids in Polymer Solution at Low Solvent Velocities

C. Gutsche, F. Kremer

We already present a first direct experimental observation of jamming-induced drag-enhancement on colloids pulled through a solution of $\lambda$-DNA (used here as a monodisperse model polymer) with an optical tweezer [1]. The experiments have shown a drag force which is larger than expected from the Stokes formula and the independently measured viscosity of the DNA solution. We attribute this to the accumulation of DNA in front of the colloid and the reduced DNA density behind the colloid. Now this former measurements are expanded to very low solvent velocities, which lead to a nonlinear response based on soft shape and high flexibility the DNA-coils have on this slow approaches. Therefore the resolution of our optical tweezers setup was increased up to 5 fN. Preliminary results are shown in Fig. 3.12.

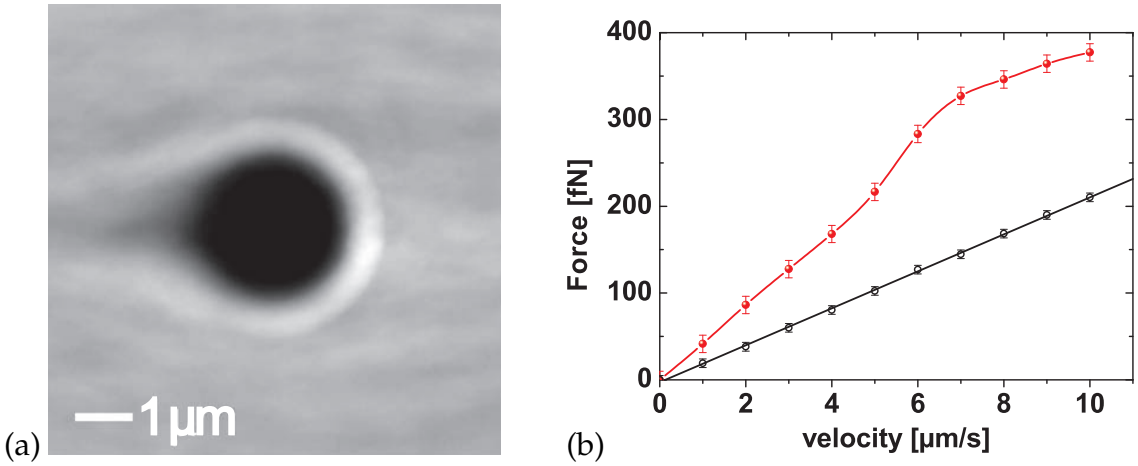


**Figure 3.12:** (**a**) Polymer density around the colloid averaged over 2000 snapshots of the system by Brownian Dynamics simulations. *Lighter colors* denote higher DNA concentration. (**b**) Drag force on colloids in $\lambda$-DNA as a function of the pulling velocity (*red dots*). Also shown is the Stokes force on the colloids (*black open circles* fitted with *solid black line*) in pure water.

[1] C. Gutsche et al.: J. Chem. Phys. **129**, 084 902 (2008)

## 3.13 DNA Condensation under the Action of the Protein TmHU as Studied on a Single Molecule Level

C. Wagner, M. Salomo, U.F. Keyser, C. Gutsche, F. Kremer

The interaction of the histone-like protein TmHU (from Thermotoga maritima) to DNA is analyzed on a single molecule level by use of optical tweezers [1, 2]. This technique provides a nm-resolution in positioning a micron-sized colloid and an accuracy of ±50 fN in measuring the forces acting on it. As a further refinement, our set-up is now accomplished with a fast feed-back loop (regulation frequency: 30 Hz) which allows to carry out the experiment under conditions of a constant and adjustable force. The proceeding of the condensation and its dependence on the applied force (2 – 40 pN) is investigated (Fig. 3.13). At a pre-stretching of 2 pN the length of the DNA is reduced by about 80 %. At higher forces, the reaction is disrupted at an incomplete level. The process shows two distinct regimes that can be related to different organizational levels. The condensation also shows a pronounced dependence on the concentration. By stretching the TmHU/DNA-complex, it is possible to disrupt the proteins from the DNA. The length of the smallest event conforms with the results of a simulated rupture.

[1] M. Salomo et al.: Microsc. Res. Techn. **70**, 938 (2007)
[2] M. Salomo et al.: Molec. Biol. **359**, 769 (2006)

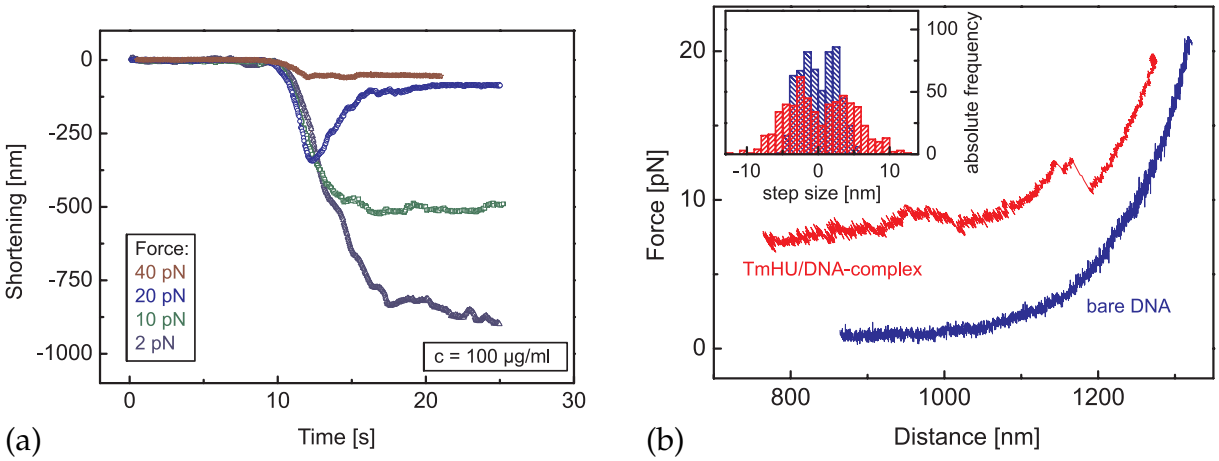


**Figure 3.13:** (**a**) The TmHU-induced condensation of the DNA at different force levels. The proceeding of the condensation of the DNA as well as the shortening depend on the applied force. (**b**) Stretching the TmHU/DNA-complex ($v$ = 5 nm/s) after the condensation at a force level of 10 pN (*red line*) compared to stretching of bare DNA (*blue line*). The complex shows a plateau at 5 – 15 pN as well as an increased noise. Inset: Comparison of the step size of the curves. In case of the TmHU-DNA-Complex there are seen larger steps. These are interpreted as the disruption of single proteins from the DNA strand.

## 3.14 DNA Binding under the Action of the Protein E.coli HU as Studied on a Single Molecule Level

C. Krause, C. Wagner, M. Salomo, J. Reinmuth, F. Kremer

In contrast to eucariotic histone proteins, not much is known about the interaction of procaryotic histone-like proteins with DNA. Optical Tweezers enable one to analyse the binding of the histone-like proteins TmHU (from Thermotoga maritima) and E.coli HU-protein (from Escherichia coli) to DNA on a single molecule level [1, 2]. The proteins act on the DNA by condensating it.

By use of a fast feedback-loop that allows to carry out the experiments under constant force conditions the action of TmHU on DNA has been investigated. TmHU consists of 90 amino acids residues and has a molecular mass of 9994 Da per monomer. In solution it exists as a homodimer containing an a-helical "core" from which two b-arms protrude. Values vor $K_d$ for DNA vary from 5.6 to 73 nM depending on the method and the length of the DNA. The Protein causes within a few seconds a shortening of the DNA-length about 80 %. The dependence on the applied force and the protein concentration allowed to unravel the kinetic and energetic of the reaction. Now similar experiments on E.coli HU are ready to be realized. This HU-protein mainly exists as a heterodimer containing two homologous subunits a and b, 9.5 kDa each. As can easily be seen from Fig. 3.14, HU E.Coli binds to DNA very differently in comparison with TmHU. Values for $K_d$ for dsDNA can vary from 200 to 2500 nM according to the experimental set-up. From the literature it is known that an introduction of Hu E.Coli results in a decrease in the end-to-end length after approximately 800 s [4]. In our Optical Tweezers experiments we now expect to detect a significant difference to the reaction with TmHU.

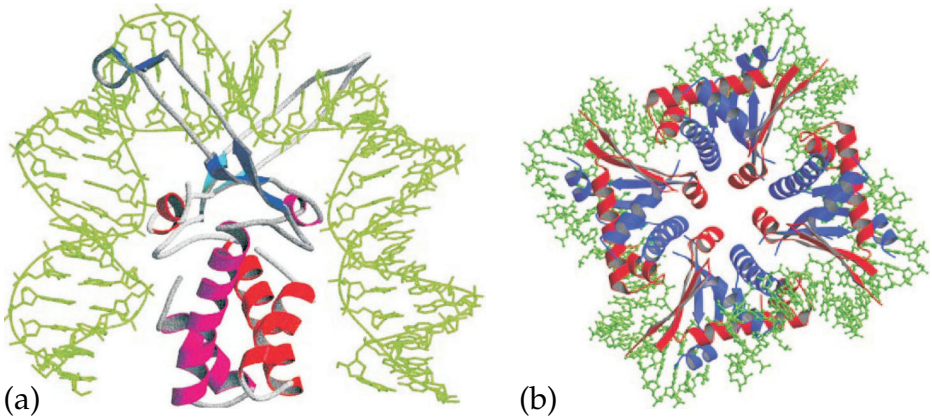


**Figure 3.14:** (**a**) DNA binds to TmHU by bending it with an angle of 160° around the protein. (**b**) Stereoviews of modeled HUab octameric unit of the left-handed multimer with DNA fragment as a repeating unit of a spiral structure. The a-subunit is in *red*, and the b-subunit is in *blue*. [3]

[1] M. Salomo et al.: Microsc. Res. Techn. **70**, 938 (2007)
[2] M. Salomo et al.: Molec. Biol. **359**, 769 (2006)
[3] F. Guo, S. Adhya: Proc. Nat. Acad. Sci. **104**, 4309 (2007)
[4] J. van Noort et al.: Proc. Nat. Acad. Sci. **101**, 6969 (2004)

## 3.15 TmHU-DNA Binding Studied by Atomic Force Microscopy

H. Brutzer, M. Salomo, U.F. Keyser, F. Kremer

In contrast to the well-characterized processes of formation and destabilization of complexes from eukaryotic histones with DNA, little is known about interactions between histone-like proteins from prokaryotes and DNA. These proteins also kink and bend DNA leading to chromatin-like structures. The histone-like HU protein is nearly ubiquitous in all bacteria. Especially TmHU from Thermotoga maritima exhibits some extraordinary properties, such as the protection of DNA inside the bacterium against thermal denaturation. Experiments with optical tweezers suggest the existence of a threshold protein concentration for the formation of TmHU-DNA complexes [1]. Here we use atomic force microscopy to study the concentration dependence by alternative means and minimize influence by external forces. The end-to-end distance and the height of the complexes were measured in dependence of protein concentration (50 – 5000 nM). With increasing protein concentration the end-to-end distance decreases from 70 to 38 nm while the height increases from 0.7 to 2.2 nm for 250 bp dsDNA, indicative of the formation of a globular structure of the TmHU-DNA complex (Fig. 3.15). Most likely this originates from a secondary organizational level during TmHU-DNA binding observed in optical tweezers experiments.

[1] M. Salomo et al.: Microsc. Res. Techn. **70**, 938 (2007)

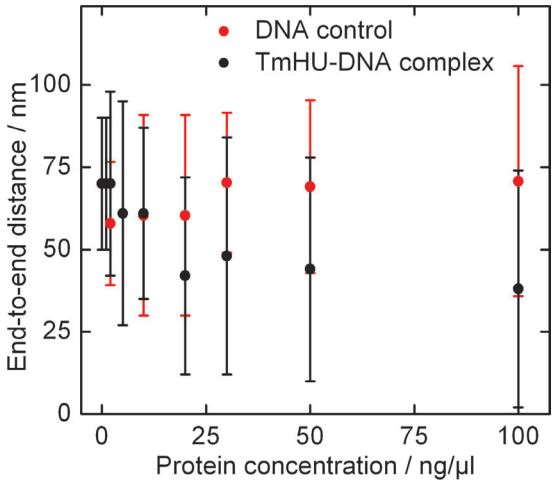


**Figure 3.15:** End-to-end distance dependence of TmHU-DNA complexes on protein concentration. TmHU compacts the DNA above a concentration of 20 ng/ml.

## 3.16 Optical Tweezers to Investigate Receptor–Ligand Interactions on a Single Contact Level

M. Salomo, C. Wagner, F. Kremer

The extraordinary features of optical tweezers [1, 2] having a nm-resolution in positioning a micron-sized colloid and an accuracy of (±50 fN) in measuring the forces acting on it, enable one to study the interaction within a single receptor–ligand contact. For that

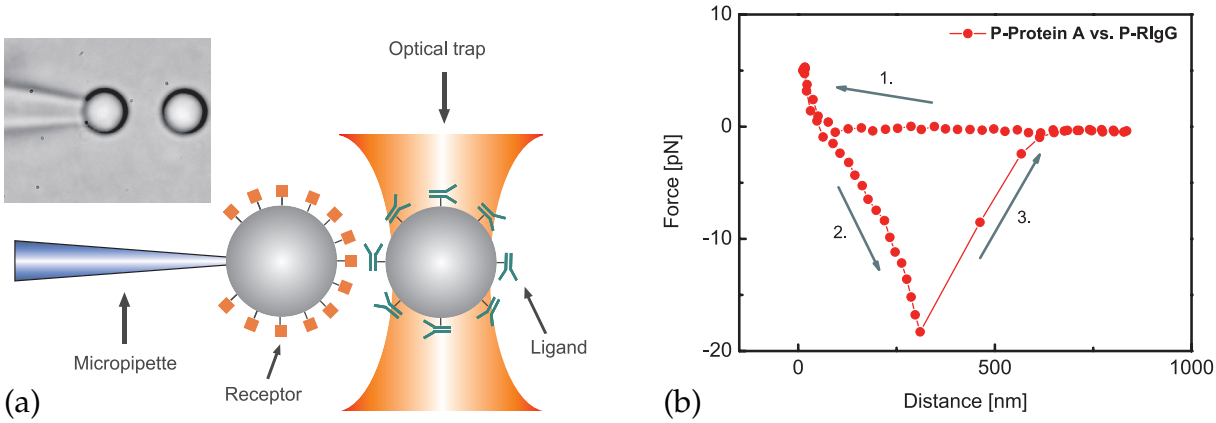


**Figure 3.16:** (**a**) Micro-image of the two colloids and scheme of the experimental setup. For investigating the interaction between a receptor–ligand pair, the particular interaction partners are immobilized on the surface of microparticles. One of the particles is held by a micropipette, the other one is trapped by the optical tweezers. (**b**) Force–distance trace. The particles are approached until a force of 5 pN is reached (*1*). Afterwards the particles are pulled apart. Due to a single contact between the P-Protein A and the Immunoglobuline P-RIgG the particle in the optical trap is shifted out of the equilibrium position in the optical trap (*2*). When the force reaches a certain level, the rupture of the binding between the receptor and the ligand can be observed (*3*) [1].

ligand and receptor molecules are immobilized on the surface of two different colloids. By holding one of these by a micropipette and the other in the optical trap, it is possible to approach the particles until a certain contact force of typically 5 pN is reached (Fig. 3.16). Directly afterwards the particles are pulled apart. If a receptor–ligand contact was established, the forces of interaction cause the particle in the optical trap to be shifted out of the equilibrium position in the optical trap. This approach benefits additionally from the chance for the identical pair of colloids the measurements can be repeated many times. Furthermore it is possible to modify the surrounding medium (pH, ion concentration, etc.) and to study its effect on the binding-characteristics.

It is the goal of the present project to advance this approach to a novel automated screening technique in single molecule bio-nano-technology. For that multifold hard- and software developments have to be initiated.

[1] M. Salomo et al.: Microsc. Res. Techn. **70**, 938 (2007)
[2] K. Kegler et al.: Phys. Rev. Lett. **98**, 058 304 (2007)
[3] M. Salomo et al.: Eur. Biophys. J. **37**, 927 (2007)

## 3.17 Localized Heating Effects in Micro-Capillaries and Nanopores

J.H. Peters, U.F. Keyser

Optical tweezers are a powerful and widely used experimental tool in biological physics including single molecule investigations. The strongly focused laser-beam in such a setup can reach power densities in the order of 108 W/cm$^2$ that cause significant heating exceeding 10 K per Watt of incident laser power for a 1064-nm-Laser [1, 2]. As the reaction constants of biomolecules are temperature dependent, heating effects should be considered in biophysical experiments. The ionic current through a channel or pore depends on the local temperature in a well-defined manner and hence (i) can be used for temperature measurements with high spatial resolution [1] (ii) map out the ionic current profiles in micron sized capillaries [3]. We compare experiments using nanopores and micro-capillaries with numerical finite element calculations and investigate the dependence of heating effects on parameters like geometry and thermal conductivity of water and nanopore material (Fig. 3.17). We were able to confirm earlier findings as the logarithmic dependence of the maximal temperature on the size of the system [2] and also gain a more detailed insight into the temperature distribution found in optical tweezers. The is also a strong correlation with impurities in the glass.

[1] U.F. Keyser et al.: Nano Lett. **5**, 116 104 (2005)
[2] E. Peterman et al.: Biophys. J. **84**, 1308 (2003)
[3] L.J. Steinbock et al.: Biosens. Bioelectron. **24**, 2423 (2009), doi:10.1016/j.bios.2008.12.026

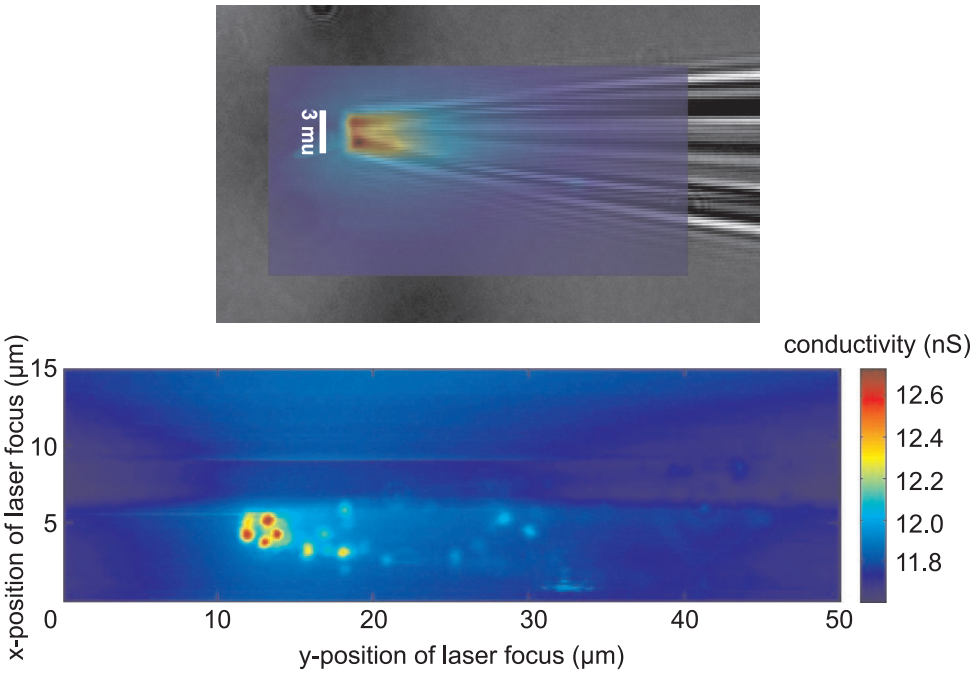


**Figure 3.17:** *Top*: Microscope image (*grey*) and ionic current map of a micron-scale glass capillary. *Red* denotes high ionic current and thus high temperature and *blue* denotes low ionic current Temperature-distribution generated by a focussed (gaussian). *Bottom*: Ionic conductance map as a function of laser position of a capillary with impurities attached to the glass. The Laser-beam is strongly adsorbed by the impurities and leads to significant and localized heating patterns detected by the ionic current measurements (*green*, *yellow* and *red spots* in the graph). These correlate with optical microscope images (not shown).

## 3.18 Modeling of Colloidal Transport in Capillaries

G. Stober, L.J. Steinbock, U.F. Keyser

We dynamically model the passage of micron-sized colloids through micro-capillaries in silicon [3, 4]. The computer model is able to reproduce the signal shape, the transition time and the amplitude and baseline current with an accuracy of approximately 35 %. This is achieved by computing the electrical field in the fluidic cell in dependence from the geometry of the capillary orifice. Further, the model physics includes a numerical implementation of a Hagen-Poisseuille flow profile in dependence of a free adjustable fluidic cell geometry, the colloid size, the ion mobility, the ionic strength, the colloid charge and coatings as well as the applied voltage [1, 2]. A simulated signal is given in Fig. 3.18 and shows a quantitative agreement with a measured signal (Fig. 3.18b).

Additionally, the simulation of the gaussian noise allows to test the custom written detection algorithm to determine the detection threshold for smallest observable colloids.

[1] U.F. Keyser et al: Rev. Sci. Instrum. **77**, 105 105 (2006)
[2] C. Gutsche et al.: Phys. Rev. E **76**, 031 403 (2007)
[3] L.J. Steinbock et al.: Biosens. Bioelectron. **24**, 2423 (2009), doi:10.1016/j.bios.2008.12.026
[4] G. Stober et al.: J. Appl. Phys. **105**, 084 702 (2009), doi:10.1063/1.3095761

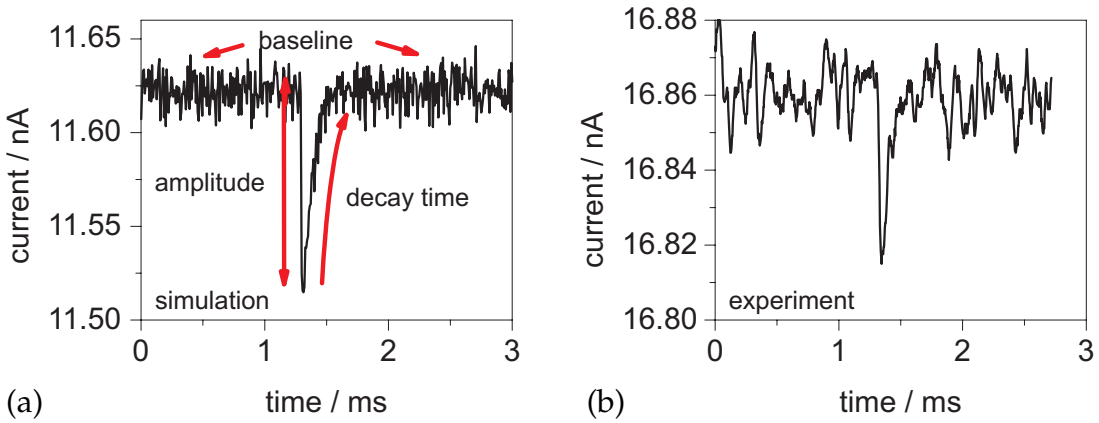


**Figure 3.18:** (**a**) Current as a function of time calculated for a typical capillary geometry showing a sudden rise to the maximum amplitude and a gradual decay. The geometry of the capillary required to use two different taper in the simulation, due to a not gradual opening of the orifice. This simulation was carried out with similar settings as in the experiment, which used a colloid of diameter 1 µm and a capillary with diameter of 3.5 µm and a taper (1) length of 70 µm and a taper (2) with 930 µm. The NaCl concentration was 20 mMol. (**b**) The graph shows a detected colloid for a similar capillary.

## 3.19 Sensing DNA-Coatings of Microparticles Using Micropipettes

L.J. Steinbock, G. Stober, U.F. Keyser

The resistive pulse technique is widely used to detect the size of small particles in aqueous solutions. This work demonstrates that a few tens of DNA molecules and thus the charges on a particle can be simply detected by pressure-driven translocation through a microcapillary based Coulter counter [1]. The typical opening of the capillaries ranges from 2 to 6 µm. The custom-built system gives optical access using a high numerical aperture objective allowing to observe colloids passing the sensing volume by optical means. We show the feasibility of our setup by distinguishing colloids with one and two micron diameters. Our measurements prove that a few ten strands of DNA bound to the colloids can be detected. This can be achieved by simple comparison of current amplitudes for blank and coated colloids at low salt concentrations (2 – 40 mMol NaCl). Our results clearly demonstrate that the Coulter counter can be used to detect the surface charges on colloids (Fig. 3.19). Moreover, the results are in good agreement with a dynamical computer model taking into account the full geometry of the capillary [2].

[1] L.J. Steinbock et al.: Biosens. Bioelectron. **24**, 2423 (2009), doi:10.1016/j.bios.2008.12.026
[2] G. Stober et al.: J. Appl. Phys. **105**, 084 702 (2009), doi:10.1063/1.3095761

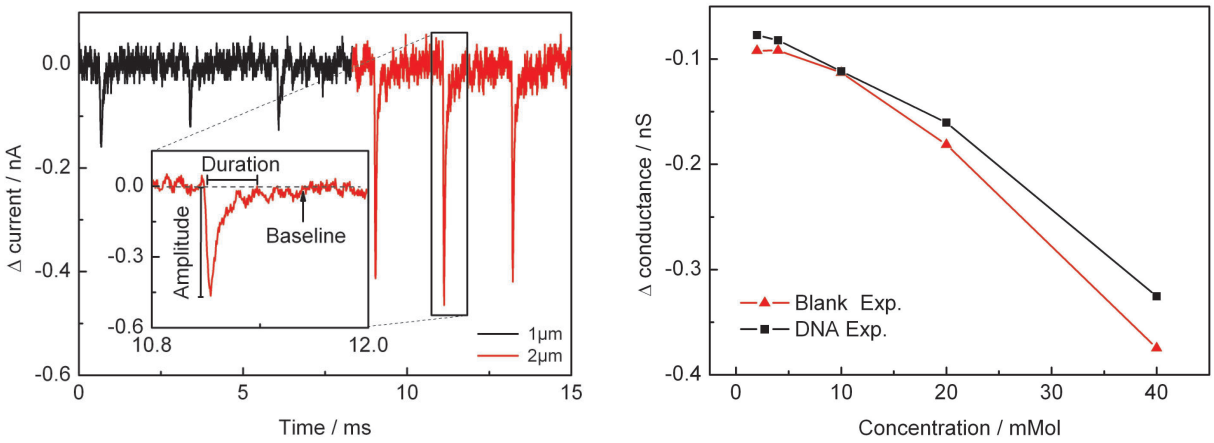


**Figure 3.19:** *Left*: Characteristic current signal (Δ current) as a function of time showing peaks caused by the translocation of 1-µm (*black*) and 2-µm colloids (*red*). For better presentation the mean current was subtracted. The inset illustrates the characteristics of a single translocation event. The start of an event is defined once a certain current threshold is surpassed. The difference between the baseline and peak current is defined as event amplitude. Once the current reaches the baseline level the translocation event is defined as finished. The start and termination point determines the duration of the translocation event. The Δ current divided by the actual potential gives the Δ conductance value. *Right*: Δ conductance values as function of the NaCl concentration during translocation of blank and DNA-labeled colloids as *red* and *black lines*, respectively. The capillary was 6 µm wide, colloid diameter was 1 µm and the pressure 10 mbar. Due to the charge of the grafted DNA molecules the Δ conductance shows higher values for the DNA than for the blank colloids. The standard error of the fits was less than 1 % of the actual Δ conductance value and lie therefore within the data points.

## 3.20 Funding

*DFG-Teilprojekt im Rahmen des Schwerpunktprogramms "Nano- und Mikrofluidik: Von der molekularen Bewegung zur kontinuierlichen Strömung" SPP 1164*
Prof. Dr. F. Kremer
Kr 1138/14-2 (2006 – 2008)

*DFG-Teilprojekt im Rahmen des Schwerpunktprogramms "Nano- und Mikrofluidik: Von der molekularen Bewegung zur kontinuierlichen Strömung" SPP 1164*
Prof. Dr. F. Kremer
Kr 1138/14-3 (2008 – 2010)

*DFG-Projekt "Confinement effects on the molecular dynamics of polymers with special architectures"*
Prof. Dr. F. Kremer, Dr. A. Serghei
Kr 1138/17-1 (2006 – 2008)

*DFG-Projekt "Physicochemical characterisation of ionic liquids-mediated peptide acylation reactions"*
Prof. Dr. F. Kremer
Kr 1138/18-1 (2006 – 2008)

*DFG-Projekt "In-situ Untersuchung der Wechselwirkungskräfte an Polyelektrolytbürsten"*
Prof. Dr. F. Kremer
Kr 1138/20-1 (2006 – 2008)

*FOR877, DFG-Projekt "From local constraints to macroscopic transport: Dynamics of DNA under tension and confinement"*
Prof. Dr. F. Kremer, Prof. Dr. K. Kroy
Kr 1138/21-1 (2007 – 2010)

*SPP, "Polymer-Festkörper-Kontakte: Grenzflächen und Interphasen", DFG-Teilprojekt "Interfacial dynamics of polymers in interaction with solid substrates"*
Prof. Dr. F. Kremer
Kr 1138/23-1 (2008 – 2011)

Prof. Dr. F. Kremer is Principal Investigator and Lecturer in the International Research Training Group "Diffusion in Porous Materials" headed by Prof. Dr. J. Kärger and Prof. Dr. F. Kapteijn.

Prof. Dr. F. Kremer is Principal Investigator in the "Leipzig School of Natural Sciences - Building with Molecules and Nano-Objects" in the framework of a Graduate School funded by the "Federal Excellence Initiative". Several PhD projects are supported by that.

## 3.21 Organizational Duties

F. Kremer

- Director of the Institute of Experimental Physics I (until May 2008)
- Project Reviewer: Deutsche Forschungsgemeinschaft (DFG)
- Editor: J. Coll. Polym. Sci.
- Member of Editorial Board: Macromol. Rapid Commun., Macromol. Chem. Phys., Polym. Adv. Technol.

## 3.22 External Cooperations

**Academic**

- Max-Planck-Institute for Microstructure, Halle, Germany
  M. Alexe, F. Bordusa
- Delft University of Technology, The Netherlands
  C. Dekker
- Leibniz-Institut für Oberflächenmodifizierung, Leipzig, Germany
  D. Hirsch
- University of California, Santa Barbara, USA
  Y.W. Kim

- Universität Konstanz, Germany
  M. Krüger
- Universität Düsseldorf, Germany
  C.N. Likos
- Lund University, Sweden
  P. Linse
- Technische Universität München, Germany
  V. Lobaskin, R. Netz
- Technische Universität Dresden, Germany
  M. Mertig
- Universität Stuttgart, Germany
  J. Harting, M. Rauscher
- Institute of Entomology, Ceske Budejovice, Czech Republic
  A. Sponner
- Leibniz-Institut für Polymerforschung, Dresden, Germany
  A. Drechsler, M. Stamm, A. Synytska, P. Uhlmann
- Brown University, Providence, USA
  D. Stein
- University of Oxford, UK
  F. Vollrath
- Universität Bayreuth, Germany
  W. Zimmermann

**Industry**

- Novocontrol, Hundsangen, Germany
- Comtech GmbH, München, Germany
- Freudenberg Dichtungs- und Schwingungstechnik KG, Weinheim, Germany
- Kempchen Dichtungstechnik GmbH, Leuna, Germany
- inotec FEG mbH, Markkleeberg, Germany
- MicroFAB, Bremen, Germany

## 3.23 Publications

**Journals**

B. Berns, H. Deligöz, B. Tieke, F. Kremer: *Conductive Composites of Polyurethane Resins and Ionic Liquids*, Macromol. Mater. Eng. **293**, 409 (2008)

G. Dominguez-Espinosa, A. Synytska, A. Drechsler, C. Gutsche, K. Kegler, P. Uhlmann, M. Stamm, F. Kremer: *Optical Tweezers to measure the interaction between Poly(acrylic acid) Brushes*, Polymer **49**, 4802 (2008)

C. Gutsche, F. Kremer, M. Krüger, M. Rauscher, R. Weeber, J. Harting: *Colloids dragged through a polymer solution: experiment, theory and simulation*, J. Chem. Phys. **129**, 084 902 (2008)

C. Iacob, J. Sangoro, A. Serghei, S. Naumov, Y. Korth, J. Kärger, C. Friedrich, F. Kremer: *Charge transport and glassy dynamics in imidazole-based liquids*, J. Chem. Phys. **129**, 1 (2008)

K. Kegler, M. Konieczny, G. Dominguez-Espinosa, C. Gutsche, M. Salomo, F. Kremer, C.N. Likos: *Polyelectrolyte-Compression Forces between Spherical DNA Brushes*, Phys. Rev. Lett. **100**, 118 302 (2008)

O. Otto, C. Gutsche, F. Kremer, U.F. Keyser: *Optical tweezers with 2.5 kHz bandwidth video detection for single-colloid-electrophoresis* Rev. Sci. Instrum. **79**, 023 710 (2008)

J.R. Sangoro, C. Iacob, A. Serghei, C. Friedrich, F. Kremer: *Universality of charge transport in glass-forming ionic liquids*, Phys. Chem. Chem. Phys. **11**, 913 (2008), doi:10.1039/b816106b

J.R. Sangoro, C. Iacob, A. Serghei, S. Naumov, P. Galvosas, J. Kärger, C. Wespe, F. Bordusa, A. Stoppa, J. Hunger, R. Buchner, F. Kremer: *Electrical conductivity and translational diffusion in the 1-butyl-3-methyllimidazolium tetrafluoroborate ionic liquid*, J. Chem. Phys. **128**, 212 509 (2008)

J.R. Sangoro, A. Serghei, S. Naumov, P. Galvosas, J. Kärger, C. Wespe, F. Bordusa, F. Kremer: *Charge transport and mass transport in imidazolium based ionic liquids*, Phys. Rev. E **77**, 051 202 (2008)

A. Serghei, H. Huth, C. Schick, F. Kremer: *Glassy dynamics in thin polymer layers having a free upper interface*, Macromolecules **41**, 3636 (2008)

A. Serghei, F. Kremer: *Broadband dielectric studies on the interfacial dynamics enabled by use of nanostructured electrodes*, Rev. Sci. Instrum. **79**, 026 101 (2008)

A. Serghei, F. Kremer: *Metastable states of arrested glassy dynamics, possibly mimicking confinement effects in thin polymer films*, Macromol. Chem. Phys. **209**, 810 (2008)

R. Zorn, M. Mayorova, D. Richter, A. Schönhals, L. Hartmann, F. Kremer, B. Frick: *Effect of nanoscopic confinement on the microscopic dynamics of glass-forming liquids and polymers studied by inelastic neutron scattering*, AIP Conf. Proc. **982**, 79 (2008)

**submitted**

A. Serghei, M. Tress, J.R. Sangoro, F. Kremer: *Electrode polarization and its scaling laws*, submitted to Phys. Rev. Lett. (2008)

## 3.24 Graduations

**Diploma**

- Oliver Otto
  *Single Colloid Electrophoresis using Optical Tweezers*
  February 2008
- Carolin Wagner
  *Einzelmolekül-Kraftspektroskopie zur Untersuchung der Protein-DNA-Wechselwirkung am Beispiel von TmHU*
  September 2008

**Master of Science**

- Jan Henning Peters
  *Effects of Laser-induced Heating in a Nanopore- and Microcapillary-Systems*
  November 2008

**Bachelor**

- Robert Seifert
  *Molecular dynamics of polymers confined in ultra-thin films*
  July 2008

## 3.25 Guests

- Dr. Lidia Okrasa, Dr. Agnieszka Slazak
  Department of Molecular Physics, Technical University of Lodz, Poland
  November – December 2008

## 3.26 Awards

- Periklis Papadopoulos
  Peter Debye Prize for Young Investigatiors for Excellence in Dielectric Research 2008 of the international Dielectric Society (IDS)

# 4

# Physics of Interfaces

## 4.1 Introduction

The activities of our group in 2008 were dominated by the transition into the second funding period of our International Research Training Group (IRTG) 'Diffusion in Porous Materials', including the presentation of our achievements during the past four years and the defense of our proposal for continuation, in front of a prominent international review panel. In addition to the aspired, wonderful outcome, namely the extension of the (Dutch-NWO and German-DFG) sponsorship till 2013, with the Groups of Profs. Krijn de Jong and Bert Weckhuysen (DECHEMA Awardee 2007) from Utrecht University and of Profs. Jürgen Haase, Harald Krautscheid and Friedrich Kremer from Leipzig University, as well as with Prof. Roger Gläser on the Chair of Chemical Technology, we received prominent reinforcement. It was this novel input which notably ensured the intensification of the exchange of our students, with as much as five longer stays of our students in the Netherlands in 2008, namely of Rungroj Chanajaree with Prof. Coppens in Delft, of Muslim Dvoyashkin with Prof. Benes in Eindhoven, of Marcel Gratz with Profs. Kopinga and Magusin in Eindhoven, of Aleksey Khokhlov with Prof. Kapteijn in Delft and of Konstantin Ulrich with Prof. Petra de Jongh in Utrecht.

The activities of the IRTG were in particular *catalyzed* by the presence of our Amsterdam IRTG partner, Prof. Rajamani Krishna, who was awarded a DFG Mercator Professorship at Leipzig University. His immediate influence notably contributed to a number of ambitious publication projects (including two PRL papers as a respectable outcome) which quite decisively promoted the progress in the work of our IRTG PhD students.

Among the manifold contacts all over the world, our IRTG notably benefitted from those with US scientists, including Profs. D.M. Ruthven, University of Maine, presently back to Leipzig as a Humboldt Research Awardee, and D.B. Shah, University of Ohio, Cleveland, who sustains close contact with us as a former Mercator professor of our University. Particular emphasis deserves the cooperation with Prof. P. Monson, Amherst University, Massachusetts. His lecture series and numerous discussions during a longer stay in Leipzig initiated two fundamental papers on the interrelation between adsorption dynamics and hysteresis. Following his invitation to Amherst, one of our IRTG students (Sergej Naumov) had a most productive (and agreeable) stay in the US.

We are particularly pleased that, within the frame of a joint initiative with the institute of inorganic chemistry, we are going to welcome Prof. R.Q. Snurr, Northwestern University Evanston. Following a stay in our group as a Humboldt Fellow in 1994,

he is now honoured with the Leibniz Professorship of our University. We are looking forward to intensify our joint efforts in exploring the microdynamics of guest molecules in *metal-organic framework* (MOFs), within the frame of a recently established DFG priority programme. Finally, we enjoy the continued collaboration with our former colleague Prof. S. Vasenkov, now at University of Florida, Gainesville, in a further DFG priority programme on Molelcular Modelling.

Our research activities, together with those of our partners, led to two further supra-regional research units, namely to an international research group dedicated to the diffusion in zeolites, jointly sponsored by DFG, CNRS, EPSRC and NSF, and to the *Saxonian* DFG Research Unit 'From Local Constraints to Macroscopic Transport', ensuring the long-term exploration of molecular dynamics under confinement as one of the hot topics within the priority research project *From molecules and nano-objects to multifunctional materials and processes* (PbF1: Von Molekülen und Nanoobjekten zu multifunktionalen Materialien und Prozessen) of Leipzig University.

It is with great sadness that we must report that Professor Harry Pfeifer passed away on September 28th, 2008. He established our research group, the department of Physics of Interfaces, and chaired it until 1994. We have lost an outstanding scientist, an excellent mentor and a good friend. His interest in our work continued to the end and he would certainly have been delighted to learn that Rustem Valiullin who, a couple of years ago, joined us as a Humboldt fellow was awarded a DFG Heisenberg fellowship in October 2008. The continuing success of this research group stands as a tribute to his memory.

*Jörg Kärger*

## 4.2 Surface Permeabilities: An Unexploited Field

D. Tzoulaki, L. Heinke, J. Li*, J. Kärger

*Department of Chemistry and Chemical Biology, Rutgers University, Piscataway, USA

Within the scope of investigating a MOF material, attention was attracted by crystals of Zn(tbip) [1], synthesized by the group of Prof. Jing Li (Rutgers University, USA). These crystals are characterized as "guest-free microporous metal organic frameworks" (GFMMOFs) and demonstrate an unusually high structural and thermal stability (they remain intact upon repeated heating at 330 °C). Zn(tbip) (tbip = 5-*tert*-butyl isophthalate) are elongated, hexagonally prismatic crystallites and possess a 3D framework with 1D channels running along the longitudinal axis.

Figure 4.1 provides the results of adsorption and desorption runs with a particularly large number of permeability data for one crystal. Propane profiles provide us both the boundary concentrations and surface fluxes which are used to determine the surface permeability for each value of boundary concentration. These permeabilities are indicated in Fig. 4.1 as large bullets and are obtained by (6) uptake and (6) release experiments either under constant (5 runs for each process) or variable (1 run for each process) pressure for propane. The projection of each large bullet on the bottom plane gives the corresponding pair of the equilibrium and boundary concentration, provided by the respective transient profiles monitored by interference microscopy.

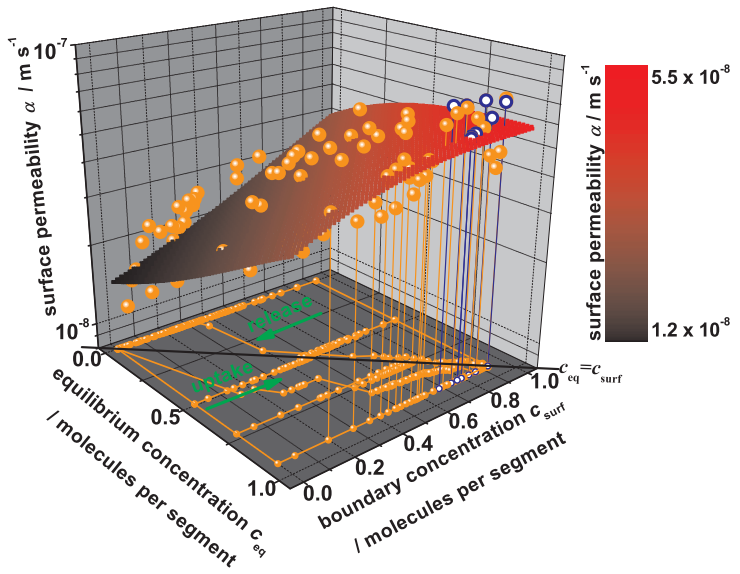


**Figure 4.1:** Surface permeability as a function of the equilibrium and the boundary concentration of the crystal. Large bullets stand for surface permeabilities. Their projection on the bottom plane gives the corresponding pair of equilibrium and boundary concentration. The *inserted surface* (varying from *black to red*) represents the best fit to a dependency $\alpha = \alpha\left(\frac{c_{eq}+c_{surf}}{2}\right)$. The *open blue symbols* refer to the uptake under constant external pressure for an initial concentration of 0.5 to a final concentration of 0.9 molecules per segment.

It has been found that the transport diffusion coefficient remains, in princple, the same in each crystal, since the pore space in every crystallite of the sample should be identical [2]. On the contrary, the surface permeabilities readily vary between different crystals [3].

[1] L. Pan et al.: J. Am. Chem. Soc. **128**, 4180 (2006)
[2] L. Heinke et al.: Phys. Rev. Lett. **102**, 065 901 (2009)
[3] D. Tzoulaki et al.: *Assessing surface permeabilities from transient guest profiles in nanoporous host materials*, Angew. Chem., in press

## 4.3 Diffusion Measurements at Elevated Temperatures

F. Hibbe, T. Binder, S. Schlayer, J. Kärger

Interference microscopy (IFM), as introduced by Kärger et al. in 1978 [1] and brought to systematical usage by Ulf Schemmert in 2001 [2], is a powerfull tool to investigate mass transport in nanoporous, transparent host systems. After one decade filled with interesting and so far unseen experimental results but only few advancements concerning the experimental setup itself, the experimental setup and the methods used for data preparation could be improved significantly.

New computer programs allow to reduce the time needed for data analysis from several days down to few hours and help to correct systematical errors done during the experiments, leading to better signal-to-noise ratios and smoother concentration profiles (Fig. 4.2a). The experimental setup was improved by adding a temperature

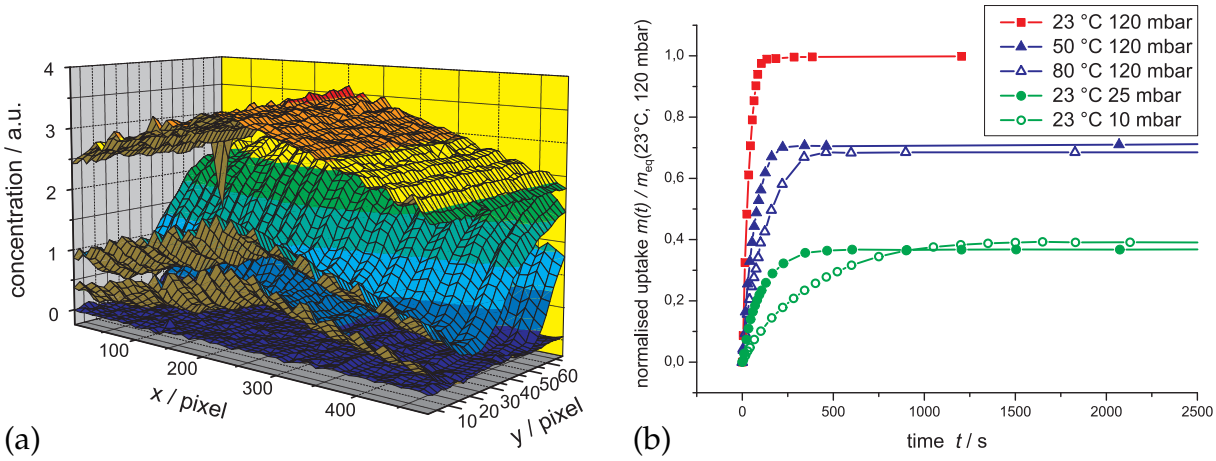


**Figure 4.2:** (**a**) Time dependent, transient concentration profiles of propane in ferrierite obtained by interference microscopy. (**b**) Uptake of propane in ferrierite for variable temperatures und gas preasures.

control device, wich allows us to control the temperature during the experiment in the range from room temperature up to approximatly 100 °C. With this device, it is now possible to investigate the influence of elevated temperatures on the velocity of mass transport, the total amount of adsorbed material $m_{eq}$ (Fig. 4.2b) and the barriers that often occur on crystal surfaces and hinder the transport process [3].

[1] J. Kärger et al.: Feingerätetechnik 27. Jg. **12**, 539 (1978)
[2] U. Schemmert: PhD Thesis, Universität Leipzig (2001)
[3] L. Heinke et al.: Adsorption **23**, 215 (2007)

## 4.4 Adsorption and Diffusion of Alkanes in $Cu_3(BTC)_2$ Crystals Investigated Using FTIR Microscopy and Molecular Simulations

C. Chmelik, L. Heinke, M. Wiebcke*, J. Caro*, J.M. van Baten†, R. Krishna†, J. Kärger

*Institut für Physikalische Chemie und Elektrochemie, Leibniz University Hannover
†Van 't Hoff Institute for Molecular Sciences, University of Amsterdam, The Netherlands

In recent years there has been a remarkable upsurge in research activity on metal-organic frameworks (MOFs), in view of several potential applications in storage, separations, and catalysis. In the development of separation technologies using MOFs, data are required on both adsorption and diffusion of guest molecules.

The current work focuses on one important MOF, i.e. CuBTC ($Cu_3(BTC)_2$ with BTC = benzene-1,3,5-tricarboxylate). Our major objective is to gain insights into the adsorption and diffusion of a variety of linear and branched alkanes in CuBTC, with a view to examining the potential of this material in alkane separations. Our study uses a combination of molecular simulations (Configurational-Bias Monte Carlo (CBMC) for adsorption, and MD for diffusion), and Infra-red Microscopy (IRM) [1].

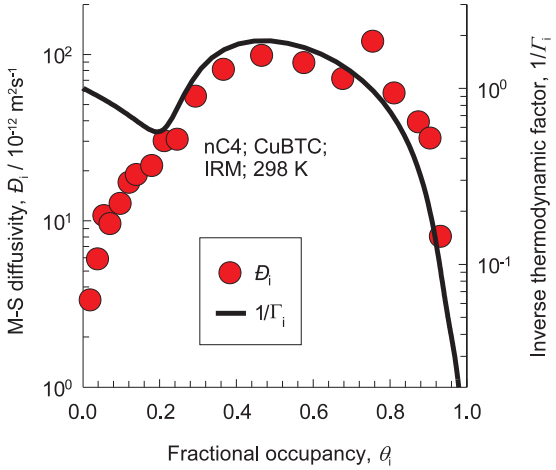


**Figure 4.3:** Occupancy dependence of the Maxwell–Stefan diffusivity $Đ_i$, and the inverse thermodynamic factor $1/\Gamma_i$ of *n*-butane in CuBTC. The symbols represent $Đ_i$ values backed out from IRM experiments, and the continuous solid lines are derived from IRM isotherm fits.

Both, experiments and simulations show strong inflection characteristics in the adsorption isotherms. The primary cause of the inflection is due to the strong preference for adsorption within, and in the regions close to the mouths of tetrahedral pockets. The isotherm inflection has a significant influence on the dependence of the Maxwell–Stefan diffusivity, $Đ_i$, on the fractional occupancy, $\Theta_i$. Both IRM experiments and simulations show that the $Đ_i - \Theta_i$ behaviour appears to be influenced by the loading dependence of the inverse thermodynamic factor $1/\Gamma_i = \mathrm{d}\ln\Theta_i/\mathrm{d}\ln p_i$ (Fig. 4.3). This work highlights the rich features of adsorption and diffusion of alkanes in CuBTC. Our study provides a platform for further research on diffusion in CuBTC and will aid in separation technology development using MOFs.

[1] C. Chmelik et al.: Micropor. Mesopor. Mater. **117**, 22 (2009)

## 4.5 Diffusion of *n*-Butane/iso-Butane Mixtures in Individual Silicalite-1 Investigated Using Infrared Microscopy

C. Chmelik, L. Heinke, J.M. van Baten*, R. Krishna*, J. Kärger

*Van 't Hoff Institute for Molecular Sciences, University of Amsterdam, The Netherlands

Adsorption and diffusion of *n*-butane/iso-butane mixtures in individual silicalite-1 crystals has been investigated using infrared (IR) microscopy and computer simulations [1]. The experimental data of the equilibrium sorption isotherm have been found to be in excellent agreement with the isotherm obtained from CBMC simulations (Fig. 4.4a). The simulation results could be used to calibrate the IR data enabling the determination of absolute concentration in the experiments. The *n*-butane counter-uptake under presence of iso-butane has been investigated for different initial iso-butane loadings

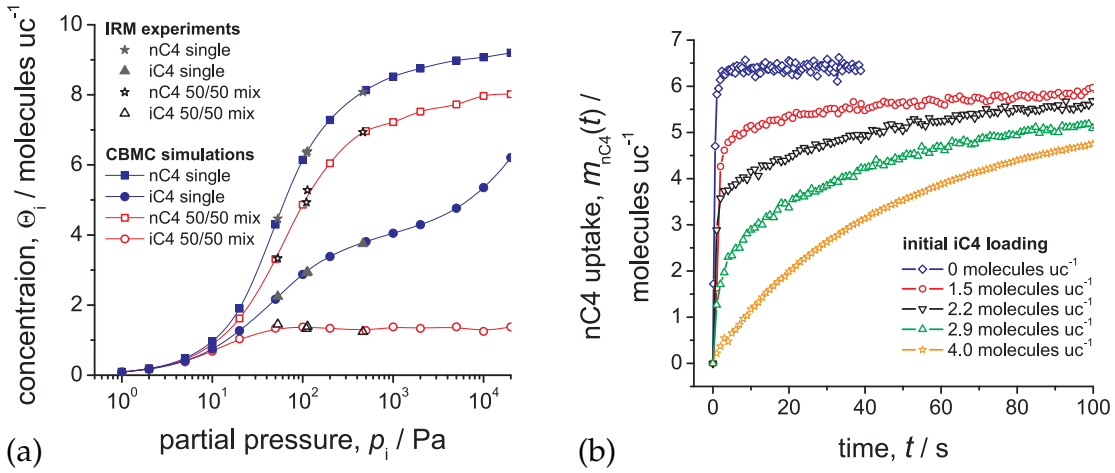


**Figure 4.4:** (**a**) CBMC isotherms for single components (*connected full symbols*) and 50:50 gas mixture (*connected open symbols*) of nC4 and iC4 in silicalite-1. The simulations are compared with experimental results obtained by IRM. (**b**) Impact of different initial iC4 loadings on the *counter-uptake* of nC4. The rate of nC4 is determined by the availability of free sites, i.e. by the release of iC4.

between zero and 4 molecules per unit cell (Fig. 4.4b). The *n*-butane uptake was found to be limited by the availability of free sites rather than the *n*-butane diffusivity. The availability of free sites, in turn, is determined by the rate at which iso-butane desorbs from the crystal. The large difference in the diffusivity by about two orders of magnitude implicates that the much more immobile iso-butane is able to *shield* network regions from *n*-butane by occupying and blocking channel intersections, which act as preferred sites for iso-butane. A site-percolation threshold given by the number of iso-butane molecules blocking these *traffic junctions* has been found to nicely describe the fraction of network regions which are initially inaccessible for *n*-butane. The reported work is relevant not only in the modelling and design of zeolite membrane permeation processes, but also for catalytic processes in which one of the reactants (such as iso-alkanes, or benzene) is located preferentially at the intersections of MFI-type crystals.

[1] C. Chmelik et al.: *Diffusion of n-butane/iso-butane Mixtures in Silicalite-1 Investigated Using Infrared (IR) Microscopy*, Micropor. Mesopor. Mater. (2009), in press

## 4.6 Dynamics of Triblock Copolymers in SBA-15

K. Ulrich, P. Galvosas, F. Grinberg*, J. Kärger, J. Vernimmen†, V. Meynen†, P. Cool†

*Institute of Neurosciences and Biophysics Medicine, Research Centre Jülich
†Department of Chemistry, University of Antwerpen, Belgium

Amphiphilic symmetric triblock copolymers (BCP) find widespread applications in drug delivery, gene therapy and in molecular engineering. In particular Pluronic BCPs are used as templates for synthesising the silica-based SBA-15 materials with cylindrical pores [1]. Recently it was demonstrated that invaluable information on the influence of the phase states and structure morphology on molecular diffusion of BCP can be

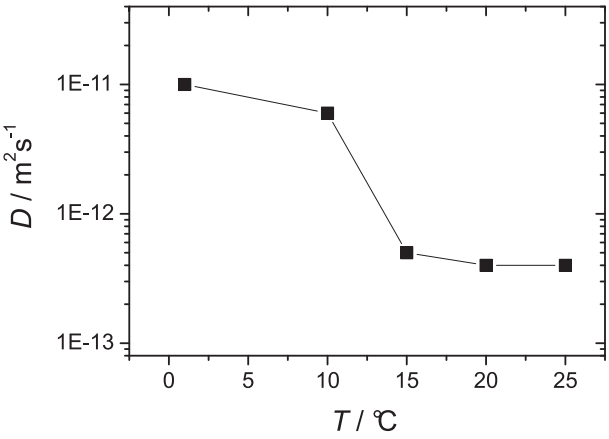


**Figure 4.5:** Diffusion coefficients $D$ of the polymer P123 confined in SBA-15 as a function of temperature.

obtained with the help of the PFG NMR [2]. In spite of the wide-spread use of self-assembling molecules in synthesis of the novel mesoporous materials, there is little knowledge about the phase and transport properties of such systems when they are confined in pores. Understanding the molecular dynamics of the BCPs in SBA-15 has a great importance for modifying and optimizing synthesis routes. The purpose of this work is the study of the effects of the nanoscaled confinements on molecular self-assembly and self-diffusion of BCP.

The diffusivity of Pluronic P123 ((EO)20-(PO)70-(EO)20) was measured using PFG NMR in combination with ultra-high magnetic field gradients. This technique allows monitoring translational dynamics in the range of 100 nm and several microns First diffusion study was performed with the P123 + water system confined in the mesoporous SBA-15. Figure 4.5 shows diffusion of Pluronic P123 in SBA-15. With decreasing temperatures, the molecular diffusivity increases step-like. This is a consequence of the increasing solubilisation of the PO block below 15 ℃ which counteracts self-assemblage. In fact, yielding a diffusivity close to that of PEO in solution, the Pluronics diffusion now occurs by individually dissolved chains rather than by chain aggregations. The results obtained can be discussed in terms of the constraints imposed by specific molecular ordering and pore walls on the diffusion mechanisms.

[1] W.J.J. Stevens et al.: J. Phys Chem. B. **110**, 9183(2006)
[2] K. Ulrich et al.: Phys. Rev. Lett. **102**, 98 (2009)

## 4.7 Assessing the Pore Critical Point of a Confined Fluid by Diffusion Measurement

M. Dvoyashkin, P. Zeigermann, R. Valiullin, J. Kärger

Supercritical fluids (SCF) represent a special class of fluids with physical properties typical for both liquids and gases. With high densities as in the liquid state but, at the same time, possessing dynamical properties typical of gases (high diffusivity, low

viscosity), these fluids have become a powerful tool of modern chemical industry. The use of SCF in such processes like heterogeneous catalysis, preparation of novel mesoporous materials, separation, etc., may not only enhance their productivity but also leads to completely new technological solutions and material properties.

In this study, by means of pulsed the field gradient NMR technique, we investigated diffusion properties of confined *n*-pentane molecules undergoing phase transition to the supercritical state within mesopores [1, 2]. Two porous glass materials as host systems have been used: Vycor particles of about 500 μm size having an internal mesoporous structure with a mean pore diameter of about 5 nm and ERM FD121 with particles of 140 – 200 μm size and with a pore diameter of about 15 nm.

The measured diffusivities of the bulk fluid and of the fluid in the pores are found to increase with increasing temperature following an Arrhenius law [3], with a difference in the absolute values caused by the tortuosity of the porous space (Fig. 4.6). As expected, for the bulk fluid the transition to the supercritical state takes place at the bulk critical temperature, i.e. at 470 K for *n*-pentane. Around this temperature, the diffusion coefficient increases by more than one order of magnitude in a temperature range of only about 7 K.

Most importantly, however, around a certain temperature (ca. 438 K for Vycor and ca. 458 K for ERM) below the bulk critical temperature a remarkable deviation from the Arrhenius pattern in the intrapore diffusivities is observed. We anticipate that this occurs due to the transition of the intrapore fluid to the supercritical, more mobile state. Noteworthy, in the vicinity of this temperature the diffusivity of the bulk liquid does not show any appreciable deviation from the normal behavior. Importantly, such type of measurements can directly provide the pore critical temperature of fluids introduced into porous solids.

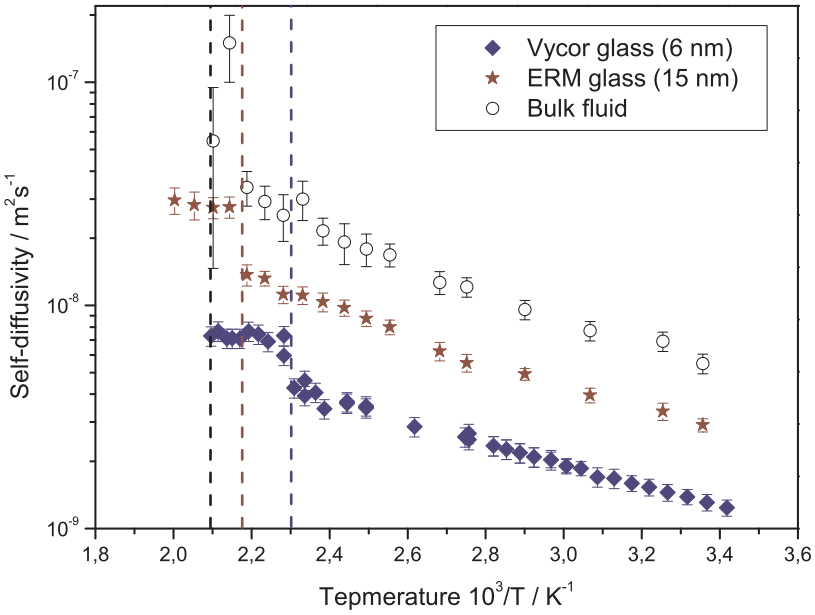


**Figure 4.6:** Arrhenius plot of the bulk (*open circles*) and pore fluid (*solid symbols*) diffusivities for *n*-pentane in Vycor porous glass (*diamonds*) and ERM (*stars*) as a function of temperature. The *vertical dashed lines* show the positions of the bulk (*black line*) and pore critical points for Vycor (*brown*) and ERM (*blue*).

[1] M. Dvoyashkin et al.: Adsorption **13**, 197 (2007)
[2] M. Dvoyashkin et al.: J. Am. Chem. Soc. **129**, 10 344 (2007)
[3] R. Valiullin, M. Dvoyashkin: Adsorption **13**, 239 (2007)

## 4.8 Network Effects within Independent Pores

S. Naumov, R. Valiullin, J. Kärger

Adsorption of gases by mesoporous materials at subcritical temperatures is often accompanied by the phenomenon of hysteresis, i.e., the amount adsorbed depends on whether the gas pressure of the surrounding atmosphere is increased (adsorption branch) or decreased (desorption branch). Such a behavior is generally associated with confinement effects upon condensation and evaporation transitions occurring in pores. In addition to shifts of the transition pressures as compared to the bulk one, variation of pore sizes within a material may lead to evaporation or condensation occcuring over a range of pressures. In the simplest way, this may be governed by the distribution of the pore sizes. It has already long ago been noted that for an array of independent pores with different pore sizes both desorption and adsorption branches should be affected in the same way, i.e., these two branches should be parallel to each other. Experiments, however, often reveal asymmetric hysteresis loops. This is typically the case for materials with highly networked pore structures, such as random porous glasses, and the asymmetry of the hysteresis is generally considered as a consequence of the interconnectivity of the pores.

Recently, porous silicon (PSi) materials, obtained using electrochemical etching of single crystals, have emerged as a promising, potential candidate for studying the effects of pore structure on phase equilibria in pores. It has been shown that by proper tuning of the fabrication conditions PSi with independent, linear pores up to a few

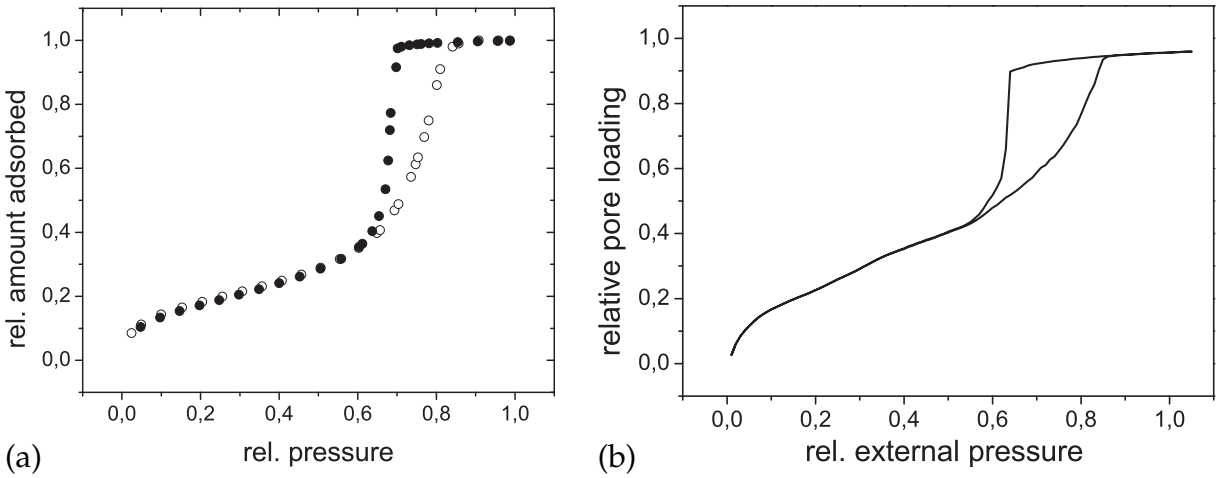


**Figure 4.7:** (**a**) Adsorption (*open symbols*) and desorption (*black symbols*) isotherms for nitrogen in porous silicon at 77 K as a function of pressure. (**b**) Adsorption and desorption isotherms calculated by means of the mean field theory for the model of linear channels with mesoscalic disorder.

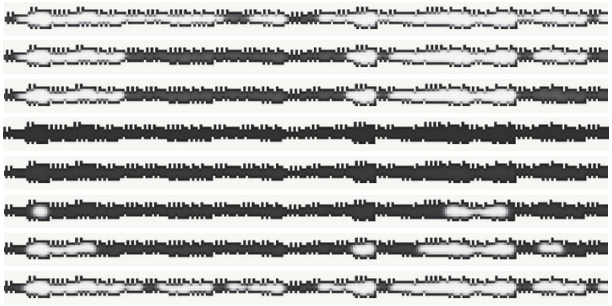

**Figure 4.8:** The fluid density profiles in linear pores obtained using MFT calculations. Adsorption is followed by desorption.

hundred micrometres in length can be obtained. A number of different experimental methods have been used to verify the absence of the intersections between individual channels [1]. Importantly, the fabrication procedure also allows some control of the shape of the pores [2]. Given such attractive options for structural control, PSi has been extensively used for experimental studies. However, the experiments revealed some unexpected, apparently counterintuitive results. The main observation is the similarity of the sorption behavior in the linear independen channles of PSi to that of the disordered 3D pore network (Fig. 4.7a).

In light of such challenging experimental results, we have performed a study using mean field theory (MFT) of a lattice gas [3] of how disorder in linear pores may affect sorption behavior. It was found that all the experimental findings described above can be comprehensively explained taking account of strong mesoscalic disorder of the pore diameter as shown in Fig. 4.8.

[1] S. Naumov et al.: Phys. Rev. E Rapid **78**, 060 601 (2008)
[2] A. Khokhlov et al.: New J. Phys. **9**, 272 (2007)
[3] P. Monson: J. Chem. Phys. **128**, 0021 (2008)

## 4.9 Freezing Kinetics in Linear Pores with Disorder

D. Kondrashova, A. Khokhlov, R. Valiullin, J. Kärger

Recent progress in the synthesis of nanoporous materials with controlled structural properties made it possible to address various phenomena occurring in mesoscalic molecular systems. Among them, different aspects of fluid phase transitions could now be related to the structural properties of mesoporous matrices. In this work, we take advantage of the option to prepare mesoporous silicon with linear, tailor-made pores and thus to study the process of freezing of a fluid under well-defined conditions of confinement [1]. In an ideal cylindrical pore one expects a reduction of the freezing temperature in proportion to the pore size. In the material under study, however, freezing starts already before the transition temperature corresponding to the average pore size is reached. This is referred to the fact that the material possesses a certain degree of disorder, namely a pore size distribution along the pore axis.

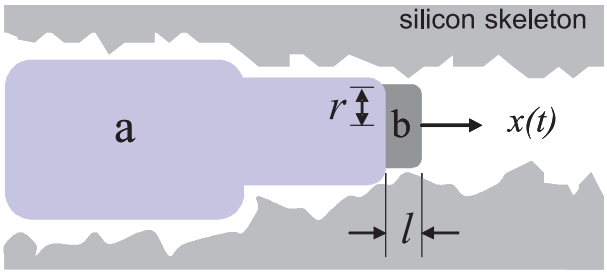


**Figure 4.9:** Freezing front propagation into a disordered linear pore of mesoporous silicon.

In this work, we have experimentally studied the kinetics of this process using NMR. We found it to be very slow and to depend on temperature. Thus, at sufficiently high temperatures, power-law dependencies are typically observed in a certain range of the observation times. We suggest a simple thermodynamical model capturing the main features observed in the experiments. It takes account of the fact that the propagation of the solidification front into a pore having a certain degree of disorder (Fig. 4.9) may require overcoming temperature- and pore-size-dependent barriers in the free energy [2]. This, thus, leads to the activated character of the freezing process under certain conditions, where the geometrical disorder in the pore structure results in a very broad range of characteristic microscopic times. As a particular point, computer simulations performed with the use of this model predict that, at a certain temperature, the solidification front may exhibit a behavior typical of Sinai diffusion [3].

[1] M. Dvoyashkin et al.: J. Chem. Phys. **129**, 154 702 (2008)
[2] R. Denoyel, R.J.M. Pellenq: Langmuir **18**, 2710 (2002)
[3] C. Monthus, T. Garel: Phys. Rev. E **78**, 041 133 (2008)

## 4.10 Crystallization of Zeolite MFI under Super-Gravity, Studied in situ by $^{11}$B MAS NMR Spectroscopy

E.E. Romanova, F. Scheffler*, D. Freude

*Department for Technical Chemistry, Otto-von-Guericke University, Magdeburg

Zeolites find extensive use in industrial applications as catalysts, adsorbent, selective membranes and ion exchangers. Their performance in these applications is strongly determined by structure type, crystal size and morphology [1]. The synthesis of zeolite crystals in space has attracted attention, since micro-gravity offers convection- and sedimentation-free conditions [2]. Crystals of different size and character compared to those grown on earth upon standard gravity of 1 g could be synthesized aboard the International Space Station (ISS), see Kirschhock et al. [3] and Manning et al. [4]. Opposite to micro-gravity, the understanding of the crystal growth mechanism under high-gravity conditions is still poorly investigated. There are only a few groups who have performed zeolite crystallization under conditions of elevated gravity up to 100 g [5, 6]. However, macro-gravity is an important complement to micro-gravity; and corresponding investigations are less expensive.

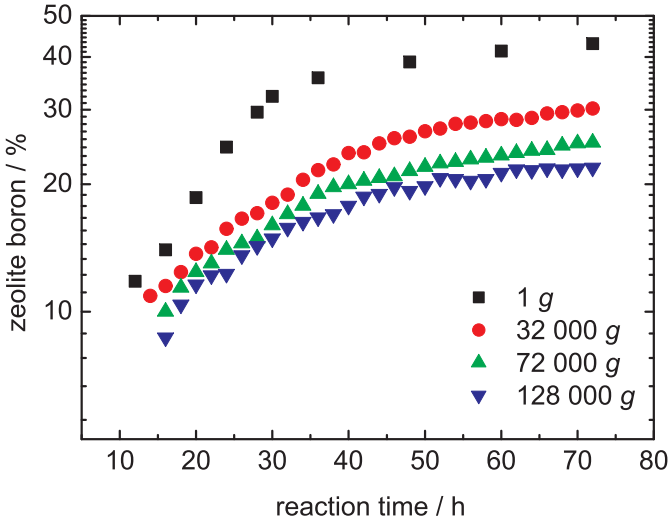


**Figure 4.10:** Semi-logarithmic plot of the percentage of the boron, which moved from the synthesis mixture into the zeolite framework.

The present $^{11}$B MAS NMR study demonstrates in situ the synthesis of MFI-type zeolite under macro-gravity up to 128 000 g. The centrifugal acceleration $a$ of material having the distance $r$ to the rotational axis leads to an elevated gravity $a = \omega^2 r$, where $\omega$ denotes the MAS angular frequency. The MAS frequency was varied from 2 to 4 kHz. Correspondingly, the synthesis of zeolites was carried out under gravity of 32 000 g as well as under 72 000 g and 128 000 g at the reaction temperature of 95 ℃. The same synthesis has been performed in an oven at 95 ℃ in a steel vessel and in a non-rotating quartz tube. The products of the syntheses in the oven were investigated by $^{11}$B MAS NMR spectroscopy at room temperature. Three parameters of crystallization were determined from Fig. 4.10. The first parameter is the crystallization onset which corresponds to the time at which we observe 10 – 12 % of the total boron in the zeolite. We obtain 12 h, 14 h, 16 h and 24 h for 1 g, 32 000 g, 72 000 g, and 128 000 g, respectively. The second parameter is the yield of crystallization, which corresponds to the percentage of boron after 72 h. The values are 43.0 %, 30.2 %, 25.1 % and 21.9 % for 1 g, 32 000 g, 72 000 g, and 128 000 g, respectively. As a third parameter we determined the rate of crystallization from the slope of the plots in Fig. 4.10. Rates of 1.3 %, 0.5 %, 0.4 % and 0.4 % were found for 1 g, 32 000 g, 72 000 g, and 128 000 g, respectively.

The statements derived from the three parameters are that the crystallization onset increases from 12 to 24 h, the crystallization rate decreases from 1.3 % to 0.4 % and the yield of crystallization decreases from 43.0 % to 21.9 %, for 1 g and 128 000 g, respectively. Although the parameters of crystallization degrades with increasing gravity, the difference between crystallization under 128 000 g, 72 000 g, and 32 000 g is relatively low. Then the conclusion is that the increase of gravity from 1 g to 128 000 g degrades significantly the synthesis condition, but the parameters downgrade by less than one order of magnitude

[1] R. Xu et al.: *Chemistry of Zeolites and Related Porous Materials: Synthesis and Structure*, (Wiley, Weinheim 2007)
[2] Z.A.D. Lethbridge et al.: Micropor. Mesopor. Mater. **79**, 339 (2005)
[3] C. Kirschhock et al.: Stud. Surf. Sci. Catal. **154**, 139 (2004)

[4] M.P. Manning et al.: Stud. Surf. Sci. Catal. **154**, 147 (2004)
[5] H.H. Xu et al.: Zeolites **19**, 119 (1997)
[6] Y. Kiyozumi et al.: Nippon Kagaku Kaishi **4**, 320 (1995)

## 4.11 Polysaccharide Salt Hydrogels for Controlled Internal Curing of Hydrating Cements

K. Friedemann, F. Stallmach, J. Kärger

Using non-destructively operating low-field $^1$H NMR relaxometry, hydrogels of different polysaccharides were investigated for their suitability for controlling the release of internal water during hydration of ordinary Portland cements. The polysaccharide hydrogels (calcium and aluminium carboxlates and sulfates) differ with respect to the chemical structure, the functional groups as well as the cations stabilizing the gel structure. It was found that they release the water to the cement mainly during the accelerated period of cement hydration. The transition of water starts at a degree of hydration of about 0.1. The water in the hydrogels is consumed completely by the cement hydration at a degree of hydration of approximately 0.7 (Fig. 4.11a). Based on our results of NMR relaxometry the development of the volume fractions of water inside the hydrogel, of the capillary bound water, of water in gel pores, of the solid hydration products and of the unhydrated cement was quantified according to Powers hydration model [1] (Fig. 4.11b). The results are discussed in detail in [2].

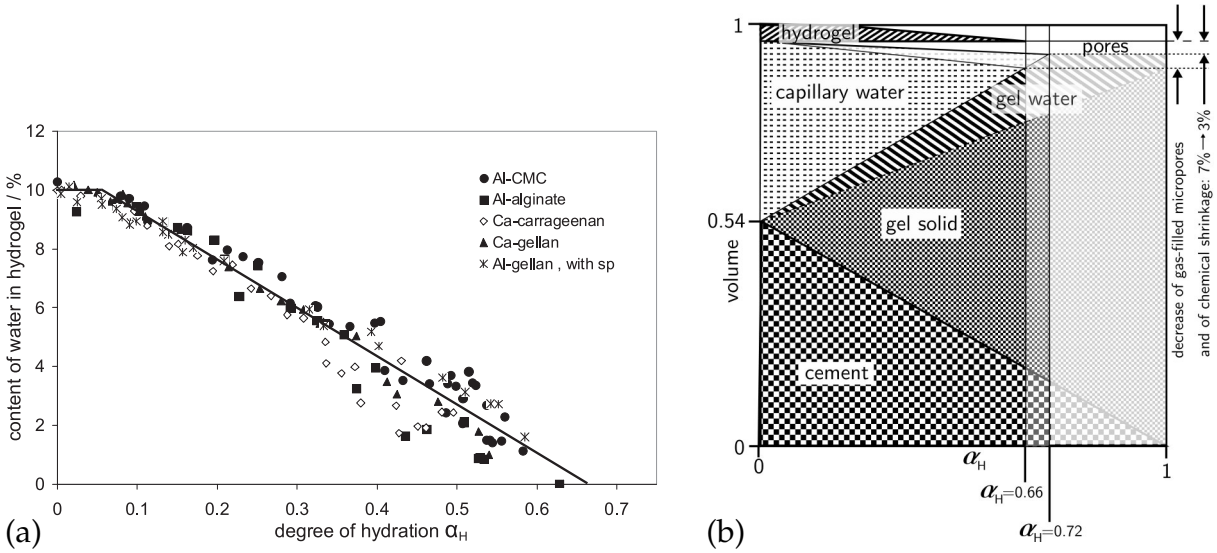


**Figure 4.11:** (**a**) The content of water in five different hydrogels in dependence on the degree of hydration. The initial water content (10 %) refers to the relative amount of water, detected inside of the hydrogel directly after sample preparation. (**b**) Volumetric phase distribution in dependence on the degree of hydration $\alpha_H$ for a hydrating cement with internal curing by hydrogel, $w/c_0 = 0.275 + 0.025$. It is shown that $\alpha_H$ is increased and the extent of chemical shrinkage can be reduced by internal curing.

[1] T.C. Powers, T.L. Brownyard: J. Am. Concrete I. **43**, 101 (1946)
[2] K. Friedemann et al.: Cement Concrete Comp. **31** 244 (2009)

## 4.12 Self-Diffusion in CuBTC Monitored by PFG NMR

M. Wehring, J. Gascon*, F. Kapteijn*, F. Stallmach

*DelftChemTech, Delft University of Technology, Netherlands

In the field of synthesised porous materials the invention of metal organic frameworks (MOF) has attracted a great deal of attention during the last years. So far most of the studies about host-guest interactions of hydrocarbons inside the pores of the MOFs are computer simulations or adsorption studies. For the development of applications using MOFs like gas separation, gas storage or heterogeneous catalysis the knowledge of diffusion of adsorbed hydrocarbons is important.

This study focuses on the MOF copper(II) benzene-1,3,5-tricarboxylate ($Cu_3(BTC)_2(H_2O)_3$ (CuBTC)), which was first synthesised by Chui et al. [1]. In the current work, the self-diffusion of butane and butene adsorbed in CuBTC is investigated experimentally by ($^1$H) pulsed field gradient nuclear magnetic resonance (PFG NMR)[2]. The self-diffusion measurements were carried out in a temperature range from 193 K to 353 K and the activation energy of self-diffusion were determined. The spin echo attenuations show a strictly mono-exponential behaviour (Fig. 4.12a). Depending on the temperature, the intracrystaline self-diffusion coefficient varies between $10^{-11}$ m$^2$s$^{-1}$ and $10^{-10}$ m$^2$s$^{-1}$ (Fig. 4.12b). The activation energy of butane (8.5 kJ/mol) is found to be slightly smaller than that of butene (9.7 kJ/mol) [3].

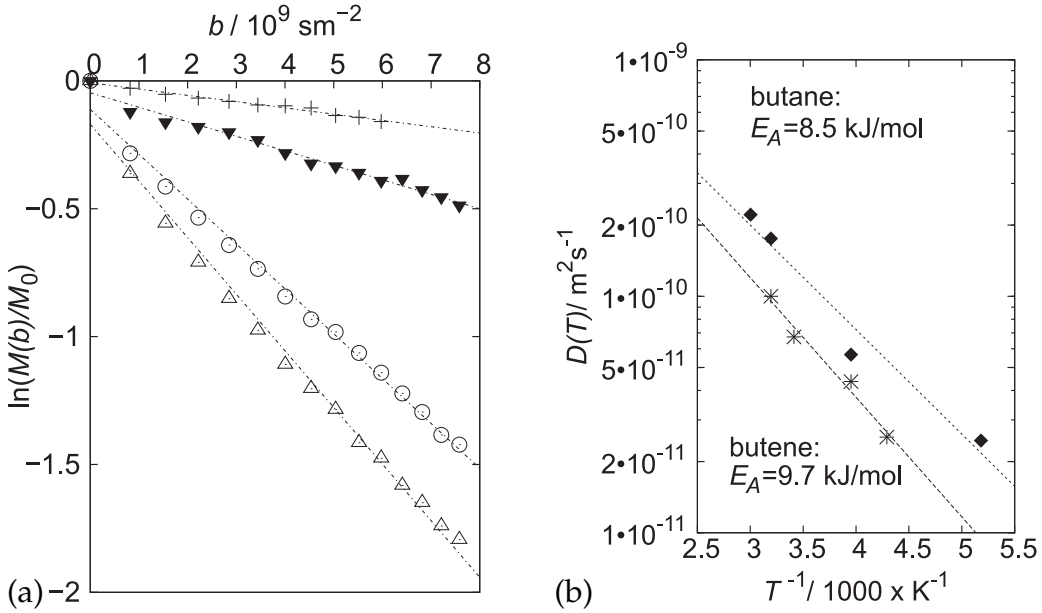


**Figure 4.12:** (**a**) Spin echo attenuation of butane adsorbed in CuBTC for temperatures of $T$ = 193 K (+), 253 K (▼), 313 K (○), 333 K (△). (**b**) Intracrystalline self-diffusion coefficients of butane (*black diamonds*) and butene (*stars*), with the corresponding activation energies of self-diffusion.

[1] S.S.Y. Chui et al.: Science **283**, 1148 (1999)
[2] F. Stallmach, P. Galvosas: Ann. Rep. NMR Spectrosc. **61**, 51 (2007)
[3] M. Wehring et al.: Poster at the 1. Int. Conf. Metal Organic Frameworks and Open Framework Compounds (MOF2008), Augsburg, Germany, 08. – 10. October 2008

## 4.13 Molecular Exchange of *n*-Pentane in NaX Zeolite Investigated by DEXSY

M. Gratz, P. Galvosas

We recently investigated the exchange behaviour of *n*-pentane among its free phase and a phase being confined in the microporous NaX zeolite. Therefore we used the diffusion exchange spectroscopy (DEXSY) as suggested in [1], which was adapted to the use of ultra-high pulsed magnetic field gradients [2] as outlined in [3]. The DEXSY experiment consists of two NMR spin echo experiments, which are separated by a mixing time $\tau_m$. The pairs of pulsed field gradients as incorporated in each spin echo sub-sequence are raised independently, thus leading to a 2D NMR signal map. With the help of an inverse 2D Laplace transformation of this map one may obtain the distribution $p(D_1, D_2)$, which is shown for a mixing time of 500 ms in Fig. 4.13a.

Starting with small mixing times $\tau_m$, molecules are not able to pass over to the other phase, thus not changing their motional behaviour. Hence, the transformed map yields only two diagonal peaks ($D_1 = D_2$). For increasing mixing times, off-diagonal (exchange) peaks raise, since for longer $\tau_m$ the probability for a molecule to migrate from the zeolite to the free phase ($D_1 < D_2$) and vice verse ($D_1 > D_2$) increases.

An analysis of the growth of all occurring peaks (Fig. 4.13b) yields an exchange time of $\tau_{\text{exch}} = (460 \pm 50)$ ms (see [3] for details). This value is much bigger than that, one would expect for an exchange process, which is limited by intra-crystalline diffusion only. Thus, we conclude, that the exchange is also controlled by the surface of the zeolite.

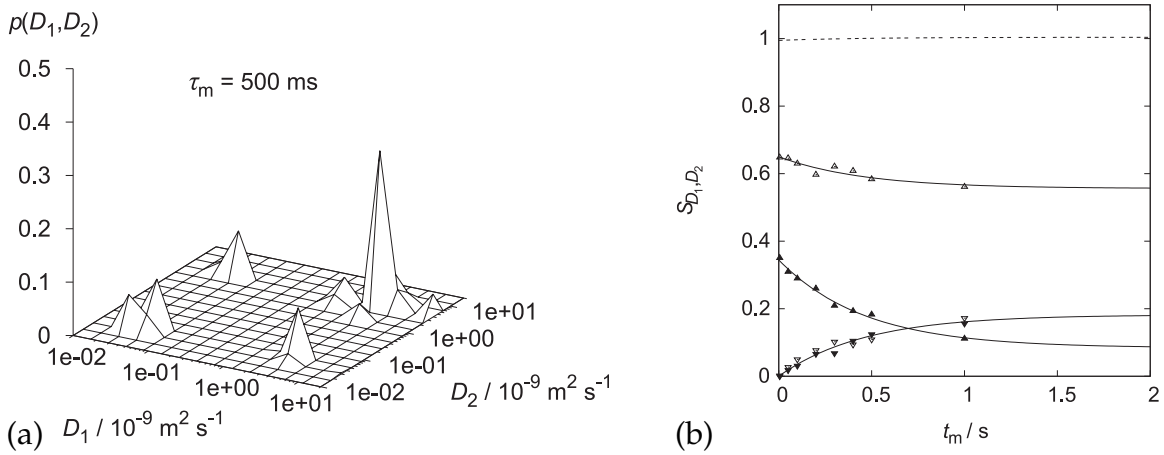


**Figure 4.13:** Results of the DEXSY experiments: **(a)** Exchange map from the DEXSY using the mixing time $\tau_m = 500$ ms. **(b)** Intensities of the exchange peaks (▽ and ▼) and the free (△) and adsorbed peaks (▲) and their corresponding fits (*solid line*), as well as the sum of all intensities (*dashed line*).

[1] P.T. Callaghan et al.: Magn. Reson. Imaging **21**, 243 (2003)
[2] P. Galvosas et al.: J. Magn. Reson. **151**, 260 (2001)
[3] M. Gratz et al.: *Multidimensional NMR diffusion studies in microporous materials*, Micropor. Mesopor. Mater. (2009), in press

## 4.14 Funding

*Alkan- und Alken-Aktivierung in der heterogenen Säurekatalyse. In situ-C-13 und H-1 MAS NMR-Untersuchungen der Kinetik des Isotopen- Scramblings (C-13, H-2) im Reaktionsverlauf.*
Prof. Dr. D. Freude
DFG Fr 902 / 15-2

*Combined NMR Studies of Diffusion and Reaction.*
Prof. Dr. D. Freude
im DFG GRK 1056/1, International Research Training Group "Diffusion in Porous Materials"

*Anwendungen der Doppelrotations- und Multiquanten-Messtechnik für Hochfeld-NMR-Untersuchungen an O-17-Kernen in porösen Festkörpern.*
Prof. Dr. D. Freude, Dr. H. Ernst
DFG Fr 902/16-2

*Computersimulation und analytische Untersuchungen zum Einfluss der Kristallgrenze auf den Austausch von Gastmolekülen zwischen Zeolith-Nanokristallen und der Umgebung*
Dr. S. Fritzsche, Prof. Dr. S. Vasenkov
DFG Fr 1486/2-1, SPP 1155 "Molekulare Modellierung und Simulation in der Verfahrenstechnik"

*Studying Zeolitic Diffusion by Interference and IR Microscopy.*
Prof. Dr. J. Kärger
DFG Ka 953/18-3, International Research Group "Diffusion in Zeolites"

*Bestimmung mikroskopischer Kenngrößen der Molekültranslation in Schüttungen nanoporöser Partikel mittels PFG NMR und Monte-Carlo-Simulation.*
Prof. Dr. J. Kärger
DFG Ka 953/19-1

*Confinement Effects on Diffusion and Reaction in Zeolites, Studied by Dynamic MC Simulations, PFG NMR and Interference/IR Microscopy.*
Prof. Dr. J. Kärger
im DFG GRK 1056/1, International Research Training Group "Diffusion in Porous Materials"

*In situ study and development of processes involving nanoporous solids.*
Prof. Dr. J. Kärger
EU-Projekt NMP3-CT-2004-500895

*PFG NMR studies of zeolitic diffusion.*
Prof. P. Galvosas, Prof. Dr. J. Kärger
DGF Ga 1291/1-2

*PFG NMR investigations on formulated catalysts; Bestimmung von Diffusionskoeffizienten an Katalysatoren.*

Prof. Dr. J. Kärger, Dr. F. Stallmach
BASF AG

*Fourier-Transform-PFG-NMR mit starken Feldgradientenimpulsen zur selektiven Selbstdiffusionsmessung.*
Prof. Dr. J. Kärger, Dr. F. Stallmach
DFG Ka 953/16-1

*Innovative Zugabestoffe für die Innere Nachbehandlung von Hochleistungsbeton unter Berücksichtigung der räumlichen und zeitlichen Wasserbilanz.*
Prof. Dr. J. Kärger, Dr. F. Stallmach
DFG Ka 953/22-2

*Intelligent design of nanoporous sorbents.*
Prof. Dr. J. Kärger, Despina Tzoulaki
EU-Projekt CT-2004-005503

*Fluid Transport in Porous Rocks and Sediments from Near-Surface Aquifers Studied by NMR and MRI.*
Dr. F. Stallmach
im DFG GRK 1056/1, International Research Training Group "Diffusion in Porous Materials"

*NMR and MRI studies of aquifer rocks; NMR- and MRI-Untersuchungen an Aquifergesteinen.*
Dr. F. Stallmach, Prof. Dr. J. Kärger
UFZ Halle/Leipzig GmbH

*Messung intrakristalliner Diffusions-Reaktions-Profile in Zeolithen mittels IR-Imaging.*
Prof. Dr. J. Kärger
DFG Ka 953/20-1

*Messung von Phasenübergängen in mesoskopisch beschränkten Systemen: kombinierter Einsatz von NMR und Molekulardynamik.*
Prof. Dr. J. Kärger, Dr.R. Valiullin
DFG Ka 953/21-1

*Untersuchung der Diffusion in heterogenen Systemen mit PFG-MAS-NMR-Spektroskopie.*
Dr. A. Pampel, Prof. Dr. J. Kärger
DFG Pa 907/3-1

*PFG NMR Untersuchung der Transporteigenschaften von Fluiden in Mesoporen in der Nähe des kritischen Punktes*
Prof. J. Kärger, Dr. R. Valiullin
DFG Ka 953/25-1

*P8 Particle Dynamics in Nano-Structured Channels*
Prof. J. Kärger, Dr. R. Valiullin, Prof. Janke
DFG Ka 953/27-1

*ZP Zentralprojekt gemeinsam beantragter Mittel für die sächsische Forschergruppe*
Prof. J. Kärger
DFG Ka 953/28-1

*Network of Excellence: Inside Pores*
Prof. J. Kärger, Dr. F. Grinberg
EU-Projekt 23120 562

*Mercator-Professur*
Prof. Dr. Rajamani Krishna
Le 758/25-1

## 4.15 Organizational Duties

D. Freude
- Membership in Editorial Boards: Solid State NMR; Diff. Fund. (Online Journal)
- Referee: Chem. Phys. Lett., J. Chem. Phys., J. Phys. Chem., J. Magn. Res., Solid State NMR

P. Galvosas
- Referee: Magn. Reson. Imag., J. Magn. Reson., Concept. Magn. Reson.
- Faculty board member
- Grievance committee member (Prüfungskommission)
- General advisor for physic study affairs (Studienfachberater für Physik)
- Deputy institutional ERASMUS coordinator

F. Grinberg
- Membership in "AMPERE Division of Spatially Resolved Magnetic Resonance" Polish German Radiospectroscopy Group (PGRG)
- Membership in Editorial Boards: Diff. Fund. (Online Journal, Editor)

J. Kärger
- Speaker of the International Research Training Group (DFG, NWO) "Diffusion in Porous Materials", the DFG-Research Group "From Local Constraints to Macroscopic Transport" and the International Research Group (CNRS, DFG, EPSRC, NSF) "Diffusion in Zeolites"
- Membership in the Programme Committee "Magnetic Resonance in Porous Media" (Bologna 2006, Boston 2008, Leipzig 2010), "Fundamentals of Adsorption" (Giardini Naxos, Sicily, Italy 2007, Kyoto, Japan 2010), International Zeolite Conference (Peking 2007, Sorento, Italy 2010), in the permanent DECHEMA committees Zeolites and Adsorption and in the Board of Directors of the Magnetic Resonance Centre (MRZ) of Leipzig University
- Membership in Editorial Boards: Micropor. Mesopor. Mater. (European Editor), Diff. Fund. (Online Journal, Editor); Adsorption
- Referee: Phys. Rev., Phys. Rev. Lett., Europhys. Lett., J. Chem. Phys., J. Phys. Chem., Langmuir, Micropor. Mesopor. Mater., Phys. Chem. Chem. Phys., J. Magn. Res., Nature, Angew. Chem.
- Reviewer: Deutsche Forschungsgemeinschaft, National Science Foundation (USA)

F. Stallmach
- Referee: Micropor. Mesopor. Mater., Angew. Chem., J. Am. Chem. Soc., J. Magn. Res., J. Phys. Chem.
- Reviewer: Deutsche Forschungsgemeinschaft, Swiss National Science Foundation (SNF)

R. Valiullin
- Membership in Scientific Advisory Committee "Int. Bologna Conf. Magn. Reson. Porous Media (Ampere Event)"
- Referee: J. Phys. Chem., Phys. Rev., Adsorption, Micropor. Mesopor. Mater.

## 4.16 External Cooperations

**Academic**

- Academy of Sciences of the Czech Republic, J. Heyrovsky Institute of Physical Chemistry, Prague, Czech Republic
  Dr. Kocirik, Dr. Zikanova
- Delft University, DelftChemTech, The Netherlands
  Prof. Kapteijn
- Institut de Recherches sur la Catalyse, CNRS, Villeurbanne, France
  Dr. Jobic
- GeoForschungsZentrum Potsdam (GFZ), Germany
  A. Förster, H.-M. Schulz
- Helmholtz Zentrum für Umweltforschung UFZ Halle-Leipzig GmbH, Leipzig, Germany
  Prof. Kopinke, H.-R. Gläser, I. Mitreiter, S. Oswald
- Institut Francais du Petrole, Malmaison, France
  Dr. Methivier
- Max-Planck-Institut für Kohlenforschung, Mülheim, Germany
  Dr. Schmidt, Prof. Schüth
- Max-Planck-Institut für Metallforschung, Stuttgart, Germany
  Dr. Majer
- Russian Acadademy of Sciences, Boreskov Institute of Catalysis, Siberian Branch, Novosibirsk, Russia
  Dr. Stepanov
- Technische Universität München, Lehrstuhl Technische Chemie 2, Germany
  Prof. Lercher
- University Medical Center Hamburg-Eppendorf, Hamburg, Germany
  Dr. M. Koch
- Università di Sassari, Dipartimento Chimica, Sassari, Italy
  Prof. Demontis, Prof. Suffritti

- Universiät Eindhoven, Schuit Institute, The Netherlands
  Prof. van Santen
- Universität Erlangen Nürnberg, Deptartment for Chemical Engineering, Erlangen, Germany
  Prof. Emig, Prof. Schwieger
- Universität Hannover, Institute of Physical Chemistry, Germany
  Prof. Caro, Prof. Heitjans
- Universität Leipzig, Institut für Analytische Chemie, Germany
  Prof. Berger
- Universität Leipzig, Institut für Technische Chemie, Germany
  Prof. Einicke, Prof. Papp, Prof. Gläser
- Universität Leipzig, Institut für Anorganische Chemie, Germany
  Prof. Krautscheid
- Universität Leipzig, Institut für Medizinische Physik und Biophysik, Germany
  Prof. Arnold, Prof. Gründer, Prof. Huster
- Technische Universität Dresden, Institut für Biophysik, Germany
  Prof. Brunner
- Universität Stuttgart, Institut für Technische Chemie, Germany
  Prof. Hunger, Prof. Weitkamp
- University Athens, Deptartment for Chemical Engineering, Greece
  Prof. Theodorou
- University of Amsterdam, The Netherlands
  Prof. Krishna
- University of Maine, Deptartment for Chemical Engineering, Orono, USA
  Prof. Ruthven
- Cleveland University, USA
  Prof. Shah
- University of Edinburgh, UK
  Prof. Brandani
- Westfälische Wilhelms-Universität Münster, Institut für Physikalische Chemie, Germany
  Prof. Schönhoff
- Victoria University of Wellington, MacDiarmid Institute for Advanced Materials and Nanotechnology, School of Chemical and Physical Sciences, New Zealand
  Prof. Callaghan
- Ludwig-Maximilians-Universität München, Department of Chemistry and Biochemistry, Germany
  Prof. Bräuchle, Dr. C. Jung
- Martin-Luther-Universität Halle-Wittenberg, Fachbereich Chemie/Technische Chemie, Germany
  Dr. D. Enke

- University of Massachusetts, Department of Chemical Engineering, Amherst, USA
  Prof. P.A. Monson

**Industry**

- Air Prod & Chem Inc., Allentown, USA
  Dr. Coe, Dr. Zielinski
- BASF, Ludwigshafen, Germany
  Dr. Müller, Dr. Nestle, Dr. Rittig
- Cepsa, Madrid, Spain
  Dr. Perez
- Grace, Worms, Germany
  Dr. McElhiney
- Resonance Instruments Ltd., Witney, UK
  J. McKendry
- SINTEF, Oslo, Norway
  Prof. Stöcker
- Südchemie, Berlin, Germany
  Dr. Tissler, Dr. Tufar, Dr. Lutz
- StatoilHydro, Stavanger, Norway
  C. v. d. Zwaag
- HeidelbergCement, Baustoffe für Geotechnik GmbH & Co. KG, Ennigerloh, Germany
  A. Märten, J. Dietrich A. Märten, J. Dietrich
- Volkswagen AG, Wolfsburg/Isenbüttel, Germany
  R. Scheffler

## 4.17 Publications

**Journals**

C. Chmelik, L. Heinke, J. Kärger, W. Schmidt, D.B. Shah, J.M. van Baten, R. Krishna: *Inflection Behaviour in the Loading Dependence of the Maxwell-Stefan Diffusivity of iso-Butane in MFI Zeolite*, Chem. Phys. Lett. **459**, 141 (2008)

M. Dvoyashkin, A. Khokhlov, R. Valiullin, J. Kärger, *Freezing of Fluids in Disordered Mesopores*, J. Chem. Phys **129**, 154 702 (2008)

M. Fernandez, A. Pampel, R. Takahashi, S. Sato, D. Freude, J. Kärger: *Revealing Complex Formation in Acetone-n-Alkane Mixtures by MAS PFG NMR Diffusion Measurement in Nanoporous Hosts*, Phys. Chem. Chem. Phys. **10**, 4165 (2008)

K. Friedemann, W. Schönfelder, F. Stallmach, J. Kärger: *NMR Relaxometry During Internal Curing of Portland Cements by Lightweight Aggregates*, Mater. Struct. **41**, 647 (2008)

M. Gratz, P. Galvosas: *Investigation of Molecular Exchange Using DEXSY with Ultra-High Pulsed Field Gradients*, Proc. Magn. Reson. Porous Media **1081**, 91 (2008)

L. Heinke, C. Chmelik, J. Kärger: *Determining the Transport Diffusivity from Intracrystalline Concentration Profiles*, Stud. Surf. Sci. Catal. **174**, 607 (2008)

L. Heinke, P. Kortunov, D. Tzoulaki, M.J. Castro, P.A. Wright, J. Kärger: *Three-Dimensional Diffusion in Nanoporous Host-Guest Materials, Directly Monitored by Interference Microscopy*, Europhys. Lett. **81**, 26002 (2008)

L. Heinke, J. Kärger: *Assessing One-Dimensional Diffusion in Nanoporous Materials from Transient Concentration Profiles*, New J. Phys. **10**, 023 035 (2008)

L. Heinke, J. Kärger: *Mass Transfer in One-Dimensional Nanoporous Crystals with Different Surface Permeabilities* Diff. Fund. **9**, 2.1 (2008)

G. Kalies, P. Bräuer, M. Szombathely: *Design of Liquid/Solid Adsorption Isotherms by Energy Distribution Functions*, J. Coll. Interf. Sci. **331**, 329 (2008)

J. Kärger: *Comment on "PFG NMR Self-Diffusion of Small Hydrocarbons in High Silica DDR, CHA and LTA Structure" (Micropor. Mesopor. Mater. **109**, 327 (2008))*, Micropor. Mesopor. Mater. **116**, 715 (2008)

J. Kärger: *Comment on "Diffusionandadsorption Selectivities of Hydrocarbons over FCC Catalysts" (Chem. Eng. J. **132**, 67 (2007))*, Chem. Eng. J. **145**, 522 (2008)

A.G. Khokhlov, R.R. Valiullin, J. Kärger, N.B. Zubareva, M.A. Stepovich: *Estimation of Pore Sizes in Porous Silicon by Scanning Electron Microscopy and NMR Cryoporometry*, J. Surf. Invest. X-ray, Synchr. Neutr. Techn. **2**, 919 (2008)

A.G. Khokhlov, R.R. Valiullin, M.A. Stepovich, J. Kärger: *Characterization of Pore Size Distribution in Porous Silicon by NMR Cryoporosimetry and Adsorption Methods*, Colloid J. **70**, 507 (2008)

M. Krutyeva, J. Kärger: *NMR Diffusometry with Beds of Nanoporous Host Particles: An Assessment of Mass Transfer in Compartmented Two-Phase Systems*, Langmuir **24**, 10 474 (2008)

S. Naumov, A. Khokhlov, R. Valiullin, J. Kärger: *Understanding Capillary Condensation and Hysteresis in Porous Silicon: Network Effects within Independent Pores*, Phys. Rev. E **78**, 060 601 (2008)

S. Naumov, R. Valiullin, J. Kärger, R. Pitchumani, M.-O. Coppens: *Tracing Pore Connectivity and Architecture in Nanostructured Silica SBA-15*, Micropor. Mesopor. Mater. **110**, 37 (2008)

S. Naumov, R. Valiullin, P.A. Monson, J. Kärger: *Probing Memory Effects in Confined Fluids via Diffusion Measurements*, Langmuir **24**, 6429 (2008)

E.E. Romanova, C.B. Krause, A.G. Stepanov, W. Schmidt, J.M. van Baten, R. Krishna, A. Pampel, J. Kärger, D. Freude: $^{1}$H *NMR Signal Broadening in Spectra of Alkane Molecules Adsorbed on MFI Type Zeolites* Solid State Nucl. Magn. Reson. **33**, 65 (2008)

D. Tzoulaki, L. Heinke, W. Schmidt, U. Wilczok, J. Kärger: *Exploring Crystal Morphology of Nanoporous Hosts from Transient Guest Profiles*, Angew. Chem. Int. Ed. **47**, 3954 (2008)

D. Tzoulaki, W. Schmidt, U. Wilczok, J. Kärger: *Formation of Surface Barriers on Silicalite-1 Crystal Fragments by Residual Water Vapour as Probed with Isobutane by Interference Microscopy*, Micropor. Mesopor. Mater. **110**, 72 (2008)

K. Ulrich, M. Sanders, F. Grindberg, P. Galvosas, S. Vasenkov: *Application of PFG NMR with High Gradient Strength for Studies of Self-Diffusion in Lipid Membranes on the Nanoscale*, Langmuir **24**, 7365 (2008)

S. Zschiegner, S. Russ, R. Valiullin, M.-O. Coppens, A.J. Dammers, A. Bunde, J. Kärger: *Normal and Anomalous Diffusion of Non-Interacting Particles in Linear Nanopores*, Eur. Phys. J. **161**, 109 (2008)

**Books**

F. Grinberg: *NMR of constrained fluids*, in *Magnetic Resonance Imaging*, ed. by J. Seymour, S. Codd (Wiley, Weinheim 2008) p 534

G. Kalies: *Der flüssige Zustand*, in *Alles fließt, Dimensionen des Wassers*, ed. by E. Schenkel, A. Lempert (Peter Lang Verlag für Wissenschaften, Frankfurt am Main 2008) p 55

J. Kärger: *Application of IR Spectroscopy, IR Microscopy, and Optical Interference Microscopy to Diffusion in Zeolites*, in *Adsorption and Diffusion*, ed. by H. Karge, J. Weitkamp (Springer, Berlin 2008) p 135

J. Kärger: *Determination of Diffusion Coefficents in Porous Media*, in *Handbook of Heterogeneous Catalysis*, ed. by G. Ertl, H. Knözinger, F. Schüth, J. Weitkamp (Wiley, Weinheim 2008) p 1714

J. Kärger: *Diffusion Measurements by NMR Techniques*, in *Adsorption and Diffusion*, ed. by H. Karge, J. Weitkamp (Springer, Berlin 2008) p 85

J. Kärger: *Single-File Diffusion in Zeolites*, in *Adsorption and Diffusion*, ed. by H. Karge, J. Weitkamp (Springer, Berlin 2008) p 329

J. Kärger, R. Valiullin: *History-Dependent Molecular Dynamics in Nanoporous Host Matrices*, in *Physik-Statistik-Informationen*, ed. by W. Eisenberg, U. Renner, S. Trimper, B. Fritzsche, K. Vogelsang (Universitätsverlag Leipzig, Leipzig 2008) p 74

R. Valiullin, J. Kärger: *Anomalous Molecular Dynamics in Confined Spaces*, in *Anomalous Transport: Foundations and Applications*, ed. by R. Klages, G. Radons, I.M. Sokolov (Wiley, Weihnheim 2008)

**in press**

C. Chmelik, L. Heinke, J.M. van Baten, R. Krishna: *Diffusion of n-Butane/iso-Butane Mixtures in Silicalite-1 Investigated Using Infrared (IR) Microscopy*, Micropor. Mesopor. Mater.

K. Friedemann, F. Stallmach, J. Kärger: *Carboxylates and Sulfates of Polysaccharides for Controlled Internal Water Release During Cement Hydration*, Cement Concrete Comp.

M. Gratz, M. Wehring, P. Galvosas, F. Stallmach: *Multidimensional NMR Diffusion Studies in Microporous Materials*, Micropor. Mesopor. Mater.

D. Tzoulaki, L. Heinke, J. Li, H. Lim, D. Olson, J. Caro, R. Krishna, C. Chmelik, J. Kärger: *Assessing Surface Permeabilities From Transient Guest Profiles in Nanoporous Materials*, Angew. Chem.

**Talks**

C. Chmelik, F. Grinberg, J. Kärger: *The Evidence of Microscopic Diffusion Measurement: Surprises and Miracles* (invited plenary lecture), 1. Int. Workshop Nanopor. Mater. Energy Env. (NAPEN 2008), Chania, Crete, Greece, 12. – 15. October 2008

C. Chmelik, L. Heinke, J. Kärger, W. Schmidt, J.M. van Baten, R. Krishna: *Inflection in the Loading Dependence of the Maxwell-Stefan Diffusivity of iso-Butane in MFI-type Zeolites*, 1. Int. Workshop Nanopor. Mater. Energy Env. (NAPEN 2008), Chania, Crete, Greece, 12. – 15. October 2008

C. Chmelik, L. Heinke, J. Kärger, M. Wiebcke, J. Caro, J.M. van Baten, R. Krishna: *Adsorption and Diffusion of Alkanes in $Cu_3BTC_2$ Crystals Investigated Using FTIR Microscopy and Molecular Simulations*, 1. Int. Workshop Nanopor. Mater. Energy Env. (NAPEN 2008), Chania, Crete, Greece, 12. – 15. October 2008

C. Chmelik, J. Kärger, R. Krishna, M. Wiebcke, J. Caro: *Adsorption and Diffusion of Guest Molecules in Single $Cu_3BTC_2$ Crystals Studied by FTIR Microscopy*, 20. Deutsche Zeolith-Tagung, Halle, Germany, 05. – 07. March 2008

C. Chmelik, J. Kärger, M. Wiebcke, J. Caro, J.M. van Baten, R. Krishna: *Adsorption and Diffusion of Alkanes in Single $Cu_3BTC_2$ Crystals Studied by IR Microscopy and Molecular Simulations*, 235. ACS National Meeting - Spring 2008, New Orleans, USA, 06. – 10. April 2008

C. Chmelik, S. Naumov: *Diffusion Measurements in Porous Glasses* (invited talk), Institute for Chemistry, Martin-Luther-University Halle-Wittenberg, Halle, Germany, 19. December 2008

M. Dvoyashkin, R. Valiullin, J. Kärger, R. Gläser, W.-D. Einicke: *Diffusion of Supercritical Fluids in Mesoporous Materials Studied by PFG NMR*, 11. Eur. Meeting Supercritical Fluids, Barcelona, Spain, 04. – 07. May 2008

M. Gratz, P. Galvosas: *Investigation of Molecular Exchange Using DEXSY with Ultra-High Pulsed Field Gradients*, 9. Int. Bologna Conf. Magn. Reson. Porous Media (MRPM9), Cambridge, USA, 13. – 17. July 2008

F. Grinberg: *Diffusion and Structure in Self-Assembling Fluids Studied by NMR*, AMPERE NMR School, Wierzba, Poland, 22. – 28. June 2008

F. Grinderg: *Self-Assembly and Molecular Diffusion of Amphiphilic Blockcopolymers in Mesopores*, 9. Int. Bologna Conf. Magn. Reson. Porous Media (MRPM9), Cambridge, USA, 13. – 17. July 2008

G. Kalies: *Synthesis, Characterization and Adsorptive Application of Nanoporous Solids*, Minisymposium for Particle Synthesis, Friedrich-Alexander-University Erlangen-Nürnberg, Erlangen, Germany, 08./09. Juni 2008

G. Kalies: *Kontrolle der treibenden Kräfte für Keimbildung und Wachstum bei der Nanopartikelsynthese*, Minisymposium for Particle Synthesis, Friedrich-Alexander-University Erlangen-Nürnberg, Erlangen, Germany, 08./09. Juni 2008

J. Kärger: *The Beauty of Transient Concentration Profiles and their Evidence for Understanding Mass Transfer in Nanoporous Materials*, colloquium at the Northwestern University, Evanston, USA, 10. October 2008

J. Kärger: *The Evidence of Microscopic Diffusion Measurement: Surprises and Miracles*, colloquium at the EXXON-MOBIL research center, Clinton, USA, 23. October 2008

J. Kärger: *The Evidence of Microscopic Diffusion Measurement: Surprises and Miracles*, colloquium at the University of Massachusetts, Amherst, USA, 17. October 2008

J. Kärger: *The Potentials of Diffusion Measurement by NMR: Exploring the Rate-Determining Steps of Mass Transfer in Nanoporous Materials*, colloquium at Rutgers University, Piscataway, USA, 24. October 2008

J. Kärger: *Studying Guest Diffusion in Nanoporous Hosts by Monitoring Transient Concentration Profiles*, 7. Brazil. Meeting Adsorption, Campina Grande, Brasil, 25. – 27. June 2008

J. Kärger: *Unprecedented Options to Study Diffusion in Zeolites by Monitoring Transient Concentration Profiles*, 58. Canad. Chem. Eng. Conf., Ottawa, Canada, 19. – 22. October 2008

J. Kärger, A. Märcker, J. Gabke: *Physikalische Spielereien*, 129. Sonntagsvorlesung an der Fakultät für Physik und Geowissenschaften, Universität Leipzig, Germany, 9. March 2008

S. Naumov: *Diffusion Processes in Mesoporous Adsorbents Probed by PFG NMR*, 20. Deutsche Zeolith-Tagung, Halle, Germany, 05. – 07. March 2008

S. Naumov: *Overview of the Department of Interface Physics*, 1. Young Res. Meeting INSIDE POReS, Delft, The Netherlands, 10./11. February 2008

S. Naumov: *Phase Transitions under Confinement: Deeper Insight using NMR*, AMPERE NMR School, Wierzba, Poland, 22. – 28. June 2008

D. Tzoulaki: *Silicalite-1 Crystals: A Study of their Morphology by means of Interference Microscopy*, 18. Int. Congress Chem. Proc. Eng. (CHISA 2008), Prague, Czech Republic, 24. – 28. August 2008

D. Tzoulaki: *Unprecedented Insight into MOF Transport Properties by Monitoring Transient Concentration Profiles*, 1. Int. Conf. Metal Organic Frameworks and Open Framework Compounds (MOF2008), Augsburg, Germany, 08. – 10. October 2008

**Posters**

C. Chmelik, L. Heinke, J. Kärger, W. Schmidt, J.M. van Baten, R. Krishna: *Inflection in the Loading Dependence of the Maxwell-Stefan Diffusivity of iso-Butane in MFI-type Zeolites*, 1. Int. Workshop Nanopor. Mater. Energy Env. (NAPEN 2008), Chania, Crete, Greece, 12. – 15. October 2008

C. Chmelik, L. Heinke, J. Kärger, M. Wiebcke, J. Caro, J.M. van Baten, R. Krishna: *Adsorption and Diffusion of Alkanes in $Cu_3(BTC)_2$ Crystals Investigated Using FTIR Microscopy and Molecular Simulations*, 1. Int. Conf. Metal Organic Frameworks and Open Framework Compounds (MOF2008), Augsburg, Germany, 08. – 10. October 2008

C. Chmelik, L. Heinke, J. Kärger, M. Wiebcke, J. Caro, J.M. van Baten, R. Krishna: *Adsorption and Diffusion of Alkanes in $Cu_3BTC_2$ Crystals Investigated Using FTIR Microscopy and Molecular Simulations*, 1. Int. Workshop Nanopor. Mater. Energy Env. (NAPEN 2008), Chania, Crete, Greece, 12. – 15. October 2008

C. Chmelik, L. Heinke, D.B. Shah, J. Kärger, J.M. van Baten, R. Krishna: *Loading Dependence of the iso-Butane Diffusivity in Silicalite-1 Studied by IR Microscopy and Computer Simulations*, 4th Int. FEZA Conf., Paris, France, 02. – 06. September 2008

L. Heinke, C. Chmelik, S. Khajavi: *Diffusion of Water in Sodalite*, IRTG Meeting Diff. Porous Mater., Leipzig, Germany, 18. February 2008

L. Heinke, C. Chmelik, J. Kärger: *Analysing Transient Concentration Profiles in Nanoporous Host Materials*, 4th Int. FEZA Conf., Paris, France, 02. – 06. September 2008

L. Heinke, J. Kärger: *IR Microscopy and Analytical Methods for Analyzing Intracrystalline Concentration Profiles*, IRTG Meeting Diff. Porous Mater., Leipzig, Germany, 18. February 2008

L. Heinke, P. Kortunov, D. Tzoulaki, J. Kärger: *Exchange Dynamics at the Interface of Nanoporous Materials with their Surroundings*, 20. Deutsche Zeolith-Tagung, Halle, Germany, 05. – 07. March 2008

L. Heinke, D. Tzoulaki, C. Chmelik, J. Kärger: *Determining the Transport Parameters in Nanoporous Materials from Transient Concentration Profiles*, 1. Int. Conf. Metal Organic Frameworks and Open Framework Compounds (MOF2008), Augsburg, Germany, 08. – 10. October 2008

L. Heinke, D. Tzoulaki, C. Chmelik, J. Kärger: *Diffusion of Guest Molecules in MOFs: A Detailed Analysis of Transient Concentration Profiles*, 1. Int. Conf. Metal Organic Frameworks and Open Framework Compounds (MOF2008), Augsburg, Germany, 08. – 10. October 2008

L. Heinke, D. Tzoulaki, C. Chmelik, R. Krishna, J. Kärger: *Analysing Time-Dependend Concentration Profiles in Nanoporous Host Materials* Nanostruct. Mater. Membr. Trainings Course, Patras, Greece 18. – 27. June 2008

M. Gratz, C. Horch, S. Schlayer, P. Galvosas: *Methodical Aspects of 2D NMR Spectroscopy under Conditions of Ultra-High Pulsed Field Gradients*, 9. Int. Bologna Conf. Magn. Reson. Porous Media (MRPM9), Cambridge, USA, 13. – 17. July 2008

E.E. Romanova, F. Grinberg, J. Kärger, D. Freude: *Binary Liquid Mixtures and Liquid Crystals Confined in Porous Glasses Studied by MAS PFG NMR*, AMPERE NMR School, Wierzba, Poland, 22. – 28. June 2008

E.E. Romanova, F. Grinberg, J. Kärger, D. Freude: *MAS PFG NMR Diffusion Studies of Liquid Crystals and Liquid Mixtures Confined in Porous Glasses*, 9. Int. Bologna Conf. Magn. Reson. Porous Media (MRPM9), Cambridge, USA, 13. – 17. July 2008

F. Stallmach, P. Galvosas, K. Friedemann: *Understanding T2 Relaxation Times in Hardening Cement Pastes Using the NMR Exchange and the Powers' Hydration Models*, 9. Int. Bologna Conf. Magn. Reson. Porous Media (MRPM9), Cambridge, USA, 13. – 17. July 2008

D. Tzoulaki: *Playing with Intracrystalline Concentration Profiles: A Detailed Study of Zn(tbip) MOF Material*, 1. Int. Workshop Nanopor. Mater. Energy Env. (NAPEN 2008), Chania, Crete, Greece, 12. – 15. October 2008

D. Tzoulaki: *The Striking Influence of the Amount of Silica on the Diffusion Properties of SAPO STA-7 Samples investigated by Interference Microscopy*, 20. Deutsche Zeolith-Tagung, Halle, Germany, 05. – 07. March 2008

K. Ulrich, F. Grinberg, M. Krutyeva: *Molecular Dynamics and Structure of Self-Assembling Systems Studied by NMR Techniques*, EUROMAR-2008, St. Petersburg, Russia, 06 – 11. July 2008

M. Wehring, J. Gascon, F. Kapteijn, F. Stallmach: *Self-Diffusion of Hydrocarbons in CuBTC*, 1. Int. Conf. Metal Organic Frameworks and Open Framework Compounds (MOF2008), Augsburg, Germany, 08. – 10. October 2008

M. Wehring, J. Gascon, P. Magusin, F. Stallmach: *High-Resolution NMR Diffusion Measurements in Metal-Organic Frameworks*, 20. Deutsche Zeolith-Tagung, Halle, Germany, 05. – 07. March 2008

M. Wehring, P.C.M.M. Magusin, S. Amirjalayer, R. Schmid, F. Stallmach: *NMR Studies of Mobility on Ferrocene Adsorbed in MOF-5*, 72. DPG Spring Meeting, Berlin, Germany 25. – 29. February 2008

## 4.18 Graduations

**Doctorate**

- Christian Chmelik
  *Orts- und zeitaufgelöste Untersuchungen der intrakristallinen Diffusion in Zeolithen mittels FTIR-Mikroskopie*
  February 2008
- Moises Fernandez Perez
  *Mixture diffusion in porous media studied by MAS PFG NMR*
  June 2008
- Oraphan Saengsawang
  *Rotation and diffusion of n-pentane in the zeolite ZK5*
  July 2008
- Wiete Schönfelder
  *Studying petrophysical and geotechnical parameters by multi-dimensional NMR methods*
  July 2008
- Konstantin Ulrich
  *Diffusion measurements in nanomaterials using PFG NMR with ultra-high magnetic field gradients*
  September 2008
- Stephan Zschiegner
  *Self- and transport diffusion in narrow pores in the Knudsen regime*
  October 2008

**Diploma**

- Marcel Gratz
  *Nutzung von ultra-hohen gepulsten magnetischen Feldgradienten zur Untersuchung von Korrelation und Austausch in mehrdimensionalen NMR-Experimenten*
  January 2008
- Florian Hibbe
  *Interferenzmikroskopische Untersuchung der Temperaturabhängigkeit transienter Konzentrationsprofile in nanoporösen Materialien*
  November 2008
- Carsten Horch
  *Konstruktion und Aufbau eines Messsystems zur NMR-Relaxometrie unter hohen statischen Gasdrücken*
  December 2008

## 4.19 Guests

- Rajamani Krishna
  Van't Hoff Institute for Molecular Science, Amsterdam, The Netherlands
  15. February – 14. July 2008

- Alexander Stepanov
  Boreskov Institute of Catalysis, Novosibirsk, Russia
  30. April – 01. July 2008 and 01. November 2008 – 31. March 2009
- Mikkail Stepovich
  University of Kaluga, Russia
  10. October – 31. December 2008
- Sergey Vasenkov
  Department of Chemical Engineering, University of Florida, Gainesville, USA
  21. July – 04. August 2008
- Peter Moson
  Department of Chemical Engineering, University of Massachusetts, Amherst, USA
  15. June – 31. July 2008

## 4.20 Awards

- Dr. Rustem Valiullin
  Heisenberg Fellowship (DFG)

# 5

# Soft Matter Physics

## 5.1 General Scientific Goals - Polymers and Membranes in Cells

In his book "What is Life?", Schrödinger recognized the immense challenge to explain biological processes by basic physics and chemistry. Consequentially, traditional medical physics had predominately the role to develop devices for medicine such as sophisticated imaging solutions (X-ray, NMR, multiphoton) or laser scalpels. Commencing with Watson and Crick, science has gained tremendous insight into the molecular basis of biological cells. Over 25 000 genes encode the information of human life, and their subsequent transcription and translation add to the complexity of molecular interactions resulting in an insurmountable combinatorial number of relations. Recent progress in biosciences towards a more quantitative description opens a challenging and new pathway for medical physics to use physics underlying biological processes to directly impact diagnosis and therapy. Despite that this approach is still in its infancy, it may redefine medical physics. This kind of research is based on fundamental biological physics and has in its ideal case applied aspects in medical physics. By identifying cellular subunits acting as independent functional modules this complexity becomes tractable and the fundamental physical principles of these modules can be studied.

A prototypical example for such a module is the intracellular scaffold known as the cytoskeleton. The cytoskeleton is the key structural element in cellular organization and is an indicator of pathological changes in cell function. It is a compound of highly dynamic polymers and molecular motors as active nano-elements inside cells. The cytoskeleton mechanically and chemically senses a cell's environment achieving a high sensitivity by using processes such as stochastic resonance. This active polymeric scaffold generates cellular motion and forces in the tens of nanoNewton sufficiently strong to push rigid AFM cantilevers out of the way. These forces are generated by molecular motor-based nano-muscles and by polymerization through mechanisms similar to Feynman's hypothetical thermal ratchet. A new type of polymer physics describes these active polymer networks since the nano-sized motors overcome the inherently slow, often glass-like Brownian polymer dynamics. This results in novel self-organization of the polymer scaffolds and rapid switching between different ordered states. This organization of the cytoskeleton is tightly controlled in cells. Thus, suspended cells' biomechanical properties are well-defined and distinguish different cellular states and

cell types with confidence levels of more than 95 % (metastatic from non-metastatic cancer cells, stem cells from differentiated cells in adult tissues, etc.). Since cell elasticity depends highly nonlinear on cytoskeletal composition already small changes in a cell's state are measurable by biomechanical changes and recent polymer theories can be used to deduce the cytoskeletal part of a cell's proteomic condition. Recently, the optical stretcher, a photonic device developed in our laboratory, was demonstrated within a clinical study as a highly sensitive non-invasive tool for mechanical classification of cancer cells [1]. The device's versatility was drastically improved by integration of the capability to rotate cells under observation [2]. The cytoskeleton uses up to 30 % of cellular ATP, which is a cell's fuel. Optical gradient forces due to cells' dielectric nature can manipulate the cytoskeleton's consequential active and dynamical state. Opto-molecular coupling between laser light and cytoskeletal processes permits optical control of neuronal growth. The specific opto-molecular influence on membrane and cytoskeletal transport is complex. Cells cannot modulate diffusion by the parameters found in the Einstein equation (temperature, viscosity, molecular size).

Consequentially, cells exhibit rich multifaceted intracellular transport including motor-driven motion and anomalous subdiffusion, which can be probed by the use of nanoparticles as tracers. The cytoskeleton as active, soft condensed matter, with structures on nanometer and micron scales representative of individual proteins and cells, calls forth new biological and polymer physics. Our research group's goals center on unraveling this new physics of the cytoskeleton. The current and future research goals are summarized in the following sections.

*Josef A. Käs*

[1] T. Remmerbach et al: Cancer Res. **69**, 1728 (2009)
[2] M. Kreysing et al: Opt. Express **16**, 16 984 (2008)

## 5.2 The Optical Cell Rotator

T. Kießling, A. Fritsch

The optical cell rotator (OCR) is a modified dual-beam laser trap for the holding and controlled rotation of suspended dielectric microparticles, such as cells. In contrast to optical tweezers, OCR uses two counter-propagating divergent laser beams, which are shaped and delivered by optical fibers. The rotation of a trapped specimen is carried out by the rotation of an asymmetric laser beam [1]. Experiments were performed on human erythrocytes, promyelocytic leukemia cells (HL60), and cell clusters (MCF-7). Since OCR permits the rotation of cells around an axis perpendicular to the optical axis of any microscope and is fully decoupled from imaging optics, it could be a suitable and expedient tool for tomographic microscopy (Fig. 5.1).

[1] M. Kreysing et al.: Opt. Express **16**, 16984 (2008)

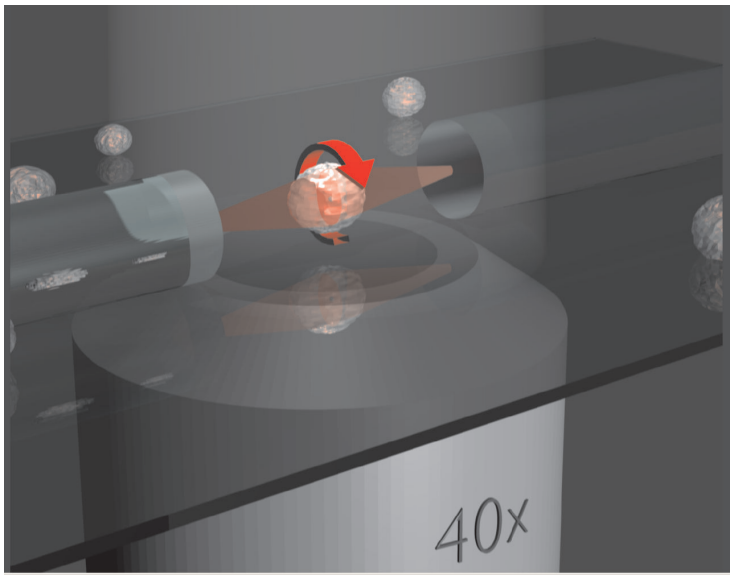


**Figure 5.1:** Illustration of the optical cell rotator.

## 5.3 Diffusion of Nano-Particles in Inhomogeneous Lipid Membranes

F. Rückerl, D. Martin*, M. Forstner†, C. Selle, J. Käs

*Department of Physics, Lawrence University, Appleton, USA
†Department of Physics, Syracuse Biomaterials Institute, Syracuse University, USA

Lipid membranes play a fundamental role in vital cellular functions such as signal transduction. Many of these processes rely on lateral diffusion within the membrane, which is generally a complex fluid containing ordered microdomains. Langmuir monolayers are often used as simple models for such biological membranes. The possibility to change their composition and phase state in a very controlled manner as well as the access to a large observation area makes them a versatile tool for the investigation of membrane related interactions.

In our group we investigate the interaction of single, partially charged nanoparticles with lipid microdomains by experiments and Monte Carlo simulations. We address the effect of such interactions on diffusive transport by studying lateral diffusion in a phase-separated Langmuir phospholipid monolayer via single-particle tracking. The attractive dipole–dipole interactions between condensed phase domains and diffusing probe beads lead to transient confinement at the phase boundaries, causing a transition from 2D to 1D diffusion. The electric dipole field changes with increasing size of the domain. This change from single dipole ($E \propto 1/r^3$) to semi-infinite domain characteristics ($E \propto 1/r$), significantly influences the motion of the particle (Fig. 5.2). Small immobile domains ($R = 1\,\mu\text{m}, E(r) \propto 1/r^{1.1}$) confine the movement of the tracer to the boundary of the domain whereas for large domains ($R \geq 10\,\mu\text{m}, E(r) \propto 1/r$) its motion is only temporarily hindered [1].

Using Brownian dynamics simulations, the long-term diffusion constant for such a system is found to have a sensitive, Boltzmann-like dependence on the interaction

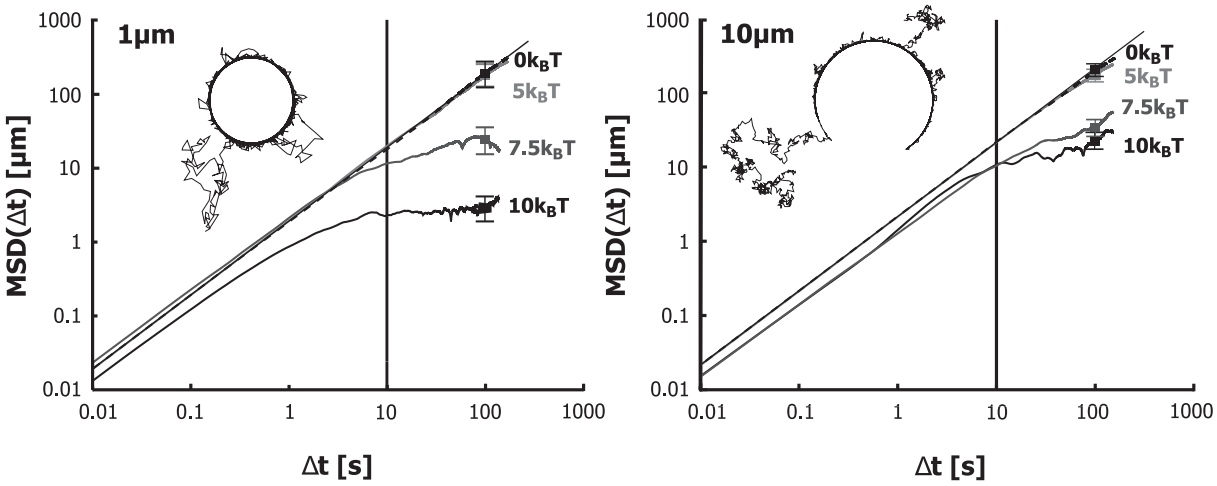


**Figure 5.2:** Mean square displacement ($MSD(\Delta t)$) for two different domain sizes (*left*: 1 µm, *right*: 10 µm) at varied potential depths (0, 5, 7.5 and $10k_BT$). The thin straight line represents a normal diffusing particle ($\alpha = 1$, $MSD(\Delta t) = 4D\Delta t^{\alpha}$. The trajectory segments were chosen to start 10 s before the first contact, indicated by the *vertical line*. For both domain sizes a typical track at a potential depth of $10k_BT$ is shown as an *inset* (not to scale).

strength. In addition, this interaction strength is shown to be a strong function of the ratio of domain to particle size [2]. As similar interactions are expected in biological membranes, the modulation of diffusive transport dynamics by varying interaction strength and/or domain size may offer cells selective spatial and temporal control over signaling processes.

[1] F. Rückerl et al.: Langmuir **24**, 3365 (2008)
[2] M. Forstner et al.: Phys. Rev. E **77**, 051 906 (2008)

## 5.4 Errors in Two-Particle Tracking at Close Distances

M. Gyger, F. Rückerl, J. Käs, J. Ruiz-García*

*Instituto de Física, Universidad Autónoma de San Luis Potosí, Mexico

Tracking single and multiple particles is of great importance for many physical investigations in a variety of different areas. It is essential to find and eliminate sources of systematic errors in the particle position determination (PPD) and to determine the limits of its applicability to a given problem. Particularly when measuring the interactions between colloids at close distances, artifacts in the image taking process pose a great problem.

By means of a simulation technique, we investigated the accuracy of the PPD using 2D Gaussian and Gaussian-like fitting functions (Fig. 5.3). For the distance between the two colloidal particles this revealed a systematic overestimation of the inter-particle distance of up to 1.9 % of the particle diameter for the Gaussian fitting function. This deviation can be explained by the differences between the intensity distribution of the overlap of the simulated particles and the linear superposition of the Gaussian functions [1]. Modifications of the fitting functions can reduce the systematic error significantly.

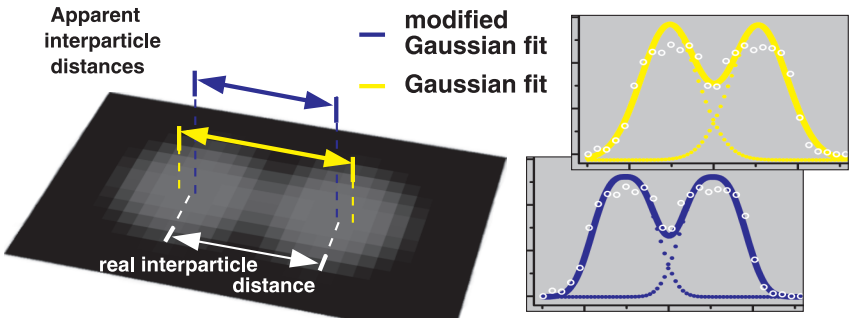


**Figure 5.3:** Effect of different fitting functions for particles at close distances. The simple gaussian function (*yellow*) leads to a systematic over estimation of the inter-particle distance. The modified function (*blue*) reproduces the inter-particle distance more accurately.

[1] M. Gyger et al.: J. Colloid Interf. Sci. **326**, 382 (2008)

## 5.5 Growing Actin Networks Form Lamellipodium and Lamellum by Self-Organization

F. Huber, B. Stuhrmann, B. Gentry, D. Strehle, D. Smith, M. Steinbeck, C. Vogt, S. Ehrig, M. Dogterom*, T. Pollard†, M. Rao‡

*Institute for Atomic and Molecular Physics, Foundation for Fundamental Research on Matter, Amsterdam, The Netherlands
†Department of Molecular Cellular and Developmental Biology, Yale School of Medicin, Yale University, New Haven, USA
‡Raman Research Institute, Bagalore, India

Cell migration is associated with the dynamic protrusion of a thin actin-based cytoskeletal extension at the cell front. This extension has been shown to consist of two different substructures, the lamellipodium and the lamellum, which differ in their kinetic and kinematic properties as well as their molecular composition. While the formation of the lamellipodium is increasingly well understood, organizational principles underlying the emergence of the lamellum are just beginning to be unravelled.

We developed a 2D Monte-Carlo simulation [1] and an analytical description [2] that include chemical reaction kinetics, actin monomer diffusion, and filament transport to investigate the formation of growing actin networks in migrating cells. We could demonstrate the system's ability to form two distinct networks by self-organization (Fig. 5.4). We found a characteristic transition in filament lengths and a distinct maximum of depolymerization, both within the leading $1-2\,\mu$m of the cell, in agreement with experimental data (Fig. 5.5). Moreover, we investigated the complex interplay between ADF/cofilin and tropomyosin and propose a mechanism that leads to spatial separation of, respectively, ADF/cofilin- or tropomyosin-dominated compartments. Tropomyosin is found to play an important role in stabilizing the lamellar actin network. Furthermore, the influence of filament severing and annealing on the network properties is explored [1]. With both the simulation and the analytical model we contribute

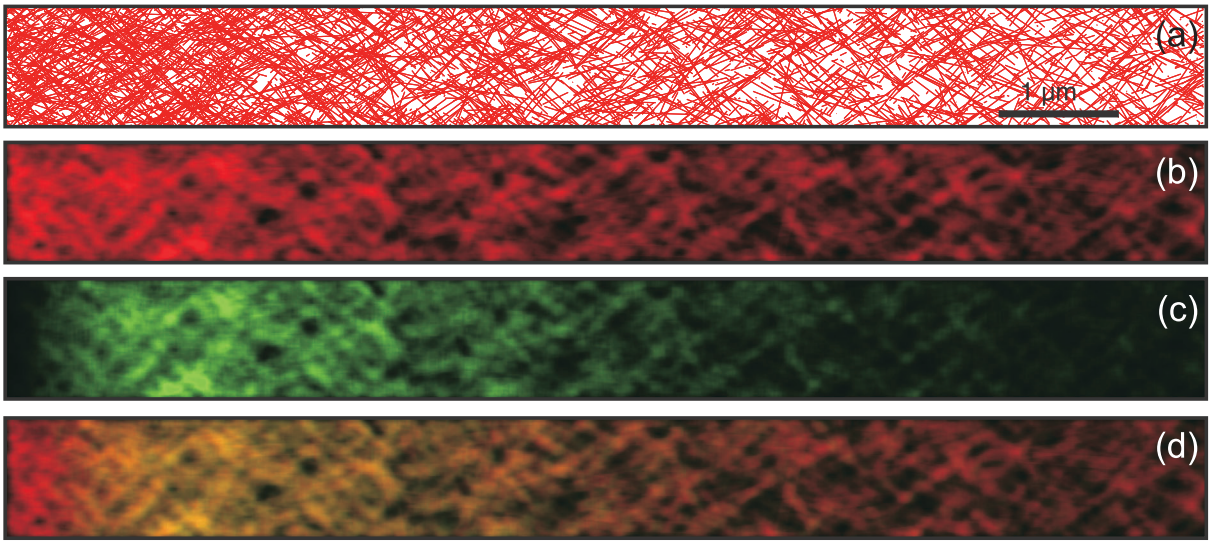


**Figure 5.4:** Computer generated pseudo-fluorescence signals. The simulated F-actin network (**a**) is coarsegrained using a Gaussian blur to mimic the optical resolution limit of light microscopy (see text), yielding pseudo-fluorescence F-actin (**b**) and ADF/cofilin-F-actin (**c**) signals. (**d**) An overlay of F-actin and ADF/cofilin-F-actin signals is in qualitative agreement with experimental data [4].

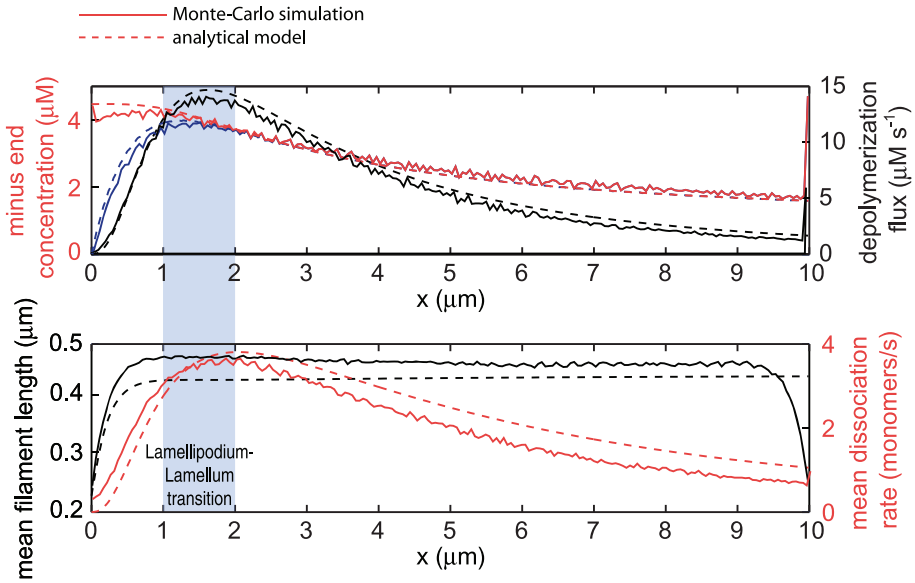


**Figure 5.5:** Mathematical model solutions suggesting the compartmentalization of the calculated network into lamellipodium and lamellum. Criteria for the distinction are the position of the depolymerization flux maximum (*top*) and the difference in mean filament lengths (*bottom*). Computer simulation data (not shown) agree reasonably well with the solutions of the mathematical model (< 25 % deviation at each data point).

to a fundamental understanding of how cells organize their molecular components to achieve movement.

In addition, an experimental attempt to model lamellipodial actin network growth in vitro was established and already lead to first results [3]. Future research will aim

towards combining all three modeling approaches in order to gain a deeper insight into the self-organization of cellular actin networks.

[1] F. Huber et al.: Biophys. J. **95**, 5508 (2008)
[2] B. Stuhrmann et al.: J. Theor. Biol. (2009), in press
[3] D. Smith et al.: Biophys. Rev. Lett. **4**, 181 (2009)
[4] T. Svitkina et al.: J. Cell Biol. **145**, 1009 (1999)

## 5.6 Funding

*MS CartPro – Multiparametric Monitoring and Steering of Mesenchymal Stem Cell derived Cartilage Formation in 3D Production Systems*
Prof. Dr. J.A. Käs, Dr. J. Guck
BMBF-Project MS CartPro (FKZ: PTJ – BIO/ 31P4282)

*Untersuchungen der altersabhängigen Modulation der Elastizität von Hautzellen durch physiologische Stressoren*
Prof. Dr. J.A. Käs, F. Wetzel
Beierdorf AG – Forschungsvertrag

*Leipzig School of Natural Sciences – Building with Molecules and Nano-objects* (BuildMoNa)
Prof. Dr. E. Hey-Hawkins, Prof. Dr. M. Grundmann, Prof. Dr. J.A. Käs

*Single Particle and Polymer Tracking in Two-Dimensional Energy-Landscapes*
Prof. Dr. J. Kärger, Prof. Dr. F. Cichos, Prof. Dr. J.A. Käs
DFG-Forschergruppe, SFG FOR 887

*Optical Stretcher zur hochaufgelösten Darstellung und Analyse von einzelnen Zellen*
Prof. Dr. J.A. Käs
Carl-Zeiss MicroImaging GmbH – OSDA - Forschungsvertrag

*DFG Graduiertenkolleg "InterNeuro"*
Prof. Dr. J.A. Käs, Dr. J. Guck
GRK 1097

*Active Biomimetic Systems (Active BIOMICS)*
Prof. Dr. J.A. Käs, Dr. J. Guck
Projektnr.: 2312 0 385

*Donation to the Softmatter Physics Division from Ms. H. Reifert / stipend payment*
Prof. Dr. J.A. Käs

*Donation to the Softmatter Physics Division from Ms. M. Duda*
Prof. Dr. J.A. Käs

## 5.7 Organizational Duties

J.A. Käs

- Advisory committee for soft matter physics, NASA, USA
- Chair, scientific advisory board, Evacyte Inc., USA
- CNRS review committee, Institute Curie, Paris
- Referee: Nature, Phys. Rev. Lett., Phys. Rev. E, Biophys. J., Biophys. Biochem. Acta, Biochemistry, Proc. Nat. Acad. Sci., Eur. Biophys. J., Langmuir
- Grant review: National Science Foundation (NSF); Deutsche Forschungsgemeinschaft (DFG), Alexander von Humboldt Foundation, Deutsche Studienstiftung, Centre National de la Recherche Scientifique (CNRS)

## 5.8 External Cooperations

**Academic**

- MD Anderson Cancer Center, Houston, USA
  Prof. Dr. Michel Follen
- Center for Nonlinear Dynamics, Austin, USA
  Prof. Dr. Harry Swinney
- University of Texas at Austin, USA
  Prof. Dr. Ken Shih, Prof. Dr. Mark Raizen
- Institute Curie, Paris, France
  Prof. Dr. Jean-Francois Joanny
- École Supérieure de Physique et de Chimie Industrielles (ESPCI), Paris, France
  Prof. Dr. Jacques Prost
- CEA/Saclay, France
  Prof. Dr. Marie-France Carlier
- Princeton University, USA
  Prof. Dr. Robert Austin
- University of Saarbrücken, Germany
  Prof. Dr. Walter Zimmermann
- Max-Planck-Institute for Colloids and Interfaces, Potsdam-Golm, Germany
  Prof. Dr. Reinhardt Lipowsky
- Max-Planck-Institute for Complex Systems, Dresden, Germany
  Prof. Dr. Frank Jülicher

**Industry**

- Carl Zeiss MicroImaging GmbH, Jena, Germany
  Dr. C. Dietrich
- Beiersdorf AG, Hamburg, Germany
  Dr. T. Blatt

- Euroderm GmbH, Leipzig, Germany
  Dr. A. Emmendörffer
- Evotec GmbH, Dresden, Germany
  Dr. T. Bauer
- FAUN GmbH, Leipzig, Germany
  F. Fischer
- GeSim GmbH, Dresden, Germany
  Dr. S. Howitz
- JPK Instruments, Berlin, Germany
  T. Jähnke
- Niendorf & Hamper, Hamburg, Germany
  Prof. A. Niendorf
- Qiagen GmbH, Hilden, Germany
  Dr. T. Singer

## 5.9 Publications

**Journals**

M.B. Forstner, D.S. Martin, F. Rückerl, J.A. Käs, C. Selle: *Attractive membrane domains control lateral diffusion*, Phys. Rev. E **77**, 051 906 (2008)

M. Gyger, F. Rückerl, J.A. Käs, J. Ruiz-García: *Errors in two particle tracking at close distances*, J. Colloid Interf. Sci.**326**, 382 (2008)

F. Huber, J.A. Käs, B. Stuhrmann: *Growing actin networks form lamellipodium and lamellum by self-assembly*, Biophys. J. **93**, 5508 (2008)

M.K. Kreysing, T. Kießling, A. Fritsch, C. Dietrich, J.R. Guck, J.A. Käs: *The optical cell rotator*, Opt. Express, **16**, 16 984 (2008)

F. Rückerl, J.A. Käs, C. Selle: *Diffusion of Nanoparticles in Monolayers is Modulated by Domain Size*, Langmuir, **24** 3365 (2008)

M. Semmling, O. Kreft, A.M. Javier, G.B. Sukhorukov, J.A. Käs, W.J. Parak: *A novel flow-cytometry-based assay for cellular uptake studies of polyelectrolyte microcapsules*, Small **4**, 1763 (2008)

**Books**

K. Franze, A. Reichenbach, J.A. Käs: *Biomechanics of the CNS*, in *Mechanosensitivity of the Nervous System*, ed. by A. Kamkin, I. Kiseleva (Springer, Dordrecht 2008)

**in press**

B. Stuhrmann, F. Huber, J.A. Käs: *Self-organization of lamellum and lamellipodium from a common nucleation source: a mathematical analysis* J. Theor. Biol.

**Talks**

J.A. Käs: *Feeling For Cancer Cells with Light* (lecture), 1. Trieste Workshop New Approaches Diagnose Treat Cancer, Trieste, Italy, 16. – 17. October 2008

J.A. Käs: *Feeling for Cells with Light*, Conf. Nonlin. Microsc. Opt. Control, Münster, Germany, 19./20. February 2008

J.A. Käs: *Feeling for cells with light* (lecture), FEBS Workshop "Mechanics and Dynamics of the Cytoskeleton", Potsdam, Germany, 22. – 26. June 2008

J.A. Käs: *Feeling for cells with light* (lecture), Physikalische Kolloquium, University of Duisburg–Essen, Germany, 2. July 2008

J.A. Käs: *Feeling for Cells with Light* (lecture), PIERS Symp. 2008, Hangzhou, China, 23. – 26. March 2008

J.A. Käs: *From Single Cell Biomechanics To Cancer Diagnostics and Nerve Regeneration*, Conf. Interfaces of Life, Chennai, India, 07. – 18. January 2008

J.A. Käs: *Optical deformability as a new cell marker*, SPIE Conf. Opt. Photon., San Diego, 10. – 14. August 2008

J.A. Käs: *Optische Finger: Wie fühlt man Zellen mit Licht?* (lecture), Symp. Photonics meets Life Sciences, University of Jena, Germany, 22. September 2008

J.A. Käs: *Passive and active single cell biomechanics* (lecture), 3. Symp. of the Centre of Integrated Bioanalysis, Fraunhofer Institute, Potsdam-Golm, Germany, 19. June 2008

J.A. Käs: *Soft Brains, Signal Amplification through Noise, and Taking the Bull by its Horns* (lecture), Department of Physics, Indian Institute of Science, Bangalore, India, 12. – 16. May 2008

J.A. Käs: *Soft brains, signal amplification through noise, and taking the bull by its horns* (lecture), Workshop "Bio meets nano", Haus der Dechema, Frankfurt am Main, Germany, 03./04. November 2008

**Patents**

J. Guck, J.A. Käs: *Optical Stretcher* U.S. Patent # 6067859

J. Guck, J.A. Käs: *Optical Stretcher*, European Patent # 1059871 for Germany, Great Britain, France, Switzerland, Italy and Spain

J. Guck, J.A. Käs, M. Kreysing: *Anordnung und Verfahren zur berühungslosen Ausrichtung und Drehung von Partikeln durch anisotrope, elektromagnetische Strahlungsfelder*, Europäisches Patent # 193549811

J.A. Käs, M. Raizen, V. Milner, T. Betz, A. Ehrlicher: *Optical Cell Guidance*, U.S. Patent # 7435568, European and Asian patents are pending

## 5.10 Graduations

**Doctorate**

- Michael Gögler
  *Force Production and Cell Edge Dynamics of Fish Keratocytes*
  April 2008
- Daniel Koch
  *Stochastic Lamellipodium Dynamics and Forces in Cell Motility*
  April 2008

**Diploma**

- Tobias Kießling
  *Novel Application of Lasers in Cytometry*
  January 2008
- Markus Streicher
  *Development of a Single Laser Stretcher*
  February 2008
- Anatol Fritsch
  *Biomechanics of Tumor Spheroids*
  February 2008
- Daniela Kolbe
  *Rastertransmissions - Ionenmikroskopie einzelner lebender und fixierter Zellen*
  April 2008
- Christoph Leuze
  *Construction and testing of a realistic head phantom for assessment of radiofrequency power deposition in MRI*
  October 2008
- Roland Stange
  *Entwicklung eines mikrofluidischen Chips zur optomechanischen Analyse und Sortierung von Zellen*
  December 2008

**Master**

- Kenechukwu David Nnetu
  *Opto-rheological Characterization of the Metastatic Potential of Cells*
  January 2008
- José Alvarado
  *Biomechanics of Actin Bundles*
  November 2008

**Bachelor**

- Paul Heine
  *Biomechanics of Actin Bundles*
  Oktober 2008
- Ralf Kohlhaas
  *Neuronal Guidance on Laser Modified Polyacrylamide Surfaces*
  November 2008

## 5.11 Guests

- Prof. Dr. Madan Rao
  Raman Research Institute, Bangalore, India
  7. – 8. February 2008
- Prof. Dr. Ernst-Ludwig Florin
  Center for Nonlinear Dynamics, University of Texas at Austin, USA
  20. May 2008
- Prof. Dr. Timo Schinköthe
  TumorTec GmbH
  28. August 2008
- Dr. Kay Gottschalk
  Ludwigs-Maximilian-Universität, München, Germany
  27. – 28. August 2008
- Dr. Tilo Pompe
  Leibniz-Institut für Polymerforschung, Dresden, Germany
  24. October 2008
- Daniel E. Minner
  Indiana University Purdue University Indianapolis (IUPUI), USA
  01. – 30. November 2008

## 5.12 Awards

**Awards**

- Prof. Dr. Josef A. Käs
  Wolfgang-Paul Prize awarded by the Alexander von Humboldt Foundation
- Prof. Dr. Josef A. Käs
  Distinguished Lecturer, SigmaXi Academic Honor Society, USA
- Prof. Dr. Josef A. Käs
  Adjunct Professor, Department of Biomedical Engineering, University of Texas at Austin
- Dr. Kristian Franze
  Klaus Tschira Preis für verständliche Wissenschaft 2008, Klaus Tschira Stiftung

# II

# Institute for Experimental Physics II

# 6

# Magnetic Resonance of Complex Quantum Solids

## 6.1 Introduction

The electronic properties of quantum-solids in which the electrons exhibit strong correlations with each other or with the lattice are particularly rich and will be of special importance in future functional materials. In addition, such solids are challenging for experiment, as well as theory, as the more than twenty-year history of high-temperature superconductivity shows: we still do not understand the electronic structure of these systems and new systems that were just discovered this year. One particular aspect of strongly correlated electronic materials is their tendency towards nano-scale electronic phase separation. Even in perfect lattices, electronic nano-structures can form. The investigation of such materials requires the use of methods that can give detailed information. Here, magnetic resonance, on nuclei and electrons, is of particular interest as they not only have atomic scale resolution, but also yield bulk information in contrast to surface techniques. As one might expect, the material properties can be quite different from the bulk near the surface.

*Jürgen Haase*

## 6.2 Two-Component Behaviour of High-Temperature Superconductors from NMR

J. Haase, C.P. Slichter*, G.V.M. Williams†

*Department of Physics, University of Illinois at Urbana-Champaign, USA

†The MacDiarmid Institute and Industrial Research Limited, Wellington, New Zealand

Most NMR experiments on high-temperature superconductors, in particular spin shift measurements, have been interpreted in terms of a single component. New NMR experiments presented here on Cu and O in $La_{1.85}Sr_{0.15}CuO_4$, from which uncertainties from the Meissner effect have been removed experimentally by recording apical oxygen spectra, are in disagreement with single-component behaviour in the temperature dependence of the spin susceptibility. Instead, it can be explained within a two-component

model that was used to explain early uniform susceptibility measurements. With this it is possible to determine the temperature dependences of the two susceptibilities, even below the transition temperature $T_c$, from NMR. It is found that one of the susceptibilities is constant above $T_c$ and drops exponentially at lower temperatures, while the one that carries the pseudogap feature starts to decrease at much higher temperatures and continues to do so below $T_c$.

## 6.3 Cw and Pulsed ESR Spectroscopy of Cupric Ions in the Metal-Organic Framework Compound $Cu_3(BTC)_2$

B. Jee, A. Pöppl

The metal-organic framework (MOF) compound $Cu_3(BTC)_2(H_2O)_3 \times H_2O$ (BTC = benzene 1,3,5-tricarboxylate) was prepared by solvothermal synthesis under ambient pressure and structurally characterized by powder X-ray diffraction and nitrogen adsorption at 77 K. X- and Q-band cw electron spin resonance (ESR) (Fig. 6.1) and hyperfine sublevel correlation spectroscopies (HYSCORE) were used to explore the coordination state and location of the Cu(II) ions in the porous coordination polymer. Cupric ions were found to be present in two different chemical environments [1]: (a) $Cu(II)_2$ clusters in the paddle-wheel building blocks of the $Cu_3(BTC)_2$q network giving rise to an antiferromagentically coupled spin state in accordance with previous susceptibility measurements [2]. However, the cross-linking of the paddle-wheels by the BTC linker lead to an additional spin exchange among dimers as evidenced by the characteristics of

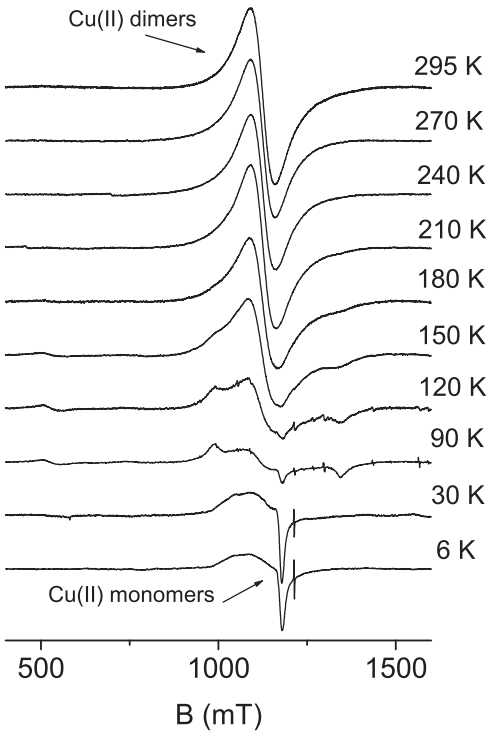


**Figure 6.1:** Q-band cw ESR spectra of $Cu_3(BTC)_2$.

the $S = 1$ ESR signal of their excited spin state. (b) In addition, paramagnetic monomer Cu(II) species are accommodated in the pore system of $Cu_3(BTC)_2$ material. They coordinate to adsorbed water molecules and form $[Cu(H_2O)_6]^{2+}$ complexes, which are inhomogeneously distributed over the $Cu_3(BTC)_2$ pore system.

[1] A. Pöppl et al.: J. Phys. Chem. C **112**, 2678 (2008)
[2] X.X. Zhang et al.: J. Appl. Phys. **87**, 6007 (2000)

## 6.4 Temperature Stability and Photodimerization Kinetics of $\beta$-Cinnamic Acid and Comparison to its $\alpha$-Polymorph as Studied by Solid-State NMR Spectroscopy Techniques and DFT Calculations

I. Fonseca, M. Bertmer

Photoreactions of the $\alpha$- and $\beta$-polymorphs of *trans*-cinnamic acid were studied by $^{13}C$ CPMAS solid-state nuclear magnetic resonance spectroscopy, and the reactants and products were spectroscopically characterized in detail [1]. Chemical shifts and chemical shift anisotropy tensors calculated using density functional theory (DFT) were found to be in good agreement with the experimental results and helped to identify the polymorphs and the individual assignments of reactant and photoproduct carbon atoms. The $\beta$-polymorph is metastable. Its transformation into the $\alpha$-cinnamic acid polymorph is monitored by temperature-dependent $^{13}C$ NMR spectroscopy. The transformation occurs at a very slow rate at room temperature but is highly accelerated at elevated temperatures. Analysis of the kinetics of the photoreaction shows that the $\beta$-polymorph progresses at a slower rate compared to that of $\alpha$-cinnamic acid (Fig. 6.2).

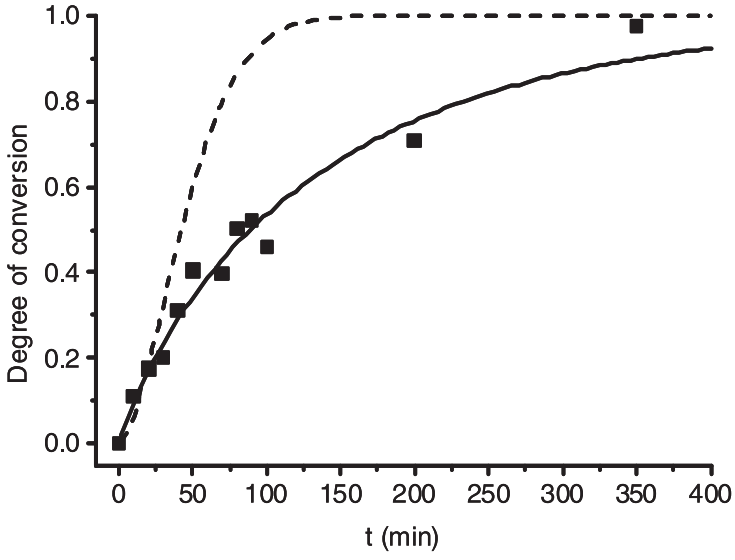


**Figure 6.2:** Photodimerization curve for $\beta$-cinnamic acid (dots and solid line) in comparison to that of $\alpha$-cinnamic acid (dashed line).

Based on chemical shift tensor values of reactants and products as obtained from 2D PASS spectra, the difference in reaction rates is suggested to be due to the higher amount of molecular reorientation of functional groups upon photoreaction and the larger distance between the reacting double bonds.

[1] I. Fonseca et al.: Phys. Chem. Chem. Phys. **10**, 5898 (2008)

## 6.5 Jahn–Teller Effect in $BaTiO_3$:$Cr^{5+}$ An Electron Paramagnetic Resonance Study

R. Böttcher, H.T. Langhammer*, T. Müller†

*Physikalisches Institut, Martin-Luther-Universität Halle-Wittenberg
†Chemisches Institut, Martin-Luther-Universität Halle-Wittenberg

Electron paramagnetic resonance (EPR) spectra of chromium defects with $3d^1$ electron configuration incorporated on Ti sites in single crystal and powdered ceramics of $BaTiO_3$ (BTO) were investigated in the temperature range 50 K to 220 K at 34 GHz (Q band). Single-crystal and powder measurements allow the unambiguous determination of the full $g$ tensor in the ferroelectric rhombohedral phase whereas in the orthorhombic phase only the determination of the principal values of the $Cr_I^{5+}$ $g$ tensor was successful. The Jahn–Teller Effect stabilizes the vibronic ground state of the $3d^1$ electron of the $Cr_I^{5+}$ ion and leads to a tetragonally compressed defect-$O_6$ octahedron with the point symmetry $D_{4h}$. The spontaneous electrical polarisation present in the ferroelectric phases of BTO appears as a further perturbation. The quadratic field effect reduces the $D_{4h}$ symmetry of the $Cr_I^{5+}$ defect centre and produces an additional $g$ tensor breaking the tetragonal symmetry of the Zeeman term. For symmetry reasons one of the principal axes of the rhombic $g$ tensor must be directed along one ⟨110⟩ direction. The angles of the other two principal axes with respect to the ⟨001⟩ axes are dependent on the absolute value of the spontaneous polarisation. The difference in the temperature behaviour of the single-crystal and powder spectra can be explained by the presence of internal stress in the grains of the ceramic samples which increases the JT energy of the $3d^1$ electron.

## 6.6 Funding

*Controlling Mesoscopic Phase Separation*
J. Haase
EU-FP6,CoMePhS, NMP4-CT-2005-517039

*Advanced Signal-Processing for Ultra-Fast Magnetic Resonance Spectroscopic Imaging, and Training*
J. Haase
EU-CORDIS-FP6, MRTN-CT-2006-035801

*EuroMagNET, JRA NMR*
J. Haase
EU, RII3CT-2004-506239

*Magnetic Ground State and Dynamics in High-Temperature Superconductors*
J. Haase, O.P. Sushkov, B. Keimer
EU, DP0881336

*Study of doped nanocrystals with advanced EPR techniques of the paramagnetic centers in nano- and micrometer-sized SiC*
A. Pöppl
DFG Po 426/7-1

*Host-guest interactions and magnetic ordering in MOFs studied by electron and nuclear spin resonance spectroscopy*
A. Pöppl
DFG Po 426/8-1

*Characterization of the [2+2] Photodimerization of cinnamic acid and its derivatives with solid-state NMR*
M. Bertmer
DFG Be 2434/2-2

*Fabrication and physical properties of ferroelectrics confined in nanoporous materials*
D. Michel, E.V. Charnaya
DFG Mi 390/25-1

## 6.7 Organizational Duties

M. Bertmer
- Referee: Angew. Chem., Chem. Mater., Solid State Nucl. Magn. Reson.

R.-M. Böttcher
- Referee: Phys. Rev., J. Phys. Cond. Mat., Langmuir, J. Magn. Reson.

J. Haase
- Dean of Faculty
- Director of the Magnetic Resonance Center Leipzig (MRZ)
- Referee: Phys. Rev.

A. Pöppl
- Referee: J. Magn. Reson., J. Am. Chem. Soc., Phys. Chem. Chem. Phys., Chem. Phys. Lett.
- Reviewer: German-Israel-Foundation for Scientific Research and Development (GIF)

## 6.8 External Cooperations

**Academic**

- Laboratoire National des Champs Magnétiques Pulsés, Toulouse, France
  Prof. Dr. G. Rikken

- Department of Physics, University of Illinois at Urbana-Champaign, USA
  Prof. Dr. C.P. Slichter
- School of Physics, University of New South Wales, Sydney, Australia
  Prof. Dr. O.P. Sushkov
- Department of Electrical and Computer Engineering, University of Illinois at Urbana-Champaign, USA
  Prof. Dr. A.G. Webb
- The MacDiarmid Institute and Industrial Research Limited, Wellington, New Zealand
  Dr. G.V.M. Williams
- Dresden High Magnetic Field Laboratory, Forschungszentrum Dresden-Rossendorf, Germany
  Prof. Dr. J. Wosnitza
- Department of Chemistry, Washington University, St. Louis, USA
  S.E. Hayes
- Abteiltung Chemie, Universität Koblenz-Landau, Koblenz, Germany
  G.E. Schaumann
- Cavendish Laboratory, Department of Physics, University of Cambridge, UK
  Prof. Dr. P. Littlewood
- Physikalisches Institut, Martin-Luther-Universität Halle–Wittenberg, Germany
  Dr. H.T. Langhammer
- Faculty of Physics, University of Vilnius, Lithuania
  Prof. Dr. J. Banys
- Advanced Materials Science, Institut für Physik, Universität Augsburg, Germany
  Prof. Dr. M. Hartmann
- Anorganisch-chemisches Institut, Technische Universität München, Germany
  Prof. Dr. K. Köhler
- Institute of Semiconductor Physics, National Academy of Sciences of Ukraine (NASU), Kiev, Ukraine
  Prof. Dr. E.N. Kalabukhovaa
- Laboratoire de Physique de l'Etat Condenseé, Faculté des Sciences, Université du Maine, Le Mans, France
  Prof. Dr. A. Kassiba

**Industry**

- NMR-Service, Erfurt, Germany
  M. Braun
- Bruker BioSpin, Rheinstetten, Germany
  F. Engelke

## 6.9 Publications

**Journals**

S.V. Baryshnikov, C. Tien, E.V. Charnaya, M.K. Lee, D. Michel, W. Böhlmann: *Dielectric properties of mesoporous sieves filled with $NaNO_2$*, Ferroelectrics **363**, 177 (2008)

S.V. Baryshnikov, C. Tien, E.V. Charnaya, M.K. Lee, D. Michel, W. Böhlmann, N.P. Andriyanova: *Dielectric and NMR studies of superionic AgI embedded in mesoporous silica matrices*, Phys. Solid State **50**, 1342 (2008)

S.V. Baryshnikov, C. Tien, E.V. Charnaya, M.K. Lee, D. Michel, W. Böhlmann, N.P. Andriyanova: *Superionic phase transition in AgI embedded in molecular sieves*, J. Phys. Condens. Mat. **20**, 025 214 (2008)

R. Böttcher, H.T. Langhammer, T. Müller, H.-P. Abicht: *3C-6H phase transition in $BaTiO_3$ induced by Fe ions: an electron paramagnetic resonance study*, J. Phys. Cond. Mat. **20**, 505 209 (2008)

V. Degirmenci, F. Erdem, O. Ergun, A. Yilmaz, D. Michel, D. Üner: *Synthesis and NMR Characterization of Titanium and Zirconium Oxides Incorporated in SBA-15*, Topics Catal. **49**, 204 (2008)

O.F. Erdem, D. Michel: *Study of Thermal Mobility by Means of $^1H$ NMR Magic-Angle Spinning Sideband Analysis*, Appl. Magn. Reson. **34**, 135 (2008)

O.F. Erdem, A. Pampel, D. Michel: *Slow Motion of Confined Molecules: NMR and Briadband Dielectric Spectroscopy Investigation*, J. Nanosci. Nanotechnol. **8**, 887 (2008)

I. Fonseca, S.E. Hayes, B. Blümich, M. Bertmer: *Temperature stability and photodimerization kinetics of beta-cinnamic acid and comparison to its alpha polymorph as studied by solid-state NMR spectroscopy techniques together with DFT calculations*, Phys. Chem. Chem. Phys. **10**, 5898 (2008)

J. Haase, C.P. Slichter, G.V.M. Williams: *Two-component behaviour of high-temperature superconductors from NMR*, J. Phys. Cond. Mat. **20**, 434 227 (2008)

H.T. Langhammer, T. Müller, R. Böttcher, H.-P. Abicht: *Structural and optical properties of chromium-doped hexagonal barium titanate ceramics*, J. Phys. Cond. Mat. **20**, 085 206 (2008)

R.C. Nieuwendaal, M. Bertmer, S.E. Hayes: *An Unexpected Phase Transition during the [2+2] Photocycloaddition Reaction of Cinnamic Acid to Truxillic Acid: Changes in Polymorphism Monitored by Solid-State NMR*, J. Phys. Chem. B **112**, 12920 (2008)

A. Pöppl, S. Kunz, D. Himsl, M. Hartmann: *CW and Pulsed ESR Spectroscopy of Cupric Ions in the Metal-Organic Framework Compound $Cu_3(BTC)_2$*, J. Phys. Chem. **112**, 2678 (2008)

D. Rybicki, C. Kapusta, W. Tokarz, H. Stepánková, V. Procházka, J. Haase, Z. Jirák, D.T. Adroja, J.F. Mitchell: *The 55Mn Nuclear Magnetic Resonance study of high Sr doped $La_{2-2x}Sr_{1+2x}Mn_2O_7$ ($x = 0.5 - 0.8$)*, Phys. Rev. **78**, 184 428 (2008)

D.V. Savchenko, A. Pöppl , J. Hoentsch, E.N. Kalabukhova, Y. Bulois, A. Kassiba: *Intrinsic defects in SiC nonaoparticles as studied by pulsed electron paramagnetic resonance*, Solid State Commun., **146**, 83 (2008)

P. Sedykh, J. Haase, D. Michel, E.V. Charnaya: *Investigation of barium titanate nanoparticles by* $^{137}$*Ba NMR*, Ferroelectrics **363**, 215 (2008)

C. Tien, E.V. Charnaya, M.K. Lee, S.V. Baryshnikov, D. Michel, W. Böhlmann: *Nature of the* $^{2}$3*Na spin relaxation increase near the ferroelectric phase transition in bulk and confined sodium nitrite*, Ferroelectrics **366**, 177 (2008)

C. Tien, E.V. Charnaya, M.K. Lee, S.V. Baryshnikov, D. Michel, W. Böhlmann: *NMR studies of structure and ferroelectricity for Rochelle salt nanoparticles embedded into mesoporous sieves*, J. Phys. Condens. Mat. **20**, 215 205 (2008)

O. Weichold, B. Tigges, M. Bertmer, M. Moeller: *A comparative study on the dispersion stability of aminofunctionalised silica nanoparticles made from sodium silicate*, J. Coll. Interf. Sci. **324**, 105 (2008)

G.V.M. Williams, S. Richter, J. Haase, C.U. Jung, H.-G. Lee, S.-I. Lee: *Magnetization and Cu nuclear magnetic resonance study of* $Sr_0.9La_0.1Cu_{1-x}Ni_xO_2$, Phys. Rev. **78**, 104 522 (2008)

**Talks**

J. Haase: *Elektrischer Strom und Leipziger Physik*, Festkolloquium zu Ehren von Herrn Prof. Dr. Werner Holzmüller, Universität Leipzig, Germany, 11. February 2008

J. Haase: *Evidence for two components in high-*$T_c$ *superconductivity*, Laboratory of Solid State Theory, University of Tartu, Estland, April 2008

J. Haase: *Hochtemperatur-Supraleitung*, 123. öffentlicher Experimentalvortrag, Universität Leipzig, Germany, 20. January 2008

J. Haase: *Hochtemperatur-Supraleitung, alte und neue Einsichten mit der magnetischen Kernresonanz*, Universität Göttingen, Germany, 09. June 2008

J. Haase: *NMR and Recent Progress in High-Temperature Superconductivity*, Rocky Mountain Conference, Breckenridge, USA, 27. – 31. July 2008

D. Rybicky: *Spatial variation of local hole density in Hg* $Ba_2CuO_4$+ *from* $^{6}$3*Cu NMR*, Second CoMePhS Workshop in Controlling Phase Separation in Electronic Systems, Nafplion, Greece, 30. September – 04. October 2008

J. Haase: *Uniform Spin-Response in the Cuprate Superconductors*, The MacDiarmid Institute and Industrial Research Limited New Zealand, Wellington, New Zealand, February 2008

## 6.10 Graduations

**Diploma**

- Susanne Richter
  *Kernresonanzspektroskopie an Hochtemperatursupraleitern*
  June 2008

**Bachelor**

- Damaris Kröber
  *EPR studies of $Cu_3BTC_2$ metal organic framework compounds*
  September 2008

## 6.11 Guests

- Adil Ayouch, PhD
  Faculté des Sciences, Université du Maine, Le Mans, France
  March – July 2008
- Dr. Rafail Rakhmatullin
  Physics Faculty, Kazan State University, Russia
  March – May 2008
- Dr. G.V.M. Williams
  The MacDiarmid Institute and Industrial Research Limited, Wellington, New Zealand
  July – September 2008

# 7

# Nuclear Solid State Physics

## 7.1 Introduction

Our research is focused on two main fields: materials sciences (analysis and modification) and life sciences. The latter one includes quantitative microscopy of elemental distributions in biological samples (mainly for neuroscience), the targeted irradiation of living cells with counted single ions for low dose radiobiology, and a new ion beam based biotechnological method to create areas of confined cell growth for patterned cell cultures. For material analysis we use the standard ion beam analytical methods with the broad as well as the focussed beam, for wich we successfully introduced channeling techniques on the micrometer scale. We could also extend the capabilities for 3D-density and elemental analysis by introducing the limited angle tomography for the scanning microbeam.

The high energy proton or helium-ion beam is also used to modify the physical properties of solids (resists, semiconductors and carbon based materials) by ion irradiation. We create high aspect ratio and free standing microstructures in positive and negative resists and in several types of semiconductors. In carbon based materials we are able to change the electronic properties, which is highly interesting for the study of intrinsic ferromagnetism in these systems.

Our working horse is the high-energy ion-nanoprobe LIPSION with specifications which are unique in Germany and belongs to the best systems worldwide. A careful re-adjustment of the ion optical system lead to a major improvement which opened new high current applications that are usually not feasible on focussed microbeams. Over the last ten years, since the first beam in 1998, we have developed to one of the leading high-energy ion-nanobeam laboratories in the world. This was recognized by the international community by awarding us to host the next international conference on nuclear microprobe technology and applications ICNMTA in 2010.

We have also a longterm expertise in perturbed angular correlation of $\gamma$-rays (TDPAC). This method is used to determine the nuclear quadrupole interactions of materials like $TiO_2$ bulk and $TiO_2$ nano-particles and nano-wires. TDPAC is especially suited to assess in-vitro the solubility of these nano-particles in body fluids without separation of the particles and solution. This information is absolutely necessary to determine probable health risks after incorporation of nano-particles.

A few technical remarks: After the breakdown of our X-ray detector in June 2007, the repair process at the manufacturer lasted till May 2008 with moderate success.

The detector performance dramatically degraded which complicated X-ray analysis. Therefore, we ordered a new X-ray detector (from a different supplier), that will be delivered in April 2009. Nevertheless, standard μPIXE analyses could be performed. The TDPAC laboratory equipment was extended by a fully digital TDPAC-spectrometer that has been developed to improve the experimental setup and the data acquisition.

Our research was financially supported by the European Commission, the Deutsche Forschungsgemeinschaft, and the Federal German Excellence Initiative that we gratefully acknowledge. We also acknowledge the fruitful cooperation with our partners in academic and industries.

*Tilman Butz*

## 7.2 Lattice Distortion and Atomic Displacements in Proton-Induced Freestanding GaN Thin Layer Splitting

A. Guittoum*, O. Moutanabbir†, S. Jankuhn, R. Krause-Rehberg*

*Department of Physics, Martin-Luther-University Halle-Wittenberg, Halle
†Max Planck Institute of Microstructure Physics, Halle

The modification of GaN structural, electrical, and optical properties by ion implantation has attracted a great deal of attention [1]. However, in spite of more than a decade of extensive investigations, there are yet several unexplored aspects and unexplained phenomena. In particular, the influence of the implantation of hydrogen ions at intermediate fluences is still poorly understood. It was demonstrated that annealing above 500 ℃ of hydrogen-implanted GaN (peak concentration ≈ 12 %) leads to the formation

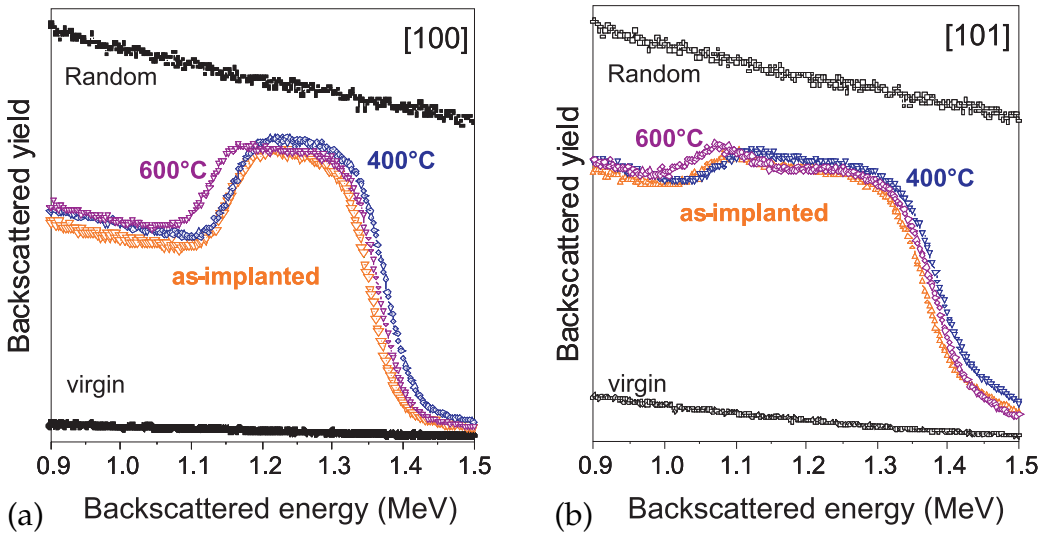


**Figure 7.1:** RBS/C spectra of as-implanted and annealed (at 400 ℃ and 600 ℃) GaN. For comparison spectra (random and channeled) of unimplanted material are also shown. (**a**) Channeling along [100] direction; (**b**) channeling along [101].

of extended internal surfaces. This phenomenon is technologically highly relevant as it could bridge the gap between cost and quality in the fabrication of GaN-based devices [2]. Our objective is to unveil the underlying physics and the atomic processes involved in hydrogen ion splitting of GaN thin layers. Due to the complexity of the microstructure produced immediately after implantation, we have employed several techniques to probe the nature of ion-induced defects and their thermal evolution leading to the splitting. Rutherford backscattering spectrometry in channeling mode (RBS/C) is the technique of choice to investigate the atomic displacements and lattice distortion. A set of GaN substrates implanted at the optimal dose of $2.6 \times 10^{17}$ cm$^{-2}$ at 50 keV and annealed at different temperatures were analyzed by RBS/C using a 2-MeV $He^+$ beam. From the RBS/C spectra, we note the presence of a damage-related peak localized at 1.25 MeV for as-implanted and annealed samples (Fig. 7.1). The damage peaks for ion channeling along the [101] direction are wider than that obtained for [100]. For the annealed sample at 600 °C, the RBS/C spectrum indicates the existence of a shoulder which appears beyond the damage-related peak. The appearance of this shoulder coincides with the formation of nanoscopic cracks [3] and also with the positronium formation [4].

[1] S.O. Kucheyev et al.: Mater. Sci. Eng. R **33**, 107 (2001), doi:10.1016/S0927-796X(01)00028-6
[2] O. Moutanabbir et al.: Electrochem. Solid State Lett. **12**, H105 (2009), doi:10.1149/1.3066081
[3] O. Moutanabbir et al.: Appl. Phys. Lett. **93**, 031 916 (2008), doi:10.1063/1.2955832
[4] O. Moutanabbir et al.: Talk at Int. Workshop Positron Studies of Defects, Prague, Czech Republic, 01. – 05. September 2008

## 7.3 Characterization and Elemental Analysis of Nano- and Microdimensional Structures using PIXE and RBS

C. Meinecke, C. Czekalla*, J. Vogt, A. Rahm, T. Butz

*Semiconductor Physics

Due to the current research in materials science, like in semiconductor physics, the production of micro- and nanostructures raises more interest for basic researchers. The aim is to control the electronic, magnetic and optical properties by variation of the elemental composition and feature size. During the last few years we developed an elemental characterization of different micro- and nanostructures using ion beam analysis with an expected spatial resolution of 100 nm, which is unique in the world. New analytical experiments using focused high energy ion beams can reveal, apart from stoichiometry and morphology, also the lattice structure of the micro- and nanostructures. The application of ion channeling like channeling-RBS and channeling-STIM to these new nanostructures, reveals lattice distortions. This project characterizes sub-micrometer structures of different shapes and compositions (heterostructures, coated structures, homogeneous doped structures etc.) to learn more about growth procedures, electronic

and magnetic properties, elemental distributions of multilayered microstructures and crystal quality using focused high energy ions.

## 7.4 Ion Beam Analysis of Doped and Undoped ZnO as well as BGaAs and BGaP Thin Films

C. Meinecke, D. Spemann, J. Vogt, T. Butz

In collaboration with the divisions of Semiconductor Physics and Superconductivity and Magnetism, respectively, ZnO thin films, nominally undoped, alloyed with Mg, P, Co and Ga grown epitaxially on *c*-plane sapphire by pulsed laser deposition (PLD) were investigated.

In order to determine the elemental composition as well as the film thicknesses the films were analysed by Rutherford Backscattering Spectrometry (RBS) and Particle Induced X-Ray Emission (PIXE) using a $H^+$ ion beam.

The knowledge of the composition of the Mg, P, Co and Ga doped ZnO films is required to understand the optical and electronic properties. Additionally, sensitive trace element analysis was carried out on some of the films in order to quantify the influence of extrinsic impurities on the magnetic properties of the samples.

Furthermore, the crystalline quality and the incorporation of boron in BGaAs and BGaP thin films grown by MOVPE (V. Gottschalch, Institute of Anorganic Chemistry) were investigated using RBS/channeling as well as nuclear reaction analysis under channeling conditions. For this purpose, the proton yield from the $^{10}B(\alpha,p)^{13}C$ nuclear reaction excited by 2.3 MeV $He^+$ ions was recorded under channeled incidence into the [001], [011] and [111] axis of the thin film material. The reduction of the proton yield was nearly identical with the reduction of the RBS yield from the same depth interval. From this it could be concluded that more than 90 % of the incorporated Boron atoms are located on substitutional lattice sites.

## 7.5 Channeling Contrast Microscopy – Spatially-Resolved Ion Channeling at Lipsion

N. Liebing, D. Spemann, T. Butz

Ion channeling is an established technique since 1950 [1]. The channeling effect relies on the regular arrangement of atoms in a crystal. The atomic rows or planes can be considered as strings or sheets of charge. The average of the individual atomic potentials can be described as a continuum potential. The channeled ions are steered by the rows or planes and suffer only small angular scattering. Therefore, the alignment of a major direction of a crystal (rows or planes) leads to a large reduction in the rate of energy loss and scattering probability. This steering ability gives rise to a number of phenomena useful for the investigation of the crystal structure. Anything that disturbs this regular arrangement can be studied using this technique.

The traditional channeling technique with a broad, unfocused beam is limited to distinguish between different types of defects and delivers information about their

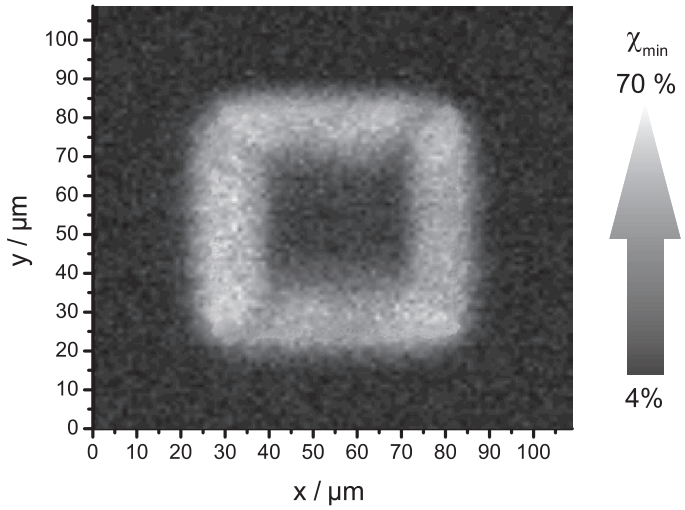


**Figure 7.2:** CCM image ($106 \times 106$ µm$^2$) of Si (along [100]) irradiated on a $54 \times 54$ µm$^2$ area with 2 MeV $^4He^+$ ions. The dechanneling at the outer edges of this area which was swollen shows up in *light grey*.

depth distribution. However, the exact nature of the defect cannot be determined unambiguously. Spatially resolved information cannot be produced using conventional broad beam channeling analysis.

The nuclear microprobe offers the capability to raster a sample with a focused beam. This allows to study crystalline materials using the traditional channeling technique in addition with spatial information from the sample (Fig. 7.2). The spatially resolved channeling techniques are called Channeling Contrast Microscopy (CCM) [3] and Channeling Scanning Transmission Ion Microscopy (CSTIM) [2]. CCM has now been established at the ion nanoprobe LIPSION. In general for CCM a very high accuracy in sample motion is required. Therefore, a eucentric two-axis goniometer was installed and a new software was developed for an automated alignment procedure which links the data acquisition with the goniometer control.

A first application of CCM was the investigation of the ion beam induced swelling of a silicon single crystal [4]. For this purpose the beam was aligned with the [100] axis and the normalized RBS yield ($\chi = Y_{\text{aligned}}/Y_{\text{random}}$) was monitored. As can be seen the ion beam induced swelling leads to a misalignment of the crystallographic axis at the outer edge of the irradiated area with respect to the ion beam (Fig. 7.2). This results in an increased back-scattering yield.

Furthermore, we studied the dependency of the dechanneling due to swelling on scan area and ion fluence (Fig. 7.3). Whereas the minimum yield $\chi_{\text{min}}$ of the total scan area increases significantly with ion fluence due to the contribution of the misalignment in the outer edge, good channeling conditions remain in the center of the scan.

Crystal defects influence the electrical properties of materials in different ways. Thus, the imaging of the crystal quality is an important application for ion microbeams in the field of materials analysis of semiconductors. Channeling Contrast Microscopy offers the capability to perform these analyses even for µm-sized samples. Further developments focus on the introduction of CSTIM (high resolution single ion technique) which allows a better spatial resolution without having ion beam induced swelling as a limiting factor, but requires thin samples.

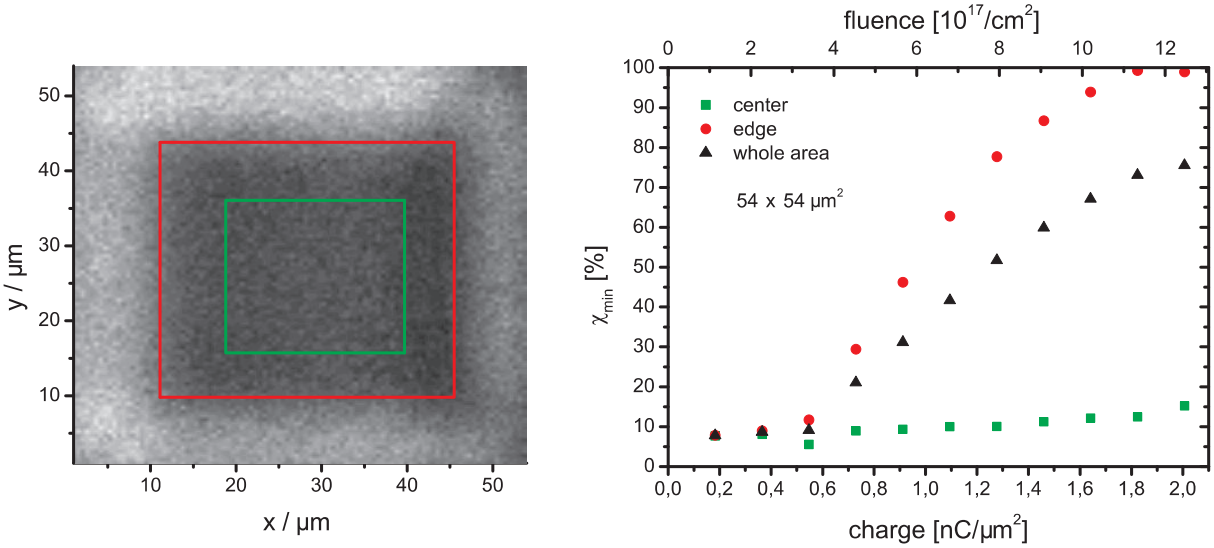


**Figure 7.3:** *Left*: CCM image of a Si crystal irradiated with 2 MeV $^4He^+$ ions. *Right*: Minimum yield $\chi_{min}$ extracted from the regions indicated in the CCM image as a function of ion fluence. Whereas the dechanneling in the total scan area increases remarkably with ion fluence due to the contribution of the misalignment in the outer edge, good channeling conditions remain in the center of the scan.

[1] L.C. Feldman et al.: *Materials analysis by ion channeling: Submicron crystallography* (Academic Press, New York 1982)
[2] M. Cholewa et al.: Nucl. Instrum. Meth. **54**, 397 (1991)
[3] C.J. McCallum et al.: Appl. Phys. Lett. **42**, 827 (1983)
[4] N. Liebing: Diplomarbeit, Universität Leipzig (2009)

## 7.6 Modification of Electric Transport Properties of Carbon-Based Systems by MeV-Ion Beam Irradiation

A. Arndt, D. Spoddig*, P. Esquinazi*, T. Butz

*Superconductivity and Magnetism Workgroup

In a cooperation between the groups of Nuclear Solid State Physics and Superconductivity and Magnetism a newly developed experimental setup was realized to determine the electric properties of multi graphene layers *during* the ion irradiation. Furthermore, also the electric transport properties should be investigated in situ. In the frame of this work a special sample holder and a suitable electromagnet was build to fit into the LIPSION chamber for the external beam with exit nozzle. The sample holder allows the in situ resistance and magneto-transport measurements. The used ions were 2.25-MeV protons with a fluence between $9\times10^{12}$ cm$^{-2}$ and $6\times10^{15}$ cm$^{-2}$. After the proton irradiation, the samples exhibits an increase of resistance and a reduction of the magneto-resistance effect. This effect is correlated with the ion-induced ferromagnetic

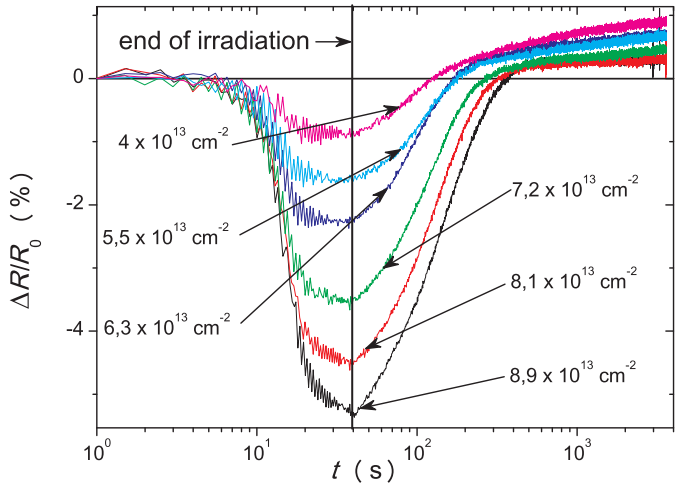


**Figure 7.4:** In-situ measurement of electric resistance during irradiation with quoted fluence values.

order within the graphene system. During the actual investigations this behavior was not established in the samples. Surprisingly, during the in situ irradiation measurements of the resistance a clearly visible reduction in the electric resistance could be observed within the used fluence range. Furthermore, after the minimum of the resistance a relaxation behaviour was found. Figure 7.4 shows this effect in the normalized resistance values. The figure depicts six resistance curves of a multi graphene system of 60 nm thickness. Between the starting point ($t$ = 0 s) and the end point ($t$ = 40 s) of the irradiation process, the resistance drops by up to 5 % of the initial value. After this irradiation the resistance exhibits a relaxation curve to a resistance value higher than the initial one of each irradiation process (0.2 % up to 1 %). This process is still not fully understood. One part of this process could be identified as a thermal relaxation process due to the temperature increase during the irradiation. Another possible effect could be the recombination of the induced vacancies and interstitial carbon atoms.

## 7.7 Development of New Proton-Beam Writing Techniques and Creation of 3D Microstructures in III–V Semiconductors

F. Menzel, D. Spemann, J. Lenzner*, W. Böhlmann†, T. Butz

*Semiconductor Physics Workgroup
†Superconductivity and Magnetism workgroup

The work with the new method of grayscale lithography by proton-beam writing (PBW) was developed further leading among other things to the creation of a Fresnel lens in negative resist (Fig. 7.5a). However, detailed investigations concerning the improvement of the structure quality produced by this technique, especially the surface roughness, has to be to carried out.

Furthermore a new approach for the creation of 3D resist structures using masks and homogeneous ion irradiation was developed. Thereby the mask absorbs part of

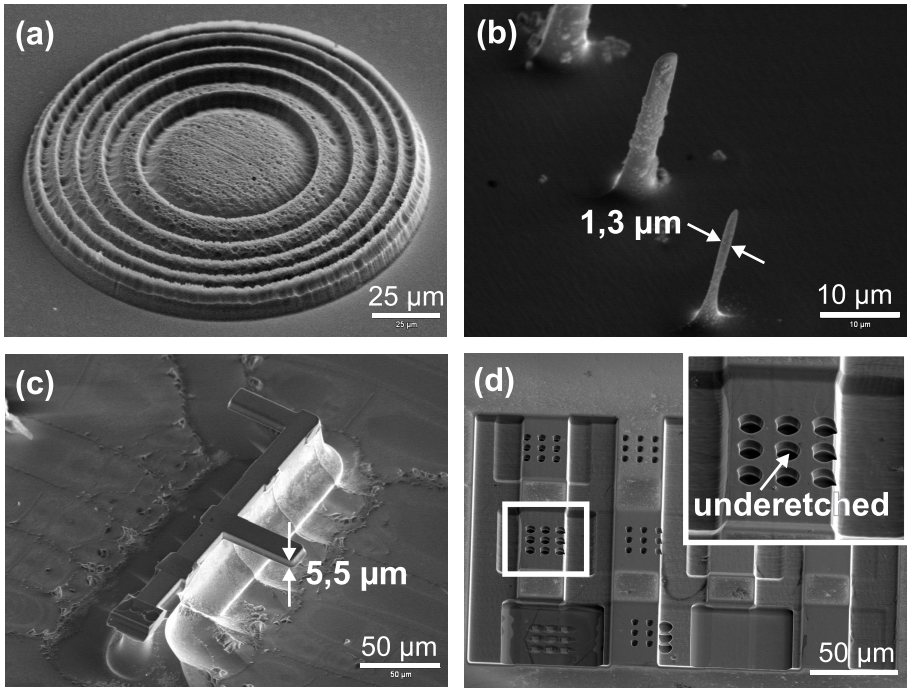


**Figure 7.5:** SEM images of microstructures in different materials created by PBW followed by a chemical or electrochemical etch procedure: (**a**) Fresnel lens in the negative ma-N resist, (**b**) micro pillars in *p*-type GaAs, (**c**) self-supporting structure in *p*-type InP, and (**d**) 3D and partly underetched microstructure in SI GaAs.

the primary ion energy leading to a lateral distribution of ions with different energies and penetration depths in the irradiated negative-resist layer beneath the mask. Due to the different exposure depths 3D freestanding resist structures result.

Experiments dealing with the creation of microstructures in GaAs and InP by PBW and electrochemical etching were continued. In *p*-type GaAs an increase of the etch current density leads to high aspect microstructures with vertical side walls and with heights of some tens of micrometers as well as with lateral dimensions down to ~ 1 µm (Fig. 7.5b). In *p*-type InP similar microstructures as well as self-supporting microstructures (Fig. 7.5c) already shown for *p*-type Si and GaAs were created successfully. Furthermore, the irradiation of SI GaAs with 1.125 MeV $H_2^+$-molecules and different fluences leads to partly underetched multilevel microstructures due to the influence of the irradiation fluence on the electrochemical etch rate (Fig. 7.5d).

## 7.8 Creating Mircofluidic Devices using Proton-Beam Writing

R. Feder, F. Menzel, C. Meinecke, C. Chmelik*, J. Kärger*, T. Butz

*Department of Interface Physics

The creation of microfluidic devices in polymethylmethacrylat (PMMA) using proton-beam writing (PBW) for diffusion measurements in organic crystals and zeolites is in

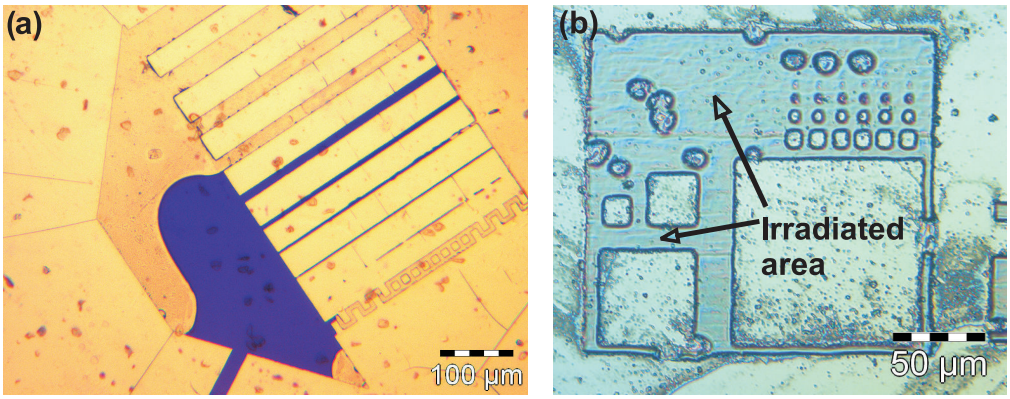


**Figure 7.6:** Different test structures created with PBW in PMMA: (**a**) for ink flowing through enclosed micro channels and (**b**) for experiments showing the negative resist behavior of PMMA after high-fluence irradiation.

progress. PBW is a direct writing technique using a focused beam of MeV protons to create 3D structures in different resist and semiconductor materials down to the submicrometer range. Because the height of the structures is given by the irradiation range of the protons, the farbricated channels are up to 90 µm deep. After developing the PMMA the structures were coupled on a substrate by thermal bonding. A microfluidic test structure with ink flowing through the channels only powered by capillary forces is shown in Fig. 7.6a.

The chamber for the diffusion experiments will be linked with two capillaries for evacuation and for Xe gas inlet, to establish a defined atmosphere surrounding the crystal. Installing this construction into the LIPSION nanoprobe irradiation chamber allows in-situ PIXE and RBS measurements of the diffusion process. A possible effect of the inner boundaries given by the crystal structure to the diffusion could be determined by these experiments. Another task of the experiments was to analyse the characteristics of PMMA influenced by different irradiation fluences. PMMA is usually a positive resist, so irradiated arrays dissolve during the development. At fluences which are about ten times higher than necessary for normal exposure (0.5 pC/µm$^2$) PMMA crosslinks. This crosslinked PMMA is resistant against aceton and can be used as a high resolution negative resist.

## 7.9 Creation of Microstructures in Silicon for Acoustic Applications by Proton-Beam Writing

U. Scholz, F. Menzel, E. Twerdowski*, W. Grill*, T. Butz

*Solid State Optics and Acoustics Workgroup

Micromachined Si structures have been produced for acoustic applications like mode converters. Different arrays of upright and inclined rods with heights ranging from 10 – 50 µm and different array sizes and distances between the rods were created by proton-beam writing (PBW) and subsequent electrochemical etching of Si. These structures were investigated using an ultrasonic microscope at frequencies of 86 MHz in

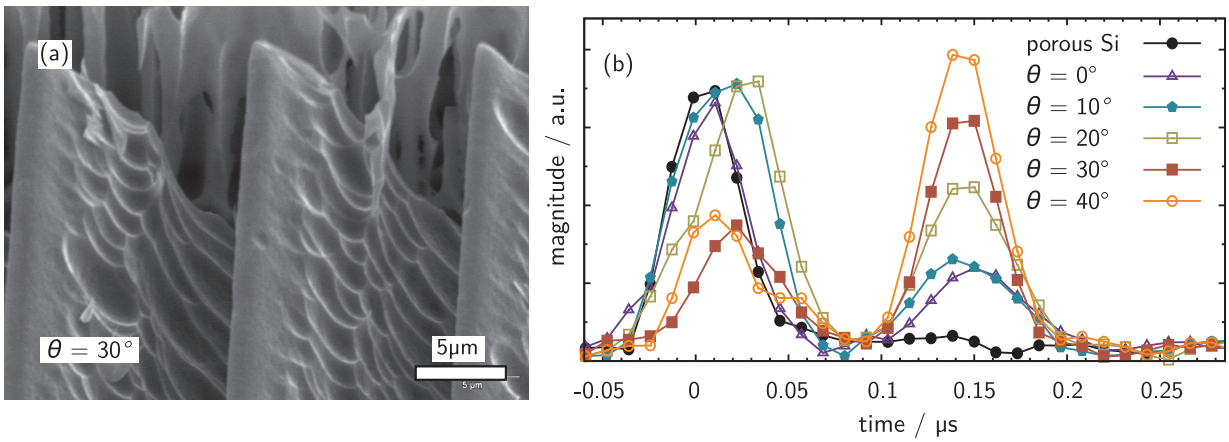


**Figure 7.7:** (**a**) SEM image of micromachined 30° inclined walls with a lateral distance of 10 µm in a Si sample. (**b**) Transients of the magnitude obtained by scanning the micromachined ≈ 430 µm thick sample in tomography mode at different places on the sample.

holography mode. The comparison of measured and simulated holographic patterns show significant differences between structured and unstructured silicon surfaces indicating a transverse/longitudinal mode conversion of acoustic waves at the structured surfaces.

In order to increase this effect of mode conversion, arrays of silicon walls with different inclination angles $\theta$ have been produced (Fig. 7.7a). Acoustic tomography measurements reveal different intensities of acoustic transmission which can be ascribed to mode conversion depending on $\theta$ (Fig. 7.7b).

## 7.10 Improvement of the Ion-Microprobe Performance

M. Rothermel, T. Reinert

After the rebuild of the target chamber of the Leipzig high-energy nanoprobe, the probe forming system was realigned. The system consists of two separated quadrupole doublets, an aperture and an object diaphragm. The magnetic quadrupoles were aligned by successively adjusting the position of each lense's line foci to the ion optical axis. Watching the line foci on a glass with the online microscope in the chamber, the alignment process was effective and precise. Thus, just a small residual, intrinsic rotational misalignment remained, which is essentially reduced by a correction lens. To further improve the performance of the system, experimental grid shadow patterns were taken and compared with ion optical simulations (Fig. 7.8). These reveal dominant spherical aberrations of the system and a parasitic octupole field (0.3 % contribution) superimposed on the third quadrupole. The simulation allows to design a corrective octupole field (Fig. 7.8c) that will be installed in front of the third quadrupole lense.

The grid shadow technique also allows to determine the optimal position where the aperture diaphragm has to be set. Thus, the influences from spherical aberrations on the beam focus can be minimized.

Performance tests yielded proton microbeam currents of 8.3 nA with 1.5 µm beam spot and for a 2 µm beam 17.2 nA which are the best values compared to other micro-

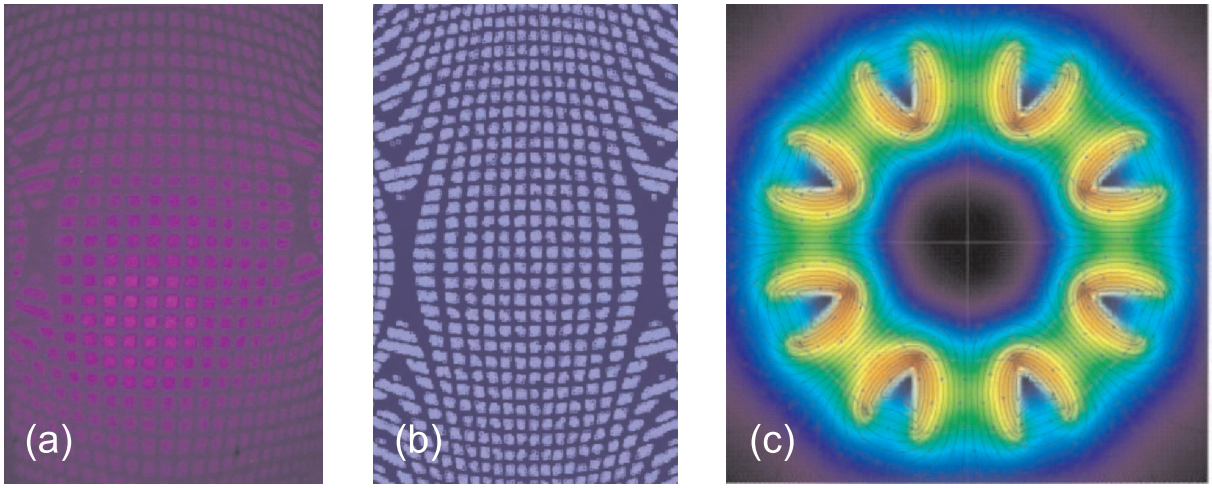


**Figure 7.8:** (**a**) Experimental grid shadow pattern. (**b**) Ion optical simulation of the experiment gives the 0.3 % contribution of a parasitic octupole field. (**c**) Design of a corrective field.

probes worldwide. Since the analysis of minor and trace elemental distribution with a spatial resolution in the micrometer or sub-micrometer range commonly involves large data acquisition times, the reached high beam currents reduce the measurement time without loosing sensitivity. Thus, larger numbers of samples can be analyzed which ensures sufficient statistics in e.g. in biological studies.

We gratefully acknowledge the financial support of the Leipzig Graduate School of Natural Sciences BuildMona.

## 7.11 Limited-Angle STIM and PIXE Tomography of Cells

T. Andrea, M. Rothermel, T. Butz, T. Reinert

The technique of scanning transmission ion micro-tomography (STIM-T) has been successfully employed in recent years at LIPSION and has proved to be a valuable method for the three-dimensional visualization of the density distribution of micro-samples with sub-micron resolution [1]. This technique requires that STIM projections covering an angular range of 180° be taken which makes a free-standing sample necessary.

In order to overcome the difficulties posed by this requirement for the preparation of single cells the most recent development at LIPSION has focused on limited-angle tomography as an alternative. STIM tomography experiments using 1.9 MeV $^4He^+$-ions have been conducted of the unicellular organism *thaumatomonas coloniensis* [2] fixed on a 0.9 μm PE foil. With this setup only an angular range of about 120° could be covered. The missing projections were supplemented by an iterative algorithm developed for limited-angle tomography. The 3D reconstruction of the cell revealed a dense region in the centre. At this stage, however, the resolution was still insufficient to image the contours of organelles definitely (see Fig. 7.9a).

By the combination of STIM and PIXE (particle induced X-ray emission) tomography elemental as well as density information can be obtained. A specimen of the organism *euglena gracilis* fixed on a 4 μm nylon foil was investigated using 1.8-MeV hydrogen molecules for STIM and 2.25-MeV protons for PIXE tomography. Missing

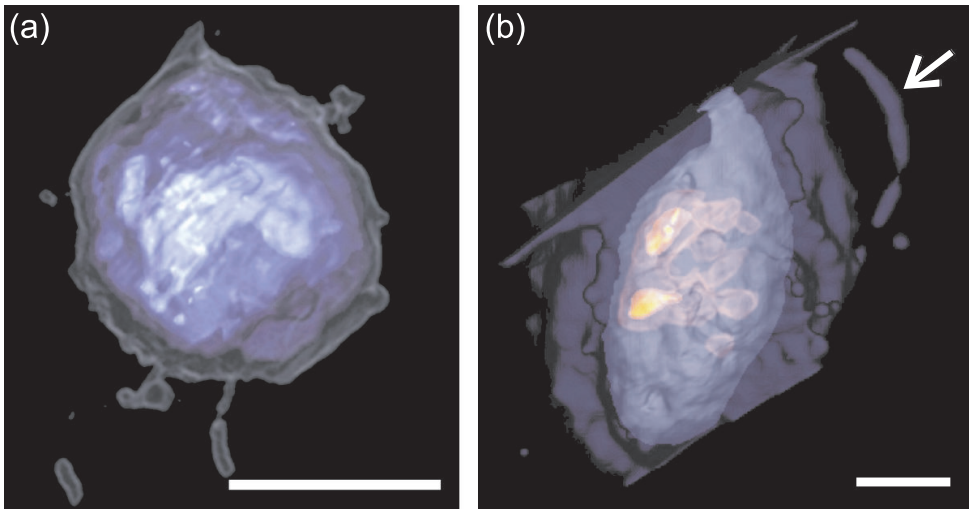


**Figure 7.9:** (**a**) Reconstruction of *thaumatomonas coloniensis*. Isosurfaces of ascending density are represented by brightening shades of blue. A dense structure is visible in the centre. (**b**) Reconstructed density (*blue*) and phosphorus (*yellow*) distribution of *euglena gracilis*. The *arrow* points to the flagellum. Reconstruction artefacts persist at low densities. *Scalebars*: 5 μm.

projections were supplemented iteratively. After reconstruction the 3D density distribution was superimposed with the phosphorus distribution revealing intracellular structures (see Fig. 7.9b).

The combination of limited-angle STIM and PIXE tomography is a very fruitful one since STIM has a better resolution and PIXE is more sensitive to intracellular structures [3].

[1] M. Schwertner et al.: Ultramicroscopy **106**, 574 (2006)
[2] C. Wylezich et al.: J. Eukaryot. Microbiol. **54**, 347 (2006)
[3] T. Andrea: Diplomarbeit, Universität Leipzig (2009)

## 7.12 Quantitative Element Microscopy of Human Hippocampi of Opiate Abusers

M. Weber*, S. Wernicke*, A. Fiedler†, T. Reinert

*Institut für Rechtsmedizin, Medizinische Fakultät
†Paul-Flechsig Institut für Hirnforschung, Medizinische Fakultät

Metal-binding metallothioneins (MT) with a strong neuroprotective effect in the mammalian brain were shown to be upregulated in the brains of morphine intoxicated rats. Data from animal models of addiction hint at an e.g. impaired zinc homeostasis. This might particularly affect the large neuroplastic potential of the hippocampus and would reduce capabilities of cognition and memory. However, semi-quantitative analysis of MT protein expression in human hippocampi by means of immunohistochemistry revealed no significant difference of MT expression in drug addicts versus

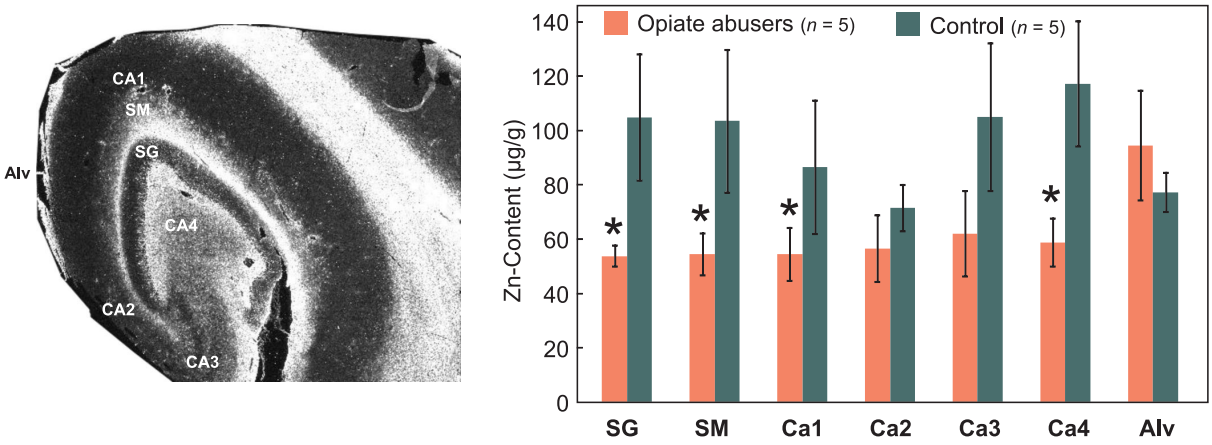


**Figure 7.10:** *Left*: Micrograph of the hippocampus with its regions (*SG*: stratum granulare, *SM*: stratum moleculare, *CA1, CA2, CA3, CA4, Alv*: alveus). *Right*: Zn-content of the regions for opiate abusers and the control group (*error bars*: standard error). Significantly lower concentrations are flagged by an *asterisk*.

age and gender matched controls. Thus, we assumed that the amount of bound metals such as zinc could be affected, while the antibody-recognized protein expression remains constant.

In order to quantitatively compare the concentrations of zinc and other relevant elements (P, S, Ca, Fe, Ni, Cu) we performed a µPIXE study of the hippocampal structures of unstained DePeX embedded brain sections of five opiate abusers and five control individuals. We analysed the hippocampal regions stratum granulare (SG), stratum moleculare (SM), CA1, CA2, CA3, CA4, and alveus (Alv).

Zinc concentrations were found to be significantly decreased in the hippocampi of the addicts in the stratum granulare ($p = 0.028$), the stratum moleculare ($p = 0.047$, the CA1 ($p = 0.093$) and the CA4 ($p = 0.050$). Except for the alveus where the zinc concentration was higher in the drug addicts all other regions showed a slight trend to lower zinc concentrations in the drug addicts (Fig. 7.10). The amount of Fe was slightly higher in the hippocampi of the addicts than in the controls in all regions except stratum moleculare and CA4. However, statistical analysis for each region revealed no significant differences.

## 7.13 Quantification and Localisation of Trace Elements in Parkinsonian Brain: A Proton-Beam Microscopy Study

N. Barapatre, M. Morawski*, T. Arendt*, T. Butz, T. Reinert

*Paul-Flechsig Institut für Hirnforschung, Medizinische Fakultät

The Parkinson's disease is characterised by the severe loss of dopaminergic neurones in the *substantia nigra* (SN) of the brain. These neurones also possess a browny-black pigment called neuromelanin (NM; Fig. 7.11a), which chelates and accumulates metal

(a) 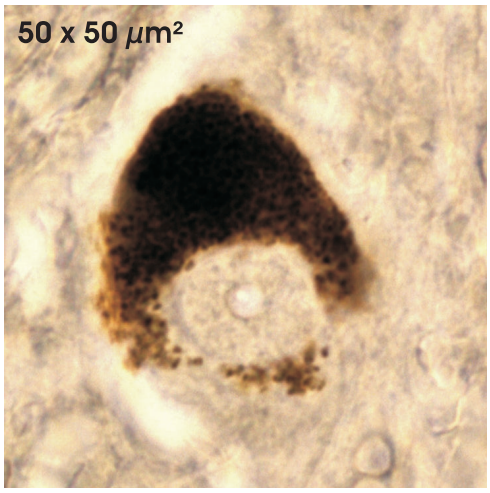


(b) 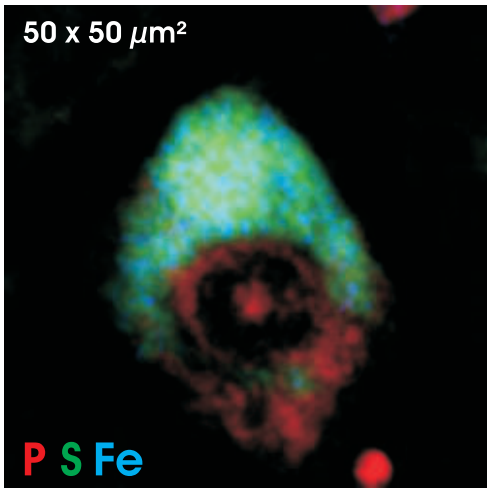


**Figure 7.11:** (**a**) An optical picture of a neuron containing the browny-black pigment neuromelanin. (**b**) A three-element map of the same neurone showing phophorous, sulphur and iron distribution. *Turquoise colour* is due to overlap of *blue* (Fe) and *green* (S).

ions. The role of neuromelanin in the regulation of trace metal ions has come under scrutiny, since an overload of iron in the SN of Parkinsonian brain has been reported in many studies [1]. In general, these studies do not provide information on the localisation of iron overload within the SN. With the help of proton beam microscopy one can locate and quantify metal ions with trace element sensitivity [2]. The trace element concentration in the SN of three Parkinsonian cases was compared with three controls. Particularly, the trace metal content bound to NM and in the extra-cellular region was analysed. Surprisingly, no significant difference was found in the Fe content either bound to neuromelanin or in the extracellular region when the mean of three Parkinsonian cases was compared against the mean of three controls. The Ca and K content bound to neuromelanin as well as in the extra-cellular region was significantly altered. Also, the Cu content in the extra-cellular region was significantly lower in the Parkinsonian cases.

This work was supported by the Deutsche Forschungsgemeinschaft in the framework of GRK InterNeuro.

[1] M. Götz, et al.: Ann. N.Y. Acad. Sci. **1012**, 193 (2004)
[2] T. Reinert, et al.: Nucl. Instrum. Meth. B **249**, 734 (2006)

## 7.14 High Throughput Targeted Cell Irradiation with Single Ions for Low-Dose Radiobiological Experiments

T. Koal, R. Werner, T. Butz, T. Reinert

For low-dose radiobiological effects (Bystander effect - deviation from the linear no threshold dose response model) targeted single cell irradiation with counted sin-

gle ions is required. For this purpose, a reliable recognition software of cell nuclei/compartments, based on dark-field microscopic images to avoid UV-light, and a platform for high-precision ion irradiation of the detected targets were developed. It delivers single ions in air with a lateral precision of 0.5 μm. This allows precise irradiation of cell nuclei and other cell structures. A new in-house program *Cellcognition* was developed using the Matlab platform. The software recognizes the cell nuclei positions in dark field microscope pictures (no staining and no UV-illumination is needed) within a few seconds on a standard PC with a high correctness of > 96 %. The missing 4 % were caused by bi-nucleated cells, grains in the Mylar foil or blurred cells. These false positive detections can be manually discarded during the workflow of Cellcognition. For transforming the cell coordinates into beam coordinates two microscopes are necessary (offline at cell laboratory and online at the irradiation platform) as well as fiducial markers on the irradiation Petri dishes (a commercial 35-mm Petri dish with the bottom replaced by a 2.5-μm Mylar foil or a $Si_3N_4$ membrane window).

In the high current mode (~ 1 nA), as an initial calibration, the program also recognizes reference beam positions on a glass substrate positioned in the focus plane of the cells for the determination of the beam spot positions. In the low-current mode (< 1 fA) a STIM (Scannig Transmission Ion Microscopy) measurement of a reference structure (a grid with a dimension of $2 \times 2\,mm^2$) will be performed with the maximum scan size ($2 \times 2\,mm^2$) using $4095 \times 4095$ pixels. The structure can be recognized in the STIM image as well as in the online microscope image. This allows a projection of the cell coordinate system onto the beam coordinate system.

For the hit verification crosses with the dimension of $3 \times 3$ μm and a fluence of $10 \times 10^8$ protons/$\mu m^2$ were written on an artificial test structure ($10 \times 10$ circles with 3 μm in diameter) in Mylar foil at predetermined coordinates. The crosses on the test structure showed a hit accuracy of ± 1.5 μm at the recognized coordinates.

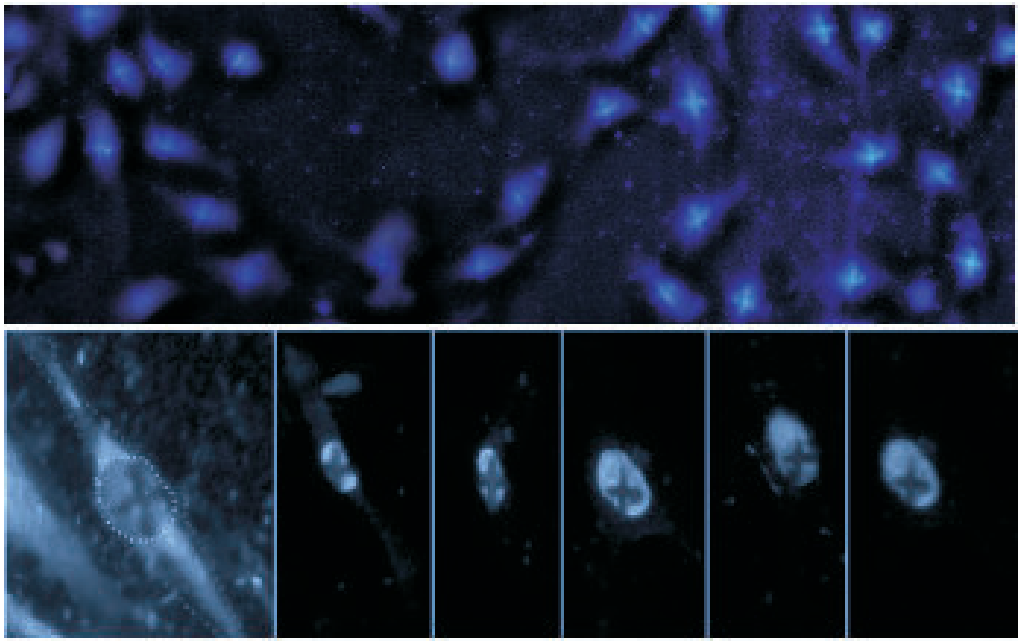

**Figure 7.12:** *Top*: Fluorescent crosses (10 μm × 10 μm) in Mylar at the located nuclei positions. *Bottom*: DAPI stained nuclei show reduced fluorescence due to DNA destruction after irradiation.

These tests were extended to irradiation experiments with living cells (EaHy, human Fibroblasts). The hit accuracy tests with cells on Mylar foil were also carried out with a high fluence instead of single ions. Fluorescent crosses were written at recognized positions with the ion beam. Additionally, the (post irradiation) DAPI stained nuclei showed a reduced fluorescence at the irradiated areas which confirms the accuracy. The crosses for the nucleus hit verification are shown in Fig. 7.12. The target hit accuracy is in total better than $\pm 2\,\mu$m.

The Petri dishes have to be in a vertical position due to the horizontal beam at LIPSION. Therefore, the online experimental procedure comprises medium removal and medium refilling. The fast irradiation ($\sim 5000$ ions/s) allows the irradiation setup to irradiate up to 1500 cells in less than 1.5 minutes including Petri dish handling time.

We gratefully acknowledge the financial support by the NOTE IP 036465 (FI6R), Euratom specific programme for research and training on nuclear energy, 6th FP of the EC.

## 7.15 Spatially Confined Cell Growth for Biological Experiments

R. Werner, T. Koal, T. Butz, T. Reinert

Cell–cell communication (Bystander effects) after low dose irradiations is mostly unknown. There are two possibilities: direct cell–cell communication via gap junctions and cell–cell communication via media. For the investigation of these effects the compartmentalization of Petri dishes is a good way to exclude the direct communication. AGAR, a water-insoluble, cell-repellent polysaccharide was applied to the surface of Petri dishes, silicon nitride ($Si_3N_4$) irradiation windows, and multi-electrode arrays.

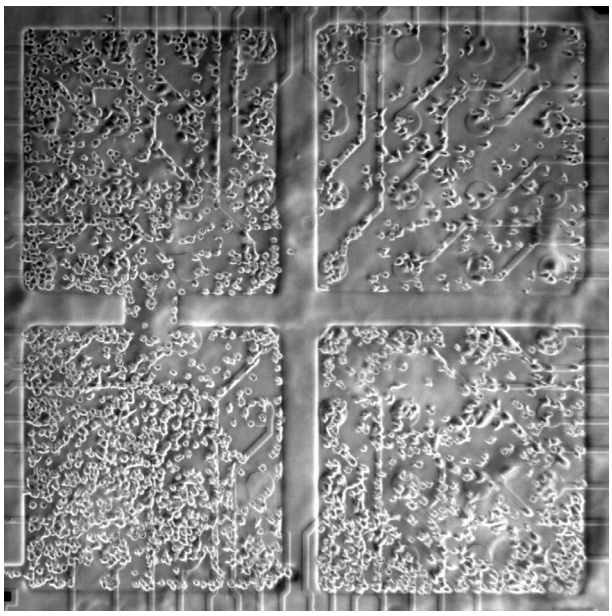

**Figure 7.13:** Confined cell growth on a multi-electrode array in four areas, of which the two left are connected (image size $1.8 \times 1.8\,\text{mm}^2$).

The compartmentalization was achieved by proton beam writing. This irradiation destroys the polysaccharide into water-soluble monosaccharides. Irradiated parts were developed in PBS solution. Seeded cells could only adhere in the areas were the AGAR was removed. The rest is removed via cleaning with PBS or medium. With a new exit nozzle we can irradiate the Petri dishes in air. This allows us to increase the production of structured Petri dishes per hour significantly. Now we are able to produce structured Petri dishes with a maximum size of $2 \times 2\,\mathrm{mm}^2$ with an accuracy of $< 2\,\mu\mathrm{m}$. With proton beam writing we are able to create any possible 2D structure. For further biological research, multi-electrode arrays were structured (see Fig. 7.13). This allows impedance spectroscopy of the cells in the four areas after a selective targeted irradiation of cells in just one area. We want to study whether the cellular response of unirradiated cells depends on the signaling via direct cell–cell communication.

We gratefully acknowledge the financial support by the NOTE IP 036465 (FI6R), Euratom specific programme for research and training on nuclear energy, 6th FP of the EC.

[1] S. Rohr et al.: Eur. J. Physiol. **446**, 125 (2003)

## 7.16 Synthesis of $TiO_2$ Nanowires

S. Ghoshal, L.S. Chang, T. Butz

$TiO_2$ nanowires with diameters of $2-3\,\mathrm{nm}$ and length up to $100\,\mathrm{nm}$ were synthesized via a hydrothermal route. They were characterized by X-Ray diffraction and high-resolution transmission electron microscopy (HRTEM). They were found to grow in the $TiO_2$(B) modification with "b" being the long axis. Subsequently they were impregnated with a 4 M HCl solution containing carrier-free $^{44}$Ti ($t_{1/2} = 60\,\mathrm{y}$). After drying the label was diffused into the wires at 180 °C for two hours. This temperature is enough to diffuse the label a few lattice spacings. We performed Time Differential Perturbed Angular Correlation (TDPAC) measurements on the daughter $^{44}$Sc and obtained two discrete signals for the nuclear quadrupole interaction. The prominent one resembles the value obtained for bulk anatase where the minority fraction is ascribed to the probe atoms close to the surface with an assumed OH-termination. Stable suspensions with $^{44}$Ti-labelled nanoparticles were produced. The measured re-orientation correlation time via TDPAC agrees with the particle size as determined by HRTEM.

## 7.17 A Time Differential Perturbed Angular Correlation Study of Ultrapure Hafnium Metal

S.K. Das, S.C. Bedi, T. Butz

Hf metal crystallizes in the hcp strucure. By thermal neutron activation, $^{181}$Hf ($t_{1/2} = 42\,\mathrm{d}$) is produced which is a suitable isotope for Time Differential Perturbed Angular Correlation (TDPAC) of $\gamma$-rays. Contrary to expectations, one does not find 100 % of all probe atoms in an axially symmetric electric field gradient. Three further signals are observed with about 3 – 5 % of the total signal intensity and asymmetry parameters

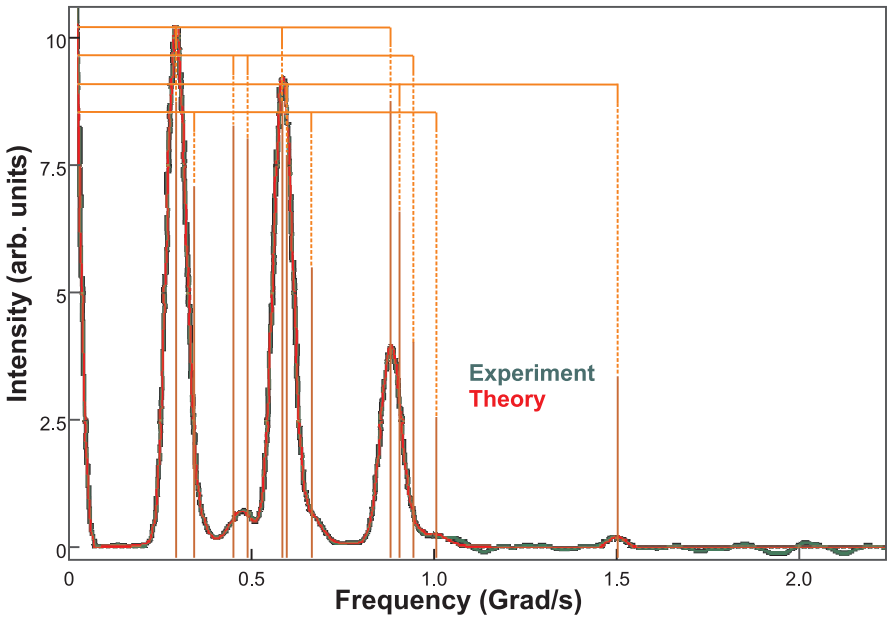


**Figure 7.14:** Cosine-transformed TDPAC spectrum of $^{181}$Hf($\beta^-$)$^{181}$Ta in ultrapure Hf metal.

of 0, about 0.5, and about 0.9 (see Fig. 7.14). The samples contain only 110 ppm Zr, much too low for being responsible for the extra signals. Moreover, Zr and Hf are chemically very similar. Thus we have to look for another explanation. These extra signals are tentatively assigned to one, two, and three atoms on interstitial positions. One of the signals has axial symmetry and requires a first coordination shell with three-fold rotation axis. Incidentally, this signal resembles the signal observed in $\omega$-Zr on B-sites with double occupancy. Heterophase fluctuations have been proposed long time ago for the group-IVb metals based on Mößbauer and neutron diffraction data. We believe that the recoil during prompt de-excitation of $^{181}$Hf in a highly excited state after thermal neutron capture might lead to such metastable configurations because at about 100 ℃ these extra signals are essentially lost. Heating and quenching experiments are under way to clarify the situation.

## 7.18 Funding

*CELLION: Studies of cellular response to targeted single ions using nanotechnology*
Prof. Dr. T. Butz
EU-Project: MRTN-CT-2003-503923 2

*Leipzig School of Natural Sciences - Building with Molecules and Nano-objects (BuildMona)*
Prof. Dr. T. Butz
GSC 185/1

*DFG Graduiertenkolleg Interdisciplinary Approaches in Cellular Neurosciences (InterNeuro)*
Prof. Dr. T. Butz
GRK 1097

*Non-Targeted Effects of ionising Radiation – NOTE*
Prof. Dr. T. Butz
EU Integrated Project FI6R-036465

## 7.19 Organizational Duties

T. Andrea
- Referee: Nucl. Instrum. Meth. B

T. Butz
- Dean of the Faculty for Physics and Geosciences
- Vertrauensdozent der Studienstiftung des deutschen Volkes
- Sprecher der Ortsgruppe Leipzig des deutschen Hochschulverbandes
- Co-tutor for students of Tautenburg (astrophysics), LMU München (astrophysics), DESY/Zeuthen (particle physics)
- external Expert Scientific Committee on Consumer Products, DG Sanco, Brüssel
- Reviewer: DFG, Studienstiftung des deutschen Volkes
- Referee: J. Physics C, Phys. Rev. B, Chem. Rev., Phys. Rev. Lett., J. Biol. Inorg. Chem., Nucl. Instrum. Meth. B, Hyperfine Interact., Israeli Science Foundation, Alexander von Humboldt Foundation

T. Koal
- Referee: Nucl. Instrum. Meth. B

C. Meinecke
- Referee: Nucl. Instrum. Meth. B

F. Menzel
- Referee: Nucl. Instrum. Meth. B

T. Reinert
- Referee: Nanotoxicology, Nucl. Instrum. Meth. B

M. Rothermel
- Referee: Nucl. Instrum. Meth. B

D. Spemann
- Referee: Nucl. Instrum. Meth. B

## 7.20 External Cooperations

**Academic**

- Centre d'Etudes Nucléaires de Bordeaux Gradignan (CENBG), Bordeaux, France
  Prof. P. Moretto
- European Organization for Nuclear Research (CERN), Genf, Switzerland
  ISOLDE Collaboration

- Institute of Physics, Kraków, Poland
  Dr. Z. Stachura
- Leibniz-Institut für Oberflächenmodifizierung (IOM), Leipzig, Germany
  Dr. K. Zimmer, Dr. J. Gerlach
- Royal Veterinary and Agricultural University (KVL), Copenhagen, Denmark
  Dr. L. Hemmingsen
- Max-Planck-Institute for Demographic Research, Rostock, Germany
  A. Fabig
- Center for Ion Beam Applications, National University of Singapore
  Prof. F. Watt, Dr. T. Osipowicz
- Paul-Flechsig-Institut, Universität Leipzig, Germany
  Prof. T. Arendt, Dr. M. Morawski
- Institut für Rechtsmedizin, Medizinische Fakultät, Universität Leipzig, Germany
  Dr. M. Weber, S. Wernicke
- Institut für Laboratoriumsmedizin, Klinische Chemie und Molekulare Diagnostik, Medizinische Fakultät, Universität Leipzig, Germany
  Prof. J. Thiery, Dr. D. Teupser
- Microanalytical Research Centre, The University of Melbourne, Australia
  Prof. D. Jamison
- Technische Universität Wien, Austria
  Prof. K. Schwarz, Prof. P. Blaha
- Universität Hannover, Germany
  Arbeitskreis Prof. P. Behrens, Arbeitskreis Prof. C. Vogt
- Universitätskliniken Leipzig, Germany
  Prof. Dr. G. Hildebrandt
- Martin-Luther-University Halle-Wittenberg, Germany
  Dr. A. Guittoum, Prof. R. Krause-Rehberg
- Max-Planck-Institut für Mikrostrukturphysik, Halle, Germany
  Dr. O. Moutanabbir

**Industry**

- Qimonda Dresden GmbH, Germany
  M. Jerenz
- Solarion GmbH, Leipzig, Germany
  Dr. A. Braun
- Roth & Rau AG, Germany
  Dr. R. Böhme
- Dechema, Germany
  Dr. E. Zschau, Self-employed expert in materials research

## 7.21 Publications

**Journals**

J. Barzola-Quiquia, R. Höhne, M. Rothermel, A. Setzer, P. Esquinazi, V. Heera: *A comparison of the magnetic properties of proton- and iron-implanted graphite*, Eur. Phys. J. B**61**, 127 (2008), doi:10.1140/epjb/e2008-00047-7

M. Brandt, H. von Wenckstern, H. Schmidt, A. Rahm, G. Biehne, G. Benndorf, H. Hochmuth, M. Lorenz, C. Meinecke, T. Butz, M. Grundmann: *High electron mobility of phosphorous-doped homoepitaxial ZnO thin films grown by pulsed laser deposition*, J. Appl. Phys. **104**, 013 708 (2008), doi:10.1063/1.2953066

T. Butz: *Powder perturbation functions in angular correlations for distributions of electric fieldgradient tensor components: analytical expressions for* $I = 1$, Phys. Scr. **78**, 015 801 (2008), doi:10.1088/0031-8949/78/01/015801

E. Gontier, M.-D. Ynsa, T. Bíró, J. Hunyadi, B. Kiss, K. Gáspár, T. Pinheiro, J.-N. Silva, P. Felipe, J. Stachura, W. Dabros, T. Reinert, T. Butz, P. Moretto, J.-E. Surlève-Bazeille: *Is there penetration of titania nanoparticles in sunscreens through skin? A comparative electron and ion microscopy study*, Nanotoxicology **2**, 218 (2008), doi:10.1080/17435390802538508

R. Höhne, P. Esquinazi, V. Heera, H. Weishart, A. Setzer, D. Spemann: *The influence of iron, fluorine and boron implantation on the magnetic properties of graphite*, J. Magn. Magn. Mater. **320**, 966 (2008), doi:10.1016/j.jmmm.2007.09.019

F. Menzel, D. Spemann, J. Lenzner, W. Böhlmann, G. Zimmermann, T. Butz: *Creation of GaAs microstructures using the nuclear nanoprobe LIPSION*, Semicond. Sci. Technol. **23**, 125 028 (2008), doi:10.1088/0268-1242/23/12/125028

S.-B. Ryu , S.K. Das, T. Butz, W. Schmitz, C. Spiel, P. Blaha, K. Schwarz: *Nuclear quadrupole interaction at* $^{44}$Sc *in the anatase and rutile modifications of* $TiO_2$*: Time-differential perturbed-angular-correlation measurements and ab initio calculations*, Phys. Rev. B **77**, 094 124 (2008), doi:10.1103/PhysRevB.77.094124

Q. Xu, H. Schmidt, S. Zhou, K. Potzger, M. Helm, H. Hochmuth, M. Lorenz, C. Meinecke, M. Grundmann: *Magnetic and transport properties of* $Cu_{1.05}Cr_{0.89}Mg_{0.05}O_2$ *and* $Cu_{0.96}Cr_{0.95}Mg_{0.05}Mn_{0.04}O_2$ *films*, Thin Solid Films **516**, 8543 (2008), doi:10.1016/j.tsf.2008.05.012

Q. Xu, L. Hartmann, H. Schmidt, H. Hochmuth, M. Lorenz, A. Setzer, P. Esquinazi, C. Meinecke, and M. Grundmann: *Magnetotransport properties of* $Zn_{90}Mn_{7.5}Cu_{2.5}O_{100}$ *films*, Thin Solid Films **516**, 1160 (2008), doi:10.1016/j.tsf.2007.06.145

Q. Xu, H. Schmidt, S. Zhou, K. Potzger, M. Helm, H. Hochmuth, M. Lorenz, A. Setzer, P. Esquinazi, C. Meinecke, M. Grundmann: *Room temperature ferromagnetism in ZnO films due to defects*, Appl. Phys. Lett. **92**, 082 508 (2008), doi:10.1063/1.2885730

Q. Xu, H. Schmidt, H. Hochmuth, M. Lorenz, A. Setzer, P. Esquinazi, C. Meinecke, M. Grundmann: *Room temperature ferromagnetism in Nd- and Mn-codoped ZnO films due to defects*, J. Phys. D: Appl. Phys. **41**, 105 012 (2008), doi:10.1088/0022-3727/41/10/105012

**Books**

T. Butz: *Aufnahme und Speicherung von Nanopartikeln durch die Haut*, in *Nanotechnologie – Grundlagen, Anwendungen, Risiken, Regulierung*, ed. by A. Scherzberg, J.H. Wendorff (De Gruyter, Berlin 2008) p 81

**Talks**

T. Andrea, M. Rothermel, T. Butz, T. Reinert: *STIM tomography of Biological Samples*, 11. Int. Conf. Nucl. Microprobe Technol. Appl., Debrecen, Hungary, 20. – 25. July 2008

T. Butz: *Selected Properties of Common Nanomaterials*, SCCP-Meeting, Bruxelles, Belgium, 2. July 2008

T. Butz: *Wissen und Wissenslücken zum Thema Hautpenetration von Nanopartikeln*, Bundesinstitut für Risikobewertung, Berlin-Dahlem, Germany, 18. September 2008

T. Butz: *Gibt es ein Risiko von Nanomaterialien aus dermatologischer Sicht?*, Bundesinstitut für Risikobewertung, Berlin-Marienfelde, 10. November 2008

T. Koal, T. Butz, T. Reinert: *Detection of Cell Nuclei on Bright Field Microscope Pictures without UV Fluorescent Markers and Accuracy Check with Proton Beam Writing in PET foil*, 8. Int. Workshop Microbeam Probes of Cellular Radiation Response, Chiba, Japan, 13. – 15. November 2008

T. Koal, M. Hohlweg, T. Butz, T. Reinert: *Development of new techniques to arrange and recognize cells for radiobiological ion micro-beam experiments*, 72. DPG Spring Meeting, Berlin, Germany 25. – 29. February 2008

C. Meinecke, A. Rahm, M. Grundmann, T. Butz: *Quantitative Elemental Characterisation of Mg-, Mn- and Co doped ZnO Nanowires and Films*, 11. Int. Conf. Nucl. Microprobe Technol. Appl., Debrecen, Hungary, 20. – 25. July 2008

F. Menzel, D. Spemann, T. Koal, T. Butz: *PBW at the high energy nanoprobe LIPSION*, 3. Int. Workshop Proton Beam Writing, Debrecen, Hungary, 20. – 25. July 2008

F. Menzel, D. Spemann, T. Koal, J. Lenzner, T. Butz: *Application of proton beam writing for grayscale lithography in negative resist materials*, 11. Int. Conf. Nucl. Microprobe Technol. Appl., Debrecen, Hungary, 20. – 25. July 2008

M. Rothermel: *Sub-micron ion beam analysis and material modification - applications in physics and biology*, 1. BuildMoNa Workshop, Leipzig, Germany, 16./17. October 2008

M. Rothermel: *The high energy ion nanoprobe LIPSION - a tool for sub-micron research in physics and biology*, 42. Zakopane School of Physics, 19. – 24. May 2008

**Posters**

N. Barapatre, T. Reinert, T. Butz, D. Teupser, J. Thiery: *Trace element mapping of atherosclerotic lesions in mice - A pilot study at the LIPSION laboratory*, 11. Int. Conf. Nucl. Microprobe Technol. Appl., Debrecen, Hungary, 20. – 25. July 2008

A. Fiedler, M. Morawski, T. Reinert, G. Brückner, T. Arendt: *Intraneuronal analyses of iron and iron proteins*, 6. FENS Forum Eur. Neurosci., Geneva, Switzerland, 12. – 16. July 2008

T. Koal, T. Butz, T. Reinert: *Detection of cell nuclei on bright field microscope pictures without UV fluorescent markers and accuracy check with Proton Beam Writing in PET foil*, German Biophys. Soc. Meeting 2008, Berlin, Germany, 28. – 30. September 2008

T. Koal, T. Butz, T. Reinert: *From cell detection to cell irradiation - Status report on LIPSION facility*, 8. Int. Workshop Microbeam Probes of Cellular Radiation Response, Chiba, Japan, 13. – 15. November 2008

T. Koal, T. Butz, T. Reinert: *Gezielter Einzelionenbeschuß lebender Zellen für radiobiologische Experimente am LIPSION*, 7. Research Festival Leipzig, Germany, 12. December 2008

C. Meinecke, M. Brandt, M. Grundmann, J. Vogt, T. Butz: *Characterization and elemental analysis of nano- and microdimensional structures using PIXE and RBS*, 72. DPG Spring Meeting, Berlin, Germany 25. – 29. February 2008

F. Menzel, D. Spemann, J. Lenzner, W. Böhlmann, G. Zimmermann, T. Butz: *Fabrication of microstructures in III-V semiconductors by proton beam writing*, 11. Int. Conf. Nucl. Microprobe Technol. Appl., Debrecen, Hungary, 20. – 25. July 2008

A. Müller, G. Benndorf, S. Heitsch, H. Hochmuth, C. Meinecke, M. Grundmann: *Optical investigations of hexagonal $Mg_xZn_{1-x}O$ thin layers in UV spectral range*, 72. DPG Spring Meeting, Berlin, Germany 25. – 29. February 2008

T. Koal, M. Hohlweg, F. Menzel, T. Butz, T. Reinert: *Development of New Techniques to Arrange and Recognise Cells for Radiobiological Ion Microbeam Experiments*, 11. Int. Conf. Nucl. Microprobe Technol. Appl., Debrecen, Hungary, 20. – 25. July 2008

M. Rothermel, J.L. Barzola-Quiquia, T. Reinert, C. Nilsson, P. Esquinazi, T. Butz: *Ion beam analysis and material modification at LIPSION*, 1. Scientific Symposium of Build-MoNa, Leipzig, Germany, 07./08. February 2008

M. Rothermel, T. Butz, T. Reinert: *Rearranging a nanoprobe: line foci, grid shadow patterns and performance tests*, 11. Int. Conf. Nucl. Microprobe Technol. Appl., Debrecen, Hungary, 20. – 25. July 2008

M. Rothermel, T. Reinert, C. Nilsson, T. Butz: *The new comfort at the LIPSION nanoprobe.*, 11. Int. Conf. Nucl. Microprobe Technol. Appl., Debrecen, Hungary, 20. – 25. July 2008

M. Weber, A. Fiedler, S. Wernicke, T. Reinert: *IQuantitative element microscopy of human hippocampi of opiate abusers*, 6. FENS Forum Eur. Neurosci., Geneva, Switzerland, 12. – 16. July 2008

Q. Xu, H. Schmidt, S. Zhou, K. Potzger, M. Helm, H. Hochmuth, M. Lorenz, C. Meinecke, M. Grundmann: *Magnetic properties of amorphous p-type conducting* $CuCr_{0.93}Mg_{0.05}Mn_{0.02}O_2$, 72. DPG Spring Meeting, Berlin, Germany 25. – 29. February 2008

## 7.22 Graduations

**Diploma**

- Marcus Hohlweg
  *Entwicklung strukturierter Petrischalen und Ionenbeschuss lebender Zellen zur Untersuchung des Bystander-Effektes unter Ausschluss von Zell–Zell-Kommunikation über Gap-Junctions*
  January 2008
- Daniela Kolbe
  *Rastertransmissions-Ionenmikroskqopie einzelner lebender und fixierter Zellen*
  March 2008

## 7.23 Guests

- Dr. Ling-Shao Chang
  Sun Yat Sen University, Taipei, Taiwan
  October 2007 – June 2008
- Dr. Shamik Ghoshal
  Bhabha Atomic Research Centre, Mumbai, India
  November 2007 – June 2008
- Dr. J. Škopek
  Charles University, Praha, Czech Republic
  September 2007 – March 2008

# 8

# Semiconductor Physics

## 8.1 Introduction

Based on our advances in ZnO materials technology, namely pulsed-laser deposition, we have achieved exciting results in 2008. ZnO microwires were found to exhibit lasing on whispering gallery modes. We have fabricated nanowires wrapped with quantum wells and Bragg reflectors, and nanowire *p*–*n*-diodes. We show that our all-oxide microcavities remain in the strong coupling regime beyond 400 K. High transconductance ZnO MESFETs have been fabricated with Schottky gates and as programmable FeFETs with ferroelectric gates. You are invited to read up on these latest results and further work, e.g. detailed analysis of the recombination in bulk $Mg_xZn_{1-x}O$ and MgZnO/ZnO quantum wells and defect analysis in ZnO.

We are very grateful to our funding agencies which are acknowledged individually in the short notes. On January 1st 2008 the DFG Sonderforschungsbereich 762 "Functionality of Oxide Interfaces" has started its work. Also the support by the State of Saxony via Landesinnovations-Stipendien deserves a special mentioning. The work of our students and researchers together with our academic and industrial partners near and far was fruitful and enjoyable and thus it is with pleasure that the semiconductor physics group presents their progress report.

*Marius Grundmann*

## 8.2 Whispering Gallery Mode Lasing in ZnO Microwires

C. Czekalla, C. Sturm, R. Schmidt-Grund, B.Q. Cao*, M. Lorenz, M. Grundmann

*present address: Department of Electrical and Electronic Systems Engineering, Kyushu University, Fukuoka, Japan

Whispering gallery mode (WGM) lasing has been observed in single zinc oxide (ZnO) microwires using spatially resolved photoluminescence spectroscopy (micro PL). In a WGM resonator, the light wave circulates around the hexagonal cross section due to total internal reflection at the resonator boundaries. For the visible spectral range, this has already been demonstrated in ZnO wires [1].

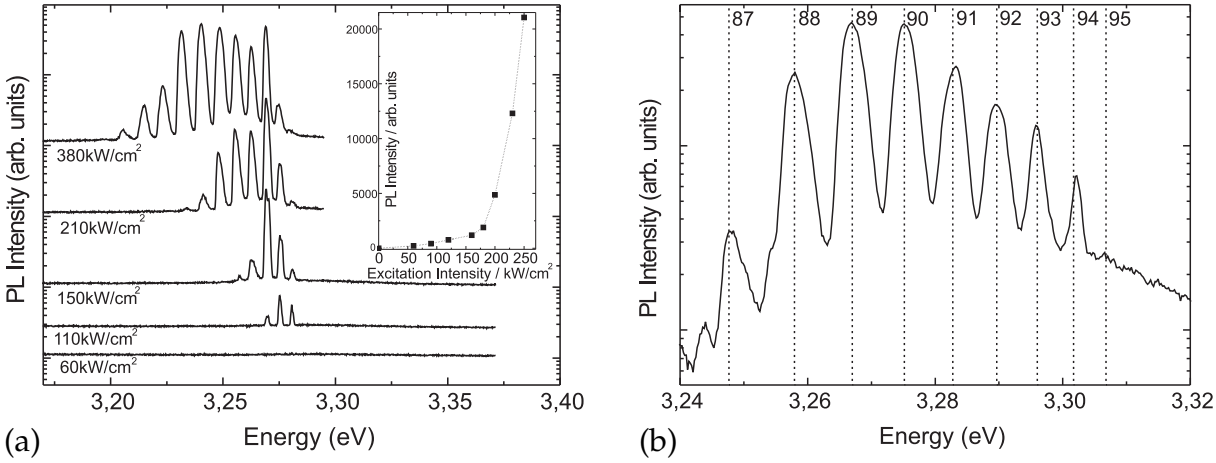


**Figure 8.1:** (**a**) Emission spectra for different excitation intensities as indicated taken from a single microwire at a temperature of 10 K in a semi-logarithmic plot. The *inset* shows the highly superlinear dependence of the emitted intensity on the excitation intensity. (**b**) Comparison of a typical lasing spectrum to the energy positions calculated from the WGM model with indicated interference orders $N$ in a semi-logarithmic plot.

The investigated microwires have diameters in the range between 1 μm and 20 μm. At a temperature of 10 K, sharp peaks arise from the PL spectra as the excitation intensity is increased as shown in Fig. 8.1a. The number of observed peaks increases with increasing excitation intensity and the peaks show a highly superlinear dependence of the emitted intensity on the excitation intensity, a clear indication for lasing as shown in the inset of Fig. 8.1a. From the FWHM of the peaks, quality factors around 5000 are obtained. The energetic position of the lasing peaks suggests an electron hole plasma (EHP) as gain mechanism.

The energetic peak positions can be calculated from a simple plane wave model [1, 2]. As shown in Fig. 8.1b, the calculated values fit the experimentally observed peak positions. From the temperature dependence of the lasing threshold intensity, the characteristic temperature $T_0$ of the microlasers was determined to be 30 K. This small value is most likely caused by an inefficient radiative recombination at higher temperatures.

Further work will be directed towards coupling the WGMs to the emission of a quantum well grown as a core shell structure around the microwires.

This work was supported by the DFG within FOR 522 and the EU within NANDOS and SANDiE and by the Leipzig School of Nano-Science BuildMoNa.

[1] T. Nobis et al.: Phys. Rev. Lett. **93**, 103 903 (2004), doi:10.1103/PhysRevLett.93.103903
[2] C. Czekalla et al.: Appl. Phys. Lett. **92**, 241 102 (2008), doi:10.1063/1.2946660

## 8.3 Strong Light–Matter Coupling up to 410 K

C. Sturm, H. Hilmer, R. Schmidt-Grund, C. Czekalla, H. Hochmuth, M. Grundmann

The strong coupling between light and matter in microresonators forms new bosonic quasi particles which are called exciton-polaritons. Due to their quantization in energy

and momentum and their tiny particle mass (about 9 orders of magnitude smaller than those of atoms) they are promising candidates for the realization of Bose–Einstein-Condensation above room temperature and the realization of new devices such as ultra-low threshold lasers [1]. We investigated the exciton-polaritons in a ZnO based resonator consisting of a half wavelength ZnO cavity embedded between two Bragg reflectors made of 10.5 layers of YSZ (yttria stabilized zirconia) and $Al_2O_3$. For the preparation of this resonator we refer to the contribution of H. Hilmer et al. (Sect. 8.4) in this research report.

The exciton-polariton modes were observed by means of photoluminescence (PL) and reflectivity (R) measurements at temperatures 10 – 410 K for emission angles or rather angles of incidence in the range 0 – 76° (6 – 76° for R). The PL spectra for 10 K and 410 K are shown in Fig. 8.2a,b. Instead of a pure exciton and cavity-photon mode dispersion a lower polariton branch (LPB) is observable. Its dispersion changes from a photonic one to an excitonic one with varying angle. The upper polariton branch is not observable due to the strong absorption of ZnO in this spectral range [2].

For the determination of the exciton–photon coupling strength we analyzed the dispersion of the LPB in its energy and broadening. Therefore we use for simplification a $2 \times 2$ coupling Hamiltonian, i.e. assuming the coupling of one photon mode with one exciton mode (that with the lowest ground state energy). The energy of the LPB is than given by

$$E_{\mathrm{LPB}}(\varphi) = \frac{1}{2}\left((E_{\mathrm{X}} - E_{\mathrm{C}}(\varphi)) - \sqrt{(E_{\mathrm{X}} - E_{\mathrm{C}}(\varphi))^2 + 4V^2}\right), \tag{8.1}$$

with the complex energy of the uncoupled exciton mode $E_{\mathrm{X}}$, the complex energy of the uncoupled cavity-photon mode $E_{\mathrm{C}}$, the coupling strength $V$ and the emission angle $\varphi$. The angular dependence of the uncoupled cavity-photon mode was calculated by the approach suggested by Panazarini et al. [3] taking into account the optical thickness of all layers of the complete resonator structure. Besides the thickness of each layer the according refractive index has to be known which was determined by spectroscopic ellipsometry from single layers with properties similar to the respective layers within the whole resonator structure. In the case of the ZnO we removed all excitonic contributions from the refractive index in order to exclude coupling effects.

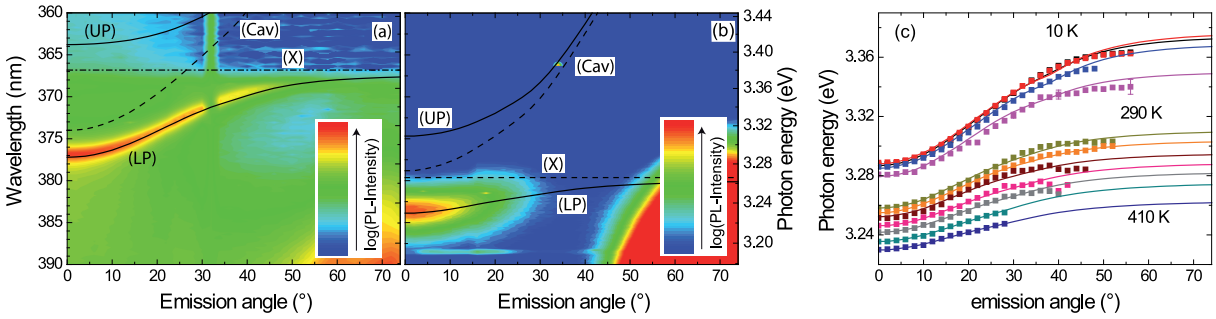


**Figure 8.2:** (**a**,**b**) Photoluminescence spectra in a half-logarithmic false colour scale for 10 K (**a**) and 410 K (**b**). The *solid lines* represent the calculated lower (LP) and upper polariton branch (UP) whereas the *dashed lines* represent the uncoupled exciton mode (X) and the uncoupled cavity-photon mode (Cav). (**c**) The experimentally observed (*symbols*) and calculated (*solid lines*) energy of the lower polariton branch.

By applying this model, the observed dispersion of the LPB, or rather its angular dependence, can be described very well (Fig. 8.2c). We obtain a maximum coupling strength of 51 meV in PL and 55 meV in R at 10 K, which is one of the largest for inorganic semiconductors. The difference in the coupling strength for PL and R can be attributed to different formation processes of the excitons in these experiments. This leads to a different exciton density and therefore to a different occupation of the LPB. With increasing temperature the coupling strength decreases. Responsible for this is the decreasing exciton oscillator strength based on the reduction of the static dielectric constant. For 410 K we obtain for the coupling strength 43 meV in PL and 35 meV in R. This is the highest reported temperature for the formation of exciton-polaritons. Besides the coupling strength, the exciton energy and the cavity-photon energy decreases with increasing temperature. However, the redshift of the exciton energy is much stronger affected than those of the cavity-photon and so the detuning of the resonator, i.e. the difference between the cavity and the exciton energy at zero in-plane wavevector, increases from −65 meV to 7 meV.

Above 410 K the dispersion of the LPB shows a small blue shift. However, the presence of a strong coupling regime cannot be confirmed since the LPB is only observable at small angles and the uncertainty for these temperatures is very large. Furthermore, using the determined temperature behaviour of the exciton-polaritons, the splitting between these two branches is smaller than their broadening. Therefore we call this the intermediate coupling regime. In order to reach the strong coupling regime up to the predicted temperature of 560 K [4] the exciton-oscillator strength has to be increased by improving the crystal quality of the ZnO cavity or by using quantum wells as active medium.

This work was supported by the DFG in project Gr 1011/20-1.

[1] A. Kavokin, G. Malpuech: *Cavity Polaritons* (Elsevier, Amsterdam 2003)
[2] S. Faure et al.: Phys. Rev. B **78**, 235 323 (2008), doi:10.1103/PhysRevB.78.235323
[3] G. Panzarini et al.: Phys. Rev. B **59**, 5082 (1999), doi:10.1103/PhysRevB.59.5082
[4] M. Zamfirescu et al.: Phys. Rev. B **65**, 161 205R (2005), doi:10.1103/PhysRevB.65.161205

## 8.4 Ellipsometry on Microresonators Grown by Pulsed-Laser Deposition

H. Hilmer, C. Sturm, R. Schmidt-Grund, J. Sellmann, J. Lenzner, H. Hochmuth, M. Lorenz, B. Rheinländer, M. Grundmann

Much effort has been devoted to the investigation of exciton-polaritons in the past decades. These bosonic particles can be formed in a microresonator, where light strongly interacts with matter, which generates physical effects opening a wide field of new applications such as ultra-low threshold lasers and optical amplifiers. ZnO is a promising material to realize this far above room temperature [1].

Our ZnO microresonator has been grown on *c*-plane sapphire substrate by means of pulsed-laser deposition and consists of two Bragg reflectors (BR), each made of 10.5 pairs yttria stabilized zirconia (YSZ) and $Al_2O_3$, surrounding a half-wavelength ZnO

cavity, which acts simultaneously as active medium. The substrate temperature during growth was chosen to be about 650 ℃ and oxygen pressures in the range of 0.002 mbar to 0.02 mbar were applied. For thickness control ellipsometry measurements were essential as well as for the calculation of the reflectivity of the BR. It is $R_{\max} = 99.2\,\%$ at 3.26 eV for 10.5 layer pairs. Scanning transmission electron microscopy images (Fig. 8.3a) show homogeneous layers without voids and with smooth and planar interfaces throughout the layer stack. Also a passive microresonator, where the ZnO layer has been omitted to form a YSZ-cavity, was fabricated in order to investigate the resonator system without coupling effects.

Usually the formation of exciton-polaritons is observed by means of photoluminescence (PL) and reflection (R) experiments. In contrast to these techniques, spectroscopic ellipsometry provides a very sensitive additional information: the phase. The ellipsometric parameters $\Psi$ and $\Delta$ are defined by:

$$\rho = \frac{r_\mathrm{p}}{r_\mathrm{s}} = \tan\Psi e^{i\Delta} \,. \tag{8.2}$$

The ellipsometric parameter $\Delta$ is the phase difference between the phases of light polarised parallel ($r_\mathrm{p}$) and perpendicular ($r_\mathrm{s}$) to the plane of incidence. In idealised simulations of $\Psi$ and $\Delta$ of a passive microresonator using the transfer matrix method, a multitude of structures can be investigated. Especially, the symmetry of the line shapes in $\Delta$ (Fig. 8.3b) provides information on the ideality of the resonator structure, when $\Psi$ spectra are almost identical. Thereby, we are able to distinguish the tuning relation, i.e. the spectral shift of the stopband, of the bottom and top BR with respect to each other in $\Delta$ (Fig. 8.3b). This immediately provides information which is also a valuable input for the growth.

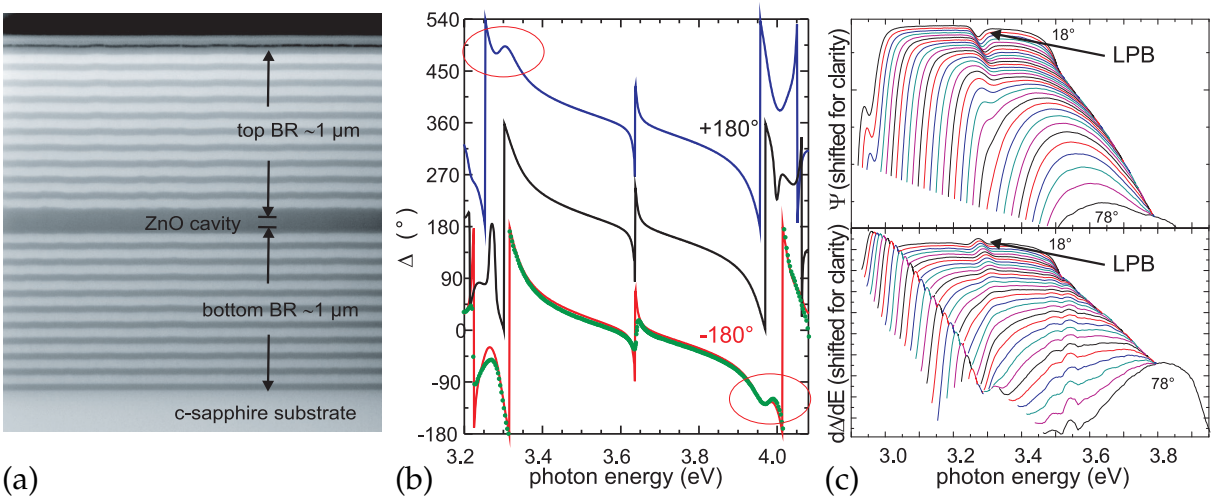


**Figure 8.3:** (**a**) Scanning transmission electron microscopy image of a ZnO resonator consisting of a half-wavelength ZnO cavity embedded between two 10.5-pair YSZ/$Al_2O_3$ Bragg reflectors on *c*-plane sapphire. The *dark layers* are ZnO and YSZ, the *bright layers* $Al_2O_3$. (**b**) $\Delta$ spectra for tuned (*black*) and detuned passive microresonators (*blue*: bottom BR shifted to higher and top BR to lower energies, and *red*: vice versa) compared to experiment (*green*). The *encircled regions* reveal the detuning situation. (**c**) Experimental data of the dispersion of the lower polariton branch (LPB) in the ellipsometric parameters $\Psi$ and the 1st derivative of $\Delta$ of the ZnO microresonator.

Investigating the ZnO resonator with ellipsometry, both $\Psi$ and $\Delta$ spectra in the range of $(18-78)^\circ$ clearly show the dispersion of the lower polariton branch (Fig. 8.3c). The evaluation of this dispersion and also temperature- and angle-dependent PL and R spectra reveal the resonator to be in the strong coupling regime even above room temperature (see also Sect. 8.3).

[1] M. Zamfirescu et al.: Phys. Rev. B **65**, 161 205R (2002), doi:10.1103/PhysRevB.65.161205

## 8.5 Core/Shell ZnO/ZnMgO Quantum Wells on Free-Standing ZnO Nanowires

J. Zúñiga Pérez*, B.Q. Cao†, C. Czekalla, H. Hilmer, J. Lenzner, M. Lorenz, M. Grundmann

*Centre de Recherche sur l'Hétéro-Epitaxie et ses Applications (CRHEA), Centre National de la Recherche Scientifique (CNRS), Valbonne, France

†present address: Department of Electrical and Electronic Systems Engineering, Kyushu University, Fukuoka, Japan

Low-area density ZnO nanowire arrays, growing perpendicularly to the substrate, are synthesized with high-pressure pulsed-laser deposition. The introduction of a ZnO buffer layer enables us to fabricate individual nanowires several micrometers apart (area density < 0.1 nanowire/$\mu m^2$), suppressing any shadowing effect by neighbouring nanowires during subsequent growth. In order to reduce the nanowires area density, a combination of low- and high-pressure PLD growth methods were employed for growing a ZnO buffer layer and the ZnO core nanowires (Fig. 8.4a), respectively. These low density ZnO nanowires, whose *c*-axis is perpendicular to the substrate surface,

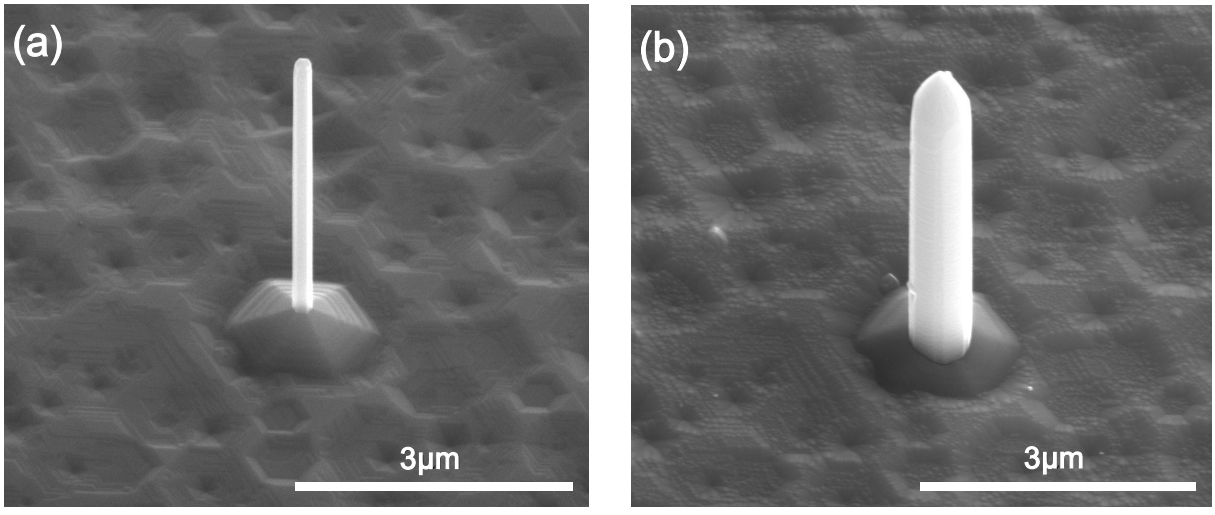


**Figure 8.4:** SEM images (recorded at a 45° tilt angle) of exactly the same nanowire after the core (**a**) and shell (**b**) growths.

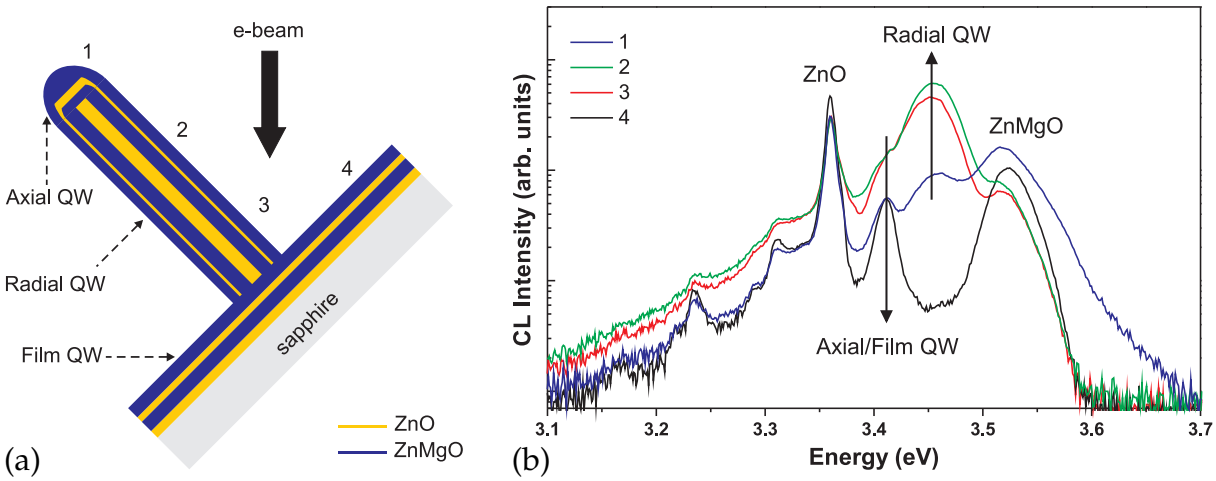


**Figure 8.5:** Schematic diagram of a single ZnO/ZnMgO QW wire as oriented in the CL cryostat (**a**). CL spectra ($T$ = 10 K, $U$ = 15 kV, $I$ = 150 pA) (**b**) measured at the locations indicated in (**a**).

are then used as templates to grow ZnO/ZnMgO core-shell nanowires heterostructures with conventional low-pressure pulsed-laser deposition (Fig. 8.4b and Fig. 8.5). Cathodoluminescence measurements (Fig. 8.5) as well as transmission electron microscopy show that a sharp interface forms between the ZnO core and the ZnMgO shell. Based on these findings, we have grown a series of radial ZnO/ZnMgO quantum wells with different thicknesses that exhibit quantum confinement effects, with thicker quantum wells emitting at lower energies. Spatially resolved cathodoluminescence confirms the homogeneity of the quantum well structure along the full nanowire length of about 3 μm.

This work was supported by the EU within NANDOS and by the Alexander von Humboldt Foundation.

## 8.6 Strong Indications for *p*-Type Conductivity of ZnO:P Nanowires

B.Q. Cao*, M. Lorenz, G. Zimmermann, M. Grundmann

*present address: Department of Electrical and Electronic Systems Engineering, Kyushu University, Fukuoka, Japan

The reproducible growth of *p*-type conducting ZnO with high structural quality and acceptable stability over time is still a challenge of the current ZnO research. There are numerous reports on *p*-type conductivity of heteroepitaxial ZnO thin films doped with potential acceptor elements as for example nitrogen, phosphorous, arsenic, or antimony. In most publications, the reproducibility and stability of *p*-type conductivity is not mentioned and it was often found that the *p*-type conductivity of these ZnO thin films reversed to *n*-type after few days or weeks. Therefore, supported by the recent advances of ZnO nanowire growth, *p*-type doping of ZnO nano- and microwires became an interesting issue. Because of the 1D growth mode of nanowires perpendicular to a substrate surface, strain effects are expected to be minimized for nanowires

in comparison to hetero- or homoepitaxial thin films. We have found three independent indications for reproducible and about one-year stable *p*-type conductivity of phosphorous-doped ZnO (ZnO:P) wires: (1) Low-temperature cathodoluminescence of single ZnO:P nanowires exhibits phosphorus-acceptor-related peaks: ($A^0$,X), (e,$A^0$), and DAP [1], (2) bottom-gate field-effect transistors (FET) using undoped (*n*-type) ZnO and ZnO:P wires showed opposite transfer characteristics [2], and (3) the rectifying *I*–*V* characteristics of the ZnO:P-nanowire / ZnO:Ga-film junctions [3].

We use both high-pressure pulsed-laser deposition (PLD) and carbothermal evaporation to grow ZnO-based nano- and microwires, respectively. By simply adding $P_2O_5$ into the source targets of both processes, phosphorous-doped ZnO nano- and microwires could be grown successfully. In cathodoluminescence (CL) spectra of single selected ZnO:P nano- and miocrowires, acceptor-related peaks ($A^0$,X), (e,$A^0$), and DAP were found. This peak assignment was further confirmed by temperature-dependent CL spectra and appropriate fits of the peak-energy shifts and by spatial CL maps individually extracted for selected peaks [1, 2]. Furthermore, undoped (naturally *n*-type) ZnO and ZnO:P microwires were used to built bottom-gate FETs and opposite transfer characteristics were found for undoped and P-doped wires [2]. As a third independent indication for a stable (within one year) *p*-type conductivity of the phosphorous-doped ZnO wires, we presented all-ZnO *p*–*n*-junctions defined by ZnO:P nanowire arrays grown on ZnO:Ga layers on sapphire substrates, as shown schematically in Fig. 8.6. The *p*–*n*-junctions were grown by two-step pulsed-laser deposition on *a*-plane sapphire substrates using a Ga-doped ZnO thin film as *n*-type conducting material. On top of these *n*-type films, phosphorous-doped ZnO nanowires were prepared by high-pressure PLD. Rectifying *I*–*V* curves with threshold voltage of about 3.2 V and a forward/reverse current ratio of 100 at ±3.5 V were measured reproducibly on these junctions, as shown in Fig. 8.7.

Because the time between the growth of the first *p*–*n*-junctions and the electrical measurements is now about one year, we can state a corresponding time stability of the ZnO junctions. In total about 20 junction samples were grown, from which about 10 showed the typical rectifying behaviour of Fig. 8.7. Finally, electroluminescence spectra could be accumulated with pulsed current excitation on selected junctions which showed a weak, diffuse blue-green emission.

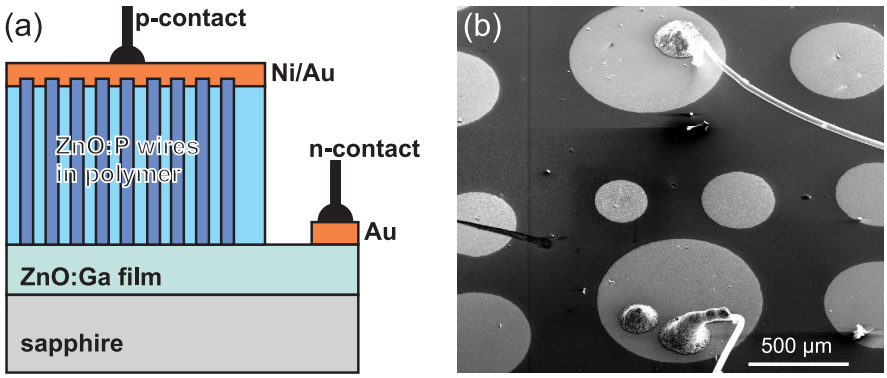


**Figure 8.6:** (**a**) Scheme of the ZnO:P / ZnO:Ga *p*–*n*-junctions including one *p*- and one *n*-contact. The SEM image (**b**) is a top view on the Ni–Au contact pads on top of the embedded ZnO:P nanowire array. The connection to the top contact is made with silver glue.

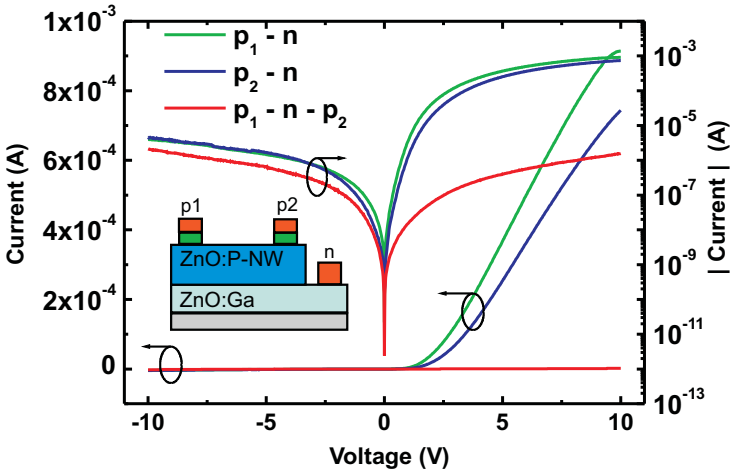


**Figure 8.7:** Rectifying *I–V* curves of two typical ZnO *p–n*-junctions on the same substrate, denoted $p_1$–$n$ and $p_2$–$n$, plotted in linear and logarithmic current scale. In addition, the *I–V* characteristics of these two *p*-contacts is shown, which corresponds to the $p_1$–$n$–$p_2$ configuration of two opposite *p–n* diodes. This curve is dominated by the leakage currents of the two diodes.

This work was supported by the EU within NANDOS and by the DFG within FOR 522.

[1] B.Q. Cao et al.: Nanotechnology **18**, 455 707 (2007), doi:10.1088/0957-4484/18/45/455707
[2] B.Q. Cao et al.: Phys. Stat. Sol. RRL **2**, 37 (2008), doi:10.1002/pssr.200701268
[3] M. Lorenz et al.: *Stable p-type ZnO:P nanowire / n-type ZnO:Ga film junctions, reproducibly grown by two-step pulsed laser deposition*, J. Vac. Sci. Technol. B (2009), in press

## 8.7 Photonic-Wire Resonators with Concentric Bragg Reflectors

R. Schmidt-Grund, H. Hilmer, J. Zúñiga-Pérez*, A. Hinkel, C. Sturm, C. Czekalla, G. Zimmermann, B. Rheinländer, M. Grundmann

*Centre de Recherche sur l'Hétéro-Epitaxie et ses Applications (CRHEA), Centre National de la Recherche Scientifique (CNRS), Valbonne, France

We demonstrate the possibility of the growth of lateral concentric Bragg reflectors (BR) on ZnO nano-pillars and show hints for such a resonator to be in the regime of strong exciton-photon coupling. Compared to the planar case, the reduction of the cavity mode volume in such pillar-resonators along with a simultaneously high quality factor of the resonator opens the opportunity for (i) the enhancement of the lateral confinement in classical pillar-resonators in order to increase the emission rates in the regime of weak exciton–photon coupling (Purcell effect), (ii) to enhance the exciton–polariton coupling strength in the strong-coupling regime, and (iii) to be used for 2D confinement in free-standing photonic wire resonators. Compared to 1D confinement, additional cavity modes occur due to the quantization of the cavity-photon *k*-vector in two dimensions, leading to a complex system of exciton-polaritons with multiple branches, which

are considered to provide much more efficient channels for the scattering of exciton-polaritons to their ground state in order to undergo Bose–Einstein condensation.

We use here free standing ZnO nano-pillars as cavity and active medium which are low-densely arranged on the substrate. This dilute arrangement is very important for the growth of the concentric BR as well as for the subsequent optical characterization. As BR materials we use YSZ (Yttrium stabilized $ZrO_2$) as high-index material and $Al_2O_3$ as low-index material. The nano-pillar resonators have been fabricated by pulsed-laser deposition (PLD) in three steps. First, a ZnO nucleation layer with a thickness of about 1 µm has been deposited by low-pressure PLD (oxygen background pressure $p(O_2)$ = 0.02 mbar) at temperatures of $T$ = 650 °C. This rough nucleation layer assures low density growth of nano-pillars in step two. In this second step, the ZnO nano-pillars are grown by a high-pressure PLD process ($p(O_2)$ = 100 mbar, $T$ = 750 °C, Fig. 8.8a). Nano-pillars with 5 – 10 µm in length and diameters of 50 – 800 nm have been obtained. In step three, the nano-pillars were coated with the YSZ/$Al_2O_3$ shell Bragg reflectors (8.5 pairs) by low pressure ($p(O_2)$ = 0.002 mbar), low-temperature ($T$ = 150 °C) oblique-incidence PLD (OIPLD). The use of such low temperatures is mandatory in order to obtain amorphous Bragg reflector materials. In the OIPLD process, the direction of the plasma flow is tilted by 30° with respect to the pillar axis and the sample rotates with 1.5 rpm with the rotation axis parallel to the pillar axis (Fig. 8.8b). Thus, a very homogeneous coating of the nano-pillars with concentric Bragg reflectors with well defined layer thickness has been reached in the lateral, in the azimuthal, as well as in the longitudinal direction (Fig. 8.9).

In order to investigate the structure of the lateral optical modes of the ZnO nano-pillar resonators, we have cleaved the sample in such a manner, that some of the pillars are located directly at the breakline. This enables us to focus a probe light beam with a microscope setup on the lateral surface of the pillar resonators. As probe,

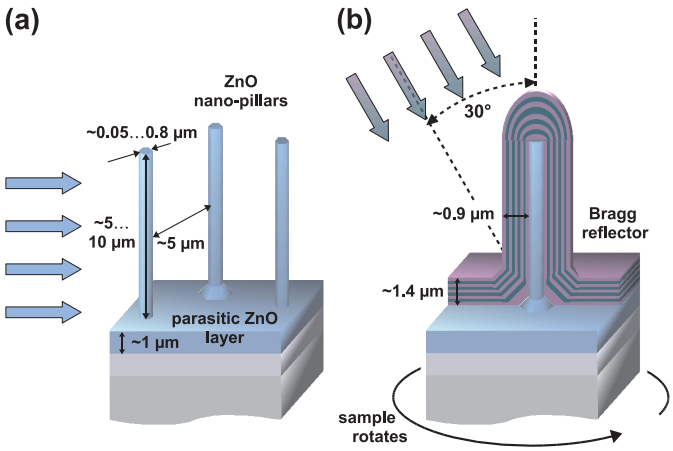


**Figure 8.8:** Fabrication principles of the ZnO nano-pillar resonators. Steps two and three are shown in the parts (**a**) and (**b**), respectively. In each part, the arrows indicate the direction of the PLD plasma flow.

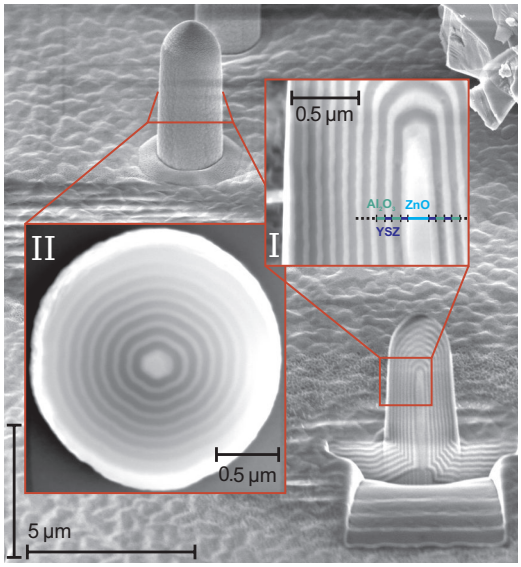


**Figure 8.9:** SEM images of coated ZnO nano-pillars. *Insets I* and *II* present an enlarged section of a longitudinal cut pillar and a cross-section cut, respectively.

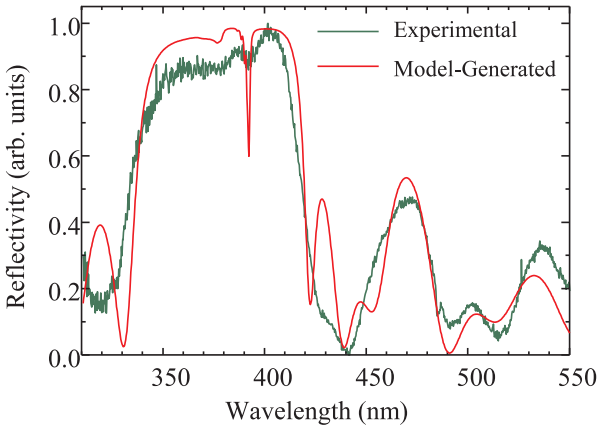


**Figure 8.10:** Reflectivity of a lateral surface of a ZnO nano-pillar resonator ($d \sim 250$ nm) with concentric Bragg reflectors. The dips at 375 nm and 390 nm correspond to resonator modes.

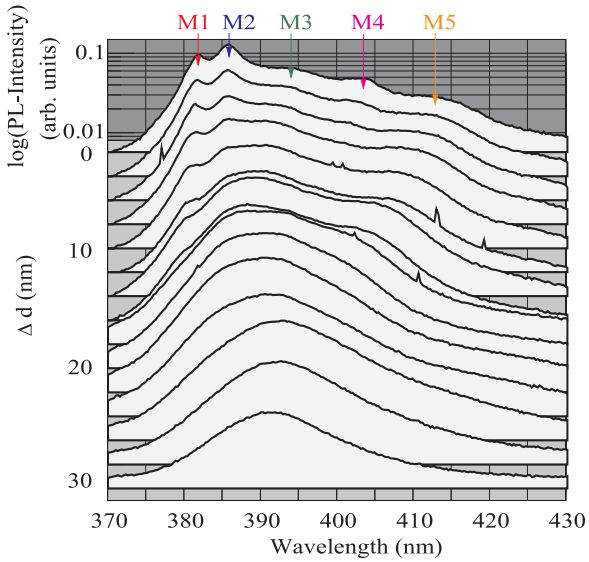


**Figure 8.11:** Experimental PL spectra of a resonator ($d \sim 300$ nm) as a function $\Delta d$ during the lateral PL-scan. The most prominent resonator modes are indicated by arrows.

we use a laser beam with a spot diameter of 1 µm for spatially resolved photoluminescence (PL) investigations and a white-light beam with a spot diameter of 4 µm for spatially resolved reflection measurements. In Fig. 8.10, spectra of the reflectivity taken from a lateral surface of a coated pillar are shown together with preliminary model calculations for the case of 1D confinement. The Bragg stop-band can be recognized clearly along with several resonator modes. Please note, by using such a 1D model we can reproduce the layer thicknesses of the BR very well but cannot obtain quantitatively correct values the thickness of the cavity. Fig. 8.11 shows spectra of the PL for different positions at the lateral surface of a pillar-resonator. As the ZnO pillars changes their diameter $d$ as a function of the longitudinal position ($\Delta d/d \sim 10\,\%$), the energetic position of the cavity modes could be varied in this manner and therewith the detuning between the cavity and exciton modes. From the thickness dependence of the observed modes we have found strong hints for the resonator to be in the strong-coupling regime, which is a subject for further investigations.

This work was supported by the DFG within FOR 522.

## 8.8 ZnO-Based Metal–Semiconductor Field-Effect Transistors with Ag-, Pt-, Pd-, and Au-Schottky Gates

H. Frenzel, A. Lajn, M. Brandt, H. von Wenckstern, G. Biehne, H. Hochmuth, M. Grundmann

Metal-semiconductor field-effect transistors (MESFETs) were fabricated by reactive dc sputtering of either Ag, Pt, Pd, and Au as Schottky gate contacts on ZnO thin

**Table 8.1:** Overview of the measured sample properties at room temperature.

| Sample MESFET | $d$ [nm] | $n$ [$cm^{-3}$] | $\mu_{Hall}$ [$cm^2/Vs$] | $\mu_{ch}$ [$cm^2/Vs$] | $g_{max}$ [S/cm] | on/off ratio | max. slope [mV/dec] |
|---|---|---|---|---|---|---|---|
| Ag | 20 | $2.8\times10^{18}$ | 9.3 | 6.3 | 37.5 | $1.2\times10^{8}$ | 81 |
| Pt | 26 | $2.4\times10^{18}$ | 12.1 | 11.4 | 46.9 | $4.5\times10^{6}$ | 83 |
| Pd | 26 | $2.4\times10^{18}$ | 12.1 | 12.8 | 52.7 | $2.6\times10^{5}$ | 156 |
| Au | 20 | $1.5\times10^{18}$ | 43.9 | 23.9 | 61.3 | $1.6\times10^{3}$ | 282 |

films grown by pulsed-laser deposition on *a*-plane sapphire substrates. Three samples with nominally equal channel thickness and doping concentration were prepared. Two of them were used to process MESFETs with Ag- and Au-gates, respectively. On the third layer, MESFETs wit Pt- and Pd-gates were fabricated. The oxygen partial pressure was kept between 0.02 mbar and 0.04 mbar; the growth temperature was 620 °C. The channel thickness as well as an overview of measured electrical parameters at room temperature is given in Tab. 8.1. All four gate metals were deposited by reactive dc-sputtering as described in [1]. Non-reactively dc-sputtered Au was used as ohmic source/drain contacts and the capping layer on the gate.

*I–V* measurements were performed between 25 °C and 150 °C in order to test figures of merit and reliability of the MESFETs. A comparison of room-temperature transfer characteristics at source–drain voltage $V_{SD} = 2\,V$ is shown in Fig. 8.12. All MESFETs show a strong field effect. The Ag-MESFET has the highest on/off-ratio of $1.2\times10^8$ with very low off-current in the sub-picoampere range applying an off-gate-voltage of only $V_G = -1.4\,V$. The Pt-, Pd-, and Au-MESFETs exhibit larger leakage currents, which increase the off current. Nevertheless, for Pt, the on/off-ratio is still $4.5\times10^6$, whereas it is only $2.6\times10^5$ for Pd and $1.6\times10^3$ for Au. The off-gate-voltages of the devices with Pt, Pd, and Au are smaller than for the Ag-sample reflecting the higher off-currents. The differences in the characteristics can be explained by slightly different channel thicknesses and the different Schottky contacts barrier heights and built-in potentials resulting in a different depletion layer depth.

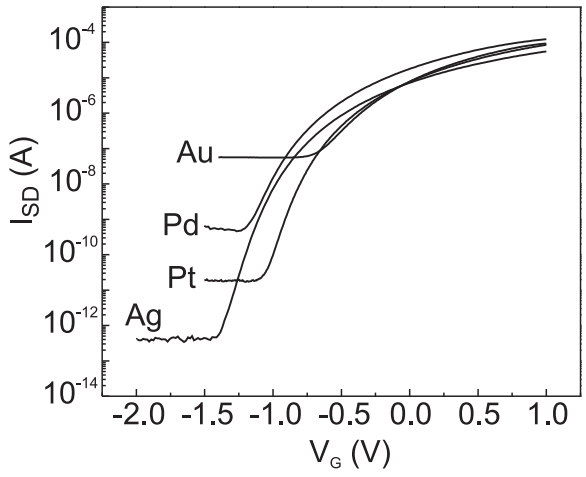


**Figure 8.12:** *I–V* transfer characteristics of MESFETs with Ag-, Pt-, Pd and Au-Schottky-gate contacts at room temperature.

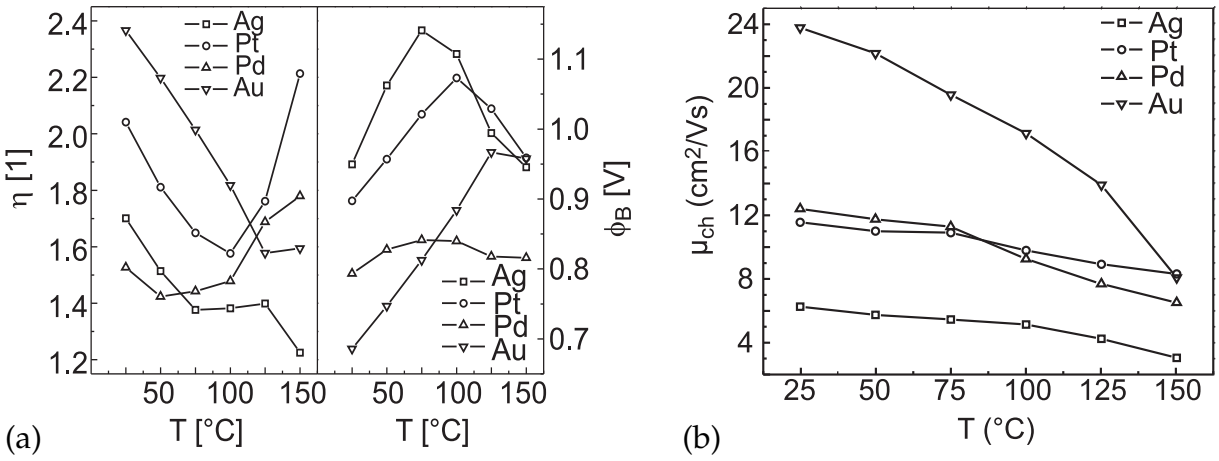


**Figure 8.13:** (**a**) Ideality factor (*left*) and Schottky barrier height (*right*), and (**b**) channel mobility of Ag, Pt, Pd, and Au Schottky-gate MESFETs at elevated temperatures.

Figure 8.13a,b depicts Schottky barrier heights $\Phi_B$ and ideality factors $\eta$ of the Schottky-gate contacts at elevated temperatures. Ag, Pt, and Au show similar behavior, in contrast to Pd. For the Pd Schottky contact, $\eta$ is increasing with increasing temperature while $\Phi_B$ stays constant at values around 0.82 V. For the MESFETs with Ag, Pt, and Au, an annealing effect was observed. Until 100 °C (for Au until 125 °C), $\eta$ is decreasing, whereas $\Phi_B$ is increasing up to maximum values of 1.14 for Ag, 1.07 for Pt, and 0.97 for Au. A further increase in temperature leads to irreversible degradation of the Schottky contacts and the ideality factors are increasing while the Schottky barrier heights are decreasing again.

Figure 8.13c shows the temperature dependence of the Ag-, Pt-, Pd-, and Au-MESFET's channel mobilities $\mu_{ch}$. All samples show a monotonic decrease in $\mu_{ch}$ with increasing temperature due to increasing optical phonon scattering. However, a change in slope is observed in the curves of Ag, Pt, and Pd at certain temperatures. For Pt- and Pd-gated devices, the slope increases at 75 °C. It is steeper for the Pd-sample indicating a faster degradation of the MESFET. For Ag, the slope increases not until 100 °C yielding into a similar slope as for the Pt sample. This indicates that the Pd- and Pt-MESFETs are stable until 75 °C, whereas Ag-MESFETs are stable until 100 °C. For Au, no particular slope change, but a smooth increase of the slope is observed. The apparent channel mobility of Au degrades more drastically as compared to Ag, Pt, and Pd.

Although, the Ag-MESFET has the smallest channel mobility in this study, the electrical properties such as ideality factor, Schottky barrier height, on/off-ratio, and off-current are the best. Despite the higher leakage current, Pt is similar to Ag. The lower Schottky barrier and higher leakage currents disqualify Pd and Au for the use in high-quality MESFETs. However, the reactively sputtered Au Schottky contacts on ZnO are close to the best reported in literature [2].

[1] H. Frenzel et al.: Appl. Phys. Lett. **92**, 192 108 (2008), doi:10.1063/1.2926684
[2] C.A. Mead et al.: Phys. Lett. **18**, 218 (1965), doi:10.1016/0031-9163(65)90295-7

## 8.9 Electrical Properties of Reactively Sputtered Ag, Au, Pd, and Pt Schottky Contacts on n-type ZnO Thin Films

A. Lajn, H. von Wenckstern, Z. Zhang, C. Czekalla, G. Biehne, J. Lenzner, H. Hochmuth, M. Lorenz, M. Grundmann, S. Wickert* C. Vogt,* R. Denecke*

*Wilhelm-Ostwald-Institut für Physikalische und Theoretische Chemie, Universität Leipzig

We fabricated highly rectifying Ag, Au, Pd and Pt Schottky contacts (SC) on heteroepitaxial ZnO thin films by reactive sputtering in an argon/oxygen-atmosphere. This method of contact fabrication had been introduced by Allen et al. [1] for high quality AgO-SCs on ZnO single crystals. SCs permit the characterization of defects by space-charge spectroscopy and the fabrication of devices, e.g. field-effect transistors [2].

The zinc oxide thin film was grown on a 2 inch diameter *a*-plane sapphire wafer by pulsed-laser deposition (PLD) at 710 °C in an oxygen partial pressure of 0.02 mbar. The first layer of the SCs was deposited by reactive sputtering of the respective metal in an $O_2$/Ar-atmosphere. Subsequently, a metallic capping layer was sputtered in pure argon using the same metal.

X-ray photoelectron spectroscopy (XPS) was performed to determine the degree of oxidation of the reactively sputtered contact materials. The spectra recorded for the gold film reveal only electrons with binding energies attributed to elementary gold. Oxygen-containing species were not detected. Consequently, the gold film is metallic and not oxidized. For the Ag, Pd and Pt films emission of electrons from oxygen core levels is detected. As zinc-related electrons were not measured, also O related electrons from ZnO would be beyond the escape depth and thus, the oxygen stems from the contact material.

Photocurrent measurements revealed the necessity to cover the oxidic contact material with a conducting capping layer to form an equipotential surface. This can be explained by the low conductivity of the oxidic contact material. Strong fluctuations of the photocurrent signal among the contact area were not found, indicating the homogenous contact formation.

To characterize the electrical properties of the SCs current–voltage ($I$–$V$) and capacitance–voltage measurements ($C$–$V$) and temperature-dependent $I$–$V$ measurements ($I$–$V$–$T$) were carried out.

Highly rectifying SCs were fabricated with all four metals (see Fig. 8.14). The current transport in these diodes can be well described by thermionic emission. This model involves the series and parallel resistance of the diode, $R_S$ and $R_P$, respectively, the effective barrier height $\Phi_{eff}$ and the voltage dependence of the barrier by the ideality factor $n$. By fitting the forward $IV$ characteristics the SC parameters were extracted at room temperature (see Tab. 8.2). All SCs show ideality factors $n < 1.6$ and effective barriers $> 0.65$ eV. The low measured effective barrier heights, compared to the Schottky–Mott model, are attributed to lateral variations of the barrier height [3]. This was modeled assuming a Gaussian distribution of the barrier heights with a voltage-dependent mean barrier height $\Phi_{B,m}(V) = \Phi_{B,m}(0\,V) + \rho_2 V$ and a voltage-dependent standard deviation $\sigma^2(V) = \sigma^2(0\,V) + \rho_3 V$. Since current flows preferentially over the lower barrier paths,

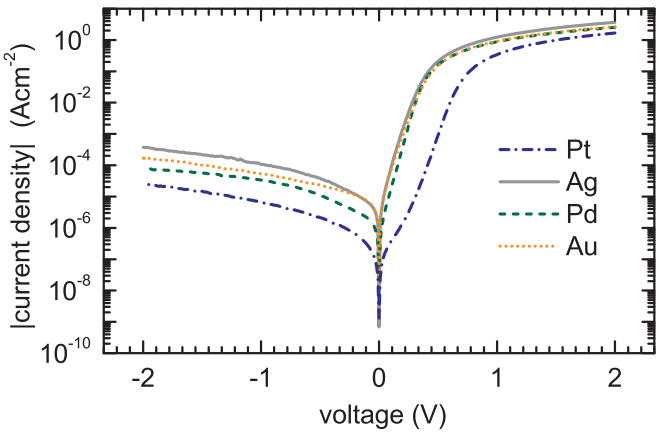


**Figure 8.14:** Current–voltage characteristics of the best SCs on ZnO.

**Table 8.2:** Parameters of the best Ag, Au, Pd and Pt contacts, determined by *I–V*, *C–V* and *I–V–T*.

| | *I–V* | | *C–V* | | *I–V–T* | | | |
|---|---|---|---|---|---|---|---|---|
| contact material | $\Phi_{\mathrm{eff}}$ [eV] | $n$ | $\Phi_{\mathrm{m}}$ [eV] | $\sigma$ [eV] | $\Phi_{\mathrm{m}}$ [eV] | $\sigma$ [eV] | $\rho_2$ | $\rho_3$ [eV] |
| Pt | 0.84 | 1.59 | 1.34 | 0.16 | 1.27 | 0.14 | −0.13 | −0.021 |
| Au | 0.69 | 1.36 | 1.22 | 0.16 | 0.96 | 0.14 | 0.06 | −0.014 |
| Ag | 0.66 | 1.57 | 1.35 | 0.19 | 1.04 | 0.14 | −0.33 | −0.029 |
| Pd | 0.73 | 1.25 | 1.20 | 0.15 | 1.23 | 0.15 | −0.29 | −0.027 |

the *e*ffective barrier height determined by *I–V* at finite temperature is smaller than the *m*ean barrier height.

The *C–V* mean barriers heights range for all metals between 1.2 and 1.35 eV (see Tab. 8.2). Using the previously measured mean and effective barrier heights, the standard deviation was calculated (Tab. 8.2, column 4). In order to compare the standard deviations and the mean barrier heights, temperature-dependent *I–V* measurements were carried out. $\Phi_{\mathrm{B,m}}$ and $\sigma$ were again calculated this time using the Gaussian barrier model, employing the effective barrier heights extracted from the *I–V* characteristics for each temperature. Additionally the voltage dependency of the distribution parameters $\Phi_{\mathrm{B,m}}$ and $\sigma$ was calculated. The model adequately describes the measured data between 320 and 200 K. For lower temperatures possibly a second, lower barrier, tunnelling or trap-assisted tunnelling should be considered.

For Pt and Pd the mean barrier heights determined by *C–V* and *I–V–T* are approximately equal. The *C–V* mean barrier height for Pd of 1.20 eV accords despite of the metal oxidation well with resistively evaporated Pd-SCs being purely metallic [3]. The mean barrier height for Pt is according to the Schottky–Mott model expected to have the observed value. Please note, that the Schottky Mott model considers an ideal metal in contact with a semiconductor.

In case of gold and silver the *C–V* mean barrier height is significantly higher, than the *I–V–T* value. For gold SCs, smaller values of 0.6 − 0.7 eV, which are close to our previously measured effective barrier, are commonly reported. Schottky–Mott theory predicts significantly higher barrier heights, as our *C–V* and *I–V–T* also reveal. For silver oxide SCs mean barrier heights of 1.2 eV in maximum are reported on high quality single

crystals [1]. Thus, the $C$–$V$ measurement might overestimate the barrier height due to charging effects of the oxidic contact material, as the $I$–$V$–$T$ value of 1.04 eV compared to the $C$–$V$ value of $\Phi_{B,m} = 1.35$ eV indicates. The voltage coefficients $\rho_2$ of the mean barrier height are negative except for gold, but vary significantly in magnitude. The values of $\rho_3$ vary between −14 meV and −29 meV for all SCs, which is in accordance to the value reported for metallic Pd SCs [3]. As $\rho_3$ is negative, the Gaussian distribution narrows with increasing bias, such that the barrier height distribution becomes more homogeneous.

This work was supported by the DFG within SFB 762.

[1] M. Allen et al.: Appl. Phys. Lett. **91**, 053 512 (2007), doi:10.1063/1.2768028
[2] H. Frenzel et al.: Appl. Phys. Lett. **92**, 192 108 (2008), doi:10.1063/1.2926684
[3] H. von Wenckstern et al.: Appl. Phys. Lett. **88**, 092 102 (2006), doi:10.1063/1.2180445

## 8.10 Interface Effects in ZnO Metal–Insulator–Semiconductor and Metal–Semiconductor Structures

H. Frenzel, H. von Wenckstern, A. Lajn, M. Brandt, G. Biehne, H. Hochmuth, M. Lorenz, M. Grundmann

ZnO metal–insulator–semiconductor (MIS) and metal–semiconductor (MES) field-effect transistors were fabricated by pulsed-laser deposition to study the influence of interface scattering on the lateral electronic transport. Channel mobilities were increased by successive elimination of electron-scattering mechanisms by means of different ZnO transistor types: heteroepitaxial MISFET, MESFET and high-electron-mobility transistor (HEMT) on *a*-plane sapphire substrate as well as homoepitaxial MESFET on ZnO substrate.

The three heteroepitaxial FETs were grown under an oxygen partial pressure of 0 002mbar and a growth temperature of 650 °C on *a*-plane sapphire substrate. For the heteroepitaxial MISFET, the ZnO channel thickness was 500 nm. An $Al_2O_3/HfO_2/Al_2O_3$ sandwich structure was used as insulating top-gate oxide to suppress gate leakage current [1]. The thicknesses were 50 nm for $Al_2O_3$ and 40 nm for $HfO_2$, respectively. The source, drain and gate contacts were structured using photolithography, lift-off processes and thermal evaporation of Ti/Au. The heteroepitaxial MESFET had a channel thickness of 20 nm. The Schottky-gate contact was reactively DC-sputtered using Ag as reported in [2] and covered by an Au capping layer which was also used for the source and drain contacts. The channel of the heteroepitaxial HEMT consited of a $Zn_{0.9}Mg_{0.1}O/ZnO/Zn_{0.9}Mg_{0.1}O$ single quantum well (QW) heterostructure with a QW thickness of 5 nm and a barrier thickness of 100 nm. The barrier was doped with 0.5 % Ga to provide free charge carriers for the transport. As a fourth type of samples, a homoepitaxial MESFET was grown on ZnO substrate, which was pre-treated as described in [3]. The 65 nm thick ZnO-channel was doped with 0.01 % P and grown at $3 \times 10^{-4}$ mbar and 730 °C. The contacts for the latter two FETs were fabricated as for the heteroepiaxial MESFET.

Figure 8.15a shows the transfer characteristic and channel mobility of a normally-on top-gate MISFET with an on-off-ratio of $\sim 10^5$. The leakage current is below $10^{-10}$ A due to the high conduction band offset between ZnO and $Al_2O_3$ and the use of a sandwich structure which introduces additional interfaces to interrupt current paths within

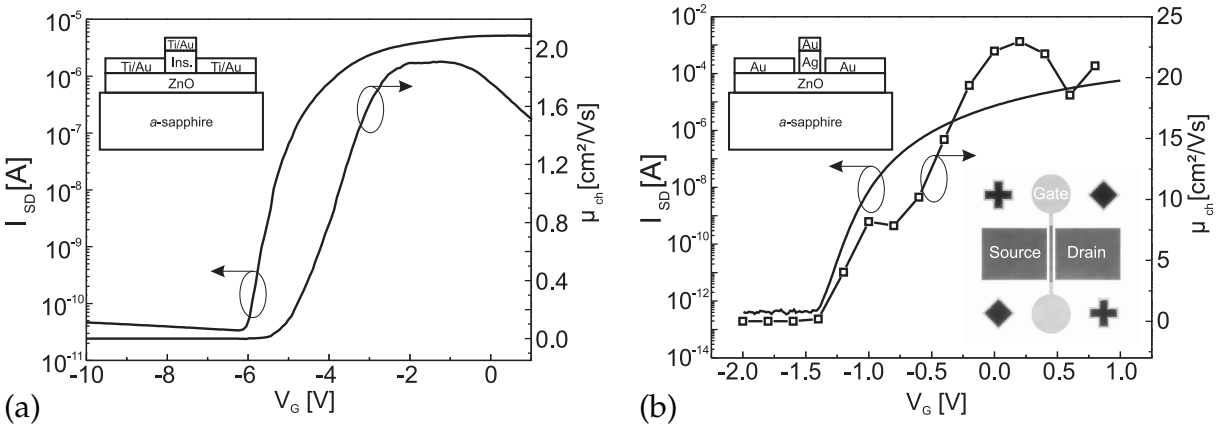


**Figure 8.15:** Transfer characteristic and channel mobility of a heteroepitaxial MISFET (**a**) and MESFET (**b**) [2].

the insulator. The maximum slope in the transfer characteristic is 300 mV/dec. However, the maximum channel mobility calculated as in [4] is only 1.9 $cm^2$/Vs, which is about a factor of 10 lower than the Hall mobility. This is due to electron scattering at $ZnO/Al_2O_3$-interface states. The interface-trapped charge-density was measured by admittance spectroscopy to be in the range of $10^{12}\,eV^{-1}cm^{-2}$.

The scattering at surfaces is eliminated in the heteroepitaxial MESFET (Fig. 8.15b) since the electrons are kept away from the surface by the depletion layer of the Ag-Schottky contact [2, 5]. This leads to an average channel mobility of 11 $cm^2$/Vs which equals the Hall mobility. The maximum channel mobility is 23 $cm^2$/Vs as depicted in Fig. 8.15b. An on-off ratio of $\sim 10^8$ with a very low leakage current $< 10^{-12}$ A and a maximum slope of only 100 mV/dec could be achieved.

A further increase of the mobility can be achieved using a 2D electron gas (2DEG) in a ZnMgO/ZnO/ZnMgO-QW heterostructure. As can be seen in the inset of Fig. 8.16, charging of the QW has been observed by current–voltage ($I$–$V$) measurements around

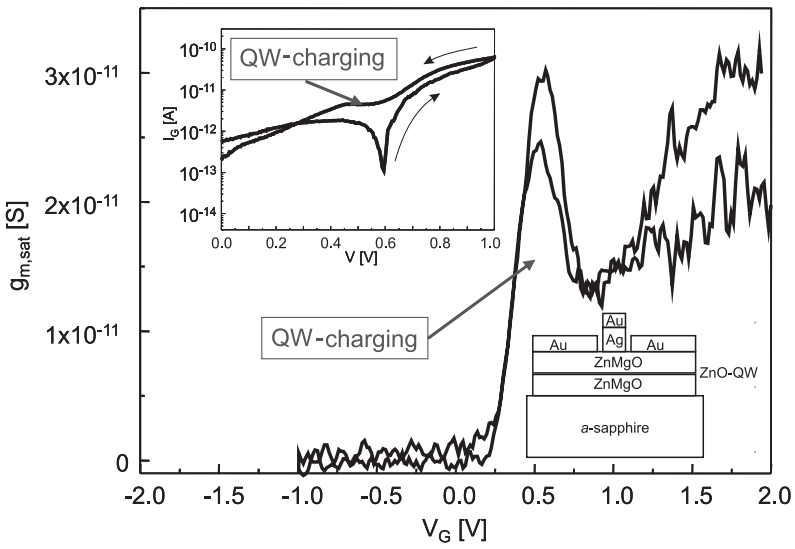


**Figure 8.16:** Forward transconductance of a heteroepitaxial HEMT. *Inset*: $I$–$V$ measurement of the gate Schottky contact.

0.5 V. At the same voltage, the forward transconductance of the HEMT reveals a sharp increase which is directly proportional to the channel mobility. However, the source–drain current is rather small due to low carrier injection through the ZnMgO:Ga barrier.

In order to reduce scattering at grain boundaries and interfaces of structural defects, a homoepitaxial MESFET has been investigated. Atomic force microscopy showed a 2D growth of the channel layer with $c/2$-steps and less grain boundaries as compared to heteroepitaxy. The dislocation density is given by the substrate and lies in the range of $10^5$ cm$^{-2}$. From temperature-dependent Hall experiments the room-temperature mobility is obtained as 150 cm$^2$/Vs and can be fitted (not shown) without grain boundary scattering. However, from $I$–$V$ measurements on the MESFET, a channel mobility of only 50 cm$^2$/Vs could be determined. Possibly, a current through the substrate causes the lower mobility and an overestimation of the net doping concentration.

This work was supported by the DFG within SFB 762.

[1] S. Chang et al.: Appl. Phys. Lett. **92**, 192 104 (2008), doi:10.1063/1.2924769
[2] H. Frenzel et al.: Appl. Phys. Lett. **92**, 192 108 (2008), doi:10.1063/1.2926684
[3] H. von Wenckstern et al.: Phys. Stat. Sol. RLL **1**, 129 (2007), doi:10.1002/pssr.200701052
[4] R.L. Hoffman: J. Appl. Phys. **95**, 5813 (2004), doi:DOI:10.1063/1.1712015
[5] B. van Zeghbroeck: ece-www.colorado.edu/ bart/book/book/index.html

## 8.11 Defects in Zinc Implanted ZnO

M. Schmidt, M. Ellguth, H. von Wenckstern, R. Pickenhain, M. Grundmann, G. Brauer*

*Institute of Ion Beam Physics and Materials Research, Forschungszentrum Dresden-Rossendorf, Dresden, Germany

Undoped ZnO is n-type conducting due to low formation energies of donor-like defects under either zinc- or oxygen-rich conditions [1]. In this study intrinsic defects were created by the implantation of high energy (250 keV) zinc ions into a ZnO thin film. The defect studies were carried out by the capacitance spectroscopic methods thermal admittance spectroscopy (TAS) and deep level transient spectroscopy (DLTS). A comparison between the defects found in an as-grown reference sample and those in the Zn-implanted and thermally annealed one gives a hint to intrinsic defects, that are stable or preferentially formed under zinc rich conditions.

On a 2-inch sapphire substrate the ZnO thin film was deposited by pulsed-laser deposition (PLD). The sample was then divided into parts acting as implanted and reference specimen. After the ion implantation, the sample was thermally annealed in oxygen atmosphere at approx. 970 K for 45 min. The Schottky contacts, essential for capacitance spectroscopy, were realised by resistively evaporated palladium.

By TAS and DLTS three traps have been observed (Tab. 8.3), a shallow donor T1, in literature attributed to the interstitial zinc [2], the (in ZnO almost omnipresent) deep level E3 [3], and the deep level T2 [4]. The concentrations of T1 and T2 were increased in the zinc implanted and annealed sample. Since an increase of zinc interstitials by the implantation of zinc ions into ZnO can be expected, the increase of T1 supports its suggested attribution to the zinc interstitial. Using DLTS with different reverse voltages

**Table 8.3:** Binding energie $E_d$ and electron capture cross-section $\sigma_n^{th}$ of the investigated traps obtained from Arrhenius analysis.

| sample | $E_d$ [meV] | $\sigma_n^{th}$ [$10^{-16}$ cm$^2$] |
|---|---|---|
| T1 | 30 ± 7 | 1500 |
| T2 | 190 ± 15 | 1 |
| E3 | 300 ± 10 | 2 |

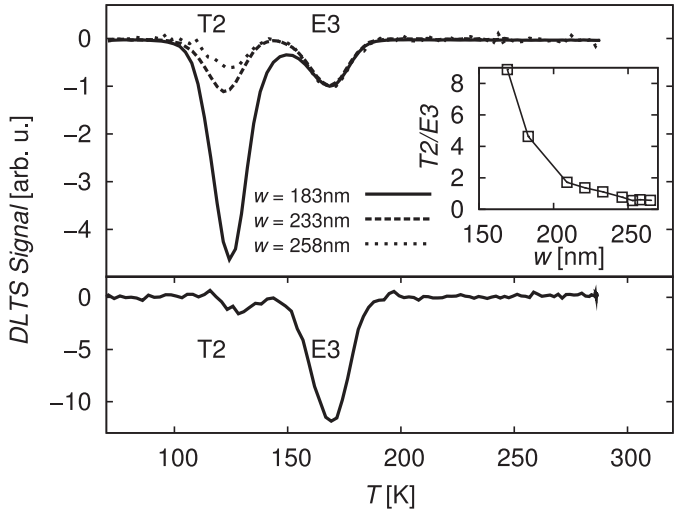


**Figure 8.17:** DLTS spectra of the as-grown (*bottom*) and the zinc implanted and annealed sample (*top*). Using different reverse voltages for the DLTS measurements, a spatial dependence of the T2/E3 ratio, which roughly follows the calculated profile of the implanted zinc ions, was measured.

and therefore different space charge region widths $w$, a spatially varying concentration of T2 was recorded in the implanted and annealed sample (Fig. 8.17). It roughly follows the calculated (SRIM) Zn ion distribution and is therefore a proof for the intrinsic nature of T2. Within the error bars of the DLTS experiment, the E3 concentration remained unchanged by the zinc implantation, which gives reason to assume E3 to be of extrinsic origin. More detailed information on these studies can be found in [4].

[1] A. Janotti, C.G. Van de Walle: J. Cryst. Growth **287**, 58 (2006), doi:10.1016/j.jcrysgro.2005.10.043
[2] J. Sann et al.: Phys. Rev. B **76**, 195 203 (2007), doi:10.1103/PhysRevB.76.195203
[3] F.D. Auret et al.: Superlat. Microstruct. **39**, 17 (2006), doi:10.1016/j.spmi.2005.08.021
[4] M. Schmidt et al.: *Defects in Zinc implanted ZnO thin films*, J. Vac. Sci. Technol. B (2009), in press

## 8.12 Defect Characterisation by Optical Deep Level Transient Spectroscopy in ZnO

M. Ellguth, M. Schmidt, H. von Wenckstern, R. Pickenhain, M. Grundmann

We conducted optical deep level transient spectroscopy (ODLTS) experiments on ZnO thin films with evaporated Pd Schottky contacts. These are designed to calculate photo

**Table 8.4:** Signatures and references as well as thermal emission rates at $T_R$ = 300 K of deep levels detected in the samples by DLTS.

| deep level | $E_c - E_t$ [meV] | $\sigma_{n,app}$ [cm$^2$] | $e_n^{th}(T_R)$ [s$^{-1}$] | ref. |
|---|---|---|---|---|
| X1 | 239 | $5.1\times10^{-10}$ | $3.90\times10^{12}$ | – |
| X2 | 229 | $7.1\times10^{-15}$ | $8.00\times10^{7}$ | – |
| E3 | 293 | $4.0\times10^{-16}$ | $3.78\times10^{5}$ | [1] |
| E4 | 555 | $7.9\times10^{-13}$ | $2.96\times10^{4}$ | [1] |
| T3 | 626 | $9.6\times10^{-15}$ | $2.31\times10^{1}$ | [2] |
| T2 | 194 | $1.0\times10^{-16}$ | $4.36\times10^{6}$ | [3] |

cross-section spectra of particular deep levels detected in thermal DLTS. The photo cross-section $\sigma^o_{n,p}$ is a measure of the probability of optically excited electron transitions from the occupied deep level into the conduction band ($\sigma^o_n$) or from the valence band onto the empty defect ($\sigma^o_p$). It depends on the optical transition matrix element between the wave functions of the defect and the involved energy band, as well as on the density of states of that energy band and electron-lattice coupling due to local modes of the defect. Experimentally, they can be determined via the optical emission rate $e^o_{n,p}(h\nu) = \Phi(h\nu)\,\sigma^o_{n,p}(h\nu)$, where $\Phi$ is the photon flux. The $e^o_n$ was determined from the DLTS signal recorded at a fixed temperature and simultaneous monochromatic illumination of the sample through the semitransparent Schottky contact. The deep levels found in two samples by thermal DLTS are listed in Tab. 8.4. Strong response to the illumination was found for the defects X1, X2, E4 and T2. The E3 level was not observed to emit electrons under optical excitation and has been estimated to have a photo cross section at least 4 orders of magnitude smaller than E4. The X1 and X2 levels were not suited for investigation by ODLTS due to the shallow energetic position or an insufficient concentration. The T3 level exhibited a notably weaker optical response than E4 but has to be investigated further. For the E4 and T2 level the photo cross-sections are depicted in Fig. 8.18. Both photo cross-section spectra show an exponential decay towards the low energy limit of the measurement. For a comparison of the optical threshold energy with the energetical distance of the deep level to the conduction band

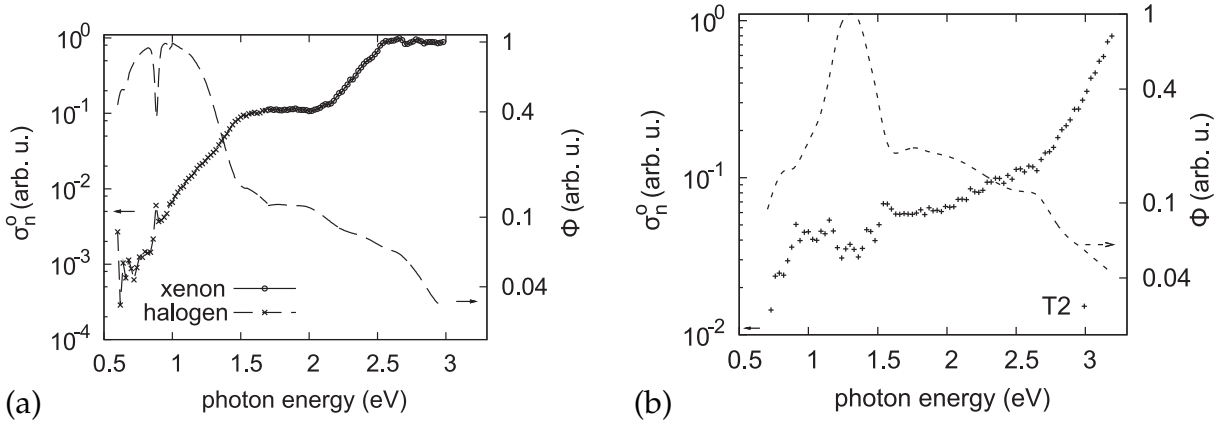


**Figure 8.18:** (**a**) Photo cross-section of E4 in relative units determined from two experiments using either a halogen or xenon lamp (*dashed line*: lamp spectrum). (**b**) Photo cross-section of T2.

edge, the lower photon energies have to be investigated in more detail. Thereby, the lattice distortion in the vicinity of the defect can be judged. In case of E4, the present results already point to a weak lattice distortion.

This work was supported by the DFG within SPP 1136.

[1] F.D. Auret et al.: Appl. Phys. Lett. **80**, 1340 (2002), doi:10.1063/1.1452781
[2] A.Y. Polyakov et al.: Appl. Phys. Lett. **83**, 1575 (2003), doi:1.1604173
[3] M. Schmidt et al.: *Defects in Zinc implanted ZnO thin films*, J. Vac. Sci. Technol. B (2009), in press

## 8.13 Ag-Related Defect State in ZnO Thin Films

H. von Wenckstern, A. Lajn, A. Laufer*, B.K. Meyer*, H. Hochmuth, M. Lorenz, M. Grundmann

*I. Physikalisches Institut, Justus-Liebig-Universität Gießen

Recently, the $\epsilon(0/-1)$ transition energy of $Ag_{Zn}$ was calculated using density functional theory with local density approximation to be 0.4 eV above the valence band maximum [1] contradicting older experimental results attributing a very deep level situated 0.23 eV below the conduction band minimum to $Ag_{Zn}$ [2] similar to the situation for $Cu_{Zn}$ [3].

We investigated the properties of $AgO_x$/ZnO Schottky diodes. The *c*-axis oriented ZnO thin films were grown by pulsed-laser deposition on *a*-plane sapphire substrates. The Schottky contacts were realized by reactive sputtering of Ag [4] onto the sample surface.

Thermal admittance spectroscopy (TAS) was carried out between 10 and 330 K under zero bias applying frequencies between 1 kHz and 5 MHz. Figure 8.19a depicts the capacitance $C$ and the conductance normalized by the frequency $G/\omega$ for $\omega = 1.1\times10^6\,s^{-1}$. Four defect levels (E30, E65, E100, E300) with thermal activation energies of 30, 65, 100 and 300 meV, respectively, are recognizable by the steps of $C(T)$ or the

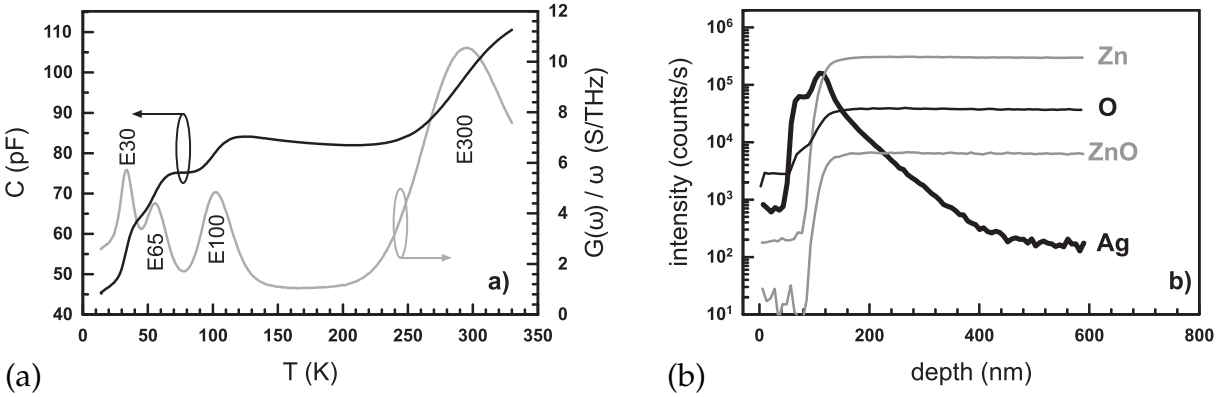


**Figure 8.19:** (**a**) $C(T)$ and $G(T)/\omega$ for $\omega = 1.1\times10^6\,s^{-1}$ of silver oxide diode on undoped ZnO. (**b**) Depth profile of relative concentrations of Zn, O, ZnO and Ag determined by secondary ion mass spectroscopy.

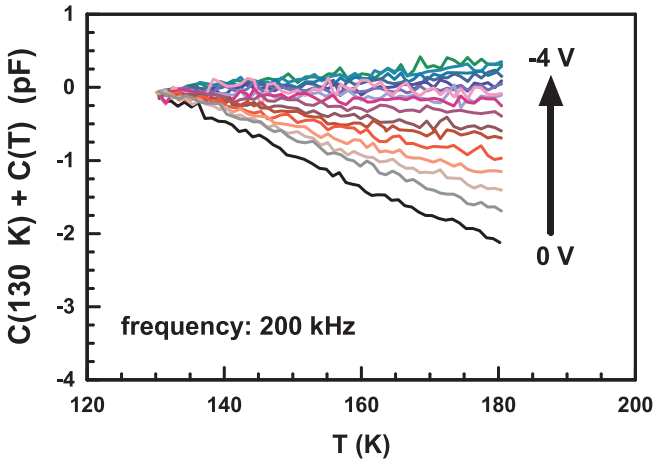


**Figure 8.20:** $C(T)$ with respect to its 130 K value for reverse bias ranging from 0 to −4 V in steps of 0.25 V.

maxima of $G(T)/\omega$ already reported [5, 6]. Interestingly, $C$ decreases for temperatures $T$ between 125 and 215 K. Such behavior has not been reported for ZnO; it is not observed in other diode structures as Pd/ZnO or Pt/ZnO. Variations of the dc bias, applied to the Schottky diode, alter its depletion width $W$ and with that the probing volume. Higher reverse bias increases $W$; the probing volume shifts towards the substrate. Figure 8.20 depicts $C(T)$ for different reverse bias and $\omega = 1.1 \times 10^6\,\mathrm{s}^{-1}$. For visibility $C(T)$ is drawn with respect to its value at 130 K. The decrease of $C(T)$ reduces with increasing reverse bias implying that it is connected to a defect with depth-dependent concentration.

Secondary ion mass spectroscopy depicted in Fig. 8.19b reveals that Ag diffuses from the Schottky contact into the ZnO thin film. Even though the contacts were prepared at room temperature and the diodes were not exposed to temperatures higher than 360 K, Ag is detected 400 nm below the surface. For Pd/ZnO Schottky contacts the metal/semiconductor interface is sharp appositely to the fact that a decrease of $C(T)$ with increasing $T$ was not observed for Pd/ZnO. The Ag depth profile correlates well with the disappearance of the decrease of $C(T)$ altogether suggesting that a defect created by the diffusion of Ag causes the anomalous behavior of $C(T)$.

The diffusion of Ag into heteroepitaxial ZnO thin films creates a defect level causing a decrease of $C(T)$ as $T$ is increased from 120 K to 215 K (depicted in Fig. 8.20) not observed for silver oxide diodes on high-quality bulk ZnO. From that, one can speculate that the larger number of crystal defects (grain boundaries, dislocations) in the ZnO thin film promotes a much faster diffusion of Ag compared to that in the ZnO bulk crystal. Further, the decrease of $C(T)$ suggests that the indiffusion of Ag creates a defect complex rather than a simple point defect. A reconfiguration of the defect complex for $T > 120$ K changes its electronic structure and charge state leading to a smaller capacitance. Besides the decrease of the capacitance, we did not detect a donor-like defect level possibly introduced by interstitial Ag. This is in agreement with calculations showing that the formation energy of Ag on interstitial site is high [1].

This work was supported by the DFG within SPP 1136.

[1] Y. Yan et al.: Appl. Phys. Lett. **89**, 181 912 (2006), doi:1063/1.2378404
[2] Y. Kanai: Jpn. J. Appl. Phys. **30**, 2021 (1991), doi:10.1143/JJAP.30.2021
[3] G. Heiland et al.: Solid State Phys. **8**, 191 (1959), doi:10.1016/S0081-1947(08)60481-6

[4] H. Frenzel et al.: Appl. Phys. Lett. **92**, 192 108 (2008), doi:10.1063/1.2926684
[5] F.D. Auret et al.: Physica B **401-402**, 378 (2007), doi:10.1016/j.physb.2007.08.192
[6] F.D. Auret et al.: J. Phys. Conf. Series **100**, 042 038 (2008), doi:10.1088/1742-6596/100/4/042038

## 8.14 Electronic Coupling in MgZnO/ZnO Double Quantum Wells

J. Zippel, M. Lange, J. Lenzner, G. Benndorf, M. Lorenz, H. Hochmuth, M. Grundmann

The electrical and optical properties of quantum well heterostructures have been investigated with considerable interest in the last years. Coupled double quantum well structures, where the two wells are separated by a thin barrier involve both, fundamental physical properties and the importance for different optoelectronic devices such as modulators, tunable light sources or quantum cascade lasers. Zinc oxide (ZnO) based quantum wells have achieved great attention due to their potential applications in optoelectronic devices operating in the blue–ultraviolet region of the spectrum. The large exciton binding energy in ZnO of 60 meV [1] enables excitonic emission up to room temperature and makes ZnO a promising candidate concerning the realization of exciton-based lasing devices.

In order to get insight in the electronic coupling of $Mg_xZn_{1-x}O$/ZnO double quantum wells (DQW), structures were prepared with pulsed-laser deposition either consisting of two quantum wells with same well width $L_W$ separated by a thin $Mg_xZn_{1-x}O$ barrier layer, so-called symmetric DQWs or structures with two quantum wells of different $L_W$, so-called asymmetric DQWs. Figure 8.21a depicts the shift of the cathodoluminescence peak in dependence of the thickness of the $Mg_xZn_{1-x}O$ barrier layer at a temperature of $T = 10$ K. Clearly a redshift of the maximum with decreasing thickness $L_W$ is observed.

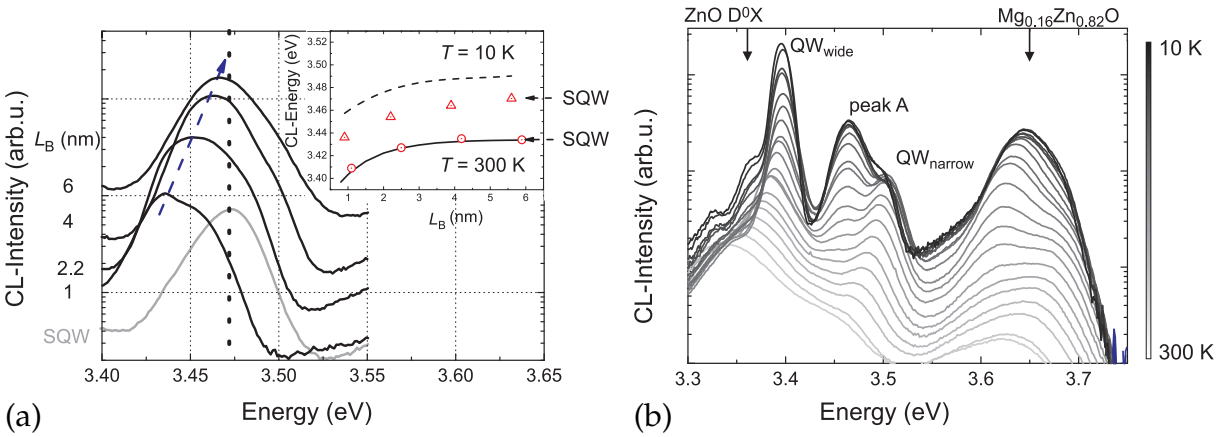


**Figure 8.21:** (**a**) Cathodoluminescence of different symmetric double quantum wells in dependence of the thickness of the $Mg_xZn_{1-x}O$ barrier layer separating the two quantum wells. The inset shows the comparison with an effective mass approximation based solution of the Schrödinger equation. (**b**) Temperature-dependent cathodoluminescence of an asymmetric DQW with $L_{W(wide)} = 4.6$ nm, $L_{W(narrow)} = 1.9$ nm and $L_B = 4$ nm.

The behaviour can be described using a simple effective mass approximation based solution of the Schrödinger equation. In the inset of Fig. 8.21a a very good agreement at room temperature is shown, whereas at 10 K a rigid deviation is obvious, which may be due to the Stokes Shift, i.e. the difference between luminescence and absorption measurement at low temperatures [2].

For the asymmetric DQWs we use temperature-dependent cathodoluminescence to investigate the luminescence characteristic. In Fig. 8.21b the luminescence from $T = 300$ K down to $T = 10$ K is shown. At about 200 K a third peak (peak A) between the luminescence maximum of the wide QW [$QW_{wide}$] and the narrow QW [$QW_{narrow}$] appears and becomes more intense relative to the narrow QW at about 100 K. The theoretical model to calculate the transition energies, suggests the assignment of the new luminescence peak to a spatially indirect transition between the wide and the narrow quantum well. This behaviour indicates the tunneling of either the electrons and/or the holes in the system.

[1] B.K. Meyer et al.: Phys. Stat. Sol B **241**, 231 (2004), doi:10.1002/pssb.200301962
[2] T. Makino et al.: J. Appl. Phys. **93**, 5929 (2003), doi:10.1063/1.1563295

## 8.15 Recombination Dynamics of Excitons in MgZnO/ZnO Quantum Wells

M. Stölzel, A. Müller, G. Benndorf, M. Grundmann

We investigated low temperature recombination dynamics of excitons in MgZnO/ZnO Quantum Wells (QWs) using time-resolved photoluminescence spectroscopy. The samples were grown by pulsed-laser deposition on *a*-plane sapphire substrates with a ZnO buffer layer. The QWs differ in width reaching from 1 to 6.5 nm.

The samples were excited by a frequency-doubled/-tripled femtosecond Ti:Sa laser tuned to resonant and non-resonant excitation (see inset of Fig. 8.22a). The corresponding transients detected on the QW maximum are shown in Fig. 8.22a. For resonant

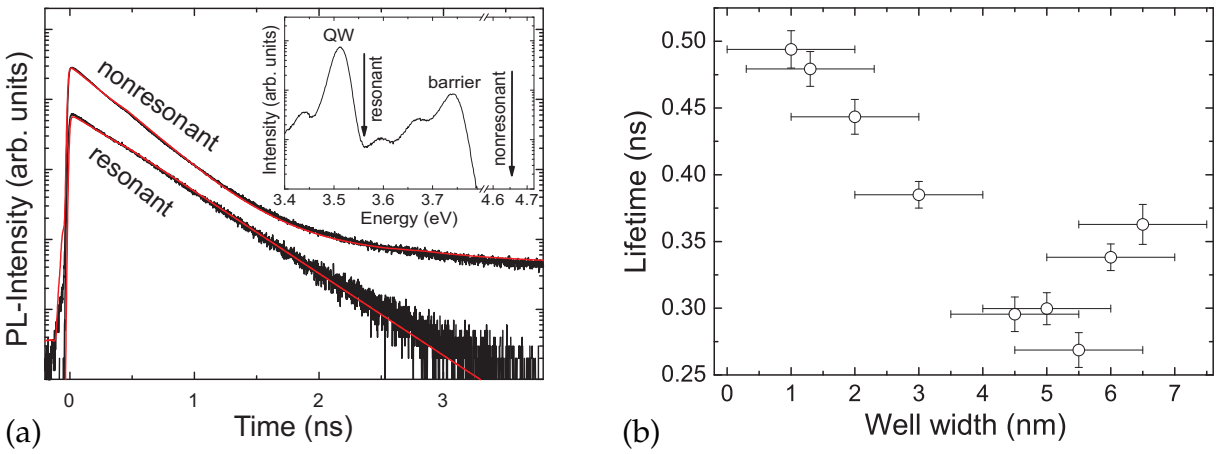


**Figure 8.22:** (**a**) Transients of the QW luminescence for resonant and non-resonant excitation together with the respective fits. (**b**) Luminescence lifetime in dependence of the quantum well width.

excitation we observe a monoexponential decay. When the barrier is excited, the QW decay is superposed by a second, non-exponential decay which matches the temporal behavior of the barrier luminescence.

The transients measured on the high energy side of the QW show a fast process in addition to the monoexponential decay, which is attributed to the relaxation of the hot excitons due to the emission of acoustic phonons. This is confirmed by time delayed spectra, which show a shift of the QW peak to lower energies with time.

The luminescence lifetime of the excitons in QWs with different well widths is shown in Fig. 8.22b. The lifetime decreases down to 4.5 nm and increases for smaller QWs similar to results obtained by Chia et al. [1]. They attribute the increase to localization preventing the migration to non-radiative recombination centers. In contrast to [2], we find no evidence for the quantum-confined Stark effect (QCSE) which would result in a major increase of lifetime for the wider wells.

[1] C.H. Chia et al.: Phys. Stat. Sol. B **229**, 863 (2002), doi:10.1002/1521-3951(200201)229:2<863::AID-PSSB863>3.0.CO;2-3
[2] T. Guillet et al.: Superlatt. Microstruct. **41**, 352 (2007), doi:10.1016/j.spmi.2007.03.030

## 8.16 2D Electron Gases in MgZnO/ZnO Heterostructures

H. von Wenckstern, J. Zippel, A. Lajn, M. Brandt, G. Biehne, H. Hochmuth, M. Lorenz, M. Grundmann

The density of 2D electron gases (2DEG) formed at wurtzite semiconductor heterojunctions exceeds that of zincblende semiconductor heterojunctions by far. The reason is that semiconductors crystallizing in the non-centrosymmetric wurtzite crystal structure are piezoelectric; charges induced by the change of polarization at a hetero-interface contribute to the density of the 2DEG ($n_{2D}$).

For ZnO thin films grown on sapphire substrates, however, a degenerate layer forms at the ZnO/sapphire interface hampering an unambiguous determination of $n_{2D}$ by Hall effect measurements even at low temperatures $T$ [1] making a depth resolved determination of the charge density necessary.We applied capacitance–voltage ($C$–$V$) spectroscopy to Zn-face MgZnO/ZnO heterostructures (HS) to obtain depth profiles of their apparent carrier concentration. This allows an unambiguous determination of $n_{2D}$ usually obtained from Hall effect measurements.

The samples were grown by pulsed-laser deposition at $T \sim 650\,^{\circ}\mathrm{C}$ and an oxygen partial pressure of 0.016 mbar. The thickness of the ZnO and MgZnO layer is 100 and 300 nm, respectively. The MgZnO layers are either nominally undoped or contain 0.5 wt. % Ga to increase the donor concentration. Schottky contacts with areas $A$ between $4\times10^{-4}$ and $4.9\times10^{-3}\,\mathrm{cm}^2$ were realized by reactive dc-sputtering of Pd at room temperature. The diode layout was adopted from [2] to ensure a low series resistance. The current density ($j_d$) vs. voltage ($U$) characteristic of a $Mg_{0.2}Zn_{0.8}O$:Ga/ZnO HS is shown in the inset of Fig. 8.23b. Regarding thermionic emission only, the ideality factor and the barrier height are 1.3 and 0.85 eV, respectively. The Pd Schottky contacts are highly rectifying; the current ratio $I(+1\,\mathrm{V})/I(-1\,\mathrm{V})$ is $3\times10^5$.

Figure 8.23a depicts a room-temperature (RT) $C$–$V$ measurement of a $Mg_{0.2}Zn_{0.8}O$:Ga/ZnO HS obtained using a probing frequency of 100 kHz. The discharge of the 2DEG

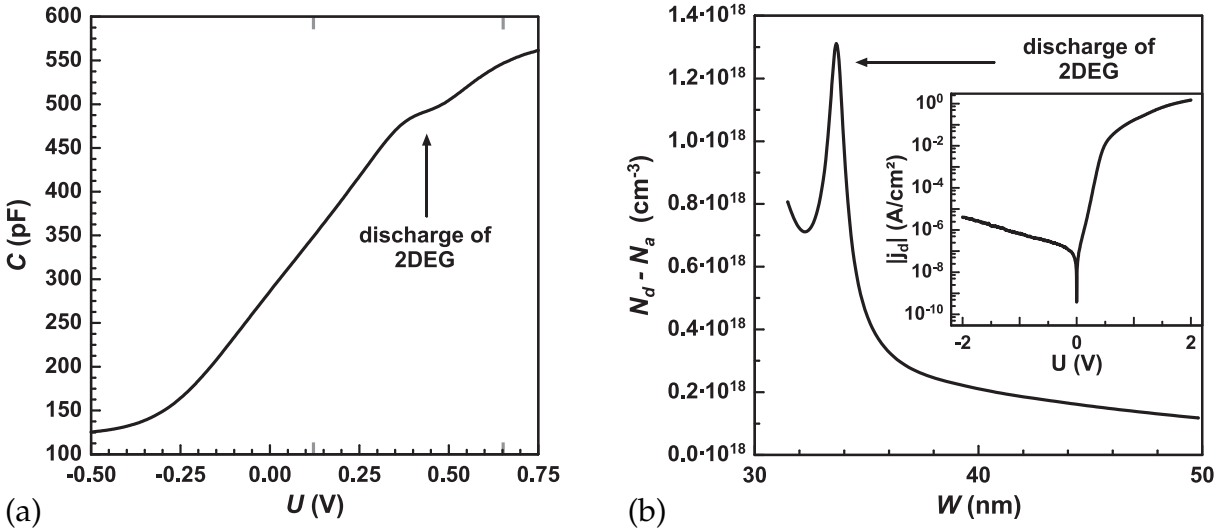


**Figure 8.23:** (**a**) Capacitance versus voltage of a Pd Schottky diode containing a MgZnO:Ga/ZnO HS using a probing frequency of 100 kHz. The *grey markers* enclose the voltage domain used for the calculation of the apparent doping concentration shown in (**b**). The *inset* of (**b**) depicts the diodes $j_d$–$U$ characteristic at room temperature.

is clearly observed between 0.4 V and 0.5 V. For voltages larger than 0.7 V the bands are essentially flat; the capacitance of the space charge region breaks down. As the reverse bias exceeds −0.4 V the space charge region extends into the degenerately conducting layer close to the ZnO/sapphire interface and $C$ depends only weakly on the applied reverse bias. The apparent carrier distribution $N_d - N_a$ is calculated by:

$$(N_d - N_a)(z) = \frac{C^3}{e\epsilon\epsilon_0 A^2}\frac{dU}{dC} \qquad \text{with} \qquad z = \frac{\epsilon\epsilon_0 A}{C}\,, \tag{8.3}$$

$e$ is the elementary charge, $\epsilon_0$ is the vacuum permittivity, $\epsilon = 8.27$, and $z$ is the depletion layer width. The apparent carrier distribution in the vicinity of the HS is depicted in Fig. 8.23b. The sharp peak at $z \sim 33$ nm is due to accumulated electrons confined at RT within the triangular potential well formed at the MgZnO/ZnO interface. Integrating the area below the accumulation peak yields the density of the 2DEG: $n_{2D} = 4\times10^{11}$ cm$^{-2}$. This value is clearly lower than expected from the change of the polarization [3] which cannot be explained by the compressive strain of the MgZnO layer introducing a piezoelectric polarization oppositely directed to $P_{sp}$. This is further illustrated by the fact that $n_{2D}$ is only $2\times10^{11}$ cm$^{-2}$ for an undoped $Mg_{0.2}Zn_{0.8}O$/ZnO HS having the same lattice mismatch as the Ga doped $Mg_{0.2}Zn_{0.8}O$:Ga/ZnO HS. The charge density $\sigma$ induced by the change of the polarization at the interface of the HS is compensated by free electrons. Their concentration in $Mg_{0.2}Zn_{0.8}O$ is not sufficient to fully compensate $\sigma$. Ga-doping increases the free electron concentration (FEC) resulting in a higher $n_{2D}$ as observed for the $Mg_{0.2}Zn_{0.8}O$:Ga/ZnO HS. However, the 2DEG density is far below expected values of some $10^{13}$ cm$^{-2}$ since the FEC is still not sufficient to compensate $\sigma$. Similar behavior was recently reported for MgZnO grown on a ZnO substrate; $n_{2D}$ was with $10^{12}$ cm$^{-2}$ clearly lower than predicted [4]. For HS grown on sapphire substrates $n_{2D}$ determined from Hall effect measurements is above $10^{13}$ cm$^{-2}$ [5, 6] and independent of the Mg-content [6]. This suggest strongly, that 2DEGs have formed

at both the MgZnO/ZnO and the ZnO/sapphire interface which cannot be separated by Hall effect measurements. Therefore, *C*–*V* spectroscopy is the tool of choice to resolve 2DEGs even at multiple MgZnO/ZnO HS individually.

[1] H. von Wenckstern et al.: Appl. Phys. A **88**, 135 (2007), doi:10.1007/s00339-007-3966-0
[2] H. von Wenckstern et al.: Appl. Phys. Lett. **88**, 092 102 (2006), doi:10.1063/1.2180445
[3] A. Tsukazaki et al.: Science **315**, 1388 (2007), doi:10.1126/science.1137430
[4] A. Tsukazaki et al.: Appl. Phys. Express **1**, 055 004 (2008), doi:10.1143/APEX.1.055004
[5] K. Koike et al.: Jap. J. Appl. Phys. **43**, L1372 (2004), doi:10.1143/JJAP.43.L1372
[6] H. Tampo et al.: J. Cryst. Growth **301-302**, 358 (2007), doi:10.1016/j.jcrysgro.2006.11.169

## 8.17 Photoluminescence Properties of PLD Grown ZnO/$Zn_{1-x}Cd_xO$/ZnO Double Heterostructures

M. Lange, C. Dietrich, G. Benndorf, C. Czekalla, M. Lorenz, M. Grundmann

For optoelectronic devices based on ZnO-heterostructures bandgap engineering is necessary. An increase of the bandgap is often realized with $Mg_yZn_{1-y}O$ whereas an decrease is possible with $Zn_{1-x}Cd_xO$. Efforts to obtain structures with an emission at lowest possible energies with $Zn_{1-x}Cd_xO$ alloys by pulsed-laser deposition (PLD) and more details to the growth conditions have already been reported [1]. Now we have studied the origin of the $Zn_{1-x}Cd_xO$ luminescence of this Cd double heterostructure with temperature-dependent photoluminescence (PL) measurements for different samples with slightly changed growth conditions.

In Fig. 8.24 the logarithm of the PL intensity $I$ normalized on the maximum value $I_{Max}$ is plotted as function of the spectral position and the temperature for one sample. In another subfigure the logarithm of the integrated PL intensity $I_{Int}$ normalized on the maximum value $I_{Int,Max}$ as function of the inverse thermal energy for the same sample and a further one with comparable growth conditions but different behavior are presented.

For the $Zn_{1-x}Cd_xO$ as well as for the ZnO luminescence with increasing temperature the luminescence intensity decreases. Following the peak position of the free A-Exciton in ZnO, a shift to lower energies for increasing temperature is observed due to the decrease of the bandgap. For the peak of the $Zn_{1-x}Cd_xO$ luminescence the behavior is different showing an so-called S-shape behavior. It is typical for temperature-dependent studies of peak position for layers having potential fluctuations, e.g. alloys or quantum wells [2]. By fitting a part of the S-shape the standard derivation of the potential fluctuations can be estimated; values between 16 to 20 meV are observed with larger values for the samples showing also larger FWHM for the $Zn_{1-x}Cd_xO$ peak.

The quenching of the $Zn_{1-x}Cd_xO$ luminescence with increasing temperature can be fitted with an Arrhenius equation using as one parameter the thermal activation energy of the process causing the loss of intensity. For all the studied samples except one the determined thermal activation energy had values of 14 to 15 meV. Hence the authors think that a level depopulation of the level of the donor Al on Zn site is the process

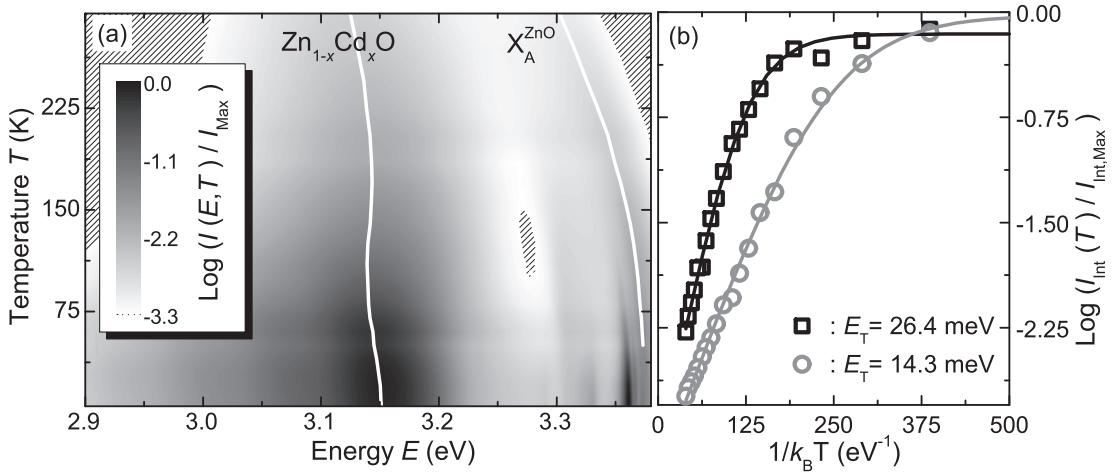


**Figure 8.24:** (**a**) Logarithm $I(E,T)$ over $I_{\mathrm{Max}}$ as function of the spectral position and the temperature for a Cd-DHS deposited with 50 pulses CdO and a substrate temperature $T_{\mathrm{S}} \sim 600$ ℃ and an oxygen partial pressure $p(\mathrm{O_2}) = 2\times10^{-3}$ mbar. The *solid lines* indicate peak positions. The *patterned area* shows areas with an intensity less than the minimal value of the scale. (**b**) Logarithm of $I_{\mathrm{Int}}(T)$ over $I_{\mathrm{Int,Max}}$ as function of the inverse thermal energy for two samples showing very different thermal activation energies although exhibiting related luminescence spectra.

causing this quenching and hence the origin of the luminescence at low temperatures should be a donor bound exciton.

For one sample a value of 27 meV is observed that is much larger than the localization energy of the typical observed donor bound excitons in ZnO. Hence a different process is expected to be the reason for the quenching for that sample although comparable growth conditions were used. Confinement effects might be a possible reason for this enhancement, but in transmission electron microscopy (TEM) images no contrast due to a $\mathrm{Zn_{1-x}Cd_xO}$-layer could be observed.

[1] M. Lange et al.: In *The Physics Institutes of Universität Leipzig, Report 2007*, ed. by M. Grundmann (Universität Leipzig 2008) p 163
[2] J. Christen et al.: Phys. Rev. B **42**, 7213 (1990), doi:10.1103/PhysRevB.42.7213

## 8.18 Excitonic Transitions in $\mathrm{Mg_xZn_{1-x}O}$ Thin Films ($x \leq 0.06$)

C. Dietrich, M. Lange, G. Benndorf, J. Lenzner, M. Grundmann

$\mathrm{Mg_xZn_{1-x}O}$ thin films with $x \leq 0.06$ grown by pulsed-laser deposition on *a*-plane sapphire substrate material and an $\mathrm{Mg_{0.4}Zn_{0.6}O}$ buffer layer were investigated using temperature-dependent photoluminescence spectroscopy (PL). In samples with $x \leq 0.03$ spectrally separated excitonic transitions could be observed for free and bound excitonic recombinations (Fig. 8.25a) despite alloy broadening. One peak could be observed for Mg-contents $x > 0.03$ (Fig. 8.25b).

The observed transitions $\mathrm{I_{6a}}$ and $\mathrm{X_A}$ are assigned to the Al-donor [1] bound excitons and the free excitons according to their energetic separation and distance to the band

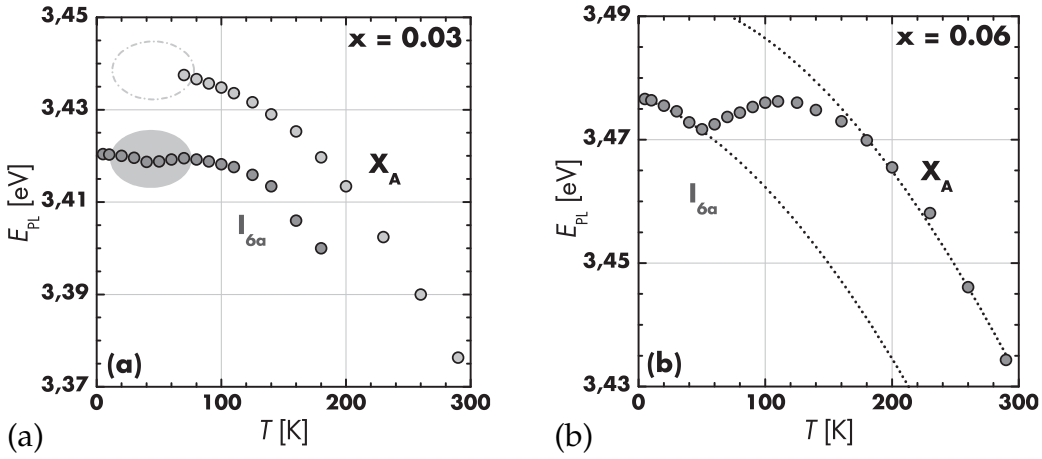


**Figure 8.25:** (**a**) Temperature dependence of $E_{PL}$ for transitions $I_{6a}$ and $X_A$ in $Mg_{0.03}Zn_{0.97}O$. The *grey area* marks the regime of thermalization in local potential fluctuations. This behavior couldn't be observed for transition $X_A$ due to alloy broadening. (**b**) Temperature dependence of $E_{PL}$ for PL-maximum in $Mg_{0.06}Zn_{0.94}O$.

gap. At $T = 5\,K$ the donor bound excitons dominate the spectrum. At temperatures above 100 K, even up to room temperature, the transition of the free excitons dominates the spectra due to the thermalization of the bound excitons.

From the temperature dependence of the PL intensity, the characteristic thermal activation energy $E_T$ of the $Mg_{0.03}Zn_{0.97}O$ sample was determined to be 13.1 meV. The corresponding value for the $Mg_{0.06}Zn_{0.94}O$ sample was determined to be 13.4 meV. This energy is most likely attributed to the required energy $E_{loc}$ for the ionization of a donor bound exciton into a neutral donor and a free exciton. Nevertheless, an increase of $E_{loc}$ means an increase of the donor binding energy.

Increasing the temperature affects the spectral position of these peaks. The $Mg_xZn_{1-x}O$ thin films with $x = 0.03$ showed a weak S-shape, the samples with $x = 0.06$ a strong S-shape behaviour. This S-shape is typically attributed to the formation of local potential fluctuations within the incorporation of Mg atoms into the crystal [2].

In summary, the strong S-shape of $E_{PL}$ for samples with $x > 0.03$ can be explained due to three appearing mechanisms: the crossover from transition $I_{6a}$ to $X_A$, the increase of the binding energy and alloy localization effects.

[1] B.K. Meyer et al.: Phys. Stat. Sol. B **241**, 231 (2004), doi:10.1002/pssb.200301962
[2] A. Müller et al.: Solid State Commun. **148**, 570 (2008), doi:10.1016/j.ssc.2008.09.045

## 8.19 Localized and Impurity Bound Exciton Transition in $Mg_xZn_{1-x}O$ ($x > 0.06$)

A. Müller, M. Stölzel, G. Benndorf, M. Grundmann

The exciton dynamics in $Mg_xZn_{1-x}O$ thin films have been investigated using time-resolved photoluminescence spectroscopy (TRPL). For Mg contents above 6 %, free and bound exciton transitions cannot be resolved using standard photoluminescence

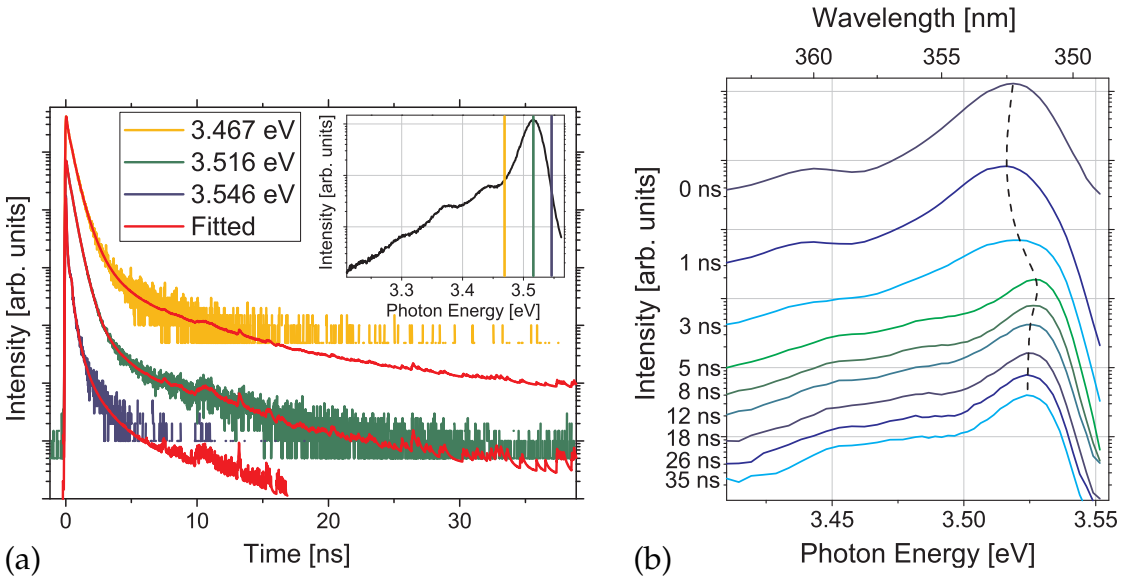


**Figure 8.26:** (**a**) Selected transients of the $Mg_{0.08}Zn_{0.92}O$ sample at $T = 2\,K$ for three different emission energies. The spectral positions are marked in the *inset*. (**b**) Delayed luminescence spectra calculated from the transients.

due to the large alloy broadening. Therefore, the nature of the luminescence is not well understood.

For low temperature TRPL measurements, we observed a blue shift of the luminescence maximum for increasing time, which is shown in Fig. 8.26b. This indicates that there are at least two processes visible. The measured transients (Fig. 8.26a) could be fitted using the sum of a stretched exponential for the fast process and a power law model for the slow decay.

Time integrated intensities for both processes are shown in Fig. 8.27a. The fast process shows the intensity maximum at 3.517 eV, while the maximum of the power

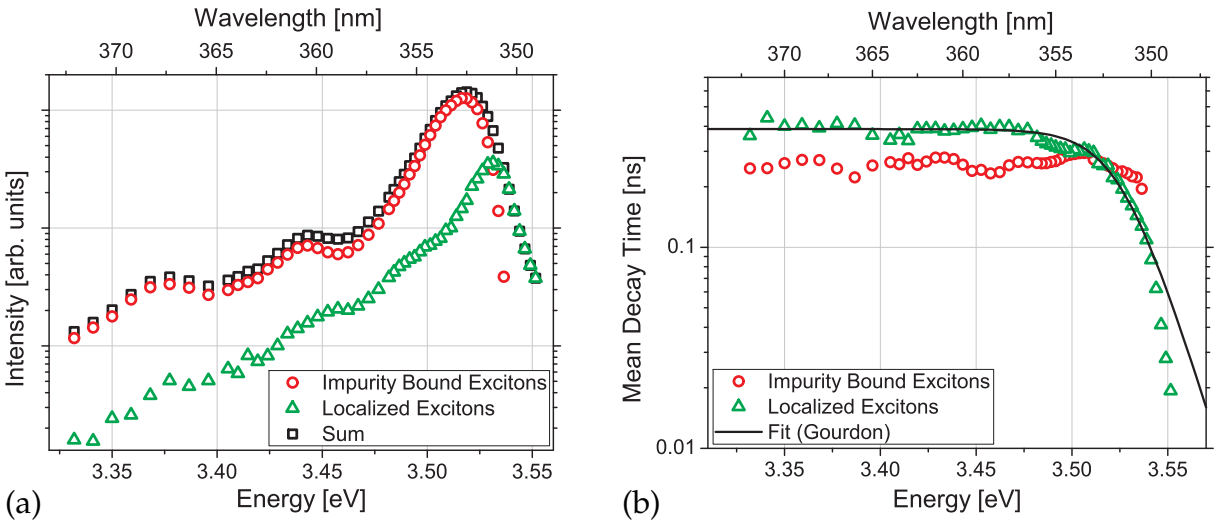


**Figure 8.27:** Spectral dependence of the (**a**) time-integrated PL intensities and (**b**) mean decay times for both processes, calculated from the fits to the transients of the $Mg_{0.08}Zn_{0.92}O$ sample for $T = 2\,K$. The *solid line* is a fit according to Gourdon et al. [1].

law decay is shifted 15 meV to higher energies. Therefore, we attribute the low energy process to an impurity bound exciton transition, which shows a spectrally constant mean decay time of 250 ps. The slow tail is attributed to excitons localized within alloy potential fluctuations.

In contrast to ZnO, these excitons are trapped within random potential minima and cannot reach an impurity. Due to the fast exciton relaxation to lower potential minima, the mean decay time decreases at high emission energies. This can be described by a model from Gourdon et al. [1] for mixed crystals. For an exponentially distributed density of states, they predict an exponential decrease of the observed decay time at high energies. A fit according to this model is shown in Fig. 8.27b.

The emission shows a broad distribution of decay times, which is often observed for random potential distributions in alloyed crystals, but also quantum dot ensembles. It can be explained by taking into account the different localized states or built-in electric fields which influence the expected decay time of a single exciton.

[1] C. Gourdon, P. Lavallard: Phys. Stat. Sol. B **153**, 641 (1989), doi:10.1002/pssb.2221530222

## 8.20 Ferroelectric Thin-Film Field-Effect Transistors Based on Zno/$BaTiO_3$ Heterostructures

M. Brandt, H. Frenzel, H. Hochmuth, M. Lorenz, M. Grundmann, J. Schubert*

*Institut für Bio- und Nanosysteme and Center of Nanoelectronic Systems for Information Technology, Forschungszentrum Jülich, Germany

Ferroelectric materials are used in a wide range of electronic applications. Among these one of the most interesting fields is the application in nonvolatile memory elements, which makes direct use of the ferroelectric polarization. Ferroelectric memory devices are either capacitive or resistive memory elements, which differ in their readout mechanism. The readout of capacitive elements is destructive, resulting in the need to re-write the data into the memory cell. On the contrary the readout of a resistive memory element is non-destructive, resulting in a faster operation of the device. The most prominent resistive non-volatile memory element based on ferroelectrics is the ferroelectric field effect transistor (FeFET).

Based on the observations made in preliminary structures [1], we conclude that the $BaTiO_3$/ZnO system should be a candidate for the formation of FeFETs in all-oxide heterostructure. Field-effect transistors have been successfully prepared employing ZnO/$Ba_xSr_{1-x}TiO_3$ (BST) heterostructures [2]. However, the used BST has been polycrystalline, and was not ferroelectric at room temperature due to its composition.

ZnO thin films of 30 nm thickness were grown by pulsed laser deposition (PLD) on ex-situ prepared BTO templates. These templates have been likewise prepared by PLD and consist of a BTO layer of a thickness of 800 nm, deposited on a lattice-matched Nb doped $SrTiO_3$ (100) (STO:Nb) substrate. However, for the hexagonal ZnO, a twelvefold in-plane symmetry was found by XRD $\phi$-scans indicating the presence of two 30° rotational domains.

FeFET structures have been patterned by photolithography. The ZnO was etched by phosphoric acid in order to form the ZnO channels. Ohmic source and drain contacts have been deposited by DC-sputtering of Au onto the ZnO without overlapping onto the underlying BTO layer. Current–voltage ($I$–$V$) as well as FET output and transfer characteristics have been measured on the BTO-based heterostructures. Very low leakage currents have been observed at 5 V gate voltage in a reference sample ($j_l < 10\times10^{-9}$ A/cm$^2$). From the hysteresis in the ($I$–$V$) curve, the coercive field and spontaneous ZnO polarization is estimated [3]. Including the thickness of the respective layers and the ZnO dielectric constant a coercive field of $E_C = (12.5\pm1)$ kV/cm was obtained being in good agreement with literature values [4]. The ZnO polarization was calculated to be $P_{ZnO} = (0.2\pm0.05)$ μC/cm$^2$. This value is about one order of magnitude below literature values [5–8]. We assume that this is caused by the coexistence of two different ZnO polarities, namely the O-face and the Zn-face polarity in the sample, reducing the apparent ZnO polarization. This assertion is supported by the observation of the 30° rotational domains [9].

Field-effect measurements on the samples show a saturation behavior of the source–drain current upon an increase of the source–drain voltage in the output characteristic. The saturation voltage follows the theoretically expected quadratic behavior. The FeFETs are normally-on with a threshold voltage of $V_T = -2.4$ V; the source–drain current can be varied by at least 6 orders of magnitude within a change in $V_G$ of 7 V, reaching values of up to 10 μA. The field-effect mobility was calculated and reached a maximum of 0.27 cm$^2$/Vs, which is significantly lower than the mobility in bulk ZnO at room temperature. However, the value is close to that reported in literature for bottom gate MISFETs [10]. The transistor structures have been poled by an increased gate voltages ($V_G \approx 20$ V) and the transfer characteristic has been recorded between $V_G = 0$ V and $V_G = 5$ V. After that, a sufficiently large negative "erase" voltage (e.g. $V_G = -7$ V) was applied and the transfer characteristic was recorded again. The process was repeated multiple times in order to check for reproducibility. The results of these experiments are given in Fig. 8.28a. The transistor can be switched into two polarization states and the transfer characteristics in both states differ largely. The ratio of the currents in both operation states reach values of up to 1000 (Fig. 8.28b), depending on the gate voltage.

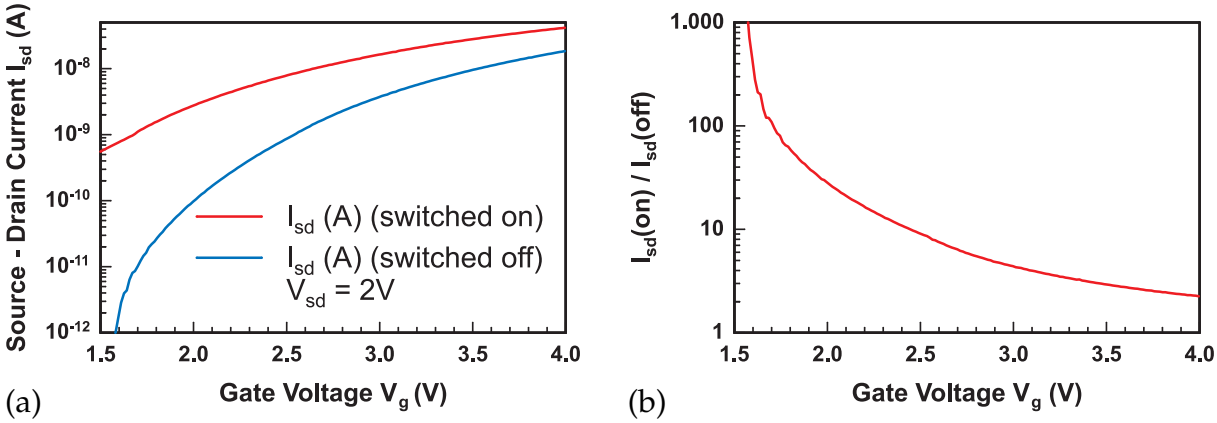


**Figure 8.28:** (**a**) Transfer characteristics of a ZnO/BTO MISFET after applying a forward and backward pulse, respectively. (**b**) Ratio of the current in the permanent on and the permanent off state.

This work has been supported by the DFG within SFB 762.

[1] N. Ashkenov et al.: Thin Solid Films **486**, 153 (2005), doi:10.1016/j.tsf.2004.11.226
[2] J. Siddiqui et al.: Appl. Phys. Lett. **88**, 212 903 (2006), doi:10.1063/1.2204574
[3] M. Brandt et al.: *Ferroelectric thin film field-effect transistors based on ZnO/$BaTiO_3$ heterostructures*, J. Vac. Sci. Technol. B (2009), in press
[4] W.J. Lin et al.: J. Appl. Phys. **77**, 6466 (1995), doi:10.1063/1.359121
[5] F. Bernardini et al.: Phys. Rev. B **56**, R10 024 (1997), doi:10.1103/PhysRevB.56.R10024,
[6] V. Voora et al.: J. Elec. Mat. **37**, 1029 (2008), doi:10.1007/s11664-008-0461-0
[7] Y. Kim et al.: Appl. Phys. Lett. **90**, 101 904 (2007), doi:10.1063/1.2711289
[8] J. Jerphagnon et al.: Appl. Phys. Lett. **18**, 245 (1971), doi:10.1063/1.1653649
[9] I. Ohkubo et al.: Surf. Sci **443**, L1043 (1999), doi:10.1016/S0039-6028(99)01024-9
[10] R.L. Hoffman et al.: Appl. Phys. Lett. **82**, 733 (2003), doi:10.1063/1.1542677

## 8.21 Structural and Optical Properties of $BaTiO_3$ Thin Films

S. Schöche, R. Schmidt-Grund, C. Sturm, H. Hochmuth, M. Lorenz, M. Grundmann

Ferroelectric oxides are of scientific and technological interest due to their potential for applications in various electronic and optoelectronic devices. Because of its high static dielectric constant, remanent polarization, and transparency in the visible spectral range, especially tetragonal barium titanate (BTO) is a suitable material for thin film capacitors, optical resonators, piezoelectric devices, or waveguide modulators. A coupling of the ferroelectric polarization of BTO with the static polarization of wurtzite ZnO gives rise to applications as non-volatile memories or transparent field effect transistors [1]. High-quality thin films and a detailed knowledge of the dielectric function are required to create and investigate these devices.

The BTO layers have been grown by pulsed-laser deposition. It is known from literature that tetragonal BTO single crystals show a birefringence ($\Delta n = n_\perp - n_\parallel$) of about 0.05 in the visible spectral range with optical axis parallel to the *c*-axis [2]. Therefore the BTO layers were deposited on cubic $SrTiO_3$ substrates (STO) of (100), (110), and (111) orientation to be able to proof an optical anisotropy. The chemically and thermally treated (100)-oriented STO substrates provide straight steps of height one unit cell. The surface is $TiO_2$-terminated. A thermal treatment of the substrates of (110) orientation leads to a smooth surface with steps of various heights.

The crystalline quality and surface morphology of the BTO-layers were investigated using X-Ray diffraction (XRD) and atomic force microscopy (AFM). All thin films on (100)-oriented STO are strained and only show (001) orientation. According to literature [3], an decrease of the *c*-lattice constant for increasing film thickness was observed. A relaxation of the layers is visible above a critical film thickness of about 50 nm connected with a growth mode change from layer-by-layer to island growth [4]. Below, all layers show a *c*-lattice constant of 0.424 nm which is much higher then the *c*-lattice constant of the single crystal ($c = 0.403$ nm). The growth mode change can also be seen in the surface morphology. Below the critical thickness steps of full and half

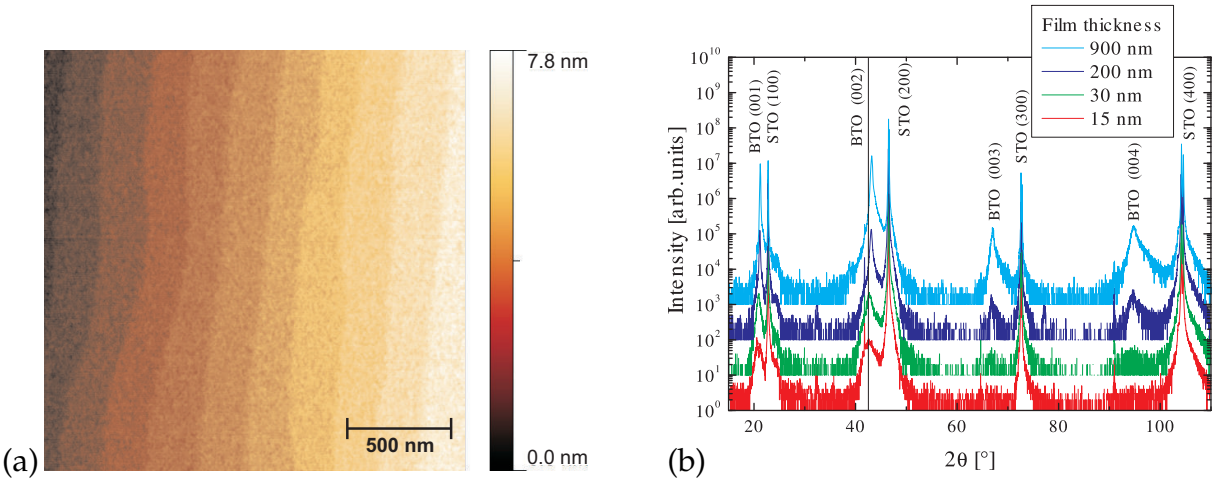


**Figure 8.29:** (**a**) AFM image of an (001)-oriented BTO layer of 45 nm thickness on STO (100) substrate. (**b**) XRD- $2\theta$-$\omega$-Scan of (001)-oriented BTO thin films of different thickness.

unit-cell height are visible (Fig. 8.29a). For the (110)- and (111)-oriented thin film no thickness dependence of the layer lattice constants is measurable. All of these samples are strained and show a smooth surface with roughness lower than 1 nm.

Spectroscopic ellipsometry was used to determine the optical properties of the BTO thin films in the spectral range (0.75 – 5) eV. Müller-matrix (MM) measurements were applied to (110)-oriented BTO films for four different orientations of the optical axis with respect to the plane of incidence. Non-vanishing off-diagonal elements indicate that BTO thin films show an optical anisotropy as the single crystal does. The ellipsometry data have been analyzed by using a layer-stack model including the STO substrate, the BTO film, and a surface layer with model dielectric functions (MDF) for the BTO films and the STO substrate. An uniaxial model containing 4 Gauß–Lorentz oscillators for each direction (parallel and perpendicular to the optical axis which lies in the sample plane) was used to describe the DF of BTO. The resulting index of refraction is shown in Fig. 8.30a.

Because the birefringence of $\Delta n = 0.02$ for the (110)-oriented layers is smaller than that of the single crystal value and no dependence of the ellipsometric data on the in

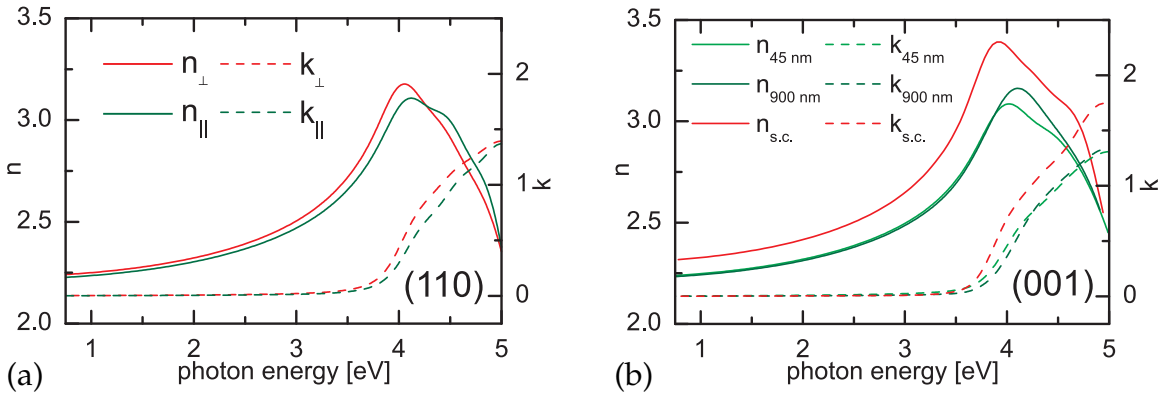


**Figure 8.30:** (**a**) Complex index of refraction for (110)-oriented BTO thin films (uniaxial model). (**b**) Complex index of refraction for (001)-oriented BTO-films of different thicknesses and of a bulk single crystal (isotropic model).

plane sample orientation was found, an isotropic model is used to describe the DF of the (001)-oriented BTO thin films. A change of complex refractive index with varying film thickness is observed (Fig. 8.30b) which we relate to the strucural differences (Fig. 8.29b). For the (111)-oriented thin films, a small anisotropy is expected as well, but the measured off-diagonal MM elements are smaller than the measuring accuracy of the ellipsometer. That means an isotropic model can be assumed even for the (111)-oriented BTO thin films.

This work was supported by the DFG within SFB 762.

[1] B.N. Mbenkum et al.: Appl. Phys. Lett. **86**, 091 904 (2005), doi:10.1063/1.1862778
[2] S.H. Wemple et al.: J. Phys. Chem. Sol. **29**, 1797 (1968), doi:10.1016/0022-3697(68)90164-9
[3] A. Petraru et al.: J. Appl. Phys. **101**, 114 106 (2007), doi:10.1063/1.2745277
[4] Y.S. Kim et al.: Appl. Phys. Lett. **86**, 102 907 (2005), doi:10.1063/1.1880443

## 8.22 Temperatur-Dependent Dielectric Function of Non-Polar ZnO

P. Kühne, R. Schmidt-Grund, C. Sturm, M. Brandt, M. Grundmann

ZnO is a direct semiconductor which crystallizes in the wurtzite structure. Non-polar surfaces like *a*- or *m*-plane are of special interest since they avoid electric fields at interfaces, which will influence the performance of optoelectronic devices. In this work we study the temperature dependence of the dielectric functions (DF) of non-polar *m*-plane bulk ZnO single crystals by means of spectroscopic ellipsometry in the spectral range 0.75 – 4.5 eV and for temperatures 10 – 460 K. Especially, we give emphasis to the sample preparation and the calibration of effects introduced by the cryostat system. The used commercial ellipsometer was equipped with an UHV cryostat system because ellipsometry is very sensitive to surface contamination. By using such an system, we have minimized the condensation of ice or other residual gases on the sample at low temperatures to an negligible amount (Fig. 8.31a).

The ellipsometry spectra are influenced by the cryostat windows, especially if they are strained. Therefore the influence of lateral shifts of the light spot on the windows and the tilt of the windows were investigated. Effects of angular rotations and p- and s-amplitude changes imposed by the windows were modelled. A very good agreement between meassurements with and without windows was reached (Fig. 8.31b).

A further important effect is surface roughness of the sample because it also alters the ellipsometric spectra. The degree of crystallinity of surface-near regions often is poor, which screens the bulk properties in surface sensitive experiments like ellipsometry. As received from the manufacturer, the surface of the bulk crystals was dominated by scratches and impurities, as found from atomic force (AFM) and scanning electron microscopy (SEM) (Fig. 8.32a). To improve the quality, the sample was thermal annealed in oxygen at 900 °C. Scratches and impurities were removed and atomic steps appeared. Such surface now exhibits a high degree of crystallinity (Fig. 8.32b).

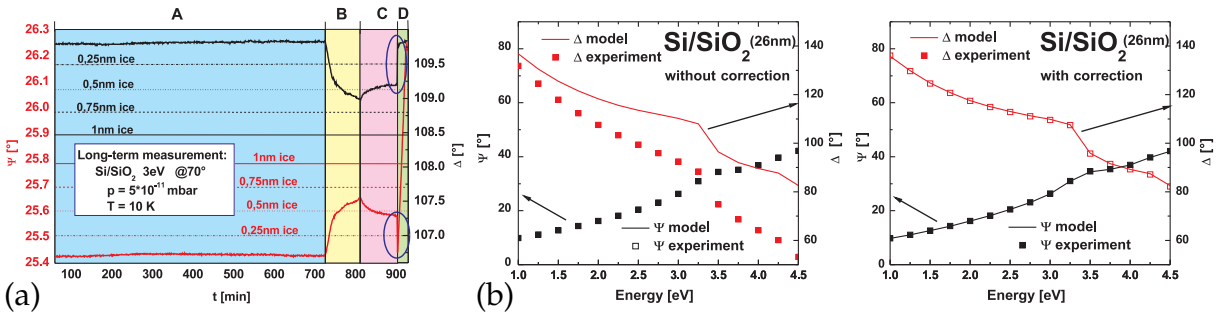


**Figure 8.31:** (**a**) Dynamic scan of the ellipsometric parameters $\Psi$ (*red line*) and $\Delta$ (*black line*) taken from an ZnO bulk single crystal at 10 K. Over 12 hours the pressure within the cryostat was $5\times10^{-11}$ mbar (region A). During this time, no adsorption is recognizable. The *horizontal lines* represent values of $\Psi$ and $\Delta$ for the hypothetical presence of thin adsorbate films. In region B, the bleeder was opened and the pressure was set to $1\times10^{-9}$ mbar, a growth of 0.6 nm adsorbate takes place. In region C, the bleeder was closed again and the heater was switched on in region D. Now, desorption of the adsorbate takes place. (**b**) Effects introduced by the cryostat windows. Experimental (*symbols*) ellipsometric data without (*left*) and with (*right*) window corrections taken from an $Si/SiO_2$ sample within the cryostat. The solid lines represent the model calculations.

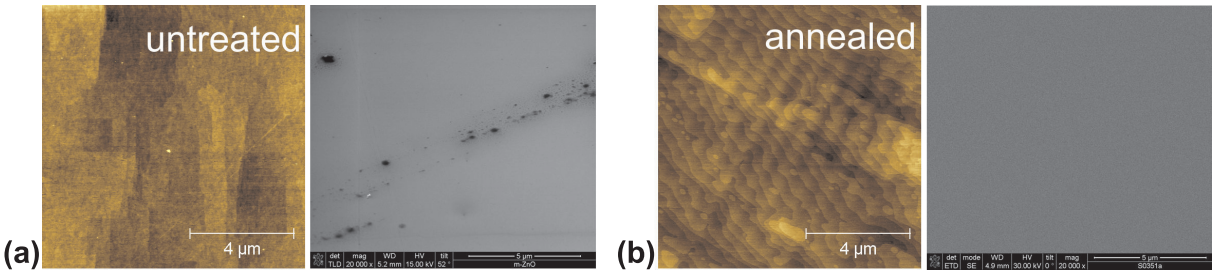


**Figure 8.32:** Sample surfaces before (**a**) and after annealing (**b**). For each case AFM (*left*) and SEM (*right*) images are shown.

For ZnO, the DF is a tensor with two independent components parallel ($\epsilon_{\parallel}$) and perpendicular ($\epsilon_{\perp}$) to the crystal axis. For *m*-plane ($1\bar{1}00$) orientated crystals, the optical axis is located in the surface plane. Due to the absence of mode conversion, $\epsilon_{\perp}$ and $\epsilon_{\parallel}$ can be found by standard (isotropic) ellipsometry, if the optical axis is orientated perpendicular (sc) or parallel (pc) to the plane of incidence. As we have applied standard ellipsometry for these two orientations of our bulk crystal, which exhibits an almost clean and atomic flat surface, the pseudo-DF is similar to the actual materials DF $\epsilon_{\perp}$ or $\epsilon_{\parallel}$, but with residually contributions from the respective other tensor component. In Fig. 8.33a, spectra of the imaginary part of the pseudo-dielectric function $\langle\varepsilon_2\rangle$ are shown as function of the temperature for the orientations pc and sc.

The data-analysis was performed in two steps. First, in order to determine the thickness of the surface layer, in the transparent spectral region a layer stack model was applied which consists of the half-infinite bulk ZnO, which dielectric function was approximated by a cauchy function, and a Bruggemann effective medium surface layer, accounting for the remaining roughness. Then the same model was used for the whole spectrum, but the ZnO DF was replaced by a line shape model DF after [1]. The obtained dielectric function of ZnO near the band gap is dominated by polarizabilities

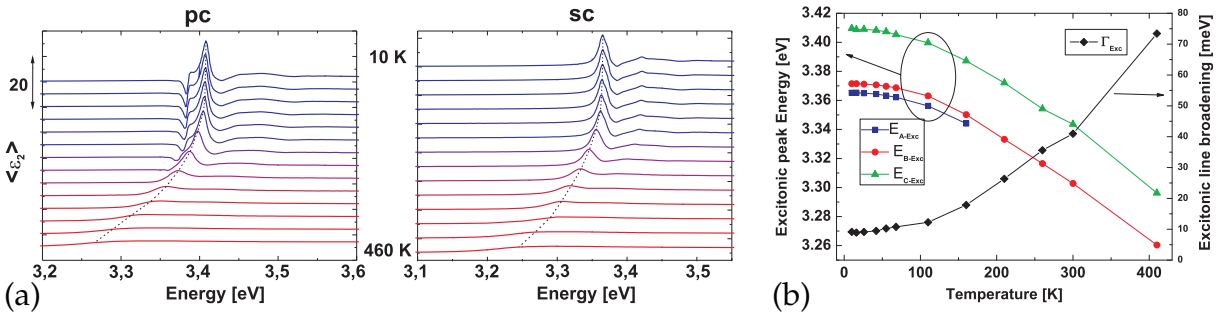


**Figure 8.33:** (**a**) $\langle \epsilon_2 \rangle$ for the two measured orientations pc and sc for temperatures from 10 K to 460 K. (**b**) Temperature dependence of the line shape model parameters A- (*blue*), B- (*red*), and C- (*green*) exciton-energy and exciton-broadening (*black*). The *lines* are guides to the eye.

of free discrete and unbound excitons, exciton–phonon complexes [2], and band-to-band transitions. The temperature dependence of the line shape model parameters exciton-energies and -broadening are shown in Fig. 8.33b.

[1] H. Yoshikawa, S. Adachi: Jpn. J. Appl. Phys. **36**, 6237 (1997), doi:10.1143/JJAP.36.6237
[2] W.Y. Liang, A.D. Yoffe: Phys. Rev. Lett. **20**, 59 (1968), doi:10.1103/PhysRevLett.20.59

## 8.23 Dopant Activation in MgZnO:P Thin Films Grown on ZnO by Pulsed-Laser Deposition

M. Brandt, H. von Wenckstern, C. Meinecke, T. Butz, H. Hochmuth, M. Lorenz, M. Grundmann

Growth of ZnO and its ternary compounds on ZnO substrates facilitates the deposition of thin films with both high structural quality and low impurity concentration. ZnO substrates show atomic steps of $c/2$ height and are perfectly suitable for epitaxial growth after a thermal annealing step [1]. Undoped MgZnO samples grow in the step flow mode and show very high structural and optical quality. High electron peak mobilities of 800 $cm^2/Vs$ at 70 K and 170 $cm^2/Vs$ at room temperature have been observed in homoepitaxial ZnO:P thin films [2]. However, the films remained *n*-type.

We have grown $Mg_xZn_{1-x}O$:P thin films ($x < 0.05$) on ZnO substrates with very good structural properties and electron mobilities comparable to that of homoepitaxial ZnO:P films. The phosphorous dopant was thermally activated and, in contrast to the ZnO:P thin films, an increase in the resistivity has been observed depending on the oxygen partial pressure applied during growth.

The composition of the films has been determined by proton induced X-ray emission (PIXE), employing irradiation with 1.1 and 1.25 MeV protons at the LIPSION [3] ion beamline. With increasing oxygen partial pressure, the concentration of both Mg and P decreases equally. It is known that Mg replaces Zn. In concordance with a defect model for Sb and As doped samples [4] it has been calculated, that phosphorous is incorporated mainly on the Zn site as well [5]. This hypothesis is supported by the present results.

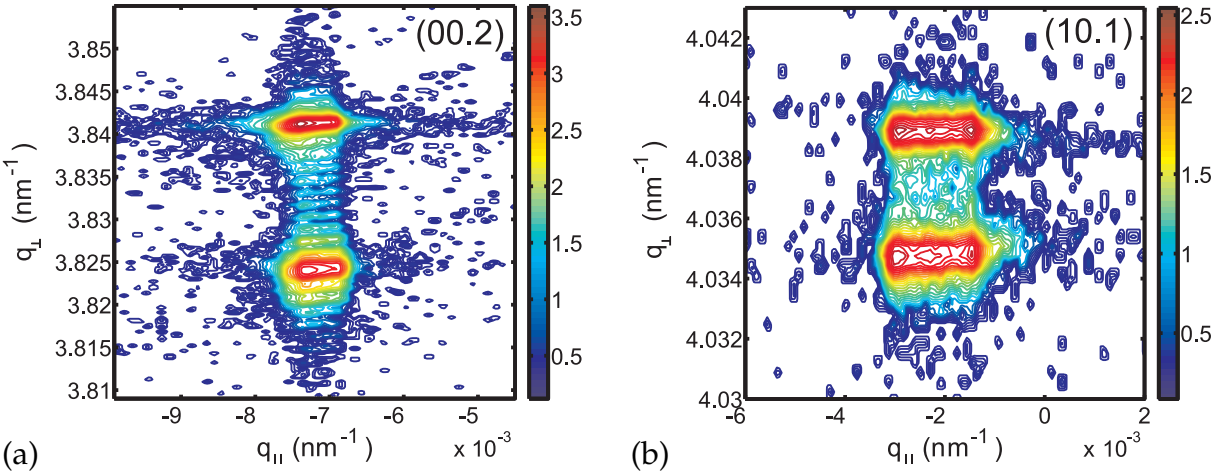


**Figure 8.34:** HR-XRD reciprocal space maps of the symmetric (00.2) (**a**) and the asymmetric skew (10.1) (**b**) reflex of a homoepitaxial MgZnO:P film grown at $2\times10^{-3}$ mbar.

Reciprocal space maps of the symmetric (00.2) (Fig. 8.34a) and the asymmetric skew (10.1) (Fig. 8.34b) reflex of the MgZnO:P sample with the highest Mg and P concentration are shown exemplarily. As can be seen, the peak positions only differ in the out-of-plane direction but have the same in-plane value. Therefore the growth is pseudomorpic for all samples grown at oxygen partial pressures below 0.1 mbar.

The temperature dependence of the Hall-mobility is depicted in Fig. 8.35a). High electron mobilities have been observed in the MgZnO:P samples grown at oxygen partial pressures below 0.1 mbar. The maximal values are comparable to that in the previously discussed homoepitaxial ZnO:P samples [2] underlining the very high structural quality of the samples.

From the temperature dependence of the free carrier concentration the donor activation energy $E_D$ and concentration $N_D$ was determined using a single donor model. As the donor concentration is in the $10\times10^{17}$ cm$^{-3}$ range, the activation energy is reduced by the beginning overlap of the donor states. The donor activation energy follows

$$E_D = E_{D0}\left(1-\left(\frac{N_D}{N_C}\right)^{1/3}\right), \tag{8.4}$$

as given in [6]. Here $N_C$ denotes the critical donor concentration and $E_{D0}$ is the donor activation energy in the dilute limit. From a fit to the experimental data we derive a critical concentration of $N_C = (8.3\pm1)\times10^{18}$ cm$^{-3}$ and a donor activation energy of $E_{D0} = (56\pm3)$ meV, which is close to the activation energy of the effective mass donor (Fig. 8.35b).

In order to investigate thermal activation effects of the dopant, the MgZnO:P layers have been annealed in a 700 mbar oxygen atmosphere at 850 ℃ for 5 min. The samples grown at the highest oxygen partial pressures $p_{O_2} = 0.016$ mbar and $p_{O2} = 0.1$ mbar show the highest increase in resistivity by 6 and 4 orders of magnitude, respectively, indicating an increase in the acceptor concentration.

This work has been supported by the DFG within SFB 762 and FOR 404.

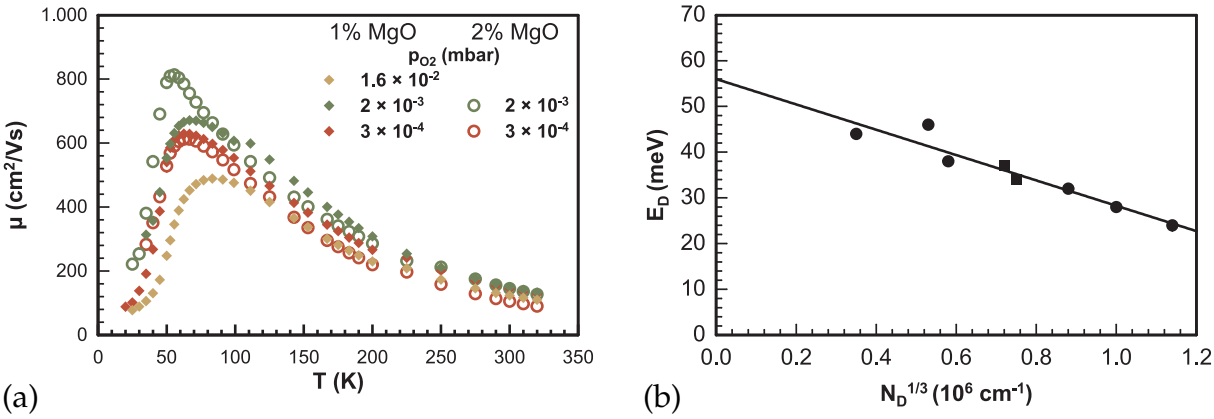


**Figure 8.35:** (**a**) Electron mobility versus temperature in MgZnO:P thin films, with a nominal MgO content of 1 wt. % and 2 wt. %, respectively, as labeled. (**b**) Donor activation energy versus donor concentration in ZnO:P (*squares*) and MgZnO:P (*circles*) thin films. The *curve* is a least squares fit to (8.4).

[1] H. von Wenckstern et al.: Phys. Stat. Sol. RRL **1**, 129 (2007), doi:10.1002/pssr.200701052
[2] M. Brandt et al.: J. Appl. Phys. **104**, 013 708 (2008), doi:10.1063/1.2953066
[3] J. Vogt et al.: Microchim. Acta **133**, 105 (2000), doi:10.1007/s006040070078
[4] S. Limpijumnong et al.: Phys. Rev. Lett. **92**, 155 504 (2004), doi:10.1103/PhysRevLett.92.155504
[5] W.-J. Lee et al.: Phys. Rev. B **73**, 024 117 (2006), doi:10.1103/PhysRevB.73.024117
[6] M. Grundmann: *The Physics of Semiconductors* (Springer, Berlin 2006), doi:10.1007/3-540-34661-9

## 8.24 Strain Control of Homoepitaxial MgZnO:P Thin Films

M. Lorenz, M. Brandt, G. Zimmermann, H. von Wenckstern, M. Grundmann

A major obstacle for electrically pumped light emitting ZnO devices is the difficulty to reproducibly obtain *p*-type conducting ZnO with good time stability. Although acceptor elements as for example nitrogen or phosphorus can be incorporated into ZnO, the electrical activation of these acceptors is not well understood up to now. We have demonstrated homoepitaxial growth of ZnO thin films doped with phosphorus and/or alloyed with magnesium by pulsed-laser deposition on *c*-plane O-face ZnO substrates [1, 2]. In-plane lattice matched, pseudomorphic growth could be confirmed for MgO concentration up to 4 wt. % and/or up to 1 wt. % $P_2O_5$ in the PLD source target [2]. The resulting perpendicular strain of the films is a balance between Mg induced tensile strain and P initiated compressive strain. In this way, a strain engineering of homoepitaxial ZnO thin films was performed for strain values from −0.18 % to +0.75 % [2]. As an example, Fig. 8.36 shows HR-XRD reciprocal space maps (RSM) of two selected samples with compressive (E1917) or tensile strain (E2000). The different strain development is obvious by the different separation of the film peaks in relation to the substrate peaks.

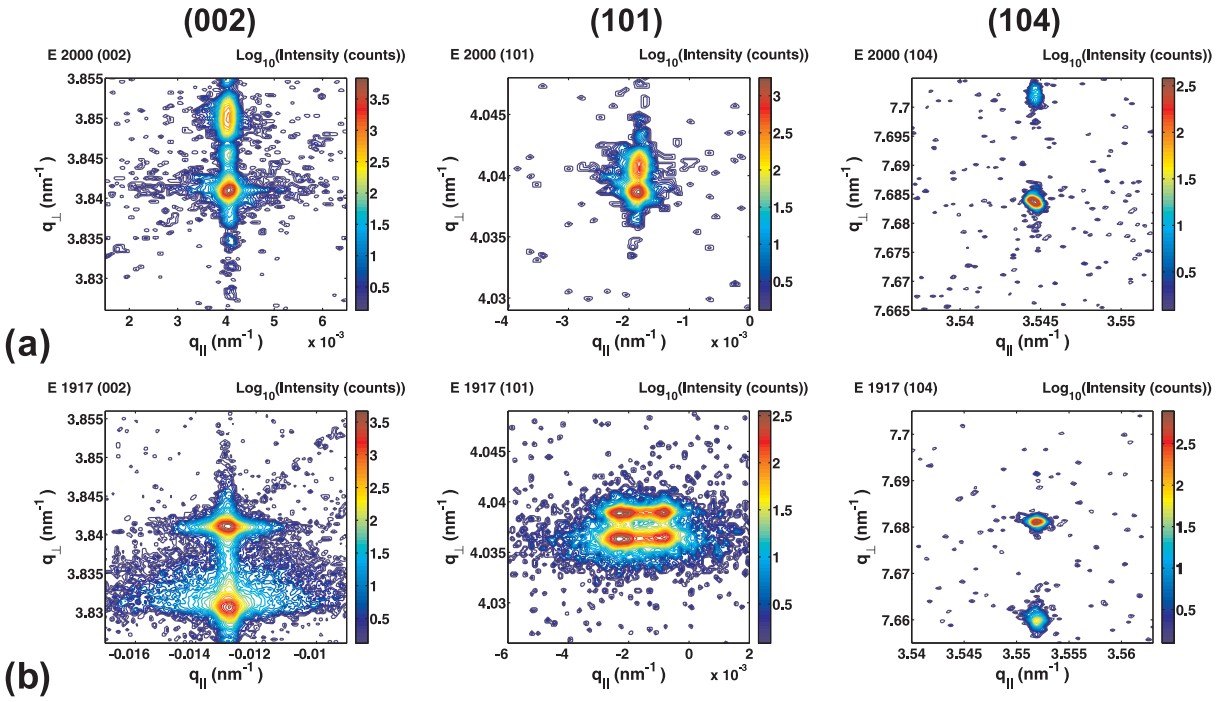


**Figure 8.36:** HR-XRD reciprocal space maps (RSM) of the (002), (101) and (104) reciprocal lattice points of two homoepitaxial samples: row (**a**) E2000 with tensile strain and row (**b**) E1917 with compressive strain. In the center of the maps is the substrate peak with higher intensity, and above (**a**) or below (**b**) is the weaker film peak. RSM (101) in row (**b**) is broadened due to twisted crystalline domains of both film and substrate. The perfect vertical alignment of (104) film and substrate peaks demonstrate the pseudomorphic in-plane lattice match [2].

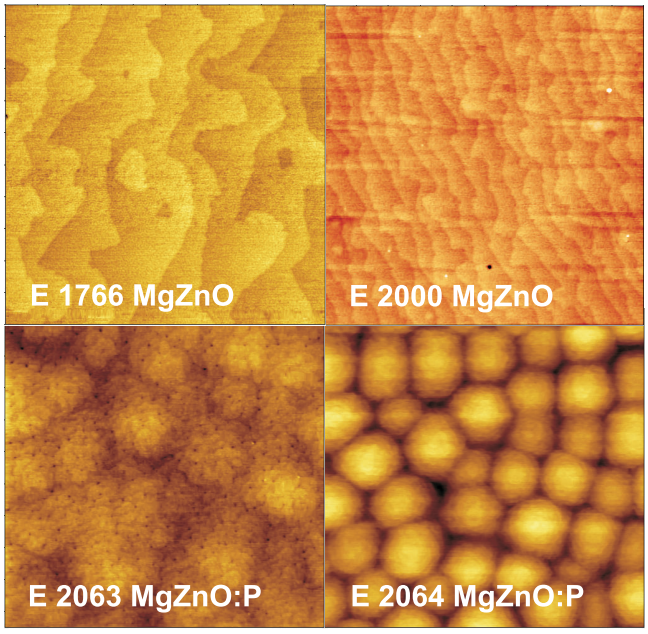


**Figure 8.37:** AFM surface images of four selected homoepitaxial ZnO:Mg,P films. The scan size is $2 \times 2\ \mu m^2$ for all images, the $z$-scales are 2.16 nm (E1766), 2.5 nm (E2000), 3.25 nm (E2063), and 5.5 nm (E2064). Large-area ZnO monolayer terraces with step height $c$ or $c/2$ coresponding to 2D growth are obtained for homoepitaxial MgZnO films, whereas MgZnO:P films show monolayer terraces on a more granular structure [2].

An increasing density of *c*-plane defects with increasing phosphorus dopant concentration, i.e. increasing strain, was found in TEM cross sections and SAD patterns [2]. The FWHM of ZnO(002) XRD rocking curves of homoepitaxial films taken from the separated film peak was in the range 27 to 50 arcsec without much impact of dopant concentration. More important for narrow film rocking curves is the structural substrate quality, which was considerably improved by preselection of batches by the supplier. As shown in the AFM images of Fig. 8.37, 2D layer by layer growth with monolayer terraces was observed for MgZnO films on ZnO, whereas for doped MgZnO:P films a combined 2D plus 3D Stransky–Krastanov growth mode was found.

The electrical properties of these films are discussed in Sect. 8.23.

This work is supported by the DFG within SFB 762 and by the Graduate School BuildMoNa.

[1] M. Lorenz et al.: *Homoepitaxial ZnO thin films by PLD: Structural properties*, Phys. Stat. Sol. C **5**, 3280 (2008), doi:10.1002/pssc.200779504
[2] M. Lorenz et al.: Proc. SPIE Photonics West – OPTO 2009, 7217-23 (2009), doi:10.1117/12.817017
[3] M. Brandt et al.: *High electron mobility of phosphorus-doped homoepitaxial ZnO thin films grown by pulsed-laser deposition*, J. Appl. Phys. **104**, 013 708 (2008), doi:10.1063/1.2953066

## 8.25 Mid-Infrared Spectroscopy of Organic–Inorganic Interfaces

K. Goede, M. Grundmann

Peptide adhesion to semiconductors is widely seen as a valuable model system for organic–inorganic matter interaction. However, the impact of the molecular conformation on the adhesion results and the kind of molecule–substrate binding have so far not seen due research interest. This comes despite it is known [1, 2] that mutating or randomising a peptide's amino-acid content can result in a complete change in its adhesion behaviour. Any biotechnological application of such hybrid systems demands precise knowledge of the organic–inorganic interface [2, 3].

We have employed Fourier-Transform Infrared (FTIR) spectroscopy to detect thin films of 12-mer peptides on semiconductor substrates in the mid-infrared (MIR) [4].The characteristic spectral signature of the respective organics is clearly visible in such curves, and extremely low amounts down to the pmol range have been detected even at room temperature. As an example, Fig. 8.38 shows absorptance curves from 7 pmol of a freshly prepared sample of the peptide AQNPSDNNTHTH on GaAs (100) and of the same peptide after 9-month storage. In the latter case, obviously ~ 80 % of all molecules have been cracked into amino-acid pieces, which has been confirmed by chromatography and mass spectrometry.

This access to key biochemical information such as age-induced degeneration or point mutations with a fast and easy-to-use setup may prove to be relevant for biotechnological applications. Another central finding is the small water content of these amino-acid and peptide films, although they have been prepared by using a watery solution. While it is known that the investigated peptides are largely unfolded in watery

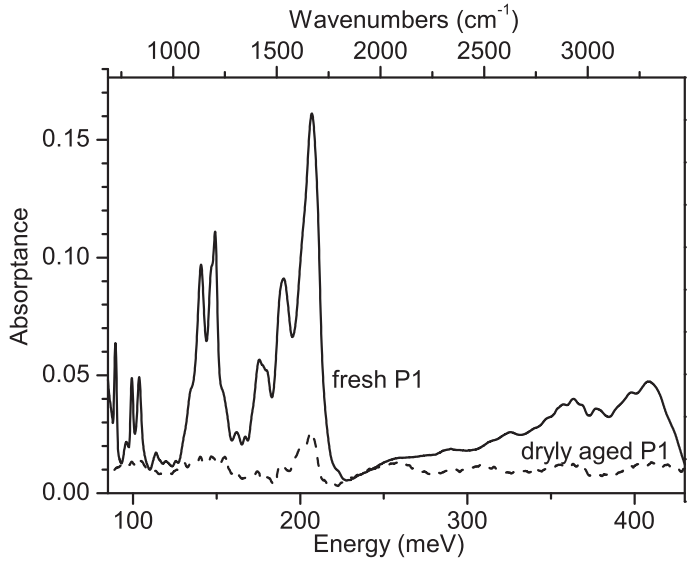


**Figure 8.38:** MIR absorptance of the peptide AQNPSDNNTHTH on a freshly prepared sample and after a storage time of 9 months. In the 200-meV region, the two distinct amide bands from the backbone binding have nearly vanished on the aged sample.

solution, there are indications that the approach to an attractive substrate by a peptide molecule might stabilise folded conformations. This will change the absorption fingerprint of those molecules. By intentionally broadening the optical focus region, the molecular monolayer directly at the hybrid interface to the substrate and thus its conformation and binding situation should be spectroscopically accessible in the near future.

[1] K. Goede et al.: Nano Lett. **4**, 2115 (2004), doi:10.1021/nl048829p
[2] M. Bachmann, K. Goede, A. Beck-Sickinger, M. Grundmann, A. Irbäck, W. Janke: *Microscopic mechanism of specific peptide adhesion to semiconductor substrates* (2009), submitted
[3] K. Goede et al.: Langmuir **22**, 8104 (2006), doi:10.1021/la0605236
[4] K. Goede, D. Stender, M. Grundmann: *Infrared spectroscopy of peptide and amino-acid thin films on semiconductors*, in preparation

## 8.26 Alloy Droplet Formation and Separation During the VLS Growth of GaAs Nanowires by MOVPE

J. Bauer*, V. Gottschalch*, A. Vogel*, J. Lenzner

*Semiconductor Chemistry Group, Faculty of Chemistry

The growth of GaAs nanowires (NW) on GaAs $(\bar{1}\bar{1}\bar{1})_{As}$ substrate via the "vapor–liquid–solid" (VLS) mechanism was studied by metal-organic vapor phase epitaxy (MOVPE). In particular the transient effects in the liquid Au–Ga(–As) alloy prior to and after the GaAs growth step in the MOVPE process sequence were focussed.

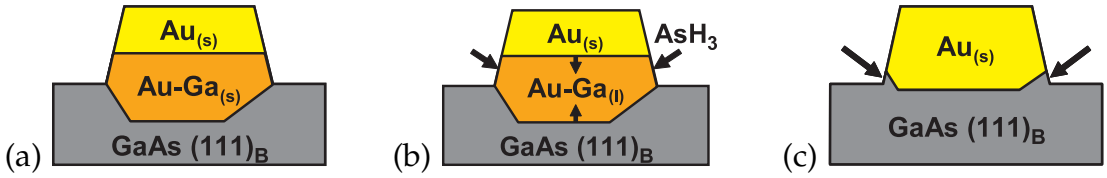


**Figure 8.39:** Schematics of the initial Au–GaAs reaction. (**a**) $T < 390\,^{\circ}\mathrm{C}$: formation of a solid Au–Ga alloy at the Au/GaAs interface. (**b**) $T = 390-420\,^{\circ}\mathrm{C}$: partial melting of the Au–Ga alloy and phase separation as a result of the external arsenic supply. (**c**) final state: solid gold particle ($\alpha$-Au–Ga phase) with a characteristic socket (marked by *arrows*).

The MOVPE sequence was as follows: Starting point was a 6 nm gold film evaporated on GaAs $(\bar{1}\bar{1}\bar{1})_{\mathrm{As}}$ substrate. The sample was heated to $400-530\,^{\circ}\mathrm{C}$ in $AsH_3/H_2$ atmosphere. After a period of 2 min trimethylgallium (TMG) was turned on additionally for further 2 min (GaAs growth step). Finally the sample was cooled down maintaining the arsine supply.

First, the initial Au–GaAs reaction prior to the GaAs growth step (Fig. 8.39) was investigated by scanning electron microscopy (SEM) and $\Omega/2\,\Theta$ X-ray diffraction (XRD): During heat-up to the GaAs-NW growth temperature gold plateaus arise from the continuous gold film. At the Au/GaAs interface a Au–Ga alloy layer is formed which melts at $390-420\,^{\circ}\mathrm{C}$. As a result of the arsine supply the liquid alloy interlayer is macroscopically separated in $\alpha$-Au–Ga phase and a characteristic GaAs socket below the plateaus. The Au/GaAs interface consists of inclined $\{1\bar{1}\bar{1}\}_{\mathrm{Ga}}$ and the $(\bar{1}\bar{1}\bar{1})_{\mathrm{As}}$ plane. Possibly, the liquid alloy interlayer is not completely separated when the GaAs growth step starts.

After GaAs NW growth characteristic morphology regions were observed (Fig. 8.40c): 1) The NW foot region is formed during initial NW growth. In this period the droplet composition and the Au/GaAs interface geometry changes. 2) Then the alloy particle reaches a (kinetical stabilized) quasi-stationary equilibrium state resulting in

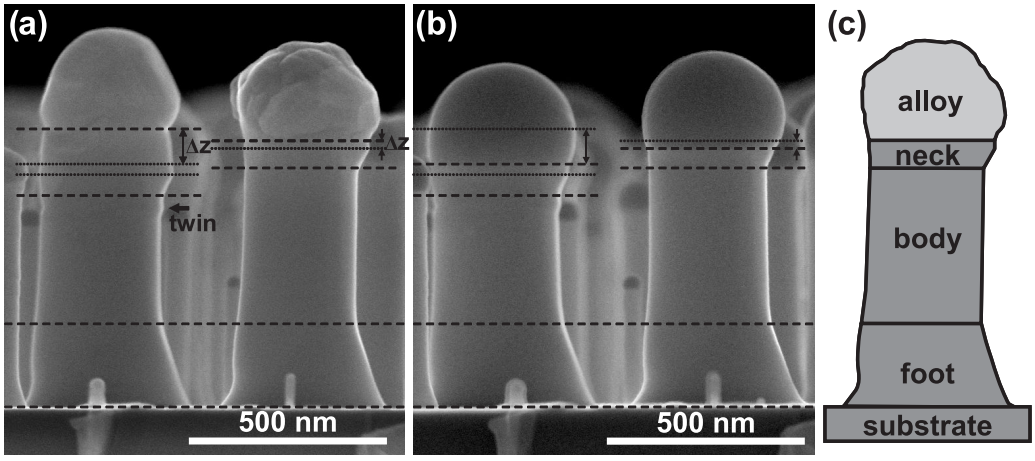


**Figure 8.40:** GaAs NW (2 min, 480 °C, V/III = 10, $p_{\mathrm{TMG}} = 0.36$ Pa) on GaAs $(\bar{1}\bar{1}\bar{1})_{\mathrm{As}}$ substrate grown from a 6 nm thick gold film. (**a**) After growth the sample was cooled down with further arsine supply. (**b**) The sample from (**a**) was treated for 2 min at 480 °C in $AsH_3/H_2$ atmosphere. The cooling down was performed without further arsine supply. (**c**) Habitus of the right GaAs NW in (**a**) representing the majority of GaAs NW.

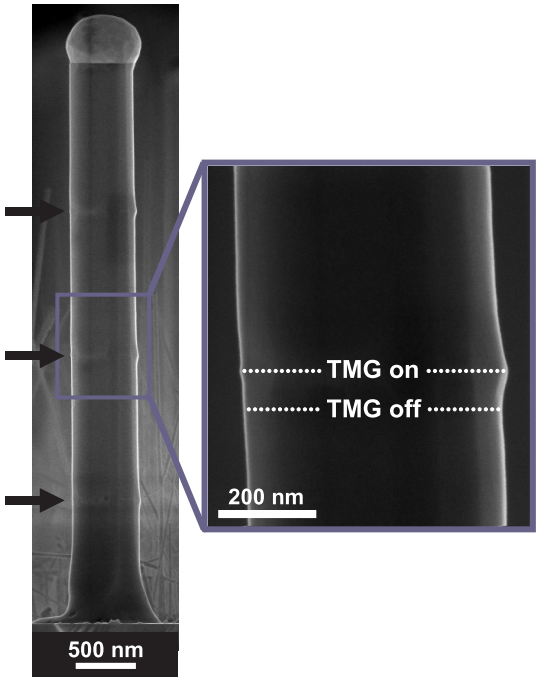


**Figure 8.41:** GaAs NW with *in-situ* markers (see the *arrows*).

the column-like NW body region. 3) After switching off the TMG supply maintaining the arsine flow the laterally extended NW neck region is formed. In this case the necessary amount of gallium for GaAs deposition originates from the reservoir in the Au–Ga droplet. When TMG and arsine are switched off simultaneously no neck region appears.

During slow cooling down with further arsine supply the Au–Ga alloy is completely separated into $\alpha$-Au–Ga phase and GaAs neck region and the resulting gold particle shows well-defined facets (see left NW in Fig. 8.40a). In contrast, a fast cooling down results in polycrystalline solidification of the liquid Au–Ga alloy in Au–Ga phases and GaAs. The particle morphology is undefined in that case (see right NW in Fig. 8.40a).

In Fig. 8.40b the sample was heated up again with arsine supply and cooled down without arsine. The neck region is almost completely solved by the alloy particle. From the neck extention the alloy composition during GaAs NW growth was estimated to $Au_{0.74}Ga_{0.26}$ (V/III = 10) which is in liquid state at growth temperature.

The usage of interrupts during GaAs NW growth allowed the *in-situ* creation of markers. In Fig. 8.41 the TMG supply was interrupted three times for 5 min each. During switching off the TMG flow the situation is similar to the formation of the neck region accompanied by the increase of the NW diameter. When the TMG is switched on again the quasi-stationary growth state is reached after a short transient growth. As a result a local diameter increase (*in-situ* marker) is left by the TMG interruption. With increasing interruption period from 5 s to 5 min the diameter increase extends.

The experiments further suggest a complete macroscopic separation of the alloy droplet after 5 – 30 min TMG interruption. In contrast, related results show that the initial GaAs NW growth, i.e. the alloy formation, is completed after about 50 s. With increasing V/III ratio (arsine partial pressure) the separation period decreases and the initial growth period increases.

This work was supported by the DFG within FOR 522.

# 8.27 PECVD of Cylindrical $SiO_x$/Si Bragg Reflectors on GaAs Nanowires

V. Gottschalch*, K. Mergenthaler*, J. Bauer*, H. Paetzelt*, T. Gühne*, H. Hilmer, R. Schmidt-Grund

*Semiconductor Chemistry Group, Faculty of Chemistry

In recent years, attention has been devoted to the plasma-enhanced chemical vapor deposition (PECVD) of dielectric Bragg Reflectors (BRs) because of their potential application in optoelectronic devices. Due to its high refractive index difference ($n_{Si} - n_{SiO_x} \approx 2$) a high reflectivity can be reached with just a small number of layer pairs [1]. HCSEL (horizontal cavity surface-emitting laser) structure with a cleaved facet and an ion beam etched out-coupler facet, coated with PECVD $SiO_x$/Si Bragg mirror, was successfully fabricated [2, 3]. Dielectric BR´s are promising for the tree dimensional confinement of the light in micro-resonators and to enhance the external efficiency of microcavity light emitters. We studied the deposition behaviour of BRs on planar GaAs substrates and GaAs nanowire arrays.

Well-ordered GaAs nanowire arrays were grown by selective-area metal-organic vapor-phase epitaxy (SA MOVPE) [4]. The growth conditions for SA MOVPE of GaAs nanowires on $(\bar{1}11)_{As}$ GaAs substrates were $T = 800\,°C$, the V/III = 260 and $p_{TMGa} = 0.001\,4$ mbar. The nanowires have an average radius of 130 nm and a length of 1600 nm at the growth time of 20 min. The nanowires have a hexagonal cross-section and a top plane parallel to the substrate surface.

The $SiO_x$/Si BR have been prepared by PECVD at 13.56 MHz in a Plasmalab 80 plus reactor. All depositions have been carried out at 22 mW/cm$^2$, 1 torr and at a temperature of 300 °C. Gas mixtures of $SiH_4$ (2 % in $N_2$) and $N_2O$ have been used.

The optical properties were studied using spectroscopic ellipsometry (SE) on planar samples. The morphology and layer thickness of as-deposited BR on nanowires were analysed by means of scanning electron microscopy (SEM).

The calculated reflectivity spectrum at normal incidence of a $SiO_x$/Si Bragg reflector designed for GaAs is shown in Fig. 8.42.

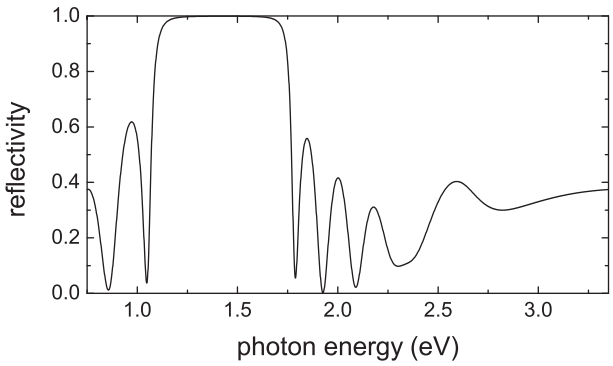


**Figure 8.42:** Reflectivity of the $SiO_x$/Si Bragg reflector on planar GaAs substrate; 5 layer pairs: thickness of $SiO_x$/Si ≈ 149 nm, thickness of Si ≈ 73 nm, the reflectivity spectrum was simulated using the optical constants determined from single layer analysis.

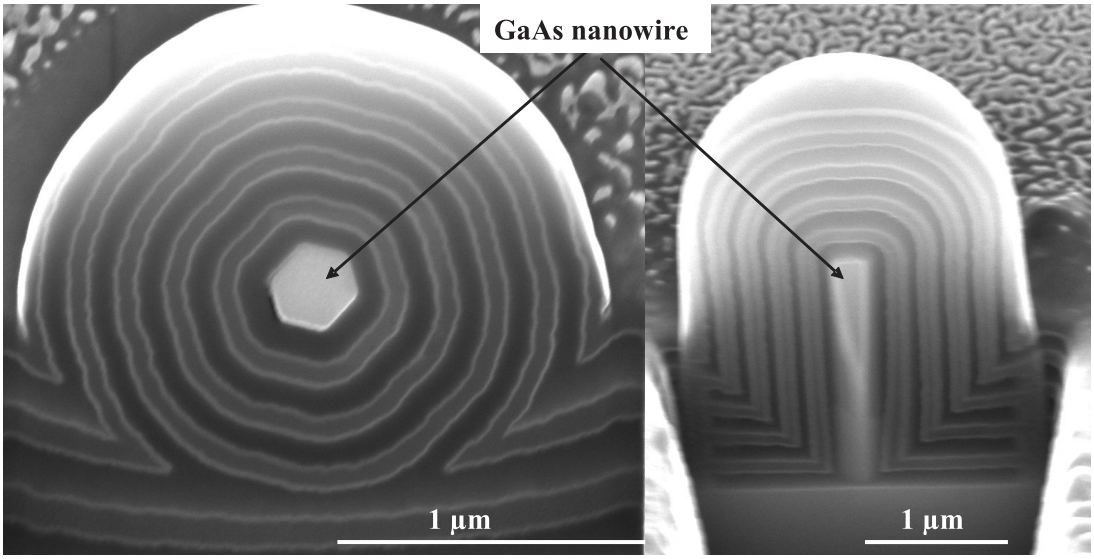


**Figure 8.43:** SEM images of a $SiO_x$/Si Bragg reflector deposited on well-ordered GaAs nanowires grown by SA MOVPE.

In Fig. 8.43, we display two sections of GaAs nanowires embedded in a cylindrical $SiO_x$/Si Bragg reflector. The deposition conditions are the same as of the planar sample (Fig. 8.42).

The SEM images reveal very homogeneous layer thicknesses, smooth interfaces of BR layers, and the conservation of the GaAs nanowires morphology. The formation of the BR on the planar top-surface and the planar area of substrate is visible. The ratio of the layer ticknesses of both areas is 0.88 and the BR of nanowire shifted to shorter wavelength.

Such cylindrical BRs are attractive for nanowires with the $(\bar{1}11)_{As}$ top facet and the cavity is formed along the axis of the nanowire.

This work was supported by the DFG within FOR 522.

[1] V. Gottschalch et al.: Thin Solid Films **416**, 224 (2002), doi:10.1016/S0040-6090(02)00704-6
[2] T. Gühne et al.: Laser Phys. **16**, 441 (2006), doi:10.1134/S1054660X06030042
[3] J. Kovac et al.: Laser Phys. Lett. **4**, 200 (2007), doi:10.1002/lapl.200610092
[4] H. Paetzelt et al.: J. Cryst. Growth **310**, 5093 (2008), doi:10.1016/j.jcrysgro.2008.06.065

## 8.28 Pulsed VLS Growth Mode of GaAs Nanowires Using MOVPE

V. Gottschalch*, G. Wagner*, J. Bauer*, H. Paetzelt*, J. Lenzner

*Semiconductor Chemistry Group, Faculty of Chemistry

Nanowires have remarkable properties and much potential for realizing new optoelectronic devices. The preparation of freestanding GaAs wires with diameters ranging

from few to hundreds nanometers is typically based on the vapor–liquid–solid (VLS) growth mechanism and involves the use of initiators or catalysts such as Au or other metals. However, the VLS growth process is complicated and the fundamental aspects of the growth mechanism (droplet formation, reaction with the substrate and their influence on the formation of wurtzite phase) are under inspection [1].

We investigated pulsed MOVPE growth and analysed the structure of GaAs nanowires. In particular, the segments of sphalerite and wurtzite type structure were determined with respect to important growth parameters.

The growth investigation based on conventional metal–organic vapor-phase epitaxy (MOVPE) technique using trimethylgallium (TMG) and $AsH_3$. Prior to growth, we deposited thin gold films of 3, 6 and 20 nm thickness on $(\bar{1}11)_{As}$ GaAs substrates. The gold films and their interactions with the MOVPE precursor were characterized using various X-ray diffraction techniques.

Fig. 8.44 shows XRD $\Theta/2\Theta$ scans (*ex-situ* after cooling down) of the reaction of the gold film (6 nm thickness) with TMG at 480 °C. Supplying 20 s of TMG the (111) gold peak at $2\Theta = 38.2°$ disappeared and polycrystalline Au–Ga alloys were generated.

The growth of GaAs nanowires has been performed by low-pressure MOVPE ($p_{tot}$ = 50 mbar) in a commercial AIX 200 reactor using the pulsed growth mode (PGM). During the PGM the TMG and $AsH_3$ were introduced alternately into the reactor. Figure 8.45 shows the schematic diagram of wire growth. The pulse sequence of TMG

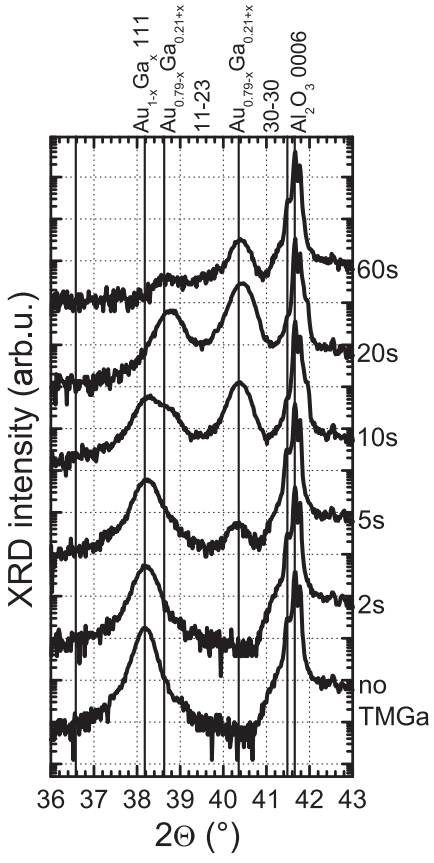


**Figure 8.44:** X-ray diffraction pattern ($\Theta/2\Theta$ scans) obtained on 6 nm Au/$(\bar{1}11)$GaAs specimens at different TMG treatments.

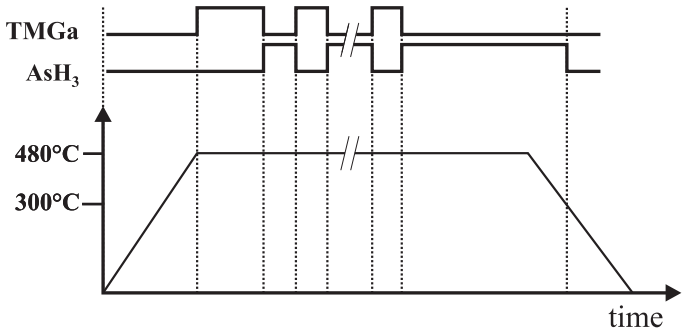


**Figure 8.45:** Schematic diagram of wire growth, one deposition cycle consisted of separate pulses of TMG and $AsH_3$; after the TMG pulse followed a 2-s $H_2$ pulse, after the $AsH_3$ pulse followed a 5-s $H_2$ pulse.

and $AsH_3$ was 10 s. The partial pressure of TMG and $AsH_3$ were $3.6\times10^{-3}$ mbar and $7.1\times10^{-2}$ mbar, respectively. The growth was started with a 20-s TMG pulse, this first step is the formation of $Au_mGa_n$ droplets and can be formally described with the following reaction:

$$m\,\mathrm{Au}^{\mathrm{s}} + n\,\mathrm{Ga(CH_3)_3^{v}} + 3n\,\mathrm{H} \longrightarrow \mathrm{Au}_m\mathrm{Ga}_n^{\mathrm{l}} + 3n\,\mathrm{CH_4}^{v}\ . \tag{8.5}$$

After finishing TMG supply, we started in the second step ($AsH_3$ pulse) the decomposition of $AsH_3$ at the droplet, the As-(super)saturation of the Au–Ga-alloy and the crystallization of GaAs. This process of the $AsH_3$ reaction with the AuGa-alloy can be formally described:

$$\mathrm{Au}_m\mathrm{Ga}_n^{\mathrm{l}} + n\,\mathrm{AsH_3^{v}} \longrightarrow n\,\mathrm{GaAs}^{\mathrm{s}} + m\,\mathrm{Au}^{\mathrm{s}} + 3n/2\,\mathrm{H_2}\ . \tag{8.6}$$

After 12 such pulse sequences of TMG and $AsH_3$, the samples were cooled in an $AsH_3$ atmosphere. The growth temperature was 480 ℃.

Fig. 8.46 shows a scanning electron micrograph of GaAs wires grown on $(\bar{1}11)_{\mathrm{As}}$ GaAs substrate covered with a 3-nm gold film. The switching sequences are visible and marked. The diameters of the wires were in the range of 80 – 100 nm. Vertical growth rates of 1.6 – 2.0 nm/s were measured.

The GaAs wires are covered with Au droplets at the top. Diffraction patterns obtained after nanowire growth at 480 ℃ showed strong 111 GaAs and 111 Au peaks indicating that pure gold or gold with a small concentration of Ga ($\alpha$-Au–Ga alloy) crystallized on top of the wires. Additionally, the phi-scans of 331 GaAs and 311 Au diffraction peaks indicate the following orientation relationships:

$$(\bar{1}11)\mathrm{GaAs} \parallel (111)\mathrm{Au}\,; \quad \langle 110\rangle\mathrm{GaAs} \parallel \langle 110\rangle\mathrm{Au}\ . \tag{8.7}$$

Wires grown on substrates with a thin gold film of 20 nm thickness showed decreased diameters ranging from 20 – 80 nm, the growth rates were increased to 2.3 – 2.6 nm/s.

The structural properties of the nanowires were determined with high-resolution transmission electron microscopy (HRTEM). Figure 8.47 shows the HRTEM image of cross section of a GaAs wire. This image and selected area diffraction pattern revealed the existence of sphalerite (sph) and wurtzite (w) type structure in the GaAs wires.

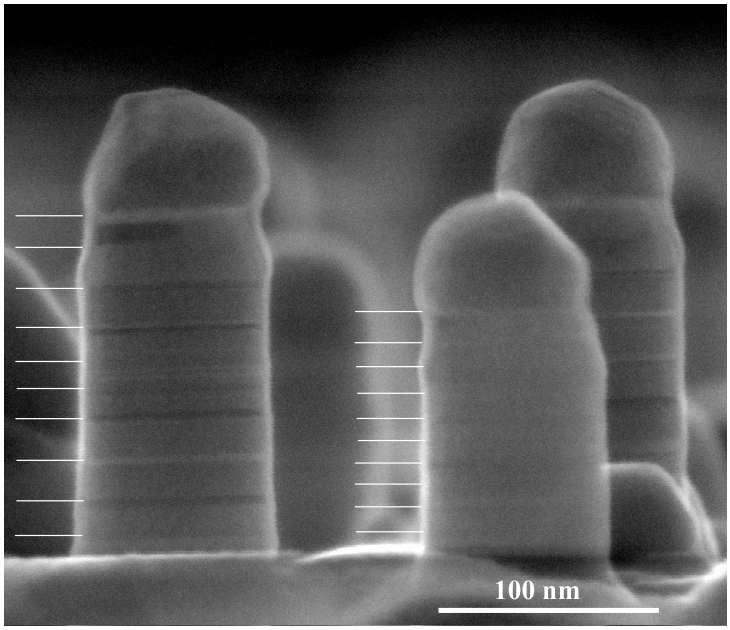


**Figure 8.46:** SEM image of GaAs wires grown on $(\bar{1}11)_{As}$ GaAs. (110) cross-section.

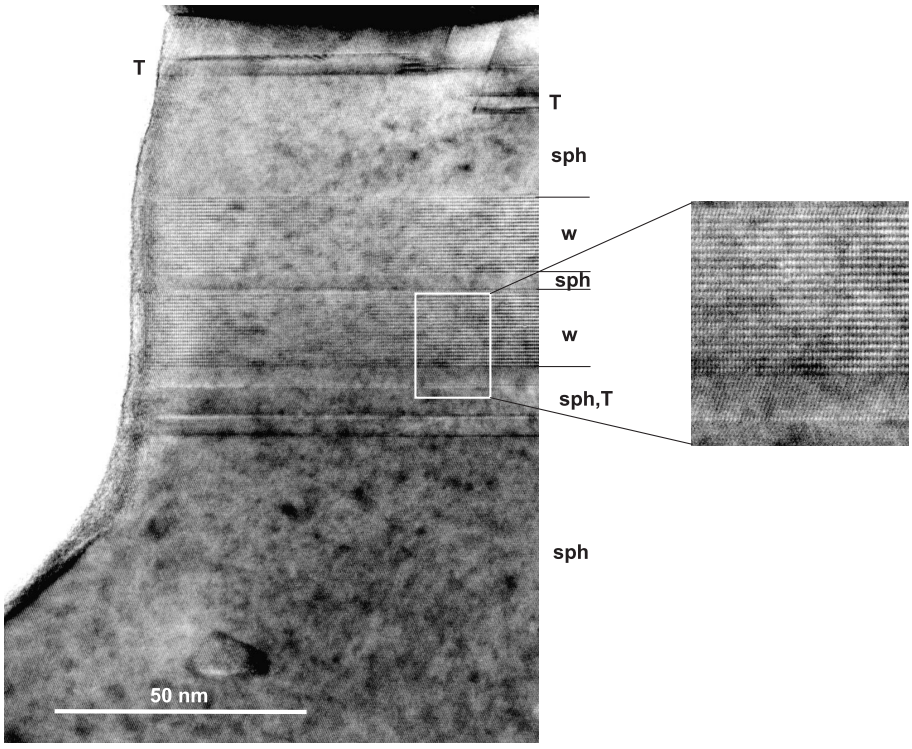


**Figure 8.47:** HRTEM image of a GaAs wire consisting of regions with sphalerite-type (*sph*) and wurtzite-type (*w*) structure. Twinning (T) exists within the sphalerite-type regions. A sphalerite–wurtzite transition is shown in the *enlarged detail*.

The foot region is from pure sphalerite type. All segments of sphalerite type structure contain stacking faults and twins. After the stabilization of the AuGa-droplet (10 s TMG supply) and the following arsine supply the NW growth is abruptly switched to wurtzite type. The occurrence of the wurtzite type structure is result of the nucleation

process, the 2D nucleation occurs preferentially at the vapor–liquid–solid phase line and high supersaturation in the droplet [2]. After the last switching sequence of TMG the NW neck region is formed. The decreasing of NW diameter results from the partial Ga consumption of the Au–Ga droplet.

To the best of our knowledge this is the first report on the formation of GaAs nanowires with wurtzite type structure grown by MOVPE.

This work was supported by the DFG within FOR 522.

[1] J. Bauer: Disseration, University of Leipzig, (2009) handed in
[2] F. Glas et al.: Phys. Rev. Lett. **99**, 146 101 (2007), doi:10.1103/PhysRevLett.99.146101

## 8.29 MOVPE Growth of $\beta$-$Ga_2O_3$

V. Gottschalch*, K. Mergenthaler*, G. Wagner*, J. Bauer*, H. Paetzelt*, C. Sturm, U. Teschner

*Semiconductor Chemistry Group, Faculty of Chemistry

Monoclinic $\beta$-$Ga_2O_3$ is a wide band gap material with a direct gap $E_g \approx 4.9$ eV and high transparency in the visible and UV region. Above 870 °C $\beta$-$Ga_2O_3$ is the most stable modification. It is a promising base material for optical device applications within the deep-ultraviolet (DUV) spectral region, high temperature gas sensors, transparent conductors, photocatalysts, and it can be used for the passivation of GaAs surfaces. Furthermore, single crystalline $\beta$-$Ga_2O_3$ substrates are applicable for the growth of GaN-based epitaxial layers and LED devices.

The MOVPE (metal-organic vapor-phase epitaxy) growth was carried out in a non-commercial horizontal cold-wall reactor at atmospheric pressure. Triethylgallium (TEG) as gallium precursor, $N_2O$ as oxygen source were separately introduced into the growth region. The flow rates of TEG and $N_2O$ were 5.2 $\mu$mol/min and 22 mmol/min, respectively. The growth rate was about 0.7 $\mu$m/h.

The $Ga_2O_3$ films were analyzed by means of high-resolution X-ray diffraction (HRXRD), scanning electron microscopy (SEM), transmission electron microscopy (TEM) and optical transmission measurements (TM).

Epitaxial layers of monoclinic $\beta$-$Ga_2O_3$ were successfully grown at 800 °C on (0001) sapphire and at 700 °C on $(\bar{1}11)_{As}$ GaAs substrates [1]. Figure 8.48a shows a cross-sectional HRTEM image of $\beta$-$Ga_2O_3$ grown at 800 °C on *c*-plane sapphire. The well-aligned $\beta$-$Ga_2O_3$ lattice planes (parallel to interface) with a distance of 0.46 nm in growth direction can be clearly seen. This distance corresponds to the $(\bar{2}01)$ *d*-spacing of $\beta$-$Ga_2O_3$. The corresponding selected area diffraction (SAD) pattern (Fig. 8.48b) also shows the crystalline nature of the layer and the in-plane arrangement of differently oriented rotational domains.

Figure 8.49 shows the cross-sectional HRTEM image of a $\beta$-$Ga_2O_3$ layer grown on $(\bar{1}11)_{As}$ GaAs. An abrupt transition between GaAs and thin film is visible. The HRTEM image shows well aligned $\beta$-$Ga_2O_3$ lattice planes with a distance of 0.46 nm corresponding to the lattice spacing of the $(\bar{2}01)$ planes.

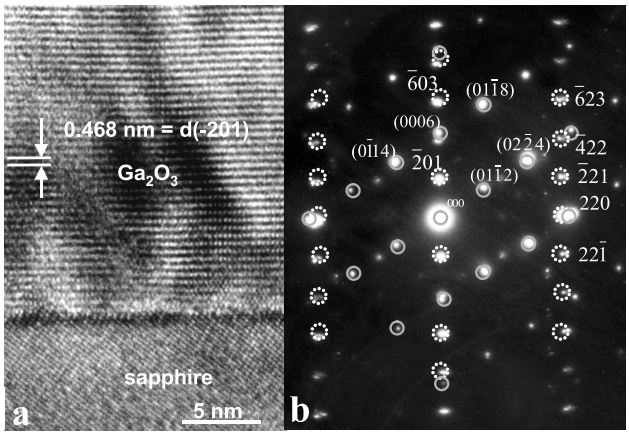


**Figure 8.48:** Cross-sectional HRTEM image (**a**) and SAD pattern (**b**) of $\beta$-$Ga_2O_3$ grown at 800 °C on *c*-plane sapphire. Electron-beam incidence is parallel to $[2\bar{1}\bar{1}0]$ sapphire. The SAD pattern stem from substrate (marked by *closed circles* and indices *with brackets*) and layer (marked by *dotted circles*, indices *without brackets*).

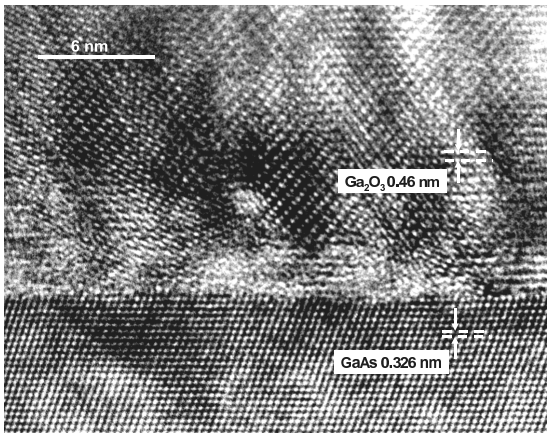


**Figure 8.49:** HRTEM image of $\beta$-$Ga_2O_3$ grown on $(\bar{1}11)_{As}$ GaAs. $(1\bar{1}0)$ TEM cross-section, electron beam direction is parallel to [110] GaAs and [010] $\beta$-$Ga_2O_3$.

By means of XRD and TEM the orientation relationship between $\beta$-$Ga_2O_3$ domains, sapphire and GaAs substrates were determined:

$$(\bar{2}01)\,\beta\text{-}Ga_2O_3 \parallel (0001)\,Al_2O_3\,, \qquad \langle 010\rangle\,\beta\text{-}Ga_2O_3 \parallel \langle 10\bar{1}0\rangle\,Al_2O_3\,, \tag{8.8}$$

$$(\bar{2}01)\,\beta\text{-}Ga_2O_3 \parallel (\bar{1}11)\,GaAs\,, \qquad \langle 010\rangle\,\beta\text{-}Ga_2O_3 \parallel \langle 110\rangle\,GaAs\,. \tag{8.9}$$

The arrangement of monoclinic $\beta$-$Ga_2O_3$ domains on threefold symmetric substrates leads to a sixfold in-plane symmetry. For deposition on $(11\bar{2}0)$, $(10\bar{1}0)$ and $(01\bar{1}2)$ oriented sapphire substrates the low-temperature modification $\beta$-$Ga_2O_3$ was observed.

Room-temperature optical transmission measurements revealed for $\beta$-$Ga_2O_3$ films deposited on *c*- and *a*-plane sapphire a high optical transmittance of over 90 % and a sharp cut-off at about 250 nm.

[1] V. Gottschalch et al.: Phys. Stat. Sol. A **206**, 243 (2009), doi:10.1002/pssa.200824436

## 8.30 Combination of Selective-Area and Vapor-Liquid-Solid Growth – GaAs Nanotree Structures

H. Paetzelt*, V. Gottschalch†, J. Bauer†, J. Lenzner

*Leibniz-Institut für Oberflächenmodifizierung, Leipzig
†Semiconductor Chemistry Group, Faculty of Chemistry

Complex nanostructures are becoming increasingly important for the development of nanoscale devices and functional nanomaterials. The aim of our investigations is

the fabrication of three-dimensional structures with GaAs-nanowires as components. We report on the combination of a catalyst-free growth of GaAs nanowires using the selective-area metal-organic vapor-phase epitaxy (SA-MOVPE) and a catalyst-assisted growth of GaAs nanowires using the vapor-liquid-solid (VLS) growth mechanism.

The SA nanowires were grown on (111)B oriented GaAs substrates partially covered with $SiN_x$. We used plasma enhanced chemical vapor deposition (PECVD) for the deposition of a thin $SiN_x$ layer ($\sim$ 15 nm) on the substrate surface [1]. The $SiN_x$ was partially removed by electron beam lithography (EBL) definition of well ordered circular openings in an electron sensitive resist and wet chemical etching using a diluted ammonium fluoride etching mixture (AF 87,5-12,5 VLSI Selectipur Merck). The radius of the openings was held constant to 250 nm and the triangular lattice with a pitch $a$ of the openings was varied from 600 to 3300 nm. The selective-area and the VLS growth were carried out using low-pressure ($p_{tot}$ = 50 mbar) MOVPE in an AIXTRON AIX200 reactor with a total gas flow into the reactor of 7000 sccm in $H_2$ atmosphere. Trimethylgallium (TMGa) was used as group-III source and arsine ($AsH_3$) was used as group-V source material in both growth modes.

The optimal growth conditions for SA-MOVPE of GaAs nanowires on (111)B GaAs substrate were found to be $T$ = 800 °C and a V/III ratio of 260 with a partial pressure of $p_{TMGa}$ = 0.001 4 mbar. Figure 8.50a shows a SEM image of a GaAs nanowires array grown on (111)B oriented GaAs substrate. The growth time was 20 min and the array pitch $a$ between the circular openings in the 15 nm thick $SiN_x$ layer was 1000 nm. We can see a uniform array of vertically aligned nanowires with a hexagonal cross section formed by six $\{1\bar{1}0\}$ side wall facets and a top plain parallel to the substrate surface. The nanowires have an average radius of $r$ = 130 nm and a height of $h$ = 1600 nm. These nanowire arrays form the basis for the second epitaxial VLS-grown nanowires. The samples were evaporated with a thin Au layer under a pressure of $p = 2\times10^{-6}$ mbar and a sample temperature of $T$ = 100 °C. The gold evaporation starts with an included angle of 45° between the nanowire axes and evaporation direction. Also the normal of one $\{1\bar{1}0\}$ sidewall facet and the evaporation direction are inplane. After the first Au layer was deposited the sample was rotated 120° in nanowire axes. This was repeated a third time so that all side-facet have nearly the same Au layer thickness of 1 nm (measured during the evaporation using an oscillating crystal).

This system forms the starting point for the epitaxy of the VLS grown GaAs nanowires. The growth temperature was $T$ = 480 °C and the TMGa and $AsH_3$ flow was held constant to 10 ml/min. So the V/III ratio was 20 which is very low in contrast to the V/III ratio during the SA-growth of 260.

During the heating the thin Au layer forms small Ga containing droplets on the $\{1\bar{1}0\}$ sidewalls and the (111)B top surface. The GaAs nanowire growth occurs when Ga and As are supplied from the sources TMGa and $AsH_3$ and supersaturation occurs in the Au–Ga–As alloy particles [3]. The nanowires nucleate from the $\{1\bar{1}0\}$ sidewalls while their growth direction is the $[\bar{1}\bar{1}\bar{1}]$B. The growth time was held to 2 min which forms nanowire with diameters of 20 to 50 nm and a length up to 1 μm. The data fits well with standard growth models (see [4]). Figure 8.50b–d show the final complex GaAs nanotree structures. Each SA nanowire is surrounded by a number of VLS nanowires (branches) which grow in the ⟨111⟩B directions. Viewed from above, the nanotrees exhibit 6 branch directions, separated by 60° (Fig. 8.50d). In dependence of the array pitch and the adjustment of the circular openings defined by EBL a docking of the

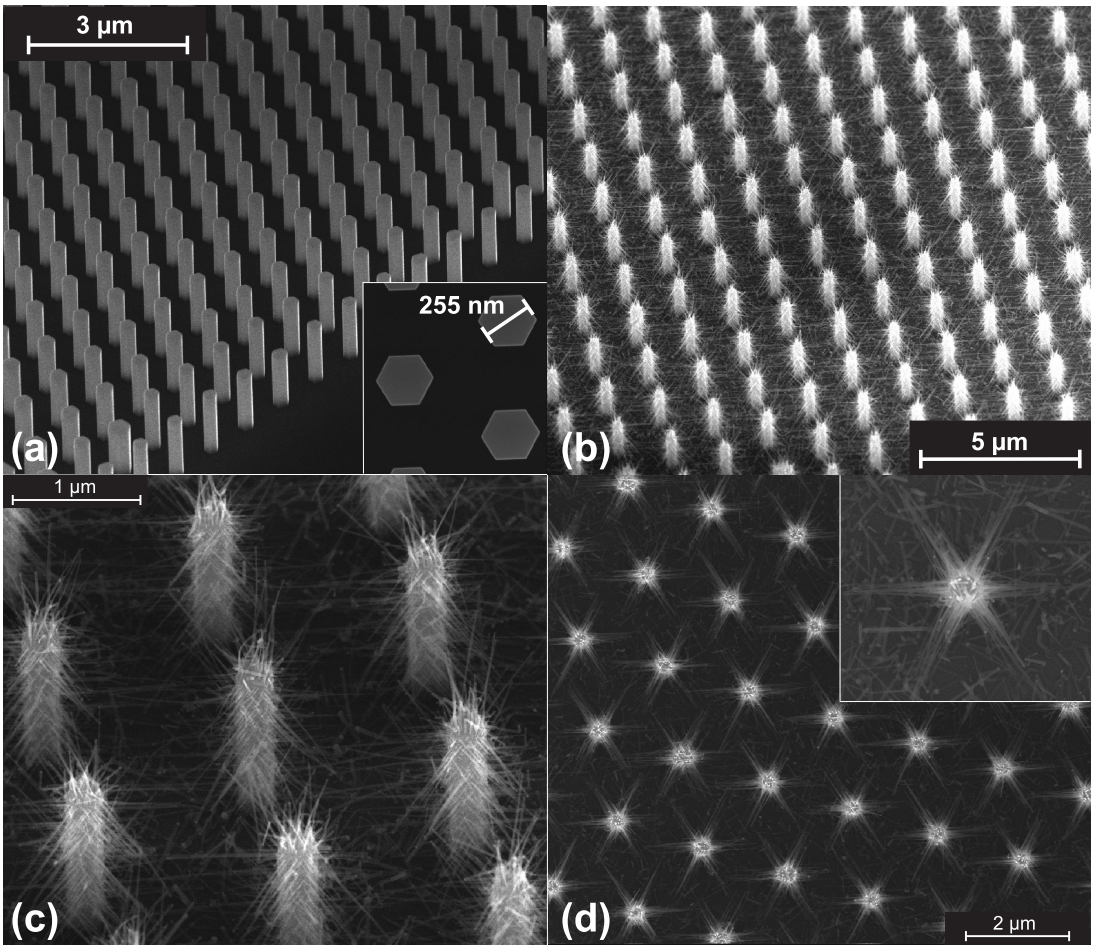


**Figure 8.50:** SEM images of (**a**) SA-MOVPE grown GaAs nanowire array titled 45° to the surface normal with an array pitch of 1 µm (*Inset*: top-view). (**b**) and (**c**) SA-MOVPE + VLS grown nanotrees array with an array pitch of 2 µm, (**d**) top-view.

VLS nanowires the next neighbor is possible and allows the realization of complex nano-networks.

This work was supported by the DFG within FOR 522.

[1] V. Gottschalch et al.: Thin Solid Films **416**, 224 (2002), doi:10.1016/S0040-6090(02)00704-6
[2] H. Paetzelt et al.: J. Cryst. Growth **310**, 5093 (2008), doi:10.1016/j.jcrysgro.2008.06.065
[3] E. Givargizov: J. Cryst. Growth **31**, 20 (1975), doi:10.1016/0022-0248(75)90105-0
[4] T. Hamano et al.: Jpn. J. Appl. Phys. **36**, L286 (1997), doi:10.1143/JJAP.36.L286

## 8.31 Funding

*One-dimensional heterostructures and nanowire arrays*
Prof. Dr. M. Grundmann, Dr. M. Lorenz
DFG Gr 1011/11-1 within DFG Forschergruppe FOR 522 *Architecture of nano- and microdimensional building blocks*

*Lateral optical confinement of microresonators*
Prof. Dr. B. Rheinländer, Dr. V. Gottschalch
DFG Rh 28/4-1 within DFG Forschergruppe FOR 522 *Architecture of nano- and microdimensional building blocks*

*Transferability of the codoping concept to ternary ZnO:(Cd,Mg)*
Prof. Dr. M. Grundmann, Dr. H. Schmidt
DFG Gr 1011/10-3 within DFG-Schwerpunktprogramm 1136 *Substitutionseffekte in ionischen Festkörpern*

*Self-assembled Semiconductor Nanostructures for New Devices in Photonics and Electronics* (SANDiE)
Coordinator: Universität Leipzig, Prof. Dr. M. Grundmann
Sixth Framework Programme, European Network of Excellence, Contract NMP4-CT-2004-500101

*Leipzig School of Natural Sciences – Building with Molecules and Nano-objects* (BuildMoNa)
Prof. Dr. M. Grundmann
GSC 185/1

*Nanophotonic and nanoelectronic Devices fom Oxide Semiconductors (NANDOS)*
Prof. Dr. M. Grundmann, Dr. M. Lorenz
EU STReP Contract No. 016 424

*Polarisationswechselwirkung in Laser-MBE Wurtzit–Perowskit-Heterostrukturen*
Dr. M. Lorenz
SFB 762/1-2008, TP A2 within SFB 762 "Funktionalität Oxidischer Grenzflächen"

*Optische Untersuchungen zur dielektrischen Funktion und ihrer Dynamik an oxidischen Heterostrukturen*
Prof. Dr. M. Grundmann, Prof. Dr. H. Gräner (Martin-Luther-Universität Halle-Wittenberg)
SFB 762/1-2008, TP B3 within SFB 762 "Funktionalität Oxidischer Grenzflächen"

*Lateraler Transport in oxidischen Feldeffekt-Strukturen*
Prof. Dr. M. Grundmann, Prof. Dr. J. Christen (Otto-von-Guericke-Universität Magdeburg), Dipl.-Phys. H. Frenzel
SFB 762/1-2008, TP B4 within SFB 762 "Funktionalität Oxidischer Grenzflächen"

*Spinabhängiges Tunneln in oxidischen Heterostrukturen*
Prof. Dr. M. Grundmann, Prof. Dr. I. Mertig (Martin-Luther-Universität Halle-Wittenberg), Dipl.-Phys. M. Schmidt
SFB 762/1-2008, TP B6 within SFB 762 "Funktionalität Oxidischer Grenzflächen"

*Bose–Einstein-Kondensation von Exziton-Polaritonen bei Raumtemperatur*
Prof. Dr. Marius Grundmann, Dr. Rüdiger Schmidt-Grund, Dipl.-Phys. Chris Sturm
DFG Gr 1011/20-1

*Herstellung und Charakterisierung von UV-Mikrokavitäten*
Dipl. Phys. H. Hilmer
Landesinnovationsstipendium im Rahmen des Europäischen Sozialfonds

*Herstellung und Charakterisierung von transparenten Feldeffekttransistoren*
Dipl. Phys. A. Lajn
Landesinnovationsstipendium im Rahmen des Europäischen Sozialfonds

*Herstellung und Charakterisierung von Quantendraht-Heterostrukturen*
Dipl. Phys. M. Lange
Landesinnovationsstipendium im Rahmen des Europäischen Sozialfonds

*Magnetische Tunnelkontakte*
Dipl. Phys. J. Zippel
Landesinnovationsstipendium im Rahmen des Europäischen Sozialfonds

## 8.32 Organizational Duties

M. Grundmann

- Direktor des Institut für Experimentelle Physik II
- Coordinator of the European Network of Excellence on 'Self-Assembled semiconductor Nanostructures for new Devices in photonics and Electronics' (SANDiE, www.sandie.org)
- Sprecher der DFG Forschergruppe 'Architektur von nano- und mikrodimensionalen Strukturelementen' (FOR 522), http://www.uni-leipzig.de/~for522
- Stellvertretender Sprecher der Graduiertenschule 'Leipzig School of Natural Sciences – Building with Molecules and Nano-objects' (BuildMoNa), http://www.buildmona.de
- Stellvertretender Sprecher des Sonderforschungsbereiches zur "Funktionalität Oxidischer Grenzflächen" (SFB 762), http://www.physik.uni-halle.de/FG
- Sprecher der Fächerübergreifenden Arbeitsgemeinschaft Halbleiterforschung Leipzig (FAHL), http://www.uni-leipzig.de/~fahl
- Mitglied des Beirat Ionenstrahlzentrum, FZR, Rossendorf
- Project Reviewer: Deutsche Forschungsgemeinschaft (DFG), Alexander von Humboldt-Stiftung (AvH), Schweizerischer Nationalfonds zur Förderung der wissenschaftlichen Forschung (FNSNF), Fonds zur Förderung der Wissenschaften (FWF)
- Referee: Appl. Phys. Lett., Electr. Lett., J. Appl. Phys., Nature, Physica E, Phys. Rev. B., Phys. Rev. Lett., Phys. Stat. Sol., Science

M. Lorenz

- Project Reviewer: United States – Israel Binational Science Foundation (BSF)
- Referee: Appl. Phys. Lett., IEEE Transact. Appl. Supercond., J. Am. Chem. Soc., J. Phys. D Appl. Phys., Thin Solid Films, J. Cryst. Growth, Mater. Lett., Appl. Surf. Sci., Appl. Phys. A, J. Phys. Chem., Mat. Sci. Eng. B, Semicond. Sci. Technol., Nanotechnology

H. von Wenckstern

- Referee: Appl. Phys. Lett., J. Appl. Phys., Thin Solid Films, Solid State Electron., Phys. Stat. Sol., Superlatt. Microstruct., J. Electron. Mater., Turk. J. Phys., J. Mater. Sci. Mater. Electron., J. Vac. Sci. Technol., Mater. Sci. Eng. B, J. Nanosci. Nanotechnol., Microelectron. Eng., J. Phys. D, J. Cryst. Growth, Surf. Sci.

## 8.33 External Cooperations

**Academic**

- Leibniz-Institut für Oberflächenmodifizierung e.V., Leipzig, Germany
  Prof. Dr. B. Rauschenbach, Prof. Dr. T. Höche, Dr. J. Gerlach
- Universität Leipzig, Fakultät für Biowissenschaften, Pharmazie und Psychologie, Germany
  Prof. Dr. A. Beck-Sickinger
- Universität Leipzig, Fakultät für Chemie und Mineralogie, Germany
  Dr. V. Gottschalch, Prof. Dr. H. Krautscheid, Prof. Dr. K. Bente
- Universität Halle-Wittenberg, Germany
  Prof. Dr. I. Mertig, Prof. Dr. W. Widdra, Prof. Dr. H. Graener
- Max-Planck-Institut für Mikrostrukturphysik, Halle/Saale, Germany
  Prof. Dr. U. Gösele, Dr. O. Breitenstein, Dr. A. Ernst, Dr. P. Werner, Dr. D. Hesse
- Forschungszentrum Dresden-Rossendorf, Germany
  Prof. Dr. M. Helm
- Technische Universität Berlin, Germany
  Prof. Dr. D. Bimberg, Dr. A. Hoffmann
- Universidade de Aveiro, Portugal
  Prof. Dr. N. Sobolev
- Chinese Academy of Sciences, Institute of Physics, Beijing, P.R. China
  Prof. Dr. Yusheng He
- Universität Gießen, Germany
  Prof. Dr. B. Meyer, Dr. D. Hofmann, Prof. Dr. J. Janek
- Universität Magdeburg, Germany
  Prof. Dr. A. Krost, Dr. A. Dadgar, Prof. Dr. J. Christen
- Universität Ulm, Germany
  Prof. Dr. F. Scholz, Prof. Dr. K. Thonke
- Universität Bonn, Germany
  Prof. Dr. W. Mader
- Universität Hannover, Germany
  Prof. Dr. M. Binnewies
- Göteborg University, Sweden
  Prof. Dr. M. Willander

- NCSR "Demokritos", Institute of Materials Science, Greece
  Prof. Dr. A. Travlos
- Univerité Joseph Fourier, Grenoble, France
  Prof. Dr. D. Le Si Dang
- University of Pretoria, South Africa
  Prof. F.D. Auret
- University of Canterbury, Christchurch, New Zealand
  Prof. S. Durbin
- University of Nebraska, Lincoln, USA
  Prof. Dr. M. Schubert
- Centre de Recherche sur l'Hétéro-Epitaxie et ses Applications (CNRS-CRHEA), Valbonne, France
  Dr. J. Zúñiga Pérez

**Industry**

- Solarion AG, Leipzig, Germany
  Dr. Alexander Braun, Dr. Andreas Rahm
- El-Mul Technologies, Yavne, Israel
  Dr. Armin Schön
- OSRAM Opto-Semiconductors GmbH, Regensburg, Germany
  Dr. V. Härle, Dr. S. Lutgen
- Freiberger Compound Materials GmbH, Freiberg, Germany
  Dr. G. Leibiger
- Q-Cells SE, Thalheim, Germany
  Dr. K. Petter

## 8.34 Publications

**Journals**

F.D. Auret, W.E. Meyer, P.J.J. van Rensburg, M. Hayes, J.M. Nel, H. von Wenckstern, H. Hochmuth, G. Biehne, M. Lorenz, M. Grundmann: *Dependence of trap concentrations in ZnO thin films on annealing conditions*, J. Korean Phys. Soc. **53**, 3064 (2008)

J. Bachmann, R. Zierold, Y.T. Chong, R. Hauert, C. Sturm, R. Schmidt-Grund, B. Rheinländer, M. Grundmann, U. Gösele, K. Nielsch: *A practical, self-catalytic, atomic layer deposition of silicon dioxide*, Angew. Chem. Int. Ed. **47**, 6177 (2008), doi:10.1002/anie.200800245

J. Bachmann, R. Zierold, Y.T. Chong, R. Hauert, C. Sturm, R. Schmidt-Grund, B. Rheinländer, M. Grundmann, U. Gösele, K. Nielsch: *Selbstkatalytische Atomlagenabscheidung von Siliciumdioxid*, Angew. Chem. **120**, 6272 (2008), doi:10.1002/ange.200800245

M. Brandt, H. von Wenckstern, H. Schmidt, A. Rahm, G. Biehne, G. Benndorf, H. Hochmuth, M. Lorenz, C. Meinecke, T. Butz, M. Grundmann: *High electron mobility of phosphorous doped homoepitaxial ZnO thin films grown by pulsed laser deposition*, J. Appl. Phys. **104**, 013 708 (2008), doi:10.1063/1.2953066

B.Q. Cao, M. Lorenz, M. Brandt, H. von Wenckstern, J. Lenzner, G. Biehne, M. Grundmann: *p-type conducting ZnO:P microwires prepared by direct carbothermal growth*, Phys. Stat. Sol. RRL **2**, 37 (2008), doi:10.1002/pssr.200701268

B.Q. Cao, M. Lorenz, H. von Wenckstern, C. Czekalla, M. Brandt, J. Lenzner, G. Benndorf, G. Biehne, M. Grundmann: *Phosphorous doped ZnO nanowires: acceptor-related cathodoluminescence and p-type conducting FET characteristics*, Proc. SPIE **6895**, 689 50*V* (2008), doi:10.1117/12.763435

C. Czekalla, J. Guinard, C. Hanisch, B.Q. Cao, E.M. Kaidashev, N. Boukos, A. Travlos, J. Renard, B. Gayral, D. Le Si Dang, M. Lorenz, M. Grundmann: *Spatial fluctuations of optical emission from single ZnO/MgZnO nanowire quantum wells*, Nanotechnology **19**, 115 202 (2008), doi:10.1088/0957-4484/19/11/115202

C. Czekalla, C. Sturm, R. Schmidt-Grund, B.Q. Cao, M. Lorenz, M. Grundmann: *Whispering gallery mode lasing in zinc oxide microwires*, Appl. Phys. Lett. **92**, 241 102 (2008), doi:10.1063/1.2946660

H. Frenzel, A. Lajn, M. Brandt, H. von Wenckstern, G. Biehne, H. Hochmuth, M. Lorenz, M. Grundmann: *ZnO metal-semiconductor field-effect transistors with Ag-Schottky gates*, Appl. Phys. Lett. **92**, 192 108 (2008), doi:10.1063/1.2926684

D. Fritsch, Heidemarie Schmidt, Rüdiger Schmidt-Grund, and Marius Grundmann: *Intensity of optical absorption close to the band edge in strained ZnO films*, J. Korean Phys. Soc. **53**, 123 (2008)

D. Hofstetter, Y. Bonetti, E. Baumann, F.R. Giorgetta, A.-H. El-Shaer, A. Bakin, A. Waag, R. Schmidt-Grund, M. Grundmann, M. Schubert: *Characterization of an optically pumped ZnO-based 3rd order distributed feedback laser*, Proc. SPIE **6895**, 68 950J (2008), doi:10.1117/12.762128

M. Lorenz, G. Wagner, A. Rahm, H. Schmidt, H. Hochmuth, H. Schmid, W. Mader, M. Brandt, H. von Wenckstern, M. Grundmann: *Homoepitaxial ZnO thin films by PLD: Structural properties*, Phys. Stat. Sol. C **5**, 3280 (2008), doi:10.1002/pssc.200779504

M. Mäder, J.W. Gerlach, T. Höche, C. Czekalla, M. Lorenz, M. Grundmann, B. Rauschenbach: *ZnO nanowall networks grown on DiMPLA pre-patterned thin gold films*, Phys. Stat. Sol. RRL **2**, 200 (2008), doi:10.1002/pssr.200802174

F. Menzel, D. Spemann, J. Lenzner, W. Böhlmann, G. Zimmermann, T. Butz: *Creation of GaAs microstructures using the nuclear nanoprobe LIPSION*, Semicond. Sci. Technol. **23**, 125 028 (2008), doi:10.1088/0268-1242/23/12/125028

A. Müller, G. Benndorf, S. Heitsch, C. Sturm, M. Grundmann: *Exciton–phonon coupling and exciton thermalization in $Mg_xZn_{1-x}O$ thin films*, Solid State Commun. **148**, 570 (2008), doi:10.1016/j.ssc.2008.09.045

S. Müller, C. Ronning, M. Lorenz, C. Czekalla, G. Benndorf, H. Hochmuth, M. Grundmann, H. Schmidt: *Intense white photoluminescence emission of V-implanted zinc oxide thin films*, J. Appl. Phys. **104**, 123 504 (2008), doi:10.1063/1.3041652

A.S. Pereira, S. Pereira, T. Trindade, A.O. Ankiewicz, M.C. Carmo, N.A. Sobolev, W. Gehlhoff, A. Hoffmann, M. Grundmann: *Surface modification of Co-doped ZnO nanocrystals and its effect on the magnetic properties*, J. Appl. Phys. **103**, 07*D* 140 (2008), doi:10.1063/1.2833300

H. Schmidt, M. Wiebe, B. Dittes, M. Grundmann: *Meyer-Neldel rule in ZnO*, Appl. Phys. Lett. **31**, 232 110 (2008), doi:10.1063/1.2819603

R. Schmidt-Grund, D. Fritsch, M. Schubert, B. Rheinländer, H. Schmidt, C.M. Herzinger, E.M. Kaidashev, M. Lorenz, M. Grundmann: *Vacuum ultraviolet dielectric function and band structure of ZnO*, J. Korean Phys. Soc. **53**, 88 (2008)

R. Schmidt-Grund, B. Rheinländer, C. Czekalla, G. Benndorf, H. Hochmuth, M. Lorenz, M. Grundmann: *Exciton-polariton formation at room temperature in a planar ZnO resonator structure*, Appl. Phys. B **93**, 331 (2008), doi:10.1007/s00340-008-3160-x

J. Sellmann, C. Sturm, R. Schmidt-Grund, C. Czekalla, J. Lenzner, H. Hochmuth, B. Rheinländer, M. Lorenz, M. Grundmann: *Structural and optical properties of $ZrO_2$ and $Al_2O_3$ thin films and Bragg reflectors grown by pulsed laser deposition*, Phys. Stat. Sol. C **5**, 1240 (2008), doi:10.1002/pssc.200777875

C. Sturm, T. Chavdarov, R. Schmidt-Grund, B. Rheinländer, C. Bundesmann, H. Hochmuth, M. Lorenz, M. Schubert, M. Grundmann: *Investigation of the free charge carrier properties at the ZnO-sapphire interface in a-plane ZnO films studied by generalized infrared ellipsometry*, Phys. Stat. Sol. C **5**, 1350 (2008), doi:10.1002/pssc.200777853

S.B. Thapa, J. Hertkorn, T. Wunderer, F. Lipski, F. Scholz, A. Reiser, Y. Xie, M. Feneberg, K. Thonke, R. Sauer, M. Dürrschnabel, L.D. Yao, D. Gerthsen, H. Hochmuth, M. Lorenz, M. Grundmann: *MOVPE growth of GaN around ZnO nanopillars*, J. Cryst. Growth **310**, 5139 (2008), doi:10.1016/j.jcrysgro.2008.07.009

H. von Wenckstern, M. Brandt, H. Schmidt, G. Benndorf, J. Zippel, H. Hochmuth, M. Lorenz, M. Grundmann: *Properties of homoepitaxial ZnO and ZnO:P thin films grown by pulsed laser deposition*, Proc. SPIE **6895**, 689505 (2008), doi:10.1117/12.768614

H. von Wenckstern, M. Brandt, H. Schmidt, C. Hanisch, G. Benndorf, H. Hochmuth, M. Lorenz, M. Grundmann: *Homoepitaxial ZnO thin films by Pulsed-Laser Deposition*, J. Korean Phys. Soc. **53**, 3064 (2008)

H. von Wenckstern, G. Biehne, M. Lorenz, M. Grundmann, F.D. Auret, W.E. Meyer, P.J.J. van Rensburg, M. Hayes, J.M. Nel: *Dependence Of Trap Concentrations in ZnO Thin Films on Annealing Conditions*, J. Korean Phys. Soc. **53**, 2861 (2008)

H. von Wenckstern, G. Biehne, M. Lorenz, M. Grundmann, F.D. Auret, W.E. Meyer, P.J.J. van Rensburg, M. Hayes, J.M. Nel: *Electronic properties of shallow level defects in ZnO grown by pulsed laser deposition*, J. Phys. Conf. Series **100**, 042 038 (2008)

V.M. Voora, T. Hofmann, M. Brandt, M. Lorenz, M. Grundmann, N. Ashkenov, M. Schubert: *Interface-charge-coupled polarization response of Pt-$BaTiO_3$-ZnO-Pt heterojunctions: A physical model approach* J. Electr. Mat. **37**, 1029 (2008), doi:10.1007/s11664-008-0461-0

V.M. Voora, T. Hofmann, M. Brandt, M. Lorenz, M. Grundmann, M. Schubert: *Electrooptic ellipsometry study of piezoelectric $BaTiO_3$-ZnO heterostructures*, Phys. Stat. Sol. C **5**, 1328 (2008), doi:10.1002/pssc.200777908

Q. Xu, L. Hartmann, H. Schmidt, H. Hochmuth, M. Lorenz, A. Setzer, P. Esquinazi, C. Meinecke, and M. Grundmann: *Magnetotransport properties of $Zn_{90}Mn_{7.5}Cu_{2.5}O_{100}$ films*, Thin Solid Films **516**, 1160 (2008), doi:10.1016/j.tsf.2007.06.145

Q. Xu, L. Hartmann, S. Zhou, A. Mcklich, K. Potzger, M. Helm, G. Biehne, H. Hochmuth, M. Lorenz, M. Grundmann, H. Schmidt: *Spin manipulation in Co doped ZnO*, Phys. Rev. Lett. **101**, 076 601 (2008), doi:10.1103/PhysRevLett.101.076601

Q. Xu, H. Schmidt, H. Hochmuth, M. Lorenz, A. Setzer, P. Esquinazi, C. Meinecke, M. Grundmann: *Room temperature ferromagnetism in Nd- and Mn-codoped ZnO films due to defects*, J. Phys. D Appl. Phys. **41**, 105 012 (2008), doi:10.1088/0022-3727/41/10/105012

Q. Xu, H. Schmidt, S. Zhou, K. Potzger, M. Helm, H. Hochmuth, M. Lorenz, C. Meinecke, M. Grundmann: *Magnetic and transport properties of $Cu_{1.05}Cr_{0.89}Mg_{0.05}O_2$ and $Cu_{0.96}Cr_{0.95}Mg_{0.05}Mn_{0.04}O_2$ films*, Thin Solid Films **516**, 8543 (2008), doi:10.1016/j.tsf.2008.05.012

Q. Xu, H. Schmidt, S. Zhou, K. Potzger, M. Helm, H. Hochmuth, M. Lorenz, A. Setzer, P. Esquinazi, C. Meinecke, M. Grundmann: *Room temperature ferromagnetism in ZnO films due to defects*, Appl. Phys. Lett. **92**, 082 508 (2008), doi:10.1063/1.2885730

S. Zhou, Q. Xu, K. Potzger, G. Talut, R. Grötzschel, J. Fassbender, M. Vinnichenko, J. Grenzer, M. Helm, H. Hochmuth, M. Lorenz, M. Grundmann, H. Schmidt: *Room temperature ferromagnetism in carbon-implanted ZnO*, Appl. Phys. Lett. **93**, 232 507 (2008), doi:10.1063/1.3048076

**Books**

M. Allen, H. von Wenckstern, M. Grundmann, S. Hatfield, P. Jefferson, P. King, T. Veal, C. McConville, S. Durbin: *Mechanisms in the Formation of High Quality Schottky Contacts to n-type ZnO*, ed. by D.P. Norton, C. Jagadish, I. Buyanova, and G-C. Yi, Mater. Res. Soc. Symp. Proc. **1035E** (MRS, Warrendale 2008) p 1035-L10-06

C. Bundesmann, R. Schmidt-Grund, M. Schubert: *Optical Properties of ZnO and Related Compounds*, in: *Transparent Conductive Zinc Oxide*, ed. by K. Ellmer, A. Klein, B. Rech, Springer Series in Materials Science Vol. 104 (Springer, Berlin 2008) p 79, doi:10.1007/978-3-540-73612-7

M. Grundmann, A. Rahm, T. Nobis, M. Lorenz, C. Czekalla, E.M. Kaidashev, J. Lenzner, N. Boukos, A. Travlos: *Growth and characterization of ZnO nano- and microstuctures*, in: *Handbook of Self-Assembled Semiconductor Nanostructures for Novel Devices in Photonics and Electronics*, ed. by M. Henini (Elsevier, Amsterdam 2008) p 293

M. Lorenz: *Pulsed Laser Deposition of ZnO-based Thin Films*, in: *Transparent Conductive Zinc Oxide*, ed. by K. Ellmer, A. Klein, B. Rech, Springer Series in Materials Science Vol. 104 (Springer, Berlin 2008) p 303, doi:10.1007/978-3-540-73612-7

R. Schmidt-Grund, C. Sturm, M. Schubert, B. Rheinländer, D. Faltermeier, H. Hochmuth, A. Rahm, J. Bläsing, C. Bundesmann, J. Zúñiga-Pérez, T. Chavdarov, M. Lorenz, M. Grundmann: *Valence Band Structure of ZnO and $Mg_xZn_{1-x}O$*, in: *Zinc Oxide and Related Materials*, ed. by D.P. Norton, C. Jagadish, I. Buyanova, and G-C. Yi, Mater. Res. Soc. Symp. Proc. **1035E** (MRS, Warrendale 2008) p 1035-L11-37

**Talks**

J. Bachmann, R. Zierold, Y.T. Chong, C. Sturm, R. Schmidt-Grund, B. Rheinländer, M. Grundmann, U. Gösele, K. Nielsch: *A practical, self-catalytic, atomic layer deposition of silicon dioxide*, 8. Int. Conf. Atomic Layer Deposition, Bruges, Belgium, 29. June – 2. July 2008

M. Brandt, H. von Wenckstern, C. Dietrich, G. Benndorf, J. Zippel, A. Abdullah, C. Meinecke, T. Butz, H. Hochmuth, M. Lorenz, M. Grundmann: *Dopant activation in homoepitaxial ZnO:P and ZnMgO:P thin films*, 5. Int. Workshop ZnO and Related Materials, Ann Arbor, USA, 22. – 24. September 2008

M. Brandt, H. von Wenckstern, H. Hochmuth, M. Lorenz, G. Biehne, G. Benndorf, C. Meinecke, T. Butz, H. Schmidt, A. Rahm, M. Grundmann: *Homoepitaxial growth of ZnO thin film by pulsed laser deposition (PLD)*, 72. DPG Spring Meeting, Berlin, Germany 25. – 29. February 2008

M. Brandt, H. von Wenckstern, H. Hochmuth, M. Lorenz, J. Zippel, J. Lenzner, G. Benndorf, M. Grundmann: *Accumulation of carriers in ZnO/MgZnO heterostructures and quantum wells*, 2. Int. Symp. TCO, Hersonissos, Crete, Greece, 22. – 26. October 2008

B.Q. Cao, M. Lorenz, A. Rahm, H. von Wenckstern, C. Czekalla, J. Lenzner, G. Benndorf, M. Grundmann: *Phosphorous doped ZnO nanowires: Acceptor-related cathodoluminescence and p-type conducting FET-characteristics*, SPIE Photonics West 2008, San Jose, USA, 19. – 24. January 2008

B.Q. Cao, M. Lorenz, H. von Wenckstern, C. Czekalla, M. Brandt, A. Rahm, J. Lenzner, G. Benndorf, G. Biehne, M. Grundmann: *Phosphorus doped ZnO wires: acceptor-related cathodoluminescence and p-type conducting FET-characteristics*, E-MRS Spring Meeting, Strasbourg, France, 26. – 30. May 2008

C. Czekalla, C. Hanisch, B.Q. Cao, M. Lorenz, M. Grundmann, J. Guinard, D. Le Si Dang, N. Boukos, A. Travlos, J. Renard, B. Gayral: *Narrow quantum dot-like luminescence lines from single ZnO/MgZnO nanowire quantum wells*, E-MRS Spring Meeting, Strasbourg, France, 26. – 30. May 2008

C. Czekalla, J. Lenzner, R. Schmidt-Grund, B.Q. Cao, M. Grundmann: *Lasing modes in ZnO microwires*, 72. DPG Spring Meeting, Berlin, Germany 25. – 29. February 2008

C. Czekalla, R. Schmidt-Grund, C. Sturm, J. Lenzner, M. Lange, M. Lorenz, M. Grundmann: *Whispering gallery mode lasing in zinc oxide microwires*, 29. Int. Conf. Phys. Semicond., Rio de Janeiro, Brasil, 27. August – 01. September 2008

M. Ellguth, M. Schmidt, A. Lajn, H. von Wenckstern, R. Pickenhain, M. Grundmann: *Modelling of the frequency and temperature dependence of ZnO Schottky diode capacitance*, 72. DPG Spring Meeting, Berlin, Germany 25. – 29. February 2008

H. Frenzel, A. Lajn, H. von Wenckstern, M. Brandt, G. Biehne, H. Hochmuth, M. Grundmann: *Transport investigations on ZnO field-effect structures*, 1. BuildMoNa Workshop, Leipzig, Germany, 16./17. October 2008

H. Frenzel, H. von Wenckstern, A. Lajn, M. Brandt, G. Biehne, H. Hochmuth, M. Grundmann: *Transparent ZnO metal-semiconductor field-effect transistors*, 5. Int. Workshop ZnO and Related Materials, Ann Arbor, USA, 22. – 24. September 2008

H. Frenzel, H. von Wenckstern, H. Hochmuth, G. Biehne, M. Lorenz, M. Grundmann: *ZnO-based MIS diodes*, 72. DPG Spring Meeting, Berlin, Germany 25. – 29. February 2008

M. Grundmann: *Epitaktische Halbleiter-Nanosysteme: Bausteine für die ZnO Nanophotonik* (invited), 4. nanoMA-Symposium, Technische Universität Chemnitz, Germany, 10. July 2008

M. Grundmann: *On the road to ZnO lasers: Homoepitaxy, p-doping and nanostructures* (invited colloquium), Max-Born-Institute Berlin, Germany, 29. May 2008

M. Grundmann: *ZnO Nanowhiskers: Transport and Optical properties* (invited), Japan–Germany Workshop Nanoelectronics (DFG-JST), Aachen, Germany, 05. – 07. March 2008

H. Hilmer, J. Sellmann, C. Sturm, R. Schmidt-Grund, H. Hochmuth, J. Zúñiga-Pérez, G. Zimmermann, J. Lenzner, C. Czekalla, G. Benndorf, M. Lorenz, B. Rheinländer, A. Serghei, M. Grundmann: *PLD growth of ZnO resonators based on all-oxide Bragg reflectors*, 72. DPG Spring Meeting, Berlin, Germany 25. – 29. February 2008

D. Hofstetter, Y.C. Bonetti, A.-H. El-Shaer, A.S. Bakin, A. Waag, R. Schmidt-Grund: *Demonstration of an ultraviolet optically pumped 3rd order ZnO-based distributed feedback laser*, SPIE Photonics West 2008, San Jose, USA, 19. – 24. January 2008

A. Lajn, H. von Wenckstern, M. Schmidt, M. Brandt, G. Biehne, H. Hochmuth, M. Lorenz, M. Grundmann: *Sputtered silver contacts on zinc oxide*, 72. DPG Spring Meeting, Berlin, Germany 25. – 29. February 2008

A. Lajn, H. von Wenckstern, Z. Zhang, C. Czekalla, G. Biehne, H. Hochmuth, M. Lorenz, M. Grundmann, S. Künzel, C. Vogt, R. Denecke: *Properties of reactively sputtered Ag, Au, Pd and Pt schottky contacts on n-type ZnO*, 5. Int. Workshop ZnO and Related Materials, Ann Arbor, USA, 22. – 24. September 2008

M. Lorenz: *Gepulste Laser-Plasmaabscheidung (PLD) von oxidischen Dünnfilmen und Nanostrukturen* (invited), Coherent-Technologieseminar, Göttingen, Germany, 19. June 2008

M. Lorenz, B.Q. Cao, G. Zimmermann, G. Biehne, C. Czekalla, H. Frenzel, H. von Wenckstern, M. Grundmann: *ZnO p–n-junctions built from n-type ZnO:Ga films and p-type ZnO:P nanowires, reproducibly grown by PLD*, 5. Int. Workshop ZnO and Related Materials, Ann Arbor, USA, 22. – 24. September 2008

M. Lorenz, B.Q. Cao, G. Zimmermann, H. von Wenckstern, M. Brandt, G. Wagner, C. Czekalla, G. Benndorf, H. Hochmuth, M. Grundmann: *Recent issues in ZnO homoepitaxy and ZnO p-type conductivity*, THIOX Workshop, Sestri Levante, Italy, 09. – 11. April 2008

M. Lorenz, G. Wagner, H. von Wenckstern, M. Brandt, A. Rahm, H. Schmidt, C. Czekalla, G. Benndorf, H. Hochmuth, M. Grundmann: *Homoepitaxial undoped and doped ZnO thin films grown by Pulsed Laser Deposition*, SPIE Photonics West 2008, San Jose, USA, 19. – 24. January 2008

C. Meinecke, A. Rahm, M. Grundmann, T. Butz: *Quantitative Elemental Characterisation of Mg-, Mn- and Co doped ZnO Nanowires and Films*, 11. Int. Conf. Nucl. Microprobe Technol. Appl., Debrecen, Hungary, 20. – 25. July 2008

F. Menzel, D. Spemann, T. Koal, J. Lenzner, T. Butz: *Application of proton beam writing for grayscale lithography in negative resist materials*, 11. Int. Conf. Nucl. Microprobe Technol. Appl., Debrecen, Hungary, 20. – 25. July 2008

A. Müller, M. Stölzel, G. Benndorf, M. Grundmann: *Time-Resolved Photoluminescence Spectroscopy on MgZnO-based Layers and Quantum Wells*, 1. BuildMoNa Workshop, Leipzig, Germany, 16./17. October 2008

M. Schmidt, G. Brauer, W. Skorupa, M. Helm, M. Ellguth, H. von Wenckstern, R. Pickenhain, M. Grundmann: *Electrical characterisation of oxygen implanted ZnO thin films*, 72. DPG Spring Meeting, Berlin, Germany 25. – 29. February 2008

R. Schmidt-Grund, C. Sturm, H. Hilmer, J. Sellmann, C. Czekalla, B. Rheinländer, J. Lenzner, H. Hochmuth, A. Rahm, M. Lorenz, M. Grundmann: *Exciton-polaritons in ZnO microcavity resonators*, 29. Int. Conf. Phys. Semicond., Rio de Janeiro, Brasil, 27. August – 01. September 2008

C. Sturm, H. Hilmer, R. Schmidt-Grund, J. Sellmann, C. Czekalla, M. Lorenz, M. Grundmann: *Strong Exciton-Photon Coupling in a ZnO based Resonator*, 5. Int. Workshop ZnO and Related Materials, Ann Arbor, USA, 22. – 24. September 2008

C. Sturm, H. von Wenckstern, R. Schmidt-Grund, M. Brandt, T. Chavdarov, B. Rheinländer, C. Bundesmann, H. Hochmuth, M. Lorenz, M. Schubert, M. Grundmann: *Determination of the free charge carrier profile in ZnO films*, 72. DPG Spring Meeting, Berlin, Germany 25. – 29. February 2008

H. von Wenckstern: *Doping, contacting, defect levels and transport properties of ZnO* (invited), Kolloquium AG Wegscheider, Universität Regensburg, Germany, 17. November 2008

H. von Wenckstern, M. Brandt, J. Zippel, A. Lajn, M. Lange, G. Benndorf, H. Hochmuth, M. Lorenz, M. Grundmann: *Polarization induced two-dimensional electron gases localized at the ZnO surface or the ZnO/ZnMgO interface*, 29. Int. Conf. Phys. Semicond., Rio de Janeiro, Brasil, 27. August – 01. September 2008

**Posters**

M. Brandt, H. Frenzel, H. Hochmuth, M. Lorenz, J. Schubert, M. Grundmann: *Ferroelectric thin film field-effect transistors based on ZnO/$BaTiO_3$ heterostructures*, 5. Int. Workshop ZnO and Related Materials, Ann Arbor, USA, 22. – 24. September 2008

M. Brandt, H. Hochmuth, M. Lorenz, N. Ashkenov, M. Schubert, V. Voora, M. Grundmann: *Epitaxial ferroelectric BTO/ZnO heterostructures*, 72. DPG Spring Meeting, Berlin, Germany 25. – 29. February 2008

C. Czekalla, R. Schmidt-Grund, C. Sturm, J. Lenzner, M. Lange, M. Lorenz, M. Grundmann: *Whispering gallery mode lasing in zinc oxide microwires*, 5. Int. Workshop ZnO and Related Materials, Ann Arbor, USA, 22. – 24. September 2008

M. Ellguth, M. Schmidt, H. von Wenckstern, R. Pickenhain, M. Grundmann: *Characterisation of deep defects in ZnO thin films by means of Optical Deep Level Transient Spectroscopy (ODLTS)*, 72. DPG Spring Meeting, Berlin, Germany 25. – 29. February 2008

H. Frenzel, A. Lajn, M. Brandt, H. von Wenckstern, G. Biehne, H. Hochmuth, M. Lorenz, M. Grundmann: *ZnO metal-semiconductor field-effect transistors with Ag Schottky gates*, 2. Int. Symp. TCO, Hersonissos, Crete, Greece, 22. – 26. October 2008

H. Frenzel, A. Lajn, H. von Wenckstern, G. Biehne, H. Hochmuth, M. Lorenz, M. Grundmann: *ZnO metal-semiconductor field-effect transistors with Ag Schottky contacts*, THIOX Meeting, Sestri Levante, Italy, , 09. – 11. April 2008

H. Frenzel, H. von Wenckstern, M. Brandt, G. Biehne, H. Hochmuth, M. Lorenz, M. Grundmann: *Lateral transport investigations on atomic interfaces in multiferroic heterostructures*, 1. Scientific Symposium of BuildMoNa, Leipzig, Germany, 07./08. February 2008

H. Frenzel, H. von Wenckstern, A. Lajn, M. Brandt, G. Biehne, H. Hochmuth, M. Lorenz, M. Grundmann: *Interface effects in ZnO metal-insulator- semiconductor- and metal-semiconductor-structures*, 29. Int. Conf. Phys. Semicond., Rio de Janeiro, Brasil, 27. August – 01. September 2008

H. Hilmer, J. Sellmann, C. Sturm, R. Schmidt-Grund, C. Czekalla, B. Rheinländer, J. Lenzner, H. Hochmuth, M. Lorenz, M. Grundmann: *PLD Growth of High-Reflective All-Oxide Bragg Reflectors for ZnO Resonators*, 29. Int. Conf. Phys. Semicond., Rio de Janeiro, Brasil, 27. August – 01. September 2008

M. Lange, S. Heitsch, G. Benndorf, C. Czekalla, H. Hochmuth, M. Lorenz, M. Grundmann: *Investigations of the Properties of MgZnO-ZnO Quantum Well Interfaces grown by Pulsed Laser Deposition*, 72. DPG Spring Meeting, Berlin, Germany 25. – 29. February 2008

M. Lange, G. Benndorf, C. Czekalla, M. Brandt, H. Hochmuth, M. Lorenz, M. Grundmann: *Temperature Dependence of Localization Effects of Excitons in CdZnO*, 5. Int. Workshop ZnO and Related Materials, Ann Arbor, USA, 22. – 24. September 2008

C. Meinecke, M. Brandt, M. Grundmann, J. Vogt, T. Butz: *Characterization and elemental analysis of nano- and microdimensional structures using PIXE and RBS*, 72. DPG Spring Meeting, Berlin, Germany 25. – 29. February 2008

F. Menzel, D. Spemann, J. Lenzner, W. Böhlmann, G. Zimmermann, T. Butz: *Fabrication of microstructures in III-V semiconductors by proton beam writing*, 11. Int. Conf. Nucl. Microprobe Technol. Appl., Debrecen, Hungary, 20. – 25. July 2008

A. Müller, G. Benndorf, S. Heitsch, H. Hochmuth, C. Meinecke, M. Grundmann: *Optical investigations of hexagonal $Mg_xZn_{1-x}O$ thin layers in UV spectral range*, 72. DPG Spring Meeting, Berlin, Germany 25. – 29. February 2008

A. Müller, G. Benndorf, S. Heitsch, M. Stölzel, H. Hochmuth, M. Grundmann: *Time-Resolved Photoluminescence Spectroscopy*, 1. Scientific Symposium of BuildMoNa, Leipzig, Germany, 07./08. February 2008

M. Schmidt, M. Ellguth, H. von Wenckstern, R. Pickenhain, M. Grundmann, G. Brauer, W. Skorupa, M. Helm: *Defects in oxygen and zinc ion implanted ZnO thin films*, 5. Int. Workshop ZnO and Related Materials, Ann Arbor, USA, 22. – 24. September 2008

R. Schmidt-Grund, H. Hilmer, C. Czekalla, B.Q. Cao, C. Sturm, M. Grundmann: *Polarisation dependence of the free discrete exciton luminescence in ZnO microwires*, 72. DPG Spring Meeting, Berlin, Germany 25. – 29. February 2008

J. Sellmann, C. Sturm, R. Schmidt-Grund, H. Hilmer, H. Hochmuth, C. Czekalla, M. Lorenz, M. Grundmann: *Structural and optical properties of $ZrO_2$ and $Al_2O_2$ thin films and Bragg reflectors grown by pulsed laser deposition*, 72. DPG Spring Meeting, Berlin, Germany 25. – 29. February 2008

C. Sturm, R. Schmidt-Grund, C. Czekalla, B. Rheinländer, J. Lenzner, G. Benndorf, H. Hochmuth, M. Lorenz, M. Grundmann: *Exciton-Photon-Coupling in ZnO Microcavities*, 2008 Latsis Symposium at EPFL, Lausanne, Switzerland, 28. – 30. January 2008

C. Sturm, R. Schmidt-Grund, J. Sellmann, H. Hilmer, B. Rheinländer, M. Lorenz, M. Grundmann: *Calculations of the optical properties of ZnO microcavities for Bose-Einstein condensation*, 72. DPG Spring Meeting, Berlin, Germany 25. – 29. February 2008

Q. Xu, H. Schmidt, S. Zhou, K. Potzger, M. Helm, H. Hochmuth, M. Lorenz, C. Meinecke, M. Grundmann: *Magnetic properties of amorphous p-type conducting $CuCr_{0.93}Mg_{0.05}Mn_{0.02}O_2$*, 72. DPG Spring Meeting, Berlin, Germany 25. – 29. February 2008

M. Ziese, M. Khalid, A. Setzer, P. Esquinazi, M. Lorenz, H. Hochmuth, M. Grundmann, D. Spemann: *Magnetic Properties of ZnO Films grown by Pulsed Laser Deposition under $N_2$ Atmosphere*, Joint Eur. Magn. Symp. JEMS08, Dublin, Ireland, 14. – 19. September 2008

## 8.35 Graduations

**Doctorate**

- Karsten Goede
  *Rasterkraftmikroskopische Untersuchungen zur Spezifität der Peptidadhäsion auf Halbleiteroberflächen*
  August 2008
- Susanne Heitsch
  *Optimierung der PLD-Abscheidung und Lumineszenzuntersuchungen an $Mg_xZn_{1-x}O$-Dünnfilmen und -Quantengrabenstrukturen*
  June 2008
- Marc Schillgalies
  *MOVPE von InGaN-basierten Halbleiterlasern im Wellenlängenbereich von 400 nm bis 450 nm*
  August 2008
- Holger von Wenckstern
  *Doping, contacting, defect levels and transport properties of ZnO*
  May 2008

**Diploma**

- Martin Ellguth
  *Untersuchung von Midgap-Zuständen im ZnO mittels optischer und kapazitätsspektroskopischer Methoden*
  November 2008
- Helena Hilmer
  *ZnO-Mikroresonatoren mit YSZ/$Al_2O_3$-Braggspiegeln hergestellt mittels PLD*
  August 2008
- Alexander Lajn
  *Reaktiv gesputterte Schottkykontakte auf epitaktischem Zinkoxid*
  Juli 2008
- Martin Lange
  *Photolumineszenz von ZnO/CdZnO-Doppelheterostrukturen und MgZnO/ZnO-Quantengrabenstrukturen*
  September 2008
- Dominik Lausch (gemeinsame Betreuung mit Q-Cells SE, Bitterfeld-Wolfen)
  *Untersuchung von Vordurchbrüchen an Siliziumsolarzellen*
  November 2008

- Nils Neubauer (extern, Humboldt-Universität, Berlin)
  *Aufbau zweier Michelson-Interferometer zur Time-Bin-Kodierung von schmalbandigen Photonen für die Quanteninformantion*
  Mai 2008
- Jan Zippel
  *Kathodolumineszenz-Untersuchungen an MgZnO/ZnO-Doppelquantengräben*
  September 2008

**Master**

- Aziz Muhemed Abdullah
  *Crystallographic properties of homoepitaxial ZnO thin films*
  September 2008

**Bachelor**

- Artjom Bergmann
  *Charakterisierung der Eigenschaften freier Ladungsträger in ZnO anhand von Hall- und Mikro-Hall-Messungen*
  September 2008
- Henning Schulte-Huxel
  *Photoluminescence Study of Cu(InGa)$Se_2$ Thin Films*
  September 2008

## 8.36 Guests

- Ekta Makhija, M.Sc.
  Indian Institute of Technology, Kanpur, India
  16. June – 21. August 2008
- Prof. Dr. Mathias Schubert
  Department of Electrical Engineering & Center for Materials Research and Analysis, University of Nebraska, Lincoln, USA
  01. – 31. August 2008 (SFB 762)
- Dr. Konstiantyn Shportko
  Lehrstuhl der allgemeinen Physik, Pädagogische M. Dragomanow-Nationaluniversität Kiew, Ukraine
  30. June – 31. July 2008 (SFB 762)
- V. Manikyala Rao Voora
  Department of Electrical Engineering & Center for Materials Research and Analysis, University of Nebraska, Lincoln, USA
  18. July – 24. August 2008 (SFB 762)
- Dr. Jesús Zúñiga Pérez
  Centre de Recherche sur l'Hétéro-Epitaxie et ses Applications (CNRS-CRHEA), Valbonne, France
  02. September – 30. November 2008 (Alexander von Humboldt Foundation)

# 9

# Solid State Optics and Acoustics

## 9.1 Introduction

The research is concentrating on the study of transport properties of elementary excitations in condensed matter of the Bosonic type (Bosonic quasi particles). Concerning the conventional description this relates mainly to acoustic and optic waves. Special interest is currently given to the influence of anisotropy but also of inhomogeniety to the dynamics of mechanical excitations. Furthermore novel schemes and first principle modeling is developed for the study and in support of applications concerning nonlinear interaction of acoustic excitations. Applications concentrate on the enhancement and application of high resolution monitoring in space and time. The respective technologies include scanning Bosonic confocal microscopy for which even a combined instrument for optical and acoustical excitations has been developed. 3D microscopic imaging is also pursued with support of novel technologies concerning microscopic holographic imaging and microscopic line holography. With relation to temporal resolution the developments pursued in cooperation with industry include refinements of electronic schemes capable of pico-second resolution. Monitoring schemes based on the scientific developments cover concerning bio-medical applications non-invasive high resolution acoustic imaging of living mesenchymal stem cells for substantial fractions of the life cycle, acoustic monitoring of cell constructs by optical and acoustic methods, monitoring of the muscle dynamics of exercising athletes. Concerning structural health and dynamic load monitoring the developments of novel detection schemes include high resolution load monitoring in flying aircrafts, monitoring of directional solidification in the Materials Science Laboratory (MSL) of the International Space Station (ISS) but also the study of transport properties of transverse acoustic waves in fluids which determine the rheological properties. The development of monitoring technologies is supported in international co-operations including combined developments with institutions in Bangladesh, India and the USA, in European projects of the 7th Framework and of the European Space Agency (ESA) and in national projects in cooperation with industry and in projects of the Bundesministerium für Bildung und Forschung (BMBF). Basic research is supported by the Deutsche Forschungsgemeinschaft and concerning efforts related to education and didactics also by the Deutsche Akademische Austauschdienst (DAAD).

*Wolfgang Grill*

## 9.2 Non-Invasive High Resolution Acoustic Monitoring of Mesenchymal Stem Cells

M. von Buttlar, W. Grill

The goal of the project is to observe adherent living stem cells non-invasively for several days with a vector-contrast scanning acoustic microscope operating at a frequency of 1.2 GHz in reflection. Time-lapse movies of the cells are generated from recorded images in magnitude and phase contrasts. Vector-contrast scanning acoustic microscopy has the advantage of providing two contrasts in a single measurement [1]: the magnitude of the ultrasound echo signal, which relates to the extinction of the ultrasonic wave, and the phase, which relates to the time-of-flight (TOF) of the ultrasonic wave. In comparison to optical fluorescence microscopy the method is based on the inherent contrast of cells which is related to their mechanical properties. Therefore, no staining of the cells is required. The mechanical setup of the ultrasound unit was re-designed for improved vibration isolation. It is mounted on a commercially available confocal laser scanning microscope (Zeiss LSM 510 laser scanning head with an Axiovert 200M inverted microscope). The inverted optical microscope allows simultaneous optical imaging of the cells from below and acoustical imaging with the ultrasound unit from above [2]. The ovine mesenchymal stem cells used in the experiments are grown on thin cover slips. A live support system for the cells was integrated into the newly constructed observation chamber. The chamber is constantly supplied with pre-mixed gas and the temperature is regulated to 37 °C. Newly developed hardware and software routines reduce artifacts by detection of lens echo offset voltages [3] and automatically adjust the focus position, which is a prerequisite for time-lapse imaging. To allow imaging under sterile conditions, a 1 µm PET thin film was introduced as an acoustic window between the cells and the focusing transducer. Even at GHz frequencies imaging through the foil with sub-cellular resolution is possible. The software chain for instrument control, data acquisition and image processing was extended to allow batch-processing for time-lapse images and the creation of pseudo-3D movies of cell locomotion and cell–cell interaction. The magnitude data serves as the texture and the phase information is used as the height map assuming constant sound velocity inside the cells. Figure 9.1 is a single frame of a time-lapsed movie showing ovine mesenchymal stem cells. This view shows an excerpt from the imaged area of $306 \times 225\,\mu m^2$. The total observation time


**Figure 9.1:** Pseudo-3D view of ovine mesenchymal stem cells created from acoustic images in magnitude and phase contrast.

was 8 hours with a new image recorded every 40 seconds. A condensed cell is visible on the left side whereas the cells on the right side are spread out on the substrate.

Support by the Federal Ministry of Education and Research (BMBF grant 0313836, MS CartPro) is gratefully acknowledged.

[1] W. Grill et al.: Physica B **263**, 553 (1999)
[2] A. Kamanyi et al.: Ultrasonics **44**, e1295 (2006)
[3] M. von Buttlar et al.: *Offset correction for scanning acoustic microscopy with phase contrast*, Proc. Int. Congress Ultrasonics, Austria, Vienna, April 2007

## 9.3 Modeling of Local Piezoelectric Coupling and Acoustic Wave Propagation in Piezoelectric Materials

M. Pluta*, A. Habib, E. Twerdowski, M. von Buttlar, M. Schmachtl†, R. Wannemacher, W. Grill

*Institute of Physics, Wroclaw Univiversity of Technology, Poland
†EPCOS AG, Surface Acoustic Wave Components, Munich

Imaging of structures through anisotropic materials is of importance in technology and quality control. Structures of electronic circuits, created on crystals are often covered by protective layers. In such situations a non-destructive detection through the substrate with a scanning ultrasonic microscope can be the solution. In case of anisotropic material distortions of the wave front are related to the group velocity and depend on the symmetry and mechanical properties of the crystal. The Phase-Sensitive Acoustic Microscope (PSAM) technique [1], delivers amplitude and phase distribution of an acoustic signal travelling through the sample. Reconstruction of the acoustic source is performed with the application of numerical back propagation. Image obtained that way is free of geometrical aberrations, but quality of the imaging is limited through diffraction and depends on the crystal properties, way of coupling to the material and on the reconstruction algorithm.

**Image Quality Criteria** Imaging process, treated as linear and stationary, may be represented through the point spread function (PSF) $h(x, y)$. The image is described then as the convolution of the object (or source) $t(x, y)$ with PSF

$$t'(x, y) = t(x, y) \otimes h(x, y) \, . \tag{9.1}$$

The Rayleigh's two point resolution criteria tells, that two points are resolved when the distance between their images is equal to the position of the first zero of the PSF. In case of aberration free imaging PSF has the form of the Airy disc, and two mutually incoherent points are resolved when the distance between them is [2]

$$\rho_R = \frac{1.22\lambda}{2\sin(\sigma)} \, , \tag{9.2}$$

where $\lambda$ is the wavelength and $\sigma$ is the half of the objective lens aperture angle. In optics the value of $\rho_R$ is modified through mutual coherence, aperture apodisation and aberrations [3]. In acoustics we assume coherent sources. In that case the resolution gets worse and the numerical factor in (9.2) becomes 1.64 instead of 1.22 [4].

The imaging quality may be estimated with the help of the spatial frequency amplitude transfer function (FTF), which is defined as the Fourier transform of PSF. The modulus of that function, which is known as modulation transfer function (MTF). Siemens star is a test pattern usually in the form of radial black and white sectors. The pattern contains a wide range of spatial frequencies. Local contrast in the image of the Siemens star image represents value of the MTF.

**Spatial Frequency Transfer Limits in Microscopic Imaging** Due to the Abbe's theory, periodic structures are observed in microscopic imaging, as long as the waves from the 1st and −1st order of diffraction may travel through the imaging system and interfere at the output to create the image. For an acoustic source of frequency, observed with the ultrasonic lens of half aperture $\sigma$, through coupling liquid, usually water of sound velocity $c_W$, the diffractive limit for observable spatial frequencies is

$$|\nu| = f \sin(\sigma)/c_W \ . \tag{9.3}$$

The limit scales up with the acoustic frequency. To compare results measured at different frequencies the results are shown in $\nu/f$ µs/mm scale. In experiments with acoustic coupling, the lens half aperture was $\sigma = 30^\circ$, water was the coupling fluid and the spatial frequencies limit was at 0.338 µs/mm, that is treated as a reference value. At $f = 3\,\mathrm{GHz}$ , a structure of about 1000 lines per millimeter would be at the resolution limit. That is close to the resolution of typical optical systems.

## Modeling

Discussion of imaging quality in ultrasonic observations through anisotropic plates is based on the model of acoustic wave propagation and the dynamic Green's function presented in earlier papers [5, 6]. The modelling and reconstruction algorithm applied is the angular spectrum (AS) technique [7] in combination with the 2D FFT.

**Acoustic Coupling** In case of observation through a solid material of the sound velocity $c_M$, with acoustic lenses coupled acoustically through a liquid $c_W$, only $G^{(n)}_{33}$ component of the Green's tensor counts. The observed resolution in that case is limited by the aperture acceptance angle. That angle is limited effectively to the value of critical angle at the solid–liquid border

$$\sin(\sigma_C) = \frac{c_W}{c_M} = \frac{s_M}{s_W} \ , \tag{9.4}$$

where $s_M$ and $s_W$ are the respective slownesses of acoustic waves.

**Coulomb Coupling** In the case of Coulomb coupling [7] the reflected charge technique is applied to obtain the effective source. The driving force is related to the local

stress, and the coupling to acoustic wave occurs mainly in the vicinity of the free surface. In that case all three modes of the acoustic wave are excited. As a result, for point-like electrodes, the observed acoustic field is a superposition of convolutions of Green's tensor components with the electric field distribution, with the piezoelectric constants playing role of the weighting factors. Similar way of coupling is assumed also on the detection side and taken to the final convolution.

## Measurements and Modeling Results

The model of angular spectrum propagation applied in our earlier research to several types of crystals, delivered results that are in good agreement with the measurements. In case of piezoelectric $LiNbO_3$ measurements results are presented in Fig. 9.2 and of numerical simulations in Fig. 9.3 for both acoustic and Coulomb coupling.

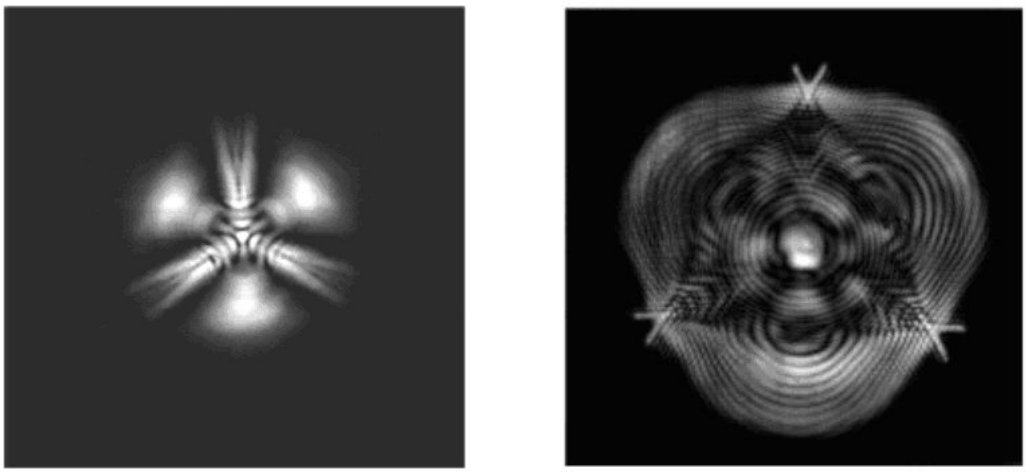

**Figure 9.2:** Amplitude of patterns obtained for $z$-cut, 5 mm thick plate of $LiNbO_3$ at frequency of 89.6 MHz. Measurements with PSAM technique for Coulomb (*left*) and acoustic coupling (*right*). Image size is $15 \times 15\,\mathrm{mm}^2$.

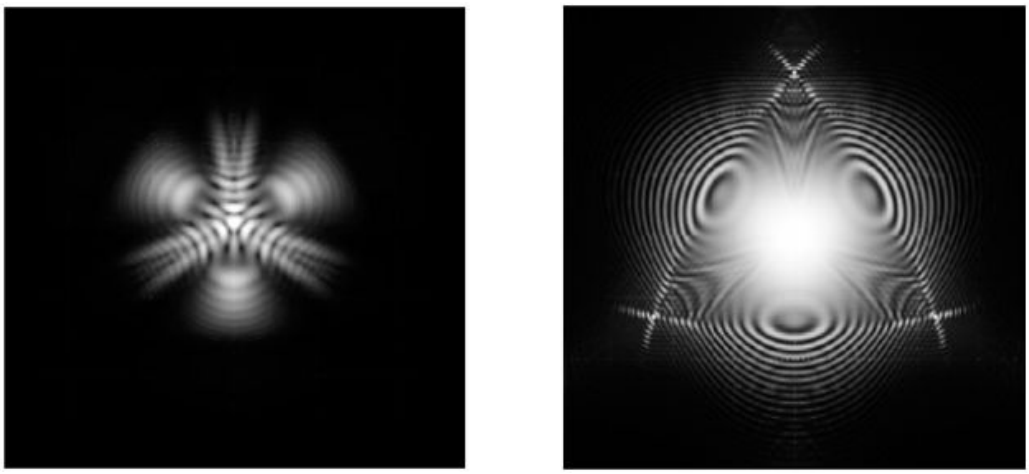

**Figure 9.3:** Numerical simulations of PSAM amplitude for parameters as in Fig. 9.2 – Coulomb coupling (*left*), acoustic coupling (*right*).

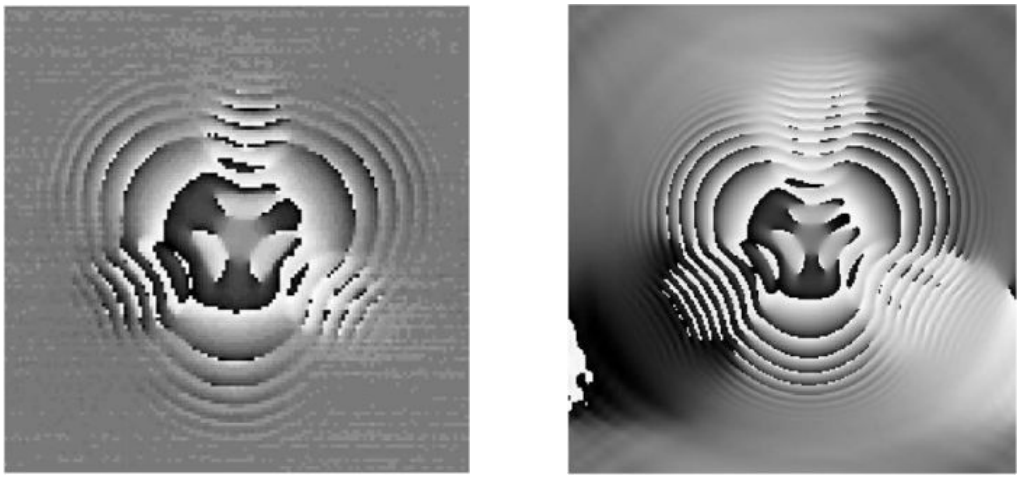

**Figure 9.4:** Measured (*left*) and simulated (*right*) ultrasonic wave phase distribution for $LiNbO_3$ along $z$-axis. In calculations 0.4° tilt of the crystal axis was assumed. Similarity of asymmetry in both pictures reveals similar tilt of the real crystal.

There are striking similarities between the measurements (Fig. 9.2) and the numerical simulations (Fig. 9.3). Especially convincing is the accuracy of the numerical model of the phase distribution in Fig. 9.4. We treat above results as the proof of the calculations accuracy.

## Numerical Inversion

Treating the 2D data collected by PSAM at the crystal surface, as complex holograms, we invert the propagation to recover the distribution of sources. The inversion is performed by a numerical AS back propagation technique, by putting $-x_3$. The MTF of such a combined imaging process (including wave propagation and calculated inversion) has the form

$$\mathrm{MTF}(\mathbf{s}_{\|}) = \left[\frac{\Lambda_{33}(\mathbf{s}_{\|})}{V_3(\mathbf{s}_{\|})}\right]^2 , \tag{9.5}$$

where $\Lambda_{33}$ is the wave coupling factor, and $V_3$ is the $z$th component of the group velocity. The PSF, of the entire imaging process may be calculated as the inverse Fourier transform of the MTF.

Images of the sinusoidal Siemens star, treated as the control object, are obtained through its convolution with PSF of the whole imaging process. Longitudinal propagation mode may be separated through time gating, and we consider independent imaging with that mode.

In the case of imaging with longitudinal waves, low spatial frequencies are transferred quite well, while the contrast vanishes gradually at middle spatial frequencies. With transversal waves resolved frequencies become a bit higher, while in addition the contrast vanishes in low spatial frequencies range. In the case of Coulomb coupling low frequencies are transferred quite well, while we observe number of artefacts in the middle frequency range. The resolution and quality of imaging is in that case much lower than in the case of acoustic coupling.

## Conclusions

Besides of the AS back-propagation, there are possible other types of inverting numerical procedures. Some of them could lead to local improvements in the MTF and resolution, but can not go beyond the cut-off spatial frequencies, determined through the critical angle for each mode. The back-propagation inversion has the advantage of ensuring that amplitudes of weak, noise-prone components are not amplified. In numerical simulation the same algorithm is applied in inversion as in forward propagation, with only a change in sign of the distance parameter. In MTF calculated for longitudinal and slow transversal modes in Si (Fig. 9.5), it is visible that imaging with ST wave brings higher resolution. But spatial frequencies transferred with ST mode are limited also on the low frequency end. It occurs due to weak acoustic coupling to shear waves propagating in directions close to the normal to the surface. In MTF calculated for acoustic coupling to $LiNbO_3$ (Fig. 9.6), both ST and FT modes are excited. They travel with velocities of close values, and can not be separated. Interferences between them harm the imaging of the the spatial frequencies related to the minima of that

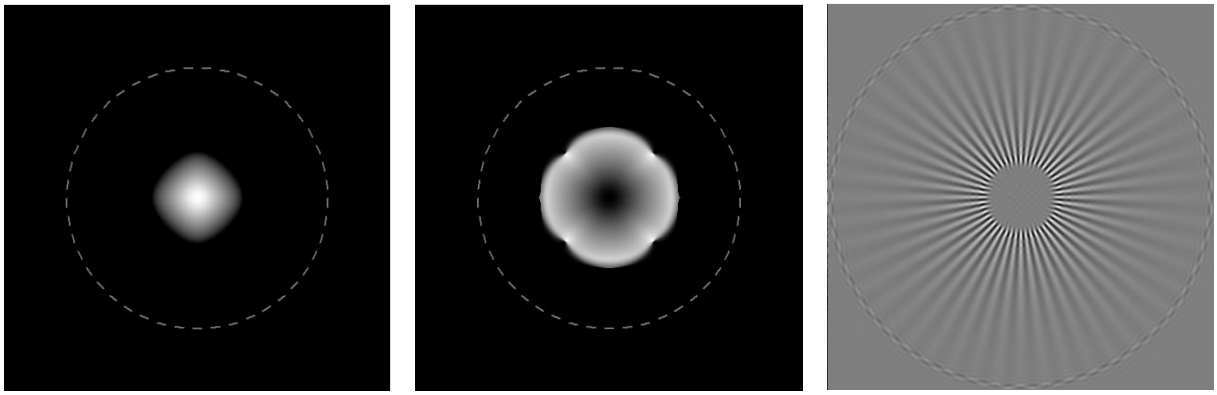

**Figure 9.5:** Imaging through Si single crystal. MTF calculated with formula (9.5), presented in $\mathbf{s}_{\|}$-space for L mode (*left*) and ST mode (*center*). Siemens star image calculated for ST mode (*right*). Side of the images is 1 μs/mm. The *right* image calculated for $x_3 = 5\,\text{mm}$, $f = 100\,\text{MHz}$ and side of the Siemens star of 5.12 mm.

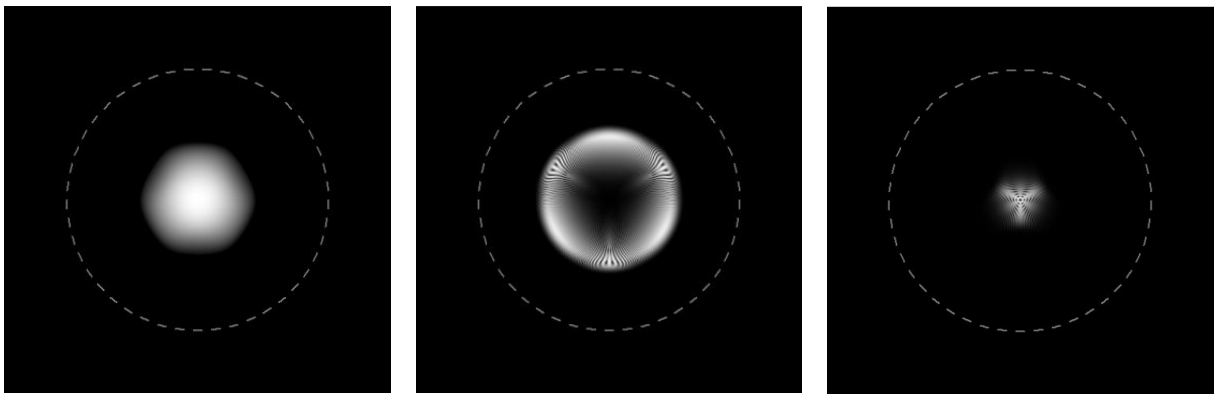

**Figure 9.6:** MTF calculated for imaging through $z$-cut $LiNbO_3$. Acoustic coupling to: L mode (*left*), to combination for ST and FT modes (*center*). Coulomb coupling (*right*) . Side of the images 1 μs/mm.

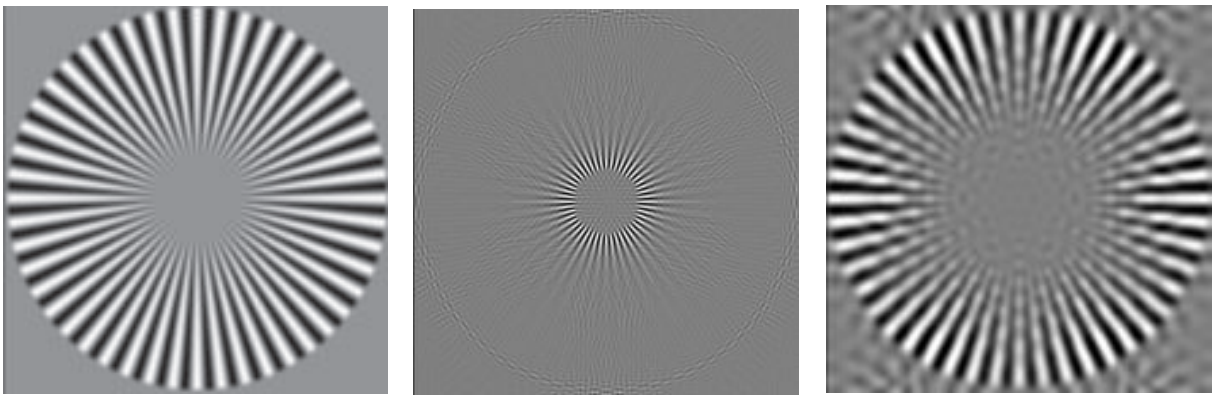

**Figure 9.7:** Images of the Siemens star calculated as for imaging through 5 mm thick *z*-cut $LiNbO_3$ at 100 MHz. Acoustic coupling to L mode (*left*), and to combination for ST and FT modes (*center*). Coulomb coupling (*right*). Side of each ot the images is 5.12 mm.

interference. Acoustic coupling is weak for low spatial frequencies, so the shear modes represent kind of middle pass filter. In the case of Coulomb coupling to $LiNbO_3$, the angular distribution of excited waves is limited, due to the finite size of the effective source (distribution of the electric field is wider than the size of the lens focus). In that case the electric field couples to both transversal modes also at low spatial frequencies. Interference of ST and FT modes is also visible. In case of Coulomb coupling (Fig. 9.7) the reconstructed image is of evidently lower quality in comparison to acoustic coupling. The resolution in each case scales with the applied ultrasonic frequency. The topic of acoustical imaging through anisotropic media is of interest because in the range of few GHz the ultrasonic resolution surpasses the one achievable in optical microscopy.

[1] W. Grill et al.: in *Advances in Acoustic Microscopy*, Vol. 2, ed. by A. Briggs, W. Arnold (Plenum, New York 1996)
[2] M. Pluta: *Mikroskopia Optyczna*, PWN, Warszawa (1982)
[3] L. Magiera, M. Pluta: Opt. Appl. **11**, 231 (1981)
[4] M. Born, E. Wolf: *Principles of Optics* (Pergamon Press, London 1980)
[5] M. Pluta et al.: Phys. Rev. B **67**, 094 117 (2003)
[6] E. Twerdowski et al.: Proc. SPIE **6935**, 693 51*U* (2008)
[7] J.W. Goodman: *Introduction to Fourier Optics* (McGraw-Hill, New York 1996)
[8] R.T. Smith, F.S. Welsh: Appl. Phys. **6**, 2219 (1971)

## 9.4 Ultrasound Diagnostics of Directional Solidification

W. Grill, E. Twerdowski, M. von Buttlar, R. Wannemacher

An ultrasonic measuring device based on guided waves has been developed in order to determine the growth rate of alloys, in particular of opaque metallic alloys. Experimental tests show that a high resolution is achievable in the determination of the position of the solid-liquid interface, down to 0.01 mm. The ultrasonic technique is therefore an appropriate tool for the measurement of the solidification velocity for stable as well as unstable solidification processes. The aim consists in the investigation of the impact

of process parameters on the resulting material properties. Controlled non-stationary growth presently appears to become a main research object for the next future, in particular in the context of industrial applications. The measurement of the solidification velocity by ultrasound is a diagnostic tool for directional solidification experiments. It was developed in the framework of the Technological Research Programme of the European Space Organization. An ultrasound pulse launched from the cold end of the sample and being reflected from the phase boundary of solidification allows to determine the position of the solid-liquid interface. Given the speed of sound in the sample the position of the phase boundary can be determined as a function of time and, hence, the solidification velocity via precise measurement of the propagation time by means of an auto-correlation technique.

In cooperation with Kayser-Threde GmbH, Munich, respective hard and software has been developed for the Materials Science Laboratory (MSL) of the International Space Station (ISS). The equipment has been provided to NASA to be transfered to the ISS with one of the next shuttle flights. Till then the project is restricted to support of the users, refinements of the evaluation software and improvements of the sample cartridges.

Funded by European Space Organization ESA/ESTEC.

## 9.5 Ultrasonic Monitoring of Athletes Muscle Dynamics and Performance

M.Z. Hossain, W. Grill

To observe muscle performance of athletes with high resolution a novel ultrasonic detection scheme has been developed in cooperation with the Bangladesh Institute of Sports (BKSP) and Analog Speed Instruments GmbH. Monitoring of the muscle dynamics is based on ultrasonic bulk waves passing the monitored muscle in lateral direction [1].

The time-of-flight from which all other data is derived is observed with the aid of a chirped excitation and digital signal compression, a scheme that has lately also been introduced for structural health and load monitoring. Synchronous monitoring of the force or pressure or the EMG-signals is provided. The achieved spatial and temporal resolution reaches ±0.02 mm and 0.01 ms respectively. The lap-top sized PC-controlled electronics is battery operated and suitable for in field monitoring. In Fig. 9.8 the determination of the reaction time initiated via visual observation of an object thrown at unpredictable time (zero in the graph) and ultrasonic monitoring of the observed gastrocnemious muscle performance is demonstrated. Monitoring is performed by customized LabVIEW software.

Details of the monitoring and of the following data analysis are demonstrated in Fig. 9.9. For contraction three different stages: acceleration, constant speed and deceleration. The relaxation phase exhibits only two different stages, acceleration and deceleration. These phases are quantitatively analyzed by respective fitting procedures used to parameterize the performance.

A so far not accessible wealth of quantitative information can be obtained by the developed scheme that is still further developed concerning additional monitoring of the variation of the ultrasonic velocity during activation, monitoring of a large number

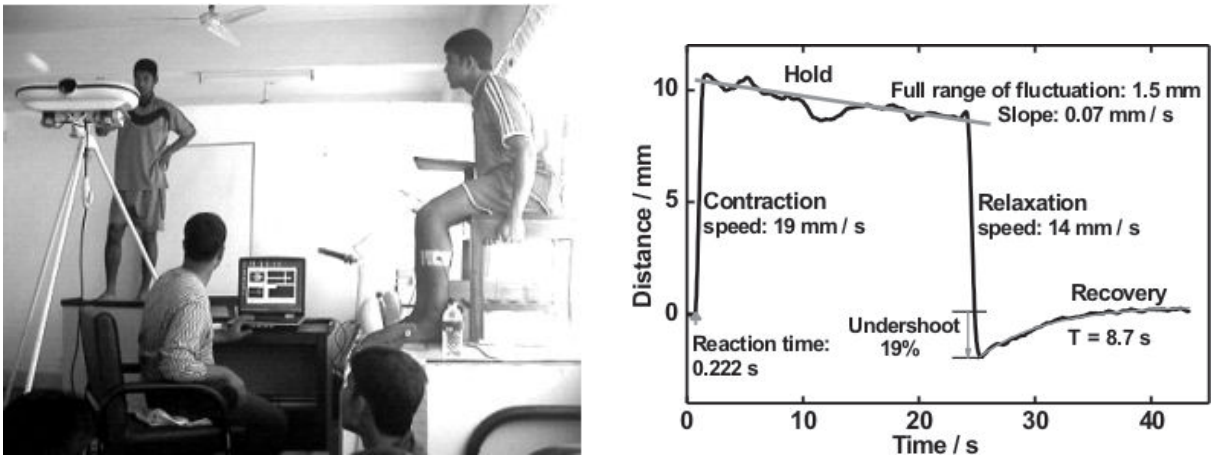


**Figure 9.8:** The image shows the throwing ball device for the visually triggered muscle activation with the athlete positioned on a chair on a table. The monitoring demonstrated in the graph with the lateral extension of the gastrocnemious muscle following triggering at time equal zero allows a quantitative analysis of the muscle movement and based on that of the athletes performance including training condition.

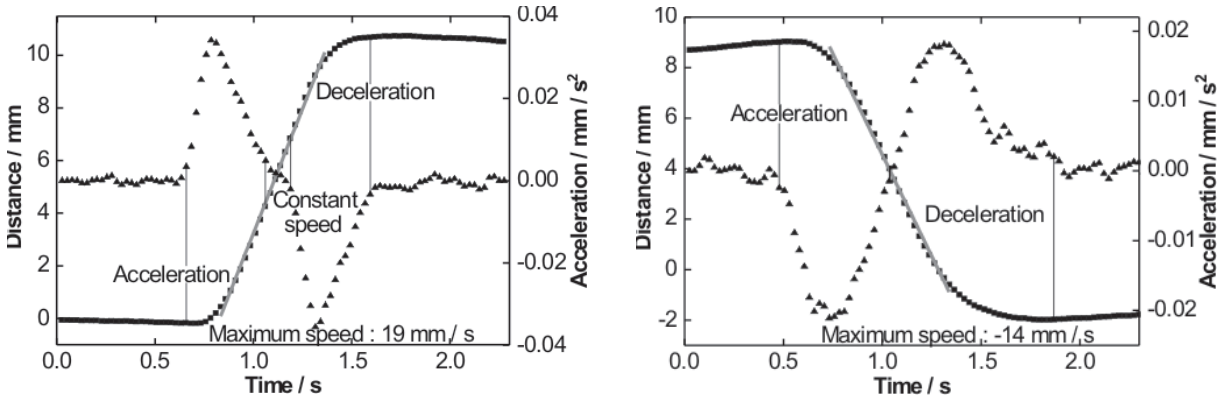


**Figure 9.9:** Detailed analysis as an example for the determination of so far not accessible parameters relating to muscle dynamics. Displayed are the transients for muscle contraction (*left*) and relaxation (*right*) and their second order derivatives. The interpretation of the different phases observed for the gastrocnemious muscle and quantitative parameters determining the observed performance are indicated by *insets*.

of athletes in field studies and synchronbous monitoring of load respectively force, and other signals including electric potentials related to nerve activation.

The developed monitoring scheme has been applied for monitoring of the gastrocnemius muscle performance during isometric contraction. Currant developments include efforts performed in cooperation with our partners to widen the field of tested application and further refine the analysis. This include for example variations of the nature of activity of the monitored muscle, other functional characteristics of skeletal muscle action like, work-limit, capacity of individual muscles or at least of a group of muscles. Continuing efforts are are also directed at the development of a radio link to allow monitoring of performing athletes.

[1] M.Z. Hossain et al.: Proc. SPIE **6935**, 693 576 (2008)

## 9.6 Determination of the Mechanical Properties of Thin Objects Deposited on Glass Slides by Gigahertz Vector-Contrast Scanning Acoustic Microscopy

E.T. Ahmed Mohamed, A. Kamanyi, M. von Buttlar, R. Wannemacher, K. Hillmann, W. Grill

Microscopic objects including living cells on planar substrates are investigated by scanning acoustic microscopy with phase and magnitude contrasts [1, 2]. The determination of sample properties related to mechanics such as density, sound velocity, and attenuation is achieved by evaluation of the relation of phase and magnitude in dependence of the variable height of the object, entering as a variable. In Fig. 9.10 the images of a chitosan deposition are presented. From the information contained in this multi-contrast image, the relation between phase and magnitude is extracted as displayed in Fig. 9.11.

Data extracted from the images are fitted to obtain the mechanical properties. The calculations are based on modeling the interferences caused by reflection from the top of the object (which is immersed in water that serves as coupling fluid) and from the interface of the object and the substrate. These properties are tested by ultrasound of longitudinal polarization at a frequency of 1.2 GHz. For homogeneous and sufficiently planar objects the contrast in magnitude and phase is a function of the properties of the substrate and the coupling fluid, which both can easily be determined in independent experiments, and of the mechanical properties of the sample under observation.

As visually experienced for oil films on water – in that case for electromagnetic waves of similar wavelength – the signal observed in reflection depends only on the height of the layer if the properties of the involved materials, in the case of fluids and gases, are constant.

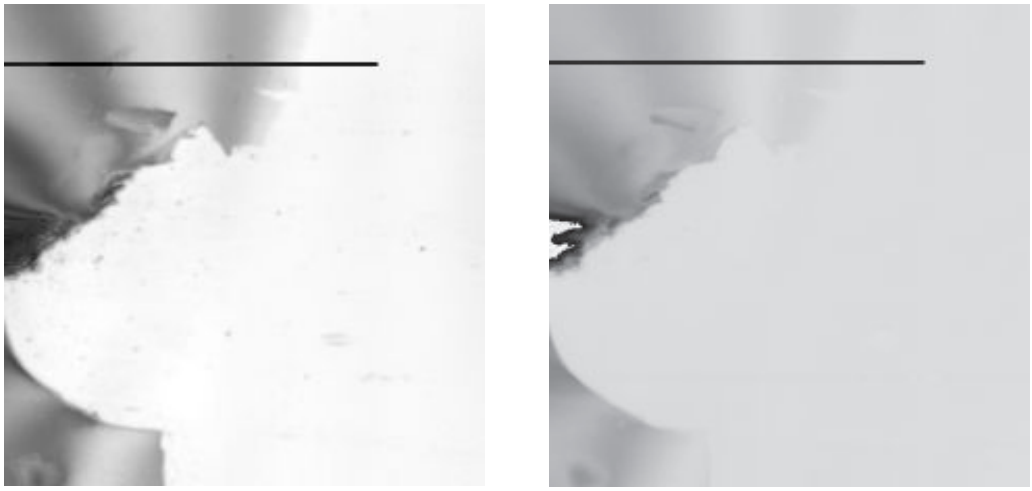

**Figure 9.10:** Images in magnitude contrast (*left*, *black* representing zero signal) and phase contrast (*right*, full gray scale of the image representing $2\pi$) of a wedge shaped chitosan layer (*darker area*) on a glass substrate. Magnitude and phase data along the area above the horizontal line are displayed in Fig. 9.11. The size of the images is $140 \times 140\ \mu m^2$.

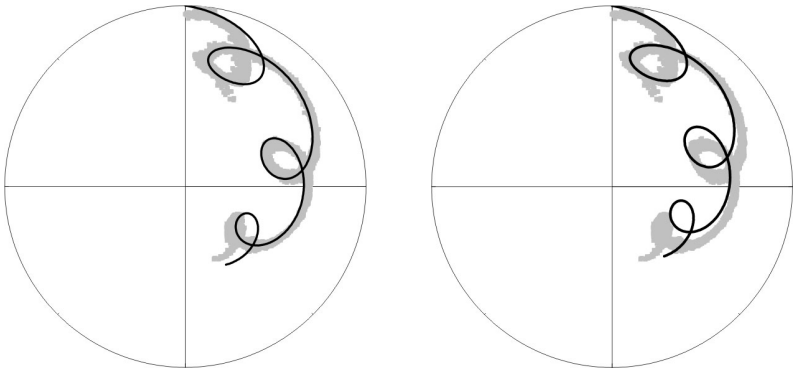

**Figure 9.11:** Polar diagram representing magnitude and phase of the observed signal with experimental values (*gray squares*) and an optimized fit to the experimental data (*black solid line*). On the *right* side, the fit is demonstrated for a velocity reduced by only 1 % with respect to the optimum fit to demonstrate the achievable resolution.

The method is demonstrated for a chitosan film deposited on a glass substrate. The scheme presented here is capable to reach a resolution of about and even below 1 % for relevant quantities in applications involving imaging at 1.2 GHz in aqueous coupling fluids.

The result of the modeling and fitting procedure depends on the relevant properties of substrate and the coupling fluid. The measured speed of the longitudinal acoustic waves in the microscope slides employed here is 5371 m/s, that of the transverse wave is 3099 m/s. The density of the glass was determined to be 2.47 g/cm. The speed of sound in water (coupling fluid) is 1489 m/s. At 1.195 GHz the attenuation coefficient for acoustic waves in water at room temperature is $0.033\,\mu\mathrm{m}^{-1}$.

The evaluation of the polar representation leads to a velocity of the longitudinal acoustic waves in the sample of 1670 m/s, a density of $1.22\,\mathrm{g/cm}^3$, and an attenuation coefficient of $0.164\,\mu\mathrm{m}^{-1}$ for a region covering a sample height of up to 2.25 μm. The optimum half opening angle for the apodization was 40°.

The demonstrated method leads to a surprising accuracy, not easily be surpassed by conventional methods applied to large samples. The observed contrast on which the evaluation is based results from water acting as coupling fluid that is replaced by the object of variable height. Even though deviations from the optimum fit are obvious in the second loop and near the third loop, a rather high resolution is obtained, since the various shape factors depend each sensitively on the mechanical parameters and each with different relative weight concerning the individual properties.

Furthermore, if sufficiently simple models are assumed for the object, the viscosity of observed objects can be determined. Since the attenuation from thermal absorption is negligible compared to that caused by viscosity, a simplified solution of the Navier–Stokes equation can be used to express the attenuation coefficient

$$\alpha = \frac{2\omega^2\eta}{3\rho v^3}\,, \tag{9.6}$$

where $\omega$ is the angular frequency of the sound wave, $\eta$ is the shear viscosity, $\rho$ is the density and $v$ is the ultrasonic speed in the sample. For the soft sample under study this leads to a projected (model dependent) shear viscosity of 0.245 Pa s.

Currently, the modeling is further refined to achieve sub-Abbe resolution in topographical images of the deposits.

Two of the authors, A. Kamanyi and W. Grill, gratefully acknowledge support by the Deutsche Forschungsgemeinschaft (DFG, grant GR566/11-2). M. von Buttlar gratefully acknowledges support by the German Ministry of Education and Research (BMBF, grant 0313836). The work has been performed in co-operation with W. Ngwa, Department of Physics, University of Central Florida, Orlando, USA.

[1] E.T. Ahmed Mohamed et al.: Proc. SPIE **6935**, 693 51Z (2008)
[2] E.T. Ahmed Mohamed et al.: Proc. SPIE **6177**, 617 716 (2006)

## 9.7 Soft Matter Acoustics: Non-Destructive Health Monitoring of Polymer Blend Films

A. Kamanyi, W. Grill

Soft condensed matter (materials which are easily deformable by external stresses, electric or magnetic fields, or even by thermal fluctuations) typically possess structures which are much larger than atomic or molecular scales. Such soft matter systems include polymer coatings, which can often be highly heterogeneous. In recent years, extensive research has been conducted to characterize the heterogeneity in coatings. Polymer coatings can contain degradation susceptible regions, and corrosion of metallic substrates has been found to occur directly underneath these regions. The sizes of these regions are believed to range from nano- to micrometers. Many micro- and spectroscopic techniques have been used either in combination or independently to provide information about the morphology and composition of multi-component polymer systems. However, these techniques lack the ability to simultaneously map morphology and volume heterogeneity in polymer coatings. The phase sensitive acoustic microscope (PSAM) provides direct spatial mapping of surface topography and volume heterogeneity non-destructively [1]. Acoustical images contain information about the elastic properties of the samples: density, stiffness respectively compressibility (elastic moduli or tensors), and acoustic attenuation. With simultaneous amplitude and phase imaging, PSAM virtually provides similar information like the topography and phase images of tapping mode atomic force microscope (AFM) when focused at the surface. Additionally, the ability of ultrasound to penetrate the surface gives it significant additional advantage, allowing non-invasive qualitative and quantitative volume investigations of materials.

Figure 9.12 shows un-annealed polymer blend films on glass and silicon substrate. The films on glass were found to be vulnerable to the water used as coupling fluid. The variations in the region marked by the arrows illustrate the susceptibility of the PS/PMMA film on glass to water. Water at the interface is often a major cause of corrosion, blistering, and disbonding of some organic coating/substrate systems. The effects observed in the un-annealed films are most probably due to adsorption of water by the film on glass. The bonds between an organic coating and a substrate of high surface-free energy ($> 100\,\mathrm{mJ/m^2}$) (like glass) are generally not thermodynamically stable in the presence of water and aqueous solutions. Consequently, water molecules

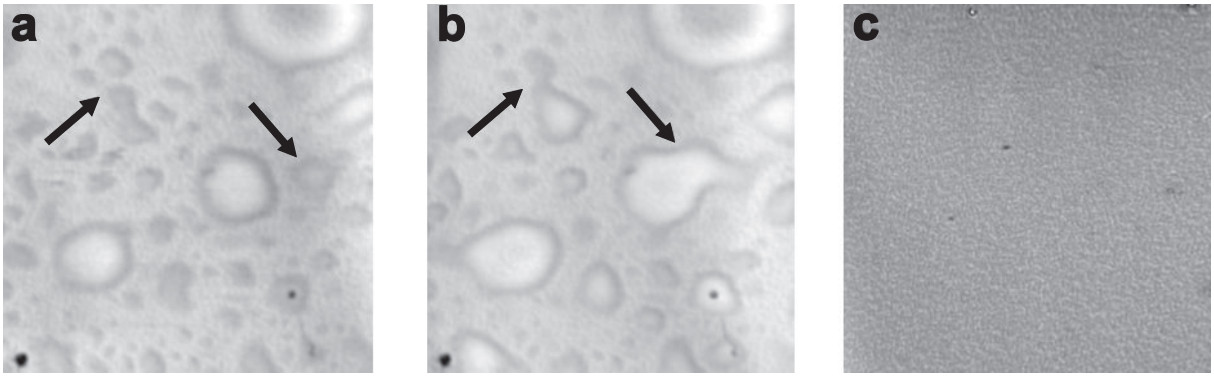


**Figure 9.12:** (**a**) $140 \times 140\,\mu m^2$ PSAM amplitude contrast image of a polystyrene-polymethylmetacrylate polymer blend film on glass substrate, (**b**) the same area after 25 s, (**c**) amplitude contrast image of similar blend film on silicon substrate remains stable.

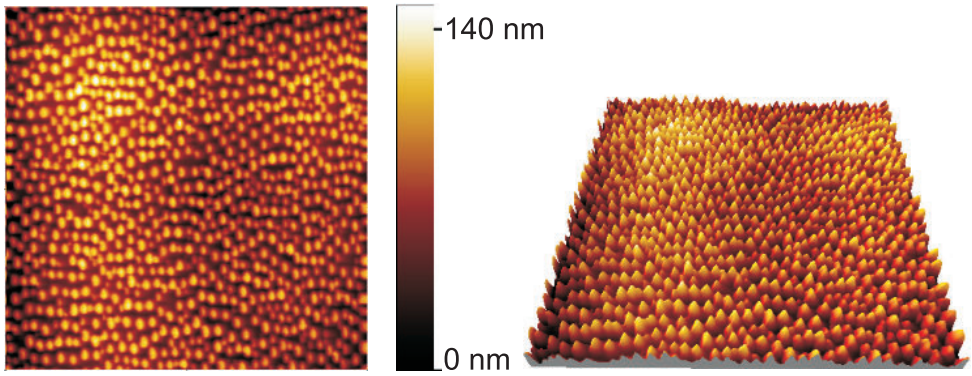


**Figure 9.13:** $32 \times 32\,\mu m^2$ AFM images for PS/PMMA films from a toluene based solution. Topography image (*left*) and corresponding 3D reconstruction from the topography image (*right*).

are likely to break these bonds and layers of water molecules are adsorbed at the coating/substrate interface. This is not observable in the AFM topography image of the same film shown in Fig. 9.13.

While this is a problem on glass, this is not the case on the silicon substrate (as is evident in Fig. 9.12). The AFM images show no difference for both substrates. For blends on glass, this vulnerability is overcome by annealing above the glass transition temperature of the individual polymer constituents. A 3D PSAM image reconstructed from the phase and amplitude contrast images is presented together with a 3D topography AFM image of the same film in Fig. 9.14.

PSAM presents certain advantages over other state-of-the-art techniques in volume monitoring of variations in morphology and elastic properties of soft matter systems as demonstrated for polymer coatings. The instability of the film relative to the blend film on glass before annealing illustrates the possibility of PSAM for monitoring coatings that have depreciated or become vulnerable to water. It is also possible with the PSAM to investigate the morphology beneath the surface. This potential can be exploited in mapping heterogeneity in coatings, and also in the non-invasive monitoring of their health.

A. Kamanyi and W. Grill gratefully acknowledge support by Deutsche Forschungsgemeinschaft (DFG grant GR566/11-2).

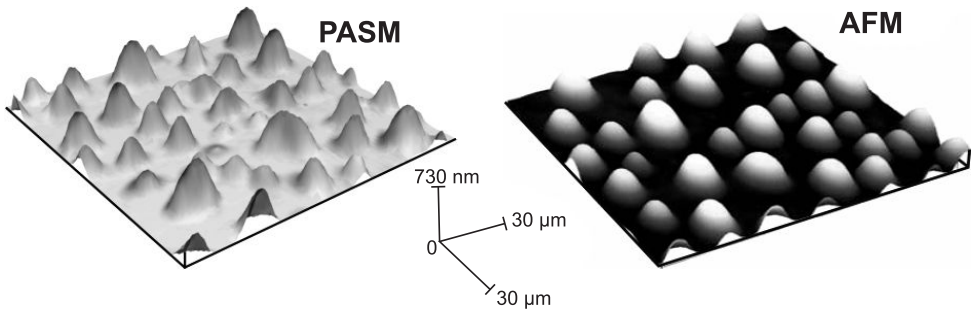


**Figure 9.14:** Comparison of topography imaging by non-invasive phase contrast acoustic imaging. Topography from phase contrast and brightness from PSAM amplitude (*left*) and 3D reconstruction from AFM topography imaging (*right*). The image shows an annealed PS/PMMA blend film on silicon substrate. Horizontal and vertitical dimensions of the images are shown in the center.

[1] A. Kamanyi et al.: Proc. SPIE **6531**, 653 106 (2007)

## 9.8 Funding

*Mesoscale Acoustics on Soft Matter Systems*
W. Grill
Gr 566/11-2

*Development of a Miniaturized Advanced Diagnostic Technology Demonstrator 'DIAMOND' - Technology Study Phase 2*
W. Grill, R. Wannemacher
European Space Organization ESA/ESTEC

*Ultrasound Diagnostics of Directional Solidification*
W. Grill, R. Wannemacher
European Space Organization ESA/ESTEC

*In-vivo Ultrasonic Holographic Imaging (within the Translational Centre for Regenerative Medicine (TRM Leipzig))*
E. Twerdowski, R. Wannemacher, W. Grill
BMBF AZA 0845 IMONIT 1040AB 50810213

*Multiparametric Monitoring and Steering of Mesenchymal Stem Cell derived Cartilage Formation in 3D Production Systems (MS CartPro)*
*Development of a 2D bioreactor with integrated phase-sensitive acoustic microscopy combined with confocal laser microscopy (AP2.2)*
*Integration of a multi-parameter online monitoring system in a 3D bioreactor (AP2.3)*
W. Grill, E. v d. Burg, M. v. Buttlar
BMBF FKZ 0313836

*Aircraft Integrated Structural Health Assesment II (AISHA II)*
W. Grill, U. Amjad, M. Pluta, H. Voigt, M. Zakir Hossain,
EU Seventh Framework Programme (FP7), Grant Agreement No. 212912

## 9.9 Organizational Duties

W. Grill

- Adjunct Professor and Member of the Graduate School, The University of Georgia, Athens, GA, USA

## 9.10 External Cooperations

**Academic**

- University of the Witwatersrand, Johannesburg, South Africa
  Prof. Dr. A. Every
- Wroclaw Institute of Technology, Wroclaw, Poland
  Dr. M. Pluta, Dr. T. Gudra
- University of Arizona, Tucson, USA
  Prof. Dr. T. Kundu
- University of Central Florida, Orlando, USA
  Prof. Dr. W. Luo, Dr. W. Ngwa
- Stanford University, USA
  Dr. K. Vodopyanov
- Johann Wolfgang Goethe-Universität, Frankfurt am Main, Germany
  Prof. Dr. J. Bereiter-Hahn
- Bernard Nocht Institute for Tropical Medicine, Hamburg
  Dr. T.W. Gilberg

**International Organizations**

- European Space Organization ESA/ESTEC

**Industry**

- Schott GLAS, Mainz, Germany
- Kayser-Threde GmbH, Munich, Germany
- EPCOS AG, Surface Acoustic Wave Components, Munich, Germany

## 9.11 Publications

**Journals**

U. Amjad, J. Ndop, E. Twerdowski, W. Grill: *Determination of the velocity of sound with high resolution by ultrasonic imaging of wedge shaped objects in transmission with vector contrast*, Proc. SPIE **6935**, 693 51C (2008)

E.T. Ahmed Mohamed, A. Kamanyi, M. von Buttlar, R. Wannemacher, K. Hillman, W. Ngwa, W. Grill: *Determination of mechanical properties of layered materials with vector-contrast scanning acoustic microscopy by polar diagram image representation*, Proc. SPIE **6935**, 693 51Z (2008)

M.Z. Hossain, E. Twedowski, W. Grill: *High speed ultrasound detection in the field of sports biomechanics*, Proc. SPIE **6395**, 693 576 (2008)

M.Z. Hossain, E. Twedowski, W. Grill: *High Speed Ultrasound Monitoring In The Field Of Sports Biomechanics*, J. Biomech. **41**, S55 (2008)

A. Kamanyi, W. Ngwa, W. Luo, W. Grill: *Effects of solvent vapor pressure and spin-coating speed on morphology of thin polymer blend films*, Proc. SPIE **6935**, 693 51X (2008)

M. Pluta, M. von Buttlar, A. Habib, E. Twerdowski, R. Wannemacher, W. Grill: *Modeling of Coulomb coupling and acoustic wave propagation in LiNbO3*, Ultrasonics **48**, 583 (2008)

K.S. Tarar, R. Meier, E. Twerdowski, R. Wannemacher, W. Grill: *A differential method for the determination of the time-of-flight for ultrasound under pulsed wide band excitation including chirped signals*, Proc. SPIE **6935**, 693 519 (2008)

E. Twerdowski, M. Pluta, R. Wannemacher, W. Grill: *Comparative evaluation of ultrasonic lenses and electric point contacts for acoustic flux imaging in piezoelectric single crystals*, Proc. SPIE **6935**, 693 51U (2008)

M. Vasiljevic, T. Kundu, W. Grill, E. Twerdowski: *Recent advances on pipe inspection using guided waves generated by electromagnetic acoustic transducers*, Proc. SPIE **6935**, 693 507 (2008)

**Talks**

M. von Buttlar, E. Ahmed Mohamed, A. Kamanyi, E. Twerdowski, W. Grill: *Long-term monitoring of mesenchymal stem cells and cell constructs by vector contrast scanning acoustic microscopy and tomography*, 11. Int. Conf. For Young Researchers: Wave Electronics and Its Applications in Information and Telecommunication Systems, St. Petersburg, Russia, 25. – 30 May 2008

M. von Buttlar, E. Twerdowski, R. Wannemacher, W. Grill: *Noninvasive Monitoring of Mesenchymal Stem Cells by 1.2 GHz Acoustic Microscopy*, Acoustics'08 Conf., Paris, France, 29. June – 04. July 2008

M.Z. Hossain, E. Twedowski, W. Grill: *High speed ultrasound detection in the field of sports biomechanics*, 15. Int. Symp. Smart Structures and Materials, Nondestructive Evaluation and Health Monitoring, San Diego, USA, 09. – 13. May 2008

M.Z. Hossain, E. Twedowski, W. Grill: *High Speed Ultrasound Monitoring In The Field Of Sports Biomechanics*, 16. Congress Eur. Soc. Biomech., Lucerne, Switzerland, 06. – 09. July 2008

A. Kamanyi: *Thin films of PS/PMMA polymer blends: A scanning acoustic microscopy study* (invited), 2. Int. Conf. Polymer Blends, Composites, IPNs, Membranes, and Gels: Macro to Nanoscales (ICBC), Kottayam, India, 22. – 24. September 2008

A. Kamanyi, W. Ngwa, W. Luo, W. Grill: *Effects of solvent vapor pressure and spin-coating speed on morphology of thin polymer blend films*, 15. Int. Symp. Smart Structures and Materials, Nondestructive Evaluation and Health Monitoring, San Diego, USA, 09. – 13. May 2008

E. Twerdowski, M. Von Buttlar, R. Wannemacher, W. Grill: *Critical cone channelling in directly bonded wafers*, Acoustics'08 Conf., Paris, France, 29. June – 04. July 2008

**Posters**

E. Ahmed Mohamed, A. Kamanyi, E. von Buttlar, R. Wannemacher, K. Hillmann, W. Ngwa, W. Grill: *Height profiling and determination of elastic properties of layered bio-materials with vector-contrast scanning acoustic microscopy using polar diagram image representation*, 7. Int. Conf. Ultrasonic Measurement and Imaging of Tissue Elasticity, Austin, USA, 27. – 30. October 2008

M. von Buttlar, E. Twerdowski, R. Wannemacher, W. Grill: *Thin foils as acoustic windows and substrates for scanning acoustic microscopy*, 15. Int. Symp. Smart Structures and Materials, Nondestructive Evaluation and Health Monitoring, San Diego, USA, 09. – 13. May 2008

M. von Buttlar, E. Ahmed Mohamed, E. Twerdowski, A. Kamanyi, R. Wannemacher, W. Grill: *Non-invasive Monitoring of Ovine Mesenchymal Stem Cells by 1.2 GHz Acoustic Microscopy*, 2. Int. Congress on Stem Cells and Tissue Formation, Dresden, Germany, 06. – 09. July 2008

M.Z. Hossain, E. Twedowski, W. Grill: *High Speed Ultrasound Monitoring In The Field Of Sports Biomechanics*, 16. Congress Eur. Soc. Biomech., Lucerne, Switzerland, 06.–09. July 2008

## 9.12 Graduations

**Doctorate**

- Evgeny Twerdowski
  *Ultrasonic transmission and holographic imaging in anisotropica media*
  June 2008

**Master**

- Umar Amjad
  *Determination of the speed of sound in solid samples by phase tracking*
  May 2008

- Rico Meier
  *Influences of stress and temperature on the time-of-flight of ultrasound in solid matter*
  June 2008

# 10

# Superconductivity and Magnetism

## 10.1 Introduction

At the Division of Superconductivity and Magnetism research is focused on the study of magnetic ordering and superconductivity in a range of materials, especially carbon-based systems and magnetic oxides. Highlight of the year 2008 was the start of two projects within the Collaborative Research Center 762 "Functionality of Oxide Interfaces" devoted to defect-induced magnetism in nominally diamagnetic oxides as well as the fabrication and study of multiferroic heterostructures.

*Pablo Esquinazi*

## 10.2 Transition from Ohmic to Ballistic Transport in Oriented Graphite

P. Esquinazi, N. García*, J. Barzola-Quiquia, J.C. González*, M. Muñoz*, P. Rödiger, K. Schindler, J.-L. Yao, M. Ziese

*CSIC Madrid, Spain

We have shown that the spreading Ohmic resistance of a quasi-2D system of size $\Omega$, thickness $t$, and with a constriction of size $W$ connecting two half-parts of resistivity $\rho$ goes as $(2\rho/\pi t)\ln(\Omega/W)$, diverging logarithmically with the size. Measurements in highly oriented pyrolytic graphite (HOPG) as well as numerical simulations confirm this relation. From this we have developed an experimental method that allows us to obtain the carriers' mean-free path $l(T)$, the Fermi wavelength $\lambda(T)$, and the mobility $\mu(T)$ directly from experiments without adjustable parameters. Measuring the electrical resistance through micro-fabricated constrictions in HOPG and observing the transition from the ohmic to the ballistic regime, we obtain that $0.2\,\mu\text{m} \le l \le 10\,\mu\text{m}$, $0.1\,\mu\text{m} \le \lambda \le 2\,\mu\text{m}$, and a mobility $5\times10^4\,\text{cm}^2/\text{Vs} \le \mu \le 4\times10^7\,\text{cm}^2/\text{Vs}$, when the temperature $T$ decreases from 270 to 3 K, see Fig. 10.1. A comparison of these results with those from literature indicates that conventional, multiband Boltzmann–Drude approaches are inadequate for oriented graphite. The upper value obtained for the mobility is much larger than that in graphene samples of micrometer size.

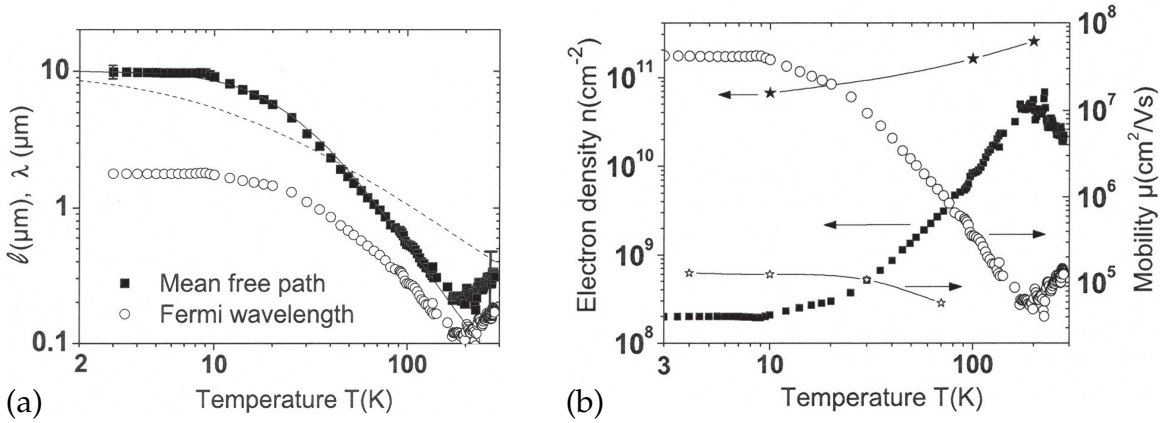


**Figure 10.1:** Upper panel: mean free path and Fermi wavelength, lower panel: carrier density and mobility of HOPG. In the lower panel the solid stars are the carrier density and the open stars are the mobility values obtained using multiband models and the Boltzmann-Drude approach.

## 10.3 Insulating Behavior of Magnetic Spots in Proton-Bombarded Graphite

K. Schindler, N. García*, P. Esquinazi, H. Ohldag†

*CSIC Madrid, Spain
†Stanford University, Stanford Synchrotron Radiation Laboratory, USA

Kelvin probe force microscopy (KPFM) measurements on micrometer small magnetic spots produced by proton bombardment on bulk graphite reveal a charge transfer from the center of the spot to an external ring with potential variation of the order of 50 mV. This is illustrated in Fig. 10.2. The total charge in the spot is neutral. The results can be well understood in terms of practically unscreened potentials, an insulating property, although the non-bombarded, surrounding graphite region exhibits good conductance. Scanning transmission X-ray microscopy measurements on magnetic spots prepared on graphitic films reveal a similar charge distribution. The insulating behavior is fundamental to understand the magnetism in graphite.

## 10.4 Epitaxial Thin Film $ZnFe_2O_4$: A Transparent Ferrimagnet

Y.F. Chen, D. Spoddig, M. Ziese

Transparent $ZnFe_2O_4$ films were fabricated by pulsed-laser deposition on $MgAl_2O_4$ substrates. Structural investigations showed epitaxial growth and a zinc to iron ratio close to 1 : 2. The films had a saturation magnetization between 0.2 T and 0.4 T at low temperatures, a Curie temperature close to 600 K and were either in a ferrimagnetic or a cluster-glass state. Figure 10.3 shows the magnetization of $ZnFe_2O_4$ films grown at various oxygen partial pressures as a function of temperature and magnetic field, respectively. Resistivity measurements showed clear semiconducting behavior with an

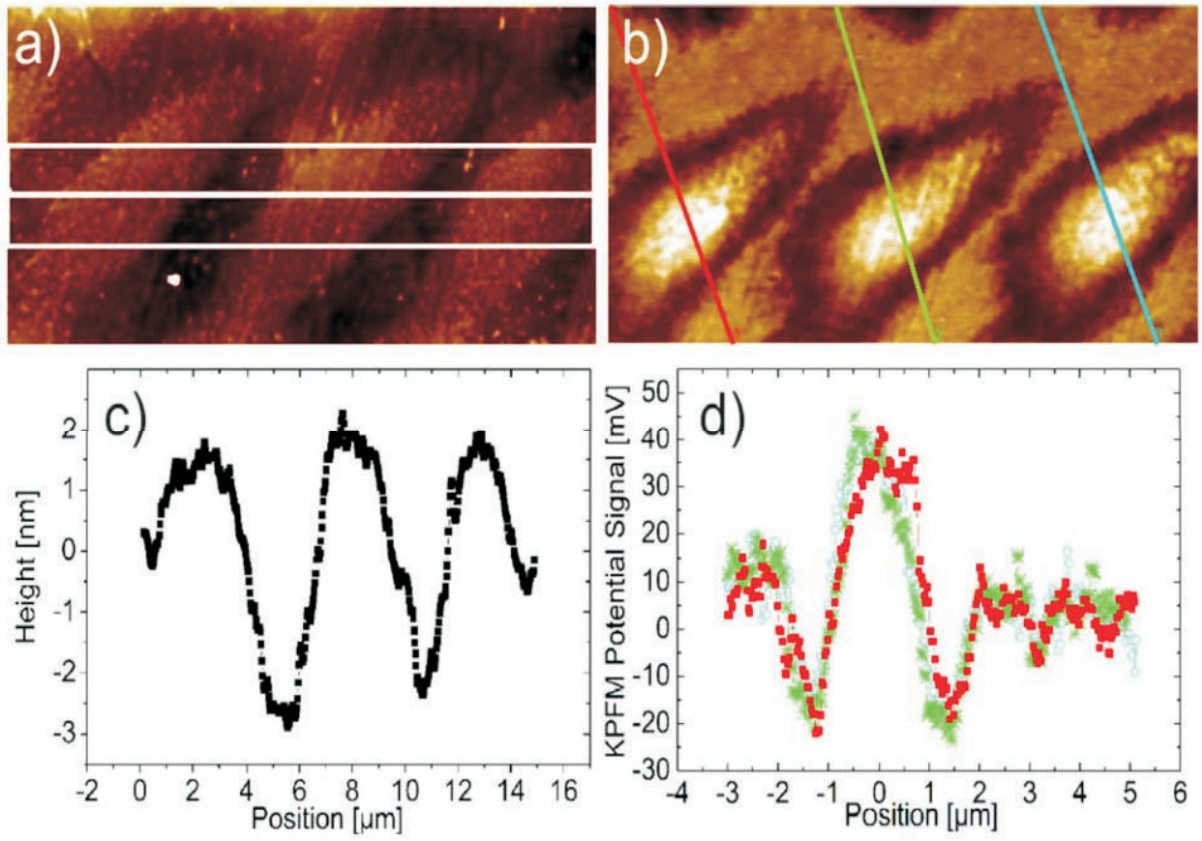


**Figure 10.2:** (**a**) AFM image showing three spots produced at a temperature of 110 K with a fluence of 0.124 nC/m$^2$ and a proton current of 1 nA on HOPG. (**b**) KPFM image of the three spots. (**c**) AFM line scans across a horizontal line through the spots. (**d**) Potential variations obtained from the KPFM line scans for the three spots of (**b**). The color of the symbol corresponds to the same color line of the corresponding spot in (**b**).

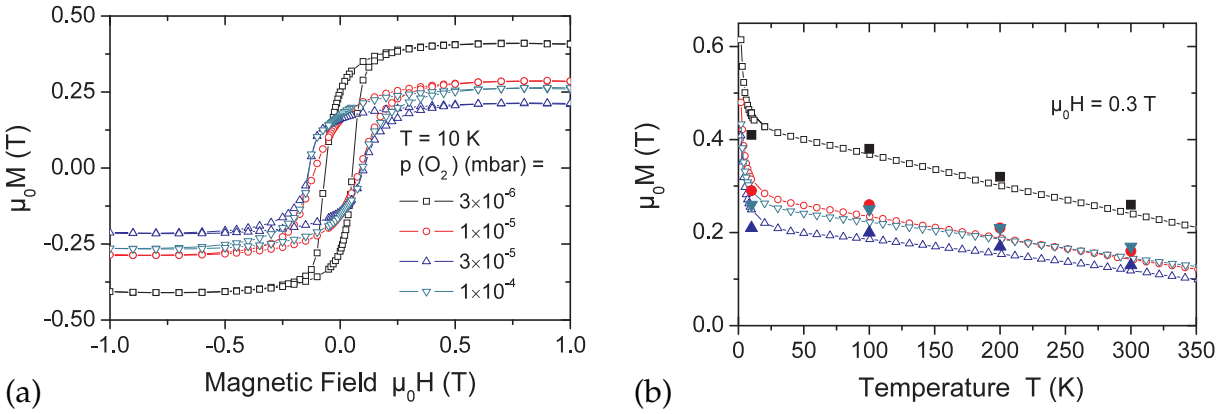


**Figure 10.3:** $ZnFe_2O_4$ films: (**a**) Magnetization versus temperature measured in an applied field of 0.3 T. The *solid symbols* indicate the saturation magnetization as determined from magnetization hysteresis loops. (**b**) Isothermal magnetization hysteresis loops recorded at 10 K.

activation energy depending on oxygen partial pressure. Ferrimagnetic, semiconducting and semi-transparent: this makes $ZnFe_2O_4$ films promising candidates for high Curie-temperature magnetic semiconductors.

## 10.5 Interfacial Strain Effects in Epitaxial Multiferroic Heterostructures of $PbZr_xTi_{1-x}O_3$ / $La_{0.7}Sr_{0.3}MnO_3$

M. Ziese, A. Setzer, P. Esquinazi, I. Vrejoiu*, B.I. Birajdar*, A. Lotnyk*, M. Alexe*, D. Hesse*

*Max-Planck-Institut für Mikrostrukturphysik, Halle

Ferroelectric $PbZr_xTi_{1-x}O_3$ and ferromagnetic $La_{0.7}Sr_{0.3}MnO_3$ films were grown on $SrTiO_3$ (100) substrates in order to fabricate multiferroic epitaxial heterostructures. Multilayers of $PbZr_{0.2}Ti_{0.8}O_3/La_{0.7}Sr_{0.3}MnO_3$ with 5 nm thin individual layers preserve good magnetic properties and have a transition temperature of about 320 K. Graded heterostructures consisting of thin $La_{0.7}Sr_{0.3}MnO_3$ films sandwiched between $PbZr_xTi_{1-x}O_3$ films of increasing Zr content were prepared. The influence of the vertically varied interfacial strain is demonstrated by the observation of different coercive fields of the $La_{0.7}Sr_{0.3}MnO_3$ films in the same heterostructure. Figure 10.4 shows magnetization hysteresis loops and the temperature dependent magnetization of two selected heterostructures as well as the ferroelectric polarization and switching current of the top PZT layer.

## 10.6 Coupled Magnetic and Structural Transitions in $La_{0.7}Sr_{0.3}MnO_3$ Films on $SrTiO_3$

M. Ziese, A. Setzer, I. Vrejoiu*, A. Lotnyk*, D. Hesse*

*Max-Planck-Institut für Mikrostrukturphysik, Halle

The magnetic properties of epitaxial $La_{0.7}Sr_{0.3}MnO_3$ films of thickness between 5 nm and 40 nm grown on $SrTiO_3$ (001) substrates were investigated. The films were very smooth, see AFM image in Fig. 10.5, and magnetically soft. The structural transition of the $SrTiO_3$ substrate induces a magnetic transition in the manganite films due to magnetoelastic coupling. Below the temperature of the structural transition additional steps in the magnetization reversal characteristics appear characterized by clearly defined coercive fields. These additional coercive fields, see Fig. 10.5, depend on the cooling history of the sample and are related to the formation of structural domains in the $La_{0.7}Sr_{0.3}MnO_3$ films induced by the substrate.

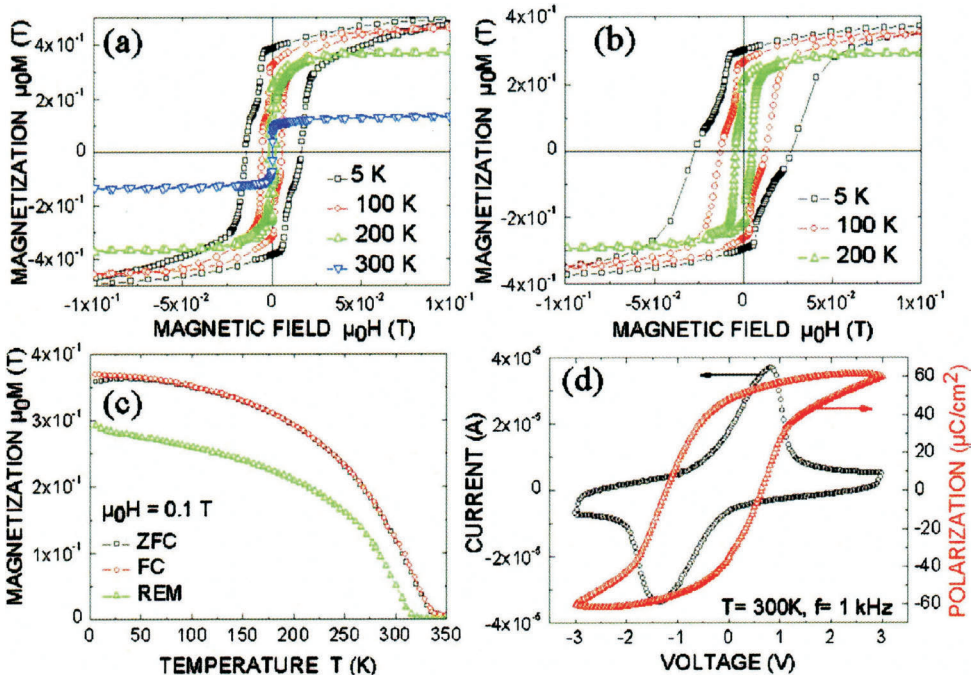


**Figure 10.4:** $La_{0.7}Sr_{0.3}MnO_3/PbZr_xTi_{1-x}O_3$ superlattices: Magnetization hysteresis loops of superlattices consisting each of three bilayer blocks with PZT composition (**a**) 30/70, 20/80 and 10/90 and (**b**) 52/48, 30/70 and 10/90. (**c**) shows the temperature-dependent magnetization and (**d**) the switching current and electric polarization hysteresis loops of the superlattice in (**b**).

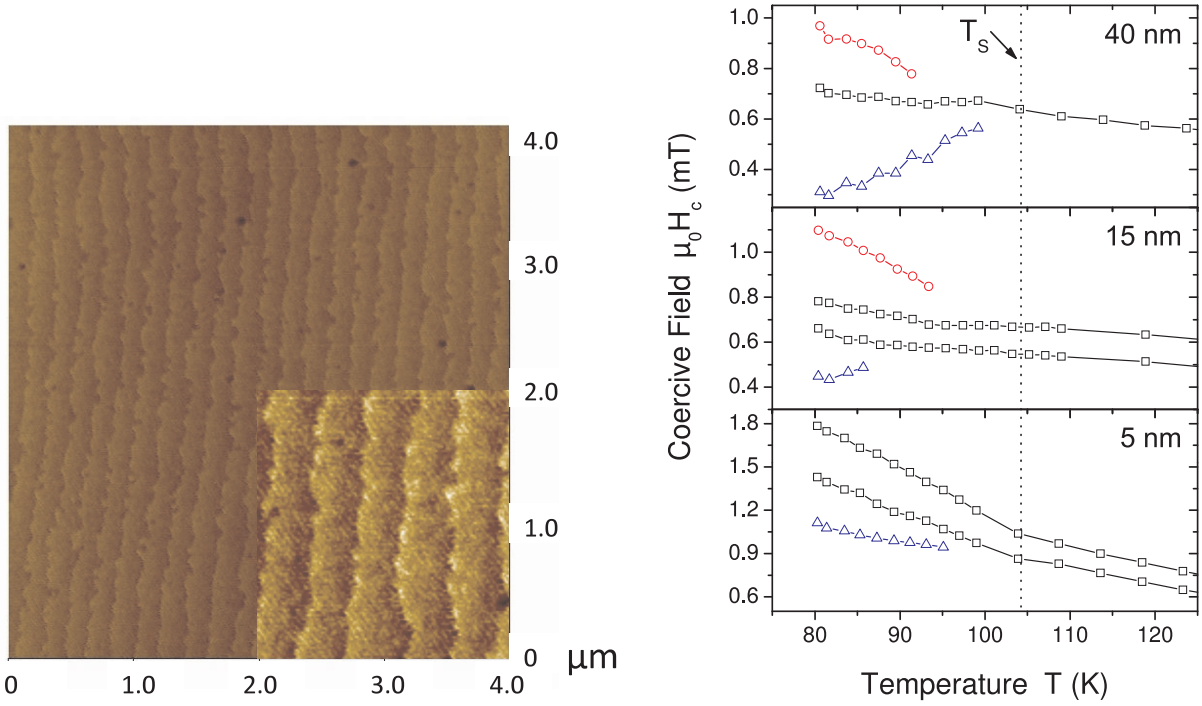


**Figure 10.5:** *Left*: AFM image of a 15 nm thick LSMO film showing a regular structure of unit cell high terraces; the *inset* shows a magnification by a linear scale factor of two of a $1 \times 1\ \mu m^2$ large area. *Right*: Coercive fields of the LSMO films of 40 nm, 15 nm and 5 nm thickness as a function of temperature.

## 10.7 Funding

*Room Temperature Ferromagnetism in Graphite and Fullerenes (FERROCARBON)*
Prof. P. Esquinazi
EU Strep No. 012881

*The origin of carbon-based magnetism and the role of hydrogen*
Prof. P. Esquinazi
DFG Es 86/11-1

*Study of intrinsic and extrinsic phenomena in the electrical transport properties of multi-graphene*
Prof. P. Esquinazi
DFG Es 86/16-1

*Defect-induced Magnetism in Oxides*
Prof. P. Esquinazi and Dr. M. Ziese
DFG SFB762 B1

*Spin-dependent Transport and Exchange-Biasing in multiferroic Heterostructures*
Dr. M. Ziese and Prof. P. Esquinazi
DFG SFB762 B5

*Magnetotransport in graphite nano-constrictions*
Prof. P. Esquinazi
DAAD

## 10.8 Organizational Duties

P. Esquinazi

- Reviewer: Deutsche Forschungsgemeinschaft (DFG), National Science Foundation (USA), German-Israeli Foundation
- Referee: Phys. Rev. Lett, Phys. Rev. B., Physica C, Phys. Lett. A, Phys. Stat. Sol., J. Low Temp. Phys., Carbon, J. Chem. Phys., Eur. J. Phys. B, J. Magn. Magn. Mater.

M. Ziese

- Reviewer: U.S.-Israel Binational Science Foundation, European Science Foundation
- Referee: APS Outstanding Referee, Phys. Rev. Lett., Phys. Rev. B., J. Phys. Condens. Matter, J. Phys. D Appl. Phys., Phys. Stat. Sol., J. Magn. Magn. Mater., Eur. J. Phys. B, Thin Solid Films

## 10.9 External Cooperations

**Academic**

- State University of Campinas, Campinas, Brazil
  Prof. Dr. Yakov Kopelevich

- Umea University, Sweden
  Dr. Tatiana Makarova
- Universidad Autónoma de Madrid, Spain
  Prof. Dr. Miguel Angel Ramos, Prof. Dr. Sebastian Vieira
- Institute for Metal Physics, National Academy of Sciences of Ukraine, Kiev, Ukraine
  Prof. Dr. V.M. Pan
- Max-Planck-Institut für Metallforschung, Stuttgart, Germany
  Dr. E.H. Brandt
- University of Ioannina, Greece
  Prof. I. Panagiotopoulos
- Institute for Materials Science, National Center of Scientific Research "Demokritos", Athens, Greece
  Dr. Nikos Moutis
- Trinity College, Dublin, Ireland
  Prof. J.M.D. Coey
- Leibniz-Institut für Festkörper- und Werkstoffforschung, Dresden, Germany
  Dr. Kathrin Dörr
- University of Sheffield, UK
  Prof. G. Gehring
- University of the Negev, Beer Sheva, Israel
  Dr. Evgeny Rozenberg
- Leibniz-Institut für Oberflächenmodifizierung, Leipzig, Germany
  Dr. K. Zimmer

## 10.10 Publications

**Journals**

J. Barzola-Quiquia, R. Höhne, M. Rothermel, A. Setzer, P. Esquinazi, V. Heera: *A comparison of the magnetic properties of proton- and iron-implanted graphite*, Eur. Phys. J. B **61**, 127 (2008)

J. Barzola-Quiquia, J.L. Yao, P. Rödiger, K. Schindler, P. Esquinazi: *Sample size effects on the transport characteristics of mesoscopic graphite samples*, Phys. Stat. Sol. A **205**, 2924 (2008)

Y.F. Chen, D. Spoddig, M. Ziese: *Epitaxial thin film $ZnFe_2O_4$: a semi-transparent magnetic semiconductor with high Curie temperature*, J. Phys. D Appl. Phys. **41**, 205 004 (2008)

P. Esquinazi, N. García, J. Barzola-Quiquia, P. Rödiger, K. Schindler, J.-L. Yao, M Ziese: *Indications for intrinsic superconductivity in highly oriented pyrolytic graphite*, Phys. Rev. B **78**, 134 516 (2008)

N. Garcia, P. Esquinazi, J. Barzola-Quiquia, B. Ming, D. Spoddig: *Transition from Ohmic to ballistic transport in oriented graphite: Measurements and numerical simulations*, Phys. Rev. B **78**, 035 413 (2008)

V. Heera, R. Höhne, O. Ignatchik, H. Reuther, P. Esquinazi: *Absence of superconductivity in boron-implanted diamond*, Diam. Relat. Mater. **17**, 383 (2008)

R. Höhne, P. Esquinazi, V. Heera, H. Weishart, A. Setzer, D. Spemann: *The influence of iron, fluorine and boron implantation on the magnetic properties of graphite*, J. Magn. Magn. Mater. **320**, 966 (2008)

N. Moutis, T. Speliotis, I. Panagiotopoulos, M. Ziese: *Magnetotransport properties of cobalt-iron pyrite films*, Thin Solid Films **516**, 2078 (2008)

S. Pruefer, M. Ziese: *Study of magnetization processes using higher harmonic ac-susceptibility*, Physica Stat. Sol. B **245**, 1661 (2008)

K. Schindler, N. Garcia, P. Esquinazi, H. Ohldag: *Insulating behavior of magnetic spots in proton-bombarded graphite*, Phys. Rev. B **78**, 045 433 (2008)

D. Spoddig, U. Köhler, M. Haak, M. Kneppe, T. Schmitte, A. Westphalen, K. Theis-Brohl, R. Meekenstock, D. You, J. Pelzl: *A comparison of ferromagnetic resonance and magneto optical Kerr effect on thin Fe films on InAs(001)*, Superlat. Microstruct. **43**, 180 (2008)

I. Vrejoiu, M. Ziese, A. Setzer, P. Esquinazi, B.I. Birajdar, A. Lotnyk, M. Alexe, D. Hesse: *Interfacial strain effects in epitaxial multiferroic heterostructures* $PbZr_xTi_{1-x}O_3$/ $La_{0.7}Sr_{0.3}MnO_3$ *grown by pulsed-laser deposition*, Appl. Phys. Lett. **92**, 152 506 (2008)

Q. Xu, L. Hartmann, H. Schmidt, H. Hochmuth, M. Lorenz, A. Setzer, P. Esquinazi, C. Meinecke, and M. Grundmann: *Magnetotransport properties of* $Zn_{90}Mn_{7.5}Cu_{2.5}O_{100}$ *films*, Thin Solid Films **516**, 1160 (2008)

Q. Xu, H. Schmidt, H. Hochmuth, M. Lorenz, A. Setzer, P. Esquinazi, C. Meinecke, M. Grundmann: *Room temperature ferromagnetism in Nd- and Mn-codoped ZnO films*, J. Phys. D Appl. Phys. **41**, 105 012 (2008)

Q. Xu, H. Schmidt, S.Q. Zhou, K. Potzger, M. Helm, H. Hochmuth, M. Lorenz, A. Setzer, P. Esquinazi, C. Meinecke, M. Grundmann: *Room temperature ferromagnetism in ZnO films due to defects*, Appl. Phys. Lett. **92**, 082 508 (2008)

M. Ziese, A. Setzer, I. Vrejoiu, B.I. Birajdar, B.J. Rodriguez, D. Hesse: *Structural, magnetic and electric properties of* $La_{0.7}Sr_{0.3}MnO_3/PbZr_xTi_{1-x}O_3$ *heterostructures*, J. Appl. Phys. **104**, 063 908 (2008)

M. Ziese, I. Vrejoiu, A. Setzer, A. Lotnyk, D. Hesse: *Coupled magnetic and structural transitions in* $La_{0.7}Sr_{0.3}MnO_3$ *films on* $SrTiO_3$, New J. Phys. **10**, 063 024 (2008)

**Talks**

M. Ziese: *Coupled magnetic and structural transitions in the $La_{0.7}Sr_{0.3}MnO_3$ / $SrTiO_3$ system*, Eur. Conf. Phys. Magn. 2008, Poznan, Poland, 24. – 27. June 2008

M. Ziese: *Structural and Magnetic Properties of $La_{0.7}Sr_{0.3}MnO_3$ / $Pb_xTi_{1-x}O_3$ Heterostructures*, Joint Eur. Magn. Symp. JEMS08, Dublin, Ireland, 14. – 19. September 2008

M. Ziese: *Coupled magnetic and structural transitions in $La_{0.7}Sr_{0.3}MnO_3$ films on $SrTiO_3$*, Joint Eur. Magn. Symp. JEMS08, Dublin, Ireland, 14. – 19. September 2008

**Posters**

Y.F. Chen, M. Ziese: *Magnetic and Magnetotransport Properties of Magnetite / Co-Ferrite Trilayers*, Eur. Conf. Phys. Magn. 2008, Poznan, Poland, 24. – 27. June 2008

M. Ziese, M. Khalid, A. Setzer, P. Esquinazi, M. Lorenz, H. Hochmuth, M. Grundmann, D. Spemann: *Magnetic Properties of ZnO Films grown by Pulsed Laser Deposition under $N_2$ Atmosphere*, Joint Eur. Magn. Symp. JEMS08, Dublin, Ireland, 14. – 19. September 2008

M. Ziese, A. Setzer, P. Esquinazi, I. Vrejoiu, D. Hesse: *Magnetoelastic Coupling of $La_{0.7}Sr_{0.3}MnO_3$ films near the structural phase transition in $SrTiO_3$*, 72. DPG Spring Meeting, Berlin, Germany 25. – 29. February 2008

M. Ziese, A. Setzer, I. Vrejoiu, A. Lotnyk, D. Hesse: *Coupled magnetic and structural transitions in $La_{0.7}Sr_{0.3}MnO_3$ films on $SrTiO_3$*, Joint Eur. Magn. Symp. JEMS08, Dublin, Ireland, 14. – 19. September 2008

## 10.11 Graduations

**Diploma**

- Ingo Hilschenz
  *Characterization of Al-Doped $MgB_2$*
  January 2008
- Thomas Scheller
  *Transport Measurements on microscopic YBCO Stripes*
  January 2008

**Bachelor**

- Holger Motzkau
  *Investigations on the temperature dependent resistivity of nano-wires prepared by ion and electron beam induced deposition*
  September 2008
- Francis Bern
  *Fabrication and Magnetoresistance Characterization of Cobalt Nanowires*
  October 2008

## 10.12 Guests

- Prof. Nicolás García (Leibniz-Professor)
  CSIC Madrid, Spain
  01. October – 31. December 2008
- Prof. Zheng Xu
  Nanjing University, China
  28. September – 03. October 2008
- Dr. Carmen Muñoz
  CSIC Madrid, Spain
  13. – 17. October 2008
- Dr. Silvia Perez de Heluani
  Universidad Nacional de Tucumán, Argentina
  12. September – 11. December 2008
- Dr. Yoram Dagan
  Tel Aviv University, Israel
  21. – 28. September 2008
- Mamadu Bah
  University of Sierra Leone, Freetown, Sierra Leone
  15. August – 26. September 2008
- Salomon W. Pohl
  Wilhelm-Ostwald-Gymnasium, Leipzig, Germany
  October – December 2008

# III

# Institute for Theoretical Physics

# 11

# Computational Quantum Field Theory

## 11.1 Introduction

The Computational Physics Group performs basic research into classical and quantum statistical physics with special emphasis on phase transitions and critical phenomena. In the centre of interest are currently the physics of spin glasses, diluted magnets and other materials with quenched, random disorder, soft condensed matter physics with focus on fluctuating paths and interfaces, biologically motivated problems such as protein folding, aggregation and adhesion as well as related properties of semiflexible polymers, and the intriguing physics of low-dimensional quantum spin systems. Investigations of a geometrical approach to the statistical physics of topological defects with applications to superconductors and superfluids and research into fluctuating geometries with applications to quantum gravity (e.g., dynamical triangulations) are conducted within a European RTN Network collaboration of 13 teams, and the statistical mechanics of complex networks is studied in collaboration with our partner university in Krakow, Poland.

The methodology is a combination of analytical and numerical techniques. The numerical tools are currently mainly Monte Carlo computer simulations and high-temperature series expansions. The computational approach to theoretical physics is expected to gain more and more importance with the future advances of computer technology, and is likely to become the third cornerstone of physics besides experiment and analytical theory. Already now it can help to bridge the gap between experiments and the often necessarily approximate calculations of analytical work. To achieve the desired high efficiency of the numerical studies we develop new algorithms, and to guarantee the flexibility required by basic research all computer codes are implemented by ourselves. The technical tools are Fortran, C, and C++ programs running under Unix or Linux operating systems and computer algebra using Maple or Mathematica. The software is developed and tested at the Institute on a cluster of PCs and workstations, where also most of the numerical analyses are performed. Large-scale simulations requiring vast amounts of computer time are carried out at the Institute on quite powerful compute servers, at the parallel computers of the University computing center, and, upon successful grant application at the national supercomputing centres in Jülich and München on IBM and Hitachi parallel supercomputers. This hierarchy of various

platforms gives good training opportunities for the students and offers promising job perspectives in many different fields for their future career.

Within the University, our research activities are closely integrated into the Graduate School "BuildMoNa": Leipzig School of Natural Sciences – *Building with Molecules and Nano-objects* funded by the German Research Foundation (DFG) within the German Excellence Initiative and the international DFH-UFA Graduate School "Statistical Physics of Complex Systems" with the l'Université Henri Poincaré Nancy, France, supported by the Deutsch-Französische Hochschule. The two Graduate Schools are both "Classes" of the Research Academy Leipzig (RAL), providing the organizational frame for hosting visiting students, offering language courses and for many other practical matters. At the post-graduate level our research projects are embedded into the "Sächsische DFG-Forschergruppe" FOR 877 *From Local Constraints to Macroscopic Transport* and into two of the priority research areas ("Profilbildende Forschungsbereiche (PbF)") and the Centre for Theoretical Sciences (NTZ) of the University. In particular the latter structures are instrumental for our cooperations with research groups in experimental physics and biochemistry.

On an international scale, our research projets are carried out in a wide net of collaborations funded by the German Academic Exchange Service (DAAD), the Alexander-von-Humboldt Foundation though an Institute Partnership with the Jagellonian University in Krakow, Poland, as well as their Fellowship Programme, and the European Commission through the RTN Network "ENRAGE": *Random Geometry and Random Matrices: From Quantum Gravity to Econophysics* and the Incoming Fellowship Programme. In 2008 and a few years to come, our group is hosting Humboldt Research Prize Winner Professor Bernd A. Berg from Florida State University, Tallahassee, USA. Further close contacts and collaborations are also established with research groups in Armenia, Austria, China, France, Great Britain, Israel, Italy, Japan, Poland, Russia, Spain, Sweden, Taiwan, Turkey, Ukraine, and the United States. These contacts are refreshed and furthered through our international Workshop series CompPhys: "New Developments in Computational Physics", taking annually place at the end of November.

*Wolfhard Janke*

## 11.2 Free-Energy Barriers of Spin Glasses

A. Nußbaumer, E. Bittner, M. Aust, F. Beyer, W. Janke

In statistical physics there is an on-going debate about the nature of the low-temperature phase of finite-dimensional spin-glass systems. The most prominent theses in the field are the replica symmetry-breaking theory and the phenomenological droplet picture (for some reviews see [1–4]).

Like in the thermodynamic limit of the mean-field spin glass, the frozen phase of a finite system shows an complicated corrugated structure. As a consequence of the disorder and frustration characterising spin glasses in general, there is a rugged free-energy landscape with probable regions and rare event-states. Consequently, conventional Monte Carlo simulations tend to get stuck in local free energy valleys.

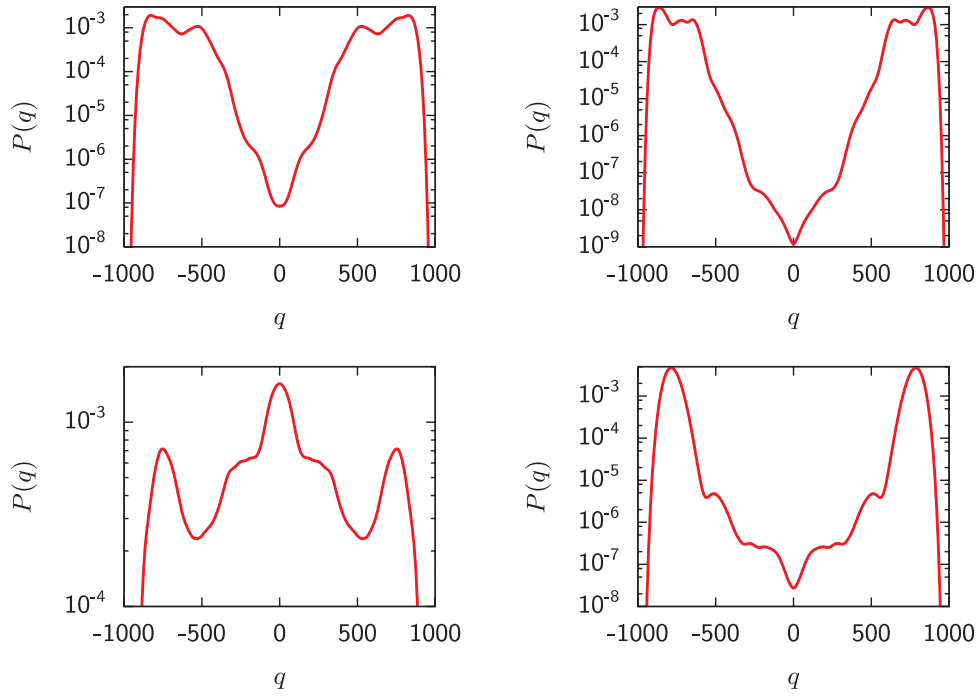


**Figure 11.1:** Distribution functions $P(q)$ of the Edwards-Anderson Ising model for four different disorder realisations on a $V = 10^3$ lattice in the low-temperature phase. While three realisations have a valley at $q = 0$, one realisation has its maximum at that point.

The project tries to solve this kind of problems using a novel, combined algorithm making use of the parallel tempering method [5] and the multioverlap Monte Carlo algorithm [6]. Large scale simulations on our local computer cluster as well as on the "JUMP" super-computer in Jülich have been performed for the Sherrington–Kirkpatrick mean-field model [7] and the Edwards-Anderson Ising model [8].

The typical outcome for different disorder realisations is shown in Fig. 11.1. To get "physical" results, several thousand different realisations must be averaged, making the vast amount of computer time needed understandable. Parts of our results can be found in [9].

[1] A.P. Young (Ed.): *Spin Glasses and Random Fields* (World Scientific, Singapore 1997)
[2] K.H. Fischer, J.A. Hertz: *Spin Glasses* (Cambridge University Press, Cambridge 1991)
[3] M. Mezard et al.: *Spin Glass Theory and Beyond* (World Scientific, Singapore 1987)
[4] K. Binder, A.P. Young: Rev. Mod. Phys. **58**, 801 (1986)
[5] K. Hukushima, K. Nemoto: J. Phys. Soc. Jpn. **65**, 1604 (1996)
[6] B.A. Berg, W. Janke: Phys. Rev. Lett. **80**, 4771 (1998)
[7] D. Sherrington, S. Kirkpartick: Phys. Rev. Lett. **35**, 1792 (1975)
[8] S.F. Edwards, P.W. Anderson: J. Phys. F **5**, 965 (1975)
[9] E. Bittner et al.: in *NIC Symposium 2008*, ed. by G. Münster et al., NIC Series, Vol. **39** (John von Neumann Institute for Computing, Jülich 2008) p 229

## 11.3 Fractals Meet Fractals: Multicritical Behavior of Self-Avoiding Walks on Percolation Clusters

V. Blavatska, W. Janke

It is well established that the scaling properties of long flexible polymer chains are perfectly described within the model of a self-avoiding walk (SAW) on a *regular* lattice [1]. In particular, for the average squared end-to-end distance $R^2$ and the number of all possible trajectories $Z_N$ of a SAW with $N$ steps on a regular lattice one finds in the asymptotic limit $N \to \infty$:

$$\langle R^2 \rangle \sim N^{2\nu_{\rm SAW}} , \qquad Z_N \sim z^N N^{\gamma_{\rm SAW}-1} , \tag{11.1}$$

where $\nu_{\rm SAW}$ and $\gamma_{\rm SAW}$ are universal exponents that only depend on the space dimensionality $d$. The properties of a SAW on a regular lattice have been studied in detail, and the values of the universal exponents in (11.1) are known by now with high precision from experiments, computer simulations and theory.

One question of great interest is the influence of structural disorder on the universal properties of a SAW, namely: does the scaling (11.1) hold with modified exponents $\nu^{p_c}_{\rm SAW}$ and $\gamma^{p_c}_{\rm SAW}$ when a SAW resides on a structurally *disordered* (diluted) lattice? The question of how do linear polymers behave in disordered media is not only of academic interest, but is also relevant for understanding transport properties of polymer chains in porous media, such as enhanced oil recovery, gel electrophoresis, gel permeation chromatography, etc. In the present project, we were interested in the special case when the disordered lattice is exactly at the percolation threshold $p_c$. Here, the SAW is allowed to have its steps only on the percolation clusters.

For simulating SAWs on percolative lattices, we used the pruned-enriched Rosenbluth method (PERM) [2]. Estimates for the critical exponents $\nu^{p_c}_{\rm SAW}$ were obtained by linear least-square fitting. Since we can construct only lattices with a finite linear size $L$, the scaling laws (11.1) only hold up to some "marginal" number of SAW steps $N_{\rm marg} \sim L^{1/\nu^{p_c}_{\rm SAW}}$. We take this into account when estimating the critical exponents by the linear least-square fitting. The thus obtained values of $\nu^{p_c}_{\rm SAW}$ for $d = 2, 3, 4$ are larger than the corresponding exponents on the pure lattice [3]; presence of disorder leads to stretching of the trajectory of self-avoiding walks. In addition we have also obtained numerical estimates for the exponents $\gamma^{p_c}_{\rm SAW}$ [4, 5].

Both a SAW and a percolation cluster are among the most frequently encountered examples of fractals in condensed matter physics. If two such fractals "meet", multifractal behavior may show up. Following early ideas [6], it was only recently proven in field-theoretical studies [7] that the exponent $\nu^{p_c}_{\rm SAW}$ alone is indeed not sufficient to completely describe the peculiarities of SAWs on percolation clusters. Instead, a whole spectrum $\nu^{(q)}$ of multifractal exponents emerges. Our numerical values for the exponents $\nu^{(q)}$ as a function of $q$ appear to be in an astonishingly perfect agreement with analytical estimates derived from $\varepsilon = 6 - d$ expansions down to $d = 2$ dimensions [8]. The properties of the associated spectral function have been analyzed as well.

[1] P.-G. de Gennes: *Scaling Concepts in Polymer Physics* (Cornell University Press, Ithaca 1979)
[2] P. Grassberger: Phys. Rev. E **56**, 3682 (1997)

[3] V. Blavatska, W. Janke: Europhys. Lett. **82**, 66 006 (2008)
[4] V. Blavatska, W. Janke: J. Phys. A **42**, 015 001 (2009)
[5] V. Blavatska, W. Janke: in *Path Integrals – New Trends and Perspectives*, ed. by W. Janke, A. Pelster (World Scientific, Singapore 2008) p 585
[6] Y. Meir, A.B. Harris: Phys. Rev. Lett. **63**, 2819 (1989)
[7] H.K. Janssen, O. Stenull: Phys. Rev. E **75**, 020 801(R) (2007)
[8] V. Blavatska, W. Janke: Phys. Rev. Lett. **101**, 125 701 (2008)

## 11.4 Critical Properties of High-Temperature XY Graphs

F. Winter*, A.M.J. Schakel†, W. Janke

*John von Neumann-Institut für Computing (NIC), Zweigstelle Deutsches Elektron Synchrotron (DESY), Zeuthen, Germany
†Institut für Theoretische Physik, Freie Universität Berlin, Germany

Based on his space-time approach to quantum mechanics, Feynman [1] developed a profound original picture of Bose–Einstein condensation. In this picture, all the particles in the system execute a random walk in space during the imaginary time interval $\hbar\beta$ ($\hbar$ is Planck's constant and $\beta$ denotes the inverse temperature). Starting and ending at the same point in space, these particle trajectories form loops. At high temperatures, the individual loops hardly overlap. However, upon lowering the temperature, individual particle trajectories start to overlap and hook up to form longer loops. A particle in such a composite loop moves in imaginary time along a trajectory that does not end at its own starting position, but at that of another particle. Whence, although the initial and final configurations are identical, the participating particles are cyclically permuted. They thereby loose their identity and become indistinguishable. Loops involving, say, $w$ particles wrap the imaginary time axis exactly $w$ times. Upon approaching the condensation temperature from above, loops with arbitrary large winding number appear and signal the formation of a Bose–Einstein condensate.

Bose–Einstein condensation in a dilute uniform Bose gas belongs to the family of critical phenomena described by the XY model which, for computational purposes, can be conveniently formulated on the lattice. The model can then, for example, be represented by graphs on the lattice. In this so-called high-temperature approach, the partition function and correlation functions are calculated by counting graphs on the lattice, with each graph representing a certain contribution. The high-temperature graphs of the XY model physically represent the spatial projections of the particle trajectories of the Bose gas.

By simulating the high-temperature graphs on a cubic lattice (see Fig. 11.2) and using observables originally introduced in the context of percolation theory, we studied the critical properties of the XY model in purely geometrical terms [2]. We determined the fractal dimension of the graphs at the critical point to be $D = 1.7626(66)$, and showed that the diverging length scale characterizing the high-temperature graphs close to the critical point coincides with the thermal correlation length. The value of the fractal dimension of the XY high-temperature graphs is between that of a self-avoiding walk, for which $D = 1.7001(32)$, and that of a Brownian random walk, for which $D = 2$.

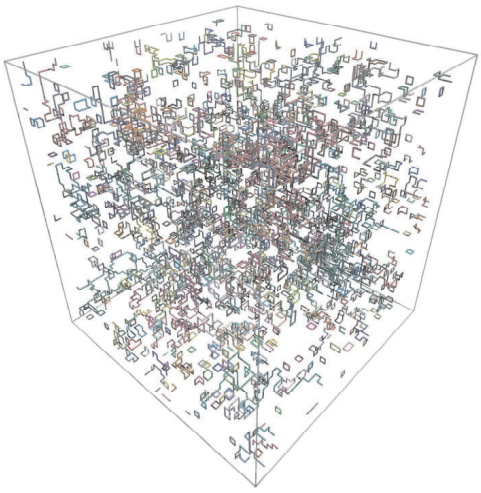

**Figure 11.2:** Typical high-temperature graphs on a cubic lattice at the temperature where, on average, a single graph spans the lattice.

[1] R.P. Feynman: Phys. Rev. **91**, 1291 (1953)
[2] F. Winter et al.: Phys. Rev. E **77**, 061 108 (2008)

## 11.5 Complex Networks and Non-Equilibrium Systems

B. Wacław, L. Bogacz*, H. Nagel, Z. Burda*, H. Meyer-Ortmanns†, J. Sopik†, W. Janke

*Institute of Physics, Jagellonian University, Krakow, Poland
†School of Engineering and Science, Jacobs University, Bremen, Germany

Complex networks [1] are a relatively new branch of physics. An enormous growth of this discipline was triggered by observing in the 90s that many networks like the Internet, the WWW, and social or biological networks display a complex structure which places them between purely random graphs and regular grids. Many models explaining their features have been proposed. However, most of them are solvable only in thermodynamic limit. We study the convergence towards limiting properties for different networks, both analytically and numerically.

We focus mainly on so-called equilibrated networks, that is graphs being maximally random under given constraints, e.g., fixed number of nodes and given degree distribution. Because typical sizes of real-world networks range from $N \sim 10^2$ (small transportation networks) to $N \sim 10^9$ (the WWW), finite-size effects are much stronger than in "classical" systems composed of atoms and particles ($N \sim 10^{23}$). For example, in scale-free networks where the degree distribution $\pi(k) \sim k^{-\gamma}$ has a power-law behavior, due to the finite size $N$, the distribution $\pi(k)$ decreases rapidly above some $k_{\text{cutoff}}$. The cutoff $k_{\text{cutoff}}$ scales as some power $\alpha$ of $N$. This effect influences many processes like percolation or disease spreading on networks. We discovered that the scaling predicted for very large networks is approached very slowly (sometimes with a logarithmic correction) and is far from being true even for $N = 10^9$ [2]. In contrast, the scaling of the maximal degree $k_{\max} \sim N^{\alpha'}$ is reached much faster and, in general, $\alpha' \neq \alpha$.

Many network models cannot be solved analytically for finite $N$ and one has to turn to Monte Carlo (MC) simulations. We developed a program [3] which generates various kinds of equilibrated networks by MC sampling. Written originally in C, the software has been rewritten in C++ in an object-oriented way and evolved into a library that can be linked to any other program [4].

Our second activity are driven diffusive systems. They are simple models of non-equilibrium systems of particles hopping between sites of a lattice, or more generally, of an arbitrary graph or network. Under certain conditions, such models exhibit condensation of particles – a single site takes an extensive number of particles. Motivated by our previous experience with zero-range processes on networks [5, 6], we study models which have pair-factorized steady states (PFSS). This means that the probability of having a certain configuration of particles factorizes over the pairs of nodes [7]. This is equivalent to an equilibrium model called SOS model [8]. The PFSS allows one to study how node–node interactions influence the condensation. We found that in one dimension the condensate, if it exists, is usually spatially extended to $W \sim N^{\alpha}$ sites, with $\alpha$ depending on the functional form of the hopping rate. We also calculated the envelope of the condensate [9]. We are currently studying the model in higher dimensions, its generalization to random graphs and the factorization over more complicated motifs (triangles, plaquettes, etc.).

This work is partially supported by an Institute Partnership grant "Krakow–Leipzig" (http://www.physik.uni-leipzig.de/~waclaw/AvH) of the Alexander-von-Humboldt Foundation and the EU-Network "ENRAGE".

[1] S. Boccaletti et al.: Phys. Rept. **424**, 175 (2006)
[2] B. Waclaw et al.: Phys. Rev. E **78**, 061 125 (2008)
[3] L. Bogacz et al.: Comput. Phys. Commun. **173**, 162 (2005)
[4] H. Nagel: http://www.physik.uni-leipzig.de/~nagel/graphgen
[5] B. Waclaw et al.: Phys. Rev. E **76**, 046 114 (2007)
[6] B. Waclaw et al.: Eur. Phys. J. B **65**, 565 (2008)
[7] M.R. Evans et al.: Phys. Rev. Lett. **97**, 010 602 (2006)
[8] S.T. Chui, J.D. Weeks: Phys. Rev. B **23**, 2438 (1981); T.W. Burkhardt, J. Phys. A **14**, L63 (1981)
[9] B. Waclaw et al.: arXiv:0901.3664

## 11.6 Thickness-Dependent Secondary-Structure Formation of Tubelike Polymers

T. Vogel, T. Neuhaus*, M. Bachmann, W. Janke

*John von Neumann-Institut für Computing (NIC), Forschungszentrum Jülich, Germany

By means of computer simulations we studied the thermodynamical behaviour of tube models for simple homopolymers as well as for exemplified hydrophobic-polar heteropolymers [1, 2]. The thickness of the tube in our simulations is controlled by a single parameter, the global radius of curvature, which depends on three-body interactions [3].

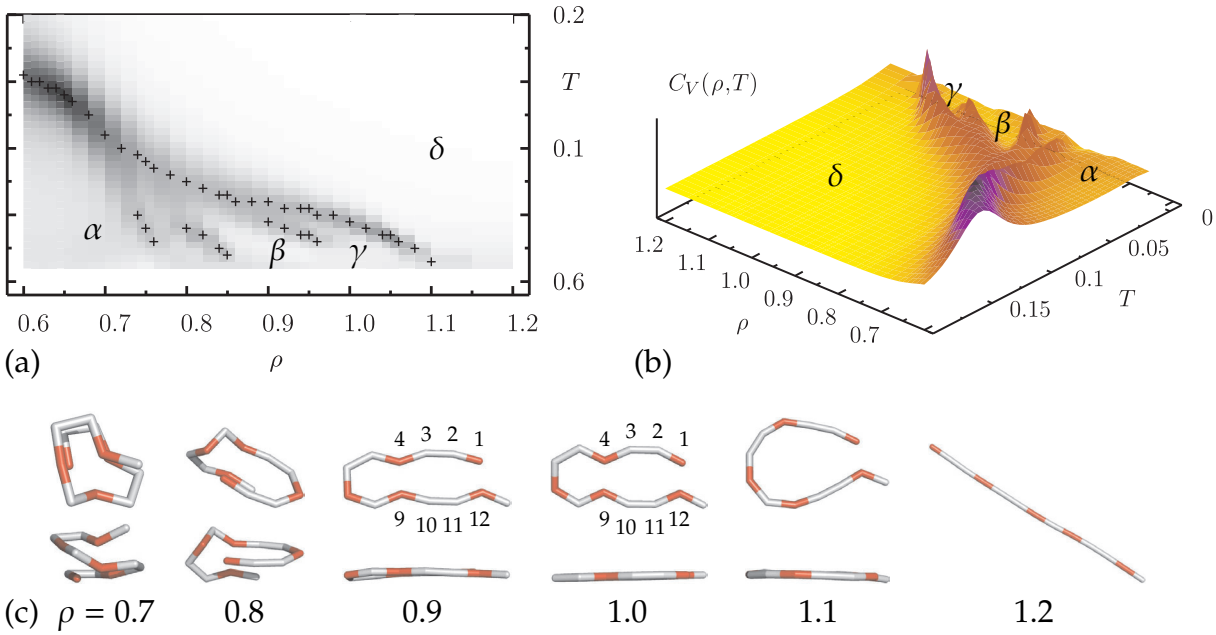


**Figure 11.3:** Pseudophase diagram and ground-state conformations of the $N = 13$ Fibonacci AB heteropolymer. (**a**) The plot shows the top-view with marked peak positions of the specific heat for various thickness parameters $\rho$, (**b**) the qualitative view of the specific-heat landscape. The pictures in (**c**) illustrate selected ground-state conformations. Conformations are shown from different viewpoints, "A" monomers are marked by red color (dark gray), "B" monomers are white.

After focusing on ground states of homopolymers and their properties in a preceding step [4], we identified dominant structural pseudophases at finite temperatures, i.e., specific-heat landscapes depending on the thickness parameter $\rho$ and temperature $T$, representing the conformational phase diagram. Independently of the polymer length, we find four major structural phases. These include helices ($\alpha$), sheetlike planar structures ($\beta$), bended rings ($\gamma$) and sprawled random coils ($\delta$). These different secondary structure phases can be assigned to different ranges of the tube thickness. The thickness parameter is therefore suitable for a classification of the structural behaviour of classes of polymers.

Particularly, we introduced the AB tube model for hydrophobic-polar heteropolymers and obtained results for specific sequences of monomers (see Fig. 11.3), which has extensively been studied before without thickness [5]. We showed that a specific monomer sequence can stabilize the general secondary structures. We find, for example, a very pronounced and stable region of $\beta$-sheet structures. We further showed that the additional introduction of a bending stiffness plays a subordinate role. This observation is necessary to relate our general results to existing results of special systems. We could in particular reproduce simulational results published within the past years for polymer models without explicit thickness as limiting case of our our study [2].

[1] T. Vogel et al.: Europhys. Lett. **85**, 10 003 (2009)
[2] T. Vogel et al.: *Thermodynamics of Tubelike Flexible Polymers*, submitted
[3] O. Gonzalez, J. Maddocks: Proc. Natl. Acad. Sci. USA **96**, 4769 (1999)
[4] T. Vogel et al.: *Ground-State Properties of Tubelike Flexible Polymers*, submitted
[5] M. Bachmann et al.: Phys. Rev. E **71**, 031 906 (2005), and references therein

## 11.7 Low-Temperature Behaviour of Elastic Lennard-Jones Polymers

S. Schnabel, M. Bachmann, W. Janke

We developed and applied sophisticated Monte Carlo computer simulation methods to investigate the low-temperature behaviour of an off-lattice model for flexible elastic homopolymers. In this model beads interact via truncated Lennard-Jones potentials and adjacent beads are additionally bonded by a FENE bond potential [1]. Special interest laid on so-called solid-solid transitions, which became accessible by the introduction of a new order parameter that refers to Platonic, Archemedean, and Johnson solids.

Considering the ground-state structures of homopolymers of different sizes, it soon turned out that the obtained structures show wide similarities to low-energy conformations of atomic Lennard-Jones clusters. We mainly found icosahedral structures (see Fig. 11.4) with Mackay or anti-Mackay overlayers [2] and were able to document transitions between both types [3].

As it is well known from former research on Lennard-Jones clusters [4], non-icosahedral structures might play an important role at low temperatures. However, due to the complex shape of the state space it is difficult to identify such structures with standard Monte Carlo methods. Therefore, we divided the conformational space by classifying all structures with respect to the occurrence of icosahedral cells. We then modified the scheme of multicanonical Monte Carlo sampling and applied different weight functions for different classes of conformations. In consequence, we were able to overcome the broken-ergodicity problem and to investigate the solid-solid transitions between structures of icosahedral and non-icosahedral type at extreme low temperatures [5].

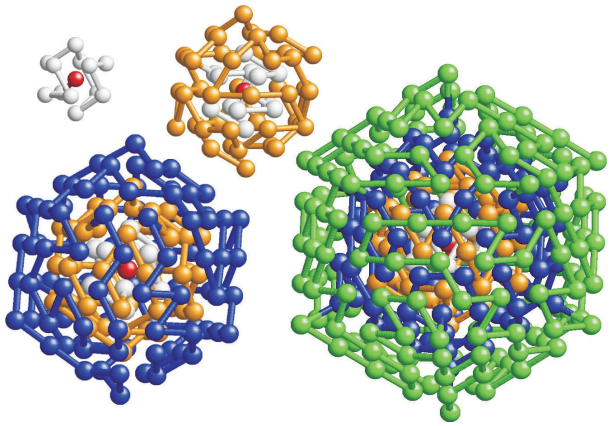

**Figure 11.4:** Ground-state conformations for homopolymers of "magic" sizes ($N$ = 13, 55, 147, 309) that form complete icosahedra. Due to the high symmetry and the almost spherical shape, these structures are of high stability and dominate the low-temperature behaviour of these polymers.

[1] R.B. Bird et al.: *Dynamics of Polymeric Liquids*, 2. Ed. (Wiley, New York 1987)
[2] J.A. Northby: J. Chem. Phys. **87**, 6166 (1987)
[3] S. Schnabel et al.: *Surface Effects in the Crystallization Process of Elastic Flexible Polymers*, submitted

[4] V.A. Sharapov et al.: Phys. Rev. Lett. **98**, 105 701 (2007)
[5] S. Schnabel et al.: *Elastic Lennard–Jones Polymers meet Clusters – Differences and Similarities*, submitted

## 11.8 Statistical Mechanics of Aggregation and Crystallization for Semiflexible Polymers

C. Junghans*, M. Bachmann, W. Janke

*Max-Planck-Institut für Polymerforschung, Mainz, Germany

Cluster formation and crystallization of polymers are processes which are interesting for technological applications, e.g., as new materials with certain mechanical properties or nanoelectronic organic devices and polymeric solar cells. From a biophysical point of view, the understanding of (de)fragmentation in semiflexible biopolymer systems like actin networks and also peptide oligomerization is of substantial relevance. This requires a systematic analysis of polymeric cluster formation processes, in particular, for small polymer complexes on the nanoscale, where surface effects are competing noticeably with structure-formation processes in the interior of the aggregate.

By means of multicanonical computer simulations, we have investigated thermodynamic properties of the aggregation of interacting semiflexible polymers. We analyzed a mesoscopic bead–stick model, where nonbonded monomers interact via van der Waals forces. The aggregation of semiflexible polymers turns out to be a process, in which the constituents experience strong structural fluctuations [1], similar to peptides in coupled folding-binding cluster formation processes. In contrast to a recently studied related proteinlike hydrophobic-polar heteropolymer model [2, 3], aggregation and crystallization are separate processes here. However, in analogy to the heteropolymer study, we find that the first-order-like aggregation transition of the complexes is accompanied by strong system-size dependent hierarchical surface effects. These are called backbending effects, because the caloric (or microcanonical) temperature decreases with increasing energy. This is a direct consequence of the fact that the aggregation of polymers is a phase-separation process with entropy reduction [4].

[1] C. Junghans et al.: *Statistical Mechanics of Aggregation and Crystallization for Semiflexible Polymers*, submitted
[2] C. Junghans et al.: Phys. Rev. Lett. **97**, 218 103 (2006)
[3] C. Junghans et al.: J. Chem. Phys. **128**, 085 103 (2008)
[4] D.H.E. Gross: *Microcanonical Thermodynamics* (World Scientific, Singapore 2001)

## 11.9 Conformational Mechanics of Polymer Adsorption Transitions at Attractive Substrates

M. Möddel, M. Bachmann, W. Janke

We used thermal fluctuations of energetic and structural quantities obtained by multicanonical computer simulations to identify a variety of pseudophases of a semiflexible

off-lattice homopolymer near an attractive substrate. Introducing a solvent parameter $\epsilon_s$, that is related to the strength of the surface attraction, the solubility-temperature phase diagram is constructed and discussed (Fig. 11.5) [1].

Although the computational expense for an accurate exploration of such a broad parameter range restricted us to investigate rather short chains, we identified the following conformational pseudophases and pseudophase transitions:

- Crystalline structures in the regimes of compact phases: We identified maximally compact desorbed conformations in bulk (DC) or adsorbed at the substrate (AC), semi-spherical compact conformations (AC2a) that are distorted by the surface but not layered, double-layer conformations (AC2b), and single-layer conformations (AC1).

- Adsorbed conformations in the globular and expanded (random-coil) phases: Here, three conformational pseudophases were distinguished: unstructured 3D surface-attached globular conformations (AG), expanded dissolved but planar adsorbed conformations (AE1), and 3D expanded random-coil-like adsorbed conformations (AE2).

- Desorbed conformations: Compact conformations (DC) are separated by the freezing transition from globular conformations (DG). At even higher temperatures above the well known $\theta$-transition, random-coil conformations are found (DE).

These results are in nice quantitative coincidence with recent lattice results [2] which demonstrates the ability of such coarse-grained models to capture the general adsorption behavior of polymers near attractive surfaces.

With the density of states, estimated in the multicanonical recursion, we then performed a microcanonical analyses that focused on the adsorption transition, where a convex intruder of the microcanonical entropy can be observed for short chains. A typical signal for a phase separation process. This, however, vanishes for increasing chain lengths and decreasing surface attraction.

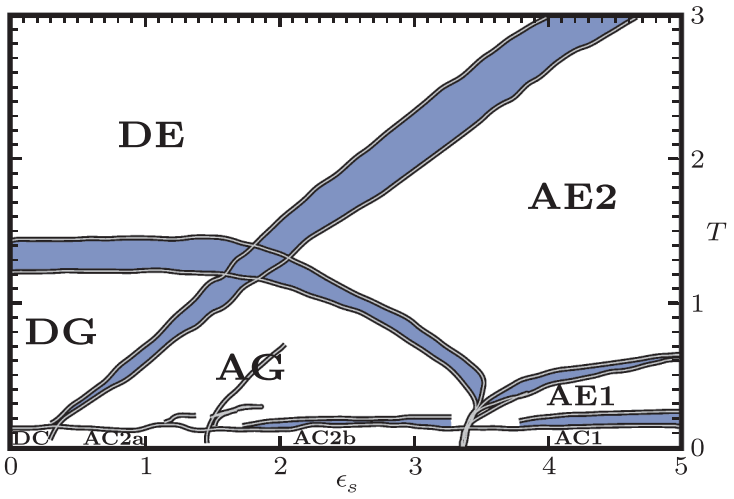


**Figure 11.5:** Phase diagram of the 20mer. The colored stripes separate the individual conformational phases described in the text.

[1] M. Möddel et al.: J. Phys. Chem. B **113**, 3314 (2009)
[2] M. Bachmann, W. Janke: Phys. Rev. Lett. **95**, 058 102 (2005); Phys. Rev. E **73**, 041 802 (2006); Phys. Part. Nucl. Lett. **5**, 243 (2008)

## 11.10 Microscopic Mechanism of Specific Peptide Adhesion to Semiconductor Substrates

M. Bachmann, K. Goede*, A.G. Beck-Sickinger†, M. Grundmann*, A. Irbäck‡, W. Janke

*Institute for Experimental Physics II, Semiconductor Physics Workgroup
†Institut für Biochemie
‡Computational Biology & Biological Physics Division, Lunds Universitet, Lund, Sweden

In the past few years, the interest in hybrid interfaces formed by "soft" molecular matter and "hard" solid substrates has rapidly grown as such systems promise to be relatively easily accessible candidates for novel biosensors or electronic devices. The enormous progress in high-resolution microscopy and in biochemical engineering of macromolecules is the major prerequisite for studies of hybrid systems and potential applications [1]. One particularly important problem is the self-assembly and adhesion of polymers, proteins, or protein-like synthetic peptides to solid materials such as, e.g., metals [2] and semiconductors [3–5]. Peptide and substrate-specific binding affinity is particularly relevant in pattern recognition processes [6]. Basic theoretical considerations of simplified polymer–substrate and protein–substrate models have predicted complex pseudophase diagrams [7, 8].

In bacteriophage display experiments, only a few peptides out of a library of $10^9$ investigated sequences with 12 amino acid residues were found to possess a particularly strong propensity to adhere to (100) gallium-arsenide (GaAs) surfaces [3]. The sequence-specificity of adsorption strength is a remarkable property, but the question remains how it is related to the individual molecular structure of the peptides. We expect that *relevant* mutations of sites in the amino-acid sequence can cause a change of the binding affinity. Indeed, one key aspect of our study is to provide evidence that proline is a potential candidate for switching the adsorption propensities to cleaned (100) silicon (Si) substrates.

In this project, we show by means of experimental and computational analyses that the adsorption properties of mutated synthetic peptides at semiconductors exhibit a clear sequence-dependent adhesion specificity. Our simulations of a novel hybrid peptide-substrate model reveal the correspondence between proline mutation and binding affinity to a clean silicon substrate. After synthesizing the theoretically suggested amino-acid sequences with different binding behaviour, we could confirm the relevance of the selective mutations upon adhesion in our subsequent atomic force microscopy experiments [9].

[1] M. Sarikaya et al.: Nature Mat. **2**, 577 (2003)
[2] S. Brown: Nature Biotechnol. **15**, 269 (1997)
[3] S.R. Whaley et al.: Nature **405**, 665 (2000)
[4] K. Goede et al.: Nano Lett. **4**, 2115 (2004)
[5] K. Goede et al.: Langmuir **22**, 8104 (2006)

[6] T. Bogner et al.: Phys. Rev. Lett. **93**, 268 108 (2004)
[7] M. Bachmann, W. Janke: Phys. Rev. Lett. **95**, 058 102 (2005); Phys. Rev. E **73**, 041 802 (2006)
[8] M. Bachmann, W. Janke: Phys. Rev. E **73**, 020 901(R) (2006)
[9] M. Bachmann et al.: *Microscopic Mechanism of Specific Peptide Adhesion to Semiconductor Substrates*, submitted

## 11.11 Quantum Critical Phenomena in Uniform and Mixed Heisenberg Spin Chains

R. Bischof, W. Janke

By means of quantum Monte Carlo (QMC) simulations (continuous imaginary time loop algorithm) [1] and quantum reweighting methods [2] we investigate quantum critical phenomena and low-temperature properties of various versions of the 1D quantum Heisenberg model, which is one of the most fundamental models of quantum magnetism and is related to high-temperature superconductors [3]. Furthermore it exhibits various zero-temperature quantum critical phenomena, depending on the specific choice of spins and different types of coupling mechanisms. Specifically, we have investigated the uniform $S = 1/2$ Heisenberg spin chain with bond alternation and alternating quantum chains of mixed spins, consisting of two different kinds of spin, $S_a$ and $S_b$, that appear alternatingly in pairs [4].

The low-temperature properties of quantum spin chains depend significantly on the size of spins involved. Uniform chains of half-odd integer spins have no energy gap between the ground state and first excited states (i.e., they are quantum critical), whereas chains with integer spins do show an excitation gap [5]. Above that, spin chains can be driven to and away from criticality by tuning appropriate parameters (such as bond alternation, exchange anisotropy, next-nearest-neighbour interaction, spin–phonon coupling, etc.). While there exists wide literature about quantum critical phenomena in uniform chains, mixed spin chains have yet rarely been considered.

The twist order parameter, as introduced in [6], is well suited to signal quantum phase transitions between different valence bond configurations in various 1D quantum spin systems. At non-zero temperature we have found the formation of a plateau in the twist order parameter around the (zero temperature) quantum critical point. We have investigated the possibility that this plateau is related to the quantum critical region that fans out from the quantum critical point. However, up to the present accuracy of our simulations the data does not support this conjecture [7].

Supplemented by exact Lanczos diagonalisation and extrapolation algorithms we could extract estimates of the critical exponents of the mixed spin models under investigation. We are currently examining the presence of multiplicative logarithmic corrections in mixed spin chains. These corrections have been found in the uniform $S = 1/2$ Heisenberg model [8].

[1] B.B. Beard, U.J. Wiese: Phys. Rev. Lett. **77**, 5130 (1996); H.G. Evertz: Adv. Phys. **52**, 1 (2003)
[2] M. Troyer et al.: Braz. J. Phys. **34**, 377 (2004)

[3] A. Auerbach: *Interacting Electrons and Quantum Magnetism* (Springer, New York 1994)
[4] K. Takano: Phys. Rev. Lett. **82**, 5124 (1999); Phys. Rev. B **61**, 8863 (2000); Z. Xu et al.: Phys. Rev. B **67**, 214 426 (2003)
[5] F.D.M. Haldane: Phys. Rev. Lett. **50**, 1153 (1983)
[6] M. Nakamura, S. Todo: Phys. Rev. Lett. **89**, 077 204 (2002)
[7] R. Bischof, W. Janke: in *Path Integrals – New Trends and Perspectives*, ed. by W. Janke, A. Pelster (World Scientific, Singapore 2008) p 514
[8] C.J. Hamer et al.: Phys. Rev. Lett. **68**, 214 408 (2003); T. Papenbrock et al.: Phys. Rev. B **68**, 024 416 (2003)

## 11.12 Unconventional Quantum Criticality in 2D Dimerized Heisenberg Models

S. Wenzel, W. Janke, S. Wessel*

*Institut für Theoretische Physik III, Universität Stuttgart, Germany

Low-dimensional quantum spin systems are a central research topic in condensed matter physics as they effectively explain many of ordering phenomena in real life materials (e.g. magnetism in the clean cuprates). In the particular the antiferromagnetic Heisenberg model defined by the Hamiltonian

$$\mathcal{H} = \sum_{\langle i,j \rangle} J_{ij} \mathbf{S}_i \mathbf{S}_j = \sum_{\langle i,j \rangle} J_{ij} \left( S_i^x S_j^x + S_i^y S_j^y + S_i^z S_j^z \right) \tag{11.2}$$

is at the forefront of such research. Repeated interest in this model stems from the possibility to study the effect of competing interactions or quantum fluctuations on the ground-state properties of an interacting many-body quantum system. Motivated by the pressure induced disorder-order quantum phase transition in Mott insulators like $TlCuCl_3$ [1], we address in this project so-called dimerized Heisenberg models, in which the lattice spins $\mathbf{S}_i$ interact via two different non-equivalent couplings $J$ and $J'$,

$$\mathcal{H} = J \sum_{\langle i,j \rangle} \mathbf{S}_i \mathbf{S}_j + J' \sum_{\langle i,j \rangle'} \mathbf{S}_i \mathbf{S}_j \,, \qquad \alpha = J'/J \,, \tag{11.3}$$

in a regular manner as depicted in Fig 11.6. Access to quantum critical physics can be gained by varying the parameter $\alpha = J'/J$. In this project, we have carried out extensive quantum Monte Carlo simulations based on the stochastic series expansion (SSE) approach [2] of the quantum phase transition in dimerized Heisenberg models in order to verify the applicability of the nonlinear sigma model (NLSM) to characterize quantum critical phenomena. This theory predicts a standard 3D $O(3)$ description for Heisenberg models.

Our most surprising result is that of a novel universality class triggered by special geometric arrangements of the strong couplings $J'$ in Fig. 11.6c. While we find total agreement with $O(3)$ criticality for the ladder and plaquette models of Fig. 11.6(a,b), our Monte Carlo data for the staggered model indicates different critical exponents $\beta/\nu$

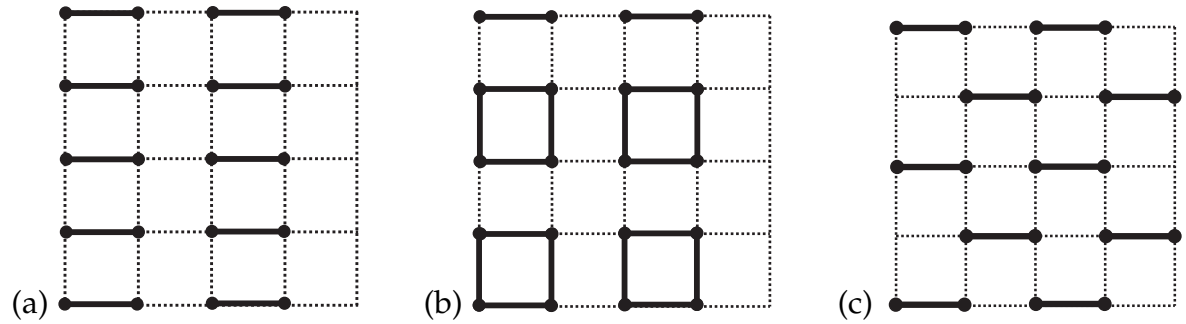


**Figure 11.6:** Examples of dimerized Heisenberg models on the square lattice in form of (**a**) the ladder model, (**b**) the plaquette model, (**c**) the staggered model. Dashed bonds indicate couplings $J$ whereas thick bonds indicate $J'$ interactions.

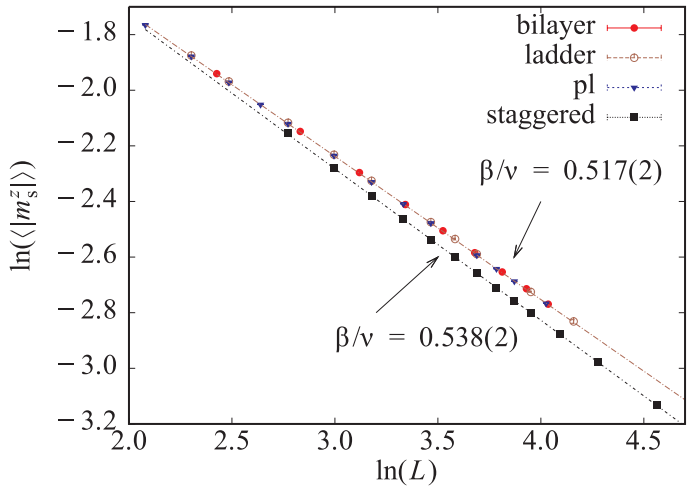


**Figure 11.7:** Finite-size scaling analysis of the sublattice magnetization in different dimerized Heisenberg models at the quantum critical point. The data for the staggered model indicates a deviation from the anticipated value $\beta/\nu = 0.5188(3)$ [3].

characterizing the sublattice magnetization order parameter $m_s^z$. This effect is illustrated in Fig. 11.7, where a finite-size analysis of the magnetization at the quantum critical point is performed [4, 5].

In case of the staggered model, further simulations show deviations from the standard theory in experimentally accessible quantities like the critical uniform magnetic susceptibility at finite temperatures. Initial analytical derivations and simulations of other dimerized Heisenberg models suggest that the novel unconventional behaviour could be related to topological terms that appear in the effective action in certain cases. In result, the Heisenberg model continues to be an even richer playground of quantum phenomena than anticipated until today.

Work supported by the Studienstiftung des deutschen Volkes and BuildMoNa.

[1] C. Rüegg et al.: Phys. Rev. Lett. **93**, 257 201 (2004)
[2] A.W. Sandvik, J. Kurkijärvi: Phys. Rev. B **43**, 5950 (1991); O.F. Syljuasen, A.W. Sandvik: Phys. Rev. E **66**, 046 701 (2002)
[3] M. Campostrini et al.: Phys. Rev. B **65**, 144 520 (2002)
[4] S. Wenzel et al.: Phys. Rev. Lett. **101**, 127 202 (2008)
[5] S. Wenzel, W. Janke: Phys. Rev. B **79**, 014 410 (2009)

## 11.13 Thermodynamics of Heisenberg Ferromagnets in a Magnetic Field

I. Juhász Junger*, D. Ihle*, L. Bogacz†, W. Janke

*Theory of Condensed Matter Workgroup
†Department of Information Technologies, Faculty of Physics, Astronomy and Applied Computer Science, Jagellonian University, Krakow, Poland

The thermodynamic properties magnetization, magnetic susceptibility, transverse and longitudinal correlation lengths, and specific heat of 1D ferromagnetic chains and of 2D ferromagnet layers with arbitrary spin $S$ in a magnetic field are investigated by a second-order Green-function theory. In addition, quantum Monte Carlo simulations for $S = 1/2$ and $S = 1$ are performed by using the stochastic series expansion (SSE) method [1]. Good agreement between the results of both approaches is found [2]. The field dependence of the position of the maximum in the temperature dependence of the susceptibility fits well to a power law at low fields and to a linear increase at high fields. The maximum height decreases according to a power law in the whole field region. The longitudinal correlation length may show an anomalous temperature dependence: a minimum followed by a maximum with increasing temperature.

Considering the specific heat in one dimension and at low magnetic fields, two maxima in its temperature dependence for both the $S = 1/2$ and $S = 1$ ferromagnets are found. For $S > 1$, only one maximum occurs, as in the 2D ferromagnets. Relating the theory to experiments on the $S = 1/2$ quasi-one-dimensional copper salt TMCuC [$(CH_3)_4NCuCl_3$], a fit to the magnetization as a function of the magnetic field yields the value of the exchange energy, which is used to make predictions for the occurrence of two maxima in the temperature dependence of the specific heat.

[1] A.W. Sandvik, J. Kurkijärvi: Phys. Rev. B **43**, 5950 (1991); O.F. Syljuasen, A.W. Sandvik: Phys. Rev. E **66**, 046 701 (2002)
[2] I. Juhász Junger et al.: Phys. Rev. B **77**, 174 411 (2008)

## 11.14 Universal Aspects of the Evaporation/Condensation of Ising Droplets

A. Nußbaumer, E. Bittner, W. Janke

In a seminal work [1] we showed in 2006 that the behaviour of droplets that live on a 2D Ising lattice, with a Hamiltonian defined as

$$H = -J \sum_{\langle ij \rangle} \sigma_i \sigma_j \,, \qquad \sigma_i = \pm 1 \,, \tag{11.4}$$

is compatible with the prediction made by Biskup et al. [2, 3] already for relatively small system sizes $L$. There, an analytical curve is derived that, adapted to the case of the Ising model, yields the amount of magnetisation that is consumed in the largest droplet of the

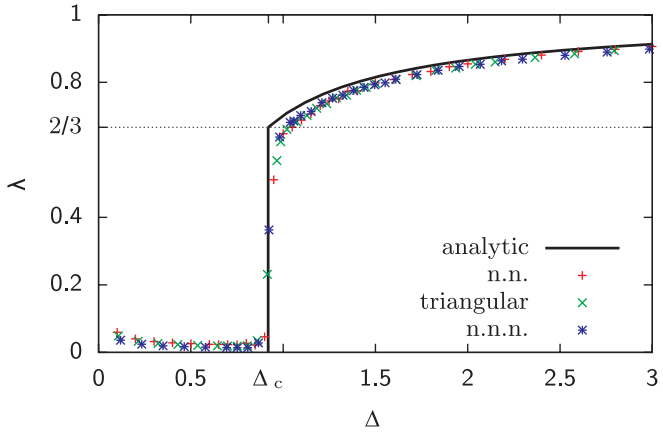


**Figure 11.8:** The fraction $\lambda$ of the excess magnetisation that builds up the largest droplet in dependence of the parameter $\Delta$ that in turn is a function of the magnetisation and some system specific constants, like the spontaneous magnetisation and others. Independent of the three different lattice types (square lattice nearest-neighbour (n.n.): +, triangular: $\times$, and square lattice next-nearest-neighbour (n.n.n.): $*$) the theoretical curve (solid line) is nicely approached. The small differences to the theoretical prediction can be attributed to the finite size ($L = 640$) of the simulated systems.

system. With the help of computer simulations, using the so-called "multicanonical" algorithm [4], we were able to obtain precise results for systems up to size $L = 640$ – even in the two-phase region, where the metastable behaviour of a solid or liquid and a gaseous phase with an greatly increased autocorrelation time makes the relative errors larger. The details of our investigations can be found in [5].

By extending our work of 2006, we redid our simulation using different lattice types. Using our numerical data we now have strong arguments that the rigorous results of Biskup et al. for the 2D square lattice Ising model with nearest neighbour (n.n.) interactions are indeed independent of the underlying geometry of the lattice and the range of interactions (see Fig. 11.8), providing thus a universal description of the evaporation/condensation process.

As a future prospect, we intend to look at the 3D case and possibly also add some off-lattice simulations using a Lennard–Jones potential.

[1] A. Nußbaumer et al.: Europhys. Lett. **75**, 716 (2006)
[2] M. Biskup et al.: Europhys. Lett. **60**, 21 (2002)
[3] M. Biskup et al.: Commun. Math. Phys. **242**, 137 (2003)
[4] B.A. Berg, T. Neuhaus: Phys. Rev. Lett. **68**, 9 (1992)
[5] A. Nußbaumer et al.: Phys. Rev. E **77**, 041 109 (2008)

## 11.15 Anisotropy of the Interface Tension of the 3D Ising Model

E. Bittner, A. Nußbaumer, W. Janke

In many physical systems with discrete symmetry the anisotropy of the interface tension can play an important role for various phenomena, including equilibrium

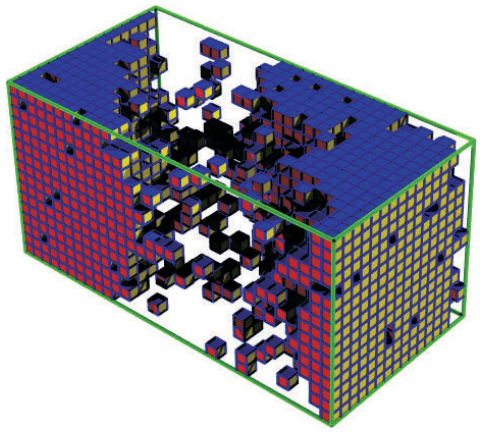

**Figure 11.9:** Plot of a typical configuration with two 110 interfaces.

droplet shapes [1] and the interfacial roughening transition [2]. For sufficiently strong anisotropy, facets, edges, or even corners can be identified in the equilibrium droplet shape. Due to the anisotropy of the interface tension in the 3D Ising model, the shape of the equilibrium droplet at some finite temperature is not spherical and has, in principle, to be determined by the Wulff construction [3]. Since the 3D Ising model with nearest-neighbour interaction is not exactly solvable, no analytical results are available for the interfacial free energy and the Wulff construction can only be done using an effective model of the angle-depending interface tension. Only for temperatures not too far below the critical temperature one can use the spherical approximation and, therefore, it is important to know how large the anisotropy is for a given temperature.

We determine the interface tension for the 100, 110 and 111 interface of the simple-cubic Ising model with nearest-neighbour interaction (see Fig. 11.9) using novel simulation methods [4]. To overcome the droplet/strip transition and the droplet nucleation barrier we use a newly developed combination of the multimagnetic algorithm with the parallel tempering method. We investigate a large range of inverse temperatures to study the anisotropy of the interface tension in detail and show that at given $T/T_c$ the anisotropy of the interface in three dimensions is larger than in two dimensions. However, down to 0.7 $T_c$ it never exceeds 3 %, so that in most cases the isotropic approximation for droplet condensation phenomena should be sufficiently accurate.

[1] J.E. Avron et al.: J. Phys. A **15**, L81 (1982)
[2] M. Hasenbusch, K. Pinn: J. Phys. A **30**, 63 (1997)
[3] G. Wulff, Z. Krist. Mineral. **34**, 449 (1901)
[4] E. Bittner et al.: *Anisotropy of the Interface Tension of the Three-Dimensional Ising Model*, Nucl. Phys. B, in print

## 11.16 Autocorrelation Times and the Parallel Tempering Algorithm

E. Bittner, A. Nußbaumer, W. Janke

We introduce a new update scheme to systematically improve the efficiency of parallel tempering Monte Carlo simulations (PT) [1] by taking into account the temperature

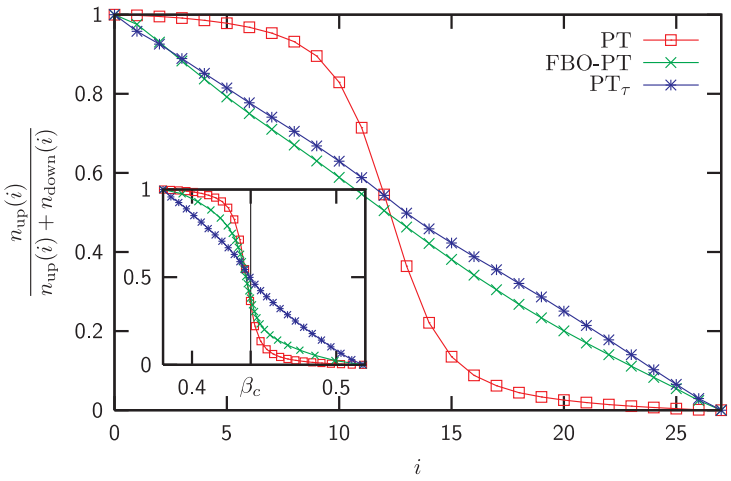


**Figure 11.10:** Fraction of replica which wander from the smallest inverse temperature $\beta$ to the largest as a function of the replica index $i$ for the 2D Ising model (with linear lattice size $L = 80$). The simulations without optimization exhibit a sharp decline close to the critical inverse temperature $\beta_c$, as one can see in the inset. Taking the canonical correlation times $\tau_{\rm can}$ into account (PT$_\tau$), the fraction decreases, for the same set of temperatures, almost linearly.

dependence of autocorrelation times. In contrast to previous attempts (FBO-PT) [2] the temperatures are not dynamically adjusted but chosen in such a way that the acceptance rate for proposed exchanges of all adjacent replica is about 50%. We show that by adapting the number of sweeps between the parallel tempering moves to the canonical autocorrelation time, the average round-trip time of a replica between the lowest and the highest temperatures is significantly decreased and, therefore, the efficiency of the parallel tempering algorithm is considerably improved, cf. Fig. 11.10. We illustrate the new algorithm (PT$_\tau$) [3] with results for the 2D Ising model and the 3D Edwards–Anderson Ising spin glass.

[1] R.H. Swendsen, J.-S. Wang: Phys. Rev. Lett. **57**, 2607 (1986); C.J. Geyer: in *Computing Science and Statistics: Proceedings of the 23rd Symposium on the Interface*, ed. by E.M. Keramidas (Interface Foundation, Fairfax Station 1991) p 156; K. Hukushima, K. Nemoto: J. Phys. Soc. Jpn. **65**, 1604 (1996)
[2] H.G. Katzgraber et al.: J. Stat. Mech. P03 018 (2006)
[3] E. Bittner et al.: Phys. Rev. Lett. **101**, 130 603 (2008)

## 11.17 Football Fever

E. Bittner, A. Nußbaumer, M. Weigel*, W. Janke

*Institut für Physik, Johannes Gutenberg-Universität, Mainz, Germany

Analyzing football score data with statistical techniques, we investigate how the not purely random, but highly co-operative nature of the game is reflected in averaged properties such as the probability distributions of scored goals for the home and away teams. As it turns out, especially the tails of the distributions are *not* well described

by the Poissonian or binomial model resulting from the assumption of uncorrelated random events. Instead, a good effective description of the data is provided by less basic distributions such as the negative binomial one or the probability densities of extreme-value statistics. To understand this behaviour from a microscopical point of view, however, no waiting time problem or extremal process need be invoked. Instead, modifying the Bernoulli random process underlying the Poissonian model to include a simple component of *self-affirmation* seems to describe the data surprisingly well and allows to understand the observed deviation from Gaussian statistics. The phenomenological distributions used before can be understood as special cases within this framework. We analyzed historical football score data from many leagues in Europe as well as from international tournaments, including data from all past tournaments of the "FIFA World Cup" series, and found the proposed models to be applicable rather universally. In particular, we analysed the results of the German women's premier football league and considered the two separate German men's premier leagues in the East and West during the cold war times and the unified league after 1990 to see how scoring in football and the component of self-affirmation depend on cultural and political circumstances [1].

The main task of the "Wissenschaftssommer" exhibition within the frame of the "Jahr der Mathematik" in July 2008 on the Augustusplatz in Leipzig was to motivate visitors to participate and to deal with the mathematical topics of the individual booths. To illustrate the meaning of statistical properties we chose the football score data described above and to incorporate the visitors we rented two football tables, see Fig. 11.11. With the help of over 2500 visitors we were able to collect more then 1000 table football results, which we analysed on-site and found a good agreement with our model. A detailed report on the results can be found in [2].

**Figure 11.11:** Football fever infected visitors of the "Wissenschaftssommer", from left to right former Foreign Minister K. Kinkel, Vice-Rector Research of the University of Leipzig Prof. Dr. M. Schlegel, Lord Mayor of Leipzig B. Jung, and Parliamentary State Secretary to the Federal Minister of Education and Research T. Rachel.

[1] E. Bittner et al.: Eur. Phys. J. B **67**, 459 (2009)
[2] E. Bittner et al.: Universität Leipzig Journal **6**/2008, 22 (2008)

## 11.18 Funding

*Excellence Initiative, Graduate School "BuildMoNa": Leipzig School of Natural Sciences – Building with Molecules and Nano-objects*
W. Janke (Principal Investigator)
DFG

*Forschergruppe 877: From Local Constraints to Macroscopic Transport*
W. Janke (Principal Investigator)
DFG

*RTN-Network "ENRAGE": Random Geometry and Random Matrices: From Quantum Gravity to Econophysics*
W. Janke (Principal Investigator)
EU MRTN-CT-2004-005616

*Host of EU Marie Curie Incoming Fellowship: SAWs on Fractals, Dr. Viktoria Blavatska (Lviv, Ukraine)*
W. Janke
EU MIF1-CT-2006-021867

*Dynamik und Statik von Spingläsern*
W. Janke
DFG Ja 483/22-1

*Phasenübergänge in Systemen mit einschränkender Geometrie*
W. Janke
DFG Ja 483/23-1 and 2

*Investigation of Thermodynamic Properties of Lattice and Off-Lattice Models for Proteins and Polymers*
M. Bachmann and W. Janke
DFG Ja 483/24-1 and 2

*Molecular Conformation Mechanics of Proteins and Polymers*
W. Janke
DFG Ja 483/24-3

*"Deutsch-Französisches Doktorandenkollegium (DFDK)" with "Co-tutelle des Thèse": Statistical Physics of Complex Systems, jointly with l'Université Henri Poincaré, Nancy I, France*
W. Janke (with B. Berche)
Deutsch-Französische Hochschule, CDFA-02-07

*Statistical Mechanics of Complex Networks*
W. Janke (with Z. Burda)

Alexander von Humboldt Foundation "Institutspartnerschaft" with the Jagellonian University, Krakow, Poland, 3.4-Fokoop-DEU/1117877

*Numerical Approaches to Protein Folding*
W. Janke (with A. Irbäck)
DAAD-STINT Collaborative Research Grant with the University of Lund, Sweden, D/05/26016

*Host of the Alexander von Humboldt Research Prize Winner Bernd A. Berg (Florida State University, Tallahassee, USA)*
W. Janke
Alexander von Humboldt Foundation

Grant for full support of 75 participants of the *International Conference ENRAGE – Random Geometry and Random Matrices: From Quantum Gravity to Econophysics, 17. – 22. May 2009*
W. Janke (Organizer)
Max-Planck-Institut für Physik komplexer Systeme, Dresden

*Monte Carlo Simulationen der Statik und Dynamik von Spingläsern*
E. Bittner, W. Janke
NIC Jülich (computer time grant for "JUMP"), hlz10

*Protein and Polymer Models*
M. Bachmann, W. Janke
NIC Jülich (computer time grant for "JUMP"), hlz11

*Quantum Monte Carlo Simulations of Quantum Spin Models*
W. Janke
NIC Jülich (computer time grant for "JUMP"), hlz12

*Dimerized Heisenberg Models*
S. Wenzel
Studienstiftung des deutschen Volkes

## 11.19 Organizational Duties

M. Bachmann

- Scientific Secretary of the Workshop *LEILAT08 – 18. Workshop on Lattice Field Theory and Statistical Physics* ITP, Universität Leipzig, 26. – 28. June 2008
- Scientific Secretary of the Workshop *CompPhys08 – 9. International NTZ-Workshop on New Developments in Computational Physics*, ITP, Universität Leipzig, 27. – 29. November 2008
- Referee: Phys. Rev. Lett., J. Am. Chem. Soc., IEEE/ACM Transact. Comput. Biol. Bioinf., Phys. Rev. A, Phys. Rev. E, J. Phys. A, Eur. J. Phys. D, Biophys. Rev. Lett., Comput. Phys. Commun., J. Comput. Chem., Macromolecules, Phys. Chem. Chem. Phys.
- Reviewer: Engineering and Physical Sciences Research Council (EPSRC) UK, National Science Foundation (NSF) USA

E. Bittner

- Scientific Coordinator of the Spring School on *Monte Carlo Simulations of Disordered Systems*, ITP, Universität Leipzig, 30. March – 04. April 2008
- Scientific Secretary of the Workshop *LEILAT08 – 18. Workshop on Lattice Field Theory and Statistical Physics* ITP, Universität Leipzig, 26. – 28. June 2008
- Co-organizer of the contribution *Football Feaver* to the "Wissenschaftssommer" exhibition within the frame of the "Jahr der Mathematik", Universität Leipzig, 28. June – 04. July 2008
- Scientific Secretary of the Workshop *CompPhys08 – 9. International NTZ-Workshop on New Developments in Computational Physics*, ITP, Universität Leipzig, 27. – 29. November 2008
- Scientific Secretary of the Workshop *CompPhys09 – 10. International NTZ-Workshop on New Developments in Computational Physics*, ITP, Universität Leipzig, 26. – 29. November 2009
- Referee: Phys. Rev. Lett., Phys. Rev. E, J. Phys. A, Eur. J. Phys. B, Comput. Phys. Commun.

W. Janke

- Director, Naturwissenschaftlich-Theoretisches Zentrum (NTZ) of the Zentrum für Höhere Studien (ZHS), Universität Leipzig
- Chairperson of the Programme Committee "Scientific Computing" of Forschungszentrum Jülich
- Member of the Scientific-Technical-Council of the Supervisory Board ("Aufsichtsrat") of the Forschungszentrum Jülich GmbH
- Editor "Computational Sciences", Lecture Notes of Physics, Springer, Berlin, Heidelberg
- Editor "Computational Physics", Central European Journal of Physics
- Member of Editorial Board: Condens. Matter Phys.
- Permanent Member of "International Advisory Board", *Conference of the Middle European Cooperation in Statistical Physics (MECO)*
- Organizer of the Spring School on *Monte Carlo Simulations of Disordered Systems*, ITP, Universität Leipzig, 30. March – 04. April 2008
- Organizer of the Workshop *LEILAT08 – 18. Workshop on Lattice Field Theory and Statistical Physics* (with A. Schiller, ITP, TET) ITP, Universität Leipzig, 26. – 28. June 2008
- Co-organizer of the contribution *Football Feaver* to the "Wissenschaftssommer" exhibition within the frame of the "Jahr der Mathematik", Universität Leipzig, 28. June – 04. July 2008
- Organizer of the Workshop *CompPhys08 – 9. International NTZ-Workshop on New Developments in Computational Physics*, ITP, Universität Leipzig, 27. – 29. November 2008
- Organizer of the 34. Conference of the Middle European Cooperation in Statistical Physics *MECO34* (with S. Trimper, Martin-Luther-Universität Halle-Wittenberg), ITP, Universität Leipzig, 29. March – 01. April 2009
- Organizer of the International Conference *ENRAGE – Random Geometry and Random Matrices: From Quantum Gravity to Econophysics*, Max-Planck-Institut für Physik komplexer Systeme in Dresden, 17. – 22. May 2009

- Organizer of the Workshop *CompPhys09 – 10. International NTZ-Workshop on New Developments in Computational Physics*, ITP, Universität Leipzig, 26. – 29. November 2009
- Member of International Organization Committee of the 10. Int. Conf. *Path Integrals* (with L.S. Schulman (USA), M. Gutzwiller (USA), A. Inomata (USA), J.R. Klauder (USA), D. Fujikawa (Japan) und Chookyu Lee (South Korea)), planned for Seoul, South Korea, Summer 2010
- Member of the Review Panel of the AQAS "Akkreditierungsverfahren" of the Master Studies Curriculum "Computer Simulation in Science", Bergische Universität Wuppertal, January 2008
- Reviewer: Humboldt-Stiftung; Deutsche Forschungsgemeinschaft (DFG); Studienstiftung des deutschen Volkes; The Jeffress Memorial Trust, Bank of America, USA; Fond zur Förderung der wissenschaftlichen Forschung (FWF), Austria; The Royal Society, UK; Engineering and Physical Sciences Research Council (EPSRC), UK; The University of Warwick, UK; Coventry University, UK; CECAM, Lyon, France; National Science Foundation (NSF), USA; Israel Science Foundation, Israel
- Referee: Phys. Rev. Lett., Phys. Rev. B, Phys. Rev. E, J. Che. Phys., Europhys. Lett., Phys. Lett. A, Phys. Lett. B, Eur. Phys. J. B, Physica A, Proc. Roy. Phys. Soc., J. Phys. A, Comput. Phys. Commun., J. Stat. Mech. Theor. Exp., New J. Phys., Int. J. Mod. Phys. C

A. Nußbaumer

- Co-organizer of the contribution *Football Feaver* to the "Wissenschaftssommer" exhibition within the frame of the "Jahr der Mathematik", Universität Leipzig, 28. June – 04. July 2008

T. Vogel

- Scientific Secretary, Naturwissenschaftlich-Theoretisches Zentrum (NTZ) of the Zentrum für Höhere Studien (ZHS), Universität Leipzig

## 11.20 External Cooperations

**Academic**

- EU RTN-Network "ENRAGE" – *Random Geometry and Random Matrices: From Quantum Gravity to Econophysics*
  research collaboration with 13 teams throughout Europe
- Deptartment of Physics, Florida State University, Tallahassee, USA
  Prof. Dr. Bernd A. Berg
- CEA/Saclay, Service de Physique Théorique, France
  Dr. Alain Billoire
- Laboratoire de Physique des Matériaux (UMR CNRS No 7556), Université Henri Poincaré, Nancy, France
  Prof. Dr. Bertrand Berche, Dr. Christophe Chatelain, Prof. Dr. Malte Henkel, Dr. Dragi Karevski

- Groupe de Physique des Matériaux, Université de Rouen, France
  Dr. Pierre-Emmanuel Berche
- School of Mathematical and Computer Sciences, Heriot-Watt University, Edinburgh, UK
  Prof. Dr. Desmond A. Johnston
- School of Physics and Astronomy, University of Edinburgh, UK
  Richard A. Blythe
- School of Mathematical and Information Sciences, Coventry University, UK
  Dr. Ralph Kenna, PD Dr. Christian von Ferber
- Department of Physics, Hacettepe University, Ankara, Turkey
  Dr. Handan Arkin, Prof. Dr. Tarik Çelik, Gökhan Gökoğlu
- Institute for Condensed Matter Physics, National Academy of Sciences, Lviv, Ukraine
  Prof. Dr. Yurij Holovatch
- Complex Systems Division, Department of Theoretical Physics, Lund University, Lund, Sweden
  Prof. Dr. Anders Irbäck, Simon Mitternacht
- John von Neumann-Institut für Computing (NIC), Forschungszentrum Jülich, Germany
  Prof. Dr. Peter Grassberger, Prof. Dr. U. Hansmann, PD Dr. Thomas Neuhaus
- Institut für Physik, Universität Mainz
  Prof. Dr. Kurt Binder, Dr. Hsiao-Ping Hsu, Dr. Martin Weigel
- Atominstitut, TU Wien, Austria
  Prof. Dr. Harald Markum, Dr. Rainer Pullirsch
- Istituto Nazionale di Fisica Nucleare, Sezione di Milano-Bicocca, Milano, Italy
  Prof. Dr. Pablo Butera
- Banaras Hindu University, Varanasi, India
  Prof. Dr. Sanjay Kumar
- Brunel University of West London, UK
  Dr. Gernot Akemann
- Institut für Theoretische Physik, Freie Universität Berlin, Germany
  Prof. Dr. Hagen Kleinert, Dr. Adriaan M.J. Schakel
- IAC-1, Universität Stuttgart
  Prof. Dr. Rudolf Hilfer
- Institut für Theoretische Physik, Universität Duisburg-Essen, Germany
  PD Dr. Axel Pelster
- Institut für Theoretische Physik, Universität Bielefeld, Germany
  Prof. Dr. Friderike Schmid
- School of Engineering and Science, Jacobs Universität Bremen, Germany
  Prof. Dr. Hildegard Meyer-Ortmanns
- Institute of Physics, Jagellonian University, Kraków, Poland
  Prof. Dr. Zdzisław Burda, Prof. Dr. Piotr Bialas, Dr. Leszek Bogacz

- Landau Institute for Theoretical Physics, Chernogolovka, Russia
  Prof. Dr. Lev N. Shchur
- Yerevan Physics Institute, Yerevan, Armenia
  Prof. Dr. David B. Saakian
- Zhejiang Institute of Modern Physics, Zhejiang University, Hangzhou, P.R. China
  Prof. Dr. He-Ping Ying, Prof. Dr. Bo Zheng

## 11.21 Publications

**Journals**

M. Bachmann, W. Janke: *Minimalistic Hybrid Models for the Adsorption of Polymers and Peptides to Solid Substrates*, Phys. Part. Nucl. Lett. **5**, 243 (2008)

B.A. Berg, W. Janke: *Multibondic Cluster Algorithm for Finite-Size Scaling Studies of Critical Phenomena*, Comput. Phys. Commun. **179**, 21 (2008)

E. Bittner, W. Janke: *A Boundary Field Induced First-Order Transition in the 2D Ising Model: Numerical Study*, J. Phys. A **41**, 395 001 (2008)

E. Bittner, A. Nußbaumer, W. Janke: *Make Life Simple: Unleash the Full Power of the Parallel Tempering Algorithm*, Phys. Rev. Lett. **101**, 130 603 (2008)

E. Bittner, A. Nußbaumer, W. Janke, M. Weigel: *Fußballfieber beim Wissenschaftssommer: Eine mathematisch-empirische Nachlese*, Universität Leipzig Journal **6**/2008, 22 (2008)

V. Blavatska, C. von Ferber, Y. Holovatch: *Scaling of Complex Polymers: New Universality Classes and Beyond*, Philos. Mag. **88**, 4085 (2008)

V. Blavatska, W. Janke: *Scaling Behavior of Self-Avoiding Walks on Percolation Clusters*, Europhys. Lett. **82**, 66 006 (2008)

V. Blavatska, W. Janke: *Multifractality of Self-Avoiding Walks on Percolation Clusters*, Phys. Rev. Lett. **101**, 125 701 (2008)

M. Hasenbusch: *The Binder Cumulant at the Kosterlitz-Thouless Transition*, J. Stat. Mech. P08 003 (2008)

M. Hasenbusch: *Monte Carlo Study of the Three-Dimensional XY Universality Class: Universal Amplitude Ratios*, J. Stat. Mech. P12 006 (2008)

M. Hasenbusch, F. Parisen Toldin, A. Pelissetto, E. Vicari: *Multicritical Nishimori Point in the Phase Diagram of the ±J Ising Model on a Square Lattice*, Phys. Rev. E **77**, 051 115 (2008)

M. Hasenbusch, F. Parisen Toldin, A. Pelissetto, E. Vicari: *Universal Dependence on Disorder of Two-Dimensional Randomly Diluted and Random-Bond ±J Ising Models*, Phys. Rev. E **78**, 011 110 (2008)

M. Hasenbusch, A. Pelissetto, E. Vicari: *The Critical Behavior of 3D Ising Spin Glass Models: Universality and Scaling Corrections*, J. Stat. Mech. L02 001 (2008)

M. Hasenbusch, A. Pelissetto, E. Vicari: *Critical Behavior of Three-Dimensional Ising Spin Glass Models*, Phys. Rev. B **78**, 214 205 (2008)

I. Juhász Junger, D. Ihle, L. Bogacz, W. Janke: *Thermodynamics of Heisenberg Ferromagnets with Arbitrary Spin in a Magnetic Field*, Phys. Rev. B **77**, 174 411 (2008)

C. Junghans, M. Bachmann, W. Janke: *Thermodynamics of Peptide Aggregation Processes: An Analysis from Perspectives of Three Statistical Ensembles*, J. Chem. Phys. **128**, 085 103 (2008)

A. Kallias, M. Bachmann, W. Janke: *Thermodynamics and Kinetics of a Gō Proteinlike Heteropolymer Model with Two-State Folding Characteristics*, J. Chem. Phys. **128**, 055 102 (2008)

A. Nußbaumer, E. Bittner, W. Janke: *Monte Carlo Study of the Droplet Formation-Dissolution Transition on Different Two-Dimensional Lattices*, Phys. Rev. E **77**, 041 109 (2008)

J. Schluttig, M. Bachmann, W. Janke: *Comparative Molecular Dynamics and Monte Carlo Study of Statistical Properties for Coarse-Grained Heteropolymers*, J. Comput. Chem. **29**, 2603 (2008)

B. Wacław, L. Bogacz, W. Janke: *Approaching the Thermodynamic Limit in Equilibrated Scale-Free Networks*, Phys. Rev. E **78**, 061 125 (2008)

B. Wacław, Z. Burda: *Counting Metastable States of Ising Spin Glasses on Arbitrary Graphs*, Phys. Rev. E **77**, 041 114 (2008)

B. Wacław, Z. Burda, W. Janke: *Power Laws in Zero-Range Processes on Random Networks*, Eur. Phys. J. B **65**, 565 (2008)

S. Wenzel, E. Bittner, W. Janke, A.M.J. Schakel: *Percolation of Vortices in the Abelian Lattice Higgs Model*, Nucl. Phys. B **793**, 344 (2008)

S. Wenzel, L. Bogacz, W. Janke: *Evidence for an Unconventional Universality Class from a Two-Dimensional Dimerized Quantum Heisenberg Model*, Phys. Rev. Lett. **101**, 127 202 (2008)

S. Wenzel, W. Janke: *Monte Carlo Simulations of the Directional-Ordering Transition in the Two-Dimensional Classical and Quantum Compass Model*, Phys. Rev. B **78**, 064 402 (2008); publisher's Note: Phys. Rev. B **78**, 099 902(E) (2008)

F.T. Winter, W. Janke, A.M.J. Schakel: *Geometric Properties of the Three-Dimensional Ising and XY Models*, Phys. Rev. E **77**, 061 108 (2008)

**Books**

M. Bachmann, W. Janke: *Thermodynamics of Protein Folding from Coarse-Grained Models' Perspectives*, in: *Rugged Free Energy Landscapes: Common Computational Approaches to Spin Glasses, Structural Glasses and Biological Macromolecules*, ed. by W. Janke, Lecture Notes in Physics **736** (Springer, Berlin 2008) p 203

M. Bachmann, W. Janke: *Conformational Transitions in Molecular Systems*, in: *Path Integrals – New Trends and Perspectives*, ed. by W. Janke, A. Pelster (World Scientific, Singapore 2008) p 531

M. Bachmann, W. Janke: *Mesoscopic Properties of Molecular Folding and Aggregation Processes*, Proc. BIFI 2008 Int. Conf. *Large Scale Simulations of Complex Systems, Condensed Matter and Fusion Plasma*, Zaragoza, Spain, 6.–8. February 2008, ed. by P. Bruscolini, J. Clemente-Gallardo, P. Echenique, J.F. Sáenz-Lorenzo, F. Castejón, AIP Conf. Proc. Volume **1071**, 1 (2008)

R. Bischof, W. Janke: *Critical Exponents of Mixed Quantum Spin Chain*, in: *Path Integrals – New Trends and Perspectives*, ed. by W. Janke, A. Pelster (World Scientific, Singapore 2008) p 514

E. Bittner, W. Janke: *Vortex-Line Percolation in a Three-Dimensional Complex $|\psi|^4$ Theory*, in: *Path Integrals – New Trends and Perspectives*, ed. by W. Janke, A. Pelster (World Scientific, Singapore 2008) p 493

E. Bittner, A. Nußbaumer, W. Janke: *Free-Energy Barriers of Spin Glasses*, in: *NIC Symposium 2008*, ed. by G. Münster, D. Wolf, M. Kremer, NIC Series **39** (John von Neumann Institute for Computing, Jülich 2008) p 229

V. Blavatska, W. Janke: *Self-Avoiding Walks on Fractals: Scaling Laws*, in: *Path Integrals – New Trends and Perspectives*, ed. by W. Janke, A. Pelster (World Scientific, Singapore 2008) p 585

V. Blavatska, C. von Ferber, Y. Holovatch: *Star Polymers in Correlated Disorder*, in: *Path Integrals – New Trends and Perspectives*, ed. by W. Janke, A. Pelster (World Scientific, Singapore 2008), p 549

W. Janke (Ed.): *Rugged Free Energy Landscapes: Common Computational Approaches to Spin Glasses, Structural Glasses and Biological Macromolecules*, Lecture Notes in Physics **736** (Springer, Berlin 2008)

W. Janke: *Rugged Free-Energy Landscapes – An Introduction*, in: *Rugged Free Energy Landscapes: Common Computational Approaches to Spin Glasses, Structural Glasses and Biological Macromolecules*, ed. by W. Janke, Lecture Notes in Physics **736** (Springer, Berlin 2008) p 1

W. Janke: *Monte Carlo Methods in Classical Statistical Physics*, in: *Computational Many-Particle Physics*, ed. by H. Fehske, R. Schneider, A. Weiße, Lecture Notes in Physics **739** (Springer, Berlin 2008) p 79

W. Janke, A. Pelster (Eds.): *Path Integrals – New Trends and Perspectives* (World Scientific, Singapore 2008)

A. Nußbaumer, E. Bittner, W. Janke: *Evaporation/Condensation of Ising Droplets*, in: *Path Integrals – New Trends and Perspectives*, ed. by W. Janke, A. Pelster (World Scientific, Singapore 2008) p 525

S. Schnabel, M. Bachmann, W. Janke: *Different Kinds of Protein Folding Identified with a Coarse-Grained Heteropolymer Model*, in: *From Computational Biophysics to Systems Biology (CBSB08)*, ed. by U.H.E. Hansmann, J.H. Meinke, S. Mohanty, W. Nadler, O. Zimmermann, NIC Series Vol. **40** (John von Neumann Institute for Computing, Jülich 2008) p 369

T. Vogel, M. Bachmann, W. Janke: *Freezing and Collapse of Flexible Polymers*, in: *From Computational Biophysics to Systems Biology (CBSB08)*, ed. by U.H.E. Hansmann, J.H. Meinke, S. Mohanty, W. Nadler, O. Zimmermann, NIC Series Vol. **40** (John von Neumann Institute for Computing, Jülich 2008) p 405

B. Wacław, L. Bogacz, Z. Burda, W. Janke: *Monte Carlo Methods for Generation of Random Graphs*, in: *Path Integrals – New Trends and Perspectives*, ed. by W. Janke, A. Pelster (World Scientific, Singapore 2008) p 342

**Talks**

M. Aust: *Outlook on a New Thermal Ratchet Theme Based on a Binary Liquid Mixture*, SFG-Meeting and Guest Kolloquia, Leipzig, Germany 25. September 2008

M. Bachmann: *Thermodynamics and Kinetics of a Proteinlike Heteropolymer Model*, 72. DPG Spring Meeting, Berlin, Germany 25. – 29. February 2008

M. Bachmann: *Conformation Mechanics of Molecular Structure Formation Processes*, Seminar talk, Max-Planck-Institut für Polymerforschung, Mainz, Germany, 04. March 2008

M. Bachmann: *Nanopatterns of Macromolecules*, Project meeting, Martin-Luther-Universität Halle-Wittenberg, Germany, 09. May 2008

M. Bachmann: *Conformational Mechanics of Molecular Structure Formation Processes*, Habilitation talk, Universität Leipzig, Germany, 17. July 2008

M. Bachmann: *Mesoscopic Modeling of Protein Assemblies*, Presentation at the Evaluation Panel Meeting "Computational Biology", Forschungszentrum Jülich, Germany, 07. – 08. October 2008

R. Bischof: *Quantum Phase Transitions in Mixed Quantum Spin Chains*, Seminar talk, Deutsch-Französische Hochschule (Collège Doctoral), Université Henri Poincaré, Nancy, France, 04. February 2008

R. Bischof: *Quantum Monte Carlo Investigation of Mixed Quantum Spin Chains*, Seminar talk, Universität des Saarlandes, Saarbrücken, Germany, 05. February 2008

E. Bittner: *Autocorrelation Times and the Parallel Tempering Algorithm*, 72. DPG Spring Meeting, Berlin, Germany 25. – 29. February 2008

E. Bittner: *Free-Energy Barriers in Spin Glasses: Mean-Field vs Short-Range Models*, invited talk, "ENRAGE" Network School on Monte Carlo Simulations of Disordered Systems, Leipzig, Germany, 30. March – 04. April 2008

E. Bittner: *Autocorrelation Times and the Parallel Tempering Algorithm*, 33. Conf. Middle European Cooperation Stat. Phys. (MECO33), Puchberg/Wels, Austria, 14. – 16. April 2008

V. Blavatska: *Multifractality of Self-Avoiding Random Walks on Percolation Clusters*, 72. DPG Spring Meeting, Berlin, Germany 25. – 29. February 2008

V. Blavatska: *Copolymer Stars in Porous Media*, XI. International Workshop on Complex Systems, Andalo, Italy, 17. – 20. March 2008

V. Blavatska: *Self-Avoiding Walks on Disordered Lattices: Scaling Laws*, "ENRAGE" Network School on Monte Carlo Simulations of Disordered Systems, Leipzig, Germany, 30. March – 04. April 2008

V. Blavatska: *Multifractality of Self-Avoiding Walks on Percolation Clusters*, ENRAGE Network Meeting, University of Oxford, UK, 15. – 19. September 2008

V. Blavatska: *Random Walks on Percolation Clusters: Multifractal Effects*, 9. Int. NTZ-Workshop "New Developments in Computational Physics" (CompPhys08), Leipzig, Germany, 27. – 29. November 2008

M. Hasenbusch: *The Spin-Glass Transition in the Three-Dimensional EAI Model*, invited talk, "ENRAGE" Network School on Monte Carlo Simulations of Disordered Systems, Leipzig, Germany, 30. March – 04. April 2008

M. Hasenbusch: *Strings, Interfaces and the Ising Model*, 18. Int. Workshop "Lattice Field Theory and Statistical Physics" (Leilat08), Universität Leipzig, Germany, 26. – 28. June 2008

M. Hasenbusch: *Kosterlitz-Thouless transition of thin films in the 3D XY universality class*, 9. Int. NTZ-Workshop "New Developments in Computational Physics" (CompPhys08), Leipzig, Germany, 27. – 29. November 2008

W. Janke: *Modeling and Simulation of Biological Macromolecules*, invited talk, Int. Conf. *Large-Scale Simulations of Complex Systems, Condensed Matter and Fusion Plasma* (BiFi2008), Universidad de Zaragoza, Spain, 06. – 08. February 2008

W. Janke: *Numerical Estimation of Baxter-Wu Critical Amplitudes*, 72. DPG Spring Meeting, Berlin, Germany 25. – 29. February 2008

W. Janke: *Universal Aspects of Ising Droplets*, 33. Conf. Middle European Cooperation Stat. Phys. (MECO33), Puchberg/Wels, Austria, 14. – 16. April 2008

W. Janke: *Universal Aspects of Ising Droplets*, invited talk, Atelier Nancy *Statistical Physics and Low Dimensional Systems 2008*, Université Nancy, France, 21.–23. May 2008

W. Janke: *Condensation in Zero-Range Processes on Inhomogeneous Networks*, invited talk, Workshop *Transport Processes in Physics and Biology*, Jacobs University, Bremen, Germany, 26.–28. May 2008

W. Janke: *Percolating Excitations – A Geometrical View of Phase Transitions*, invited talk, 13. Claude Itzykson Meeting, Saclay, France, 09.–11. June 2008

W. Janke: *Random Walks on Percolation Clusters I and II*, two invited talks, ENRAGE Network Meeting, University of Oxford, Oxford, UK, 15.–19. September 2008

W. Janke: *Quantum Phase Transitions in Dimerized Heisenberg Models*, invited talk, 24. Max Born Symposium, University of Wroclaw, Poland, 25.–27. September 2008

W. Janke: *Droplet Condensation and Evaporation*, ICP Seminar, Universität Stuttgart, Germany, 11. November 2008

W. Janke: *Quantum Phase Transitions of Coupled Spin Dimers*, Physik-Kolloquium der Freien Universität Berlin, Germany, 12. December 2008

M. Möddel: *Conformational Mechanics of Polymer Adsorption Transitions at Attractive Substrates*, Seminar talk, Deutsch-Französische Hochschule (Collège Doctoral), Université Henri Poincaré, Nancy, France, 13. October 2008

A. Nußbaumer: *Free-Energy Barriers of Spin Glasses*, 72. DPG Spring Meeting, Berlin, Germany 25.–29. February 2008

A. Nußbaumer: *Free-Energy Barriers of Spin Glasses*, 18. Int. Workshop "Lattice Field Theory and Statistical Physics" (Leilat08), Universität Leipzig, Germany, 26.–28. June 2008

A. Nußbaumer: *Free-Energy Barriers of Spin Glasses*, Seminar "Theory of Condensed Matter Physics", RWTH Aachen, Germany, 01. July 2008

A. Nußbaumer: *Free-Energy Barriers of Spin Glasses*, 9. Int. NTZ-Workshop "New Developments in Computational Physics" (CompPhys08), Leipzig, Germany, 27.–29. November 2008

S. Schnabel: *Conformational Transitions of Flexible Polymers*, 72. DPG Spring Meeting, Berlin, Germany 25.–29. February 2008

S. Schnabel: *Solution Behavior of Semiconductor-Binding Peptides*, 1. BuildMoNa Workshop, Leipzig, Germany, 16./17. October 2008

S. Schnabel: *Low Temperature Behavior of the Lennard-Jones Polymer*, 9. Int. NTZ-Workshop "New Developments in Computational Physics" (CompPhys08), Leipzig, Germany, 27.–29. November 2008

T. Vogel: *Ground-state Properties of Thick Flexible Polymers*, 72. DPG Spring Meeting, Berlin, Germany 25. – 29. February 2008

T. Vogel: *Freezing and Collapse of Flexible Lattice Polymers*, 18. Int. Workshop "Lattice Field Theory and Statistical Physics" (Leilat08), Universität Leipzig, Germany, 26. – 28. June 2008

B. Wacław: *A Monte Carlo Method for Generation of Random Graphs*, 72. DPG Spring Meeting, Berlin, Germany 25. – 29. February 2008

B. Wacław: *Introduction to Complex Networks*, "ENRAGE" Network School on Monte Carlo Simulations of Disordered Systems, Leipzig, Germany, 30. March – 04. April 2008

B. Wacław: *Finite-Size Effects in Growing Networks*, Seminar of Statistical Physics Division, LPTMS, CNRS Orsay, France, 24. April 2008

B. Wacław: *On the Number of Metastable States in Ising Spin Glasses*, Seminar of Statistical Physics Division, LPTMS, CNRS Orsay, France, 24. April 2008

B. Wacław: *Statistical Physics of Mass Transport Models*, invited talk, Workshop "Transport Processes in Physics and Biology", Jacobs University, Bremen, Germany, 26. – 28. May 2008

B. Wacław: *Approaching the Thermodynamic Limit: Cutoffs in Scale-Free Networks*, invited talk, CREEN Workshop, Norwich Research Park, Norwich, UK, 24. June 2008

B. Wacław: *Cutoffs and Maximal Degrees in Scale-Free Networks*, "ENRAGE" Network Meeting on Random Geometry and Random Matrices, University of Oxford, UK, 15. – 19. September 2008

B. Wacław: *Localization of Maximal Entropy Random Walk*, 9. Int. NTZ-Workshop "New Developments in Computational Physics" (CompPhys08), Leipzig, Germany, 27. – 29. November 2008

S. Wenzel: *Evidence of Unconventional Universality Class in a Two-Dimensional Dimerized Quantum Heisenberg Model*, Atelier Nancy *Statistical Physics and Low Dimensional Systems 2008*, Nancy, France, 21. – 23. May 2008

S. Wenzel: *Quantum Criticality in Dimerized Heisenberg Models*, 18. Int. Workshop "Lattice Field Theory and Statistical Physics" (Leilat08), Universität Leipzig, Germany, 26. – 28. June 2008

S. Wenzel: *The Quantum Compass Model and Extensions*, Seminar talk, Institut für Theoretische Physik III, Universität Stuttgart, 16. June 2008

S. Wenzel: *On Quantum Phase Transitions and Unconventional Behavior in a 2D Quantum Heisenberg Model*, Seminar talk, SFB/TRR 21 (Stuttgart, Ulm, Tübingen), Universität Stuttgart, 14. July 2008

S. Wenzel: *Unconventional Quantum Phase Transitions in Two-Dimensional Quantum Magnets*, 1. BuildMoNa Workshop, Leipzig, Germany, 16./17. October 2008

S. Wenzel: *Quantum Phase Transitions in Dimerized Heisenberg Models*, Condensed Matter Seminar, EPFL Lausanne, Switzerland, 19. November 2008

S. Wenzel: *Dimerized Heisenberg Models*, 9. Int. NTZ-Workshop "New Developments in Computational Physics" (CompPhys08), Leipzig, Germany, 27. – 29. November 2008

**Posters**

M. Aust, E. Bittner, W. Janke: *Equilibrium Properties of the Wang-Landau Algorithm*, 72. DPG Spring Meeting, Berlin, Germany 25. – 29. February 2008

M. Aust, E. Bittner, W. Janke: *Balance During Wang-Landau Recursion Simulations*, 9. Int. NTZ-Workshop "New Developments in Computational Physics" (CompPhys08), Leipzig, Germany, 27. – 29. November 2008

F. Beyer, E. Bittner, W. Janke: *Techniques Accelerating the Dynamics of Simulations of Complex Systems*, 72. DPG Spring Meeting, Berlin, Germany 25. – 29. February 2008

R. Bischof, W. Janke: *Formation of a Plateau in the Twist Order Parameter of the Bond Alternating Antiferromagnetic $S = 1/2$ Heisenberg Spin Chain*, 9. Int. NTZ-Workshop "New Developments in Computational Physics" (CompPhys08), Leipzig, Germany, 27. – 29. November 2008

E. Bittner, A. Nußbaumer, W. Janke, M. Weigel: *Football Fever: Goal Distributions and Non-Gaussian Statistics*, Economics and Psychology of Football 2008, Innsbruck, Austria, 29. – 30. May 2008

E. Bittner, A. Nußbaumer, W. Janke, M. Weigel: *Football Fever*, "Wissenschaftssommer" exhibition within the frame of the "Jahr der Mathematik", Leipzig, Germany, 28. June – 04. July 2008

E. Bittner, W. Janke: *Replica-Exchange Cluster Algorithm*, 9. Int. NTZ-Workshop "New Developments in Computational Physics" (CompPhys08), Leipzig, Germany, 27. – 29. November 2008

V. Blavatska, W. Janke: *Multifractal Properties of Self-Avoiding Walks on Percolation Clusters*, 33. Conf. Middle European Cooperation Stat. Phys. (MECO33), Puchberg/Wels, Austria, 14. – 16. April 2008

M. Möddel, M. Bachmann, W. Janke: *Conformational Mechanics of Polymer Adsorption Transitions at Attractive Substrates*, 72. DPG Spring Meeting, Berlin, Germany 25. – 29. February 2008

M. Möddel, M. Bachmann, W. Janke: *Conformational Mechanics of Polymer Adsorption Transitions at Attractive Substrates*, Jülich Soft Matter Days 2008, Bonn, Germany, 11. – 14. November 2008

A. Nußbaumer, E. Bittner, W. Janke: *Free-Energy Barriers of Spin Glasses*, "ENRAGE" Network School on Monte Carlo Simulations of Disordered Systems, Leipzig, Germany, 30. March – 04. April 2008

A. Nußbaumer, E. Bittner, W. Janke: *Free-Energy Barriers of Spin Glasses*, 33. Conf. Middle European Cooperation Stat. Phys. (MECO33), Puchberg/Wels, Austria, 14. – 16. April 2008

S. Schnabel, S. Mitternacht, M. Bachmann, W. Janke, A. Irbäck: *Solution Behavior of Semiconductor-Binding Peptides*, 1. Scientific Symposium of BuildMoNa, Leipzig, Germany, 07./08. February 2008

S. Schnabel, M. Bachmann, W. Janke: *Conformational Transitions of Flexible Polymers*, 33. Conf. Middle European Cooperation Stat. Phys. (MECO33), Puchberg/Wels, Austria, 14. – 16. April 2008

S. Schnabel, M. Bachmann, W. Janke: *Folding Channels for Coarse-Grained Polymer Models*, Workshop "From Computational Biophysics to Systems Biology" (CBSB08), Forschungszentrum Jülich, Germany, 19. – 21. May 2008

T. Vogel, T. Neuhaus, M. Bachmann, W. Janke: *Ground-State Properties of Thick Flexible Polymers*, "ENRAGE" Network School on Monte Carlo Simulations of Disordered Systems, Leipzig, Germany, 30. March – 04. April 2008

T. Vogel, T. Neuhaus, M. Bachmann, W. Janke: *Ground-State Properties of Thick Flexible Polymers*, 33. Conf. Middle European Cooperation Stat. Phys. (MECO33), Puchberg/Wels, Austria, 14. – 16. April 2008

T. Vogel, M. Bachmann, W. Janke: *Freezing and Collapse of Flexible Polymers*, Workshop "From Computational Biophysics to Systems Biology" (CBSB08), Forschungszentrum Jülich, Germany, 19. – 21. May 2008

T. Vogel, T. Neuhaus, M. Bachmann, W. Janke: *Ground-State Properties of Thick Flexible Polymers*, 9. Int. NTZ-Workshop "New Developments in Computational Physics" (CompPhys08), Leipzig, Germany, 27. – 29. November 2008

S. Wenzel, W. Janke: *Quantum Monte Carlo Study of the 2D Quantum Compass Model*, 1. Scientific Symposium of BuildMoNa, Leipzig, Germany, 07./08. February 2008

S. Wenzel, W. Janke: *Quantum Monte Carlo Study of the 2D Quantum Compass Model*, 72. DPG Spring Meeting, Berlin, Germany 25. – 29. February 2008

S. Wenzel, W. Janke: *Directional Ordering in the 2D Classical and Quantum Compass Model*, 33. Conf. Middle European Cooperation Stat. Phys. (MECO33), Puchberg/Wels, Austria, 14. – 16. April 2008

S. Wenzel, W. Janke: *Directional Ordering in the 2D Classical and Quantum Compass Model*, International Workshop on "Unconventional Phases and Phase Transitions in Strongly Correlated Electron Systems", Max-Planck-Institut für Physik komplexer Systeme, Dresden, Germany, 04. – 07. June 2008

S. Wenzel, L. Bogacz, W. Janke: *Criticality in Dimerized Heisenberg Models*, International Workshop on "Unconventional Phases and Phase Transitions in Strongly Correlated Electron Systems", Max-Planck-Institut für Physik komplexer Systeme, Dresden, Germany, 04. – 07. June 2008

S. Wenzel, W. Janke: *The 2D Compass Model*, 9. Int. NTZ-Workshop "New Developments in Computational Physics" (CompPhys08), Leipzig, Germany, 27. – 29. November 2008

M. Wiedenmann, A. Nußbaumer, E. Bittner, W. Janke: *Monte Carlo Study of the Evaporation/Condensation Transition of Ising Droplets*, 1. Scientific Symposium of BuildMoNa, Leipzig, Germany, 07./08. February 2008

M. Wiedenmann, A. Nußbaumer, E. Bittner, W. Janke: *Monte Carlo Study of the Evaporation/Condensation Transition of Ising Droplets*, 72. DPG Spring Meeting, Berlin, Germany 25. – 29. February 2008

## 11.22 Graduations

**Habilitation**

- Dr. Michael Bachmann
  *Conformational Mechanics of Molecular Structure Formation Processes*
  July 2008

**Diploma**

- Mathias Aust
  *Generalized Ensemble Simulations of Disordered Systems*
  May 2008
- Frank Beyer
  *Monte Carlo Simulation Techniques and Minimal Energy States in the Edwards-Anderson Spin-Glass Model*
  February 2008
- Monika Möddel
  *Thermodynamics of Molecular Adsorption Processes on Mesocopic Scales*
  May 2008
- Micha Wiedenmann
  *Monte Carlo Study of the Evaporation/Condensation Transition of 3D Ising Droplets*
  February 2008

## 11.23 Guests

- Prof. Dr. David P. Landau
  Unversity of Georgia, Athens, USA
  30. March – 02. April 2008
- Prof. Dr. Andrea Pelissetto
  University of Rome, Italy
  30. March – 02. April 2008

- Prof. Dr. Bertrand Berche, Dr. Christophe Chatelain, Jean-Charles Walter
  Université Henri Poincaré, Nancy, France
  31. March – 04. April 2008
- Andrzej Görlich
  Jagellonian University, Krakow, Poland
  31. March – 04. April 2008
- Marcin Zagorski
  Jagellonian University, Krakow, Poland
  30. March – 05. April 2008
- Prof. Dr. Bernd A. Berg
  Florida State University, Tallahassee, USA
  01. May – 30. June 2008
- PD Dr. Stefan Wessel
  Universität Stuttgart
  07. – 08. May 2008
- Christoph Junghans
  Max-Planck-Institut für Polymerforschung, Mainz
  15. – 16. May 2008
- Dr. Shura Hayryan
  Academia Sinica, Taipei, Taiwan
  16. May 2008
- Prof. Dr. Sanjay Kumar
  Banaras Hindu University, Varanasi, India
  19. May 2008
- Prof. Dr. Anders Sandvik
  Boston University, USA
  17. June 2008
- Prof. Dr. Sanjay Kumar
  Banaras Hindu University, Varanasi, India
  03. July 2008
- Prof. Dr. Robert H. Swendsen
  Carnegie Mellon University, Pittsburgh, USA
  30./31. July 2008
- Jean-Charles Walter
  Université Henri Poincaré, Nancy, France
  07. – 29. November 2008
- Prof. Dr. Peter Young
  University of California at Santa Cruz, USA
  26. – 30. November 2008
- Xavier Durang
  Université Henri Poincaré, Nancy, France
  26. – 30. November 2008

- Prof. Dr. Herbert Wagner
  Ludwig-Maximilians-Universität München
  04. – 05. December 2008

# 12

# Molecular Dynamics / Computer Simulation

## 12.1 Introduction

Using methods of statistical physics and computer simulations we investigate classical many-particle systems interacting with interfaces. One aim of the research in our group is to built up a bridge between theoretical and experimental physics. By means of analytical theories of statistical physics and computer simulations (Molecular dynamics, Monte Carlo procedures, percolation theories) using modern workstations and supercomputers we examine subjects for which high interest exists in basic research and industry as well. The examinations involve transport properties (diffusion of guest molecules) in zeolites and the structural and phase behaviour of complex fluids on bulk conditions and in molecular confinements. Especially we are interested to understand

- the diffusion behaviour of guest molecules in zeolites in dependence on thermodynamic parameters, steric conditions, intermolecular potentials and the concentration of the guest molecules,
- structure and phase equilibria of complex (aqueous) fluids in interfacial systems (e.g. pores, thin films, model membranes) in dependence on geometric and thermodynamic conditions,
- and the migration of molecules in (random) porous media by the use of percolation theories.

tayloring in microscopic detail and to compare the results with experimental data. The use of a network of PC's and workstations (Unix, Linux, Windows), the preparation and application of programs (Fortran, C, $C^{++}$), and the interesting objects (zeolites, membranes) give excellent possibilities for future careers of undergraduates, graduate students and postdocs. Our research is part of several national and international programs (DFG-Schwerpunktprogramme SPP1155 und SPP1362, an International Research Graduate Training program (IRTG 1056), a joint research project DFG/TRF-Thailand, a joint research project DAAD/TRF-Thailand and joint research projects with UOIT Oshawa and SHARCNET, Canada) and includes a close collaboration with the Institute of Experimental Physics I (Physics of Interfaces and Biomembranes) of Leipzig University and many institutions in Germany and other countries. Details are given in the list of external cooperations.

*Horst-Ludger Vörtler and Siegfried Fritzsche*

## 12.2 Phase Equilibria and Critical Behaviour of Molecular Fluids in Bulk Systems and in Micropores

H.L. Vörtler, I. Nezbeda*, M. Kettler

*Czech Academy of Sciences, Prague, Czech Republic

The research of this long-term project is based on a hierarchic modeling of the potential energy of fluids with respect to the range of the intermolecular forces. Thereby the potential of a real fluid is composed of a short ranged molecular modal that describes the structure and thermodynamics basically correct and a long-ranged perturbation term. Using virtual parameter variation techniques thermodynamic pressures and chemical potentials are simulated and from these data phase equilibria are estimated by thermodynamic integration. Critical data are found by scaling laws. This approach is applicable to both homogeneous and confined fluids. While we studied in the first parts of the project mainly homogeneous bulk fluids (square-well fluids, primitive models of water) we focus now on the influence of geometric restrictions to phase equilibria and critical properties. Particularly, we deal with the shift of critical data under confinement. We found a simple analytic relation that describes quantitatively all existing simulation data [1, 2] for the decrease of the critical temperature with increasing geometrical restrictions (i.e. decreasing pore size). To this subject a first paper [3] appeared in 2008. The behaviour of the critical pressure and density under the confinement seems to be much more complicated and is currently under study.

The long-term goals of this research are contributions to a statistical-mechanical theory of phase equilibria of inhomogeneous fluids with applications to nanoporous materials and biointerfaces.

[1] H.L. Vörtler, W.R. Smith: J. Chem. Phys. **112**, 5168 (2000)
[2] J.K. Singh, S.K. Kwak: J. Chem. Phys. **26**, 024 702 (2007)
[3] H.L. Vörtler: Collect. Czech Chem. Commun. **73**, 518 (2008)

## 12.3 Simulation of Fluid Phase Equilibria in Very Narrow Slit-Like Pores: Transition to Two Dimensions and Finite Size Effects

H.L. Vörtler, W.R. Smith*

*University of Ontario, Institute of Technology, Oshawa, Canada

This project deals with the important and less studied problem of the estimation of phase equilibria in fluid systems confined to very narrow slit-like pores, particularly in the transition range to 2D fluid monolayers. We perform extensive canonical ensemble simulations of confined square-well fluids in the subcritical vapour–liquid coexistence range and apply virtual (Widom-like) particle insertion and virtual volume variation steps to estimate isotherms of both the chemical potential and the thermodynamic

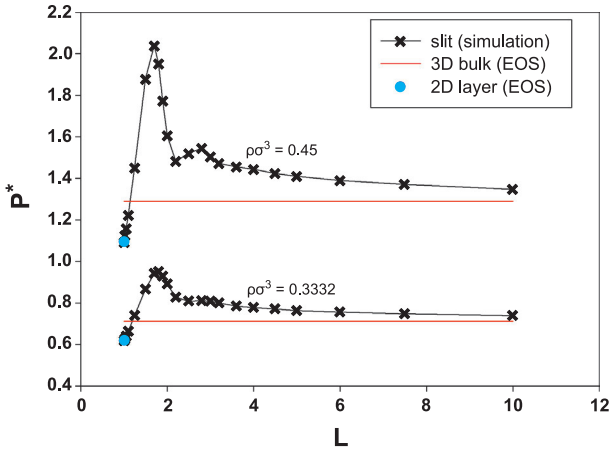


**Figure 12.1:** Spreading (thermodynamic) pressure vs. slit width in very narrow slits (for hard spheres).

(spreading) pressure. We focus on very narrow slits with width between one and two particle diameters, where for geometric reasons we expect special features related to the transition from 2D monolayers to 3D thin films. First results for the spreading pressure versus density are shown in Fig. 12.1.

For very narrow slits we observe a significant increase of the spreading pressure before for wider slits the expected decay of the pressure takes place. Of special interest is the study of finite size effects for very narrow slits in the transition range to two dimensions. Our recent detailed studies [1] of both three dimensional bulk fluids and 2D monolayers show significantly larger size effects in monolayers as in bulk fluids. Actually we study the sample size effects in the 2D/3D transition region.

The results serve as reference data for a theoretical estimation of fluid phase equilibrium data in thin films and monolayers.

The research was supported by research fund of University of Ontario Institute of Technology (research stay of H.L. Vörtler in Oshawa) and by the facilities of SHARCNET computer network (Ontario, Canada).

[1] H.L. Vörtler et al.: J. Phys. Chem. B **112**, 4656 (2008)

## 12.4 Analytical Treatment and Computer Simulations of the Influence of the Crystal Surface on the Exchange of Guest Molecules Between Zeolite Nanocrystals and the Surrounding Gas Phase

S. Fritzsche, T. Nanok, J. Gulín-González*, S. Vasenkov†

*University of Informatics Sciences, La Habana, Cuba
†University of Florida, Gainesville, USA

In the framework of the DFG priority program SPP 1155 we investigated the surface effects influencing the dynamics of adsorption of guest molecules into porous crystals.

A new analytical treatment of such processes has been developped [1, 3, 4]. Such effects are of high relevance for industrial purposes because e.g. in catalysis, relatively small crystals are used, to enhance efficiency and, furthermore, they also play an important rule in currently developed hierarchically ordered porous materials [2]. The analytical theory was tested by molecular dynamics simulations (MD) [1].

The method has now successfully been applied to new systems [5].

[1] A. Schüring: J. Phys. Chem. C **111**, 11 285 (2007)
[2] Y. Tao, H. Kanoh: J. Am. Chem. Soc. **125**, 6044 (2003), doi:10.1021/ja0299405
[3] A. Schüring: Diffus. Fund. **6**, 32.1 (2007)
[4] A. Schüring et al.: Diff. Fund. **6**, 33.1 (2007)
[5] A. Schüring et al.: *Quantification of the Mass-Transfer Coefficient of the External Surface of Zeolite Crystals by Molecular Dynamics Simulations and Analytical Treatment*, Micropor. Mesopor. Mater. (2009), in press

## 12.5 Diffusion of Water in the Zeolite Chabazite

S. Fritzsche, R. Channajaree, P.A. Bopp*, J. Kärger†

*University Bordeaux, France
†Institute for Experimental Physics I, Physics of Interfaces Workgroup

Earlier work about water in the zeolite chabazite [1, 2] has been revisited in a project in the framework of the International Research Training Group (IRTG) "Diffusion in Porous Materials". The non-monotonic dependence of the self diffusion coefficient upon the concentration of water molecules could be verified and examined in more detail and explained in MD simulations. The calculations are extremely computer time consuming and could therefore, only be done at high temperatures (600 K) in [1, 2]. High speed computing with modern supercomputers, the use of a less computer time expensive potential model (SPC water) and, parallel computing with the simulation software DL_POLY enabled now simulations even at room temperature. Moreover, the accuracy could be enhanced considerably.

For anisotropic diffusion the components of the diffusion tensor have to be used instead of a diffusion coefficient. The ratio of these components is a measure of the anisotropy. The new results yield this ratio in much better agreement with the experimental values than in [1, 2]. Rotational diffusion was now also included into this research.

Publication of the new results is in preparation. The simulations will be complemented by analytical investigations using Transition State Theory.

[1] S. Jost: PhD thesis, University of Leipzig (2004)
[2] S. Jost et al.: J. Phys. Chem. C **111**, 14 707 (2007)

## 12.6 How Do Guest Molecules Enter Zeolite Pores? Quantum Chemical Calculations and Classical MD Simulations

S. Fritzsche, S. Thompho, S. Hannongbua*, T. Remsungnen†, P.A. Bopp‡, O. Saengsawang

*Chulalongkorn University, Bangkok, Thailand
†Khon Khaen University, Khon Khaen, Thailand
‡University Bordeaux, France

This is a common project of the German DFG and the NRCT (Thailand). Effects connected with the silanol groups on the surface of zeolites with respect to diffusion have been examined in quantum chemical calculations [1] and non-equilibrium studies by Grand Canonical Molecular Dynamics [2] for the system methane silicalite–1. The adsorption dynamics was found to be influenced by the presence of the silanol groups . In the final equilibrium state the coverage of the surface by methane molecules depends upon the presence of silanol groups while the amount of adsorbed methane is not much influenced.

The surface permeability for the penetration of methane into silicalite–1 has been examined and the underlaying concept of the surface permeability has critically been discussed. The results are published in [3, 4].

[1] O. Saengsawang et al.: Stud. Surf. Sci. Catal. **158**, 947 (2005)
[2] O. Saengsawang et al.: J. Phys. Chem B **109**, 5684 (2005)
[3] S. Thompho et al.: Poster at the 20. Deutsche Zeolithtagung, Halle, 5.–7. March 2008, Abstracts p. 93
[4] S. Thompho et al.: Phys. Chem A **113**, 2004 (2009)

## 12.7 Investigation of the Rotation and Diffusion of Pentane in the Zeolite ZK5

S. Fritzsche, O. Saengsawang, A. Schüring, P. Magusin*, M.-O. Coppens†, A. Dammers†, D. Newsome†

*Eindhoven University, The Netherlands
†Delft University, The Netherlands

The rotation and diffusion of pentane in the zeolite ZK5 has been investigated. This was subject of a project (project leader S. Fritzsche) in the International Research Training Group (IRTG) “Diffusion in Porous Materials”.

The rotation of ZK5 ($\gamma$-cage) was examined experimentally in [1]. Now, MD simulation [2, 6] could find agreement and explain many features of this phenomenon. But some results in [1] could not be confirmed by the simulation. In cooperation with P. Magusin they could be reinterpreted by showing that quantities which have been assumed to be temperature independant in [1] in reality depend upon the temperature.

The diffusion of pentane in ZK5 has been investigated by new challenging methods that are combinations of transition state theory (TST) and MD simulations. In cooperation with the group of Prof. M.-O. Coppens (A. Dammers, D. Newsome, Delft University) the challenging new method of transition path sampling [3] was successfully applied to calculate one of the jump rates involved in this process [2].

But this method is not only very difficult to apply but, it is also very computer time demanding. Therefore, the newly developped method of HTCE [4] has also been used and worked very efficiently [2]. A dynamical correction (Bennett–Chandler) was computed additionally in order to take into account the recrossing events. The computed self diffusion coefficient was found within the range that has been obtained from the experiment [5]. The work resulted in a PhD thesis and the publication [6] about the rotation. The publication about the diffusion is in progress.

[1] V.E. Zorine et al.: J. Phys. Chem. B **108**, 5600 (2004)
[2] O. Saengsawang: *Rotation and Diffusion of n-pentane in the Zeolite ZK5*, PhD thesis, University of Leipzig (2008)
[3] C. Dellago et al.: Adv. Chem. Phys. **123**, 1 (2002)
[4] A. Schüring et al.: Chem. Phys. Lett. **450**, 164 (2007)
[5] P.C.M.M. Magusin et al.: Magn. Reson. Chem. **37**, 108 (1999)
[6] O. Saengsawang et al.: J. Phys. Chem. C **112**, 5922 (2008)

## 12.8 Diffusion of Guest Molecules in Metal Organic Frameworks

S. Fritzsche, K. Seehamart, S. Hannongbua[*], T. Remsungnen[†], J. Kärger[‡], C. Chmelik[‡]

[*]Chulalongkorn University, Bangkok, Thailand
[†]Khon Khaen University, Khon Khaen, Thailand
[‡]Institute for Experimental Physics I, Physics of Interfaces Workgroup

A new class of nanoporous materials that is promising for industrial applications mainly because of the possibility of 'tayloring' and the huge surface/volume ratio is the class of Metal Organic Frameworks (MOFs) [1]. Already now, after few years, the number of different MOFs that have been synthesized is larger then the number of e.g. zeolite types. Many phenomena connected with adsorption and diffusion in these materials are not yet understood. A common DFG project with experimental groups (Prof. Kärger, Leipzig, Prof. Caro, Hannover, Dr. Wiebcke, Hannover) and NRCT (Thailand, Prof. Hannongbua and other groups) started 2008 in the framework of the SPP1362. First results of quantum chemical calculations are published in [2].

In cooperation with Prof. Krishna (Amsterdam) MD simulations have been carried out that could show a surprising influence of the lattice flexibility on the concentration dependence of the self diffusion coefficient $D_S$ of ethane in the MOF Zn(tbip) [3]. Figure 12.2 shows the main result. While the simulations with rigid lattice yielded a $D_S$ that monotonically decreased with increasing ethane concentration the simulations with flexible lattice gave a $D_S$ that increased up to a maximum at a loading of about 8 ethane per unit cell. At this maximum the $D_S$ values are one order of magnitude larger

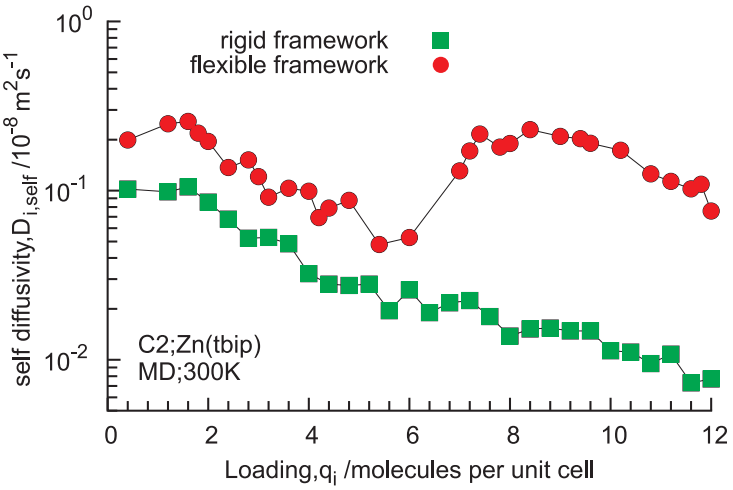


**Figure 12.2:** The self diffusion coefficient of ethane in Zn(tbip) as a function of the loading.

than with rigid lattice. At very high loadings the mutual hindrance of the diffusing ethane leads to decreasing $D_S$ as to be expected.

[1] B.F. Hoskins, R. Robson: J. Am. Chem. Soc. **112**, 1546 (1990)
[2] A. Pianwanit et al.: Chem. Phys. **349**, 77 (2008)
[3] K. Seehamart et al.: Micropor. Mesopor. Mater. (2009), in press, doi:10.1016/j.micromeso.2009.01.020

## 12.9 Funding

*Analytical Treatment and Computer Simulations of the influence of the crystal surface on the exchange of guest molecules between zeolite nanocrystals and the surrounding gas phase*
S. Fritzsche, S. Vasenkov, T. Nanok
SPP1155, DFG Fr 1486/2-3

*Diffusion of Water in the Zeolite Chabazite*
S. Fritzsche, R. Channajaree
DFG IRTG 1056

*Investigation of the rotation and diffusion of pentane in the zeolite ZK5*
S. Fritzsche, O. Saengsawang
DFG IRTG 1056

*How do guest molecules enter zeolite pores? Quantum Chemical calculations and classical MD simulations*
S. Fritzsche, S. Thompho
DFG Fr 1486/1-4

*Diffusion of Guest Molecules in Metal Organic Frameworks*
K. Seehamart

funded by a stipend of the University of Technology Isan (RMUTI), Kon Khaen, Thailand,
S. Fritzsche
SPP1362, DFG Fr 1486/5-1

*Simulation of phase equilibria in two- and three-dimensional Fluids*
W.R. Smith, H.L. Vörtler
Research fund of University of Ontario Institute of Technology (research stay of H.L. Vörtler in Oshawa) and SHARCNET computer network (Ontario, Canada)

## 12.10 Organizational Duties

S. Fritzsche
- Project leader of one project in the International Research Training Group, IRTG 1056
- Project leader of one project in the SPP1155, DFG FR1486/2-2
- Project leader of one project in the SPP1362, DFG FR1486/5-1
- Project leader of a German/Thai research project, DFG FR1486/1-4
- Referee: Chem. Phys. Lett., Micropor. Mesopor. Mater., J. Molec. Graphics Model.

H.L. Vörtler
- Speaker of the MDC workgroup
- Reviewer: Czech Science Foundation
- Referee: J. Chem. Phys., Physica A, Chem. Phys. Lett., J. Molec. Liquids, Chem. Phys.

## 12.11 External Cooperations

**Academic**

- Chulalongkorn University, Bangkok, Thailand
  Prof. Dr. S. Hannongbua
- Indian Institute of Science, Bangalore, India
  Prof. Dr. S. Yashonath
- Khon Khaen University, Khon Khaen, Thailand
  Dr. T. Remsungnen
- University Bordeaux, France
  Prof. Dr. P.A. Bopp
- Eindhoven University, Eindhoven, The Netherlands
  Prof. Dr. P. Magusin
- Technical University, Delft, The Netherlands
  Prof. Dr. M.-O. Coppens, Dr. A. Dammers, Dr. D. Newsome
- Czech Academy of Sciences, Prague & University Usti nad Labem, Czech Republic
  Prof. I. Nezbeda, Dr. M. Lisal
- University of Ontario, Institute of Technology, Oshawa, Canada
  Prof. W.R. Smith

## 12.12 Publications

**Journals**

A. Pianwanit, C. Kritayakornupong, A. Vongachariya, N. Selphusit, T. Ploymeerusmee, T. Remsungnen, D. Nuntasri, S. Fritzsche, S. Hannongbua: *The optimal binding sites of $CH_4$ and $CO_2$ molecules on the metal-organic framework MOF-5: ONIOM calculations*, Chem. Phys. **349**, 77 (2008)

O. Saengsawang, A. Schüring, T. Remsungnen, A. Loisruangsin, S. Hannongbua, P.C.M.M. Magusin, S. Fritzsche: *Rotational Motion of Pentane in the Flat Gamma Cages of Zeolite KFI*, J. Phys. Chem. C **112**, 5922 (2008)

H.L. Vörtler: *Simulation of fluid phase equilibria in square-well fluids: from three to two dimensions*, Collect. Czech. Chem. Commun. **73**, 518 (2008)

H.L. Vörtler, K. Schäfer, W.R. Smith: *Simulation of Chemical Potentials and Phase Equilibria in Two- and Three-Dimensional Square-Well Fluids: Finite Size Effects*, J. Phys. Chem. B **112**, 4656 (2008)

**Talks**

S. Fritzsche: *HTCE – A New Simulation Method in Transition State Theory for Transport in Microporous Materials*, 12. Ann. Symp. Comp. Sci. Eng. (ANSCSE 12), Ubon Ratchathanee, Thailand, 27. – 29. March 2008

A. Schüring, J. Gulin-Gonzalez, S. Vasenkov, S. Fritzsche, J. Kärger: *Simulation and Analytical Treatment of the Mass- Transfer through Zeolite Surfaces for the Ad- and Desorption of Molecules*, Int. Workshop Molec. Model., Frankfurt am Main, Germany, 10. March 2008

H.L. Vörtler, W.R. Smith: *MC Simulation of Fluid Phase Equilibria in Square-Well Fluids: From Bulk to Two-Dimensional Layers*, 9. Int. NTZ-Workshop Comp. Phys. (CompPhys08), Leipzig, Germany, 27. – 29. November 2008

**Posters**

S. Thompho, O. Saengsawang, R. Channajaree, T. Remsungnen, S. Hannongbua, A. Schüring, S. Fritzsche: *Influence of the Silanol Groups on the External Surface of Silicalite–1 on the Adsorption Dynamics of Methane*, 20. Deutsche Zeolithtagung, Halle, Germany, 05. – 07. March 2008

A. Vongachariya, A. Pianwanit, D. Nuntasri, S. Hannongbua, C. Kritayakornupong, T. Remsungnen, O. Saengsawang, S. Fritzsche: *Stability of organic frameworks and their complexes with $CO_2$ and $CH_4$ investigated by quantum chemical calculations*, 1. Int. Conf. Metal Organic Frameworks and Open Framework Compounds (MOF2008), Augsburg, Germany, 08. – 10. October 2008

## 12.13 Graduations

**Doctorate**

- Oraphan Saengsawang
  *Rotation and Diffusion of n-pentane in the Zeolite ZK5*
  July 2008

## 12.14 Guests

- Dr. T. Remsungnen
  Khon Khaen University, Thailand
  01. April – 28. June 2008

# 13

# Quantum Field Theory and Gravity

## 13.1 Geometry Dependence of the Casimir Force

M. Bordag

The vacuum of quantum fields shows a response to changes in external conditions with measurable consequences. The most prominent manifestation is the Casimir effect. It belongs to the few number of macroscopic quantum effects and it is of big importance in nanometer sizes systems. At present, the dependence of the Casimir forces on geometry is in the focus of actual research using a new representation in terms of a functional determinant. The previous results were extended to the case of a sphere in front of a plane, see [1]. The vacuum energy was studied for a spherical plasma shell providing a kind a regularization for a conducting sphere. At once this is a model for the interaction of a $C_{60}$-molecule with the vacuum of the electromagnetic field. It is shown that the ultraviolet divergences of this system can be uniquely absorbed into the classical parameters and that the vacuum energy changes sign in dependence on the plasma frequency [2].

[1] M. Bordag, V. Nikolaev: J. Phys. A **41**, 164 001 (2008)
[2] M. Bordag, N. Khusnutdinov: Phys. Rev. D **77**, 085 026 (2008)

## 13.2 Higher Order Correlation Corrections to Color Ferromagnetic Vacuum State at Finite Temperature

M. Bordag, V. Skalozub*

*Physics Faculty, Dnepropetrovsk National University, Ukraine

Topic of the investigation is the stability of the ground state of QCD with temperature and color magnetic background field by means of the calculation of the polarization tensor of the gluon field. Special attention was devoted to the investigation of the polarization tensor for the color charged gluons at finite temperature. A new technique for a parametric representation was found which allowed for an explicit separation of the Debye and the magnetic masses and, for instance, for an easy calculation of the Debye mass's field and temperature dependence, see [1, 2].

[1] M. Bordag, V. Skalozub: Phys. Rev. D **77**, 105 013 (2008)
[2] N. Khandoga et al.: J. Phys. A **41**, 164 045 (2008)

## 13.3 Casimir Effect and Real Media

M. Bordag, B. Geyer, G.L. Klimchitskaya*, V.M. Mostepanenko†

*Physics Department, North-West Polytechnical University, St. Petersburg, Russia
†Noncommercial Partnership "Scientific Instruments" of Ministry of Industry, Sciences and Technologies, Moscow, Russia

The vacuum of quantum fields shows a response to changes in external conditions with measurable consequences. The investigation of the electromagnetic vacuum in the presence of real media is of actual interest in view of current experiments as well as nanoscopic electro-mechanical devices. In recent experiments using atomic force microscopy the Casimir effect had been measured with high accuracy. This required a detailed investigation of the influence of real experimental structures on the corresponding force.

Since the year 2000, the behavior of the thermal correction to the Casimir force between real metals has been hotly debated. As was shown by several groups, the Lifshitz theory, which provides the theoretical foundation for calculations of both the van der Waals and Casimir forces, leads to different results depending on the model of metal conductivity used. To resolve these controversies, the theoretical considerations based on the principles of thermodynamics and new experimental tests were invoked. Additional, the study has to be extended to the case of dielectrics and semiconductors. In 2008 the following has been obtained:

- We have considered the *thermal Casimir effect in rectangular boxes* starting from the general expression for the Casimir free energy in the framework of Matsubara quantum field theory at nonzero temperature.

    1. The thermal correction was renormalized by subtracting counter terms proportional to the box volume, surface area, and to the sum of box sides. Using the method of zeta function regularization, a finite expression for the Casimir free energy associated with a closed volume $V$ was obtained going to zero when the characteristic dimensions of this volume go to infinity. This is achieved by a subtraction of the free energy of the black body radiation and two other geometrical contributions of quantum origin.
    2. The obtained general expression was applied to the cases of the massless scalar field with Dirichlet boundary conditions and the electromagnetic field in rectangular boxes. It was shown that physical temperature-dependent contribution to the Casimir force at zero temperature can be both positive and negative (i.e., leads to repulsion or attraction) depending on the box side lengths. This property is preserved for boxes with zero electromagnetic Casimir force at zero temperature. Numerical computations of the scalar and electromagnetic Casimir force as functions of side length and temperature for cubes have been performed.

3. The developed formalism was applied to a rectangular box divided into two sections by a movable partition consisting of ideal metal (piston). The attraction (or repulsion for a piston with Neumann boundary conditions) of the piston to the nearest face of the box does not negate the electromagnetic Casimir repulsion for boxes without a piston. However, the cases with an empty space outside the box and with another section of a larger box outside the piston are physically quite different. The proposed new approach is advantageous in comparison with the standard calculation because the former leads to meaningful results for the thermal Casimir force both for an empty box and for a box with a piston, whereas the latter is meaningful only in application to the box with a piston.

The results are published in [2, 3].

- The *application of the Lifshitz theory to real materials* was formulated observing properly the account of charge carriers. This formulation was applied to experiments on measuring the Casimir and Casimir–Polder force.

  Thereby we obtained three types of results:

  1. We confirmed the violation of the Nernst heat theorem in the standard formulation of the Lifshitz theory.
     (a) In case of two metal plates we showed that, contrary to the arguments by J.S. Høye et al. [4], the Lifshitz theory combined with the Drude model is thermodynamically inconsistent [5]. For the configuration metal-dielectric, the violation of the Nernst heat theorem in the Lifshitz theory was confirmed when the dc conductivity of the dielectric plate is included in the model of dielectric response [6].
     (b) For the configuration of an atom interacting with a cavity wall we have determined the Casimir–Polder entropy and investigated its dependence on the conductivity properties of the wall material. It was shown that for a metal wall and a dielectric wall with neglected dc conductivity the Nernst heat theorem is satisfied. At the same time, for a dielectric wall with included dc conductivity the Nernst theorem is found to be violated [7, 8].
  2. We formulated the *Lifshitz theory for real materials* and showed how to consistently apply it.
     (a) Specifically, it was justified that for all metallic-type materials (i.e., for those whose conductivity does not go to zero when the temperature vanishes) free charge carriers should be described by the plasma model in order to be in agreement with thermodynamics and consistent with all available experimental data.
     (b) As for materials of dielectric-type whose conductivity vanishes with vanishing temperature (these include insulators, doped semiconductors with a dopant concentration below critical, solids with ionic conductivity etc.), the dc conductivity arising at nonzero temperature should be neglected in the Lifshitz theory in order to avoid contradictions with thermodynamics and experiment.

(c) The physical grounds of these rules are connected with the condition of thermal equilibrium which is the basic applicability condition of the Lifshitz theory. Especially,the inclusion of the drift current into the model of dielectric response of the plate material is not compatible with the condition of thermal equilibrium and therefore leads to thermodynamic and experimental inconsistencies [7, 9, 10].

3. We compared the suggested formulation of the Lifshitz theory with the experimental data of new experiments.

   (a) The most important experiment performed in 2007 [11] is the first observation of the thermal Casimir–Polder force through the shift of center-of-mass oscillation frequency in a $^{87}$Rb Bose–Einstein condensate at a distance of a few micrometers from a fused-silica wall. We have recalculated this frequency shift by neglecting the nonzero dc conductivity of fused silica at experimental temperatures and found that the obtained results are in excellent agreement with the experimental data, thereby, confirming our rule that in Lifshitz theory the dc conductivity of dielectric materials should be disregarded [12].

   (b) Furthermore, from the measurement of the Casimir force by means of a micromachined oscillator we found new constraints on the parameters of hypothetical Yukawa-type corrections to Newtonian gravitational law; these constraints were collected and discussed in [13].

- The *interaction of hydrogen atoms and molecules with carbon nanotubes* was considered with account of repulsive exchange forces which act at the shortest separations. Using the method of phenomenological potentials, it was shown that at separations below 1 nm the exchange repulsion gives rise to the lateral force which moves hydrogen atom toward the cell center. In the position above the call center, the repulsive force cannot balance the van der Waals attraction. As a result, an atom penetrates inside the nanotube. This effect can be used for the determination of an optimal configuration of carbon nanostructures for the purposes of hydrogen storage [14].
- Finally, the book *"Advances in the Casimir Effect"* (730 pages) has been completed and submitted for publication to the Oxford University Press [1]. The first part of the book, already written in 2007, includes the foundation and general quantum field theoretic formulation of the thermal Casimir and Casimir–Polder effect. The second part of the book, written in 2008, includes the presentation of the Lifshitz theory of the van der Waals and Casimir interaction for the cases of dielectric–dielectric, metal–metal and dielectric–metal walls at both zero and nonzero temperature. In so doing, real properties of wall materials are taken into account. The application of the Lifshitz theory to atom–wall interaction is considered in thermal equilibrium and out of thermal equilibrium. A special chapter is devoted to the investigation of the Casimir force between rough and corrugated surfaces. The third part of the book is devoted to the most striking developments in the precise measurements of the Casimir force using modern laboratory techniques. This includes detailed description of 24 experiments and their comparison with theory. Special chapters are devoted to the experiments on Bose–Einstein condensation and quantum reflection, applications of the Casimir force in nan-

otechnology, and for obtaining constraints on extra-dimensional physics beyond the Standard Model from the Casimir effect.

[1] M. Bordag et al.: *Advances in the Casimir Effect* (Oxford University Press), submitted
[2] B. Geyer et al.: Eur. Phys. J. C **57**, 823 (2008)
[3] V.M. Mostepanenko: J. Phys. Conf. Ser. **161**, 012 003 (2009)
[4] J.S. Høye et al.: Phys. Rev. E **75**, 051 127 (2007)
[5] G.L. Klimchitskaya, V.M. Mostepanenko: Phys. Rev. E **77**, 023 101 (2008)
[6] B. Geyer et al.: Ann. Phys. (N.Y.) **323**, 291 (2008)
[7] G.L. Klimchitskaya et al.: J. Phys. A **41**, 432 001(F) (2008)
[8] V.B. Bezerra et al.: Phys. Rev. A **78**, 042 901, (2008)
[9] G.L. Klimchitskaya, B. Geyer: J. Phys. A **41**, 164 032 (2008)
[10] V.M. Mostepanenko, B. Geyer: J. Phys. A **41**, 164 014 (2008)
[11] J.M. Obrecht et al.: Phys. Rev. Lett. **98**, 063 201 (2007)
[12] G.L. Klimchitskaya, V.M. Mostepanenko: J. Phys. A **41**, 312 002(F) (2008)
[13] V.M. Mostepanenko et al.: J. Phys. A **41**, 164 054 (2008)
[14] G.L. Klimchitskaya et al.: J. Phys. A **41**, 164 012 (2008)

## 13.4 Quantum Field Theory of Light-Cone Dominated Hadronic Processes

B. Geyer, J. Blümlein*, D. Robaschik†, O. Witzel‡

*Institut für Hochenergiephysik, Zeuthen
†Institute for Theoretical Physics, Brandenburg Technical University, Cottbus
‡Institute for Physics, Humboldt-Universität Berlin

Light-cone dominated, polarized hadronic processes at large momentum transfer factorize into process-dependent hard scattering amplitudes and process-independent non-perturbative generalized distribution amplitudes. Growing experimental accuracy requires the entanglement of various twist as well as (target) mass contributions and radiative corrections. Their quantum field theoretic prescription is based on the nonlocal light-cone expansion [1] and the group theoretical procedure of decomposing *nonlocal, tensor-valued* QCD operators into tensorial harmonic operators with well-defined geometric twist ($\tau$ = dimension $d$ − spin $j$) developed in our previous work [2, 3].

- First, extending former work about power resp. target mass corrections for virtual Compton scattering at twist-2 [2, 4, 5], the complete target mass and finite (transverse) momentum corrections to *deeply inelastic diffractive scattering* already has been determined in the framework of quantum field theory [6].

  Now, we discussed it in detail using an equivalent formulation with the aim to derive a representation suitable for data analysis. We considered the off-cone twist-2 ligth-cone operators to derive the target mass und finite $t$ corrections of diffractive deep-inelastic scattering and deep inelastic scattering. The corrections turn out to be at most proportional to $x/|t|$, $xM^2/Q^2$, $x = x_{\rm Bj}$ or $x_{\rm P}$, which suggests

an expansion in these parameters. Their contribution varies in size considering diffrative scattering or meson-exchange processes. Relations between different kinematic amplitudes which are determined by ond and the same diffractive generalized parton distribution or its moments are derived. In the limit $t, M^2 \to 0$ one obtaines the results of [7].

- Second, the fundamental results [8] on the complete twist decomposition of generic non-local tensor operators for hadronic processes recently have been applied to *B-meson physics* [9, 10]. Thereby, two- and three-particle distribution amplitudes of heavy pseudoscalar mesons of well-defined geometric twist were introduced and their relations the conventional ones of dynamical twist have been derived. Furthermore, under the constraints of HQET, taking into account the equations of motion of the heavy meson distribution amplitudes of definite geometric twist and using the knowledge of their off-cone structure, various relations between the (sets of) independent two- and three-particle distribution amplitudes of definite geometric twist have been derived and presented using both the (double) Mellin moments and the re-summed non-local distribution amplitudes to lowest non-trivial order of light-cone distance $x^2$. Now, these off-cone results are under study to find corresponding relations to any order in $x^2$.

[1] S.A. Anikin, O.I. Zavialov: Ann. Phys. (N.Y.) **116** 135 (1978); D. Müller et al.: Fortschr. Phys. **42**, 101 (1994)
[2] B. Geyer et al.: Nucl. Phys. B **559**, 339 (1999); **618**, 99 (2001); B. Geyer, M. Lazar: Nucl. Phys. B **581**, 341 (2000), Phys. Rev. D **63**, 094 003 (2001); J. Eilers, B. Geyer: Phys. Lett. B **546**, 78 (2002)
[3] J. Eilers et al.: Phys. Rev. D **69**, 034 015 (2004)
[4] B. Geyer et al.: Nucl. Phys. B **704**, 279 (2005)
[5] B. Geyer, D. Robaschik: Phys. Rev. D **71**, 054 018 (2005)
[6] J. Blümlein et al.: Nucl. Phys. B **755**, 112 (2006)
[7] J. Blümlein, D. Robaschik: Phys. Lett. B **517**, 222 (2001); Phys. Rev. D **65**, 096 002 (2002)
[8] J. Eilers: arXiv:hep-th/0608173
[9] B. Geyer, O. Witzel: Phys. Rev. D **72**, 034 023 (2005)
[10] B. Geyer, O. Witzel: Phys. Rev. D **76**, 074 022 (2007)

## 13.5 Structure of the Gauge Orbit Space and Study of Gauge Theoretical Models

G. Rudolph, S. Charzynski, A. Hertsch, J. Huebschmann, P. Jarvis*, J. Kijowski†, M. Schmidt

*School of Physics, University of Tasmania, Hobart, Australia
†Institute for Theoretical Physics, University of Warsaw, Poland

The investigation of gauge theories in the Hamiltonian approach on finite lattices with emphasis on the role of nongeneric strata was continued. This includes, in particular,

stratified Kähler quantization for gauge groups SU(2) and SU(3) [1, 2] and the study of the question how the stratification may be encoded on the level of the algebra of observables [3]. A part of these problems was studied in collaboration with J. Huebschmann.

Based on [4], the investigations of specific models of quantum lattice gauge theory in terms of gauge invariant quantities concerning the structure of the algebra of observables and its representations were continued.

A. Hertsch completed the classification of the orbit types of the action of the group of local gauge transformations on the space of connections for arbitrary compact gauge group [5].

[1] J. Huebschmann et al.: Commun. Math. Phys. **286**, 459 (2009)
[2] J. Boehnke: *The Costratified Structure of an SU*(3)*-Lattice Gauge Model*, Diploma thesis, University of Leipzig (2008)
[3] G. Rudolph, M. Schmidt: arXiv:0708.4646 [hep-th], to appear in J. Math. Phys.
[4] J. Kijowski et al.: Ann. H. Poincaré **4**, 1137 (2003); J. Kijowski, G. Rudolph: J. Math. Phys. **46**, 032 303 (2005); Rep. Math. Phys. **55**, 199 (2005); P. Jarvis et al.: J. Phys. A **38**, 5359 (2005)
[5] A. Hertsch: *On the Gauge Orbit Stratification for Theories with Gauge Group SU*($n$), PhD thesis, University of Leipzig (2009)

## 13.6 Quantum Field Theory on Non-Commutative Geometries, Quantum Energy Inequalities, Generally Covariant Quantum Field Theory

R. Verch, P. Marecki, M. Borris, J. Schlemmer

One of the questions of recent interest is if there is a general framework for quantum field theory on non-commutative spacetimes. This question is analysed in collaboration with M. Paschke and M. Borris. On one hand, an approach to Lorentzian non-commutative geometry in the spirit of spectral geometry is being established. On the other hand, the quantization of such structures is shown to lead to simple examples of quantum field theories on non-commutative spacetimes for concrete non-commutative spacetime models. The research on these topics is in progress.

Another line of research is devoted to an extension of the framework of local general covariant quantum field theories to the case of a relation between quantum field theories on several, different dimensions. This connects to the question of how to distinguish theories of Kaluza–Klein type at the quantized level. The research work on these matters is carried out in collaboration with C.J. Fewster.

The definition and analysis of states which can be viewed as local thermal equilibrium states in quantum field theory will be extended to quantum fields in curved spacetime, with a view on application in cosmological situations. Current research work with J. Schlemmer points at a close connection between local thermal equilibrium states and quantum energy inequalities which is being further analyzed. Moreover, the validity of quantum energy inequlities in interacting quantum field models is being investigated in collaboration with C. Kopper.

A standing problem is the concept of quantum field theories on non-globally hyperbolic spacetimes. A special class of such spacetimes are certain types of rotating spacetimes. Several issues in setting up quantum field theories on such spacetimes are being studied by P. Marecki.

## 13.7 Funding

*Structure of the gluon polarization tensor in a color magnetic field background at finite temperature*
PD Dr. M. Bordag
DFG Bo 1112/16-1

*Spectral Zeta Functions and Heat Kernel Technique in Quantum Field Theory with Nonstandard Boundary Condition*
PD Dr. M. Bordag, Dr. D. Vassilevich
Heisenberg-Landau programme

*Parallel nano assembling directed by short-range field forces*
PD Dr. M. Bordag
PARNASS: Specific targeted research project within the 6th Framework Programme of EU, NMP4-CT-2005-017071

*New Trends and Applications of the Casimir Effect (CASIMIR)*
Research Networking Program der ESF (European Research Foundation)
PD Dr. M. Bordag – Member of the Steering Committee

*Improved study of the Casimir force between real metals and its application to constraints for testing extra-dimensional physics*
B. Geyer
DFG 436 RUS 113/789/0-4

*Quantum Theory of Lattice Gauge models*
A. Hertsch
IMPRS fellowship at MPI MIS

*Local thermodynamic equilibrium in cosmological spacetimes*
J. Schlemmer
IMPRS fellowship at MPI MIS

## 13.8 Organizational Duties

M. Bordag

- Referee: J. Phys. A, Phys. Rev. D, J. Math. Phys.
- Member of the Steering Committee of the ESF Research Networking Program *New Trends and Applications of the Casimir Effect (CASIMIR)*

B. Geyer

- Vertrauensdozent der Gesellschaft Dt. Naturforscher und Ärzte (GDNÄ)

- Reviewer: Deutsche Forschunggemeinschaft (DFG), Deutscher Akademischer Austausch Dienst (DAAD), Humboldt Foundation

G. Rudolph
- Referee: Class. Quant. Grav., J. Math. Phys., J. Geom. Phys., J. Phys. A, Rep. Math. Phys.
- Director of the Institute for Theoretical Physics (until September 2008)

M. Schmidt
- Referee: J. Phys. A, Int. J. Mod. Phys. A, Class. Quant. Grav., J. Gen. Relativ. Grav.

A. Uhlmann
- Board member: Rep. Math. Phys., Open Syst. Informat. Dyn.

R. Verch
- Associate Editor: J. Gen. Relat. Grav.
- Chairman of the board for the Theoretical and Mathematical Physics Section, Deutsche Physikalische Gesellschaft (DPG)
- Reviewer: Alexander von Humboldt Foundation, Mathematical Reviews
- Referee: Commun. Math. Phys., J. Math. Phys., Rev. Math. Phys., Class. Quantum Grav., Eur. Phys. J. C, Springer Lecture Notes Physics, Cent. Eur. J. Phys.

## 13.9 External Cooperations

**Academic**

- Institut für Physik / Computational Physics, Humboldt Universität zu Berlin, Germany
  Dipl.-Phys. Oliver Witzel
- DESY-Institute of High Energy Physics, Zeuthen, Germany
  Dr. Johannes Blümlein
- Institute of Theoretical Physics, Brandenburg Technical University, Cottbus, Germany
  Prof. Dr. Dieter Robaschik
- Mathematics Department, Universität Hamburg, Germany
  Dr. C. Fleischhack
- Institute for Mathematical Physics, Technical University Braunschweig, Germany
  Prof. Dr. R.F. Werner
- Department of Mathematics, University of Münster, Germany
  Dr. M. Paschke
- Polish Academy of Sciences, Center for Theoretical Physics, Warsaw, Poland
  Prof. Dr. J. Kijowski, Dr. S. Charzynski
- Polish Academy of Sciences, Mathematics Institute and University of Warsaw, Poland
  Prof. Dr. P. Hajac

- St. Petersburg University, Russia
  Prof. Yu.V. Novozhilov
- Department of Physics, North-West Polytechnical University St. Petersburg, Russia
  Prof. Dr. Galina L. Klimchitskaya
- Noncommercial Partnership "Scientific Instruments" of Ministry of Industry, Sciences and Technologies, Moscow, Russia
  Prof. Dr. Vladimir M. Mostepanenko
- National University, Dnepropetrovsk, Ukraine
  Prof. V. Skalozub
- Joint Institute for Nuclear Research, Dubna, Russia
  Dr. V. Nesterenko, Dr. I. Pirozhenko
- Centre de Physique Théorique, Ecole Polytechnique, Palaiseau, France
  Prof. C. Kopper
- Université des Sciences et Technologies de Lille, France
  Prof. Dr. J. Huebschmann
- Dipartimento di Matematica, Universita di Trento, Italy
  Prof. Dr. V. Moretti
- Department of Mathematics, University of York, UK
  Dr. C.J. Fewster
- Department of Mathematics, Connecticut State University, New Britain, USA
  Prof. Dr. T. Roman
- Department of Physics, University of South Carolina, Columbia, USA
  Prof. Dr. P. Mazur
- Lawrence Livermore National Laboratory, Livermore, USA
  Dr. G.F. Chapline
- University of Tasmania, Hobart, Australia
  Prof. Dr. P. Jarvis
- University of Newcastle, Australia
  Prof. Dr. W. Szymanski

## 13.10 Publications

**Journals**

M. Bordag, N. Khusnutdinov: *On the vacuum energy of a spherical plasma shell*, Phys. Rev. D **77**, 085 026 (2008)

M. Bordag, V. Nikolaev: *Casimir force for a sphere in front of a plane beyond proximity force approximation*, J. Phys. A **41**, 164 001 (2008)

M. Bordag, V. Skalozub: *Polarization tensor of charged gluons in color magnetic background field at finite temperature*, Phys. Rev. D **77**, 105 013 (2008)

S. Charzyński, G. Rudolph, M. Schmidt:: *On the topology of the reduced classical configuration space of lattice qcd*, J. Geom. Phys. **58**, 1607 (2008)

B. Geyer, G.L. Klimchitskaya, V.M. Mostepanenko: *Analytic approach to the thermal Casimir force between metal and dielectric*, Ann. Phys. (N.Y.) **323**, 291 (2008)

B. Geyer, G.L. Klimchitskaya, V.M. Mostepanenko: *Thermal Casimir effect in ideal metal rectangular boxes*, Eur. Phys. J. C **57**, 823 (2008)

N. Khandoga, M. Bordag, A. Ferludin, V. Skalozub: *The Green function of neutral gluons in color magnetic background field at finite temperature* , J. Phys. A **41**, 164 045 (2008)

G.L. Klimchitskaya, B. Geyer: *Problems in the theory of thermal Casimir force between dielectrics and semiconductors*, J. Phys. A **41**, 164 032 (2008)

P. Marecki: *Balanced homodyne detectors and Casimir energy densities*, J. Phys. A **41**, 164 037 (2008)

P. Marecki: *Balanced homodyne detectors in quantum field theory*, Phys. Rev. A **77**, 012 101 (2008)

V. Mostepanenko, M. Bordag (Eds.): *Papers Presented at the 8th Workshop on Quantum Field Theory under the Influence of External Conditions (QFEXT07)*, Leipzig, Germany, September 2007, Special Issue J. Phys. A **41**(16), (2008)

V.M. Mostepanenko, B. Geyer: *New approach to the thermal Casimir force between real metals*, J. Phys. A **41**, 164 014 (2008)

J. Schlemmer, R. Verch: *Local Thermal Equilibrium States and Quantum Energy Inequalities*, Ann. H. Poincare **9**, 945 (2008)

**Books**

R. Verch: *Quantum (or averaged) energy inequalities in quantum field theory*, in: *Quantum Field Thoery and Beyond*, ed. by E. Seiler, K. Sibold (World Scientific, Singapore 2008)

**in press**

B. Geyer: *On thermal Casimir force between real metals*, Proc. *60 Years of Casimir Effect*, Brasilia, Brazil, 23 – 27. June 2008, ed. by V. Dodonov

**Talks**

M. Asorey, B. Geyer, P. Lavrov , O.V. Radchenko: *Basic properties of Fedosov and Riemannian supermanifolds*, 13. Int. Conf. Selected Problems of Modern Theoretical Physics (SPMTP 08), Dubna, Russia, 23. – 27. June 2008

M. Bordag: *Beyond Proximity Force Approximation in the Casimir effect* (plenary talk), 7th Alexander Friedmann Int. Seminar Grav. Cosmol., Joao Pessoa, Paraiba, Brazil, 29. June – 05. July 2008

M. Bordag: *On the renormalization in singular background fields*, 2. Conf. Quantum Field Theoretic Models, Peterhof, Russia, 05. – 07. November 2008

M. Bordag: *Vacuum energy of a spherical plasma sheet*, Seminar at the Bogoliubov Laboratory of Theoretical Physics) (BLTP), Joint Institute for Nuclear Research (JINR), Dubna, Russia, Russia, 29. April 2008

M. Bordag: *On the renormalization in singular background fields* (plenary talk), Int. Workshop 60 years of Casimir effect, Brasilia, Brazil, 23. – 27. June 2008

B. Geyer: *Analytic approach to the thermal Casimir force between metal and dielectric* (invited), 7th Alexander Friedmann Int. Seminar Grav. Cosmol., Joao Pessoa, Paraiba, Brazil, 29. June – 05. July 2008

B. Geyer: *Generalized plasma-like permittivity and thermal Casimir force between real metals* (invited), Int. Workshop 60 years of Casimir effect, Brasilia, Brazil, 23. – 27. June 2008

B. Geyer: *Generalized plasma-like permittivity and thermal Casimir force between real metals* (invited), Workshop Quantum Vacuum 2008, Juiz de Fora, Minas Gerais, Brazil, 06. – 10. July 2008

## 13.11 Graduations

**Diploma**

- Jörn Boehnke
  *The Costratified Structure of an SU*(3)*-Lattice Gauge Model*
  October 2008

## 13.12 Guests

- Dr. S. Charzynski, Prof. Dr. J. Kijowski
  Center for Theoretical Physics, Polish Academy of Sciences, Warsaw, Poland
  17. – 22. September 2008
- Prof. Dr. Galina L. Klimchitskaya
  Department of Physics, North-West Polytechnical University, St. Petersburg, Russia
  01. March – 31. December 2008
- Prof. Dr. Vladimir M. Mostepanenko
  Noncommercial Partnership "Scientific Instruments" of Ministry of Industry, Sciences and Technologies, Moscow, Russia
  01. March – 31. December 2008

- I. Pirozhenko
  JINR Dubna
  19. November – 18. December 2008
- V. Skalozub
  University of Dnepropetrovsk, Russia
  18. November – 17. December 2008

# 14

# Statistical Physics

## 14.1 Introduction

The STP group works on the connections of statistical mechanics to quantum field theory, on the mathematical and physical aspects of renormalization group (RG) theory and on its applications to high-energy and condensed matter physics, and on quantum kinetic theory. Our methods range from mathematical proofs to computational techniques.

The RG method applied here is an exact functional transformation of the action of the system, which leads to an infinite hierarchy of equations for the Green functions. Truncations of this hierarchy are used in applications. In a number of nontrivial cases, this truncation can be justified rigorously, so that the method lends itself to mathematical studies. These mathematical aspects are also under investigation.

Another topic we study is the long-time dynamics of large quantum systems, with a view of understanding how dissipative dynamics on the macroscopic scale arises from the microscopically reversible dynamics in interesting scaling limits.

We have ongoing collaborations with the Max–Planck Institute for Solid State Research in Stuttgart, the University of British Columbia, Vancouver, the University of Munich, the University of Würzburg, the University of Mainz, and Harvard University.

The collaboration within Germany is funded via the DFG research groups FOR723, "Functional Renormalization Group for Correlated Fermion Systems". The group, established in spring, 2007, is coordinated here in Leipzig. Its members are at the univerities of Aachen, Göttingen, Heidelberg, Leipzig, and Würzburg, and at the Max-Planck-Institut für Festkörperforschung, Stuttgart.

As of September 1st, 2008, the STP group has moved to the Institute for Theoretical Physics at University of Heidelberg. Activities of the group up to that date will be reported here briefly.

I would like to take this opportunity to thank the members of the Theoretical Physics Institute and of the Physics Department for the good relations we have experienced during the seven years at this institute. My very special thanks go to Klaus Sibold for his friendship and support, and to the secretarial staff of the institute, Susan Hussack, Gabriele Menge, Gloria Salzer, and Lea Voigt.

*Manfred Salmhofer*

## 14.2 Funding

*Functional Renormalization Group for Correlated Fermion Systems*
M. Salmhofer
DFG Forschergruppe FOR723, coordinator M. Salmhofer

*Analysis and Stochastics in Complex Physical Systems*
M. Salmhofer
DFG-Forschergruppe FOR718, coordinator W. König

*Andrejewski-Vorlesungen*
M. Salmhofer
Andrejewski-Stiftung

## 14.3 Organizational Duties

M. Salmhofer

- Member of the advisory board of the *Andrejewski–Stiftung*.
  Organization of the Andrejewski lectures in Leipzig.
- Referee: Comm. Math. Phys., Phys. Rev. Lett., Phys. Rev. B, J. Stat. Phys., J. Phys. A, Found. Phys., J. Math. Phys., Eur. J. Phys.
- Reviewer: NSERC of Canada, DFG
- Associate editor: J. Math. Phys.
- Editor. Commun. Math. Phys.
- Organisation (joint with H. Gies, W. Metzner, H. Schoeller, C. Wetterich) of the international conference *Exact Renormalization Group 2008*, Internationales Wissenschaftsforum Heidelberg, 1. – 6. July 2008
- Organization of and lectures at the international school *Feynman Diagrams in Quantum Dynamics*, Oberwolfach Seminar, Mathematisches Forschungszentrum Oberwolfach, 11. – 17. Mai 2008 (joint with L. Erdös, B. Schlein, H.-T. Yau)

## 14.4 External Cooperations

**Academic**

- Max-Planck-Institut für Festkörperforschung, Stuttgart, Germany
  W. Metzner
- Institut für Theoretische Physik und Astrophysik, Universität Würzburg, Germany
  C. Honerkamp
- Mathematics Department, University of British Columbia, Vancouver, Canada
  J. Feldman
- Mathematisches Institut, Universität München, Germany
  L. Erdös
- Mathematics Department, Harvard University, Cambridge, USA
  H.-T. Yau

- Institut für Physik, Universität Mainz, Germany
  M. Reuter

## 14.5 Publications

**Journals**

L. Erdös, M. Salmhofer, H.-T. Yau: *Quantum Diffusion of the Random Schrödinger Evolution in the Scaling Limit I. The Non–recollision Diagrams*, Acta Math. **200**, 211 (2008)

J. Feldman, M. Salmhofer: *Singular Fermi Surfaces I. General Power Counting and Higher-Dimensional Cases*, Rev. Math. Phys. **20**, 233 (2008)

J. Feldman, M. Salmhofer: *Singular Fermi Surfaces II. The Two-Dimensional Case*, Rev. Math. Phys. **20**, 275 (2008)

W. Pedra, M. Salmhofer: *Determinant Bounds and the Matsubara UV Problem of Many-Fermion Systems*, Commun. Math. Phys. **282**, 797 (2008)

**Books**

L. Erdös, M. Salmhofer, H.-T. Yau: *Feynman graphs and renormalization in quantum diffusion*, in: *Quantum Field Theory and Beyond: Essays in Honour of Wolfhart Zimmermann*, ed. by E. Seiler, K. Sibold (World Scientific, Singapore 2008) p 167

**Talks**

M. Salmhofer: *Feynman graphs and renormalization in quantum diffusion*, Symposium zum 80. Geburtstag von Wolfhart Zimmermann, Schloss Ringberg, Germany, 03. – 06. February 2008

## 14.6 Graduations

**Doctorate**

- Christoph Husemann
  *Competing Orders in the Hubbard Model*
  December 2008

## 14.7 Guests

- Prof. Joel S. Feldman
  University of British Columbia, Vancouver, Canada
  23. – 27. June 2008 (Andrejewski Lectures)

# 15

# Theory of Condensed Matter

## 15.1 Introduction

Major research topics in our group include nonequilibrium phenomena and pattern formation in systems of various nature, e.g. in soft condensed matter and in biological systems. Modern analytic methods of statistical physics and computer simulations complement and stimulate each other. Cooperations with mathematicians, theoretical and experimental physicists, biologists and medical researchers in Germany, Europe and around the world are well established. Specifically we are interested in the following problems.

**Noise induced phenomena** (Behn). Noise induced non-equilibrium phase transitions are studied in coupled arrays of stochastically driven nonlinear systems. Furthermore, stability and statistical characteristics of stochastic nonlinear systems with time delay are investigated. In cooperation with the Käs-Lab (PWM) we characterize the stochastic dynamics of Lamellipodia.

**Mathematical modeling of the immune system** (Behn). Using methods of nonlinear dynamics and statistical physics, we study the architecture and the random evolution of the idiotypic network of the B-cell subsystem and describe the regulation of balance of the Th1/Th2-cell subsystem including regulatory T-cells, its relation to allergy and the hyposensitization therapy (cooperation with G. Metzner, Clinical Immunology).

**Non-equilibrium dynamics in soft-condensed-matter systems** (Kroy). The systems under investigation range from desert dunes spontaneously developing as a generic consequence of aeolian sand transport, through non-equilibrium gels of adhesive colloids and proteins, the viscoelastic mechanics of the cytoskeleton, to the non-equilibrium dynamics of single DNA molecules under strong external fields. (Related experimental work is currently in progress at EXP1: PWM, PAF.) A common feature is the presence of strong fluctuations and stochastic dynamics on the micro-scale. The emergence of macroscopic structure and (non-linear) deterministic macroscopic dynamics is to be understood. The applied methods range from analytical studies of stochastic integro-differential equations through liquid-state theories, mode-coupling theory, effective hydrodynamic equations, phenomenological modeling, to numerical simulations.

*Ulrich Behn, Klaus Kroy*

## 15.2 Stochastic Phenomena in Systems with Many Degrees of Freedom

U. Behn, S. Gütter, M. Knorr, M. Krieger-Hauwede, L. Wetzel

Arrays of spatially coupled nonlinear dynamical systems driven by multiplicative Gaussian white noise show close analogies to phase transitions in equilibrium [1]. Concepts developed to describe equilibrium phase transitions such as ergodicity breaking, order parameter, critical behaviour, critical exponents etc. have been successfully transfered to noise induced nonequilibrium phase transitions, see for example [2].

For multiplicative noise, essential characteristics of phase transitions can be found alraedy in finite arrays. In the limit of strong coupling there is a clear separation of time scales which allows to eliminate the fast degrees of freedom. The slow center of mass coordinate exhibits a critical behaviour, cf. Fig. 15.1. Analytical results for probability distribution and expectation value are confirmed by numerical simulations [3].

For infinite arrays driven by independent additive and multiplicative noise we considered several limit cases which allow analytical results for the critical values of the control parameter, the critical exponents of order parameter and susceptibility, and the ratio of susceptibility amplitudes. For example, we found a shift of the bifurcation point due to additive noise [4].

Stability and statistical properties (like the return time distribution) of stochastic systems with delayed time argument are further investigated. We study systems driven by additive or multiplicative Gaussian white noise and by dichotomous Markov processes analytically and by numerical simulations. Several stability criteria are compared. The limits of small and large delay are treated analytically [5].

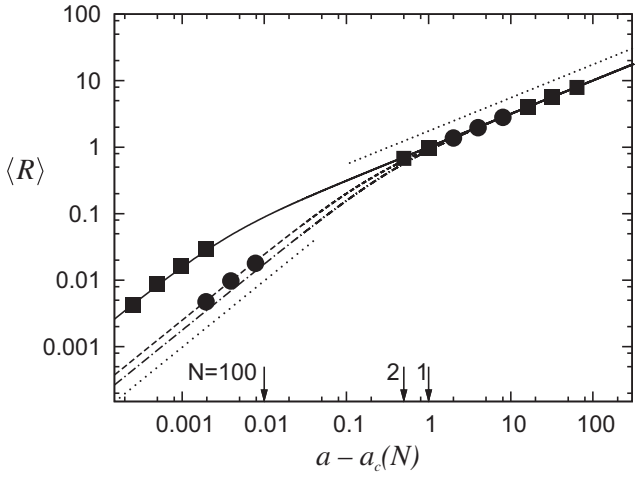


**Figure 15.1:** Crossover in the scaling behaviour of the center of mass coordinate $\langle R \rangle$ as a function of the control parameter $a - a_c(N)$ for different system sizes $N = 1$ (*dash-dotted line*), 2 (*dashed line*), and 100 (*solid line*); the lines are analytic results in the strong coupling limit. Near the critical value of $a$ we have a linear scaling as for $N = 1$ wheras in larger distance a square root behaviour as for $N \to \infty$ is found. The *dotted straight lines* have slope 1 (*left*) and slope 1/2 (*right*). The symbols show results from simulations for $N = 2$ (*circles*) and 100 (*squares*); noise and coupling strength are $\sigma^2 = 1$ and $D = 100$, respectively. The arrows indicate the crossover points.

In a joint project with the Soft Matter Physics group (J. Käs) we developed a minimal model to characterize the stochastic dynamics of Lamellipodia. The model includes underlying processes like aktin polymerization and retrograde flow and describes consistently the experimental data for various cell types [6].

[1] F. Sagués et al.: Rev. Mod. Phys. **79**, 829 (2007)
[2] T. Birner et al.: Phys. Rev. E **65**, 046 110 (2002)
[3] F. Senf et al.: arXiv:0903.2185v1 (2009)
[4] S. Gütter: Diplomarbeit, Universität Leipzig (2008)
[5] L. Wetzel: Diplomarbeit, Universität Leipzig (2008)
[6] M. Knorr: Diplomarbeit, Universität Leipzig (2008)

## 15.3 Mathematical Modeling of the Immune System

U. Behn, F. Groß, H. Schmidtchen, M. Thüne, F. Werner

The paradigm of idiotypic networks developed about 3 decades ago by Jerne [1] finds a renewed interest mainly from the side of system biology and from clinical research; for a recent review which also includes modeling see [2].

B-lymphocytes express on their membrane receptors (antibodies) of a given idiotype. Crosslinking these receptors by complementary structures (antigen or antibodies) stimulates the lymphocyte to proliferate. Thus a macroscopically large, though finite, functional network of lymphocytes, the idiotypic network, emerges. The dynamics is driven by the influx of new idiotypes randomly produced in the bone marrow and by the population dynamics of the lymphocytes themself. In our minimalistic model [3] idiotypes are represented by bitstrings. The model evolves to a highly organized dynamical architecture where groups of nodes with clearly distinct statistical characteristics can be identified. We can analytically compute size and connectivity of these groups. In a modular mean field theory mean occupation of these groups and mean life time of occupied nodes are calculated in good agreement with simulations [4]. We developed a tool which allows to detect the modules of the architecture by online monitoring the simulation, transitions between different modules can be directly observed [5]. A new representation of the link matrix between the groups is found helpful to investigate the scaling properties toward networks of realistic size. First ideas for the design of more sophisticated models (Thüne) and for the reconstruction of the networks architecture from sampling data have been developed (Schmidtchen).

T-helper lymphocytes have subtypes which differ in their spectrum of secreted cytokines. These cytokines have autocrine effects on the own subtype and cross-suppressive effects on the other subtype and regulate the type of immunoglobulines secreted by B-lymphocytes. The balance of Th1- and Th2-cells is perturbed in allergy: the response to allergen is Th2-dominated. Recently, a new type of T-lymphocytes has been identified, the regulatory T-cells (Treg) which suppress other cells. Clinical studies show that during specific immunotherapy the concentration of Tregs is increasing [8, 9]. In collaboration with G. Metzner (Institute of Clinical Immunology) we therefore extended our previous model describing the Th1/Th2 balance [6, 7] by including regulatory T-cells. For a given period of the therapeutic injections of allergen, the 3D state space is separated by the stable manifold of the unstable fixed points of a stroboscopic map into

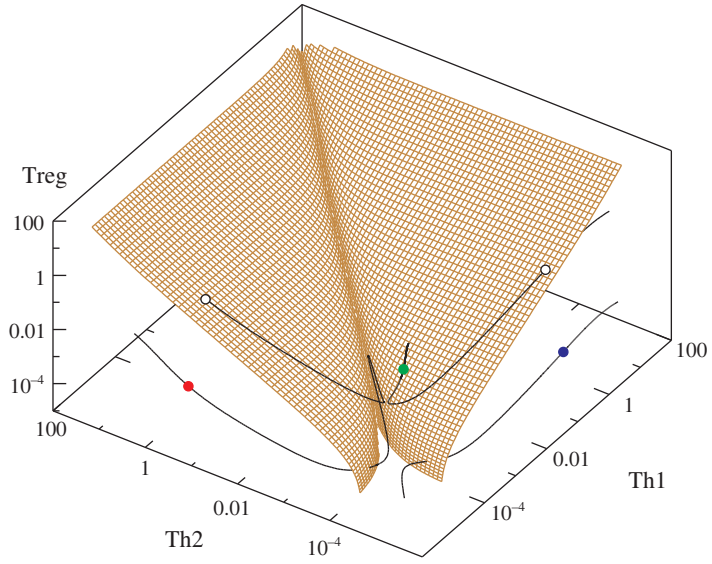


**Figure 15.2:** The figure displays the set of fixed points in the state space spanned by Th1, Th2, and Treg for varying period of allergen injections $\tau$ which is made up of 1D curves. As an example, for $\tau = 4$ the stable (•) and instable (◦) fixed points are shown along with the stable manifolds of the instable fixed points.

basins of attraction of stable fixed points, cf. Fig. 15.2. A successful therapy drives the system towards a stable fixed point where a high population of Tregs dominates both Th2- and Th1-cells, qualitatively similar to experimental findings [10].

[1] N.K. Jerne: Ann. Inst. Pasteur Immunol. **125C**, 373 (1974)
[2] U. Behn: Immunol. Rev. **216**, 142 (2007)
[3] M. Brede, U. Behn: Phys. Rev. E **67**, 031 920 (2003)
[4] H. Schmidtchen, U. Behn: in *Mathematical Modeling of Biological Systems*, Volume II, ed. by A. Deutsch et al. (Birkhäuser, Boston 2008) p 157; H. Schmidtchen et al., in preparation
[5] M. Thüne: Diplomarbeit, Universität Leipzig (2008)
[6] J. Richter et al.: J. Theor. Med. **4**, 119 (2002)
[7] R. Vogel, U. Behn: in *Mathematical Modeling of Biological Systems*, Volume II, ed. by A. Deutsch et al. (Birkhäuser, Boston 2008) p 145
[8] M. Larché et al.: Nature Rev. Immunol. **6**, 761 (2006)
[9] E. Mamessier et al.: Clin. Exp. Allergy **36**, 704 (2006)
[10] F. Groß: Diplomarbeit, Universität Leipzig (2008)

## 15.4 Glassy Dynamics of Polymer Networks

J. Glaser, L. Wolff, C. Hubert, S. Sturm, K. Kroy

Multifunctional scaffolds are the essential building blocks of living cells as well as of a broad class of modern synthetic materials. Examples range from the soft cytoskeleton of the animal cell to stiff carbon nanotube networks. These materials share universal properties and a physical description of their mechanical behavior is indispensable to

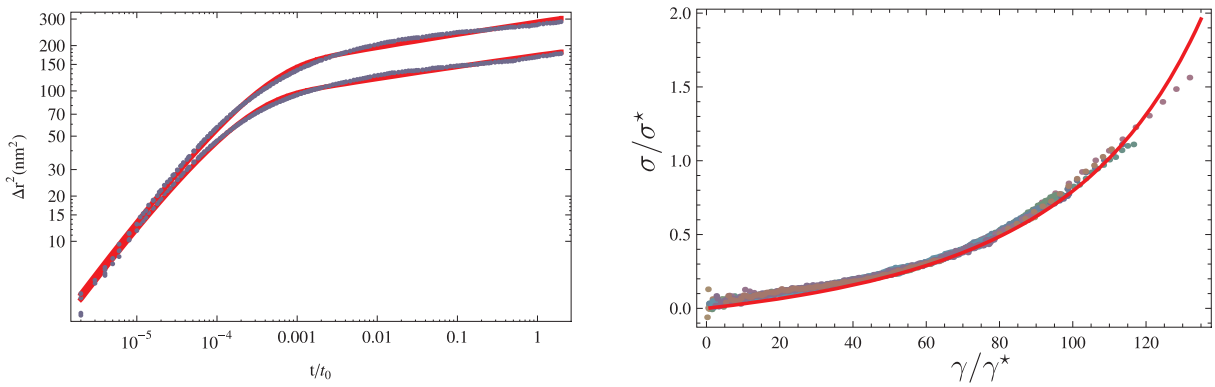


**Figure 15.3:** *Left*: Mean square displacement (MSD) of semiflexible pectin gels and comparison to the MSD of a glassy wormlike chain (GWLC) (*red curves*). *Right*: Stress–strain master relation for actin solutions sheared at constant shear rate [3], compared to the GWLC (*red solid line*).

understand, for example, the effect of stretch on airway cells, which is a major factor in asthma. A successful strategy towards understanding the universal properties of the cytoskeleton as a fibrous, polymeric scaffold has proven to be the 'bottom-up' approach [1], where the complex problem of cell mechanics is investigated in terms of the less complex mechanics of the sub-systems (e.g., in-vitro F-actin networks).

In this spirit, we are working on an extension of the well established wormlike chain model for single polymers. This extended model, the glassy wormlike chain [2–4], accounts for the properties of *networks* of stiff polymers by taking into account the stickiness and steric interactions of the polymers. From this theory, we were already able to derive quantitative results, cf. Fig. 15.3, which were applied in cooperation with experimental biophysics groups [3, 5]. The achieved results constitute a significant step towards a quantitative understanding of cell mechanics.

[1] A.R. Bausch, K. Kroy: Nature Phys. **2**, 231 (2006)
[2] K. Kroy, J. Glaser: New J. Phys. **9**, 416 (2007)
[3] C. Semmrich et al.: Proc. Natl. Acad. Sci. USA **104**, 20 199 (2007)
[4] K. Kroy: Soft Matter **4**, 2323 (2008)
[5] J. Glaser et al.: Eur. Phys. J. E **26**, 123 (2008)

## 15.5 Stiff Polymers in Random Media

M. Hennes, P. Benetatos, K. Kroy

The inside of a eukaryotic cell is a "crowded world" into which are packaged a myriad of organelles and macromolecules and it has been shown that this crowding can severely affect biochemical reactions [1]. A typical filament-like protein under such conditions appears to be subjected to highly complex and heterogeneous forces and sterical constraints. The formidable task of describing the behaviour of a polymer in such a complicated energy landscape might be tackled by assuming the chain to evolve in a random medium. The behaviour of flexible and directed polymers in random media has been extensively studied during the last decades and has found applications

in many different fields of physics [2]. Unfortunately these results cannot be applied to stiff polymers and only little work has been done so far on the influence of stochastic forces and potentials on the conformations of these objects, that play an important role in many biophysical processes. One famous example is the cytoskeleton, which confers the eukaryotic cell its mechanical stability. In this scaffold structure, the stiff filamentous protein F-actin plays a crucial role. Its persistence length can exceed the filament length and can therefore be used as a model system of a weakly bending rod [3]. The study of semidilute actin solutions via confocal video fluorescence microscopy shows a drastic reduction of the persistence length and stronger bending of the filaments as would be expected in the free case [4]. This exemplifies in vitro one possible influence of sterical hindrance: the "wiggling" of the filaments can be dramatically altered by the presence of disorder. Our theoretical investigations aim to explain qualitatively and quantitatively the new disorder induced behaviour of stiff polymers in a random environment. Recent work mainly consisted in exploring the analytical tractability of the problem inspired by methods developed in the field of flexible polymers in random disorder. Future results will be assisted by numerical simulations and hopefully lead towards a more exhaustive understanding of the meshwork cytoskeleton.

[1] R.J. Ellis: Trends Biochem. Sci. **26**, 597 (2001)
[2] T. Halpin-Healy, Y-C. Zhang: Phys. Rep. **254**, 215 (1995)
[3] J. Käs et al.: Biophys. J. **70**, 609 (1996)
[4] M. Romanowska, R. Merkel: unpublished

## 15.6 Tension Propagation in Semiflexible Polymer Networks

S. Sturm, B. Obermayer*, K. Kroy

*Arnold Sommerfeld Center for Theoretical Physics, Ludwig-Maximilians-Universität München

Governed by the tug of war between backbone tension and Brownian forces, the nonequilibrium stretching response of stiff and semiflexible biopolymers exhibits a plethora of nonlinear intermediate scaling regimes that have only recently been analyzed in a systematic fashion [1–4]. Similar mechanisms may underlie the transduction of mechanical signals through the cytoskeleton. In a crowded environment such as the cell, however, energetic and steric constraints imposed by the surrounding polymer network are bound to have a significant influence on single polymer dynamics. We try to capture the essential effects by incorporating the "Glassy Wormlike Chain" model [5] into the aforementioned theory of tension propagation. Asymptotic scaling laws for "longitudinal pulling" and "release" scenarios are discussed, cf. Fig. 15.4. We qualitatively discuss the behavior of a Glassy Wormlike Chain under transverse pulling forces.

[1] O. Hallatschek et al.: Phys. Rev. E **75**, 031905 (2007)
[2] O. Hallatschek et al.: Phys. Rev. E **75**, 031906 (2007)
[3] B. Obermayer, O. Hallatschek: Phys. Rev. Lett. **99**, 098302 (2007)

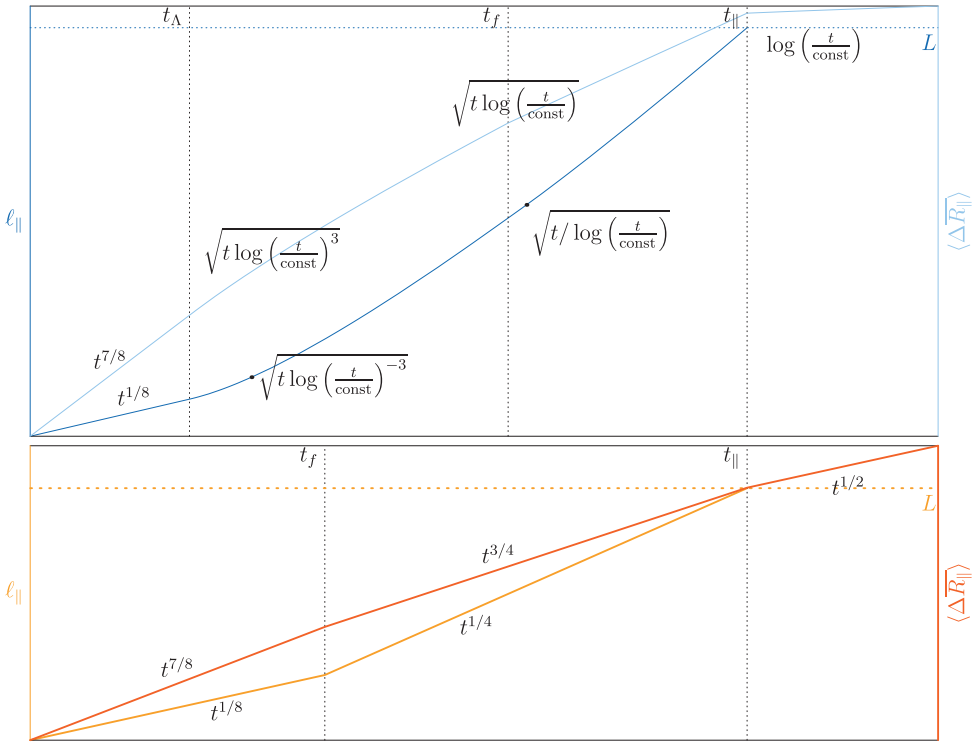


**Figure 15.4:** Longitudinal stretching response $\Delta R_\parallel$ and tension propagation length $\ell_\parallel$ for the WLC (*bottom*), GWLC (*top*).

[4] B. Obermayer et al.: Eur. Phys. J. E **23**, 375 (2007)
[5] K. Kroy, J. Glaser: New J. Phys. **9**, 416 (2007)

## 15.7 Hot Brownian Motion

R. Radünz*, D. Rings, K. Kroy, F. Cichos*

*Workgroup Molekulare Nanophotonik, Institut for Experimental Physics I

Brownian motion is abundant throughout the microscopic and mesoscopic world. Since Einstein's seminal work, there is a good understanding of this process under conditions of thermal equilibrium. Brownian motion of particles in media with inhomogeneous temperature distributions poses several new questions. A new technique called Photothermal Correlation Spectroscopy (PhCS) for the measurement of particle dynamics, which is sensitive to single metal nanoparticles down to a radius of 2.5 nm has been developed by Romy Radünz and Frank Cichos. The method is based on a fluctuation analysis of a heterodyne photothermal scattering signal created by heating the nanoparticle with an intensity modulated laser beam. In close cooperation we formulated a simple theoretical model for a suspension of heated Brownian particles. We determine the Stokes' flow around a spherical particle for radially varying viscosity and thus obtain a renormalized temperature-dependent effective viscosity $\tilde{\eta}$. Further, we deduce an effective temperature $\tilde{T}$ by which this non-equilibrium system of inhomogeneous temperature can be mapped onto a quasi-equilibrium situation. This allows us to formulate

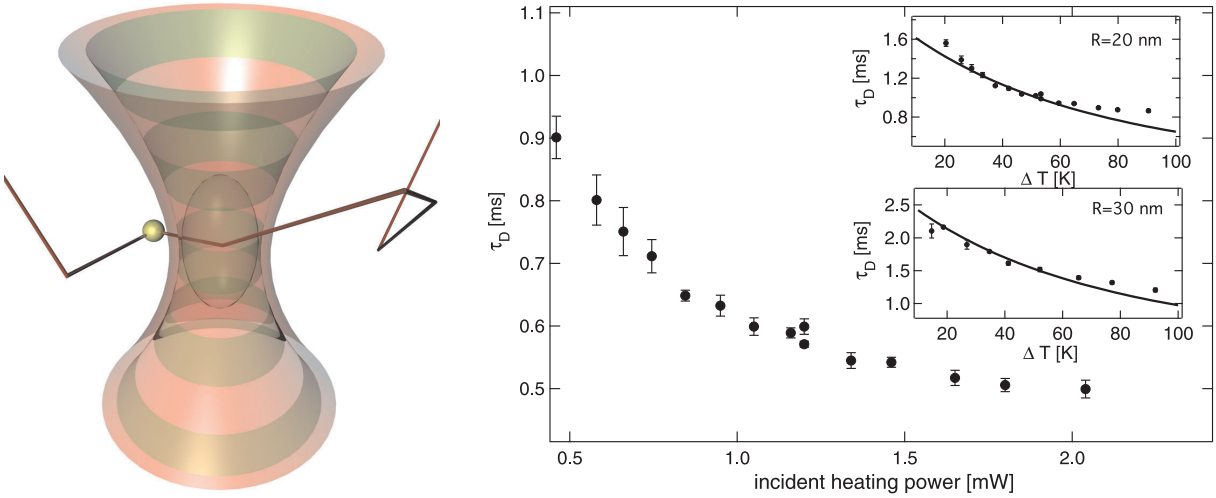


**Figure 15.5:** *Left*: PhoCS detection scheme with overlapping foci of the heating (*green*) and the detection (*red*) laser. *Right*: Experimentally determined diffusion time $\tau_D = A_{\text{focus}}/(4\tilde{D})$ of $R = 20\,\text{nm}$ particles in water at different incident heating powers. The *insets* show the diffusion times over the nanoparticle surface temperature. The *solid lines* represent the theoretical predictions.

a generalized Stokes–Einstein relation $\tilde{D} = k_B\tilde{T}/(6\pi\tilde{\eta}R)$ for the effective quantities [1], cf. Fig. 15.5. Due to the photostability of gold nanoparticles, the method promises broad applications especially in the field of high throughput biological screening.

[1] R. Radünz et al.: J. Phys. Chem. A **113**, 1674 (2009), doi:10.1021/jp810466y

## 15.8 Time-Symmetric Quantum Mechanics

A. Kramer, K. Kroy

In ordinary quantum mechanics, the state of a system depends only on the conditions given in the past. Because of phenomena like nonlocality or the collapse of the wave function, it seems to be a very puzzling theory. But according to Price [1], there seems to be no reason to treat past and future differently in microphysics. Moreover, permitting backward causation avoids the mentioned problems of interpretation. This motivates

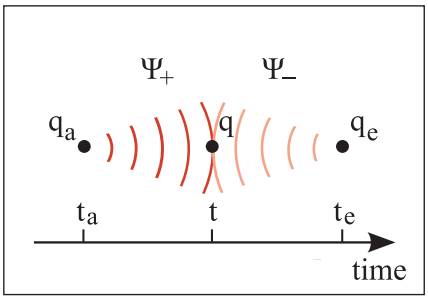


**Figure 15.6:** Determination of an event by initial and final conditions.

the search for a time-symmetric formulation of quantum mechanics that considers past as well as future conditions. In addition to a wave function $\Psi_+$, which contains the initial condition, we introduced a wave function $\Psi_-$ containing the final condition, cf. Fig. 15.6, according to Wharton [2]. From both, we constructed a new wave function for a time-symmetric description of quantum mechanics. Furthermore, we calculated conditional probabilities as a function of time-symmetric boundary conditions and developed a path integral formulation depending on past and future conditions.

[1] H. Price: *Time's Arrow and Archimedes' Point. New Directions for the Physics of Time* (Oxford University Press, New York 1996)
[2] K.B. Wharton: Found. Phys. **37**, 159 (2007), doi:10.1007/s10701-006-9089-1

## 15.9 Jahrmarkt der Wissenschaften 2008

K. Kroy, J. Glaser, D. Rings, L. Wolff, S. Schöbl, S. Sturm, C. Hubert, S. Grosser, M. Hennes, A. Kramer

*Packing Problems* is the keyword to a hands-on exhibition presented at "Jahrmarkt der Wissenschaften" within the context of 2008 being the "Year of Mathematics". From June 28 to July 04 a large number of visitors was attracted to the exhibition

**Figure 15.7:** Simple but appealing experiments demonstrate the effect of different packing configurations on e.g. density, viscosity, yield stress – attracting the interest of all ages.

tents on Augustusplatz. Among the questions addressed were "Which arrangement of spheres fills space most efficiently", "What is the densest packing of ellipsoidal objects?", "Which different phases do hard sphere systems show?", "How does DNA pack itself into a tiny cell's nucleus?". Answers to these questions, illustrating the development from Kepler's conjecture on sphere packing to Hales' proof of the problem in 2003, and implications for modern statistical physics, were presented on a set of posters and made experienceable in a variety of pedagogical experiments, cf. Fig. 15.7.

## 15.10 Funding

*Sächsische Forschergruppe*
J. Glaser
DFG FOR 877 (P3)

*The Leipzig Graduate School "Building with Molecules and Nano-objects"*
S. Sturm, L. Wolff

*Evangelisches Studienwerk Villigst, IMPRS Mathematics in the Sciences*
H. Schmidtchen

## 15.11 Organizational Duties

U. Behn

- Speaker of the Condensed Matter Theory Group
- Vertrauensdozent für die Nobelpreisträgertagungen in Lindau
- Member of PbF2
- Scientific Member of the International Max Planck Research School "Mathematics in the Sciences"
- Referee: Phys. Rev. E, J. Math. Phys.
- Reviewer: Studienstiftung des Deutschen Volkes, Santa Fe Institute, European School of Molecular Medicine, DESY, Evangelisches Studienwerk Villigst

K. Kroy

- Vice Director of the Institute for Theoretical Physics
- Organization of Faculty- & Physics-Colloquia
- Organization of "Die mitteldeutsche Physikcombo"
- Member of the graduation committee
- Member of the committee for information & communication technology
- Study counselor for physics
- Member of PbF1 and PbF2
- Principal Investigator in FG877 and The Leipzig Graduate School "Building with Molecules and Nano-objects"
- Referee: Nature, Phys. Rev. Lett., Eur. Phys. J. E, Soft Matter
- Reviewer: National Science Foundation (NSF), Deutsche Forschungsgemeinschaft (DFG), Nederlandse Organisatie voor Wetenschappelijk Onderzoek (NWO)

## 15.12 External Cooperations

**Academic**

- Max-Planck-Institute for Dynamics and Self-Organization, Göttingen, Germany
  Dr. O. Hallatschek
- University of Edinburgh, UK
  Prof. M.E. Cates
- Forschungszentrum Jülich
  Prof. R. Merkel, Dr. M. Degawa
- Technische Universität München, Germany
  Prof. A. Bausch, S. Fischer
- Massey University, Palmerston North, New Zealand
  Prof. M. Williams, R. Vincent
- Harvard School of Public Health, Boston, USA
  Prof. J. Fredberg
- University of Cambridge, UK
  Dr. P. Benetatos
- Otto-von-Guericke-Universität Magdeburg, Germany
  Prof. Dr. J. Richter
- Joint Institute for Nuclear Research, Dubna, Russia
  Prof. Dr. N.M. Plakida
- Ernst-Moritz-Arndt-Universität Greifswald, Germany
  Prof. Dr. H. Fehske
- Philipps-Universität Marburg, Germany
  Prof. Dr. G. Germano, E. Martin
- Max-Planck-Institut für Evolutionsbiologie, Plön, Germany
  Dipl.-Phys. P. Altrock
- Leibniz-Institut für Atmosphärenphysik, Kühlungsborn, Germany
  Dipl.-Phys. F. Senf
- Institut für Klinische Immunologie, Universität Leipzig, Germany
  Prof. Dr. G. Metzner
- Institut für Experimentalphysik I, Universität Leipzig, Germany
  Prof. F. Cichos, R. Radünz
- Institut für Experimentalphysik I, Universität Leipzig, Germany
  Prof. Dr. A. Käs, Dr. D. Koch

## 15.13 Publications

### Journals

S. Fischer, M.E. Cates, K. Kroy: *Dynamic scaling of desert dunes*, Phys. Rev. E **77**, 031 302 (2008)

J. Glaser, O. Hallatschek, K. Kroy: *Dynamic structure factor of a stiff polymer in a glassy solution*, Eur. Phys. J. E **26**, 123 (2008)

M. Härtel, J. Richter, D. Ihle, S.-L. Drechsler: *Thermodynamics of a one-dimensional frustrated spin-1/2 Heisenberg ferromagnet*, Phys. Rev. B **78**, 174 412 (2008)

D. Ihle, M. Pfafferott, E. Burovski, F.X. Bronold, H. Fehske: *Bound state formation and the nature of the excitonic insulator phase in the extended Falicov–Kimball model*, Phys. Rev. B **78**, 193 103 (2008)

I. Juhasz Junger, D. Ihle, L. Bogacz, W. Janke: *Thermodynamics of Heisenberg ferromagnets with arbitrary spin in a magnetic field*, Phys. Rev. B **77**, 174 411 (2008)

K. Kroy: *Dynamics of wormlike and glassy wormlike chains*, Soft Matter **4**, 2323 (2008)

### Books

J. Glaser, C. Hubert, K. Kroy: *Dynamics of sticky polymer solutions*, in: *Path Integrals – New Trends and Perspectives*, ed. by W. Janke, A. Pelster (World Scientific, Singapore 2008)

H. Schmidtchen, U. Behn: *Architecture of Randomly Evolving Idiotypic Networks*, in: *Mathematical Modeling of Biological Systems*, Vol. II, ed. by A. Deutsch, R. Bravo de la Parra, R. de Boer, O. Diekmann, P. Jagers, E. Kisdi, M. Kretzschmar, P. Lansky, H. Metz (Birkhäuser, Boston 2008) p 157

R. Vogel, U. Behn: *Th1–Th2 Regulation and Allergy: Bifurcation Analysis of the Non-autonomous System*, in: *Mathematical Modeling of Biological Systems*, Vol. II, ed. by A. Deutsch, R. Bravo de la Parra, R. de Boer, O. Diekmann, P. Jagers, E. Kisdi, M. Kretzschmar, P. Lansky, H. Metz (Birkhäuser, Boston 2008) p 145

### in press

F. Senf, P.M. Altrock, U. Behn: *Nonequilibrium phase transitions in finite arrays of globally coupled Stratonovich models: Strong coupling limit*, New J. Phys., arXiv:0903.2185v1

### Talks

U. Behn: *Randomly evolving idiotypic networks*, Invited Talk, Workshop Networks, Complexity, and Competition, Bled, Slovenia, 2. – 4. May 2008

J. Glaser: *Confined Brownian Motion of Biopolymers*, Meeting of the Saxonian Research Group, Dresden, Germany, 27. November 2008

J. Glaser: *Nonlinear rheology of a glassy solution of semiflexible polymers*, 72. DPG Spring Meeting, Berlin, Germany 25. – 29. February 2008

J. Glaser: *The glassy wormlike chain*, 1. BuildMoNa Workshop, Leipzig, Germany, 16./17. October 2008

D. Koch, M. Knorr, T. Fuhs, T. Betz, U. Behn, J. Käs: *Stochastic Lamellipodium Dynamics and Forces in Cell Motility*, 72. DPG Spring Meeting, Berlin, Germany 25. – 29. February 2008

K. Kroy: *Are we built of glass? The strange mechanics of living matter*, Kolloquium, Universität Erlangen, Germany, 07. January 2008

K. Kroy: *Are we built of glass? The strange mechanics of living matter*, Theoriekolloquium, Universität Stuttgart, Germany, 08. January 2008

K. Kroy: *Are we built of glass?*, 72. DPG Spring Meeting, Berlin, Germany 25. – 29. February 2008

K. Kroy: *Sind wir aus Glas? Die sonderbare Mechanik menschlicher Zellen*, Buchmesse Leipzig, Germany, 13. – 16. March 2008

K. Kroy: *Warum ist die Wüste nicht flach?*, Mathematik-Kolloquium, Universität Leipzig, Germany, 10. January 2008

D. Rings: *Hot Brownian motion*, Meeting of the Saxonian Research Group, Dresden, 27. November 2008

**Posters**

J. Glaser: *Packing structure and dynamics of stiff polymers*, Jülich Soft Matter Days, Bonn, Germany, 11. – 14. November 2008

C. Hubert: *Nonlinear rheology of a glassy solution of semiflexible polymers*, 72. DPG Spring Meeting, Berlin, Germany 25. – 29. February 2008

D. Rings: *Hot Brownian Motion*, Jülich Soft Matter Days, Bonn, Germany 11. – 14. November 2008

D. Rings: *Shear-Driven Cluster Aggregation: Hierarchical Algorithm and Dependence on Initial Conditions*, Crystallization and Jamming, Leiden, The Netherlands, 10. – 15. February 2008

D. Rings: *Shear-Driven Cluster Aggregation: Hierarchical Algorithm and Dependence on Initial Conditions*, 72. DPG Spring Meeting, Berlin, Germany 25. – 29. February 2008

S. Sturm: *How molecular crowding speeds up mechanotransduction*, Jülich Soft Matter Days, Bonn, Germany, 11. – 14. November 2008

S. Sturm: *Molecular crowding speeds up mechano-transduction*, 72. DPG Spring Meeting, Berlin, Germany 25. – 29. February 2008

S. Sturm: *Nonequilibrium dynamics of confined and forced single molecules*, 1. Scientific Symposium of BuildMoNa, Leipzig, Germany, 07./08. February 2008

## 15.14 Graduations

**Diploma**

- Fridolin Groß
  *Nichtlineare Populationsdynamik von T-Zellen bei Allergien: Einfluss regulatorischer T-Zellen*
  December 2008
- Susanne Gütter
  *Universalität bei rauschinduzierten Phasenübergängen im Nichtgleichgewicht*
  May 2008
- Christian Hubert
  *Zur Beschreibung von Polymernetzwerken durch das Modell der glassy wormlike chain (GWLC)*
  September 2008
- Melanie Knorr (Dipl.-Math.)
  *Stochastic Lamellipodium Dynamics in Cell Motility: Searching a Minimal Model*
  May 2008
- Sebastian Schöbl
  *Impact of disorder on flocculation and semiflexible polymer conformations*
  March 2008
- Sebastian Sturm
  *Tension propagation in semiflexible polymer networks*
  September 2008
- Mario Thüne
  *Zur Architektur idiotypischer Netzwerke: Ein minimales Modell und einfache Erweiterungen*
  December 2008
- Lucas Wetzel
  *Stability and Statistical Properties of Stochastic Delay Differential Equations*
  February 2008

**Staatsexamen**

- Andrea Kramer
  *Retrokausation und Quantenmechanik*
  November 2008

## 15.15 Guests

- Dr. P. Benetatos
  University of Cambridge
  01. October 2008 – 04. March 2009

- Dipl.-Phys. Edgar Martin
  Physikalische Chemie, Philipps-Universität Marburg
  21. – 24. April 2008

# 16

# Theory of Elementary Particles

## 16.1 Introduction

The Particle Physics Group performs basic research in the quantum field theoretic description of elementary particles and in phenomenology. Topics of current interest are conformal symmetry and its breaking in the context of supersymmetric theories, the formulation of models which realize noncommutative geometry, renormalization problems, electroweak matter at finite temperature, the lattice formulation of gauge theories, the derivation of Regge behaviour of scattering amplitudes from Quantum Chromodynamics and the related study of integrable models with and without supersymmetry. Perturbative and non-perturbative methods are applied to answer the respective questions. In perturbation theory the work is essentially analytic using computers only as a helpful tool. Lattice Monte Carlo calculations as one important non-perturbative approach however are based on computers as an indispensable instrument. Correspondingly the respective working groups are organized: in analytical work usually very few people collaborate, in the lattice community rather big collaborations are the rule. Our group is involved in many cooperations on the national and international level (DESY, Munich; France, Russia, Armenia, USA, Japan). Since elementary particles are very tiny (of the order of $10^{-15}$ m) and for the study of their interactions large accelerators producing enormously high energy are needed, it is clear that results in this direction of research do not have applications in daily life immediately. To clarify the structure of matter is first of all an aim in its own and is not pursued for other reasons. But particle theory has nevertheless a very noticeable impact on many other branches of physics by its power of providing new methodological insight. Similarly for the student specializing in this field the main benefit is her/his training in analysing complex situations and in applying tools which are appropriate for the respective problem. As a rule there will be no standard procedures which have to be learned and then followed, but the student has to develop her/his own skill according to the need that arises. This may be a mathematical topic or a tool in computer application. Jobs which plainly continue these studies are to be found at universities and research institutes only. But the basic knowledge which one acquires in pursuing such a subject opens the way to many fields where analytical thinking is to be combined with application of advanced mathematics. Nowadays this seems to be the case in banks, insurance companies and consulting business.

*Klaus Sibold*

## 16.2 Conjugate Variables in Quantum Field Theory and Natural Symplectic Structures

K. Sibold

Within standard quantum field theory we establish relations which operators conjugate to the energy-momentum operator of the theory would have. They thus can be understood as representing the effect of coordinate operators. The non-trivial commutation relations we derive constitute natural symplectic structures in the theory. The example which is based on the energy-momentum tensor of the theory is constructed to all orders of perturbation theory. The reference theory is massless $\phi^4$. The extension to other theories is indicated [1].

[1] K. Sibold: Nucl. Phys. B **811**, 363 (2009)

## 16.3 Perturbative Determination of $c_{SW}$ for Different Lattice Gauge Actions and Stout Link Clover Fermions

R. Horsley*, H. Perlt, P.E.L. Rakow†, G. Schierholz‡, A. Schiller

*School of Physics and Astronomy, University of Edinburgh, UK
†Theoretical Physics Division, Department of Mathematical Sciences, University of Liverpool, UK
‡Deutsches Elektronen-Synchrotron DESY, Germany

Lattice simulations of Wilson-type fermions at realistic quark masses for Quantum Chromodynamics require an improved action with good chiral properties and scaling behavior. A systematic improvement scheme that removes discretization errors order by order in the lattice spacing $a$ has been proposed by Symanzik [1] and developed for on-shell quantities in [2, 3]. $O(a)$ improvement of the Wilson fermion action is achieved by complementing it with the so-called clover term [3], provided the associated clover coefficient is tuned properly. Clover fermions have the lattice action for each quark flavor [3]

$$S_F = a^4 \sum_x \Big\{ -\frac{1}{2a} \left[ \bar\psi(x) \widetilde U_\mu(x) \, (1-\gamma_\mu) \, \psi(x+a\hat\mu) + \bar\psi(x) \widetilde U^\dagger_\mu(x-a\hat\mu) \, (1+\gamma_\mu) \, \psi(x-a\hat\mu) \right] + \frac{1}{a} (4 + a\, m_0 + a\, m) \, \bar\psi(x)\psi(x) - c_{SW}\, g\, \frac{a}{4}\, \bar\psi(x)\, \sigma_{\mu\nu} F_{\mu\nu}(x)\, \psi(x) \Big\} \,, \tag{16.1}$$

where

$$a m_0 = \frac{1}{2\kappa_c} - 4 \,, \tag{16.2}$$

$\kappa_c$ being the critical hopping parameter, is the additive mass renormalization term, and $F_{\mu\nu}(x)$ is the lattice field strength tensor in clover form with $\sigma_{\mu\nu} = (i/2)\,(\gamma_\mu\gamma_\nu - \gamma_\nu\gamma_\mu)$. We

consider a version of clover fermions in which we do not smear links in the clover term, but the link variables $U_\mu$ in the next neighbor terms have been replaced by (uniterated) stout links [4]

$$\widetilde{U}_\mu(x) = \mathrm{e}^{i\,Q_\mu(x)}\,U_\mu(x) \tag{16.3}$$

with

$$Q_\mu(x) = \frac{\omega}{2\,i}\left[V_\mu(x)U_\mu^\dagger(x) - U_\mu(x)V_\mu^\dagger(x) - \frac{1}{3}\mathrm{Tr}\,\left(V_\mu(x)U_\mu^\dagger(x) - U_\mu(x)V_\mu^\dagger(x)\right)\right]\,. \tag{16.4}$$

$V_\mu(x)$ denotes the sum over all staples associated with the link and $\omega$ is a tunable weight factor.

Here we present a perturbative tuning of the clover coefficient using perturbation theory of lattice QCD. In perturbation theory

$$c_{SW} = 1 + g^2\,c_{SW}^{(1)} + O\left(g^4\right)\,. \tag{16.5}$$

The one-loop coefficient $c_{SW}^{(1)}$ has been computed for the plaquette action using twisted antiperiodic boundary conditions [5] and Schrödinger functional methods [6]. Moreover, using conventional perturbation theory, Aoki and Kuramashi [7] have computed $c_{SW}^{(1)}$ for certain improved gauge actions. All calculations were performed for non-smeared links and limited to on-shell quantities.

We extend previous calculations of $c_{SW}^{(1)}$ to include stout links. This is done by computing the one-loop correction to the off-shell quark-quark-gluon three-point function. The improvement of the action is not sufficient to remove discretization errors from Green functions. To achieve this, one must also improve the quark fields

$$\psi_\star(x) = \left(1 + a\,c_D\,\vec{\not{D}} + a\,i\,g\,c_{NGI}\not{A}(x)\right)\psi(x)\,, \tag{16.6}$$

where the improvement factor $c_{NGI}$ has been introduced by [8] and has the perturbative expansion

$$c_{NGI} = g^2\,c_{NGI}^{(1)} + O\left(g^4\right)\,. \tag{16.7}$$

For the plaquette and Symanzik gauge actions we obtain the one-loop contributions of the clover improvement coefficient ($C_F = (N_c^2-1)/(2N_c)$, $N_c = 3$ for $SU(3)$)

$$\begin{aligned} c_{SW}^{(1),\mathrm{Plaq}} &= C_F\left(0.167635 + 1.079148\,\omega - 3.697285\,\omega^2\right) \\ &\quad + N_c\left(0.015025 + 0.009617\,\omega - 0.284786\,\omega^2\right)\,, \end{aligned} \tag{16.8}$$

$$\begin{aligned} c_{SW}^{(1),\mathrm{Sym}} &= C_F\left(0.116185 + 0.828129\,\omega - 2.455080\,\omega^2\right) \\ &\quad + N_c\left(0.013777 + 0.015905\,\omega - 0.321899\,\omega^2\right)\,, \end{aligned} \tag{16.9}$$

and the off-shell quark field improvement coefficient

$$c_{NGI}^{(1),\mathrm{Plaq}} = N_c\,(0.001426 - 0.011664\,\omega)\,, \tag{16.10}$$

$$c_{NGI}^{(1),\mathrm{Sym}} = N_c\,(0.002395 - 0.010841\,\omega)\,. \tag{16.11}$$

A detailed discussion can be found in [9].

[1] K. Symanzik: Nucl. Phys. B **226**, 187 (1983)
[2] M. Lüscher, P. Weisz: Commun. Math. Phys. **97**, 59 (1985) [Erratum: ibid. **98**, 433 (1985)]
[3] B. Sheikholeslami, R. Wohlert: Nucl. Phys. B **259**, 572 (1985)
[4] C. Morningstar, M.J. Peardon: Phys. Rev. D **69**, 054 501 (2004), arXiv:hep-lat/0311018
[5] R. Wohlert: DESY preprint 87/069 (unpublished)
[6] M. Lüscher, P. Weisz: Nucl. Phys. B **479**, 429 (1996), arXiv:hep-lat/9606016
[7] S. Aoki, Y. Kuramashi: Phys. Rev. D **68**, 094019 (2003), arXiv:hep-lat/0306015
[8] G. Martinelli et al.: Nucl. Phys. B **611**, 311 (2001), arXiv:hep-lat/0106003
[9] R. Horsley et al.: Phys. Rev. D **78**, 054 504 (2008), arXiv:0807.0345 [hep-lat]

## 16.4 Integrable Quantum Systems and Gauge Field Theories

S.E. Derkachov*, D. Karakhanyan†, R. Kirschner, P. Valinevich‡

*Steklov-Institute of Mathematics, St. Petersburg, Russia
†Yerevan Physics Institute, Armenia
‡St. Petersburg State University, Russia

Integrable quantum systems are applied successfully to the study of the high-energy asymptotics and of the renormalization of composite operators in gauge theories [1, 4]. These application stimulated the development of the methods of quantum systems.

The Lax matrices as particular solutions of the Yang-Baxter relation are shown to provide the appropriate formulation for the Biedenharn iterative construction of representations of the $sl(n)$ symmetry algebra from representation of the lower rank algebra. On this basis our factorisation method of constructing general Yang-Baxter solutions can be applied.

[1] L.N. Lipatov: Padova preprint DFPD-93-TH-70B; JETP Lett. **59**, 596 (1994)
[2] L.D. Faddeev, G.P. Korchemsky: Phys. Lett. B **342**, 311 (1995), arXiv:hep-th/9404173
[3] V.M. Braun et al.: Phys. Rev. Lett. **81**, 2020 (1998), arXiv:hep-ph/9805225
[4] N. Beisert: Phys. Rept. **407**, 1 (2004)
[5] S. Derkachov et al.: Nucl. Phys. B **785**, 263 (2007), arXiv:hep-th/0703076

## 16.5 Funding

*Perturbative determination of $c_{SW}$ for different lattice gauge actions and stout link clover fermions*
Supported by DFG through the DFG-Forschergruppe "Lattice Hadron Phenomenology" FOR465 and by EU Integrated Infrastructure Initiative Hadron Physics (I3HP) under contract number RII3-CT-2004-506078

*Integrable quantum systems related to gauge field theories*
Support of the visit of S.E. Derkachov (St. Petersburg) and D.R. Karakhanyan (Yerevan) by DFG, DAAD and NTZ

## 16.6 Organizational Duties

R. Kirschner
- Referee: Phys. Rev. D, Eur. Phys. J. C
- Member of the PhD commission of the faculty

A. Schiller
- Referee: Phys. Rev. D

K. Sibold
- Associated member of the Graduiertenkolleg: "Analysis, Geometrie und die Naturwissenschaften"
- Coorganizer of the "Mitteldeutsche Physik-Combo" (joint graduate lecture courses with universities Jena and Halle)
- Member of the "Beirat" of the Fachverband "Mathematische und Theoretische Grundlagen der Physik" (German Physical Society)

## 16.7 External Cooperations

**Academic**

- Nuclear Physics Institute, St. Petersburg, Russia
  Prof. L.N. Lipatov
- St. Petersburg branch of Steklov Mathematical Institute, Russia
  Dr. S.E. Derkachov
- Yerevan Physics Institute, Theory Department, Armenia
  Prof. A. Sedrakyan
- Soltan Institut of Nuclear Studies, Warsaw, Poland
  Dr. L. Szymanowski
- Sobolev Institut of Mathematics, Novosibirsk, Russia
  Dr. D.Y. Ivanov
- Universität Hamburg, Institut für Theoretische Physik & DESY, Germany
  Prof. J. Bartels
- Universität Regensburg, Institut für Theoretische Physik, Germany
  Prof. A. Schäfer, Prof. V. Braun, Dr. M. Göckeler, Dr. C. Torrero
- Humboldt-Universität Berlin, Germany
  Dr. E.-M. Ilgenfritz, Prof. M. Müller-Preussker
- Ecole Polytechnique, Paris-Palaiseau, France
  Prof. B. Pire
- NIC, Zeuthen & DESY, Hamburg, Germany
  Prof. G. Schierholz
- Edinburgh University, UK
  Dr. R. Horsley

- Department of Mathematics, Liverpool University, UK
  Dr. P.E.L. Rakow
- Parma University, Italy
  Prof. F. Di Renzo

## 16.8 Publications

### Journals

S.E. Derkachov, D. Karakhanyan, R. Kirschner, P. Valinevich: *Factorization of the R-matrix in the case of the quantum algebras* $sl_q(3)$, J. Math. Sci. **151**, 124 (2008)

S.E. Derkachov, D. Karakhanyan, R. Kirschner, P. Valinevich: *Iterative construction of* $U_q(s\ell(n+1))$ *representations and Lax matrix factorisation*, Lett. Math. Phys. **85**, 221 (2008), arXiv:0805.4724 [hep-th]

R. Horsley, H. Perlt, P.E.L. Rakow, G. Schierholz, A. Schiller: *Perturbative determination of* $c_{SW}$ *for plaquette and Symanzik gauge action and stout link clover fermions*, Phys. Rev. D **78**, 054 504 (2008), arXiv:0807.0345 [hep-lat]

### Proceedings

W. Bietenholz, N. Cundy, M. Gockeler, R. Horsley, H. Perlt, D. Pleiter, P.E.L. Rakow, G. Schierholz, A. Schiller, J.M. Zanotti: *Nucleon structure in terms of OPE with non-perturbative Wilson coefficients*, arXiv:0808.3637 [hep-lat]

N. Cundy, M. Göckeler, R. Horsley, T. Kaltenbrunner, A.D. Kennedy, Y. Nakamura, H. Perlt, D. Pleiter, P.E.L. Rakow, A. Schäfer, G. Schierholz, A. Schiller, H. Stüben, J.M. Zanotti: *Clover improvement for stout-smeared 2+1 flavour SLiNC fermions: non-perturbative results*, arXiv:0811.2355 [hep-lat]

F. Di Renzo, E.M. Ilgenfritz, H. Perlt, A. Schiller, C. Torrero: *Higher-loop gluon and ghost propagators in Landau gauge from numerical stochastic perturbation theory*, arXiv:0812.3307 [hep-lat]

R. Horsley, H. Perlt, P.E.L. Rakow, G. Schierholz, A. Schiller: *Clover improvement for stout-smeared 2+1 flavour SLiNC fermions: perturbative results*, arXiv:0809.4769 [hep-lat]

### Posters

F. Di Renzo, E.M. Ilgenfritz, H. Perlt, A. Schiller, C. Torrero: *The Landau gauge lattice ghost propagator in stochastic perturbation theory*, 26. Int. Symp. Lattice Field Theory, Williamsburg, USA, 14. – 19. July 2008, arXiv:0809.4950 [hep-lat]

# Author Index

## E



## F



## G



## H



## I



## J



## K

## L



## M



## N



## O



## P



## R

## S



## T



## U



## V



## W

## Y



## Z

Proceedings of the 9th International Conference

# PATH INTEGRALS

## NEW TRENDS AND PERSPECTIVES

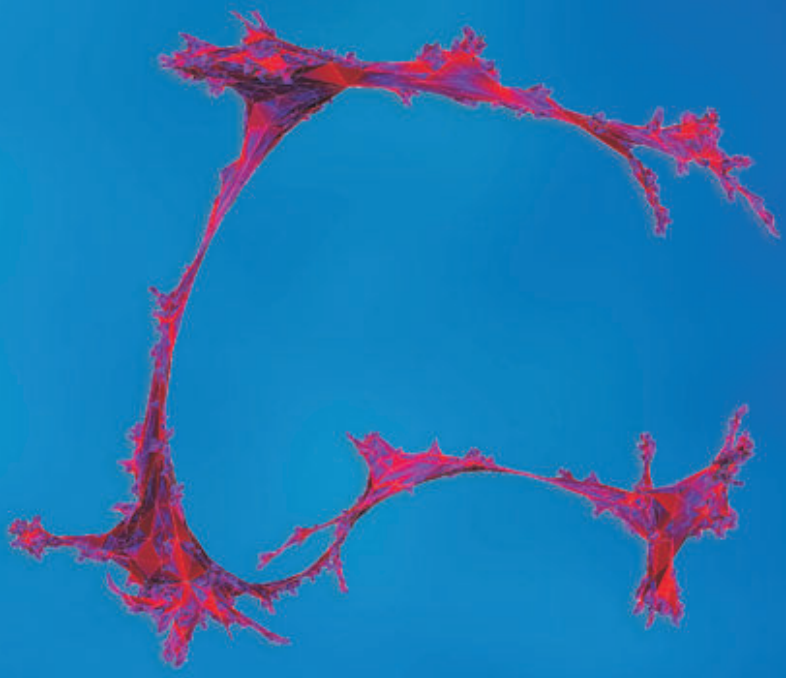

**Wolfhard Janke**
**Axel Pelster**
*editors*

World Scientific